



STIMULI-RESPONSIVE CALIX[4]PYRROLE AND CALIX[4]ARENE BASED RECEPTORS: FROM UNIMOLECULAR TO DIMERIC STRUCTURES

Pedro Miguel Mendonça Ferreira

ADVERTIMENT. L'accés als continguts d'aquesta tesi doctoral i la seva utilització ha de respectar els drets de la persona autora. Pot ser utilitzada per a consulta o estudi personal, així com en activitats o materials d'investigació i docència en els termes establerts a l'art. 32 del Text Refós de la Llei de Propietat Intel·lectual (RDL 1/1996). Per altres utilitzacions es requereix l'autorització prèvia i expressa de la persona autora. En qualsevol cas, en la utilització dels seus continguts caldrà indicar de forma clara el nom i cognoms de la persona autora i el títol de la tesi doctoral. No s'autoritza la seva reproducció o altres formes d'explotació efectuades amb finalitats de lucre ni la seva comunicació pública des d'un lloc aliè al servei TDX. Tampoc s'autoritza la presentació del seu contingut en una finestra o marc aliè a TDX (framing). Aquesta reserva de drets afecta tant als continguts de la tesi com als seus resums i índexs.

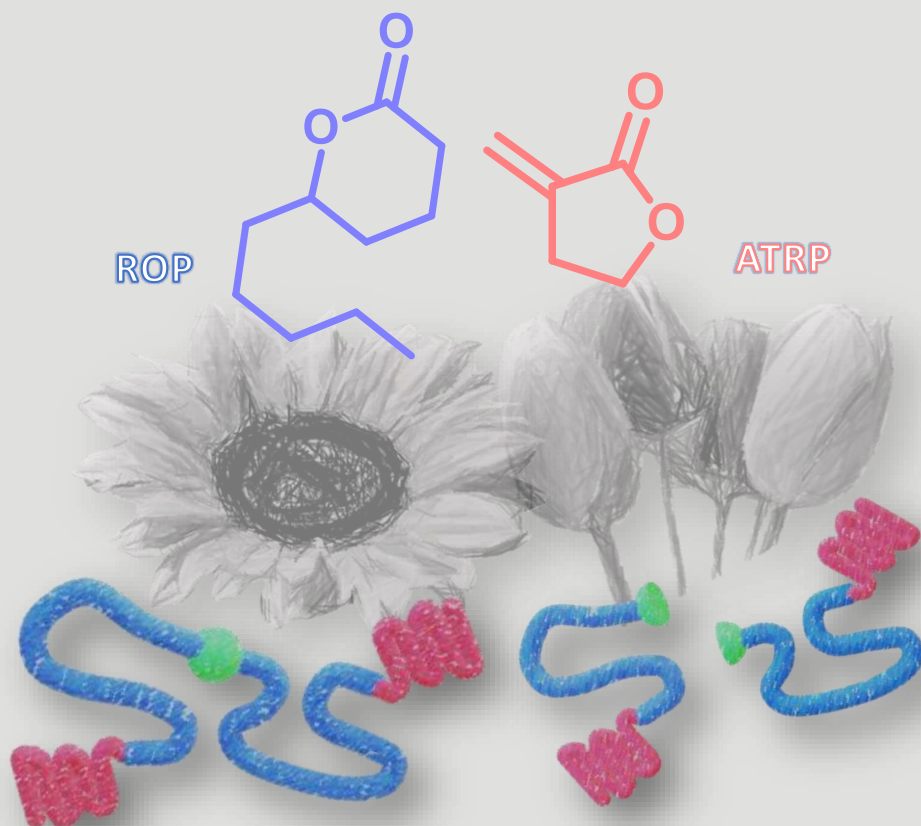
ADVERTENCIA. El acceso a los contenidos de esta tesis doctoral y su utilización debe respetar los derechos de la persona autora. Puede ser utilizada para consulta o estudio personal, así como en actividades o materiales de investigación y docencia en los términos establecidos en el art. 32 del Texto Refundido de la Ley de Propiedad Intelectual (RDL 1/1996). Para otros usos se requiere la autorización previa y expresa de la persona autora. En cualquier caso, en la utilización de sus contenidos se deberá indicar de forma clara el nombre y apellidos de la persona autora y el título de la tesis doctoral. No se autoriza su reproducción u otras formas de explotación efectuadas con fines lucrativos ni su comunicación pública desde un sitio ajeno al servicio TDR. Tampoco se autoriza la presentación de su contenido en una ventana o marco ajeno a TDR (framing). Esta reserva de derechos afecta tanto al contenido de la tesis como a sus resúmenes e índices.

WARNING. Access to the contents of this doctoral thesis and its use must respect the rights of the author. It can be used for reference or private study, as well as research and learning activities or materials in the terms established by the 32nd article of the Spanish Consolidated Copyright Act (RDL 1/1996). Express and previous authorization of the author is required for any other uses. In any case, when using its content, full name of the author and title of the thesis must be clearly indicated. Reproduction or other forms of for profit use or public communication from outside TDX service is not allowed. Presentation of its content in a window or frame external to TDX (framing) is not authorized either. These rights affect both the content of the thesis and its abstracts and indexes.



Stimuli cleavable ABA block copolymers: Synthesis of degradable thermoplastic elastomers from renewable resources.

PERE MANEL VERDUGO FERNÁNDEZ



UNIVERSITAT ROVIRA I VIRGILI
STIMULI-RESPONSIVE CALIX[4]PYRROLE AND CALIX[4]ARENE BASED RECEPTORS: FROM UNIMOLECULAR
TO DIMERIC STRUCTURES

Pedro Miguel Mendonça Ferreira

UNIVERSITAT ROVIRA I VIRGILI
STIMULI-RESPONSIVE CALIX[4]PYRROLE AND CALIX[4]ARENE BASED RECEPTORS: FROM UNIMOLECULAR
TO DIMERIC STRUCTURES

Pedro Miguel Mendonça Ferreira

UNIVERSITAT ROVIRA I VIRGILI
STIMULI-RESPONSIVE CALIX[4]PYRROLE AND CALIX[4]ARENE BASED RECEPTORS: FROM UNIMOLECULAR
TO DIMERIC STRUCTURES

Pedro Miguel Mendonça Ferreira

Pere Manel Verdugo Fernández

Stimuli cleavable ABA block copolymers: Synthesis of degradable
thermoplastic elastomers from renewable resources.

PhD Thesis

Supervised by Prof. Juan Carlos Ronda Bargalló

Department of Analytic Chemistry and Organic Chemistry



UNIVERSITAT
ROVIRA i VIRGILI

Tarragona

2020

UNIVERSITAT ROVIRA I VIRGILI
STIMULI-RESPONSIVE CALIX[4]PYRROLE AND CALIX[4]ARENE BASED RECEPTORS: FROM UNIMOLECULAR
TO DIMERIC STRUCTURES

Pedro Miguel Mendonça Ferreira



UNIVERSITAT
ROVIRA I VIRGILI

Departament de Química Analítica i Química Orgànica

C/Marcel·lí Domingo, 1

43007, Tarragona

Tel. 977558045

Prof. Juan Carlos Ronda Bargalló from the Departament of Analytical Chemistry and Organic Chemistry, Universitat Rovira i Virgili,

I STATE that the present study, entitled:

“Stimuli cleavable ABA block copolymers: Synthesis of degradable thermoplastic elastomers from renewable resources.”

Presented by Pere Manel Verdugo Fernández for the award of the degree of Doctor, has been carried out under my supervision at the Department of Analytical Chemistry and Organic Chemistry of this University.

Tarragona, 18 December 2020

Doctoral Thesis Supervisor

Prof. Juan Carlos Ronda Bargalló

UNIVERSITAT ROVIRA I VIRGILI
STIMULI-RESPONSIVE CALIX[4]PYRROLE AND CALIX[4]ARENE BASED RECEPTORS: FROM UNIMOLECULAR
TO DIMERIC STRUCTURES

Pedro Miguel Mendonça Ferreira

ABSTRACTS:

CATALÀ

Actualment, un dels majors reptes que afronta la societat es el de adaptar la nostra forma de viure de tal manera que el nostre impacte en el medi ambient sigui el mínim possible. Intentar revertir els efectes negatius que ha tingut l'activitat humana sobre la natura i el canvi climàtic es un dels majors reptes dels nostres temps. Aquest objectiu s'ha d'abordar des de diferents àmbits, entre ells de la ciència de materials. Per a un futur sostenible, en la fabricació de polímers cal substituir els compostos petroquímics, com a font de matèries primeres, per altres d'origen renovable (p. ex. olis vegetals). Però, al mateix temps, els polímers han de ser capaços de ser fàcilment degradables o reciclables un cop acabada la seva vida útil.

En aquesta tesi s'han preparat polímers fent servir monòmers d'origen renovable. La δ -decalactona, que pot ser obtinguda a partir d'àcids grassos presents a l'oli de girasol o mitjançant la fermentació del bagàs de canya de sucre y la α -metilen- γ -butirolactona (o tulipalina A), que està present en certes flors com les tulipes. Aquest monòmers han estat polimeritzats de forma controlada mitjançant les tècniques de polimerització per apertura d'anell (ROP) i polimerització radical per transferència atòmica (ATRP) respectivament. La combinació de ambdues tècniques ha permès obtenir copolímers de bloc ABA amb propietats d'elastòmer termoplàstic.

En el disseny d'aquests materials, s'han incorporat grups sensibles al punt mig del copolímer que puguin respondre a estímuls externs. Sota determinades condicions (p. ex. àcid, redox., etc.) és produeix el trencament del grup sensible, obtenint copolímers AB. Aquests copolímers AB no presenten propietats d'elastòmer termoplàstic, i per tant, es d'esperar que faciliti la seva posterior eliminació i recuperació. Aquests tipus de materials poden ser adequats per a processos en els quals es necessari la seva eliminació prèvia, com es el cas del reciclatge de paper amb adhesius.

CASTELLANO

Actualmente, uno de los mayores retos a los que se enfrenta nuestra sociedad es el de adaptar nuestra forma de vida de tal manera que nuestro impacto en el medio ambiente sea el mínimo posible. Intentar revertir los efectos negativos que ha tenido la actividad humana sobre la naturaleza y el cambio climático constituye uno de los mayores retos en la actualidad. Este objetivo debe afrontarse desde diferentes ámbitos, entre ellos el de la ciencia de materiales. Para un futuro sostenible, en la fabricación de polímeros hay que sustituir los compuestos petroquímicos, como fuente de materias primas, por otros de origen renovable (p. ej. aceites vegetales). Pero, al mismo tiempo, los polímeros han de ser capaces de ser fácilmente degradables o reciclables una vez acabada su vida útil.

En esta tesis se han preparado polímeros utilizando monómeros de origen renovable. La δ -decalactona, que puede ser obtenida a partir de ácidos grasos presentes en el aceite de girasol o mediante fermentación del bagazo de la caña de azúcar y la α -metileno- γ -butirolactona (o tulipalina A), que se encuentra en ciertas flores como los tulipanes. Estos monómeros han sido polimerizados de forma controlada mediante las técnicas de polimerización por apertura de anillo (ROP) y polimerización radical por transferencia atómica (ATRP) respectivamente. La combinación de las dos técnicas ha permitido obtener copolímeros de bloque ABA con propiedades de elastómero termoplástico.

En el diseño de estos materiales, se han incorporado grupos sensibles en el punto medio del copolímero que puedan responder a estímulos externos. Bajo ciertas condiciones (p. ej. ácido, redox., etc.) se produce la rotura del grupo sensible, dando copolímeros AB. Estos copolímeros AB no presentan propiedades de elastómero termoplástico y, por lo tanto, es de esperar que facilite su posterior eliminación y recuperación. Este tipo de materiales pueden ser adecuados en procesos, en los cuales es necesaria su eliminación previa, como en el reciclado de papel con adhesivos.

ENGLISH

Nowadays, one of the most important issues of our society is to adapt our lifestyle in a way that our impact to the environment was as minimum as possible. Trying to revert the negative effects of the human activity upon the nature and the climate change is one of the mayor challenges of our time. This purpose must be addressed from different fields, material science among them. For a sustainable future, petrochemicals as raw materials, must be substituted by other from renewable sources (e. g. vegetable oils). However, at the same time, the polymers must be able to be easily degraded or recycled once finished their useful life.

In this thesis polymers using monomers obtained from renewable resources have been synthesized. δ -Decalactone, which can be obtained from fatty acids present on sunflower oil or through the sugarcane bagasse fermentation and α -methylene- γ -butyrolactone (or tulipalin A), which is present in some flowers such as tulips. These monomers have been polymerized in a controlled manner through the Ring-Opening Polymerization (ROP) and Atom Transfer Radical Polymerization (ATRP) mechanisms respectively. The combination of these two techniques allows the obtention of ABA block copolymers with thermoplastic elastomer properties.

In the materials design, sensitive groups which can respond to external stimuli, have been incorporated at the mid-point of the copolymer. The cleavage of the sensitive group can be done under certain conditions (e. g. acid, redox., etc.), obtaining AB copolymers. These AB copolymers do not show thermoplastic elastomer properties, therefore, being more easily removable. This type of materials could be appropriate in some processes, in which its previous elimination is mandatory, such as adhesive containing paper recycling.

UNIVERSITAT ROVIRA I VIRGILI
STIMULI-RESPONSIVE CALIX[4]PYRROLE AND CALIX[4]ARENE BASED RECEPTORS: FROM UNIMOLECULAR
TO DIMERIC STRUCTURES

Pedro Miguel Mendonça Ferreira

ACKNOWLEDGEMENTS

Quisiera dedicar unas palabras a todas las personas que han hecho posible que hoy este aquí escribiendo esta tesis. También agradecer a la Generalitat de Catalunya y al Fondo Social Europeo por proporcionarme la beca necesaria para la realización de esta tesis.

Primero de todo quisiera agradecer a mi director de tesis Prof. Juan Carlos Ronda Bargalló por darme la oportunidad de trabajar en Suspol. Bajo su supervisión he aprendido mucho, no solo sobre polímeros, sino también a cómo enfrentarse a los problemas que van surgiendo durante una investigación. Gracias a él he adquirido aptitudes como la de ser resolutivo y perseverante. Además, las habilidades que he adquirido a nivel experimental durante estos cuatro años ha sido gracias a su tutela. También quisiera agradecer a la Prof. Virginia Cádiz Deleito, a la Prof. Marina Galià i Clua y al Dr. Gerard Lligadas Puig por su buena acogida en el grupo, así como sus aportaciones durante los group meetings.

También expresar mi agradecimiento a los técnicos del Servei de Recursos Científics i Tècnics (SRCiT) por su ayuda a la hora de realizar los ensayos. A Ramon Guerrero Grueso, que siempre tenía un espacio disponible para poder hacer mis interminables carbonos. A Irene Maijó Ferré y a Sònia Abelló Cros, por su gran ayuda e implicación en mis análisis de MALDI. Además, agradecer a Silvia de la Flor López, del departamento de ingeniería mecánica, por su gran ayuda en la caracterización de los materiales. Por otro lado, agradecer a Jaume Capdevila que siempre que había algún problema, especialmente informático, nos daba su apoyo.

Durante mi tesis he conocido a mucha gente, entre ellos a mis compañeros de laboratorio. Quiero agradecer la ayuda de Adrián Moreno Guerra que, aunque siempre tenía mucho trabajo, encontraba un rato para aconsejarme. El me enseñó gran parte del funcionamiento del laboratorio, desde el funcionamiento del GPC a como realizar

los pedidos, entre muchas otras tareas. A Carmen Valverde Sarmiento, que con su buen humor y actitud siempre te alegraba el día. Mi compañera de escritorio que siempre tenía alguna historia que contar, sobre todo de gatos. Nunca olvidare que tu primera llamada de teléfono fue para decirme que habías pinchado una rueda. A Nabil Bensabeh, que cuando llegué todavía estaba haciendo el máster, y a Aarón Pérez Das Dores, que llego poco después, muchas gracias por los buenos momentos. Tanto en el laboratorio como fuera de él, en las cenas que hicimos o en los congresos a los que asistimos. Aaron ahora te quedas tu a cargo del laboratorio, muchos ánimos en la recta final. También quería agradecer a Adria Roig, el único en el laboratorio que compartía mis gustos musicales, que además me ayudó muchísimo con los ensayos de DMA. Tampoco quiero olvidar a la gente que conocí fuera del laboratorio, a Xavier Montané, Rubén Donoso, Alberto Belmonte, así como a los italianos, Rita, Francesco, Mimmo, Mario y Gianmarco. Su gran acogida los primeros días al llegar a Tarragona hicieron más llevadera la llegada a una ciudad donde no conocía a nadie.

Por otro lado, y fuera del ámbito académico, quisiera agradecer a mis amigos todo el apoyo que me han dado. Porque siempre que les decía que bajaba al pueblo hacían un hueco para quedar conmigo. Cuando no venían ellos a verme a Tarragona. Gracias a ellos conseguía desconectar cuando lo necesitaba y pasar muy buenos ratos. A Eloi Manyosa Lacruz, Lamin Jadama Merino, Joan Fruitós Medina (que me ayudo con la mudanza a Tarragona), Marc Pardines Gonzalez, Albert Vázquez Moliner, Dani Puga Blanco y Arnau Fabregat Diaz, a todos muchas gracias.

Agradecer a mi familia su apoyo durante todo este tiempo. Especialmente a mis padres, Pere y Piedad, que siempre han hecho lo posible para que me vaya bien en la vida. Desde pequeño me animaron a estudiar lo que más motivase y a dar de esta forma lo mejor de mí. Gran parte de lo que soy se lo debo a ellos. Sin olvidar a mis abuelas, a Piedad, que ya no está entre nosotros, y a Emilia. Ellas siempre se han preocupado por mí y me han ayudado, por eso muchas gracias.

Por último, pero no menos importante, quiero agradecerle a mi pareja, Mercedes Villalba Mora, todo el apoyo que me ha dado todos estos años. Tú me has acompañado todo este tiempo, no solo durante el doctorado, sino también en la carrera y el máster. Sin tu ayuda, especialmente en los momentos difíciles, nunca hubiera llegado tan lejos. Siempre has sabido como animarme y hacerme coger fuerzas para seguir adelante. Así que esta tesis te la dedico a ti. Te quiero y espero que sigamos juntos mucho más tiempo. Tú y yo, ahora y por siempre.

UNIVERSITAT ROVIRA I VIRGILI
STIMULI-RESPONSIVE CALIX[4]PYRROLE AND CALIX[4]ARENE BASED RECEPTORS: FROM UNIMOLECULAR
TO DIMERIC STRUCTURES

Pedro Miguel Mendonça Ferreira

TABLE OF CONTENTS

1	INTRODUCTION	3
1.1	Brief history of thermoplastic elastomers	3
1.2	Thermoplastic elastomer: Physical and mechanical properties	4
1.2.1	Phase structure	4
1.2.2	Phase separation	6
1.3	Types of thermoplastic elastomers	7
1.3.1	Hard polymer-elastomer combinations	7
1.3.2	Branched block copolymers	7
1.3.3	Linear block copolymers	9
1.4	Thermoplastic elastomers applications	14
1.5	Advantages, limitations, and challenges for TPEs	15
1.6	Polymers from renewable resources	16
1.7	Monomers from renewable feedstocks	18
1.7.1	Direct extraction from natural feedstocks	18
1.7.2	Biotransformation of natural feedstocks	19
1.7.3	Chemical transformation of natural feedstocks	20
1.7.4	δ -Decalactone (DL)	21
1.7.5	α -Methylene- γ -butyrolactone (MBL)	23
1.8	Polyesters	26
1.8.1	Polycondensation	27
1.8.2	Ring-opening polymerization (ROP) of cyclic esters.	28
1.8.3	ROP mechanisms	37
1.9	ROP of δ-decalactone with TBD	40

1.10	Acrylic and methacrylic polymers	43
1.10.1	Poly(meth)acrylates synthesis	44
1.10.2	Poly(meth)acrylates properties	44
1.10.3	Poly(meth)acrylates applications	46
1.11	Radical polymerizations	47
1.12	Controlled radical polymerizations (CRP)	48
1.13	Atom transfer radical polymerization (ATRP)	52
1.13.1	ATRP mechanism	53
1.13.2	Catalytic systems in ATRP (Metal/ligand)	56
1.13.3	Initiator effect	58
1.13.4	The halogen exchange effect	61
1.13.5	Solvent, temperature, and reaction time	63
1.13.6	ATRP variations	64
1.14	ATRP of MBL	68
1.15	Stimuli-cleavable polymers	70
1.15.1	Redox cleavable polymers	72
1.15.2	Acid cleavable polymers	74
1.15.3	Light cleavable polymers	76
2	OVERVIEW AND OBJECTIVES	105
2.1	Overview	105
2.2	Objectives	107

3	STIMULI-CLEAVABLE POLYESTER MACROINITIATORS FROM RENEWABLE δ-DECALACTONE: SYNTHESIS, END-GROUP MODIFICATION, AND CHARACTERIZATION.	113
3.1	Synthesis of poly(δ -decalactone) as soft/rubbery block	113
3.2	End-group modification for ATRP	122
3.3	Synthesis of poly(DL) using stimuli cleavable initiators	132
4	ATOM TRANSFER RADICAL POLYMERIZATION: SYNTHESIS OF HOMOPOLYMERS AND ABA BLOCK COPOLYMERS	145
4.1	Synthesis of poly(MMA) by ATRP	146
4.2	Synthesis of poly(MBL) by ATRP	151
4.3	Synthesis of ABA block copolymers by ATRP	163
5	CLEAVAGE OF ABA BLOCK COPOLYMERS	181
5.1	Reductive cleavable polymer	181
5.2	Acid cleavable polymers	186
5.2.1	Cleavage of poly(MBL)- <i>co</i> -poly(DL)- <i>l</i> ₂ - <i>co</i> -poly(MBL)	187
5.2.2	Cleavage of poly(MBL)- <i>co</i> -poly(DL)- <i>l</i> ₃ - <i>co</i> -poly(MBL)	191
5.3	Reactive oxygen species (ROS) cleavable polymers	193

6	EXPERIMENTAL PART	213
6.1	Materials	213
6.2	Instruments and methods	215
6.3	Synthesis of stimuli-cleavable initiators	219
6.3.1	Synthesis of 1,1-bis-[3-((2-hydroxyethyl)thio)propyloxy]ethane (I ₂)	219
6.3.2	Synthesis of 3,9-bis-[2-(ethylthio)ethanol]- 2,4,8,10-tetraoxaspiro-[5.5]undecane (I ₃)	221
6.3.3	Synthesis of bis-((2-hydroxyethyl)thio)methane (I ₄)	222
6.3.4	Synthesis of (4-methoxyphenyl)-bis-[(2-hydroxyethyl)thio]methane (I ₅)	223
6.4	Synthesis of α-methylene-γ-butyrolactone (MBL)	224
6.5	Synthesis of N-(2-bromoisobutyryl)imidazole (BriB-Im)	225
6.6	Synthesis of 1,4-phenylenebis(methylene)-bis(2-bromo-isobutyrate) (I₆)	226
6.7	Synthesis of model compounds.	227
6.7.1	Synthesis of bis(DL) _{1,6-Hex} diol	227
6.7.2	Synthesis of model cleavable compounds Dod-I ₁ , Dod-I ₄ and Dod-I ₅	229
6.8	Synthesis of poly(MBL-co-DL-co-MBL) block copolymers	231
6.8.1	Synthesis of poly(DL) soft macroinitiators	231
6.8.2	Synthesis poly(MBL) hard blocks	239
6.8.3	Synthesis of block copolymers	243
6.9	Degradation of stimuli-cleavable block copolymers	247
6.9.1	Reductive cleavable block copolymer poly(MBL)-co-poly(DL)-I ₁ -co-poly(MBL)	247
6.9.2	Acid cleavable block copolymers	248
6.9.3	ROS cleavable block copolymers	251

7	GENERAL CONCLUSIONS	259
8	ANNEX	265
8.1	Acetaldehyde diallylacetal	265
8.2	1,1-Bis-[3-((2-hydroxyethyl)thio)propyloxy]ethane (I ₂)	267
8.3	3,9-Bis-[2-(ethylthio)ethanol]- 2,4,8,10-tetraoxaspiro-[5.5]undecane (I ₃)	270
8.4	Bis-((2-hydroxyethyl)thio)methane (I ₄)	272
8.5	(4-Methoxyphenyl)-bis-[(2-hydroxyethyl)thio]methane (I ₅)	273
8.6	α -Methylene- γ -butyrolactone (MBL)	274
8.7	N-(2-bromoisobutyryl)imidazole (BriB-Im)	275
8.8	1,4-Phenylenebis(methylene)-bis(2-bromoisobutyrate) (I ₆)	276
8.9	Bis(DL) _{1,6-Hex} diol	277
8.10	2,2'-Disulfanediyldiethanol didodecanoate (Dod-I ₁)	278
8.11	Bis-[(2-ethylthio)dodecanoate)methane (Dod-I ₄)	279
8.12	(4-Methoxyphenyl)-bis-[(2-ethylthio)dodecanoate]-methane (Dod-I ₅)	280
8.13	Poly(DL) _{1,8-Oct} diol	282
8.14	Poly(DL) _{1,8-Oct} BriB ester	285
8.15	Poly(DL)-I ₁ diol	288
8.16	Poly(DL)-I ₁ BriB ester	290
8.17	Poly(DL)-I ₂ diol	291
8.18	Poly(DL)-I ₂ BriB ester	293
8.19	Poly(DL)-I ₃ diol	295
8.20	Poly(DL)-I ₃ BriB ester	297

8.21	Poly(DL)-I ₄ diol	298
8.22	Poly(DL)-I ₄ BriB ester	300
8.23	Poly(DL)-I ₅ diol	302
8.24	Poly(DL)-I ₅ BriB ester	304
8.25	Poly(MMA) _{EtBriB}	306
8.26	Poly(MBL) _{EtBriB}	308
8.27	Poly(MBL)-I ₆	310
8.28	1,4-phenylenebis(methylene)-bis(2-chloroisobutyrate)	312
8.29	Poly(MBL)-co-poly(DL) _{1,8-Oct} -co-poly(MBL)	313
8.30	Poly(MBL)-co-poly(DL)-I ₁ -co-poly(MBL)	314
8.31	Poly(MBL)-co-poly(DL)-I ₂ -co-poly(MBL)	315
8.32	Poly(MBL)-co-poly(DL)-I ₃ -co-poly(MBL)	316
8.33	Poly(MBL)-co-poly(DL)-I ₄ -co-poly(MBL)	317
8.34	Poly(MBL)-co-poly(DL)-I ₅ -co-poly(MBL)	318
8.35	Cleavage product of poly(MBL)-co-poly(DL)-I ₁ -co-poly(MBL) with Bu ₃ P	319
8.36	Cleavage product of poly(MBL)-co-poly(DL)-I ₂ -co-poly(MBL) with [TFA] = 0.01 M	320
8.37	Cleavage product of poly(MBL)-co-poly(DL)-I ₂ -co-poly(MBL) with [TFA] = 0.5 M	321
8.38	Cleavage product of poly(MBL)-co-poly(DL)-I ₃ -co-poly(MBL) with [TFA] = 0.5 M	322
8.39	Deprotection product of Dod-I ₅ with DMSO/I ₂ at 90 °C	323
8.40	Cleavage products of Dod-I ₅ with TPP/O ₂ /hv	323
8.41	Oxidation product of Dod-I ₄ with H ₂ O ₂ /PTC	324
8.42	Cleavage product of poly(MBL)-co-poly(DL)-I ₄ -co-poly(MBL) with H ₂ O ₂ /TPP/hv	324
8.43	Cleavage product of poly(MBL)-co-poly(DL)-I ₅ -co-poly(MBL) with H ₂ O ₂ /TPP/hv	325

Chapter 1

Introduction

UNIVERSITAT ROVIRA I VIRGILI
STIMULI-RESPONSIVE CALIX[4]PYRROLE AND CALIX[4]ARENE BASED RECEPTORS: FROM UNIMOLECULAR
TO DIMERIC STRUCTURES

Pedro Miguel Mendonça Ferreira

1 Introduction

1.1 Brief history of thermoplastic elastomers

Thermoplastic elastomer (TPE) is a class of material that is characterized by possessing both elastomeric and plastic properties, which means that they show rubber elasticity at service temperature but can be processed at elevated temperatures as a thermoplastic.¹ The first attempts to obtain thermoplastics showing some elastomeric properties was in the 1930s with the plasticized poly(vinyl chloride) (PVC) at the B.F. Goodrich Company. By this process the mechanical properties of the material could be modulated by dissolving the PVC at high temperatures in a non-volatile solvent, such as chloronaphtalene or dibutyl phthalate, and allowing to cool obtaining a stiff but rubbery material. The properties of the material depend on the solvent (or mixture of solvents) and the solvent/polymer ratio. Increasing the solvent proportion, the material obtained in general is softer and resilient, while decreasing the solvent the material obtained is harder.² This can be seen as the first approach to obtain a thermoplastic with elastic properties. Nevertheless, more advances were done after the discovery of diisocyanate polyaddition reaction in 1937,³ which was applied by DuPont and ICI to produce the first polyurethane fibers.⁴⁻⁶ Thermoplastic polyurethanes increased in interest and, in the 1960s the Goodrich Company developed the first commercial thermoplastic elastomer polyurethane showing both good mechanical properties and processability.⁷ In the same decade, Shell developed styrene-diene block copolymers as thermoplastic elastomers which were introduced in 1966 as Kraton®.⁸ Since then, thermoplastic elastomer production has grown considerably, due to its simplified processing and low energy consumption, together with both interesting mechanical properties and recyclability.⁹ The global TPE market exceeded \$ 24 billion and the market demand reached 6.7 million tons in 2019.¹⁰

1.2 Thermoplastic elastomer: Physical and mechanical properties

As mentioned before, a TPE possess the mechanical features of elastomers (undergo linear and reversible response to strain upon an applied force) with the difference that the cross-linking, which prevents the viscous flow, is physical instead of chemical. This characteristic, in contrast with thermosets, allows the TPE to be processed and recycled as a thermoplastic. The most common processing methods for TPEs are extrusion and injection molding, but can also be processed by compression molding, transfer molding, blow molding, etc.¹¹

Elastomers elongation is allowed due to a conformational change from a compact random coil (of the rubbery segment) to an extended chain. An extended chain has only one possible conformation, resulting in low entropy. Therefore, the extended chain will spontaneously contract into a random coil, which have many possible conformations resulting in a high entropy. Thus, entropy is overcome by a mechanical force deforming the elastomer. The enthalpic factor generally do not contribute due to the small intermolecular forces involved.^{11, 12}

1.2.1 Phase structure

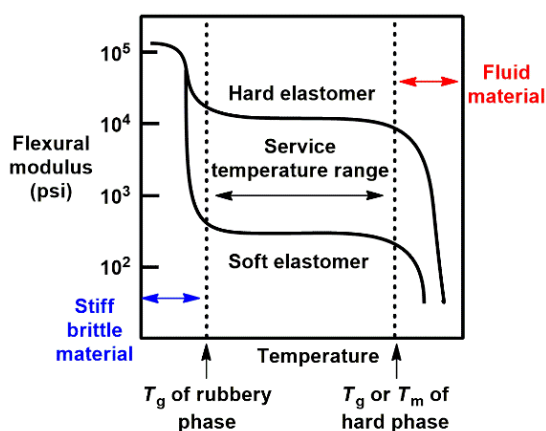


Figure 1.1 Dependence of stiffness of a typical TPE with temperature.

TPE consist in an elastic (soft) matrix that is physically crosslinked by plastic (hard) domains. The elasticity is given due to a phase segregation microstructure, caused by the incompatibility of the segments, where the hard segments are dispersed in the soft matrix. These hard segments are physically crosslinked by chain entanglements or crystalline regions. The physical crosslinking can also be formed by forces such as van der Waals interactions, dipole interactions or hydrogen bonding.¹³ Below the service temperature (below the glass transition temperature (T_g) of the rubbery segment) both phases are hard and then the material is stiff and brittle. At the service temperature (above the T_g of the rubbery segment and below the T_g or the melting temperature (T_m) of the hard segment), the soft segment is in its molten state and the hard segments prevent viscous flow of the elastic material. As temperature increases, the modulus stays relatively constant (“rubbery plateau”) until the T_g or T_m of the hard segment is reached, when the crosslink is break down and the material becomes viscous and can be processed (Figure 1.1)¹⁴. The choice of the soft segment will determine the elastic properties and the hard segment the mechanical properties, such as the tensile strength or solvent resistance. The choice of the hard segment will also determine the maximum service temperature of the material. Nowadays exist a wide variety of commercial TPE ranging different service temperature (Table 1.1).¹²

Table 1.1 Glass transition (T_g) and melting (T_m) temperatures of soft and hard phases of commercial TPE.

TPE type	Soft segment, T_g (°C)	Hard segment, T_g or T_m (°C)
SBS ^a	-90	95 (T_g)
SIS ^b	-60	95 (T_g)
SEBS ^c	-55	95 (T_g) and 165 (T_m)
SIBS ^d	-60	95 (T_g) and 165 (T_m)
Polyurethane elastomers	-40 to -60	190 (T_m)
Polyester elastomers	-40	185 to 220 (T_m)
Polyamide elastomers	-40 to -60	220 to 275 (T_m)

^a poly(Styrene-co-butadiene-co-styrene), ^b poly(Styrene-co-isoprene-co-styrene), ^c poly(Styrene-co-ethylene-co-butylene-co-styrene), ^d poly(styrene-co-isobutylene-co-styrene)

1.2.2 Phase separation

The proportion and the nature (strength of phase separation) of the two domains determines the final properties of the material.¹⁵ The hard phase gives the strength to the TPE, while the rubbery phase give the flexibility and elasticity. The two components on the polymer must be incompatible, not mutually soluble that would form a homogeneous phase; thus, the two segments may have very different structures. Segments with high molecular weight and low service temperatures also favors the phase separation. The hardness of the material will depend on the hard/soft phase ratio: hardness will increase as the hard segment proportion is increased, and hence, lowering the elasticity. The microdomains formed in phase separation will also depend on the hard/soft phase ratio, which can present different structures such as spherical, cylindrical, lamellar, etc.^{12, 14} Atomic force microscopy (AFM) is used to study the phase separation in block copolymers. It provides the surface topography together with the cartography of the microdomains and allows the characterization of the different possible morphologies (e.g. spheres, cylinders or lamellae) (Figure 1.2).¹⁶

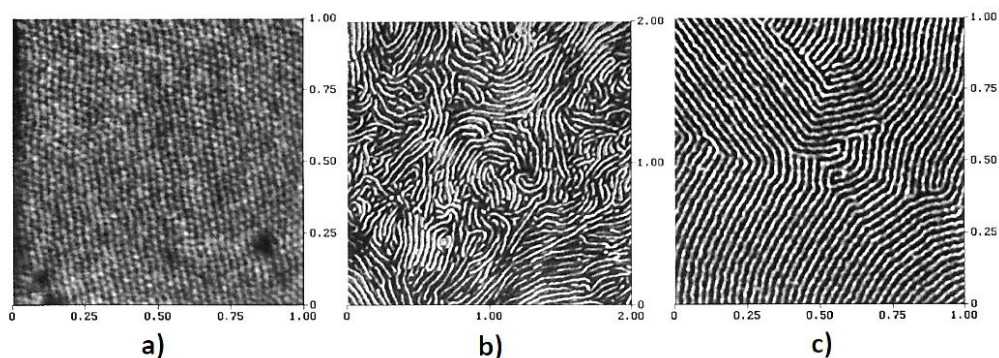


Figure 1.2 Trapping mode AFM images of ABA block copolymer TPE with different morphologies; (a) spheres, (b) cylinders and (c) lamellae.¹⁶

1.3 Types of thermoplastic elastomers

Depending on the chemical composition and morphology, thermoplastic elastomers can be divided in 3 main categories:^{12, 15, 17, 18}

1.3.1 Hard polymer-elastomer combinations

These type of TPEs are not block copolymers, but fine dispersions of hard thermoplastics with soft elastomers. The two polymers are synthesized separately and then mixed (Figure 1.3). The fine dispersion of both polymers will determine the optimum properties, then a good match of the viscosity parameters of the polymers is necessary. The solubility parameters are also important, as very different polarities will result in poor adhesion between phases.^{12, 19} Some of them are only blends, e.g. thermoplastic polyolefin blends (TPOs),²⁰ but in other cases a vulcanizing agent is added during the mixing process to crosslink the two phases, e.g. dynamically vulcanized polymer blends (TPVs).²⁰⁻²⁵ These last type cannot be considered true TPEs as they are covalently crosslinked.

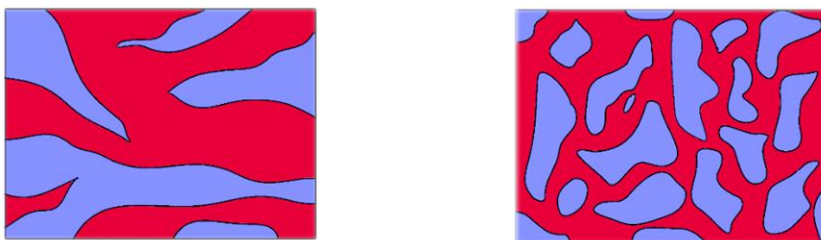


Figure 1.3 Morphology of TPV (left) and TPO (right). The hard domain represented in red and the elastomeric domain represented in blue.

1.3.2 Branched block copolymers

This type of copolymers possesses unique features such as small hydrodynamic radii, lower melt viscosity and lower solution viscosity. Furthermore, its macromolecular architecture allows the modulation of the TPE properties.¹⁵ Within this type of copolymers three different architectures are described; star branched, graft and bottle brush block copolymers. Star branched copolymers are polymers with more than two chains growing from the same center (Figure 1.4-a). If these chains have different

compositions or molecular weight the star is named miktoarm star polymer.²⁶ Usually, for TPE applications the inner block is the rubbery domain, and the hard domain are the outer block.^{15, 27} There are many examples of star branched block copolymers using acrylic monomers both for the soft block, such as n-butyl acrylate, and for the hard block, such as methyl methacrylate or plant-derived monomers such as α -methylene- γ -butyrolactone.²⁸⁻³¹

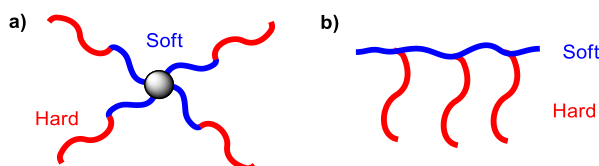


Figure 1.4 Representation of (a) $(AB)_4$ -star block copolymer and (b) graft block copolymer.

Graft copolymers consist in a main polymer chain, the backbone, with one or more side chains attached, the branches.¹⁵ The characteristics of these comb-shaped polymers are defined by three factors: (1) the molecular weight of the main chain, (2) the molecular weight of the graft chain, and (3) the distance between the graft chains (Figure 1.4-b).^{32, 33} There are many examples of graft block copolymers for TPE applications described in literature.^{34, 35} Finally, bottlebrush block copolymers are similar to the graft copolymers but the spacing between side chains are lowered and, therefore the grafting is more dense, giving a cylindrical arrangement (Figure 1.5).^{15, 30, 36} This characteristic architecture converts bottlebrush TPEs in a very interesting class of supersoft materials for medicinal chemistry,³⁷ and other applications.³⁸⁻⁴¹

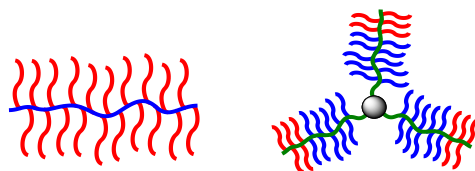
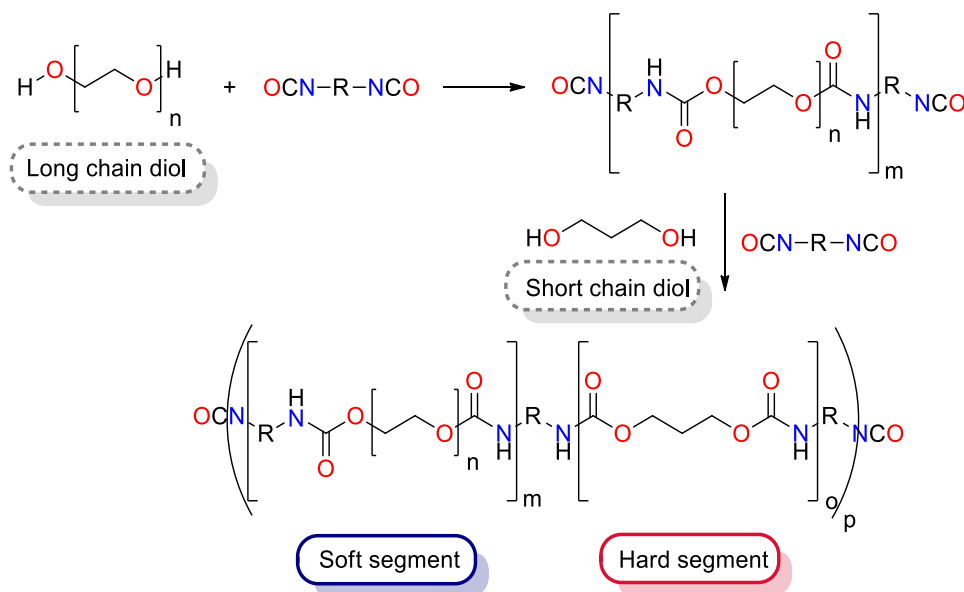


Figure 1.5 Representation of linear (left) and star (right) bottle-brush block copolymers.

1.3.3 Linear block copolymers

The most common types of linear block copolymers for TPE applications are $(AB)_n$ multiblock copolymers (MBCs), ABA triblock copolymers and ABC triblock terpolymers with A or C the hard block and B the rubbery block. The methods to obtain these structures vary from polycondensation and polyaddition reactions to controlled radical polymerizations, living anionic/cationic polymerizations, ring opening polymerizations and living coordination polymerizations.¹⁵

1.3.3.1 Multiblock copolymers (MBCs)



Scheme 1.1 Multiblock copolymer TPE based on polyurethanes.

Multiblock or segmented TPEs are linear block copolymers with a A-B-A-B-A-B... or $(A-B)_n$ structure. The hard segments (A) are crystalline thermoplastics while the soft (B) segments are amorphous elastomers. Hard segments are typically thermoplastic polyurethanes, aromatic polyesters and polyamides, whereas soft segments are usually aliphatic polyesters or polyethers. Polyurethane based TPEs are usually produced by addition of diisocyanates and mixtures of diols of different lengths. Thus, a polyether or polyester diol is reacted with an excess of a diisocyanate and then a short chain diol

(chain extender) is added (Scheme 1.1).¹² The final product is an alternating block copolymer with two different segments. The first consisting of the urethane of the long chain diol, which is amorphous and with low T_g (usually from $-100\text{ }^\circ\text{C}$ to $-45\text{ }^\circ\text{C}$). The second, the urethane formed by the short chain diol, which has a regular structure, in some cases is highly crystalline, and which possess high T_g or T_m values (usually over $100\text{ }^\circ\text{C}$). Each polymer chain possesses several hard and soft segments which are physically interconnected (Figure 1.6).

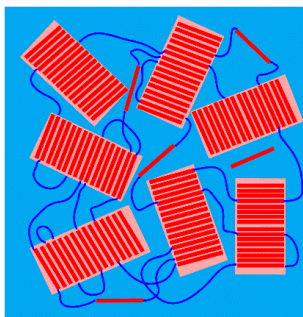
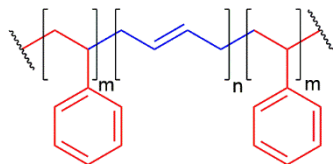


Figure 1.6 Multiblock copolymer morphology, crystalline hard segments (red) interconnected through the soft segments (blue).

The most common diisocyanates used to produce TPE polyurethanes are diphenylmethane-4,4'-diisocyanate (MDI) and 2,4-toluene-diisocyanate (TDI). The long chain diols are usually polyesters (e.g. poly(ethylene adipate)) or polyethers (e.g. poly(oxytetramethylene)glycol).^{12, 13, 42, 43} Other types of MBCs are; the polyamide-based thermoplastic elastomers (COPAs), in which the amide block forms the hard domain and the polyester, polyether-ester or polyether blocks forms the soft domain. The strong amide hydrogen-bonding allows high service temperature. Finally, there are also the polyetherester-based thermoplastic elastomer (COPEs), which combine hard crystalline aromatic polyester blocks and soft amorphous polyether blocks.^{11, 15} Several examples of multiblock copolymers for TPE applications could be found in the literature.⁴⁴⁻⁴⁶

1.3.3.2 ABA block copolymers

a)



b)

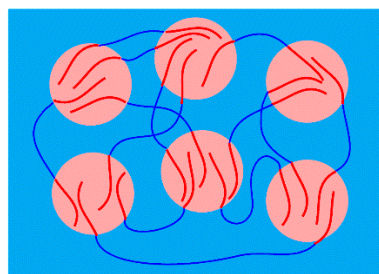


Figure 1.7 (a) Structure of styrene-co-butadiene-co-styrene (SBS) ABA block copolymer and (b) SBS morphology, hard domain (red) dispersed in a continuous elastomer phase (blue).

One of the first examples of commercial ABA type TPEs were styrene-butadiene-styrene (SBS) (Figure 1.7-a) and the styrene-isoprene-styrene (SIS) copolymers, introduced in the 1960s. The polystyrene (PS) hard segments ($T_g = 95\text{ }^\circ\text{C}$) form a separate region dispersed in a continuous phase of elastomeric polybutadiene (PB) ($T_g = -90\text{ }^\circ\text{C}$) or polyisoprene (PI) ($T_g = -60\text{ }^\circ\text{C}$).^{11, 12} The PS hard segment forms the physical crosslink preventing the soft phase to flow (Figure 1.7-b). ABA block copolymers have a much cleaner phase separation than segmented block copolymers and are typically softer.⁴⁷ This kind of TPE has been used for a wide range of applications, such as adhesives, sealants, footwear, etc. In recent years, the development of more complex ABA type TPEs has grown considerably, from the point of view of applications and mechanic performance⁴⁸ and the synthetic approaches and monomer types used.⁴⁹ The ABA block copolymers can be obtained using a variety of controlled/living polymerizations, such as nitroxide mediated polymerization (NMP), anionic/cationic polymerization, metal-catalyzed polymerization (e.g. ring opening metathesis polymerization (ROMP)) and radical polymerization. Within these techniques, there are different methodologies to obtain this type of block copolymers, one possibility is to synthesize both blocks separately and then couple them through the terminal functionality or by using a coupling reagent (Figure 1.8-1).⁵⁰⁻⁵²

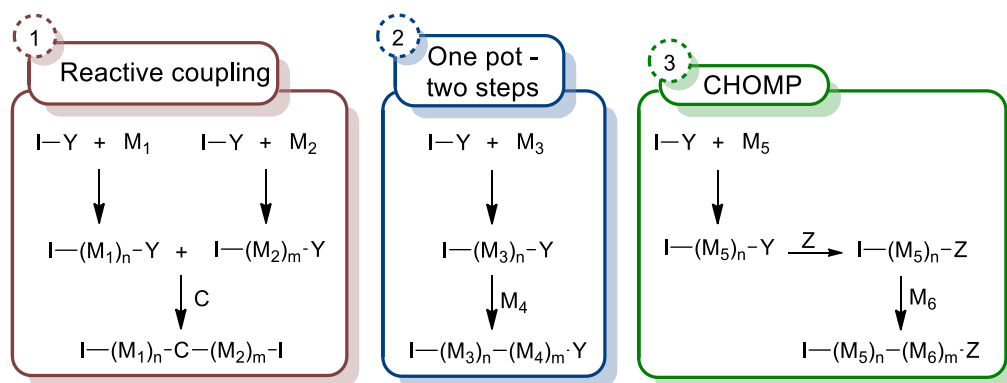


Figure 1.8 Different methodologies to obtain ABA block copolymers. (1) by reactive coupling, (2) by a one pot - two steps copolymerization and (3) by change-of-mechanism approaches. Where M_1 and M_2 can be monomers with different or the same polymerization mechanisms, M_3 and M_4 are monomers with the same polymerization mechanism and M_5 and M_6 monomers with different polymerization mechanism. Y is the active center for M_{1-5} , and Z is the active center for M_6 , and C is a coupling reagent.

However, the most straightforward route is the living or controlled polymerization of the first monomer (B) followed by the sequential living or controlled polymerization of the second monomer (A), once the first monomer is consumed (Figure 1.8-2).⁴⁹ By this way, ABA block copolymers can be obtained in a one-pot two-steps procedure without the need of purification of the first homopolymer. However, this methodology presents some limitations; on one hand, monomer reactivity must be considered, which means than the second monomer must be reactive enough to be polymerized by the macroinitiator. Thus, the order of addition of the monomers affects the efficiency of the polymerization and, hence, limiting the macromolecular architecture. In the other hand, the in-situ approach requires than monomers share the same polymerization mechanism (e.g. two acrylic monomers).

Nevertheless, the combination of two different polymerization mechanisms extends the range of monomers that can be used, allowing the obtention of a more variety of block copolymers.^{49, 53} By this approach, called change-of-mechanism polymerization (CHOMP), the first monomer is polymerized and once obtained the first block, the reactive center (appropriate for the first polymerization mechanism) is transformed (in-

situ or in a second step) to an active center appropriate for the polymerization mechanism of the second block monomer (Figure 1.8-3).⁵⁴ The CHOMP approach to obtain ABA TPEs has been applied extensively due to the variety of monomers that can be used, leading to block copolymers with properties unachievable by other methods. The ABA block copolymers have been extensively studied for the preparation of TPEs using a wide range of monomers through different polymerization mechanisms, such as, ionic polymerization,⁵⁵⁻⁵⁹ ring opening polymerization,⁶⁰⁻⁶⁶ ring opening metathesis polymerization,^{67, 68} radical polymerization,⁶⁹⁻⁷⁷ and by combination of more than one polymerization mechanism.⁷⁸⁻⁸⁰

1.3.3.3 ABC block copolymers

ABC block copolymers constitute another type of architecture which allows the obtention of TPEs. This kind of architectures are quite similar to the previously mentioned, but with the difference that the hard end blocks are different between them and also immiscible. This characteristic avoids than two hard blocks, from the same copolymer, physically crosslink in the same microdomain (loop chain), without contributing to the elastomeric behavior. In contrast when the two hard end blocks are physically crosslinked in two different microdomains (bridge chain) they do contribute to the elastomeric behavior (Figure 1.9).⁸¹⁻⁸³

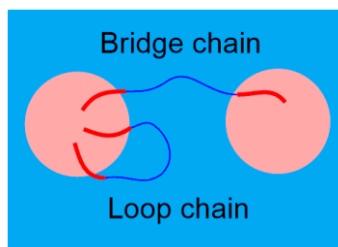


Figure 1.9 Schematic representation of ABA block copolymer bridge and loop chains.

1.4 Thermoplastic elastomers applications

TPEs are currently used in a wide range of applications, such as foams, replacement of natural rubber, thermal and electrical insulators, medical devices, household appliances, automobiles, shoes soles, sporting goods, components for construction, pipes, tires, asphalt binders and replacement of metals in many applications like in aircrafts, providing comparable strength diminishing the final weight (Figure 1.10).^{10, 11, 84-87} However, the mayor applications for TPEs are in sealants, coatings and adhesives.⁸⁸ The main difference between conventional structural adhesives, such as epoxies, and elastomeric adhesives is that the later allows a certain amount of motion between the two parts being joined, which is needed in some applications. TPE adhesives can be divided into three categories; soft structural adhesives, usually applied in the form of monomers or oligomers; pressure sensitive adhesives, typically used in tapes, labels and contact adhesives; and hot-melt adhesives, which are applied at high temperatures in liquid state and becomes solid upon cooling, typically used in sealants. These adhesives can also be applied with the aid of a solvent, taking advantage of their low solution viscosity, joining the two part upon evaporation of the solvent. TPEs are rarely used as neat polymers and are usually mixed with oils and fillers which allows tuning the final product properties.^{88, 89}



Figure 1.10 Typical applications of TPE in; automotive sector, asphalt binders, shoes soles, tires, aircrafts, adhesives and electrical insulators.

1.5 Advantages, limitations, and challenges for TPEs

The main drawbacks of TPEs, compared to thermoset rubbers, are that they suffer plastic deformation (upon tension or compression external forces), a drying process is needed prior to processing, the number of low hardness products are limited, and they soften at elevated temperatures. Nevertheless, it could be said that the advantages overcome the limitations, such as simple and fast processing, fast molding, low energy consumption, recycling of the scrap, better quality control and no curing step is necessary.⁹⁰ Due to these advantages the TPEs demand is growing and the global value of TPE is estimated to increase up to 28.27 USD billion by 2022.¹⁵ For this reason, many efforts are focused on the obtention of new TPEs with enhanced properties, which can meet the actual and future needs of the society, together with diminishing the environmental impact. This can be accomplished by replacing the fossil raw materials by renewable feedstocks, together with more convenient synthetic pathways using eco-friendly conditions,⁹¹ and designing the materials in such manner that could be recycled or degraded.^{92, 93} Moreover, sometimes it is necessary to consider, not only the degradability of the polymer itself, but the recyclability of the materials which are together with the TPE in many applications. For example, adhesives present in paper, e.g. labels or book-bindings, and cardboards, e.g. in package junctions, becomes a source of problems in terms of paper recycling. The paper contamination from adhesives, called stickies in the paper industry, causes operating problems due to the formation of deposits on the equipment and product quality defects during the process of paper recovery.^{94, 95} These adhesives are hard to remove before the recycling of paper. For this reason, there is a need for creating new TPEs able to be degraded under demand, upon external stimuli (e.g. acid or reductive media) and become easy to remove from valuable materials.⁹⁶

1.6 Polymers from renewable resources

Nowadays exist a big concern about how our society is expending the natural resources that are available. The great majority of the commercial synthetic polymers, which production have increased exponentially in the past decades, are obtained from non-renewable fossil-sourced raw materials. Even though the polymer manufacturing only consumes directly around 8% of total oil produced annually, there are estimations than with the increasing demand it will consume 20% of oil production by 2050, and also an equal quantity of oil is consumed indirectly in the production process due to the energy consumption.⁹⁷ Further, exists a big issue about the global plastic waste, many of the synthetic polymers will end in landfills, when not directly into the nature. In addition to this, most synthetic polymers are not biodegradable, remaining in the environment for years, accumulating in the oceans and affecting to ecosystems. It is considered that, apart from the incinerated materials, all the plastics than have been discarded into the environment remains unaffected (as whole items or fragments) until date.^{98, 99} There are estimations than by the 2050s the total amount of plastics produced would be around 33 billion tones. Moreover, approximately 30 % of the global plastic production is intended to PVC, polystyrene, polyurethane and polycarbonate, which are problematic materials in terms of recyclability and potential toxicity.^{100, 101}

Accordingly, in the present days an important target for polymer science and green chemistry is to satisfy both necessities; developing renewable alternatives to conventional fossil-derived raw materials, and designing materials which could be easily reused, recycled and/or degraded. In this manner, two of the twelve principles of green chemistry are being fulfilled.^{102, 103} Together with these two challenging aims, these more ecofriendly alternatives must compete, in terms of production costs, with conventional polymers. The higher price of biopolymers and their limitations for some applications (e.g. high temperature service) entails than less than 5% of the market is covered by them.¹⁰⁴ Two representative examples of commercially available

biopolymers are poly(lactic acid) (PLA), which monomer is obtained from carbohydrates fermentation (e.g. corn) and poly(hydroxyalkanoates) (PHA), synthesized directly inside microorganisms and also by carbohydrates fermentation (Figure 1.11).^{105, 106}

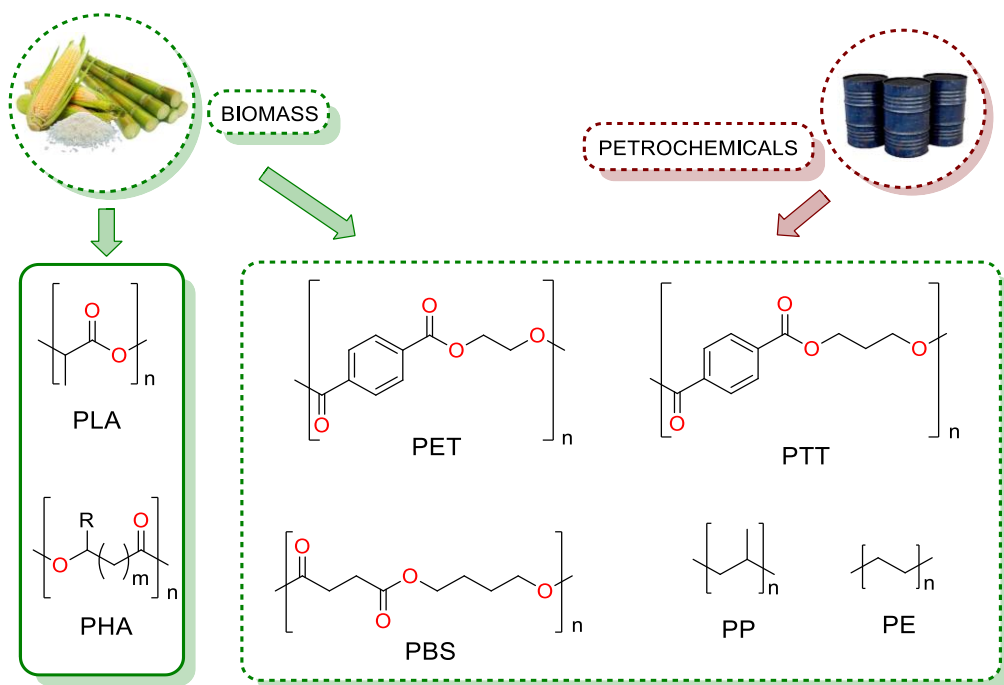


Figure 1.11 Commercially available biopolymers.

It is worth to mention that the term biopolymer not always is accompanied by the term biodegradable. Polymers traditionally obtained by petrochemicals, such as polyethylene (PE) or poly(ethylene terephthalate) (PET), can also be obtained total or partially from biomass (Figure 1.11).¹⁰⁷ But these bio-based alternatives are chemically identical to its petrochemical equivalent, then its degradation behavior will be the same.

1.7 Monomers from renewable feedstocks

There are three main methods to prepare renewable monomers:¹⁰⁴

1.7.1 Direct extraction from natural feedstocks

There are a lot of interesting compounds than can be directly extracted from plants. One of the more representative examples are vegetable oils, which are composed by a variety of fatty acid triglycerides. The composition of the fatty acids depends on the plant and the growing conditions. Oleic acid can be obtained from canola oil or from highly oleic sunflower oil, linoleic acid from soybean and sunflower seeds, linolenic acid from linseed, vernolic acid from *Vernonia galamensis* oilseed, ricinoleic acid from castor oil and erucic acid from rapeseed (Figure 1.12).^{108, 109}

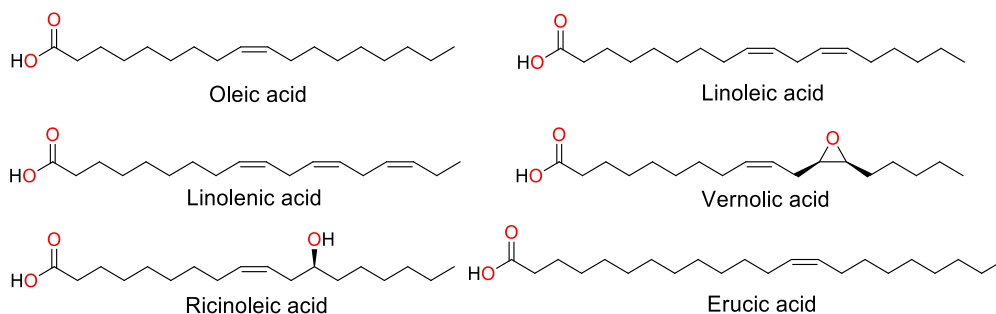


Figure 1.12 Examples of industrial fatty acids.

These fatty acids can be used directly to synthesize polymers or can be chemically modified to obtain other compounds through epoxidation, hydroformylation, hydrogenation, metathesis, oxidative cleavage among others.¹¹⁰ Other types of direct natural monomers are terpenes and terpenoids, e. g. carvone, menthol, limonene, α -pinene and myrcene (Figure 1.13), which can also be directly polymerized or used as monomer precursors. These compounds are extracted from resins collected from different trees.^{111, 112} Another interesting terpene monomer is α -methylene- γ -butyrolactone (MBL) (or tulipalin A) which is found in tulips (see section 1.7.5).

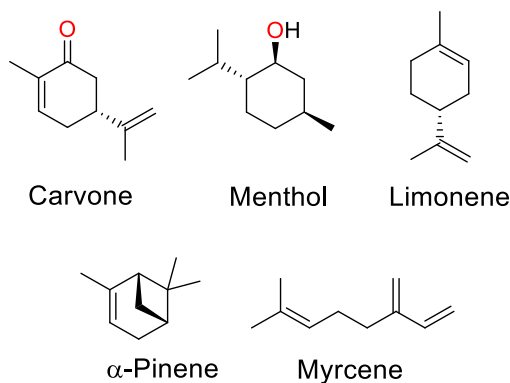


Figure 1.13 Chemical structures of common terpene and terpene derived monomers.

1.7.2 Biotransformation of natural feedstocks

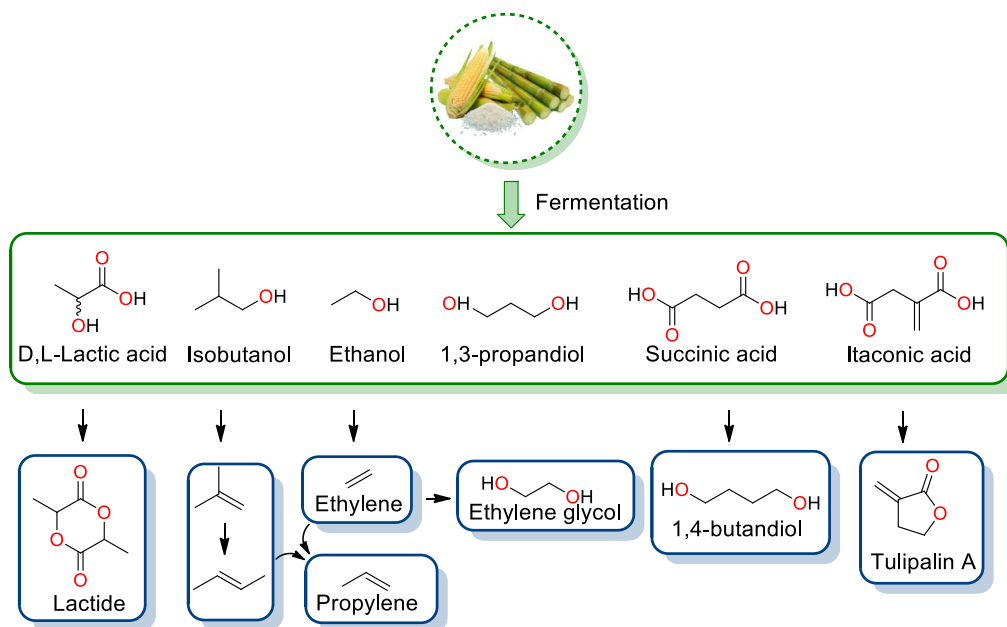


Figure 1.14 Monomers/precursors obtained from biomass fermentation (green), intermediates and monomers obtained by modification of biomass precursors (blue).

Fermentation of carbohydrates is of great interest for the obtention of monomers because biomass carbohydrates are the most abundant renewable resource. Through this pathway it is nowadays produced commercial lactic acid in large-scale, around 350 Kt/year.¹¹³ Another known example is the cost-effective process developed by DuPont

to obtain 1,3-propanediol through glucose fermentation by a genetically modified *E. coli*.¹¹⁴ From glucose a variety of precursors for polymer synthesis such as isobutanol, ethanol and succinic acid could be obtained (Figure 1.14).¹¹⁵ Other examples of compounds obtained from biomass fermentation are glutamic acid (1.7 Mt/year) and citric acid (1.6 Mt/year).¹¹⁶ Fatty acids is another natural feedstock that can be converted to useful monomers through biotransformation, e. g. the synthesis of δ -decalactone (DL) from linoleic acid and from 11-hydroxypalmitic acid (see section 1.7.4). Polymers could also be synthesized directly by microbial fermentation of fatty acids, like polyhydroxyalkanoates (PHAs) that can be obtained as homopolymers, random copolymers and block copolymers depending on the bacterial specie and growth conditions.^{115, 117}

1.7.3 Chemical transformation of natural feedstocks

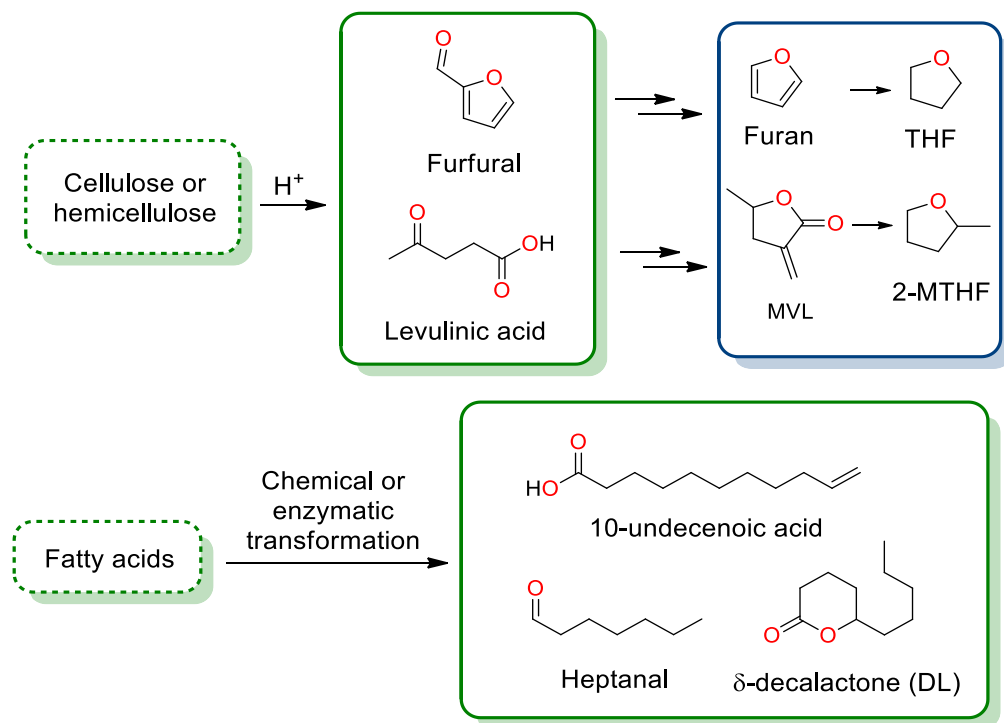


Figure 1.15 Monomers obtained by chemical or enzymatic transformation from biomass.

Finally, another source of renewable monomer involves the chemical transformation of natural feedstock. The raw material can come from agricultural or forestry wastes (mainly formed by cellulose and hemicellulose composed by C6 and C5 sugars) and from vegetable oils, rich in fatty acids. From the acidic treatment of cellulose and hemicellulose furfural and levulinic acid can be produced.¹⁰⁴ From these products other interesting derivatives as furan, tetrahydrofuran (THF), α -methylene- γ -valerolactone (MVL) and 2-methyltetrahydrofuran (2-MTHF) can be obtained (Figure 1.15).¹¹⁸ Vegetable oils are also a versatile platform to obtain valuable chemicals. One of the most important oleochemical reactions are the thermal cleavage of ricinoleic acid to form 10-undecenoic acid and heptanal¹¹⁹ and the basic cleavage to form sebacic acid¹²⁰ (decanedioic acid) and 2-octanol, through chemical transformations, but also through enzymatic and microbial processes (Figure 1.15).¹²¹⁻¹²³

1.7.4 δ -Decalactone (DL)

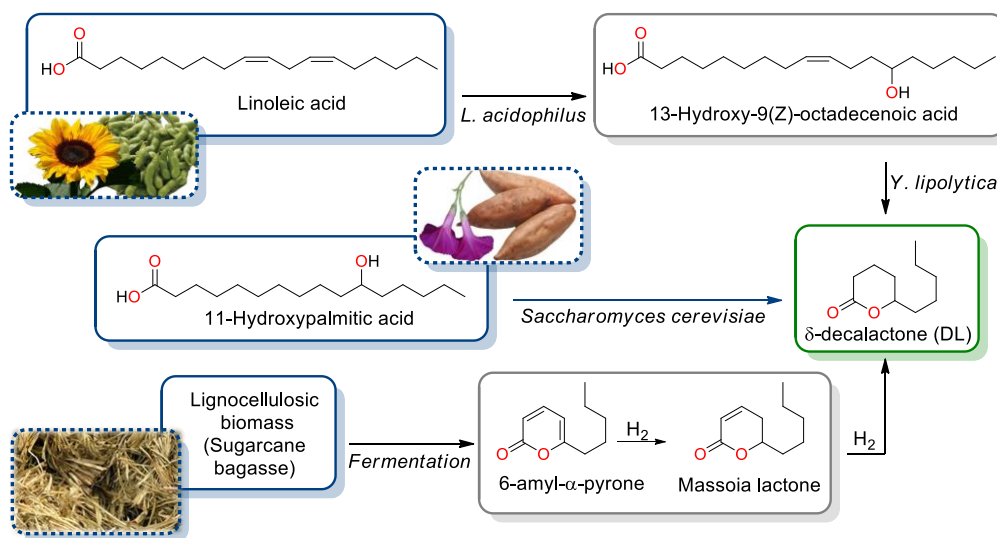


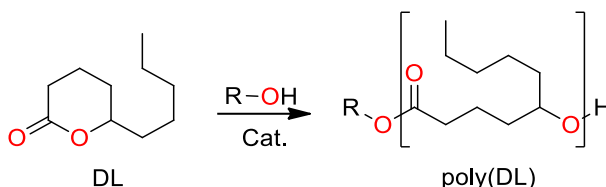
Figure 1.16 Obtention of DL from linoleic acid, 11-hydroxypalmitic acid and sugarcane bagasse.

This lactone is present naturally, among other aliphatic lactones, in foods having a high fat content such as meat, cheese, milk and coconuts. These lactones are intentionally added to foods and beverages to give flavors (peachy, coconut-like), usually in the

concentration that are found in nature (usually between 0.05 and 80 ppm).¹²⁴ δ -Decalactone can be extracted from some trees, as *Cryptocarya massoy* (an evergreen tree of *Lauraceae* family), but is present in low quantities (about 2.5 %) in heartwood oil.¹²⁵ DL can be prepared from other more available natural feedstocks such as linoleic acid, using *Lactobacillus acidophilus* and cells of *Yarrowia lipolytica*,¹²⁶ or from 11-hydroxypalmitic acid (11-hydroxyhexadecanoic acid),¹²⁷ extracted from mexican jalap (*Ipomoea orizabensis*) and sweet potato (*Ipomoea batatas*),¹²⁸ using different strains of *Saccharomyces cerevisiae*.^{129, 130} Other sources could be by hydrogenation of massoia lactone, obtained by biomass fermentation from sugarcane bagasse (Figure 1.16).^{131,}

132

- δ -Decalactone reactivity and poly(DL) properties

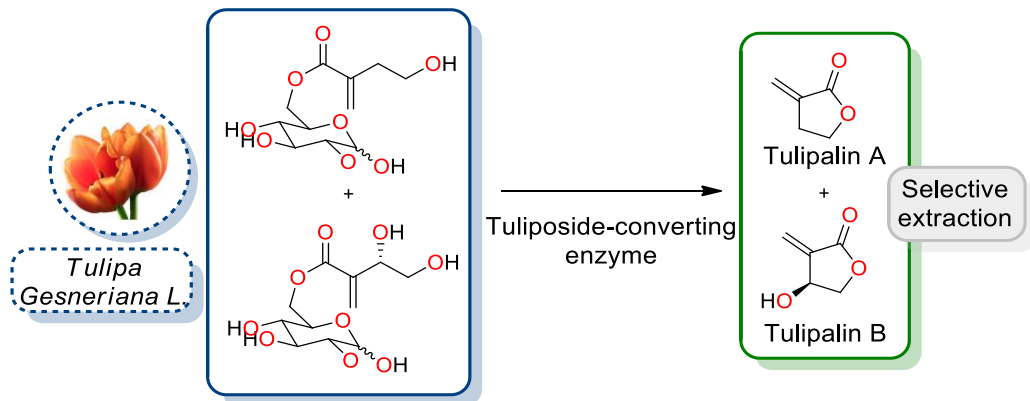


Scheme 1.2 Synthesis of poly(DL).

δ -Decalactone (DL) has been used to synthesize aliphatic non-crystalline polyesters, with low T_g values, through Ring-Opening Polymerization (ROP) (see section 1.8.2). There are many examples in the literature where DL is polymerized enzymatically (e. g. *Pseudomonas sp. lipase*)¹³³, and through acid (e. g. diphenyl phosphate (DPP))¹³⁴ or basic (e. g. 1,5,7-triazabicyclo[4.4.0]dec-5-ene (TBD))¹³⁵ catalyst (Scheme 1.2). This monomer can be polymerized in a controlled manner (polydispersity (\bar{M}_w/\bar{M}_n) below 1.2)¹³⁶ obtaining relatively high molecular weights (between 25000 and 30000 g/mol) and with a relatively high equilibrium conversion (88%).¹³⁵ The aliphatic chain at the 5-position allows the obtention of non-crystalline polymers with low glass transition temperatures ($T_g < -50$ °C), compared with the non-alkyl substituted homonym poly(δ -valerolactone) which is semicrystalline ($T_m = 55$ °C).¹³⁷ These properties make poly(DL) a suitable

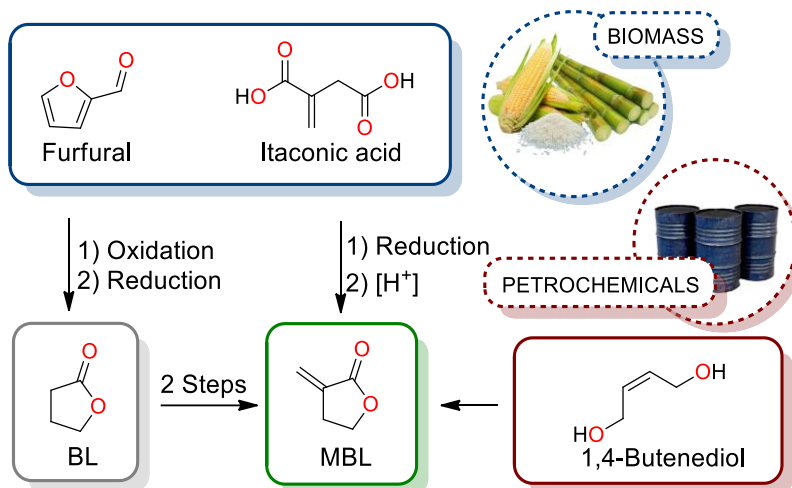
candidate as biobased soft/rubbery segment for TPE applications. Polymerization of DL is explained with more detail in section 1.9.

1.7.5 α -Methylene- γ -butyrolactone (MBL)



Scheme 1.3 Enzymatic conversion of tulipalin-glycosides, extracted from tulipa gesneriana L., to tulipalin A and B.

α -Methylene- γ -butyrolactone (MBL) or tulipalin A is a terpene plant-derived monomer, which can be considered a cyclic analog of the petro-derived monomer methyl methacrylate (MMA).¹³⁸ MBL is present in common tulip, *Tulipa Gesneriana L.*,¹³⁹ from which it can be extracted both as lactone or as glycoside (0.2-2.0% w/w fresh weight)¹⁴⁰ and can be converted to MBL through enzymatic catalysis (Scheme 1.3).¹⁴¹ However, due to the low MBL concentration in tulips, the obtention through this methods even feasible is not economically competitive. Therefore, more convenient and economic routes for the obtention of this monomer are followed for the large-scale industrial production (e. g. from 1,4-butenediol).¹⁴² Moreover, there are some, commercially available, renewable precursors from which MBL can be synthesized in a feasible way thought more conveniently routes. The most important bio-based precursors are γ -butyrolactone (BL)¹⁴³ (available from furfural)¹⁴⁴ and itaconic acid¹⁴⁵ (Scheme 1.4). Thus, using different synthetic approaches γ -butyrolactone can be conveniently transformant in MBL within two steps with acceptable yield and using economical reagents.



Scheme 1.4 Synthetic methods for the obtention of MBL from different precursors.

- **MBL reactivity and poly(MBL) properties**

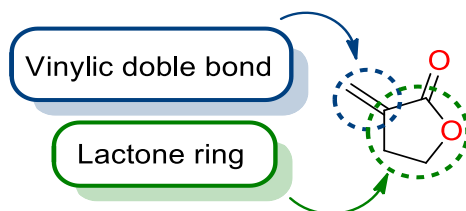
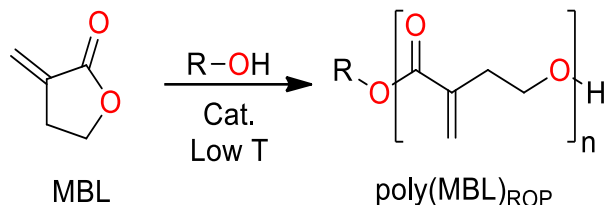


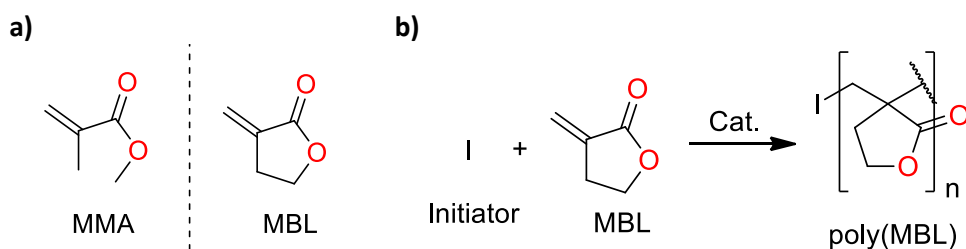
Figure 1.17 MBL reaction sites.

MBL possesses two possible polymerization sites, an exocyclic vinylic double bond and a γ -lactone ring (Figure 1.17). From the lactone ring functionality point of view, due to the low ring strain of this five-membered cyclic conformation, thermodynamics for polymer formation is unfavorable (see section 1.8.2.1). However, there are some examples in the literature where it was polymerized by ring-opening polymerization (ROP) mechanism. Using very active catalysts, together with very low temperatures, high conversions of polymers with a M_n of 30 kg/mol can be achieved.¹⁴⁶⁻¹⁴⁹



Scheme 1.5 Synthesis of poly(MBL) polyester through ROP mechanism.

However, the vinylic functionality has attracted more attention until now due to its similarity to MMA (Scheme 1.6-a). There are many examples in the literature of MBL polymerization through different mechanisms (Scheme 1.6-b), such as free radical^{139, 150} anionic,¹³⁹ reversible addition-fragmentation chain-transfer polymerization (RAFT),¹⁴⁵ coordination-addition¹⁵¹ and atom transfer radical polymerization (ATRP) (see section 1.14).¹⁵²



Scheme 1.6 (a) Comparison of MMA and MBL structures and (b) vinylic polymerization of MBL.

Poly(MBL) homopolymer is a rigid, brittle and transparent material which possesses rigid lactone rings perpendicular to the plane of the backbone creating steric hindrance (Figure 1.18). Moreover, it presents dipole-dipole interactions, which entails a restriction of the chain mobility compared with its homologous MMA.¹⁵³ This high rigidity of the chain is responsible of the high T_g value of poly(MBL), (195 °C, for atactic samples) almost double than for MMA (105 °C), and showing a better solvent resistance (only soluble in polar aprotic solvents, such as DMSO and DMF).¹³⁹ It possesses high thermal stability (major decomposition at more than 320 °C) and thermally depolymerize to monomer.¹³⁸ Thus, this polymer is an appropriate candidate for the

synthesis of the hard block in A-B-A type TPEs, and there are some examples in the literature of block copolymers using MBL for this purpose.^{70, 78}

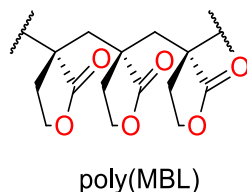


Figure 1.18 Poly(MBL) synthesized by vinylic polymerization.

1.8 Polyesters

Polyesters are a type of polymers that contain ester functional groups in the main chain. One of the first examples of this kind of polymers were reported by Carothers in 1930s by polycondensation of aliphatic diacids with aliphatic diols.^{154, 155} These firsts polyesters could not compete with other polymers such as polyamides (e. g. Nylon) due to its low melting point and susceptibility to hydrolysis. It was not until the 1940s than Whinfield and Dickson, in the research laboratories of Calico Printers' Association, developed the first commercially important aromatic polyester, poly(ethylene terephthalate) (PET) (Figure 1.19).^{156, 157} This aromatic polyester presents a high melting point (240 °C), in comparison with aliphatic polyesters, and low solubility on solvents. The hydrolytic resistance is also increased due to a more hindered hydrolytic sites caused by a close chain packaging (PET density is approx. 1.4 g/cm³).¹⁵⁷ This improved properties made PET a valuable material for commercial purposes, being able to prepare both fibers and films. Nowadays PET is one of the most produced polymers, mainly for the textile and packaging sector.

Other important polyesters, are aliphatic polyesters, such as poly(ϵ -caprolactone) (PCL) and poly(lactic acid) (PLA) (Figure 1.19). The first one is a hydrophobic semi-crystalline polyester, which was developed in the 1930s by Carothers' group.¹⁵⁸ PCL was one of the first efforts to obtain polymers which could be degraded by microorganisms, and

rapidly became widespread used in biomedical applications due to its biocompatibility.¹⁵⁹ The second one PLA, as previously mentioned, constitutes one of the first aliphatic polyesters obtained from renewable resources. Since then, the development of more complex polyesters has increased, especially for the use in more specific applications such as medical devices.¹⁶⁰ Polyesters can be synthesized through two pathways; polycondensation and ring opening polymerization (ROP).

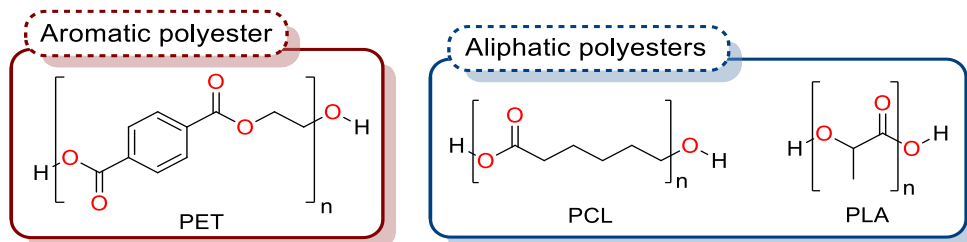
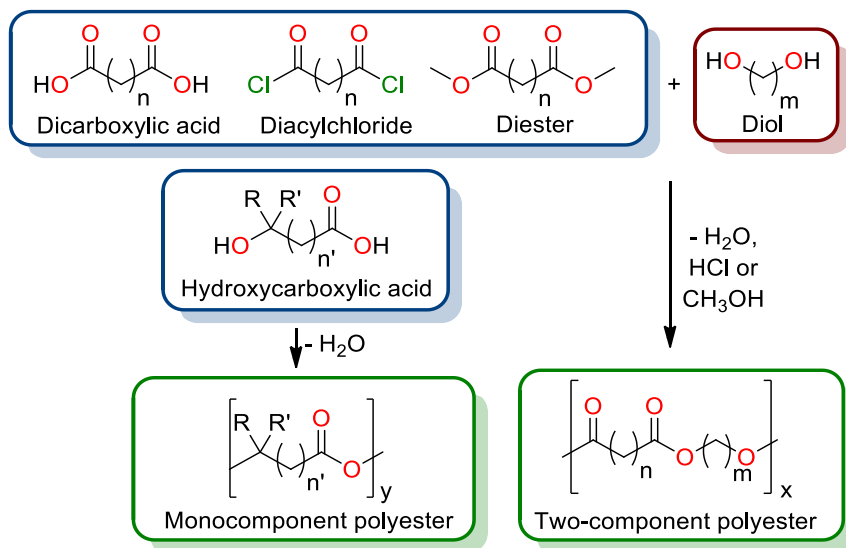


Figure 1.19 Structure of PET (aromatic polyester) and PCL and PLA (aliphatic polyesters).

1.8.1 Polycondensation



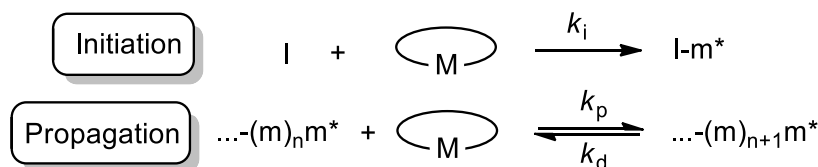
Scheme 1.7 Polyesters from polycondensation pathway.

Polycondensation consist in a stepwise reaction between bifunctional components with the elimination of small molecules. It can be performed either from

hydroxycarboxylic acids¹⁶¹, diacids and diols¹⁶², diacylchlorides and diols¹⁶³ or a diesters and a diols¹⁶⁴, with the release of water, hydrogen chloride and alcohol respectively (Scheme 1.7). Usually these reactions are catalyzed by acids¹⁶⁵, metals¹⁶⁶ or enzymes¹⁶⁷, but the driving force for this equilibrium reaction is the constant remove of the low molecular weight molecule, either by azeotropic distillation, high vacuum or using a base in the case of hydrogen chloride. The polymers obtained through polycondensation are usually polydisperse and with poor control over molecular weight and polymer architecture.

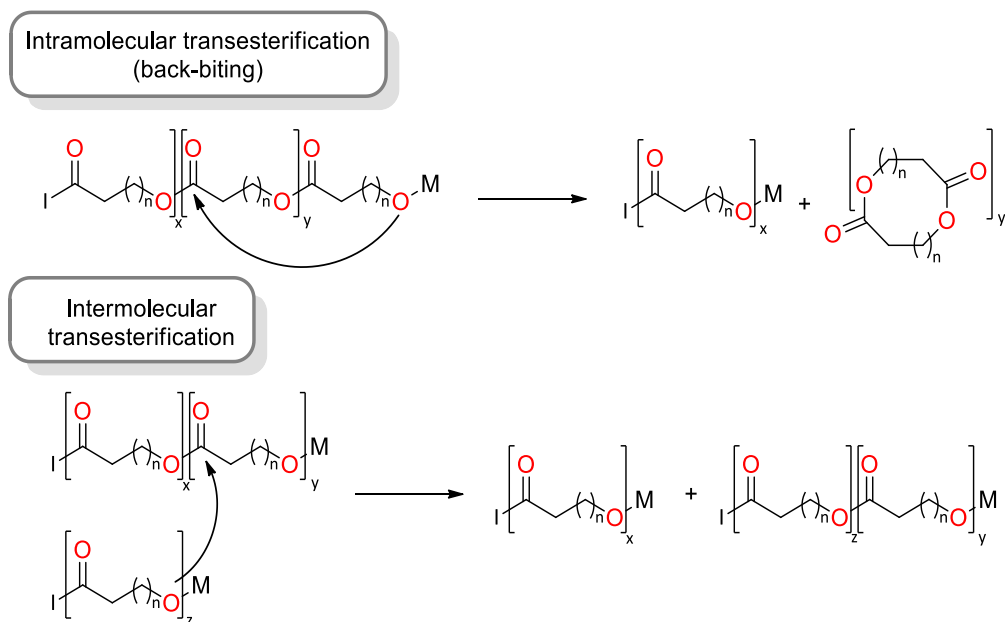
1.8.2 Ring-opening polymerization (ROP) of cyclic esters.

The second pathway to obtain polyesters is ring-opening polymerization of lactones (cyclic esters). This kind of polymerization, also known as Ring-Opening Transesterification Polymerization (ROTEP), allows the obtention of polyesters with controlled molecular weight and narrow polydispersity.¹⁶⁸ A ROP reaction begins with the addition of initiating agents (I) to a monomer (M) creating the active specie (m^*). Once initiated, the propagation step consists in an equilibrium reaction, in this case, between the monomer and the growing chain (Scheme 1.8), where m^* reacts with M incorporating to the chain and giving the opposite reaction by releasing a monomer unit. The conversion at the equilibrium will be determined by the rate constants of propagation (k_p) and depropagation (k_d) relationship. ROP reactions with high k_d value will achieve low conversions, therefore remaining a relatively high $[M]_{eq}$. once reached the equilibrium.¹⁶⁹



Scheme 1.8 Initiation and propagation steps in a ROP reaction.

The control on the molecular weight and the end group can be only achieved if k_i is higher than the k_p and, to proceed as a living process, the side reactions must be minimized. In the case of ROP of lactones two types of undesired reactions can occur. One is the intramolecular transesterification process leading to macrocyclic products and losing the chain-end.¹⁷⁰ Another unwanted reaction is the intermolecular transesterification between two polymer chains (Scheme 1.9). This may cause the loss of control in the polymer architecture, especially in block copolymers, where the monomer sequence could be randomized.¹⁷¹ The consequences in both cases is a broadening in the molecular weight distribution.^{169, 172, 173} Transesterification side reactions increases when high temperatures¹⁷⁴ and prolonged reaction times¹⁷⁵ are used.



Scheme 1.9 Representation of the transesterification side reactions involved in ROP of lactones.

1.8.2.1 Thermodynamics of ROP

The capability of a cyclic monomer to polymerize, from the thermodynamic point of view, is given by the sign of free Gibbs energy (ΔG_p) (Equation 1.1) of polymerization ($\Delta G_p < 0$). ΔH_p and ΔS_p are the enthalpy and entropy of polymerization respectively, and T is the temperature.

$$\Delta G_p = \Delta H_p - T\Delta S_p$$

Equation 1.1 General free Gibbs energy expression.

The enthalpy (ΔH_p) term mainly depends on the lactone ring strain, which is usually the driving force of the polymerization. The major contribution to the ring strain comes from the distorted bond angle values, the bond stretching, repulsion between eclipsed hydrogen atoms and non-bonding interactions between substituents.¹⁷⁶ In most cases an entropy decrease due to the loss of transitional degrees of freedom is observed,¹⁶⁹ therefore polymerization is allowed when the enthalpic term overcome the entropic contribution in the free Gibbs energy. The free Gibbs energy (ΔG_p) can be also expressed by a sum of standard free Gibbs energy (ΔG_p°) and a term associated to the concentration relationship between monomer ($[M]$) and growing chain ($[\dots - (m)_{i+1}m^*]$) (Equation 1.2).

$$\Delta G_p = \Delta G_p^\circ + RT \ln \frac{[\dots - (m)_{i+1}m^*]}{[M][\dots - (m)_i m^*]}$$

Equation 1.2 Free Gibbs energy expression as a function of the monomer concentration.

Considering the Flory's assumption that the reactivity of an active center, located in a long macromolecule, does not depend on the degree of polymerization. Then the term $\frac{[\dots - (m)_{i+1}m^*]}{[M][\dots - (m)_i m^*]}$ on Equation 1.2 can be approximate to $\frac{1}{[M]}$. Combining the obtained equation with $\Delta G_p^\circ = \Delta H_p^\circ - T\Delta S_p^\circ$ the following equation can be obtained:¹⁶⁹

$$\Delta G_p = \Delta H_p^\circ - T(\Delta S_p^\circ + R \ln[M])$$

Equation 1.3 Relationship between thermodynamic parameters and monomer concentration.

From Equation 1.3 the monomer concentration at the equilibrium ($[M]_{eq.}$) can be estimated assuming that at the equilibrium $\Delta G_p = 0$, Equation 1.4. Consequently, only when the initial monomer concentration ($[M]_0$) is higher than the monomer concentration at the equilibrium ($[M]_{eq.}$) the polymerization can be carried out ($[M]_0 > [M]_{eq.}$).

$$[M]_{eq.} = \exp\left(\frac{\Delta H_p^\circ}{RT} - \frac{\Delta S_p^\circ}{R}\right)$$

Equation 1.4 Monomer concentration at the equilibrium.

Temperature is also an important issue to consider. One extreme case are monomers possessing $\Delta H_p^\circ < 0$ and $\Delta S_p^\circ > 0$, which means that polymerization is allowed at any temperature. The other extreme case are monomers with $\Delta H_p^\circ > 0$ and $\Delta S_p^\circ < 0$, which polymerization is thermodynamically forbidden at any temperature.

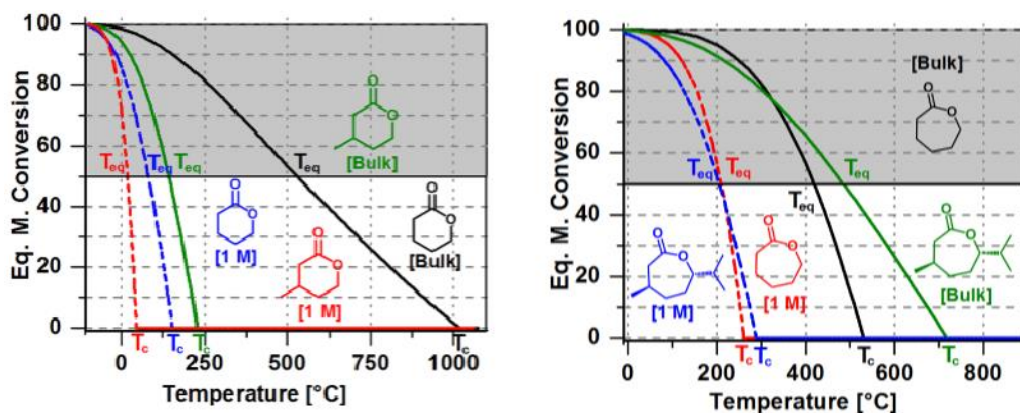


Figure 1.20 Equilibrium monomer conversion vs temperature of six-membered (left) and seven-membered (right) lactones.¹⁷⁷

However, in most cases the ΔH_p° and ΔS_p° are negative, then the highest conversions (lower $[M]_{eq.}$) are reached lowering temperature. Increasing temperature increases the $[M]_{eq.}$ and the temperature at which $[M]_{eq.} = [M]_0$ is called ceiling temperature (T_c)¹⁷⁸, above this temperature polymerization is not possible. In the other hand, the case where $\Delta H_p^\circ > 0$ and $\Delta S_p^\circ > 0$ in which $[M]_{eq.}$ decreases when increasing temperature (Figure 1.20), the critical parameter for this case is the floor temperature (T_f), below which the polymerization is not possible.¹⁶⁹ Accordingly, one of the first issues to consider is the ring size of the monomer.

- Three-membered lactones:

The α -lactones (oxiran-2-ones) are the smallest members of the cyclic esters. The fact of possessing a sp^2 carbon into a three-membered ring entails a high increase of the ring strain in comparison to its carbocycle analogue (cyclopropane).¹⁷⁹ Therefore, the α -lactones are too much reactive to be isolated and then there are not suitable candidates to become ROP monomers.

- Four-membered lactones:

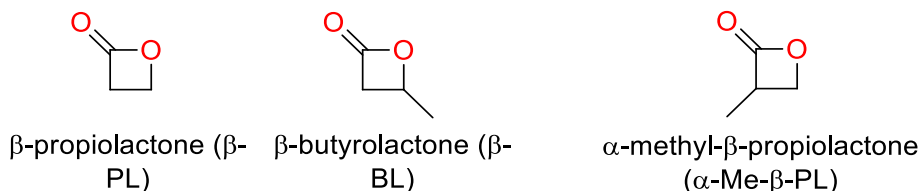
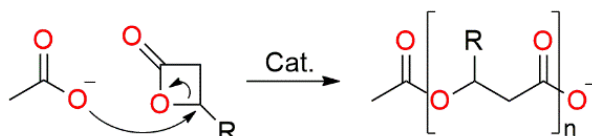


Figure 1.21 Examples of four-membered lactones.

The β -lactones (oxetan-2-ones) (Figure 1.21) possess also a high ring strain, which is responsible of its low ΔH_p° value, e.g. -82.3 kJ/mol for β -propiolactone at 298 K. This very negative polymerization enthalpy is reflected in almost complete consumption of the monomer, leading to very low $[M]_{eq.}$ value, e.g. for β -propiolactone the equilibrium concentration is $2.8 \cdot 10^{-10}$ M.¹⁷⁶ Unlike the higher member of lactones, β -lactones are usually initiated by carboxylates, such as potassium acetate crown ether complex, instead of by alkoxides.^{176, 180}

Another remarkable difference with respect to less strained lactones is the bond involved in the ring opening. In the four-membered lactones the propagating specie (carboxylate) reacts with the carbon adjacent to the ester oxygen leading to an alkyl-oxygen scission (Scheme 1.10) and the generation of another carboxylate propagating specie.¹⁸¹



Scheme 1.10 Alkyl-oxygen scission in ROP of β -lactones ($R = H$ or CH_3).

- Five-membered lactones:

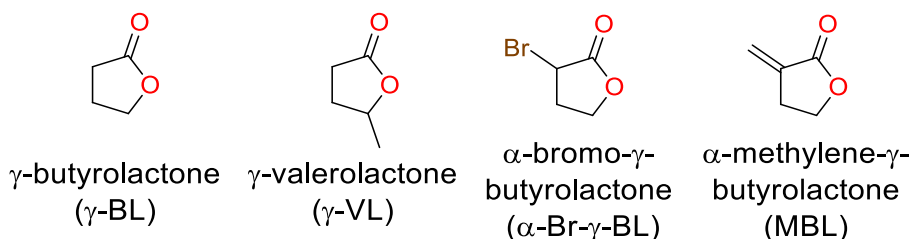


Figure 1.22 Examples of five-membered lactones.

The γ -lactones (dihydrofuran-2(3H)-ones) (Figure 1.22) are the less strained of the small lactones, because the only contribution to the ring strain comes from conformational interactions. One cause for the reduction of the strain comes from having less C-H bonds oppositions due to carbonyl group within the ring.¹⁷⁶ The ester group in a five-membered cycle has geometrical parameters (bond angle) very close to that in methyl acetate, selected as strain-free reference compound.¹⁸² This lack of strain is reflected in the ΔH_p° , being 5.1 kJ/mol, and a high $[M]_{eq.} \approx 3 \cdot 10^3$ M.¹⁷⁶ This very high monomer concentration at the equilibrium, compared with monomer concentration at bulk (13 M for γ -butyrolactone), is an evidence of the low polymerizability of the γ -lactones. However, there are examples in the recent literature where γ -butyrolactone is

polymerized in THF at - 40 °C obtaining molecular weights higher than 10 kg/mol and narrow polydispersities ($\bar{D} \approx 1.2$).¹⁴⁶ Other strategies to overcome the thermodynamic barrier is the copolymerization with more strained rings such as ϵ -caprolactone.¹⁸³

- Six-membered lactones:

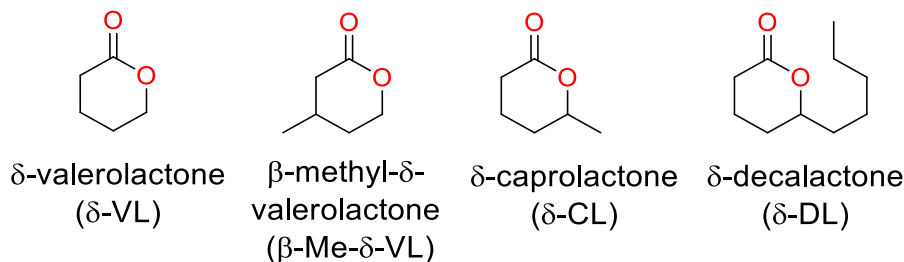


Figure 1.23 Examples of six-membered lactones.

The δ -lactones (tetrahydro-2H-pyran-2-ones) (Figure 1.23) are moderately more strained than the γ -lactones, e.g. the strain energy for γ -butyrolactone is 32.2 kJ/mol and 39.7 kJ/mol for δ -valerolactone.¹⁸⁴ The carbonyl group introduces strain into a six-membered ring due to its flat geometry,¹⁶⁹ which entails a distortion of the bond angles, especially compared with the non-strained cyclic hydrocarbon analogue cyclohexane.¹⁷⁹ Another factor influencing the strain in these cycles is the repulsion between eclipsed hydrogen atoms.

One of the first examples for the polymerization of six-membered lactones was reported at the beginning of the 1930s, Carothers et al. described the formation of a waxy solid by reacting δ -valerolactone at room temperature without catalyst for twenty-nine days.¹⁸⁵ He also described its reversible character by the formation of the starting lactone upon heating and the effect of substituents, being unable to polymerize the α -n-propyl- δ -valerolactone after twelve month of reaction. The effect of substituents on polymerization of lactones will be discussed in Section 1.8.2.2. Although having higher strain, this

kind of monomer usually have a relatively high monomer concentration at the equilibrium ($3.9 \cdot 10^{-1}$ M for δ -valerolactone at 298 K)¹⁷⁶ and therefore reaching moderate conversions. This characteristic usually makes δ -lactones unable for block copolymer synthesis through sequential addition of monomer due to the remaining monomer once reached the equilibrium. Nevertheless δ -lactones are promising candidates for the synthesis of polyesters, leading to polymers with controlled molecular weight and architectures as well as with narrow polydispersities under the appropriate polymerization conditions.^{134, 186, 187}

- Seven-membered lactones:

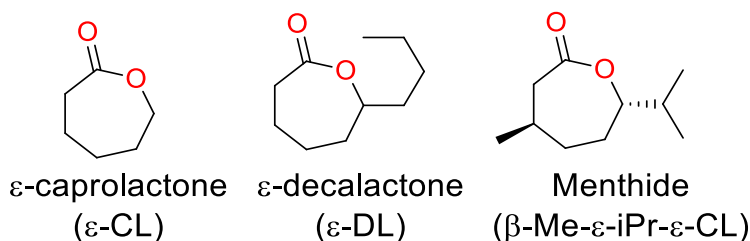


Figure 1.24 Examples of seven-membered lactones.

The ϵ -lactones (oxepan-2-ones) (Figure 1.24) are more strained than δ -lactones (with ΔH_p -28.8 and -27.4 kJ/mol for ϵ -CL and δ -VL respectively),¹⁷⁶ possessing a higher ceiling temperature (T_c) and reaching higher conversion than the six-membered lactones.¹⁷⁷ These characteristics, similar to that of six-membered lactones, makes this lactones also promising candidates for the synthesis of polymeric materials with controlled architectures and narrow polydispersities.¹⁸⁸ Consequently, ϵ -lactones derivatives have been widely studied for the synthesis of materials in different kinds of applications, such as micelles for drug encapsulation¹⁸⁹ or as thermoplastic elastomers.^{190, 191}

- Higher lactones:

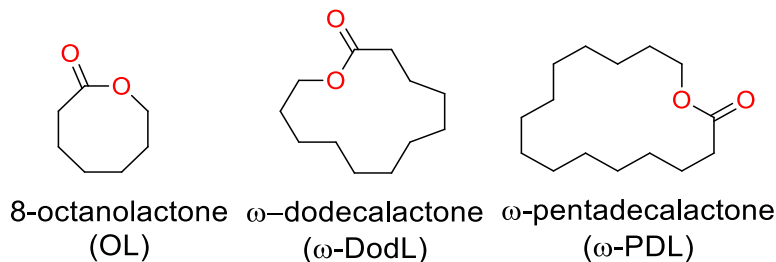


Figure 1.25 Examples of macrolactones.

Lactones with higher ring size (eight or more membered rings, Figure 1.25) presents lower ring strain as increasing in the ring size, which is reflected in an increase of enthalpy of polymerization.¹⁷⁷ The polymerization of macrolactones usually is entropy driven, due to the high flexibility of the methylene chain in the final polymer. The main drawback in the polymerization of macrolactones is that the lack of ring strain results in similar rates of polymerization and transesterification, which results in broad polydispersities ($\mathcal{D} > 2$).¹⁹²⁻¹⁹⁵

1.8.2.2 Substituent effect on the lactone ring

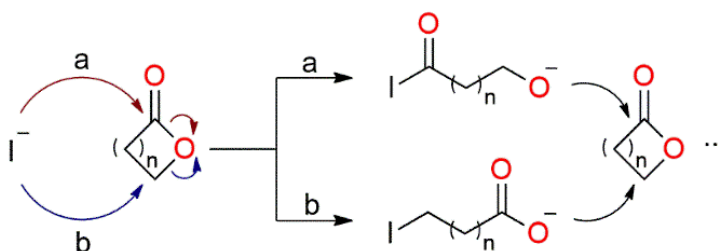
Another factor to consider about the ability of a lactone to polymerize is the substituents on the ring. It is reported that the presence of substituents in the ring decreases the conversion at the equilibrium, due to a decrease in the ring strain.¹⁸⁷ This behavior can be explained by the Thorpe-Ingold effect, in which the steric hindrance of the substituents produces a compression of the internal angle and then favoring the ring closure.¹⁹⁶ However, more recent studies reported the opposite behavior, increasing the ring strain with the presence of substituents. They reported a higher influence of the substituent on the ΔS_p° than in ΔH_p° , being magnified upon dilution. The equilibrium conversion increases when the polymerization is performed in bulk.¹⁷⁷ The length of the substituent seems to have a stronger effect than the position, the ΔH_p° of two lactones with the same substituent in different position are very similar, e. g. δ -caprolactone and β -methyl- δ -valerolactone have -13.8 and -14.3 kJ/mol

respectively. However, when comparing lactones with different length substituents at the same position the difference is magnified, e. g. ΔH_p of δ -decalactone is -20 kJ/mol.¹⁷⁷ Another consequence of having a substituent in the lactone ring is the change in the thermal properties of the resulting polyesters, e. g. lowering the T_g by increasing the length of the alkyl pendant group.^{190, 197}

1.8.3 ROP mechanisms

The ROP mechanisms can be differentiated according to the type of catalyst and mechanism of propagation; and can be classified as anionic, cationic, monomer-activated and coordination-insertion.¹⁹⁸

1.8.3.1 Anionic ROP

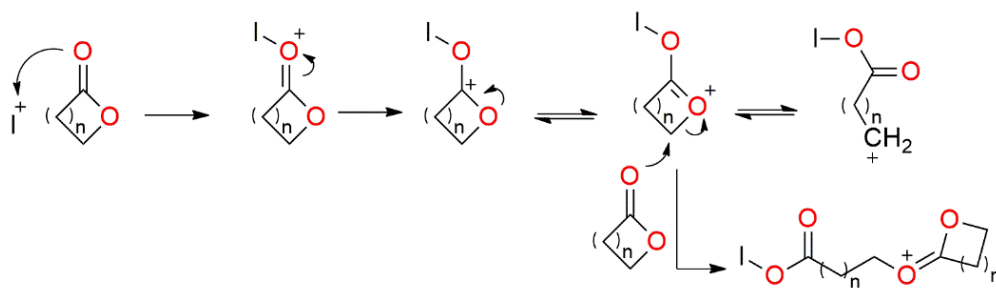


Scheme 1.11 Anionic initiation mechanism in ROP. Acyl-oxygen (a) and alkyl-oxygen (b) cleavage pathways.

This mechanism is initiated by the nucleophilic attack of a negatively charged specie to the carbonyl carbon or to the carbon bonded to the acyl oxygen (Scheme 1.11). The propagating specie is an alkoxide or a carboxylate anion respectively. Typical initiators/catalysts in anionic polymerization are radical anions, activated metal hydroxides or alkoxides, carboxylates, phosphazene bases, amines and phosphines. The anionic ROP of four-membered lactones can occur with both pathways, while larger lactones only react through the acyl-oxygen cleavage.^{168, 199} The high reactivity of the propagating specie in this mechanism, usually an alkoxide, generate cyclic oligomers as a result of post-polymerization “backbiting”.²⁰⁰

1.8.3.2 Cationic ROP

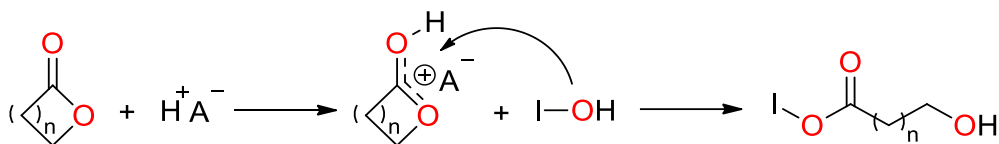
Cationic ROP polymerization of lactones can proceed through two main pathways: the chain end activated mechanism and the monomer-activated mechanism depending on the catalysts and the conditions used. In the activated chain end mechanism, the initiation specie is positively charged, and the propagation consists on the attack of a monomer to the positive propagating specie through an S_N2 type pathway (Scheme 1.12). The lactones that polymerize through this mechanism are the 4-, 6- and 7-membered rings, however with this type of mechanism control is usually difficult and low molecular weight polymers are obtained, specially due to the large extent of "backbiting".¹⁹⁹ Typical initiators used in this mechanism are protic acids such as hydrochloric acid and Lewis acids, such as boron trifluoride or aluminium chloride, which can coordinate to the carbonyl oxygen and create the reactive positive specie.²⁰¹ Other type of initiators are alkylating and acylating agents (e. g. methyl trifluoromethanesulfonate and $\text{CH}_3\text{CO}^+ \text{SbF}_6^-$) which initiates the reaction by attacking the exocyclic oxygen on the monomer.^{200, 202}



Scheme 1.12 Initiation of cationic ROP by activated chain end mechanism.¹⁶⁸

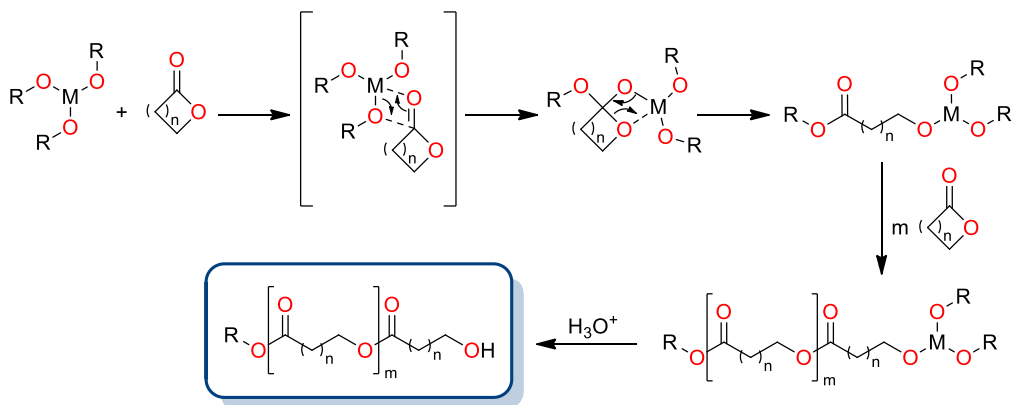
The monomer-activated mechanism consists of the activation of the carbonyl of the monomer by the catalyst, usually an acid (HA), and converting into a more electrophilic specie (Scheme 1.13). Then the initiator, usually an hydroxylic compound, attacks the carbonyl and the lactone ring is opened by the oxygen-acyl bond cleavage, creating the new propagating specie to react with another activated monomer.^{203, 204} The main

difference between this mechanism and the anionic ROP is that, in the anionic mechanism, the activated specie is the initiator/propagating specie, by the contrary, in the monomer-activated ROP the catalyst reacts with the monomer activating it for the propagation. This pathway minimizes considerably the side reactions, such as “back biting”, allowing a better control and the obtention of higher molecular weight polyesters. There are catalyst that take profit from both activations, such as 1,5,7-triazabicyclo[4.4.0]dec-5-ene (TBD).



Scheme 1.13 Initiation step at monomer-activated mechanism at ROP.

1.8.3.3 Coordination-insertion ROP



Scheme 1.14 Coordination-insertion mechanism in ROP, catalyzed by metal alkoxides.

This last mechanism is a pseudo-anionic ROP, where a metal alkoxide, e. g. aluminium isopropoxide, is used as both catalyst and initiator. The metal coordinates the carbonyl on the monomer and one of the alkoxides acts as initiator. The attack on the carbonyl carbon by the alkoxide causes the ring opening through the acyl-oxygen bond cleavage, becoming part of the polymeric chain. Then, the propagating specie is the metal

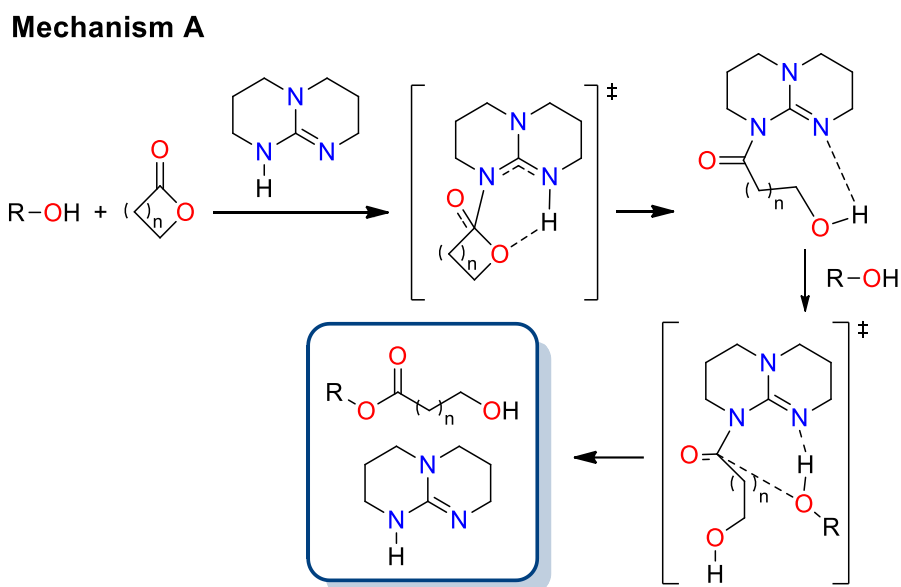
alkoxide of the opened lactone. The reaction is quenched by the hydrolysis of the metal-alkoxide end group leading to a hydroxyl chain end (Scheme 1.14).^{200, 205} This mechanism overcomes the limitations of other mechanism such as the “backbiting” on anionic or cationic mechanisms. Coordination-insertion ROP is less susceptible to produce “backbiting” side-reactions.

1.9 ROP of δ -decalactone with TBD

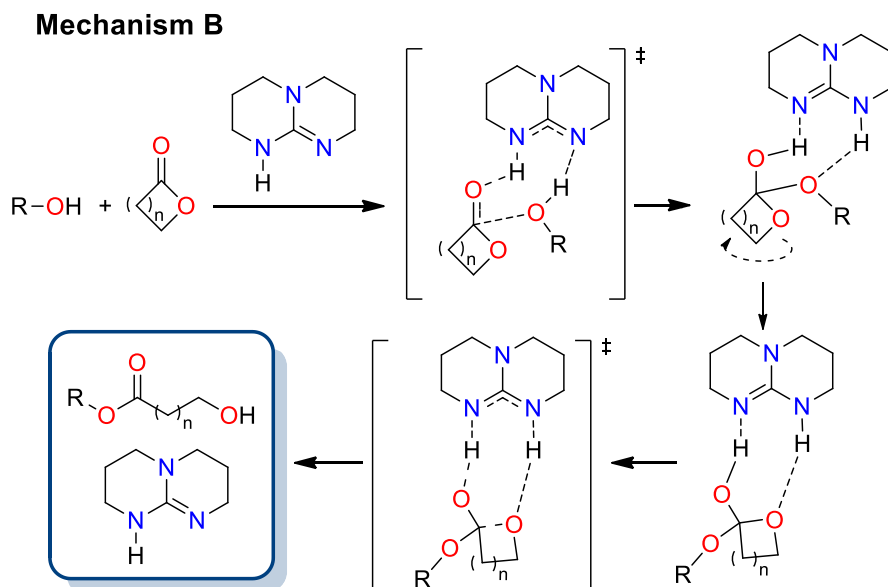
δ -Decalactone (DL) has been polymerized through activated monomer mechanism by acid catalyst (e.g. diphenyl phosphate (DPP))^{52, 134, 137} and by dual activation of monomer and initiator mechanism catalyzed by guanidine bases, such as 1,5,7-triazabicyclo[4.4.0]dec-5-ene (TBD),^{135, 136, 206-208} or by the combination of amine bases with thioureas as cocatalyst (e.g. 1,8-diazabicyclo[5.4.0]undec-7-ene (DBU) with thiourea).²⁰⁹ As six-membered lactone, the equilibrium conversion increases with concentration and by lowering temperature reaching a plateau of 88% conversion in bulk at room temperature.¹³⁵ The presence of the alkyl substituent increases the ring strain on the lactone in comparison with the non-substituted or shorter alkyl chain counterparts (ΔH_p° ; δ -valerolactone (VL) = -12.2 kJ/mol, δ -caprolactone (CL) = -13.8 kJ/mol, δ -DL = -20.0 kJ/mol). However, the alkyl group induce a negative influence on ΔS_p° , being mandatory to perform the polymerization at low temperatures and in bulk to increase the equilibrium conversion (ΔS_p° (1 M); δ -VL = -28.6 kJ/mol·K, δ -CL = -41.3 kJ/mol·K, δ -DL = -62.5 kJ/mol·K).¹⁷⁷

TBD has been demonstrated as an effective catalyst for the synthesis of poly(DL) under mild conditions and without the need of solvent. Moreover, the compatibility with sensitive groups, such as acetals and disulfides, converts TBD in an attractive catalyst for the synthesis of polyesters possessing different functionalities. These characteristics encourages us to select TBD as organocatalyst for the ROP of DL.

TBD has been extensively used as dual activation catalyst for ROP of a wide range of lactones (e.g. lactide, δ -VL and ϵ -CL) obtaining good control over the polymerization.^{198, 210-214} Two different mechanisms have been proposed in the literature for TBD-catalyzed ROP of lactones. The first pathway (mechanism A, Scheme 1.15) involves the nucleophilic attack of the imine nitrogen on the TBD to the carbonyl on the lactone. The intermediate formed reacts with an incoming alcohol, assisted by hydrogen-bonding from TBD, liberating the polymerized ester.²¹⁵ This mechanism was supported by the identification of the TBD-lactone intermediate.



Scheme 1.15 Mechanism A, or nucleophilic catalytic pathway, for TBD catalyzed ROP.²¹⁶



Scheme 1.16 Mechanism B, or acid – base catalytic pathway, for TBD catalyzed ROP.²¹⁶

However, theoretical calculations, done for δ -VL, suggest that the acid – base catalytic pathway (mechanism B, Scheme 1.16) is preferred. In this mechanism the amidine basic nitrogen establishes a hydrogen-bond with the alcohol, enhancing its nucleophilicity. This activated alcohol reacts with the lactone, whose carbonyl oxygen is also activated by hydrogen-bonding with the TBD N-H group, increasing the electrophilicity of the carbonyl carbon. A simultaneous C-O bond formation and proton transfer occurs.²¹⁶ Both mechanisms require hydrogen-bonding interactions to occur. An evidence of this effect is the different reactivity shown by TBD analogs 1,8-diazabicyclo[5.4.0]undec-7-ene (DBU) and *N*-methyl-TBD (MTBD), which were unable to form hydrogen-bond interactions.¹⁹⁸ While DBU and MTBD can polymerize lactide with good control, neither δ -VL nor ϵ -CL can be polymerized with catalyst loadings up to 20 mol %. Only with the addition of 5 mol % of a thiourea cocatalyst (TU) DBU and MTBD can polymerize these monomers.^{215, 217}

1.10 Acrylic and methacrylic polymers

Acrylic and methacrylic polymers are a group of polymers based on the polyaddition of vinylic monomers with (meth)acrylic acid structure (Figure 1.26).

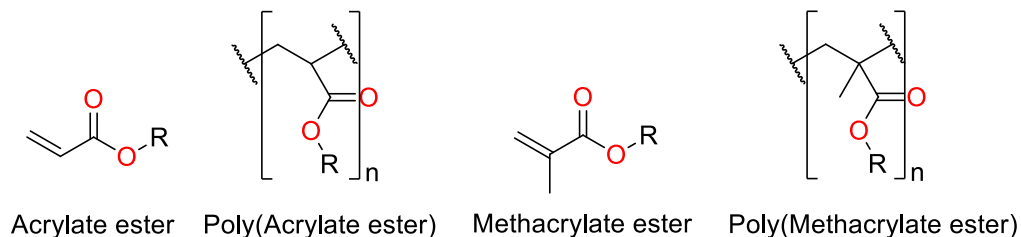


Figure 1.26 Structure of acrylic and methacrylic monomers and its corresponding polymers.

Acrylic acid and acrylate esters are known since the middle of the XIX century, but until the beginning of the XX century were not systematically investigated.²¹⁸ Encouraged by the promising properties of acrylic polymers, the industrial production of acrylate esters was developed in 1928 by Walter Bauer of Röhm & Hass.²¹⁹ Later on, at 1932, Otto Röhm and Walter Bauer patented the first polymerization of methyl methacrylate into transparent sheets as a substitute of glass.²²⁰ Then, at the middle of the 1930s, both Röhm & Hass and ICI started the mass scale production of poly(methyl methacrylate) (PMMA) and poly(methyl acrylate) (PMA).^{221, 222} During the next decades, the production of polyacrylates increased rapidly due to its wide range of applications, together with the development of improved production process.²²³⁻²²⁵ Nowadays, ethyl and butyl acrylates are the more commonly used for commercial acrylate rubbers. Within the n-alkyl methacrylate polymers, the most important is PMMA.²²⁶

1.10.1 Poly(meth)acrylates synthesis

Acrylates and methacrylates can be polymerized by both radical and anionic mechanisms.²²⁷⁻²³¹ From the industrial production point of view, the most commonly used mechanism is the free radical (see section 1.11). Anionic polymerization requires extensively purification of monomers and low reaction temperatures.²²⁵ In terms of polymerization methodology, emulsion polymerization is the most commonly used for polyacrylates synthesis. Bulk polymerization of acrylates presents high rate and heat of polymerization and results unpractical. In fact, acrylates are so reactive than can polymerize spontaneously at high temperatures without the addition of an external radical source. By the contrary, thermal initiation of methacrylates are such slow that is unpractical.²³² Suspension polymerization is also limited due to the coalescence of the soft polymer beads.²²⁴ On the other hand, methacrylates can be polymerized either homogeneously (bulk or solution) or heterogeneously (suspension or emulsion polymerization). Usually the selected method for the industrial production of PMMA will depend on the final use of the polymer.²²⁵ Until the date, polymethacrylates synthesis has been extensively studied in a wide variety of polymerization mechanism. Among these mechanism Reversible-Deactivation Radical Polymerization (RDRP) has attracted great interest for the obtention of polymers with controlled architecture and narrow molecular weight distribution (see section 1.12).

1.10.2 Poly(meth)acrylates properties

Polyacrylates are in general polymers with low glass transition temperature (T_g) (e.g. 22 °C for PMA). As the n-alkyl chain length increases results in a lower softening point polymer. This tendency changes when the alkyl chain exceeds 8 carbons due to the crystallization of the side chains.²²⁶ Thus, they are too soft, too tacky and too weak for many applications. However, this same characteristic converts polyacrylates to interesting candidates for adhesive applications. Moreover, mechanical strength can

be increased by copolymerization with monomers possessing higher T_g values (e. g. styrene, acrylonitrile, etc.).²²⁴

Table 1.2 Glass transition temperatures (T_g) of (meth)acrylic homopolymers.²²⁴

Monomer	T_g (°C)
Methyl acrylate	22
Ethyl acrylate	-8
<i>n</i> -Butyl acrylate	-43
<i>tert</i> -Butyl acrylate	55
Acrylamide	220
Acrylonitrile	105
Methyl methacrylate	105
Ethyl methacrylate	67
Methacrylamide	243

Regarding to the polymethacrylate derivatives, the presence of a α -methyl group into the backbone reduces the chain flexibility, this fact entails a higher T_g value than to the corresponding polyacrylate (e. g. 105 °C for PMMA). The T_g value is lowered when longer *n*-alkyl ester groups are present, as in the case of polyacrylates. In this case, the downward trend of the T_g is maintained until 12 carbon length, when the tendency is reversed.^{224, 226} PMMA is an amorphous polymer with clear transparency, high brilliance and high surface gloss. It is resistant to aliphatic hydrocarbons, non-polar solvents and aqueous acid and bases, but solvents such as aromatic hydrocarbons, chlorinated hydrocarbons, esters, and ketones can dissolve or swell the polymer. Water and alcohols alone are nonsolvents for PMMA (in water/alcohol mixtures can present some solubility (cosolvency)). It is a hard, rigid, but brittle material with an upper service temperature of 100 °C. These properties (good mechanical strength, excellent optical properties, good weather resistance) convert PMMA into an interesting material for many applications.²²⁵

1.10.3 Poly(meth)acrylates applications

As mentioned before, wide range of application has been found for poly(meth)acrylates or its copolymers. In the case of polyacrylates the most important areas of application are related with protection (e.g. paints, coatings and lacquers), binding (e. g. paper and textile industry) and adhesion (e. g. pressure-sensitive adhesives).²²⁴ On the other hand, polymethacrylates are more expensive than other plastic materials due to the cost of raw material. Then, they are usually used on applications where their characteristic properties (low density, resistance to fracture, transparency, etc.) are necessary for specific applications. In the case of PMMA, which is easily processed by different manners (e. g. thermoforming), is used in roofing, vehicles, machinery and instruments, pipelines and vessels for food storage and transport, optical components, etc. (Figure 1.27).²²⁵

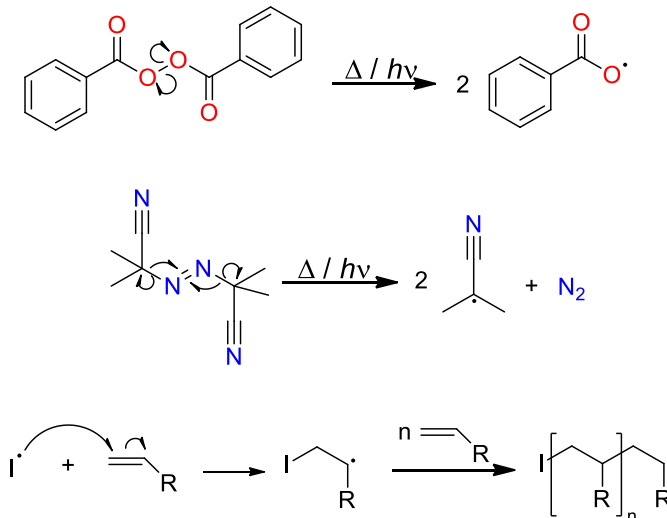


Figure 1.27 Examples of commercial products where poly(meth)acrylates are used.

1.11 Radical polymerizations

Radical polymerizations are a type of addition polymerizations in which a radical specie (initiator) reacts with a C=C double bond to form a new radical (propagating specie) which successively reacts with more monomers. The typical monomers for radical polymerization are acrylic, methacrylic, styrene and other vinylic monomers. Radical polymerizations can be classified into two main groups, free radical (FRP) and controlled polymerization (CRP).

FRP starts with an initiator molecule which can generate a radical (usually by thermal decomposition, photolysis, etc.) which adds to the monomer species (Scheme 1.17).²³³ This kind of polymerization is widely used in industry due to its tolerance to protic solvents and trace impurities in the monomer, such as oxygen or monomer stabilizers.²³⁴ Moreover, other kinds of initiators were developed, such as potassium peroxydisulphate, as water soluble initiators for biphasic polymerizations.²³⁵



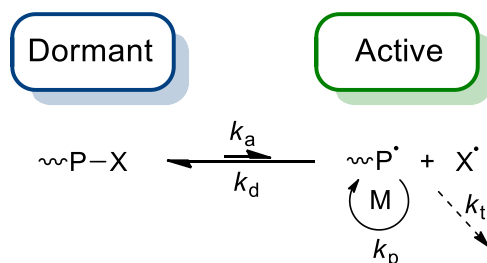
Scheme 1.17 Benzoyl peroxide (BPO) and azo-isobutyronitrile (AIBN) initiators for free radical polymerization.

However, with this kind of thermal/photochemical initiators, it is not possible to obtain a controlled architecture and narrow molecular weight distribution. The contribution

of termination processes, via radical coupling or disproportionation, is important due to the high radical concentration, which is reflected as an uncontrolled process. To overcome these, when control over the molecular weight and architecture is desired, controlled reversible-deactivation radical polymerization is generally preferred.

1.12 Controlled radical polymerizations (CRP)

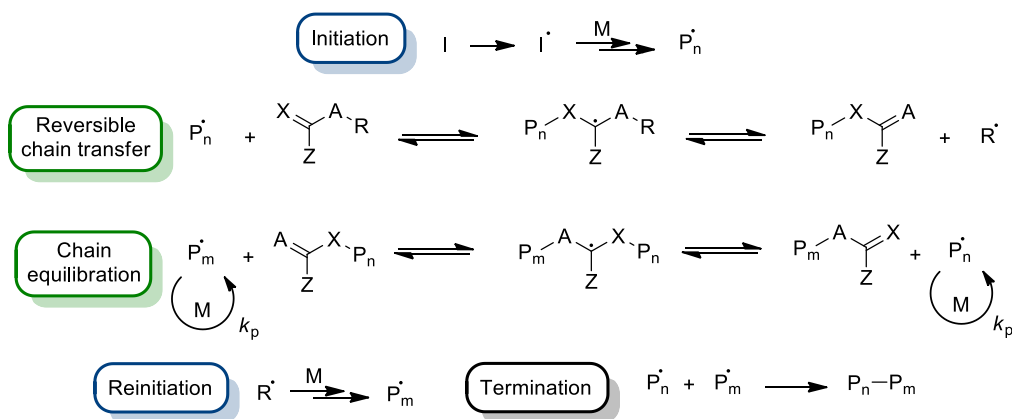
In CRP, also named Reversible-Deactivation Radical Polymerization (RDRP), the mechanism is similar, in terms of the intermediates to FRP. The main difference with the free radical process is the formation of the radical propagating species. In general, the control is achieved by maintaining the radical concentration low through a continuous equilibrium between the active growing species and a dormant species (Scheme 1.18).^{236, 237}



Scheme 1.18 Dynamic equilibrium between the dormant and the active species in PRE approach.

There are two possible types of equilibrium to control the concentration of active species. One is the persistent radical effect (PRE), in which the active species, after the incorporation of few monomers, is trapped by the persistent radical specie (X) during seconds or longer time, and then converted back to the active specie for only a period of milliseconds, leading to a low radical concentration.^{237, 238} The persistent radical specie (X) cannot terminate with each other, only can react reversibly with the growing chain, but the termination processes between growing chains are unavoidable. Because of these termination processes, the X concentration increases with time for each terminated chain. This increase in X shifts the equilibrium towards the dormant

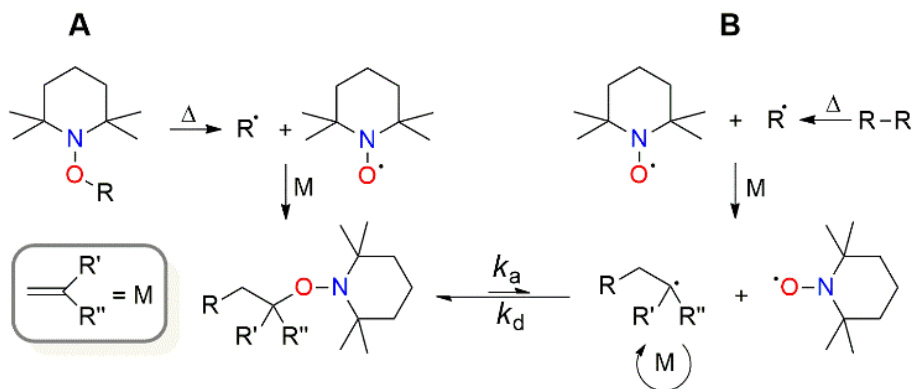
specie, lowering more the radical concentration and the probability of termination. The other type of equilibrium to control the active specie concentration is known as degenerative exchange process, or degenerative transfer (DT). This process consists in the use of conventional thermal initiators (e. g. AIBN) to initially react with monomers (M) and create the polymeric active chain (P_n) (Scheme 1.19).²³⁹ This chain is trapped by the transfer agent (TA) with the release of a new radical that will initiate another chain (R). This new propagating chain (P_m) becomes part of the equilibrium with the TA. This rapid equilibrium between the active propagating radical and the dormant polymeric chain allows control over architecture, molecular weight and polydispersity. In contrast to the PRE mechanism, in which terminations becomes lower with time, at DT terminations are constant during the reaction, and at the same time are continuously generating new growing chains. Those new growing short chains terminate faster than the long chains, allowing this way the control of polymerization. The polymer end remains attached to the transfer agent.²³⁷



Scheme 1.19 Equilibria involved in the DT process using a transfer agent (TA) where X = CH₂ or S, A = CH₂, CH₂=CHCH₂, O or S. Z is an electron stabilizing groups such as phenyl.

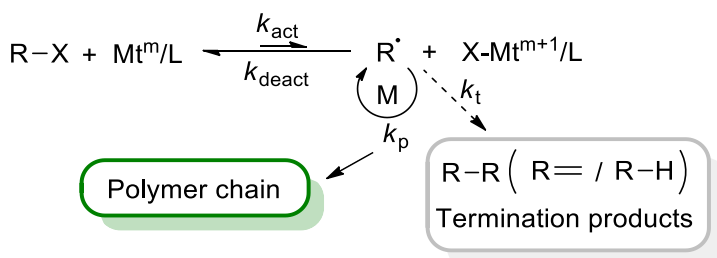
One example of polymerization by the approach of DT is Reversible addition-fragmentation chain transfer (RAFT) where the TA usually are thiocarbonylthio compounds. The most relevant methods using the PRE approach are nitroxide-

mediated polymerization (NMP) and atom transfer radical polymerization (ATRP). The NMP uses typical thermal initiators in conjunction with a nitroxide as a control agent to form the dormant species in a bicomponent initiation system (B in Scheme 1.20). It can be also initiated with an only component which thermally decomposes into the initiator and the nitroxide agent (A in Scheme 1.20).²⁴⁰



Scheme 1.20 Equilibrium on the NMP mechanism with one component (A) and two component (B) initiation systems.

ATRP consists in a dynamic equilibrium between an alkyl halide (dormant specie) and a metal complex in its lower oxidation state and an alkyl radical (active specie) and the metal complex in the higher oxidation state (Scheme 1.21).²⁴¹



Scheme 1.21 ATRP equilibrium between an alkyl halide (dormant) and the alkyl radical (active).

Each of these three techniques have its own advantage and limitations. RAFT allows the obtention of high molecular weight polymers, can be applied to a wide range of monomers and most of the chain end-group of the polymer is maintained as

thiocarbonylthio group, allowing the formation of block copolymers. However, RAFT seems to have some limitations in some block copolymer synthesis approaches. For example, in the case of using a bifunctional initiator for two types of polymerization techniques (e. g. ROP and RAFT), the macroinitiator that bears the transfer agents is also exchanged with the growing chains possessing the functional group of the radical initiator, this entails the consumption of monomer in homopolymer chains. This problem is not present in ATRP, because all the initial radicals are formed in the bifunctional initiator.²⁴² NMP share the same drawback than RAFT in terms of block copolymerization due to the use of an external radical initiator. But it is also a promising technique which can lead to relatively high molecular weight polymers with more environmentally benign reagents (without metals or sulfur compounds). Finally, ATRP is characterized by a well-defined end-group fidelity, therefore being suitable for the preparation of block copolymers. It is also appropriate for the obtention of low molecular weight polymers, due to the complete initiation in the early stages of reaction. However, the obtention of high molecular weight polymer is more challenging than RAFT, even though there are examples in the literature where high molecular weight polymers are obtained by ATRP.²⁴³ Also the number of polymerizable monomers is lower in comparison with RAFT.²⁴⁴

The aim to synthesize ABA block copolymers, starting from a polyester macroinitiators obtained by ROP, led us to decide using ATRP for the chain extension in the second stage. One advantage is the easy modification of the final hydroxyl group of a polyester to be used as macroinitiator for ATRP,²⁴⁵ and overcome the inconvenience of homopolymer formation previously mentioned.

1.13 Atom transfer radical polymerization (ATRP)

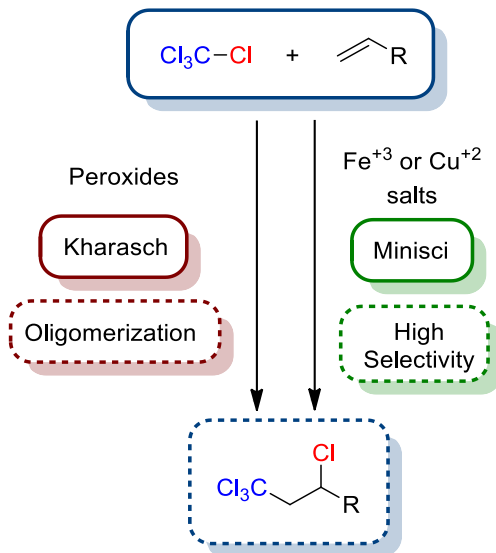


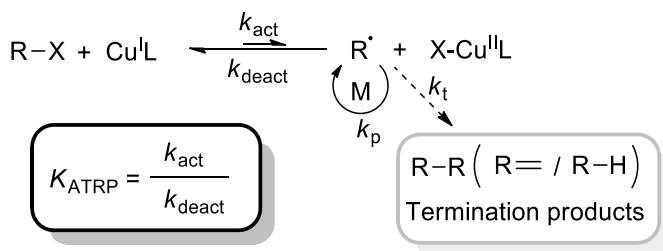
Figure 1.28 ATRA process catalyzed by peroxides (left) and transition metals (right).

Atom transfer radical polymerization was initially inspired on the Kharasch addition reaction, reported in 1945 by Morris S. Kharasch, which consist of the anti-Markovnikov addition of haloalkanes, such as chloroform or carbon tetrachloride, to olefins catalyzed by peroxides.²⁴⁶ This reaction entails the formation of oligomers and even high polymers depending on the olefin substituent (e. g. aromatic). Later in the 1961, Minisci et al. found that iron chlorides, present due to corrosion of the autoclave, inhibit acrylonitrile polymerization. They hypothesize that the first propagating radical is trapped by the iron chloride preventing to polymerize, due to a higher transfer constant, and leading to the monoadduct as major product.²⁴⁷ This process is nowadays known as atom transfer radical addition (ATRA) (Figure 1.28).²⁴⁸ In 1995, Matyjaszewski et al. take benefit of this process to develop a new controlled polymerization system using copper as catalyst. They termed this process atom transfer radical polymerization (ATRP) in analogy to ATRA. The main difference between both is than while in ATRA the ratio olefin/haloalkane is approximately 1, in ATRP the olefin is present in a large excess and this ratio will define the degree of polymerization. Matyjaszewski reported the

polymerization of styrene using 1-phenylethyl chloride as initiator and copper(I) chloride complexed by 2,2'-bipyridine as catalyst, obtaining narrow polydispersities and a good control on the molecular weight.^{249, 250}

Since then, ATRP has been widely studied for many authors for a better understanding of its mechanism,²⁵¹⁻²⁵³ kinetics,²⁵⁴⁻²⁵⁶ the effect of the different components (initiator, metal/ligand, monomer and solvent),^{257, 258} as well as for its use in the synthesis of polymers with complex architectures^{259 - 261} and different polymerization media (homogenous, heterogenous, emulsion, etc.)²⁶⁰⁻²⁶²

1.13.1 ATRP mechanism



Scheme 1.22 ATRP dynamic equilibrium.

ATRP, aside from its dynamic equilibrium (Scheme 1.22), operates like a conventional radical polymerization in terms of radical propagation. The rate of polymerization (R_p) can be expressed as in Equation 1.5, where the k_p is the rate constant of conventional radical polymerization, $[M]$ is the monomer concentration and $[R\cdot]$ is the radical concentration.

$$R_p = k_p [M] [R\cdot]$$

Equation 1.5 Radical polymerization rate equation.

Thus, in ATRP the R_p is regulated by the position of the ATRP equilibrium (Scheme 1.22 and Equation 1.6), responsible of the radical concentration. This dependence can be deduced by the combination of the Equation 1.5 and Equation 1.6 to give Equation 1.7.²⁵⁸

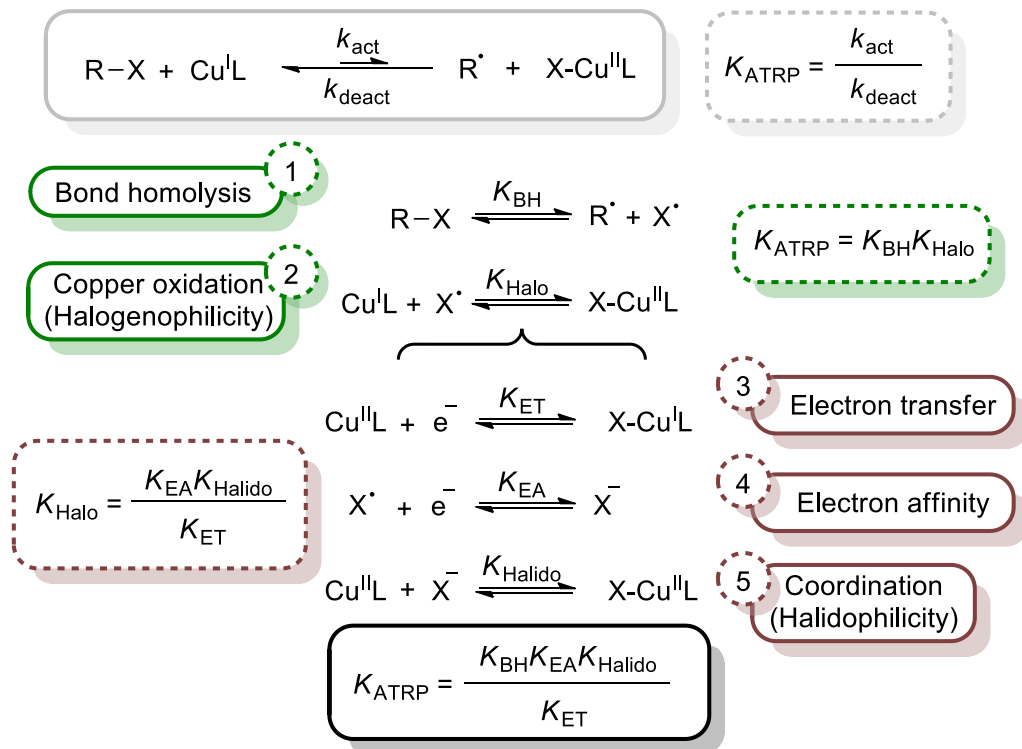
$$K_{ATRP} = \frac{k_{act}}{k_{deact}} = \frac{[R^\bullet][XCu^{II}L]}{[RX][Cu^I L]}$$

Equation 1.6 ATRP constant equation.

$$R_p = k_p[M]K_{ATRP} \frac{[RX][Cu^I L]}{[XCu^{II}L]}$$

Equation 1.7 Polymerization rate equation as function of K_{ATRP} for a given monomer.

The ATRP equilibrium (K_{ATRP}) is defined by the relative bond strengths toward homolysis of the alkyl halide bond (R-X) (K_{BH}) (Scheme 1.23-1) and the Cu^{II}-X bond of the ATRP deactivator (K_{Halo}) (Scheme 1.23-2).^{258, 263, 264} Thus, the K_{ATRP} can also be expressed as a product of these two reactions (Equation 1.8).



Scheme 1.23 Overall contributing reactions on ATRP equilibrium constant.

$$K_{ATRP} = K_{BH} K_{Halo}$$

Equation 1.8 K_{ATRP} equation as a function of R-X and X-Cu^{II}L bond formation.

The halogenophilicity, at the same time, is divided into three process; first, the oxidation of the metal in its lower oxidation state, electron transfer (ET) (Scheme 1.23-3); second, the reduction of the halogen radical to the halide anion, electron affinity (EA) (Scheme 1.23-4); and third, the formation of the deactivating specie by the coordination of the halide anion to the higher oxidation state metal complex, halidophilicity (Scheme 1.23-5).^{263, 264, 265} Therefore, a halogenophilicity rate constant (K_{Halo}) can be obtained from these three reactions (Equation 1.9).²⁵⁸

$$K_{Halo} = \frac{K_{EA}K_{Halido}}{K_{ET}}$$

Equation 1.9 Rate constant equation of halogenophilicity process.

From the combination of Equation 1.8 and Equation 1.9, an equation containing all the factors affecting the ATRP equilibrium can be obtained (Equation 1.10).

$$K_{ATRP} = \frac{K_{BH}K_{EA}K_{Halido}}{K_{ET}}$$

Equation 1.10 ATRP rate constant as a function of its different process.

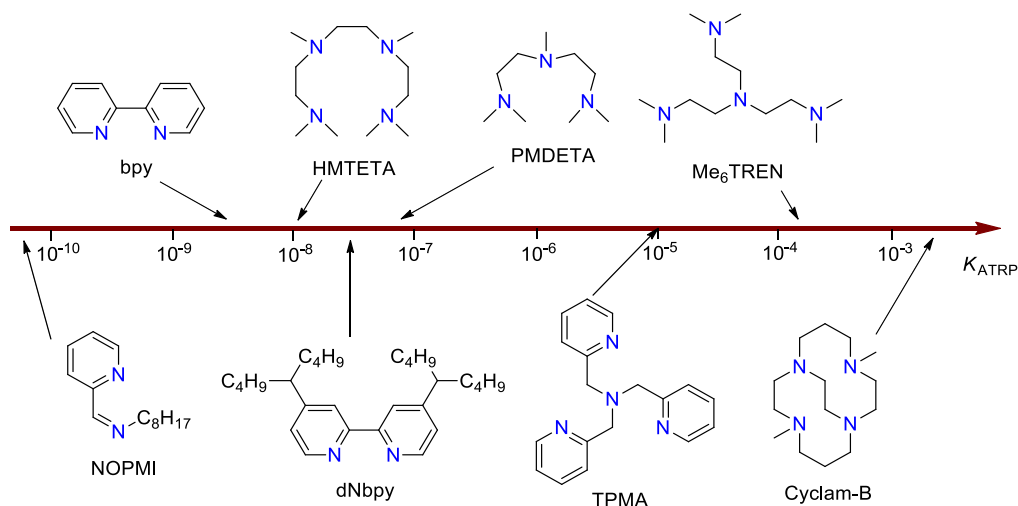
Thus, the R-X bond dissociation energy (BDE), the tendency of the halogen to be reduced by the copper complex (halogenophilicity) and the affinity of the halide to coordinate the copper in its higher oxidation state (halidophilicity) will determine the position of the ATRP equilibrium. The quantification of K_{ATRP} , for a given monomer (M) and catalyst, is a useful method to determine the true catalyst activity of a system.²⁵⁸

As mentioned before, the equilibrium between the dormant and the active radical species, not only determines the polymerization rate, but also determines the control and “livingness” of the reaction. The Cu^I/L complex must be active enough to cleave the C-X bond on the initiator (k_{act}), as well as, the X-Cu^{II}/L complex must react quickly with propagating radicals to form the dormant specie (k_{deact}). Fast deactivation of the active chain by halogen transfer favors that all the chains are growing at the same rate. This equilibrium must be shifted towards the dormant specie (C-X) in order to maintain

a low radical concentration and therefore minimize the radical-radical irreversible termination side reactions ($k_{\text{act}} \ll k_{\text{deact}}$). However, both constants must be large enough to maintain a rapid exchange and obtain a good control over the polymerization. This equilibrium is affected by many factors such as the catalytic system (metal and ligand), monomer and initiator type (important to ensure a complete initiation in the early stages), solvent and temperature.^{254, 258}

1.13.2 Catalytic systems in ATRP (Metal/ligand)

The catalytic system has a great influence on the position of the ATRP equilibrium and the dynamic exchange between the dormant and the active specie. The use of a variety of metals,²⁶⁴ such as copper,^{266, 267} iron,²⁶⁸⁻²⁷⁰ nickel,²⁷¹ has been described in the literature. The metal catalyst must have at least two accessible oxidation states separated by one electron, also it should have affinity with halogens and its coordination sphere should be expandable upon oxidation to selectively accommodate a (pseudo)halogen. Finally, the ligand must complex the metal relatively strong.²⁷² The main role of the ligand is to solubilize the metal salt in the organic solvent and to adjust the redox potential to obtain an appropriate reactivity on the dynamic exchange. Thus, by changing the ligand, the reactivity can be tuned for each specific case.²⁷² The two more common types of ligands in ATRP are phosphorous²⁶⁹ and nitrogen-based ligands.²⁶⁷ Phosphorous-based ligands are used in ATRP for most transition metals such as rhenium, ruthenium, iron, rhodium, nickel and palladium, but not for copper. The sulfur, oxygen and phosphorous based ligands are less effective coordinating copper due to inappropriate electronic effects or unfavorable binding constants, however, nitrogen-based ligands are suitable to form an active complex with copper.²⁷² Nitrogen ligands has also been used in iron-mediated ATRP.²⁷³ Nevertheless, we will focus on copper-catalyzed ATRP with nitrogen-based ligands, because it is the most studied and the polymerization of our target monomer is described in the literature using this catalytic system.⁷⁸



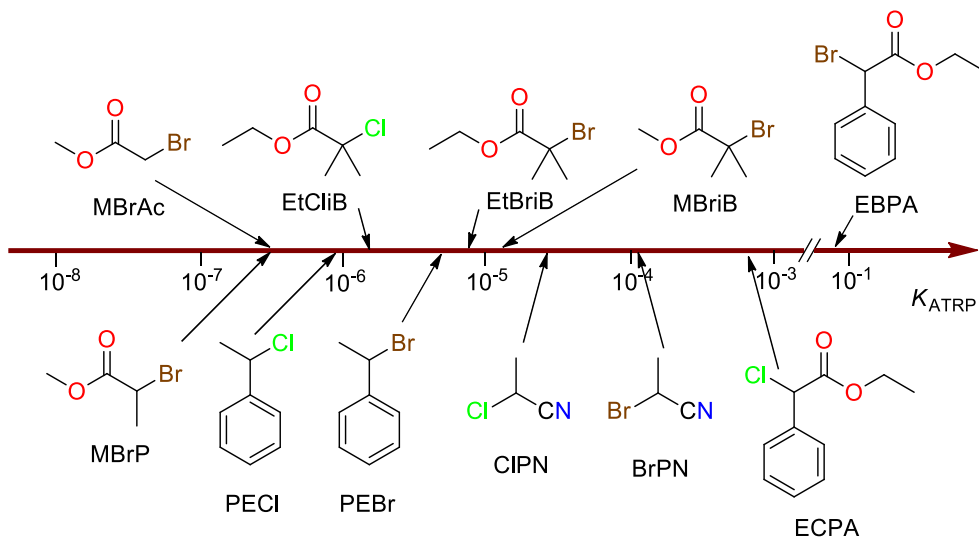
Scheme 1.24 Typical nitrogen ligands in copper-based ATRP, ordered by increasing activity.²⁵⁷

The ATRP equilibrium constant will depend on the structure of the nitrogen ligand and the number of chelating atoms (decrease in activity when decreasing the chelating atoms), as well as the steric hindrance and the type of substituent (electron-withdrawing or electron-donating groups). All these different parameters will determine the redox potential of the final complex, and consequently, the catalytic activity of the system. As a general trend, the more reducing complex the better is catalyst, and becomes more active when the Cu^{II} state is better stabilized by the ligand. The activity of the ligand decreases in the order: alkyl amine \approx pyridine $>$ alkyl imine \gg aryl imine $>$ aryl amine.²⁶⁴ The electron-withdrawing groups on the ligand entails the formation of less reducing complexes, by the contrary, ligands possessing electron-donating groups will increase the reducing character of the complex.^{257, 274} Typical ligands used in copper-based ATRP are tris[2-(dimethylamino)ethyl]amine (Me_6TREN), N,N,N',N'',N'' -pentamethyl-diethylenetriamine (PMDETA), 4,4'-di-(5-nonyl-2,2'-dipyridyl) (dNbpy), among others (Scheme 1.24). Nevertheless, not always the highest activity is the proper condition for a specific system, because high activity can result in high radical concentration and thus favoring termination side reactions with the consequent loss of control. The catalytic system must be optimized for each case.

1.13.3 Initiator effect

The main role of the initiator is to determine the number of growing polymer chains. Moreover, if initiation is fast and termination negligible, these number of growing chains are maintained constant during the progress of the reaction. The usual initiators in ATRP are alkyl halides with activating substituents on the α -carbon, such as carbonyl or aryl groups (Scheme 1.25).²⁷² However, polyhalogenated compounds (e. g. CCl_4) or compounds with a weak R-X bond, such as N-X, S-X and O-X (e. g. p-toluenesulfonyl chloride)²⁷⁵ and alkyl (pseudo)halides (e. g. alkyl diethyldithiocarbamate)²⁷⁶ can also be used as ATRP initiators.²⁷² There are many factors affecting the initiator activity. From the point of view of the initiator structure the main factor to consider is the character of the leaving atom (or group) (bond strength) and the stability of the formed radical (carbon substitution degree and radical stabilizing groups in α -position).²⁷⁷

As mentioned before, the ATRP equilibrium involves the homolytic cleavage of the alkyl halide bond (see section 1.13.1). Thus, the R-X bond dissociation energy (BDE), the tendency of the halogen to be reduced by the copper complex (halogenophilicity) and the affinity of the halide to coordinate the copper in its higher oxidation state (halidophilicity) will determine the efficiency of the initiator. For example, alkyl bromides are in general more active than alkyl chlorides, due to its lower BDE. Although alkyl iodides have a slightly lower BDE than the other alkyl halides, they are not appropriate as ATRP initiators due to its low affinity toward Cu (e.g. CuI_2 is thermodynamically unstable and cannot be isolated). Additionally, alkyl iodides are light sensitive, and the R-I bond can be heterolytically cleaved, which can entail complications in the ATRP process.^{272, 277} The standard reduction potentials of the deactivating specie $[\text{X-Cu}^{\text{II}}\text{L}]^+$ will be also affected by the halide type, decreasing in the order $[\text{I-Cu}^{\text{II}}\text{L}]^+ > [\text{Br-Cu}^{\text{II}}\text{L}]^+ > [\text{Cl-Cu}^{\text{II}}\text{L}]^+ > [\text{F-Cu}^{\text{II}}\text{L}]^+$, while the halidophilicity is in inverse order. In the case of R-F initiators, which have a very strong C-F bond,²⁷² only very active catalyst can let to activation and with a non-complete initiation.²⁷⁸ For these reasons, the most used alkyl halides in ATRP are bromides and chlorides.



Scheme 1.25 Typical ATRP initiators, ordered by increasing activity.²⁵⁷

Radical stability is another factor to consider. Tertiary radicals are more stabilized than secondary ones, and those are more stable than primary radicals, because alkyl groups give electron density (inductive effect) to the electron deficient carbon radical. Thus, the k_{act} follows the order $1^\circ < 2^\circ < 3^\circ$ (e. g. 2-bromopropionitrile is approximately 3 times more active than bromoacetonitrile).^{277, 279} The radical can also be stabilized by delocalization (resonance) in a sp^2 (or sp) system, lowering its energy by conjugation. In this way, the presence in the α -position of carbonyl, nitrile or aryl groups gives an extra radical stabilization, the order by decreasing activity follows nitrile > ester > benzyl > amide, furthermore the presence of two stabilizing groups increases even more the radical stabilization, and then improves the activation activity (e.g. phenyl acetic ester) (see Scheme 1.25).^{257, 277}

It is noteworthy to mention that to achieve a controlled ATRP, not only the activation rate constant (k_{act}), but also the deactivation rate constant (k_{deact}) must be considered. This means that not always the most active initiator is adequate for all the systems, it must be selected for each case, too active initiator can lead to terminations at early stages and a low active initiator can entail a slow and/or incomplete initiation.²⁸⁰ In

general, a good criterium for selecting a initiator is that which possess a similar structure to the resulting dormant polymeric chain, to ensure at least similar rates of initiation and propagation. For example, 1-phenylethyl bromide (PEBr) would be appropriate for polystyrene, methyl 2-bromopropionate (MBrP) for poly(methyl acrylate) and ethyl 2-bromoisobutyrate (EtBriB) for poly(methyl methacrylate).²⁷⁷ However, in ATRP of methacrylate like monomers, some additional effects have to be considered. Thus, despite the similarity of EtBriB to the dormant chain in PMMA polymerization is not well controlled at high conversions. Experimentally, the EtBriB/CuBr system for MMA shows a fast polymerization rate, as expected for this type of initiator, and low polydispersities at early stages of polymerization, probably due to the fast deactivation caused by the weak $\text{Cu}^{\text{II}}\text{-Br}$ bond. However, upon increasing conversion the molecular weight deviates from the theoretical one and an increase of polydispersity is observed (in contrast with the usual decrease in \bar{M} observed in other ATRP systems).²⁸¹ This deviation has been attributed to the so called back strain effect, causing slow initiation of EtBriB in comparison with the propagating chain due to the release of the steric strain of the dormant specie during the rehybridization from sp^3 to sp^2 configuration. This effect is only present on tertiary carbon radicals and not on the secondary ones.^{254, 281, 282} The bulky MMA penultimate unit destabilizes the dormant alkyl bromide, reduces the bond dissociation energy and, stabilize the resulting sp^2 -hybridized radical (Figure 1.29).²⁸³

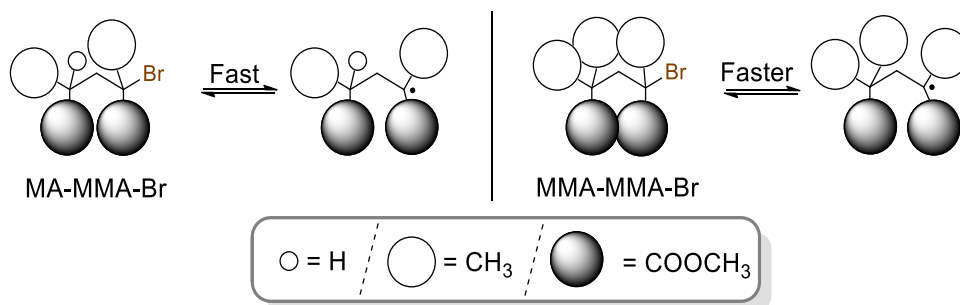


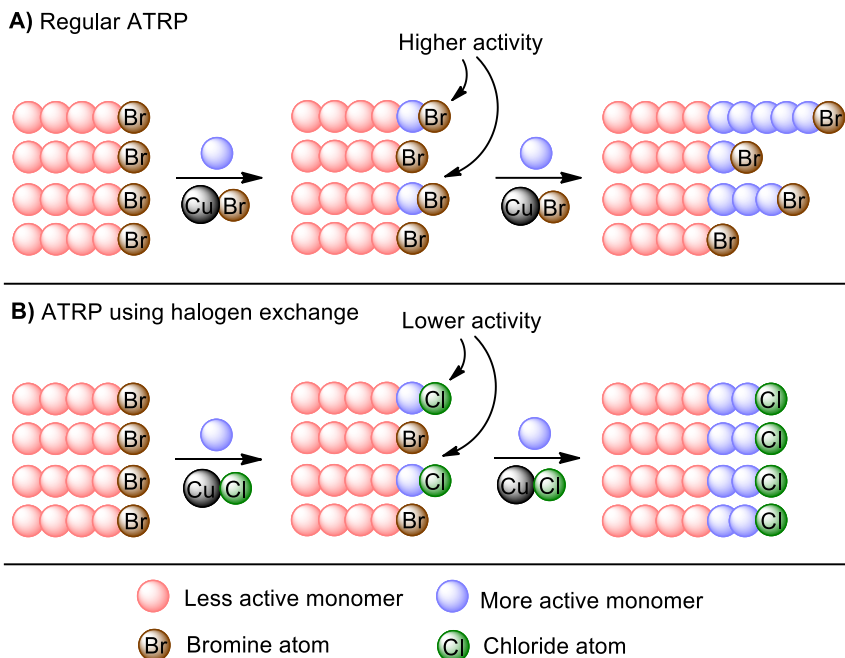
Figure 1.29 Structural comparison of dimeric MA-MMA-Br and MMA-MMA-Br. Effect of penultimate unit on activation process (back strain effect).

A more appropriate initiator for MMA would be 2-bromopropionitrile (BPN) which maintain a balance between a higher initiation rate (95 % initiation efficiency), when compared to EtBriB, and a lower capacity to give early termination, when compared to ethyl 2-bromophenylacetate (EBPA).²⁸⁰

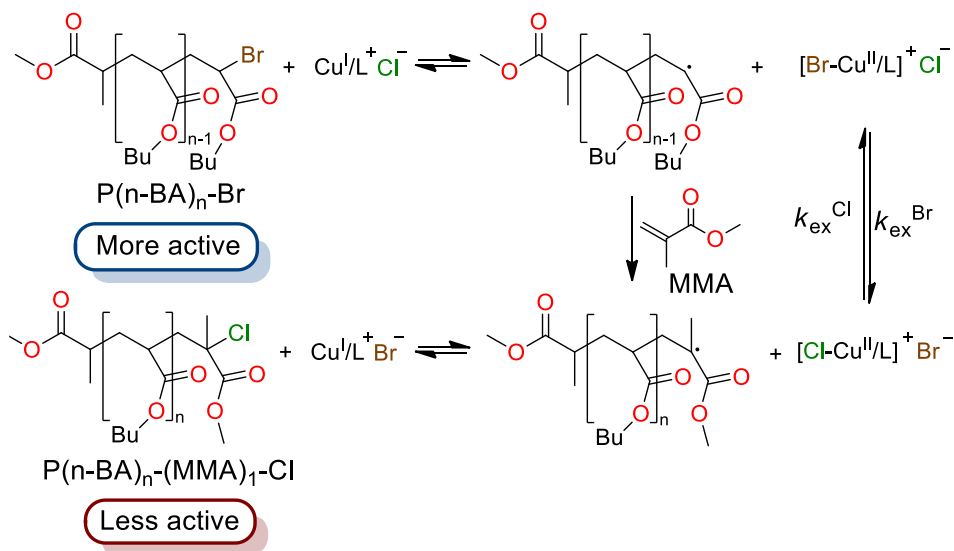
Nevertheless, sometimes the selection of the initiator is limited, especially when block copolymers, or more complex architectures, combining different polymerizations techniques are targeted.²⁸⁴ This is the reason why BriB esters encountered a widespread use, even though they are not the best initiators for methacrylate like monomers.²⁸¹ BriB units are easily incorporated to the final hydroxylic groups of a polymer (e. g. synthesized by ROP) by reacting with 2-bromoisobutyryl bromide (BriBBr).^{285, 286} Whereas other types of radical initiators would be more challenging to incorporate to a macromolecule. Nevertheless, the halogen exchange (HE) effect has been developed to overcome the problems in the initiation/propagation rate balance.²⁸⁷

1.13.4 The halogen exchange effect

The halogen exchange (HE) effect is usually used in the synthesis of block copolymers, by chain extension from macroinitiators, when the second block monomer has a higher activity towards propagation than the macroinitiator.²⁸⁸ This is the case of the polymerization of MMA using PBA-Br as macroinitiator: the alkyl bromide formed upon incorporation of the first monomer unit is more reactive than the initial macroinitiator (e.g. secondary alkyl less reactive than tertiary). This entails that some macroinitiator may remain unreacted leading to broad (\bar{M}) and/or bimodal molecular weight distribution (Scheme 1.26-A²⁸⁸).²⁸⁹ However, using copper(I) chloride instead of copper(I) bromide allows the incorporation of chloride atom at the propagating chain during the deactivation step, and after the incorporation of the first monomer unit (Scheme 1.27).



Scheme 1.26 Representative block copolymerization using a macroinitiator with a more reactive monomer (A) using copper (I) bromide (without HE) and (B) using copper (I) chloride (with HE).²⁸⁸



Scheme 1.27 HE mechanism with Cu^+/Cl^- , leading to a less reactive R-Cl propagating chain.²⁸⁸

Through this HE method the activity of a tertiary alkyl bromide can be diminished, due to the stronger nature of R-Cl bond, and therefore high initiation efficiency of the macroinitiator and simultaneous growing of all chains can be obtained (Scheme 1.26-B).²⁹⁰

1.13.5 Solvent, temperature, and reaction time

ATRP can be conducted in bulk or solution.²⁹¹ Bulk polymerization are faster than in solution but usually the use of solvent is necessary to solubilize the polymer, when it is insoluble in its own monomer, and for better solubilization of the catalyst.²⁷² There are examples of ATRP in both polar and non-polar solvents, such as toluene, diphenyl ether, acetone and dimethylformamide among others.^{258, 292, 293} Some considerations that must be taken into account about solvent selection are: first, the potential chain transfer to some solvents; second, the solvent interaction with the catalyst, e.g. coordination,²⁹³ and third, the solvolysis or elimination of HX that some end-groups can undergo at elevated temperatures and in polar solvents.²⁹⁴ In general, solvent affects the activity of the catalytic system by increasing the activation rate (k_{act}) with increasing the medium polarity, due to a better solvation of $[Br-Cu^{II}L]^+$ than $[Cu^I L]^+$ in polar solvents, presumably due to a more pronounced dipolar nature of the Cu^{II} species.²⁴⁸ However, the solvent effect on the deactivation rate (k_{deact}), which is crucial in the control of the polymerization, is still uncertain. Initial studies showed that increasing medium polarity turns slower the deactivation step and faster the activation step.²⁹⁵ However, a more recent publication concluded that both k_{act} and k_{deact} , and consequently K_{ATRP} , increase with medium polarity, but the effect is more pronounced on k_{act} than in k_{deact} .²⁹⁶ Therefore, for each case an appropriate solvent must be found to obtain an appropriate balance. It is worth to mention that the use of solvent reduces the monomer concentration, and this entails an increase of the dead chain fraction (DCF), in other words the loss of end-group functionality. This trend can be deduced from the equation developed by Zhong, et. al (Equation 1.11), where DP_T is the ratio

between the initial monomer concentration, $[M]_0$, and the concentration of the living polymers $[P-X]$, k_t is the termination rate constant, p is monomer conversion, k_p is the propagation rate constant and t is the time.^{297, 298}

$$DCF = \frac{2DP_T k_t [\ln(1-p)]^2}{[M]_0 k_p^2 t}$$

Equation 1.11 Dead chain fraction (DCF) equation.

Temperature is another important factor to consider, both radical propagation and ATRP equilibrium constants increase upon increasing temperature. The activation energy for radical propagation is higher than for radical termination, therefore higher temperatures allows better control by increasing the k_p/k_t ratio. However, higher temperatures can also lead to higher rate of chain transfer or other side reactions.^{272, 294, 299} Finally, it must be mentioned that long reaction times have, in general, a negative influence on the polymerization. Rather than reaction time, the effect is noticed at high monomer conversions, where the propagation rate is very slow, due to the low $[M]$. However, the rate of most side reactions is concentration independent, becoming significant at high conversions.²⁹⁴ Then, to not exceed 95% of conversion is important when end-group fidelity is desired. Nevertheless, the polydispersity remains unaffected by these side reactions.²⁷²

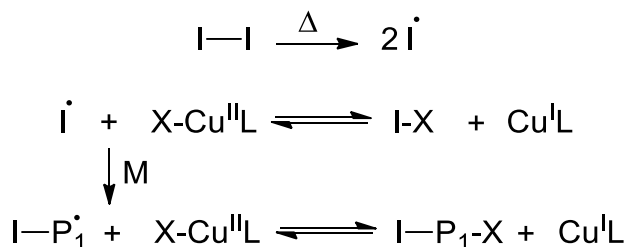
1.13.6 ATRP variations

Exists many ways to conduct ATRP. They vary mainly in the activation step and how the first radicals are generated. Here below, the main characteristics are described:

- Reverse ATRP:

In this variation the metal is used in its higher oxidation state, and a conventional free radical initiator is used to generate the active species and the formation of the dormant initiator (Scheme 1.28). This variation was developed simultaneously with the normal

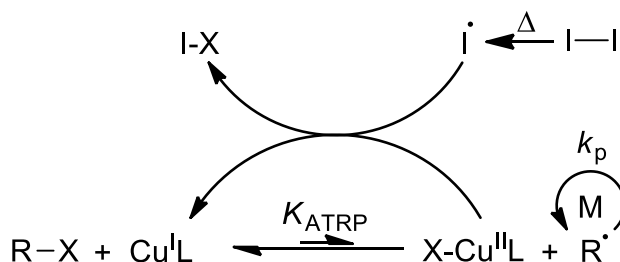
ATRP and has the limitation that the free radical initiator is incorporated to the polymer chain.^{300, 301}



Scheme 1.28 Activation step at reverse ATRP.

- Simultaneous Reverse and Normal Initiation (SR&NI) ATRP:

This variation is a combination of normal and reverse ATRP, where both free radical initiator and alkyl halide are used. The conventional free radical initiator reduces the Cu^{II} to the active specie and most of the polymer chain are initiated by the alkyl halide (Scheme 1.29).

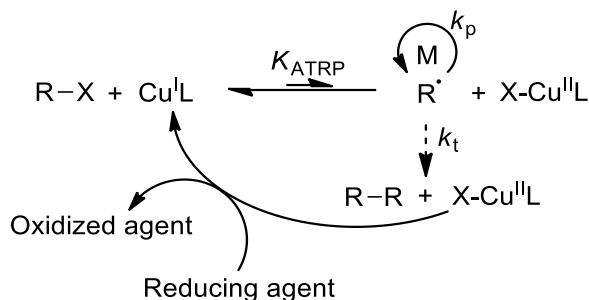


Scheme 1.29 Mechanism of SR&NI ATRP.

However, a fraction of free radical initiator is incorporated the polymer chain, this fact difficult the synthesis of block copolymers by this technique, due to the unavoidable formation of homopolymers.^{264, 302, 303}

- Activators ReGenerated by Electron Transfer (ARGET) ATRP:

In this type of ATRP a reducing agent is used (e.g. tin(II) 2-ethylhexanoate, ascorbic acid or hydrazine) to continuously regenerate the active species from the Cu^{II} species formed due to inevitable radical termination (Scheme 1.30). This allows the reduction of the copper catalyst to ppm levels.^{264, 304-306}



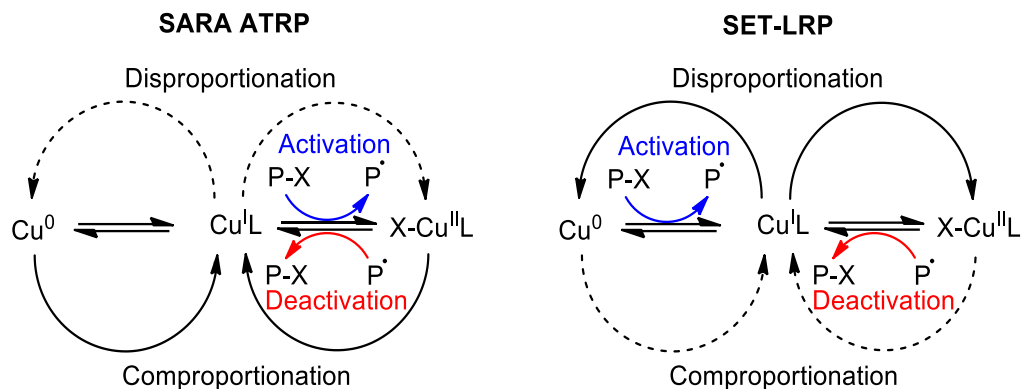
Scheme 1.30 Mechanism of ARGET ATRP.

ARGET ATRP can be considered an evolved version of SR&NI with the advantage that the reducing agent do not form radicals which can initiate and thus the polymer is only initiated by the alkyl halide. Moreover, the addition of reducing agents can be also employed for the elimination of oxygen or impurities in the medium.^{304, 307} Another benefit of reducing the amount of catalyst is that the termination side reactions are also diminished.³⁰⁸

- Initiators for Continuous Activator Regeneration (ICAR) ATRP:

This technique is quite similar to SR&NI, both uses thermal radical initiators for the reduction of the metal to the active state, however, SR&NI requires large amounts of Cu^{II} and the radical initiator is consumed rapidly at early stages of the reaction, by the contrary, in ICAR ATRP the Cu^{II} amounts are lower and the radical initiator reacts progressively during the reaction, even unreacted initiator is remained at the end of the reaction.^{303, 306}

- Supplemental Activator and Reducing Agent (SARA) ATRP:

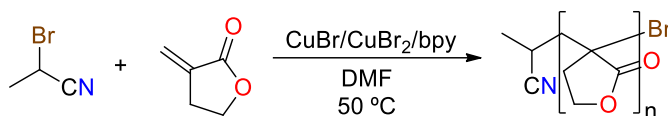


Scheme 1.31 Comparison of the proposed mechanisms for zero valence metal assisted mechanisms; SARA ATRP (left) and SET-LRP (right).

SARA ATRP consist in the use of zerovalent metals as reducing agents for the recovery of the active specie, as in the case of ARGET ATRP.³⁰⁹ The Cu^{I} is recovered by Cu^0 comproportionation with Cu^{II} formed due to terminations (Scheme 1.31).^{310, 311} However, there is a discussion about the real mechanism in zerovalent mediated living polymerization. SARA ATRP is one of the proposed mechanisms, where the only difference between the conventional ATRP is the source of Cu^{I} , which in this case comes from the comproportionation reaction of the zerovalent metal, then as ATRP process the electron transfer is through an inner sphere.^{299, 312} But another mechanism proposed by Percec et. al., named Single-Electron Transfer Living Radical Polymerization (SET-LRP), suggest an outer-sphere electron transfer. In this mechanism the real catalyst is Cu^0 that acts as electron donor, and the R-X act as electron acceptor, to form the propagating radical and the Cu^{I} specie (Scheme 1.31). This Cu^{I} disproportionate to form new Cu^0 and then deactivating Cu^{II} specie.^{313, 314} Nowadays, there is no consensus yet about the real mechanism.³¹⁵⁻³¹⁸

1.14 ATRP of MBL

The first example of MBL radical polymerization was reported at 1979 by Akkapeddi using AIBN as free radical initiator.¹³⁹ Akkapeddi noted a higher reactivity towards radical polymerization with respect to its acyclic analogous MMA. This higher reactivity was confirmed by the copolymerization of MBL with MMA, in which the MBL fraction present on the final polymer was higher than in the initial feed.³¹⁹ He attributed these results to a less steric hindrance of the methylene groups of MBL in comparison with the methyl groups of MMA. The planar structure of MBL results in a favorable interaction of the growing radical and the approaching monomer in the transition state.³²⁰ This fact is corroborated by the lower reactivity of α -methylene- δ -valerolactone (MVL), upon radical polymerization, due to the nonplanar six-membered lactone ring.³²¹ Further studies demonstrated that the ring planarity favors delocalization of the radical's spin density, conferring an extra stabilization.³²²



Scheme 1.32 First example of MBL polymerization with ATRP.

The first example of controlled radical polymerization of MBL was reported in 2008 by Matyjaszewski and Mosnáček.¹⁵² They describe the preparation of well-defined homopolymers of MBL through ATRP. The obtained polymers present a narrow molecular weight distribution ($\bar{D} = 1.09$ -1.14), as well as a good agreement between the experimental and the theoretical molecular weight. The polymerization is carried out in DMF due to the insolubility of the poly(MBL) in its own monomer. The solvent is also necessary for the catalyst solubilization. The catalytic system used for the synthesis of homopolymers was copper(I) bromide (CuBr) as metal salt, 2,2'-bipyridine (bpy) as ligand and 2-bromopropionitrile as initiator. A small amount of copper(II) bromide (CuBr₂) was added to the system to increase the rate of deactivation (Scheme 1.32).

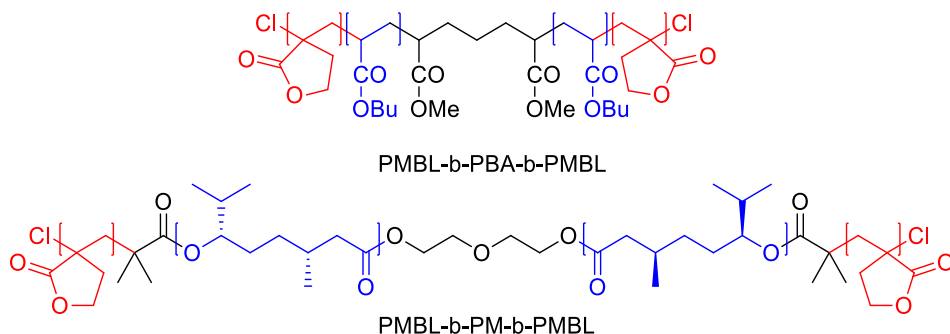


Figure 1.30 Examples of ABA thermoplastic elastomer synthesized by ATRP. Using PMBL as hard block (red) and poly(*n*-butyl acrylate) (PBA) and poly(menthilde) (PM) as soft block (blue).

They also prepared diblock and triblock copolymers from chain extension of PMMA and poly(*n*-butylacrylate) (PBA) macroinitiators. In this case, the catalytic system had to be adjusted for the preparation of block copolymers. The copper bromide was substituted for copper chloride to use the halogen exchange effect. This was necessary due to the high reactivity of MBL propagating specie with respect to bromo-terminated PMMA and PBA (see section 1.13.4). Their purpose in the synthesis of the PMBL-*b*-PBA-*b*-PMBL (Figure 1.30) was to obtain a material with thermoplastic elastomer properties.⁷⁰ The material obtained showed phase separated morphology, possessing a broad elastic plateau (approximately 250 °C between the T_g of both blocks). Shin and Hillmyer also examined the possibilities of ATRP of MBL for the synthesis of TPE. In this case, they used the bis(BriB) end-functionalized poly(menthilde) (PM) as renewable polyester macroinitiator (obtained by ROP) (Figure 1.30).⁷⁸ They obtained well-defined polymer architectures and narrow polydispersities. These block copolymers showed phase separation and the mechanical test showed a considerable elongation, strain, and elastic recovery. Thus, the characteristic properties of poly(MBL) (see section 1.7.5), with their promising applications in many fields,^{323, 324} and the capability of MBL to be polymerized in a controlled manner from a wide variety of macroinitiators, converts MBL to a potential monomer suitable for engineering thermoplastic elastomers.^{30, 79,}

1.15 Stimuli-cleavable polymers

The design of functional polymers, which can respond to environmental changes through chemical or physical transitions, is a growing area of research due to their potential applications.^{327, 328} Stimuli-responsive polymers, also known as “smart polymers”, are macromolecules which are sensitive to certain external triggers (e.g. pH and temperature).³²⁹⁻³³² These external stimuli induce a micro or nanoscale change, as morphology, bond rearrangement/cleavage and molecular motion. These changes can be reflected in their macroscopic properties, such as color, shape and functionality.³²⁷ These type of materials have been extensively studied due to their potential applicability in many fields, such as biomedicine (e.g. drug delivery, and artificial muscles),^{328, 331, 333, 334} analytics (e.g. sensors and biosensors),^{328, 335, 336} degradable materials,^{337, 338} etc.³³⁹⁻³⁴¹

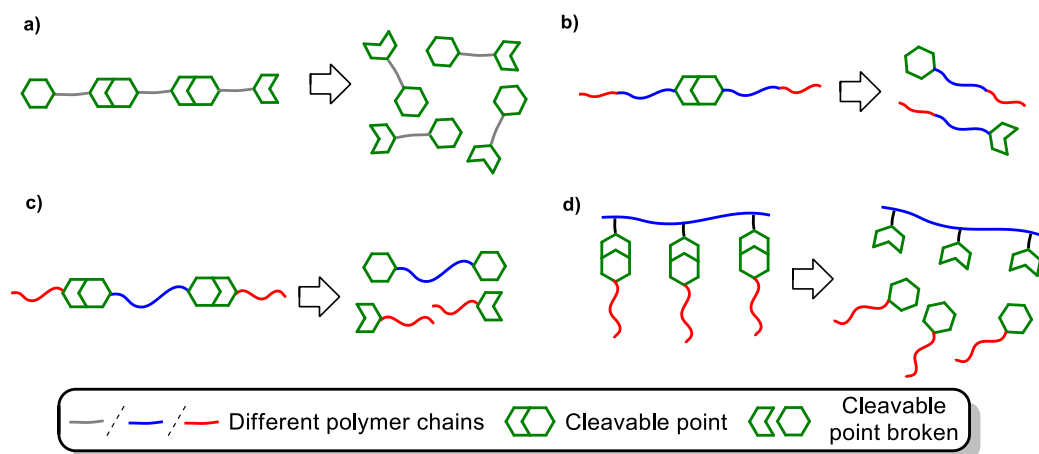


Figure 1.31 Examples of possible locations of sensitive moieties into a stimuli-cleavable polymer.

Among all the different types of stimuli-response polymers, stimuli-cleavable polymers are one of the most widely studied, being extensively applied for drug delivery systems³³³ and for enhanced degradability in polymeric materials.^{337, 338} The integration of the stimuli-responsive degradable groups could be within the polymer backbone or between block junctions. The location of the cleavable points will depend on the final

application of the polymer. If the cleavable points are within the polymer backbone the resulting degradation products are monomers or oligomers (Figure 1.31-a). If the cleavable points are on the block junctions (or in a mid-point of the polymer) the degradation products are shorter polymer chains (Figure 1.31-b, c and d). In both cases generating new functionalities at the polymer ends.

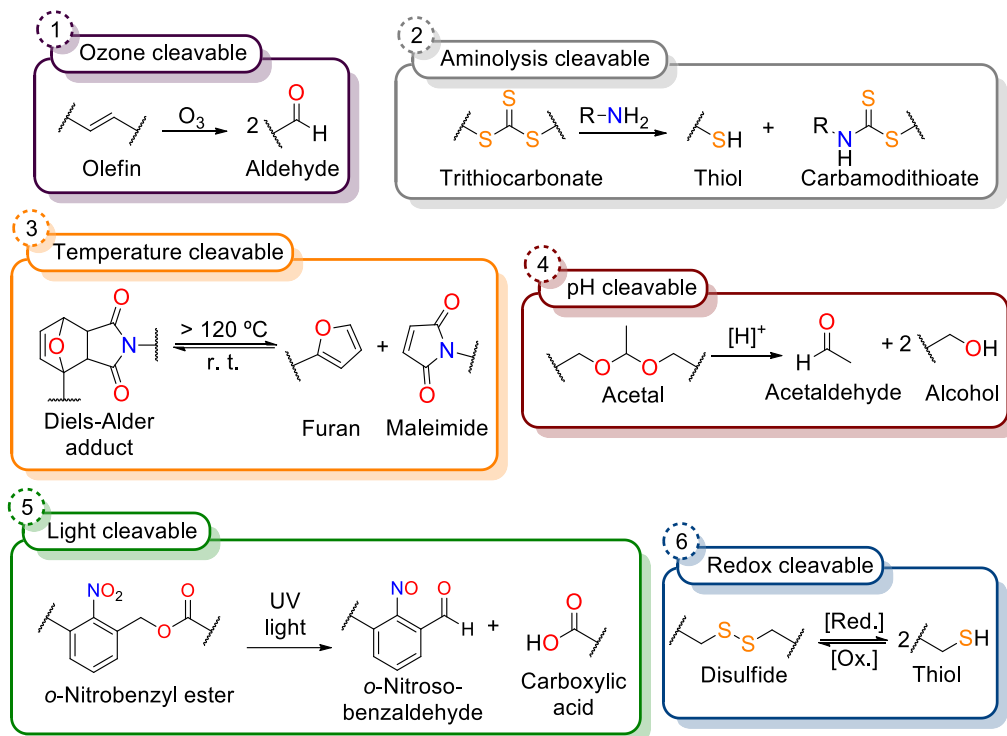


Figure 1.32 Stimuli-cleavable groups, described in the literature, for the synthesis of stimuli-responsive telechelic polymers.

In the case of the ABA block copolymer TPEs, a cleavable point in the middle of the polymer chain is enough to dramatically change its properties. The breaking of the linker between the two hard domains entails the formation of an AB diblock copolymer (Figure 1.31-b), hence, losing its elastomeric properties. One possible approach, for the synthesis of this type of stimuli-cleavable polymers, is to use a telechelic initiator with the appropriate functionality. By this way the cleavable point is located in the middle

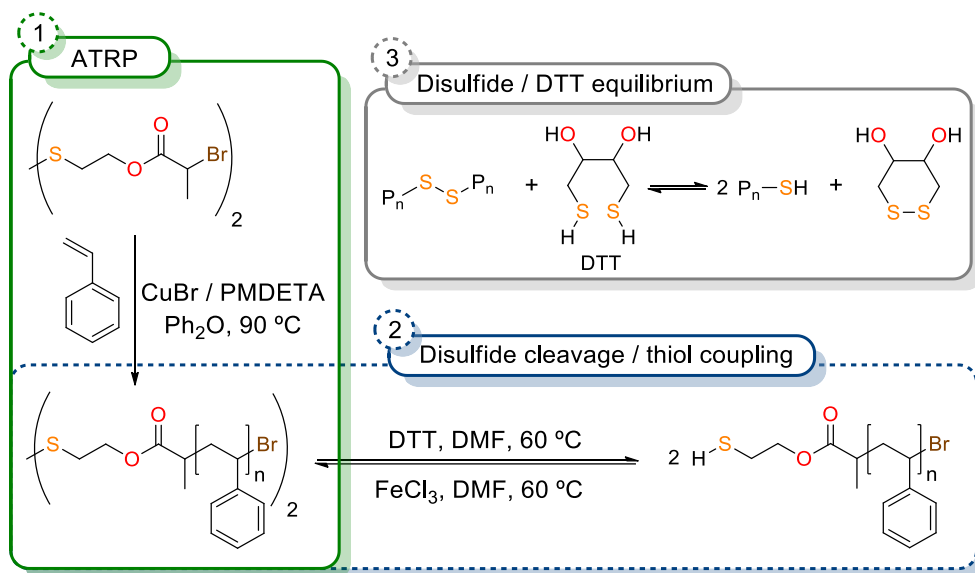
of the polymer chain.⁹⁶ This type of bifunctional initiators can possess different labile groups, sensitive to different stimuli. Figure 1.32 shows representative examples of labile groups used in the synthesis of cleavable polymers,⁹⁶ which could be broken through ozonolysis,³⁴² aminolysis,³⁴³ thermoreversible Diels-Alder,³⁴⁴ acid hydrolysis,³⁴⁵⁻³⁴⁸ light cleavage^{346, 348-350} and reduction cleavage.^{347-349, 351} The selection of the stimuli will be determined by the final application of the material. Among all the different stimuli, we have focused on the redox, acid, and light cleavable polymers. These types of stimuli have been already applied for biomedical applications,^{331, 333, 351} however their use has been scarcely considered for the preparation of TPEs. Thus, the incorporation of these type of stimuli into TPEs could be interesting in terms of reprocessing under mild conditions.

1.15.1 Redox cleavable polymers

The most noteworthy example of redox cleavable polymers are the ones which contains the disulfide group.^{338, 347-349, 351} These disulfide containing polymers can be cleaved under reductive conditions (e.g. tributylphosphine)^{348, 352-354} and by thiol – disulfide exchange reaction (e.g. glutathione (GSH) and dithiothreitol (DTT)).^{347, 349, 351, 355-358} Recently von Delius and coworkers have reported the cleavage of disulfide centered polyacrylates by exposing to ultrasound activation.³⁵⁹ Disulfide groups can also be cleaved by oxidation, using performic acid and obtaining the corresponding sulfonic acid.⁹⁶ However, by this methodology the cleavage of the disulfide group is irreversible. By the contrary, through the reduction cleavage the thiol formed can be reoxidized to the starting disulfide.^{96, 353}

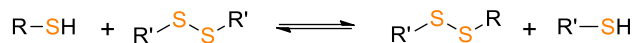
Tsarevsky and Matyjaszewski were the first to report the synthesis of a linear polymer based on a bifunctional disulfide initiator.³⁵⁵ They described the synthesis of a disulfide centered polystyrene (PS) through ATRP (Scheme 1.33-1), furthermore, they study the disulfide cleavage using DTT (Scheme 1.33-2). DTT was selected due to its efficiency upon disulfide reduction and for its solubility in a wide range of solvents, including

those that dissolve PS such as THF and DMF. They found that the disulfide cleavage was more effective in DMF than in THF since the redox potential of the disulfide bond depends on solvent polarity. The resulting cleaved polymer was analyzed through size exclusion chromatography (SEC) showing half the molecular weight of the initial polymer. Subsequently, the thiol end-groups of the cleaved polymer were coupled back to the starting disulfide using FeCl_3 (Scheme 1.33-2).



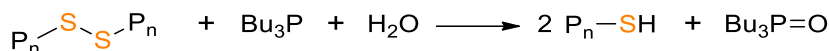
Scheme 1.33 (1) Synthesis of disulfide centered polystyrene, through ATRP. (2) Disulfide cleavage using DTT with subsequent thiol coupling using FeCl_3 . (3) Disulfide / DTT equilibrium.

Thiol-disulfide interchange is a reversible $\text{S}_\text{N}2$ reaction (Scheme 1.34) where the active nucleophile is the thiolate anion (R-S^-).³³¹ Its rate constant increases with increasing values of $\text{p}K_\text{a}$ of the thiols, since it supposes a larger thiolate fraction as well as an increased nucleophilicity of the anion formed. For this same reason, the reaction rates are faster in polar aprotic solvents, such as DMSO and DMF, which can stabilize the thiolate anion formed.



Scheme 1.34 Thiol-disulfide interchange.

By the contrary, the interchange rate in polar protic solvents, such as water and methanol, is slower. This can be explained by a higher activation energy towards the transitions state due to a more stabilized ground state in polar protic solvents.³⁶⁰



Scheme 1.35 Disulfide cleavage using tributylphosphine.

On the other hand, trialkyl phosphines (e.g. tributyl phosphine (Bu_3P)), in the presence of water, are other efficient reducing agents for disulfides (Scheme 1.35).^{348, 352, 354, 359} The main difference between the previous method and that with Bu_3P is that the reaction is irreversible due to the strength of the $P=O$ bond formed.³³¹ The advantages of Bu_3P are; higher stability towards autooxidation and high affinity to disulfide groups, meaning than large excess of reagent is not needed. Furthermore, the use of Bu_3P do not interfere with reagents usually used to react with the formed thiol (e.g. 1,3-propane sultone or ω -toluene sultone).³⁵³

1.15.2 Acid cleavable polymers

Together with the redox cleavable group, acid cleavable linkages are one of the most frequently used groups in sensitive polymers. Examples of acid labile groups used in polymers are imines, hydrazones, orthoesters and acetals (Figure 1.33).³⁶¹ These groups can be hydrolyzed under mild acidic conditions while are considerably stable in basic conditions. The two main factors affecting the hydrolysis of these compounds are; first, external factors including pH and temperature of the reaction medium and, second the structural factors including steric, resonance and inductive effects.³³¹

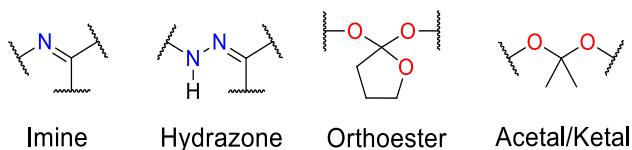
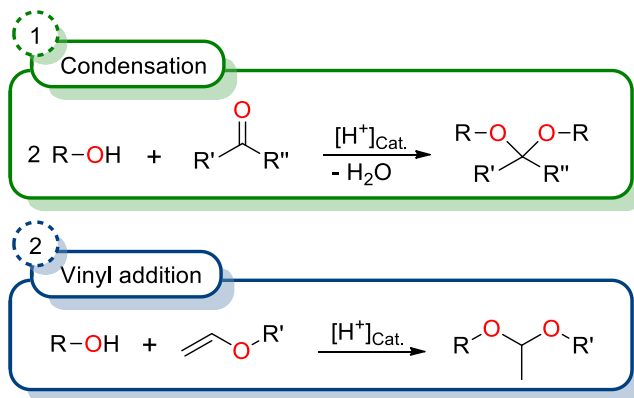


Figure 1.33 Examples of acid labile groups.

Among these labile groups, acetal and ketal groups has attracted great interest for the preparation of stimuli-cleavable polymer for many reasons: its cleavage under mild acidic conditions and low temperatures,^{346, 362-364} its ease of synthesis and its hydrolytic behavior that can be modulated depending on the substituents.³⁶⁵ Moreover, acetal moieties have already been used in different types of controlled radical polymerization, such as SET-LRP,³⁴⁸ RAFT^{357, 366} and ATRP.^{347, 348, 366} In the majority of the cases the acetal moiety remains unaffected under the polymerization conditions. Only Oh and coworkers reported some acetal hydrolysis with ARGET ATRP conditions.³⁴⁷

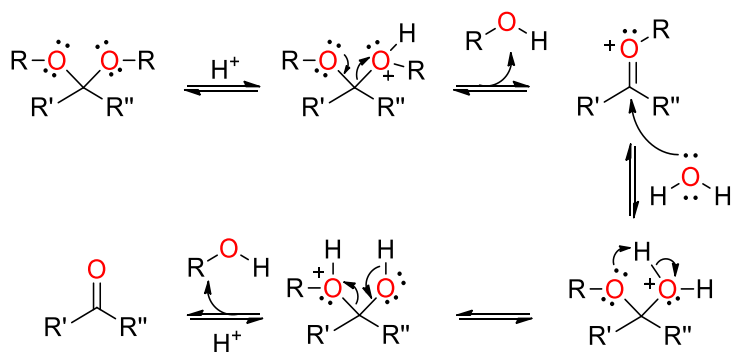


Scheme 1.36 Acetal synthesis through; (1) condensation of alcohols with aldehydes ($R'' = \text{H}$) or ketals ($R'' = \text{alkyl}$), and (2) alcohol addition to vinyl ethers.

Acetals can be synthesized from aldehydes (or ketones) and alcohols by condensation (Scheme 1.36-1)³⁶⁷ or by alcohols addition to vinyl ethers (Scheme 1.36-2),^{346, 368} both catalyzed by acid.

Acetals can be easily hydrolyzed, catalyzed by Brønsted or Lewis acids, due to the presence of lone electron pairs on oxygen atom which act as Lewis base (Scheme

1.37).^{331, 369, 370} Aside from the acidity of the medium, there are other factors affecting the hydrolysis rate of acetals. For example, the presence of carbocation-stabilizing substituents on the acetal group significantly increases the hydrolysis rate. For this reason, the hydrolysis rate of acetals prepared from ketones are usually faster than for acetals derived from aldehydes.³³¹ Cyclic acetals are more stable than similar lineal acetals, thus, linear acetals can be orthogonally deprotected in the presence of cyclic acetals.³⁷¹ Between the cyclic acetals, five-membered rings are more stable than six-membered.³³¹ Finally, the presence of basic groups, susceptible to protonation (e.g. amino groups), slows down the hydrolysis rate. The charge of the protonated basic group prevents the second protonation of the oxygen of acetal, that would lead to a positive – positive charge repulsion. Therefore, the hydrolytic behavior of an acetal moiety could be modulated by varying these parameters.³³¹

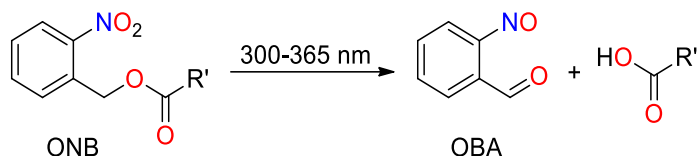


Scheme 1.37 Acetal hydrolysis mechanism in acidic medium.

1.15.3 Light cleavable polymers

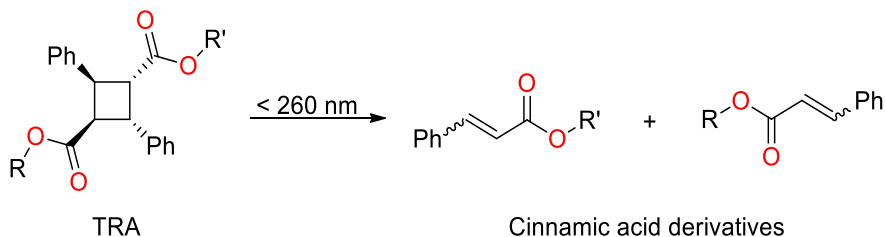
Finally, light as stimulus source has received increased attention in recent years since it is a clean and efficient stimulus which can be easily modulated. Light allows a non-invasive remote interaction with the polymer, which could be of great interest for many applications, such as controlled drug release and biomaterials.^{350, 372, 373} Light cleavable polymers, or photocleavable, are characterized for possessing a metastable photochromic group. One of the most studied photocleavable group is the α -

nitrobenzyl (ONB) ester. The ONB groups photoisomerize into an *o*-nitrosobenzaldehyde (OBA) upon UV radiation (Scheme 1.38).^{372, 374-376} This type of cleavable group has already been used in polymers prepared by controlled polymerizations, such as SET-LRP or ATRP.^{348, 377}



Scheme 1.38 Photoisomerization of *o*-nitrobenzyl (ONB) esters to give *o*-nitrosobenzaldehyde (OBA) and a carboxylic acid.

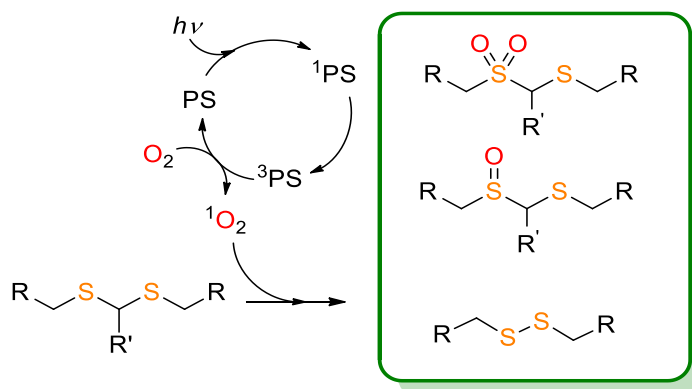
Other examples of photocleavable groups are truxillic acid (TRA) derivatives, dimers of two cinnamic acids *via* [2 + 2] cycloaddition. TRA can be cleaved under UV radiation (Scheme 1.39).³⁷²



Scheme 1.39 Truxillic acid derivatives (TRA) cleavage under UV radiation to give cinnamic acid derivatives.

More recently studies have described the use of light for the generation of reactive oxygen species (ROS), such as singlet oxygen (¹O₂). Examples of ROS are the superoxide anion and hydrogen peroxide, as well as their derived reactive species (hydroxyl radical, hypochlorous acid, peroxy radicals and singlet oxygen).³⁷⁸ These ROS are able to oxidize, and therefor to cleave, many functional groups which can be used as linkers. Some examples of ROS sensitive moieties are olefins,³⁷⁹ diselenides³⁸⁰ and thioketals.^{381, 382} Wilson et. al. first described the use of thioketals as cleavable moiety under ROS conditions.³⁸³ In this case, they used superoxide as ROS for testing the cleavage of thioketal linkages, showing great sensitivity, for further apply into *in vitro*

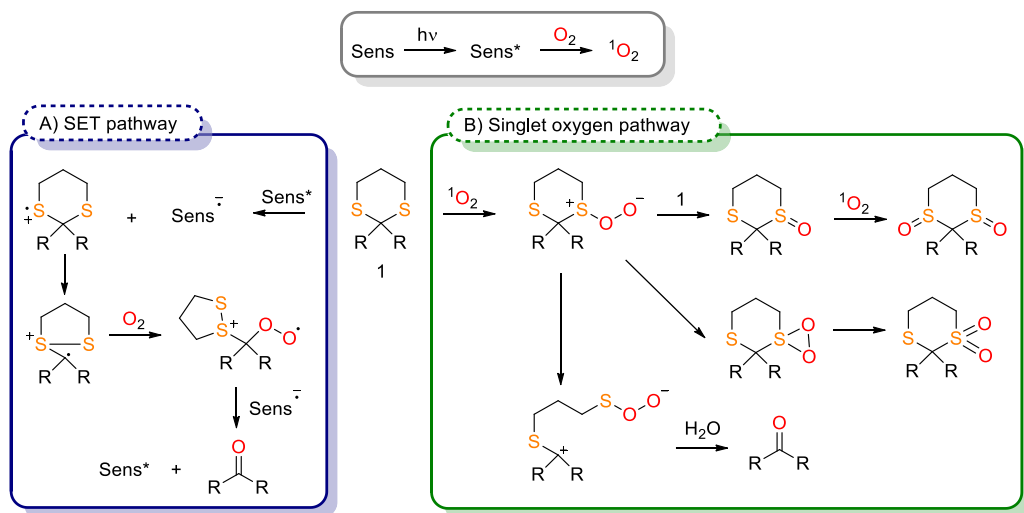
experiment where the ROS were generated by cells. Four years later Yuan et. al. reported a singlet oxygen mediated thioketal cleavage for controlled drug release.³⁸⁴ The light irradiation, in conjunction with a polyelectrolyte as photosensitizer (PS), causes the generation of $^1\text{O}_2$ responsible of the thioketal cleavage. The first step in the photooxidation of thioacetals is the caption of a photon from the photosensitizer (PS). The PS is excited to a singlet state (^1PS), which is converts to triplet PS (^3PS) responsible for the $^1\text{O}_2$ formation.³⁸⁵ Then, the $^1\text{O}_2$ reacts with the thioketal to give a mixture of sulfur species such as disulfides (RSSR), thioisulfinate (RS(O)SR) and thioisulfonates (RS(O)₂SR) (Scheme 1.40).³⁸⁶ These oxidized products could be hydrolyzed to give sulfonic acid derivatives leading to an effective cleavage of the former thioacetal.³⁸⁷



Scheme 1.40 Photooxidation of thioacetal by singlet oxygen.

It is noteworthy to mention that the cleavage products will depend on the substituents on the thioacetal. It is described in the literature that radical stabilizing substituents favor the formation of thioisulfinate products (thioisulfonate as overoxidation product) while the anion stabilizing substituents favor the formation of disulfide derivatives.³⁸⁶ Moreover, disulfides could also be oxidized through singlet oxygen leading to thioisulfonates, thioisulfonates and sulfonic acids.³⁸⁸⁻³⁹⁰

From the mechanistic point of view, two pathways are plausible depending on the thioacetal substituents and the photosensitizer used. Depending on the reduction potential of the sensitizer the mechanism would be more prone to proceed through a single electron transfer (SET) (e.g. 2,4,6-tri-(*p*-chlorophenyl)pyrylium perchlorate (TCPPClO₄) and 9,10-dicyanoanthracene (DCA)) or through singlet oxygen (e.g. methylene blue (MB) and *meso*-tetraphenylporphyrin (TPP)) pathway (Scheme 1.41).³⁹¹



Scheme 1.41 Proposed mechanistic pathways for the photo-deprotection of thioacetals through (A) single electron transfer (SET) and (B) singlet oxygen (¹O₂) pathways.³⁹¹

In SET mechanism the sensitizer in its excited state (Sens*) oxidize the thioacetal to form a cation radical intermediate which undergoes C-S bond cleavage. This new radical reacts with oxygen in its ground state to form a peroxy radical which finally is converted to the carbonyl compound. On the other hand, the singlet oxygen (¹O₂) pathway first involves the generation of ¹O₂ by the interaction of molecular oxygen with the sensitizer in its excited state (Sens*). ¹O₂ reacts with the thioacetal to give a persulfoxide intermediate. This persulfoxide can follow different reaction pathways: first, it can react with another thioacetal molecule to form two sulfoxide molecules, which could be further oxidized to disulfoxides. Second, the formation of sulfones through a thiadioxirane intermediate. And third, the formation of the parent carbonyl compound

from the cleavage of the C-S bond with subsequent hydrolysis of the carbocation formed. The singlet oxygen pathway seems to be the more convenient route for the photolytic cleavage of thioacetals moieties, as the SET mechanism leads to the formation of disulfides. The formation of disulfide would not give an effective cleavage of the polymer chain but as mentioned before, in singlet oxygen conditions the disulfide would be further oxidized to hydrolysable groups.

The capability of being deprotected under demand with a simple light stimulus, in conjunction with a sensitizer (e.g. *meso*-tetraphenylporphyrin), has emerged thioacetals and thioketals as an attractive target for the preparation of stimuli cleavable polymers. Being this method much more environmentally friendly than classical deprotection of thioacetals involving toxic heavy metals (e.g. Hg^{+2} , Ag^+ or Tl^{+3}),³⁹² it has been widely studied for biomedical applications, such as for drug delivery systems.³⁹³⁻³⁹⁹ However, in the best of our knowledge, this stimulus has never been applied for TPE applications, in which degradability is a key issue. The degradation of TPEs using light and oxygen could be of great interest for certain industrial processes, such as the removal of adhesives in paper recycling.⁴⁰⁰

- ¹ Spontak, R. J.; Patel, N. P. Thermoplastic elastomers: fundamentals and applications. *Curr. Opin. Colloid Interface Sci.* **2000**, 5, 334-341.
- ² Semon, W. L. Synthetic rubber-like composition and method of making same. *U.S. Patent US 1,929,453*. **1933**.
- ³ Bayer, O.; Rinke, H.; Siefken, L.; Orthner, L.; Schild, H. Verfahren zur herstellung von polyurethanen bzw. Polyharnstoffen. *German Patent DE 728,981*, **1937**.
- ⁴ Hanford, W. E.; Holmes, D. F. Process for making polymeric products and for modifying polymerization products. *US Patent US 2,284,896*, **1942**.
- ⁵ Christ, R. E.; Hanford, W. E. Treatment of polyesters and product therefrom. *US Patent US 2,333,639*, **1943**.
- ⁶ Coffey, D. H.; Cook, J. G.; Lake, W. H. G. Improvements in the manufacture of synthetic polymeric materials. *British Patents GB 574,134*, **1945**.
- ⁷ Schollenberger, C. S. Simulated vulcanizates of polyurethane elastomers. *US Patent US 2,871,218*, **1959**.
- ⁸ Drobny, J. G. Chapter 2. A brief history of thermoplastic elastomers. *Handbook of thermoplastic elastomers*. Ed. William Andrew (Elsevier), **2007**. ISBN 9780323221368.
- ⁹ Drobny, J. G. Chapter 17. Recent developments and trends. *Handbook of thermoplastic elastomers*. Ed. William Andrew (Elsevier), **2007**. ISBN 9780323221368.
- ¹⁰ Jibin, H.; Wenquan, C.; Shijia, Z.; Yuan, W.; Lili, H.; Shuya, L.; Hongchi, T. The research and development of thermoplastic elastomers. *SVOA Materials Science and Technology* **2020**, 2, 34-46.
- ¹¹ Shanks, R.; Kong, I. Thermoplastic elastomers. *Thermoplastic elastomers*, Ed. Prof. El-Sonbati. ISBN 978-953-51-0346-2. **2012**.
- ¹² Holden, G. *Applied plastic engineering handbook*, 1st ed., ed.; by Myer Kutz, chapter 6, p. 77-80. (Elsevier, **2011**)
- ¹³ Bonart, R. Thermoplastic elastomers. *Polymer* **1979**, 20, 1389-1403.
- ¹⁴ Drobny, J. G. Chapter 1. Introduction. *Handbook of thermoplastic elastomers*. Ed. William Andrew (Elsevier), **2007**. ISBN 9780323221368
- ¹⁵ Wang, W.; Lu, W.; Goodwin, A.; Wang, H.; Yin, P.; Kang, N.; Hong, K.; Mays, J. W. Recent advances in thermoplastic elastomers from living polymerizations: Macromolecular architectures and supramolecular chemistry. *Prog. Polym. Sci.* **2019**, 95, 1-31.
- ¹⁶ Leclère, Ph.; Rasmont, A.; Brédas, J. L.; Jérôme, R.; Aimé, J. P.; Lazzaroni, R. Phase-separated microstructures in "all-acrylic" thermoplastic elastomers. *Macromol. Symp.* **2001**, 167, 117-137.
- ¹⁷ Wang, W.; Lu, W.; Kang, H.-G.; Mays, J.; Hong, K. Chapter 5: Thermoplastic elastomers based on block, graft, and star copolymers. *Elastomers* **2017**, Publisher InTech, p 97-120.
- ¹⁸ Chemical Retrieval on the Web (CROW). <https://polymerdatabase.com/Elastomers/Elastomers.html> accessed August 14, **2019**.
- ¹⁹ Page, C. Thermoplastic elastomers of styrenic block copolymers and aliphatic thermoplastic polyurethanes. Appl. Polyone Corp. *International Patent App.* WO2008/045702A2, published 17 April **2008**.
- ²⁰ Coran, A. Y.; Patel, R. P. Thermoplastic elastomers by blending and dynamic vulcanization. *Polypropylene: Structure, blends and composites.*, **1995**, Ed. Karger-Kocsis. Published by Chapman & Hall, London. Chapter 6. ISBN 0 412 58430 1.
- ²¹ Bandyopadhyay, G. G.; Bhagawan, S. S.; Ninan, K. N.; Thomas, S. Viscoelastic behavior of polypropylene/nitrile rubber thermoplastic elastomer blends: Applications of kerner's models

for reactively compatibilized and dynamically vulcanized systems. *J. Polym. Sci. B: Polym. Phys.*, **2004**, *42*, 1417-1432.

²² Crafton, J.; Johnson, J. Thermoplastic elastomers having improved adhesive properties. *Eur. Pat. App.* EP 1672046 A1, published 21 June **2006**.

²³ Wu, M.; Wang, K.; Zhang, Q.; Fu, Q. Manipulation of multiphase morphology in the reactive blending system OBC/PLA/EGMA. *RSC Adv.*, **2015**, *5*, 96353-96359.

²⁴ Hu, X.; Kang, H.; Li, Y.; Geng, Y.; Wang, R.; Zhang, L. Preparation, morphology and superior performance of biobased thermoplastic elastomer by in situ dynamical vulcanization for 3D-printed materials. *Polymer*, **2017**, *108*, 11-20.

²⁵ Wilson, R.; Divakaran, A. V.; S, K.; Varyambath, A.; Kumaran, A.; Sivaram, S.; Ragupathy, L. Poly(glycerol sebacate)-based polyester – polyether copolymers and their semi-interpenetrated networks with thermoplastic poly(ester – ether) elastomers: Preparation and properties. *ACS Omega*, **2018**, *3*, 18714-18723.

²⁶ Khanna, K.; Varshney, S.; Kakkar, A. Miktoarm star polymers: advances in synthesis, self-assembly, and applications. *Polym. Chem.*, **2010**, *1*, 1171-1185.

²⁷ Hadjichristidis, N. Synthesis of miktoarm star (μ -Star) polymers. *J. Polym. Sci. A: Polym. Chem.*, **1999**, *37*, 857-871.

²⁸ Simal, F.; Jeusette, M.; Leclère, Ph.; Lazzaroni, R.; Roose, P. Adhesive properties of a radial acrylic block co-polymer with a rosin ester resin. *J. Adhesion Sci. Technol.*, **2007**, *21*, 559-574.

²⁹ Dufour, B.; Koynov, K.; Pakula, T.; Matyjaszewski, K. PBA – PMMA 3-arm star block copolymer thermoplastic elastomers. *Macromol. Chem. Phys.*, **2008**, *209*, 1686-1693.

³⁰ Juhari, A.; Mosnáček, J.; Yoon, J. A.; Nese, A.; Koynov, K.; Kowalewski, T.; Matyjaszewski, K. Star-like poly(*n*-butyl acrylate)-*b*-poly(α -methylene- γ -butyrolactone) block copolymers for high temperature thermoplastic elastomers applications. *Polymer*, **2010**, *51*, 4806-4813.

³¹ Pakula, T.; Koynov, K.; Boerner, H.; Huang, J.; Lee, H.-i.; Pietrasik, J.; Sumerlin, B.; Matyjaszewski, K. Effect of chain topology on the self-organization and the mechanical properties of poly(*n*-butyl acrylate)-*b*-polystyrene block copolymers. *Polymer*, **2011**, *52*, 2576-2583.

³² Hirao, A.; Goseki, R.; Ishizone, T. Advances in living anionic polymerization: From functional monomers, polymerization systems, to macromolecular architectures. *Macromolecules*, **2014**, *47*, 1883-1905.

³³ Hadjichristidis, N.; Pitsikalis, M.; Pispas, S.; Iatrou, H. Polymer with complex architecture by living anionic polymerization. *Chem. Rev.*, **2001**, *101*, 3747-3792.

³⁴ Miura, Y.; Kaneko, T.; Satoh, K.; Kamigaito, M.; Jinnai, H.; Okamoto, Y. A_xBA_x-Type block – graft polymers with soft methacrylate middle segments and hard styrene outer grafts: Synthesis, morphology, and mechanical properties. *Chem. Asian J.*, **2007**, *2*, 662-672.

³⁵ Zhou, C.; Wei, Z.; Jin, C.; Wang, Y.; Yu, Y.; Leng, X.; Li, Y. Fully biobased thermoplastic elastomers: Synthesis of highly branched linear comb poly(β -myrcene)-*graft*-poly(L-lactide) copolymers with tunable mechanical properties. *Polymer*, **2018**, *138*, 57-64.

³⁶ Sheiko, S.; Sumerlin, B. S.; Matyjaszewski, K. Cylindrical molecular brushes: Synthesis, characterization, and properties. *Prog. Polym. Sci.*, **2008**, *33*, 759-785.

³⁷ Keith, A. N.; Vatankhah-Varnosfaderani, M.; Clair, C.; Fahimipour, F.; Dashtimoghdam, E.; Lallam, A.; Sztucki, M.; Ivanov, D. A.; Liang, H.; Dobrynin, A. V.; Sheiko, S. S. Bottlebrush bridge between soft gels and firm tissues. *ACS Cent. Sci.*, **2020**, *6*, 413-419.

³⁸ Pakula, T.; Zhang, Y.; Matyjaszewski, K.; Lee, H.-i.; Boerner, H.; Qin, S.; Berry, G. C. Molecular brushes as super-soft elastomers. *Polymer*, **2006**, *47*, 7198-7206.

- ³⁹ Daniel, W. F. M.; Burdyńska, J.; Vatankhah-Varnosfaderani, M.; Matyjaszewski, K.; Paturej, J.; Rubinstein, M.; Dobrynin, A. V.; Sheiko, S. S. Solvent-free, supersoft and superelastic bottlebrush melts and networks. *Nat. Mater.*, **2015**, *15*, 183-190.
- ⁴⁰ Vatankhah-Varnosfaderani, M.; Keith, A. N.; Cong, Y.; Liang, H.; Rosenthal, M.; Sztucki, M.; Clair, C.; Magonov, S.; Ivanov, D. A.; Dobrynin, A. V.; Sheiko, S. S. Chameleon-like elastomers with molecularly encoded strain-adaptive stiffening and coloration. *Science*, **2018**, *359*, 1509-1513.
- ⁴¹ Zhang, J.; Wang, Z.; Wang, X.; Wang, Z. The synthesis of bottlebrush cellulose-*graft*-diblock copolymer elastomer via atom transfer radical polymerization utilizing a halide exchange technique. *Chem. Commun.*, **2019**, *55*, 13904-13907.
- ⁴² Kébir, N.; Campistron, I.; Laguerre, A.; Pilard, J.-F.; Bunel, C.; Couvercelle, J.-P. Use of new hydroxytelechelic cis-1,4-polyisoprene (HTPI) in the synthesis of polyurethanes (PUs): Influence of isocyanate and chain extender nature and their equivalent ratios on the mechanical and thermal properties of PUs. *e-Polymers*, **2006**, *48*.
- ⁴³ Lingier, S.; Espeel, P.; Suarez, S. S.; Türünc, O.; De Wildeman, S.; Du Prez, F. E. Renewable thermoplastic polyurethanes containing rigid spiroacetal moieties. *Eur. Polym. J.*, **2015**, *70*, 232-239.
- ⁴⁴ Wang, W.; Guo, Y.; Otaigbe, J. U. Synthesis, characterization and degradation of biodegradable thermoplastic elastomers from poly(ester urethane)s and renewable soy protein isolate biopolymer. *Polymer*, **2010**, *51*, 5448-5455.
- ⁴⁵ Martello, M. T.; Schneiderman, D. K.; Hillmyer, M. A. Synthesis and melt processing of sustainable poly(ϵ -decalactone)-*block*-poly(lactide) multiblock thermoplastic elastomers. *ACS Sustainable Chem. Eng.*, **2014**, *2*, 2519-2526.
- ⁴⁶ Zhu, Y.; Radlauer, M. R.; Schneiderman, D. K.; Shaffer, M. S. P.; Hillmyer, M. A.; Williams, C. K. Multiblock polyesters demonstrating high elasticity and shape memory effects. *Macromolecules*, **2018**, *51*, 2466-2475.
- ⁴⁷ Handlin Jr., D. L. Thermoplastic elastomers. *Encyclopedia of Materials: Science and Technology*, **2001**, Elsevier, 2nd Ed., p. 9197-9204.
- ⁴⁸ Kim, J. K. Block copolymer mechanical properties. *Encyclopedia of Materials: Science and Technology*, **2001**, Elsevier, 2nd Ed., p. 651-657.
- ⁴⁹ Hillmyer, M. A. Block copolymer synthesis. *Encyclopedia of Materials: Science and Technology*, **2001**, Elsevier, 2nd Ed., p. 9197-9204.
- ⁵⁰ Liu, N. C.; Baker, W. E. Reactive polymers for blend compatibilization. *Adv. Polym. Technol.*, **1992**, *11*, 249-262.
- ⁵¹ Orr, C. A.; Adedeji, A.; Hirao, A.; Bates, F. S.; Macosko, C. W. Flow-induced reactive self-assembly. *Macromolecules*, **1997**, *30*, 1243-1246.
- ⁵² Isono, T.; Ree, B. J.; Tajima, K.; Borsali, R.; Satoh, T. Highly ordered cylinder morphologies with 10 nm scale periodicity in biomass-based block copolymers. *Macromolecules*, **2018**, *51*, 428-437.
- ⁵³ Palmiero, U. C.; Sponchioni, M.; Manfredini, N.; Maraldi, M.; Moscatelli, D. Strategies to combine ROP with ATRP or RAFT polymerization for the synthesis of biodegradable polymeric nanoparticles for biomedical applications. *Polym. Chem.* **2018**, *9*, 4084-4099.
- ⁵⁴ Schmidt, S. C.; Hillmyer, M. A. Synthesis and characterization of model polyisoprene – polylactide deblock copolymers. *Macromolecules*, **1999**, *32*, 4794-4801.
- ⁵⁵ Varshney, S. K.; Kesani, P.; Agarwal, N.; Zhang, J. X. Synthesis of ABA type thermoplastic elastomers based on polyacrylates. *Macromolecules*, **1999**, *32*, 235-237.

- ⁵⁶ Hashimoto, T.; Namikoshi, T.; Urushisaki, M. ABA tri-block copolymer. *US Patent App.*, **2008**, US 2008/0114141 A1.
- ⁵⁷ Bolton, J. M.; Hillmyer, M. A.; Hoye, T. R. Sustainable thermoplastic elastomers from terpene-derived monomers. *ACS Macro Lett.*, **2014**, *3*, 717-720.
- ⁵⁸ Gergely, A. L.; Puskas, J. E. Synthesis and characterization of thermoplastic elastomers with polyisobutylene and polyalloocimene blocks. *J. Polym. Sci. A Polym. Chem.*, **2015**, *53*, 1567-1574.
- ⁵⁹ Hashimoto, T.; Imaeda, T.; Irie, S.; Urushisaki, M.; Sakaguchi, T. Synthesis of poly(vinyl ether)-based, ABA triblock-type thermoplastic elastomers with functionalized soft segments and their gas permeability. *J. Polym. Sci. A: Polym. Chem.*, **2015**, *53*, 1114-1124.
- ⁶⁰ Gerhard-Abozari, E.; Keul, H.; Höcker, H. Copolymers with soft and hard segments based on 2,2-dimethyltrimethylene carbonate and ϵ -caprolactone. *Macromol. Chem. Phys.*, **1994**, *195*, 2371-2380.
- ⁶¹ Kim, J.-H.; Lee, S. Y.; Chung, D. J. Synthesis and properties of triblock copolymers from L-lactide and trimethylene carbonate. *Polym. J.*, **2000**, *32*, 1056-1059.
- ⁶² Wanamaker, C. L.; O'Leary, L. E.; Lynd, N. A.; Hillmyer, M. A.; Tolman, W. B. Renewable-resource thermoplastic elastomers based on polylactide and polymethide. *Biomacromolecules*, **2007**, *8*, 3634-3640.
- ⁶³ Wanamaker, C.; Tolman, W. B.; Hillmyer, M. A. Hydrolytic degradation behavior of a renewable thermoplastic elastomer. *Biomacromolecules*, **2009**, *10*, 443-448.
- ⁶⁴ Shin, J.; Martello, M. T.; Shrestha, M.; Wissinger, J. E.; Tolman, W. B.; Hillmyer, M. A. Pressure-sensitive adhesives from renewable triblock copolymers. *Macromolecules*, **2011**, *44*, 87-94.
- ⁶⁵ Schneiderman, D. K.; Hill, E. M.; Martello, M. T.; Hillmyer, M. A. Poly(lactide)-*block*-poly(ϵ -caprolactone-co- ϵ -decalactone)-*block*-poly(lactide) copolymer elastomers. *Polym. Chem.*, **2015**, *6*, 3641-3651.
- ⁶⁶ Watts, A.; Kurokawa, N.; Hillmyer, M. A. Strong, resilient, and sustainable aliphatic polyester thermoplastic elastomers. *Biomacromolecules*, **2017**, *18*, 1845-1854.
- ⁶⁷ Switek, K. A.; Chang, K.; Bates, F. S.; Hillmyer, M. A. ABA triblock copolymers with ring-opening metathesis polymerization/macromolecular chain-transfer agent approach. *J. Polym. Sci. A: Polym. Chem.*, **2007**, *45*, 361-373.
- ⁶⁸ Ganewatta, M. S.; Ding, W.; Rahman, M. A.; Yuan, L.; Wang, Z.; Hamidi, N.; Robertson, M. L.; Tang, C. Biobased plastics and elastomers from renewable rosin via "living" ring-opening metathesis polymerization. *Macromolecules*, **2016**, *49*, 7155-7164.
- ⁶⁹ Kotani, Y.; Kato, M.; Kamigaito, M.; Sawamoto, M. Living radical polymerization of alkyl methacrylates with ruthenium complex and synthesis of their block copolymers. *Macromolecules*, **1996**, *29*, 6979-6982.
- ⁷⁰ Mosnáček, J.; Yoon, J. A.; Juhari, A.; Koynov, K.; Matyjaszewski, K. Synthesis, morphology and mechanical properties of linear triblock copolymers based on poly(α -methylene- γ -butyrolactone). *Polymer* **2009**, *50*, 2087-2094.
- ⁷¹ Wang, S.; Kesava, S. V.; Gomez, E. D.; Robertson, M. L. Sustainable thermoplastic elastomers derived from fatty acids. *Macromolecules*, **2013**, *46*, 7202-7212.
- ⁷² Liu, X.; Zhao, R.-Y.; Zhao, T.-P.; Liu, C.-Y.; Yang, S.; Chen, E.-Q. An ABA triblock containing a central soft block of poly[2,5-di(n-hexogycarbonyl)styrene] and outer hard block of poly(4-vinylpyridine): Synthesis, phase behavior and mechanical enhancement. *RSC Adv.*, **2014**, *4*, 18431-18441.

- ⁷³ Satoh, K.; Lee, D.-H.; Nagai, K.; Kamigaito, M. Precision synthesis of bio-based acrylic thermoplastic elastomer by RAFT polymerization of itaconic acid derivatives. *Macromol. Rapid Commun.*, **2014**, 35, 161-167.
- ⁷⁴ Gallagher, J. J.; Hillmyer, M. A.; Reineke, T. M. Acrylic triblock copolymers incorporating isosorbide for pressure sensitive adhesives. *ACS Sustainable Chem. Eng.*, **2016**, 4, 3379-3387.
- ⁷⁵ Ding, W.; Wang, S.; Yao, K.; Genewatta, M. S.; Tang, C.; Robertson, M. L.; *ACS Sustainable Chem. Eng.*, **2017**, 5, 11470-11480.
- ⁷⁶ Nasiri, M.; Saxon, D. J.; Reineke, T. M. Enhanced mechanical and adhesion properties in sustainable triblock copolymers via non-covalent interactions. *Macromolecules*, **2018**, 51, 2456-2465.
- ⁷⁷ Noppalit, S.; Simula, A.; Ballard, N.; Callies, X.; Asua, J. M.; Billon, L. Renewable terpene derivative as a biosourced elastomeric building block in the design of functional acrylic copolymers. *Biomacromolecules*, **2019**, 20, 2241-2251.
- ⁷⁸ Shin, J.; Lee, Y.; Tolman, W. B.; Hillmyer, M. A. Thermoplastic elastomers derived from menthene and tulipalin A. *Biomacromolecules*, **2012**, 13, 3833-3840.
- ⁷⁹ Hillmyer, M. A.; Tolman, W. B. Aliphatic polyester block copolymers: Renewable, degradable, and sustainable. *Acc. Chem. Res.*, **2014**, 47, 2390-2396.
- ⁸⁰ Ding, K.; John, A.; Shin, J.; Lee, Y.; Quinn, T.; Tolman, W. B.; Hillmyer, M. A. High-performance pressure-sensitive adhesives from renewable triblock copolymers. *Biomacromolecules*, **2015**, 16, 2537-2539.
- ⁸¹ Schmalz, H.; Böker, A.; Lange, R.; Krausch, G.; Abetz, V. Synthesis and properties of ABA and ABC triblock copolymers with glassy (A), elastomeric (B), and crystalline (C) blocks. *Macromolecules*, **2001**, 34, 8720-8729.
- ⁸² Yang, J.-X.; Pan, L.; Ma, Z.; Wang, B.; Li, Y.-S. Synthesis and properties of ABA, CBA, and CBC triblock copolymers based thermoplastic elastomers with glassy (A), elastomeric (B), and crystalline (C) blocks. *J. Macromol. Sci. A*, **2019**, 56, 225-233.
- ⁸³ Morita, H.; Miyamoto, A.; Kotani, M. Recoverably and destructively deformed domain structures in elongation process of thermoplastic elastomer analyzed by graph theory. *Polymer*, **2020**, 188, 122098.
- ⁸⁴ Rodgers, M. B. Rubber tires. *Encyclopedia of Materials: Science and Technology*, **2001**, Elsevier, 2nd Ed., p. 8237-8242.
- ⁸⁵ Amin, S.; Amin, M. Thermoplastic elastomeric (TPE) materials and their use in outdoor electrical insulation. *Rev. Adv. Mater. Sci.* **2011**, 29, 15-30.
- ⁸⁶ Kök, N. V.; Yilmaz, M.; Guler, M. Evaluation of high temperature performance of SBS + gilsonite modified binder. *Fuel*, **2011**, 90, 3093-3099.
- ⁸⁷ Qian, G.; Yao, D.; Gong, X.; Yu, H.; Li, N. Performance evaluation and field application of hard asphalt concrete under heavy traffic conditions. *Construction and building materials*, **2019**, 228, 116729.
- ⁸⁸ Drobny, J. G. Chapter 15. Applications of thermoplastic elastomers. *Handbook of thermoplastic elastomers*. Ed. William Andrew, **2007**.
- ⁸⁹ Creton, C. Elastomeric adhesives. *Encyclopedia of Materials: Science and Technology*, **2001**, Elsevier, 2nd Ed., p. 2451-2456.
- ⁹⁰ Naskar, K.; Babu, R. R. Thermoplastic Elastomers (TPEs) and Thermoplastic Vulcanizates (TPVs). *Encyclopedia of Polymeric Nanomaterials*. **2015**, Ed. Kobayashi S., Müllen K. (Springer, Berlin, Heidelberg).

- ⁹¹ Vilela, C.; Sousa, A. F.; Fonseca, A. C.; Serra, A. C.; Coelho, J. F. J.; Freire, C. S. R.; Silvestre, A. J. D. The quest for sustainable polyesters – insights into the future. *Polym. Chem.*, **2014**, *5*, 3119-3141.
- ⁹² Shin, J. Kim, Y.-W.; Kim, G.-J. Sustainable block copolymer-based thermoplastic elastomers. *Appl. Chem. Eng.* **2014**, *25*, 121-133.
- ⁹³ Zhu, Y.; Romain, C.; Williams, C. W. Sustainable polymers from renewable resources. *Nature*, **2016**, *540*, 354-362.
- ⁹⁴ Doshi, M. R.; Dyer, J. M. Paper: Recycling and recycled materials. *Encyclopedia of Materials: Science and Technology* **2001**, Elsevier, 2nd Ed., p. 6711-6720.
- ⁹⁵ Monfared, M. H. A.; Resalati, H.; Ghasemian, A.; Hubbe, M. A. Passivation of pressure sensitive adhesive stickies by addition of acrylic fibers to OCC pulp before papermaking. *Tappi J.*, **2016**, *15*, 631-639.
- ⁹⁶ Rikkou, M. D.; Patrickios, C. S. Polymers prepared using cleavable initiators: Synthesis, characterization and degradation. *Prog. Polym. Sci.*, **2011**, *36*, 1079-1097.
- ⁹⁷ Schneiderman, D. K.; Hillmyer, M. A. 50th Anniversary perspective: There is a great future in sustainable polymers. *Macromolecules* **2017**, *50*, 3733-3749.
- ⁹⁸ Barnes, D. K. A.; Galgani, F.; Thompson, R. C.; Barlaz, M. Accumulation and fragmentation of plastic debris in global environments. *Phil. Trans. R. Soc. B* **2009**, *364*, 1985-1998.
- ⁹⁹ Hopewell, J.; Dvorak, R.; Kosior, E. Plastic recycling: challenges and opportunities. *Phil. Trans. R. Soc. B* **2009**, *364*, 2115-2126.
- ¹⁰⁰ Lithner, D.; Larsson, Å.; Dave, G. Environmental and health hazard ranking and assessment of plastic polymers based on chemical composition. *Sci. Total. Environ.* **2011**, *409*, 3309-3324.
- ¹⁰¹ Rochman, C. M.; Browne, M. A.; Halpern, B. S.; Hentschel, B. T.; Hoh, E.; Karapanagioti, H. K.; Rios-Mendoza, L. M.; Takada, H.; Teh, S.; Thompson, R. C. Classify plastic waste as hazardous. *Nature* **2013**, *494*, 169-171.
- ¹⁰² Anastas, P. T.; Kirchhoff, M. M. Origins, current status, and future challenges of green chemistry. *Acc. Chem. Res.* **2002**, *35*, 686-694.
- ¹⁰³ Anastas, P.; Eghbali, N. Green chemistry: Principles and practice. *Chem. Soc. Rev.* **2010**, *39*, 301-312.
- ¹⁰⁴ Yao, K.; Tang, C. Controlled polymerization of next-generation renewable monomers and beyond. *Macromolecules* **2013**, *46*, 1689-1712.
- ¹⁰⁵ Yates, M. R.; Barlow, C. Y. Life cycle assessments of biodegradable, commercial biopolymers – A critical review. *Resour. Conserv. Recycl.* **2013**, *78*, 54-66.
- ¹⁰⁶ Getachew, A.; Woldesenbet, F. Production of biodegradable plastic by polyhydroxybutyrate (PHB) accumulating bacteria using low cost agricultural waste material. *BMC Res. Notes* **2016**, *9*, 509.
- ¹⁰⁷ Mathers, R. T. How well can renewable resources mimic commodity monomers and polymers? *J. Polym. Sci. A: Polym. Chem.* **2012**, *50*, 1-15.
- ¹⁰⁸ Metzger, J. O.; Bornscheuer, U. Lipids as renewable resources: current state of chemical and biotechnological conversion and diversification. *Appl. Microbiol. Biotechnol.* **2006**, *71*, 13-22.
- ¹⁰⁹ Lligadas, G.; Ronda, J. C.; Galià, M.; Cádiz, V. Renewable polymeric materials from vegetable oils: a perspective. *Mater. Today* **2013**, *16*, 337-343.
- ¹¹⁰ Behr, A.; Perez Gomes, J. The refinement of renewable resources: New important derivatives of fatty acids and glycerol. *Eur. J. Lipid Sci. Technol.* **2010**, *112*, 31-50.
- ¹¹¹ Wilbon, P. A.; Chu, F.; Tang, C. Progress in renewable polymers from natural terpenes, terpenoids, and rosin. *Macromol. Rapid. Commun.* **2013**, *34*, 8-37.

- ¹¹² Holmberg, A. L.; Reno, K. H.; Wool, R. P.; Epps, T. H. III Biobased building blocks for the rational design of renewable block copolymers. *Soft Matter*. **2014**, *10*, 7405-7424.
- ¹¹³ Wasewar, K. L.; Yawalkar, A. A.; Moulijn, J. A.; Pangarkar, V. G. Fermentation of glucose to lactic acid coupled with reactive extraction: A review. *Ind. Eng. Chem. Res.* **2004**, *43*, 5969-5982.
- ¹¹⁴ Emptage, M.; Haynie, S. L.; Laffend, L. A.; Pucci, J. P.; Whited, G. M. Process for the biological production of 1,3-propanediol with high titer. United States Patent Application US2003/0157674A1, published 21 August 2003.
- ¹¹⁵ Chen, G.-Q.; Patel, M. K. Plastics derived from biological sources: Present and future: A technical and environmental review. *Chem. Rev.* **2012**, *112*, 2082-2099.
- ¹¹⁶ Dodds, D. R.; Gross, R. A. Chemicals from biomass. *Science* **2007**, *318*, 1250-1251.
- ¹¹⁷ Wang, H.-h.; Zhou, X.-r.; Liu, Q.; Chen, G.-Q. Biosynthesis of polyhydroxyalkanoate homopolymers by *Pseudomonas putida*. *Appl. Microbiol. Biotechnol.* **2011**, *89*, 1497-1507.
- ¹¹⁸ Gallezot, R. Conversion of biomass to selected chemical products. *Chem. Soc. Rev.* **2012**, *41*, 1538-1558.
- ¹¹⁹ Van der Steen, M.; Stevens, C. V. Undecylenic acid: A valuable and physiologically active renewable building block from castor oil. *ChemSusChem* **2009**, *2*, 692-713.
- ¹²⁰ Multu, H.; Meier, M. A. R. Castor oil as a renewable resource for the chemical industry. *Eur. J. Lipid Sci. Technol.* **2010**, *112*, 10-30.
- ¹²¹ Serra, S.; Fuganti, C.; Brenna, E. Biocatalytic preparation of natural flavours and fragrances. *Trends Biotechnol.* **2005**, *23*, 193-198.
- ¹²² Biermann, U.; Bornscheuer, U.; Meier, M. A. R.; Metzger, J. O.; Schäfer, H. J. Oils and fats as renewable raw materials in chemistry. *Angew. Chem. Int. Ed.* **2011**, *50*, 3854-3871.
- ¹²³ Valverde, C.; Lligadas, G.; Ronda, J. C.; Galià, M.; Cádiz, V. Hydroxyl functionalized renewable polyester derived from 10-undecenoic acid: Polymer structure and post-polymerization modification. *Eur. Polym. J.* **2018**, *105*, 68-78.
- ¹²⁴ Adams, T. B.; Greer, D. B.; Doull, J.; Munro, I. C.; Newberne, P.; Portoghese, P. S.; Smith, R. L.; Wagner, B. M.; Weil, C. S.; Woods, L. A.; Ford, R. A. The FEMA GRAS Assessment of lactones used as flavour ingredients. *Food and Chemical Toxicology* **1998**, *36*, 249-278.
- ¹²⁵ Rali, T.; Wossa, S. W.; Leach, D. N. Comparative chemical analysis of the essential oil constituents in the bark, heartwood and fruits of *Cryptocarya massoy* (Oken) Kosterm. (Lauraceae) from Papua New Guinea. *Molecules* **2007**, *12*, 149-154.
- ¹²⁶ Kang, W.-R.; Seo, M.-J.; An, J.-U. Production of δ -decalactone from linoleic acid via 13-hydroxy-9(Z)-octadecenoic acid intermediate by one-pot reaction using linoleate 13-hydratase and whole *Yarrowia lipolytica* cells. *Biotechnol. Lett.* **2016**, *38*, 817-823.
- ¹²⁷ Boog, A. L. G. M.; Peters, A. L. J.; Roos, R. Process for producing delta-lactones. *Eur. Patent App.* EP 0 409 321 B1, **1994**.
- ¹²⁸ Roos, R.; Bakker, J. Process for the isolation of hydroxy fatty acid derivatives from convolvulaceae plants. European Patent EP0409320B1, published 5 October 1994.
- ¹²⁹ Boog, A. L. G.; Peters, A. L. J.; Roos, R. Process for producing delta-lactones from 11-hydroxy fatty acids. United State Patent US005215901A, published 1 June 1993.
- ¹³⁰ Romero-Guido, C.; Belo, I.; Ta, T. M. N.; Cao-Hoang, L.; Alchihab, M.; Gomes, N.; Thonart, Ph.; Teixeira, J. A.; Destain, J.; Waché, Y. Biochemistry of lactone formation in yeast and fungi and its utilization for the production of flavour and fragrances compounds. *Appl. Microbiol. Biotechnol.* **2011**, *89*, 535-547.

-
- ¹³¹ Kizer, L. E.; Morris, J. A.; Harris, G.; McLean, L. B. Process for preparing saturated lactones, products produced therefrom and organoleptic uses of said products. *Eur. Patent App.* EP 0 952 226 A1, **1999**.
- ¹³² Alam, Md. I.; Khan, T. S.; Haider, M. A. Alternate biobased route to produce δ -decalactone: Elucidating the role of solvent and hydrogen evolution in catalytic transfer hydrogenation. *ACS Sustainable Chem. Eng.* **2019**, *7*, 2894-2898.
- ¹³³ Dong, H.; Cao, S.-G.; Li, Z.-Q.; Han, S.-P.; You, D.-L.; Shen, J.-C. J. Study on the enzymatic polymerization mechanism of lactone and the strategy for improving the degree of polymerization. *Polym. Sci. A: Polym. Chem.* **1999**, *37*, 1265-1275.
- ¹³⁴ Zhao, J.; Hadjichristidis, N. Polymerization of 5-alkyl δ -lactones catalyzed by diphenyl phosphate and their sequential organocatalytic polymerization with monosubstituted epoxides. *Polym. Chem.* **2015**, *6*, 2659-2668.
- ¹³⁵ Martello, M. T.; Burns, A.; Hillmyer, M. Bulk ring-opening transesterification polymerization of the renewable δ -decalactone using an organocatalyst. *ACS Macro Lett.* **2012**, *1*, 131-135.
- ¹³⁶ Bansal, K. K.; Kakde, D.; Purdie, L.; Irvine, D. J.; Howdle, S. M.; Mantovani, G.; Alexander, C. New biomaterials from renewable resources – amphiphilic block copolymers from δ -decalactone. *Polym. Chem.* **2015**, *6*, 7196-7210.
- ¹³⁷ Schneiderman, D. K.; Hillmyer, M. A. Aliphatic polyester block polymer design. *Macromolecules* **2016**, *49*, 2419-2428.
- ¹³⁸ Agarwal, S.; Jin, Q.; Maji, S. Biobased polymers from plant-derived tulipalin A. *ACS Symposium Series* **2012**, 1105, Chapter 13, 197-212.
- ¹³⁹ Akkapeddi, M. K. Poly(α -methylene- γ -butyrolactone). Synthesis, configurational structure, and properties. *Macromolecules* **1979**, *12*, 546-551.
- ¹⁴⁰ Kollár, J.; Mrlík, M.; Moravčíková, D.; Iván, B.; Mosnáček, J. Effect of monomer content and external stimuli on properties of renewable tulipalin A-based supersorbent hydrogels. *Eur. Polym. J.* **2019**, *115*, 99-106.
- ¹⁴¹ Kato, Y.; Yoshida, H.; Shoji, K.; Sato, Y.; Nakajima, N.; Ogita, S. A facile method for the preparation of α -methylene- γ -butyrolactones from tulip tissues by enzyme-mediated conversion. *Tetrahedron Lett.* **2009**, *50*, 4751-4753.
- ¹⁴² De Wildeman, S. M. A.; De Vries, J. G.; Boogers, J. A. F. Process for the preparation of 3-methylene- γ -butyrolactone. *International Patent App.* WO2012/116977A1, published 7 September 2012.
- ¹⁴³ Murray, A. W.; Reid, R. A new synthesis of α -methylene lactones. *J. Chem. Soc., Chem. Commun.* **1984**, *2*, 132-133.
- ¹⁴⁴ Li, X.; Lan, X.; Wang, T. Highly selective catalytic conversion of furfural to γ -butyrolactone. *Green Chem.* **2016**, *18*, 638-642.
- ¹⁴⁵ Trotta, J. T.; Jin, M.; Stawiasz, K. J.; Michaudel, Q.; Chen, W.-L.; Fors, B. P. J. Synthesis of methylene butyrolactone polymers from itaconic acid. *Polym. Sci. A* **2017**, *55*, 2730-2737.
- ¹⁴⁶ Zhou, J.; Schmidt, A. M.; Ritter, H. Bicomponent transparent polyester networks with shape memory effect. *Macromolecules* **2010**, *43*, 939-942.
- ¹⁴⁷ Hong, M.; Chen, E. Y.-X. Completely recyclable biopolymers with linear and cyclic topologies via ring-opening polymerization of γ -butyrolactone. *Nat. Chem.* **2016**, *8*, 42-49.
- ¹⁴⁸ Hong, M.; Chen, E. Y.-X. Towards truly sustainable polymers: A metal-free recyclable polyester from biorenewable non-strained γ -butyrolactone. *Angew. Chem. Int. Ed.* **2016**, *55*, 4188-4193.

- ¹⁴⁹ Danko, M.; Mosnáček, J. Ring-opening polymerization of γ -butyrolactone and its derivatives: A review. *Polimery-W* **2017**, *62*, 272-282.
- ¹⁵⁰ McGraw, W. J. Lactone derivatives and methods of making. United States Patent US2624723, patented 6 January 1953.
- ¹⁵¹ Miyake, G. M.; Newton, S. E.; Mariott, W. R.; Chen, E. Y.-X. Coordination polymerization of renewable butyrolactone-based vinyl monomers by lanthanide and early metal catalysts. *Dalton Trans.* **2010**, *39*, 6710-6718.
- ¹⁵² Mosnáček, J.; Matyjaszewski, K. Atom transfer radical polymerization of tulipalin A: A naturally renewable monomer. *Macromolecules* **2008**, *41*, 5509-5511.
- ¹⁵³ Sato, K.; Koinuma, H.; Hirai, H. Polymer conformation and NMR chemical shifts, 9 poly(α -methylene- γ -butyrolactone). *Makromol. Chem.* **1984**, *185*, 771-786.
- ¹⁵⁴ Carothers, W. H.; Arvin, J. A. Studies on polymerization and ring formation. II. Poly-esters. *J. Am. Chem. Soc.* **1929**, *51*, 2560-2570.
- ¹⁵⁵ Carothers, W. H. Polymerization. *Chem. Rev.* **1931**, *8*, 353-426.
- ¹⁵⁶ Whinfield, J. R.; Dickson, J. T. Improvements relating to the manufacture of highly polymeric substances. British patent GB578079, patented 29 July 1941.
- ¹⁵⁷ Whinfield, J. R. Chemistry of "Terylene". *Nature (London)* **1946**, *158*, 930-931.
- ¹⁵⁸ Van Natta, F. J.; Hill, J. W.; Carothers, W. H. Studies of polymerization and ring formation. XXIII. ϵ -Caprolactone and its polymers. *J. Am. Chem. Soc.* **1934**, *56*, 455-457.
- ¹⁵⁹ Woodruff, M. A.; Hutmacher, D. W. The return of a forgotten polymer – Polycaprolactone in the 21st century. *Prog. Polym. Sci.* **2010**, *35*, 1217-1256.
- ¹⁶⁰ Ikada, Y.; Tsuji, H. Biodegradable polyesters for medical and ecological applications. *Macromol. Rapid Commun.* **2000**, *21*, 117-132.
- ¹⁶¹ Yoshida, Y.; Miyamoto, M.; Obuchi, S.; Ikeda, K.; Ohta, M. Preparation process of polyhydroxycarboxylic acid. European Patent EP0710684B1, patented 08 May 1996.
- ¹⁶² Takasu, A.; Oishi, Y.; Iio, Y.; Inai, Y.; Hirabayashi, T. Synthesis of aliphatic polyesters by direct polyesterification of dicarboxylic acids with diols under mild conditions catalyzed by reusable rare-earth triflate. *Macromolecules* **2003**, *36*, 1772-1774.
- ¹⁶³ Gharbi, S.; Andreolety, J.-P.; Gandini, A. Polyesters bearing furan moieties IV. Solution and interfacial polycondensation of 2,2'-bis(5-chloroformyl-2-furyl)propane with various diols and bisphenols. *Eur. Polym. J.* **2000**, *36*, 463-472.
- ¹⁶⁴ Liu, Y.; Turner, S. R. Synthesis and properties of cyclic diester based aliphatic copolyesters. *J. Polym. Sci. A, Polym. Chem.* **2010**, *48*, 2162-2169.
- ¹⁶⁵ Sokolsky-Papkow, M.; Langer, R.; Domb, A. J. Synthesis of aliphatic polyesters by polycondensation using inorganic acid as catalyst. *Polym. Adv. Technol.* **2011**, *22*, 502-511.
- ¹⁶⁶ Terzopoulou, Z.; Karakatsianopoulou, E.; Kasmi, N.; Tsanaktis, V.; Nikolaidis, N.; Kostoglou, M.; Papageorgiou, G. Z.; Lambropoulou, D. A.; Bikiaris, D. N. Effect of catalyst type on molecular weight increase and coloration of poly(ethylene furanoate) biobased polyester during melt polycondensation. *Polym. Chem.* **2017**, *8*, 6895-6908.
- ¹⁶⁷ Douka, A.; Vouyiouka, S.; Papaspyridi, L.-M.; Papaspyrides, C. D. A review on enzymatic polymerization to produce polycondensation polymers: The case of aliphatic polyesters, polyamides and polyesteramides. *Prog. Polym. Sci.* **2018**, *79*, 1-25.
- ¹⁶⁸ Labet, M.; Thielemans, W. Synthesis of polycaprolactone: a review. *Chem. Soc. Rev.* **2009**, *38*, 3484-3504.

- ¹⁶⁹ Duda, A.; Kowalski, A. Thermodynamics and kinetics of ring opening polymerization. Handbook of Ring Opening Polymerization, P. Dubois, O. Coulembier, J.-M. Raquez, Eds. Wiley-VCH Verlag: Weinheim Germany, pp. 1-51 **2009**.
- ¹⁷⁰ Zhao, W.; Wang, Q.; Cui, Y.; He, J.; Zhang, Y. Living/controlled ring-opening (co)polymerization of lactones by Al-based catalyst with different sidearms. *Dalton Trans.* **2019**, 48, 7167-7178.
- ¹⁷¹ In't Veld, P. J. A.; Velner, E. M.; Van de Witte, P.; Hamhuis, J.; Dijkstra, P. J.; Feijen, J. Melt block copolymerization of ϵ -caprolactone and L-lactide. *J. Polym. Sci. A, Polym. Chem.* **1997**, 35, 219-226.
- ¹⁷² Duda, A.; Florjanczyk, Z.; Hofman, A.; Slomkowski, S.; Penczek, S. Living pseudoanionic polymerization of ϵ -caprolactone. Poly(ϵ -caprolactone) free of cyclics and with controlled end groups. *Macromolecules* **1990**, 23, 1640-1646.
- ¹⁷³ Kowalski, A.; Duda, A.; Penczek, S. Polymerization of L,L-lactide initiated by aluminium isopropoxide trimer or tetramer. *Macromolecules* **1998**, 31, 2114-2122.
- ¹⁷⁴ Grijpma, D. W.; Pennings, A. J. Polymerization temperature effects on the properties of L-lactide and ϵ -caprolactone copolymers. *Polym. Bull.* **1991**, 25, 335-341.
- ¹⁷⁵ Dubois, Ph.; Ropson, N.; Jérôme, R.; Teyssié, Ph. Macromolecular engineering of polylactones and polylactides. 19. Kinetics of ring-opening polymerization of ϵ -caprolactone initiated with functional aluminium alkoxides. *Macromolecules* **1996**, 29, 1965-1975.
- ¹⁷⁶ Duda, A.; Penczek, S. Chapter 13: Thermodynamics, kinetics and mechanism of cyclic esters polymerization. Polymers from renewable resources; American Chemical Society: Washington, DC, Vol. 764 (**2001**), ISBN 0-8412-3646-1.
- ¹⁷⁷ Olsén, P.; Odelius, K.; Albertsson, A.-C. Thermodynamic presynthetic considerations for ring-opening polymerization. *Biomacromolecules*, **2016**, 17, 699-709.
- ¹⁷⁸ Snow, R. D.; Frey, F. E. The reaction of sulfur dioxide with olefins: the ceiling temperature phenomenon. *J. Am. Chem. Soc.* **1943**, 65, 2417-2418.
- ¹⁷⁹ Bach, R. D.; Dmitrenko, O. The effect of carbonyl substitution on the strain energy of small ring compounds and their six-member ring reference compounds. *J. Am. Chem. Soc.* **2006**, 128, 4598-4611.
- ¹⁸⁰ Adamus, G.; Kowalczyk, M. Anionic ring-opening polymerization of β -alkoxymethyl-substituted β -lactones. *Biomacromolecules* **2008**, 9, 696-703.
- ¹⁸¹ Yasuda, T.; Aida, T.; Inoue, S. Living polymerization of β -lactone catalyzed by (tetraphenylporphinato)aluminum chloride. Structure of the living end. *Macromolecules* **1983**, 16, 1792-1796.
- ¹⁸² Alemán, C.; Betran, O.; Casanovas, J.; Houk, K. N.; Hall Jr., H. K. Thermodynamic control of the polymerizability of five-, six-, and seven-membered lactones. *J. Org. Chem.* **2009**, 74, 6237-6244.
- ¹⁸³ Duda, A.; Penczek, S. Oligomerization and copolymerization of γ -butyrolactone – a monomer known as unable to homopolymerize, 1 Copolymerization with ϵ -caprolactone. *Macromol. Chem. Phys.* **1996**, 197, 1273-1283.
- ¹⁸⁴ Leitão, M. L. P.; Pilcher, G.; Meng-Yan, Y.; Brown, J. M.; Conn, A. D. Enthalpies of combustion of γ -butyrolactone, γ -valerolactone, and δ -valerolactone. *J. Chem. Thermodynamics* **1990**, 22, 885-891.
- ¹⁸⁵ Carothers, W. H.; Dorough, G. L.; Van Natta, F. J. Studies of polymerization and ring formation. X. The reversible polymerization of six-membered cyclic esters. *J. Am. Chem. Soc.* **1932**, 54, 761-772.

- ¹⁸⁶ Nakayama, Y.; Sasaki, K.; Watanabe, N.; Cai, Z.; Shiono, T. Ring-opening polymerization of six-membered cyclic esters catalyzed by tetrahydroborate complexes of rare earth metals. *Polymer*. **2009**, *50*, 4788-4793.
- ¹⁸⁷ Kim, H.; Olsson, J. V.; Hedrick, J. L.; Waymouth, R. M. Facile synthesis of functionalized lactones and organocatalytic ring-opening polymerization. *ACS Macro Lett.*, **2012**, *1*, 845-847.
- ¹⁸⁸ MacDonald, J. P.; Sidera, M.; Fletcher, S. P.; Shaver, M. P. Living and immortal polymerization of seven and six membered lactones to high molecular weights with aluminum salen and salan catalysts. *Eur. Polym. J.*, **2016**, *74*, 287-295.
- ¹⁸⁹ Kakde, D.; Taresco, V.; Bansal, K. K.; Magennis, E. P.; Howdle, S. M.; Mantovani, G.; Irvine, D. J.; Alexander, C. Amphiphilic block copolymers from renewable ϵ -decalactone monomer: prediction and characterization of micellar core effects on drug encapsulation and release. *J. Mater. Chem. B*, **2016**, *4*, 7119-7129.
- ¹⁹⁰ Olsén, P.; Borke, T.; Odelius, K.; Albertsson, A.-C. ϵ -Decalactone: A thermoresilient and toughening comonomer to poly(L-Lactide). *Biomacromolecules*, **2013**, *14*, 2883-2980.
- ¹⁹¹ Lee, S.; Lee, K.; Kim, Y.-W.; Shin, J. Preparation and characterization of a renewable pressure-sensitive adhesive system derived from ϵ -decalactone, L-lactide, epoxidized soybean oil, and rosin ester. *ACS Sustainable Chem. Eng.*, **2015**, *3*, 2309-2320.
- ¹⁹² Van der Mee, L.; Helmich, F.; de Bruijn, R.; Vekemans, J. A. J. M.; Palmans, A. R. A.; Meijer, E. W. Investigation of lipase-catalyzed ring-opening polymerizations of lactones with various ring sizes: Kinetic evaluation. *Macromolecules* **2006**, *39*, 5021-5027.
- ¹⁹³ Van der Meulen, I.; Gubbels, E.; Huijser, S.; Sablong, R.; Koning, C. E.; Heise, A.; Duchateau, R. Catalytic ring-opening polymerization of renewable macrolactones to high molecular weight polyethylene-like polymers. *Macromolecules*, **2011**, *44*, 4301-4305.
- ¹⁹⁴ Tinajero-Díaz, E.; Martínez de Ilarduya, A.; Muñoz-Guerra, S. Block and graft copolymers made of 16-membered macrolactones and L-alanine: A comparative study. *Macromol. Chem. Phys.* **2019**, *220*, 1900214.
- ¹⁹⁵ Wilson, J. A.; Ates, Z.; Pflughaupt, R. L.; Dove, A. P.; Heise, A. Polymers from macrolactones: From pheromones to functional materials. *Prog. Polym. Sci.* **2019**, *91*, 29-50.
- ¹⁹⁶ Jung, M. E.; Piizzi, G. gem-Disubstituent effect: Theoretical basis and synthetic applications. *Chem. Rev.*, **2005**, *105*, 1735-1766.
- ¹⁹⁷ Hillmyer, M. A.; Tolman, W. B. Aliphatic polyester block polymers: Renewable, degradable, and sustainable. *Acc. Chem. Res.*, **2014**, *47*, 2390-2396.
- ¹⁹⁸ Kiesewetter, M. K.; Shin, E. J.; Hedrick, J. L.; Waymouth, R. M. Organocatalysis: Opportunities and challenges for polymer synthesis. *Macromolecules* **2010**, *43*, 2093-2107.
- ¹⁹⁹ Stridsberg, K. M.; Ryner, M.; Albertsson, A.-C. Controlled ring-opening polymerization: Polymers with designed macromolecular architecture. *Adv. Polym. Sci.*, **2002**, *157*, 41-65.
- ²⁰⁰ Löfgren, A.; Albertsson, A.-C. Recent advances in ring-opening polymerization of lactones and related compounds. *J. M. C. Rev. Macromol. Chem. Phys.*, **1995**, *C35(3)*, 379-418.
- ²⁰¹ Albertsson, A.-C.; Palmgren, R. Cationic polymerization of 1,5-dioxepan-2-one with Lewis acids in bulk and in solution. *J. Macromol. Chem., Pure Appl. Chem. A33*, **1996**, *6*, 747-758.
- ²⁰² Hofman, A.; Szymański, R.; Slomkowski, S.; Penczek, S. Structure of active species in the cationic polymerization of β -propiolactone and ϵ -caprolactone. *Makromol. Chem.*, **1984**, *185*, 655-667.
- ²⁰³ Shibasaki, Y.; Sanada, H.; Yokoi, M.; Sanda, F.; Endo, T. Activated monomer cationic polymerization of lactones and the application to well-defined block copolymer synthesis with seven-membered cyclic carbonate. *Macromolecules* **2000**, *33*, 4316-4320.

- ²⁰⁴ Kim, M. S.; Seo, K. S.; Khang, G.; Lee, H. B. Ring-opening polymerization of ϵ -caprolactone by poly(ethylene glycol) by an activated monomer mechanism. *Macromol. Rapid Commun.*, **2005**, *26*, 643-648.
- ²⁰⁵ Ouhadi, T.; Stevens, C.; Teyssié, P. Mechanism of ϵ -caprolactone polymerization by aluminum alkoxides. *Makromol. Chem.*, **1975**, *1*, 191-201.
- ²⁰⁶ Tang, D.; Macosko, C. W.; Hillmyer, M. A. Thermoplastic polyurethane elastomers from bio-based poly(δ -decalactone) diols. *Polym. Chem.* **2014**, *5*, 3231-3237.
- ²⁰⁷ Ferrari, R.; Agostini, A.; Brunel, L.; Morosi, L.; Moscatelli, D. Self-assembling amphiphilic block copolymer from renewable δ -decalactone and δ -dodecalactone. *J. Polym. Sci. A Polym. Chem.* **2017**, *55*, 3788-3797.
- ²⁰⁸ Bandelli, D.; Helbing, C.; Weber, C.; Seifert, M.; Muljajew, I.; Jandt, K. D.; Schubert, U. S. Maintaining the hydrophilic – hydrophobic balance of polyesters with adjustable crystallinity for tailor-made nanoparticles. *Macromolecules* **2018**, *51*, 5567-5576.
- ²⁰⁹ Kazakov, O. I.; Datta, P. P.; Isajani, M.; Kiesewetter, E. T.; Kiesewetter, M. K. Cooperative hydrogen-bond pairing in organocatalytic ring-opening polymerization. *Macromolecules* **2014**, *47*, 7463-7468.
- ²¹⁰ Pratt, R. C.; Lohmeijer, B. G. G.; Long, D. A.; Waymouth, R. M.; Hedrick, J. L. Triazabicyclodecene: A simple bifunctional organocatalyst for acyl transfer and ring-opening polymerization of cyclic esters. *J. Am. Chem. Soc.* **2006**, *128*, 4556-4557.
- ²¹¹ Kamber, N. E.; Jeong, W.; Waymouth, R. M.; Pratt, R. C.; Lohmeijer, B. G. G.; Hedrick, J. L. Organocatalytic ring-opening polymerization. *Chem. Rev.* **2007**, *107*, 5813-5840.
- ²¹² Kiesewetter, M. K.; Scholten, M. D.; Kirn, N.; Weber, R. L.; Hedrick, J. L.; Waymouth, R. M. Cyclic guanidine organic catalyst: What is magic about triazabicyclodecene? *J. Org. Chem.* **2009**, *74*, 9490-9496.
- ²¹³ Thomas, C.; Bibal, B. Hydrogen-bonding organocatalysts for ring-opening polymerization. *Green Chem.* **2014**, *16*, 1687-1699.
- ²¹⁴ Ruiz-Cantu, L. A.; Pearce, A. K.; Burroughs, L.; Bennett, T. M.; Vasey, C. E.; Wildman, R.; Irvine, D. J.; Alexander, C.; Taresco, V. Synthesis of methacrylate-terminated block copolymers with reduced transesterification by controlled ring-opening polymerization. *Macromol. Chem. Phys.* **2019**, *220*, 1800459.
- ²¹⁵ Lohmeijer, B. G. G.; Pratt, R. C.; Leibfarth, F.; Logan, J. W.; Long, D. A.; Dove, A. P.; Nederberg, F.; Choi, J.; Wade, C.; Waymouth, R. M.; Hedrick, J. L. Guanidine and amidine organocatalysts for ring-opening polymerization of cyclic esters. *Macromolecules*, **2006**, *39*, 8574-8583.
- ²¹⁶ Simón, L.; Goodman, J. M. The mechanism of TBD-catalyzed ring-opening polymerization of cyclic esters. *J. Org. Chem.* **2007**, *72*, 9656-9662.
- ²¹⁷ Chuma, A.; Horn, H. W.; Swope, W. C.; Pratt, R. C.; Zhang, L.; Lohmeijer, B. G. G.; Wade, C. G.; Waymouth, R. M.; Hedrick, J. L.; Rice, J. E. The reaction mechanism for the organocatalytic ring-opening polymerization of L-lactide using a guanidine-based catalyst: Hydrogen-bonded or covalently bond? *J. Am. Chem. Soc.* **2008**, *130*, 6749-6754.
- ²¹⁸ Pechmann, H. V.; Röhm, O. Über α -methylen-glutarsäure, ein polymerisationsproduct der acrylsäure. *Berichte der Deutschen Chemischen Gesellschaft* **1901**, *34*, 427-429.
- ²¹⁹ Bauer, W. Processes of producing acrylic acid esters. *US Patent* US 1,829,208, **1931**.
- ²²⁰ Röhm, O.; Bauer, W. Glasersatz. *German Patent*, DE 724,229, **1932**.
- ²²¹ Hill, R. Manufacture of new polymerization products. *US Patent* US 2,117,321, **1938**.
- ²²² Röhm, O.; Bauer, W. Glass substitute and process of preparing. *US Patent* US 2,193,742, **1940**.

- ²²³ Reppe, W. Über die umsetzung von acetylene mit kohlenoxyd und verbindungen mit reaktionsfähigen wasserstoffatomen synthesen α,β -ungesättigter carbonsäuren und ihrer derivate. *Justus Liebigs Annalen der Chemie* **1953**, 582, 1-6.
- ²²⁴ Penzel, E.; Ballard, N.; Asua, J. M. Polyacrylates. *Ullmann's Encyclopedia of Industrial Chemistry*, **2018** (Wiley-VCH), Weinheim, ISBN 978-3-527-30673-2.
- ²²⁵ Albrecht, K.; Stickler, M.; Rhein, T. Polymethacrylates. *Ullmann's Encyclopedia of Industrial Chemistry*, **2013** (Wiley-VCH), Weinheim, ISBN 978-3-527-30673-2.
- ²²⁶ Saunders, K. J. Acrylic polymers. *Organic polymer chemistry*. Ed. Springer, **1988**, p. 125-148.
- ²²⁷ Zagala, A. P.; Hogen-Esch, T. E. Living anionic polymerization of methyl methacrylate at ambient temperatures in the presence of the tetraphenylphosphonium cation. *Macromolecules* **1996**, 29, 3038-3039.
- ²²⁸ Broska, D.; Fieberg, A.; Bandermann, F. Metal-free anionic polymerization of *n*-butyl acrylate. *Des. Monomers Polym.* **1998**, 1, 37-45.
- ²²⁹ Fernández-García, M.; Fernández-Sanz, M.; López Madruga, E. A kinetic study of butyl acrylate free radical polymerization in benzene solution. *Macromol. Chem. Phys.* **2000**, 201, 1840-1845.
- ²³⁰ Kumar, M. D.; Thehazhnan, P. K.; Umapathy, M. J.; Rajendran, M. Free radical polymerization of methyl methacrylate in the presence of phase transfer catalyst – A kinetic study. *Int. J. Polym. Mater.* **2004**, 53, 95-103.
- ²³¹ Kitaura, T.; Kitayama, T. Anionic polymerization of methyl methacrylate by difunctional lithium amide initiators with trialkylsilyl protection. *Polym. J.* **2013**, 45, 1013-1018.
- ²³² Stickler, M.; Meyerhoff, G. Polymerisation in substanz. *Makromol. Chem.* **1978**, 179, 2729-2745.
- ²³³ Moad, G.; Solomon, D.; *The chemistry of radical polymerization*, 2nd Ed., Elsevier, Oxford, **2006**.
- ²³⁴ Nesvadba, P.; Radical polymerization in industry. *Encyclopedia of Radicals in Chemistry, Biology and Materials*. Wiley & Sons, **2012**.
- ²³⁵ Yoganand, K. S.; Vidhya, K. R.; Umapathy, M. J. Phase transfer catalyst-induced free radical polymerization of acrylonitrile using water soluble initiator – A kinetic study. *Int. J. Polym. Mater.* **2009**, 58, 355-365.
- ²³⁶ Greszta, D.; Mardare, D.; Matyjaszewski, K. "Living" radical polymerization. 1. Possibilities and limitations. *Macromolecules*, **1994**, 27, 638-644.
- ²³⁷ Matyjaszewski, K Fundamentals of controlled/living radical polymerization. *Encyclopedia of Radicals in Chemistry, Biology and Materials*. Wiley & Sons, **2012**.
- ²³⁸ Fischer, H. The persistent radical effect: A principle for selective radical reactions and living radical polymerizations. *Chem. Rev.*, **2001**, 101, 3581-3610.
- ²³⁹ Moad, G.; Rizzardo, E.; Thang, S. H. Radical addition-fragmentation chemistry in polymer synthesis. *Polymer*, **2008**, 49, 1079-1131.
- ²⁴⁰ Nicolas, J.; Guillaneuf, Y.; Lefay, C.; Bertin, D.; Gimes, D.; Charleux, B. Nitroxide-mediated polymerization. *Prog. Polym. Sci.*, **2013**, 38, 63-235.
- ²⁴¹ Matyjaszewski, K. Atom transfer radical polymerization (ATRP): Current status and future prespectives. *Macromolecules*, **2012**, 45, 4015-4039.
- ²⁴² Palmiero, U. C.; Sponchioni, M.; Manfredini, N.; Maraldi, M.; Moscatelli, D. Strategies to combine ROP with ATRP or RAFT polymerization for the synthesis of biodegradable polymeric nanoparticles for biomedical applications. *Polym. Chem.*, **2018**, 9, 4084-4099.

- ²⁴³ Xue, L.; Agarwal, U. S.; Lemstra, P. J. High molecular weight PMMA by ATRP. *Macromolecules*, **2002**, *35*, 8650-8652.
- ²⁴⁴ Matyjaszewski, K. Controlled/living radical polymerization: State of the art in 2002. *Advances in controlled/living radical polymerization*. **2003**, Chapter 1, 2-9.
- ²⁴⁵ Plichta, A.; Kowalczyk, S.; Kamiński, K.; Wasylęczo, M.; Więckowski, S.; Olędzka, E.; Nałęcz-Jawecki, G.; Zgadzaj, A.; Sobczak, M. ATRP of methacrylic derivative of camptothecin initiated with PLA toward three-arm star block copolymer conjugates with favourable drug release. *Macromolecules*, **2017**, *50*, 6439-6450.
- ²⁴⁶ Kharasch, M. S.; Jensen, E. V.; Urry, W. H. Addition of carbon tetrachloride and chloroform to olefins. *Science*, **1945**, *102*, 128.
- ²⁴⁷ Minisci, F. Free-radical additions to olefins in the presence of redox systems. *Acc. Chem. Res.*, **1975**, *8*, 165-171.
- ²⁴⁸ Ribelli, T. G.; Lorandi, F.; Fantin, M.; Matyjaszewski, K. Atom transfer radical polymerization: Billion times more active catalyst and new initiation systems. *Macromol. Rapid Commun.*, **2019**, *40*, 1800616.
- ²⁴⁹ Wang, J.-S.; Matyjaszewski, K. Controlled/"living" radical polymerization. Atom transfer radical polymerization in the presence of transition-metal complexes. *J. Am. Chem. Soc.*, **1995**, *117*, 5614-5615.
- ²⁵⁰ Wang, J.-H.; Matyjaszewski, K. Controlled/"living" radical polymerization. Halogen atom transfer radical polymerization promoted by Cu(I)/Cu(II) redox process. *Macromolecules*, **1995**, *28*, 7901-7910.
- ²⁵¹ Percec, V.; Barboiu, B. "Living" radical polymerization of styrene initiated by arenesulfonyl chlorides and Cu^I(bpy)_nCl. *Macromolecules*, **1995**, *28*, 7970-7972.
- ²⁵² Grimaud, T.; Matyjaszewski, K. Controlled/"living" radical polymerization of methyl methacrylate by atom transfer radical polymerization. *Macromolecules*, **1997**, *30*, 2216-2218.
- ²⁵³ Tsarevsky, N. V.; Braunecker, W. A.; Matyjaszewski, K. Electron transfer reactions relevant to atom transfer radical polymerization. *J. Organomet. Chem.*, **2007**, *692*, 3212-3222.
- ²⁵⁴ Matyjaszewski, K.; Paik, H.-J.; Zhou, P.; Diamanti, S. J. Determination of activation and deactivation rate constants of model compounds in atom transfer radical polymerization. *Macromolecules*, **2001**, *34*, 5125-5131.
- ²⁵⁵ Perrier, S.; Haddleton, D. M. In situ NMR monitoring of living radical polymerization. *Reaction kinetics and catalyst evolution*. Springer, **2003**.
- ²⁵⁶ Mastan, E.; Zhu, S. A straightforward estimation of activation and deactivation parameters for ATRP systems from actual polymerization rate and molecular weight distribution data. *Macromol. Theory Simul.*, **2017**, *26*, 1600045.
- ²⁵⁷ Tang, W.; Kwak, Y.; Braunecker, W.; Tsarevsky, N. V.; Coote, M. L.; Matyjaszewski, K. Understanding atom transfer radical polymerization: Effect on ligand and initiator structures on the equilibrium constants. *J. Am. Chem. Soc.*, **2008**, *130*, 10702-10713.
- ²⁵⁸ Braunecker, W. A.; Tsarevsky, N. V.; Gennaro, A.; Matyjaszewski, K. Thermodynamic components of the atom transfer radical polymerization equilibrium: Quantifying solvent effects. *Macromolecules*, **2009**, *42*, 6348-6360.
- ²⁵⁹ Zhao, J.; Weng, Y.; Xie, D. Star-shape poly(acrylic acid)-composed glass-ionomer cements: Effect on MW and arm number on mechanical properties. *J. Appl. Polym. Sci.*, **2011**, *120*, 2390-2399.

- ²⁶⁰ Li, M.; Jahed, N. M.; Min, K.; Matyjaszewski, K. Preparation of linear and star-shaped block copolymers by ATRP using simultaneous reverse and normal initiation process in bulk and miniemulsion. *Macromolecules*, **2004**, *37*, 2434-2441.
- ²⁶¹ Jiang, J.; Zhang, Y.; Guo, X.; Zhang, H. Ambient temperature synthesis of narrow or monodisperse, highly crosslinked, and "living" polymer microspheres by atom transfer radical precipitation polymerization. *RSC Adv.*, **2012**, *2*, 5651-5662.
- ²⁶² Rusen, E.; Mocanu, A. Atom transfer radical emulsion polymerization (emulsion ATRP) of styrene with water-soluble initiator. *Colloid Polym. Sci.*, **2013**, *291*, 2253-2257.
- ²⁶³ Pintauer, T.; McKenzie, B.; Matyjaszewski, K. Toward structural and mechanistic understanding of transition metal-catalyzed atom transfer radical process. *ACS Symp. Ser.* **2003**, *854*, 130-147.
- ²⁶⁴ Braunecker, W. A.; Matyjaszewski, K. Recent mechanistic developments in atom transfer radical polymerization. *J. Mol. Catal. A Chem.* **2006**, *254*, 155-164.
- ²⁶⁵ Lin, C. Y.; Coote, M. L.; Gennaro, A.; Matyjaszewski, K. Ab Initio evaluation of the thermodynamics and electrochemical properties of alkyl halides and radicals and their mechanistic implications for atom transfer radical polymerization. *J. Am. Chem. Soc.*, **2008**, *130*, 12762-12774.
- ²⁶⁶ Matyjaszewski, K. Radical nature of Cu-catalyzed controlled radical polymerizations (Atom transfer radical polymerization). *Macromolecules*, **1998**, *31*, 4710-4717.
- ²⁶⁷ Tang, H.; Arulsamy, N.; Radosz, M.; Shen, Y.; Tsarevsky, N. V.; Braunecker, W. A.; Tang, W.; Matyjaszewski, K. Highly active copper-based catalyst for atom transfer radical polymerization. *J. Am. Chem. Soc.*, **2006**, *128*, 16277-16285.
- ²⁶⁸ Schroeder, H.; Yalalov, D.; Buback, M.; Matyjaszewski, K. Activation-deactivation equilibrium associated with iron-mediated atom transfer radical polymerization up to high pressure. *Macromol. Chem. Phys.*, **2012**, *213*, 2019-2026.
- ²⁶⁹ Wang, Y.; Kwak, Y.; Matyjaszewski, K. Enhanced activity of ATRP Fe catalyst with phosphines containing electron donating groups. *Macromolecules*, **2012**, *45*, 5911-5915.
- ²⁷⁰ Xue, Z.; Noh, S. K. Iron catalyzed atom transfer radical polymerization of methyl methacrylate using diphenyl-2-pyridylphosphine as ligand. *Macromol. Res.*, **2007**, *15*, 302-307.
- ²⁷¹ Johnson, R.; Corbin, P. S.; Ng, C.; Fraser, C. L. Poly(methyl methacrylate) with ruthenium tris(bipyridine) cores via NiBr(PR₃)₂-catalyzed atom transfer radical polymerization (ATRP). *Macromolecules*, **2000**, *33*, 7404-7412.
- ²⁷² Matyjaszewski, K. Atom transfer radical polymerization. *Chem. Rev.*, **2001**, *101*, 2921-2990.
- ²⁷³ Matyjaszewski, K. Controlled/"living" radical polymerization of styrene and methyl methacrylate catalyzed by iron complexes. *Macromolecules*, **1997**, *30*, 8161-8164.
- ²⁷⁴ Matyjaszewski, K.; Göbelt, B.; Paik, H.-j.; Horwitz, C. P. Tridentate nitrogen-based ligands in Cu-based ATRP: A structure-activity study. *Macromolecules*, **2001**, *34*, 430-440.
- ²⁷⁵ Singha, N. K.; Klumperman, B. Atom-transfer radical polymerization of methyl methacrylate (MMA) using CuSCN as the catalyst. *Macromol. Rapid Commun.*, **2000**, *21*, 1116-1120.
- ²⁷⁶ Kwak, Y.; Matyjaszewski, K. Effect on initiator and ligand structures in ATRP of styrene and methyl methacrylate initiated by alkyl dithiocarbamate. *Macromolecules*, **2008**, *41*, 6627-6635.
- ²⁷⁷ Tang, W.; Matyjaszewski, K. Effects of initiator structure on activation rate constants in ATRP. *Macromolecules*, **2007**, *40*, 1858-1863.
- ²⁷⁸ Lanzalaco, S.; Fantin, M.; Scialdone, O.; Galia, A.; Isse, A. A.; Gennaro, A.; Matyjaszewski, K. Atom transfer radical polymerization with different halides (F, Cl, Br, and I): Is the process "living" in the presence of fluorinated initiators? *Macromolecules*, **2017**, *50*, 192-202.

- ²⁷⁹ Shipp, D. A.; Matyjaszewski, K. Kinetic analysis of controlled/"living" radical polymerizations by simulations. 2. Apparent external orders of reactants in atom transfer radical polymerization. *Macromolecules* **2000**, *33*, 1553-1559.
- ²⁸⁰ Magenau, A. J. D.; Kwak, Y.; Matyjaszewski, K. ATRP of methacrylates using Cu^{II}X₂/L and copper wire. *Macromolecules*, **2010**, *43*, 9682-9689.
- ²⁸¹ Matyjaszewski, K.; Wang, J.-L.; Grimaud, T.; Shipp, D. A. Controlled/"living" atom transfer radical polymerization of methyl methacrylate using various initiation systems. *Macromolecules*, **1998**, *31*, 1527-1534.
- ²⁸² Karanam, S.; Goossens, H.; Klumperman, B.; Lemstra, P. "Controlled" synthesis and characterization of model methyl methacrylate/*tert*-butyl methacrylate triblock copolymers. *Macromolecules*, **2003**, *36*, 3051-3060.
- ²⁸³ Nanda, A. K.; Matyjaszewski, K. Effect of penultimate unit on the activation process in ATRP. *Macromolecules* **2003**, *36*, 8222-8224.
- ²⁸⁴ Bougard, F.; Jeusette, M.; Mespouille, L.; Dubois, P.; Lazzaroni, R. Synthesis and supramolecular organization of amphiphilic diblock copolymers combining poly(*N,N*-dimethylamino-2-ethyl methacrylate) and poly(ϵ -caprolactone). *Langmuir*, **2007**, *23*, 2339-2345.
- ²⁸⁵ Yuan, L.; Chen, W.; Li, J.; Hu, J.; Yan, J.; Yang, D. PEG-*b*-PtBA-*b*-PHEMA well-defined amphiphilic triblock copolymer: Synthesis, self-assembly, and application in drug delivery. *J. Polym. Sci.*, **2012**, *50*, 4579-4588.
- ²⁸⁶ Garcia, M.; Beecham, M. P.; Kempe, K.; Haddleton, D. M.; Khan, A.; Marsh, A. Water soluble triblock and pentablock poly(methacryloyl nucleosides) from copper-mediated living radical polymerisation using PEG macroinitiators. *Eur. Polym. J.*, **2015**, *66*, 444-451.
- ²⁸⁷ Matyjaszewski, K.; Shipp, D. A.; Wang, J.-L.; Grimaud, T.; Patten, T. E. Utilizing halide exchange to improve control of atom transfer radical polymerization. *Macromolecules*, **1998**, *31*, 6836-6840.
- ²⁸⁸ Peng, C.-H.; Kong, J.; Seeliger, F.; Matyjaszewski, K. Mechanism of halogen exchange in ATRP. *Macromolecules*, **2011**, *44*, 7546-7557.
- ²⁸⁹ Shipp, D. A.; Wang, J.-L.; Matyjaszewski, K. Synthesis of acrylate and methacrylate block copolymers using atom transfer radical polymerization. *Macromolecules*, **1998**, *31*, 8005-8008.
- ²⁹⁰ Braunecker, W. A.; Matyjaszewski, K. Controlled/living radical polymerization: Features, developments, and perspectives. *Prog. Polym. Sci.*, **2007**, *32*, 93-146.
- ²⁹¹ Xia, J.; Matyjaszewski, K. Controlled/"living" radical polymerization. Atom transfer radical polymerization catalyzed by copper(I) and picolylamine complexes. *Macromolecules*, **1999**, *32*, 2434-2437.
- ²⁹² De La Fuente, J. L.; Cañamero, P. F.; Fernández-García, M. Synthesis and characterization of glycidyl methacrylate/butyl acrylate copolymers obtained at low temperature by atom transfer radical polymerization. *J. Polym. Sci. A. Polym. Chem.*, **2005**, *44*, 1807-1816.
- ²⁹³ Pascual, S.; Coutin, B.; Tardi, M.; Polton, A.; Vairon, J.-P. Homogeneous atom transfer radical polymerization of styrene initiated by 1-chloro-1-phenylethane/copper(I) chloride/bipyridine in the presence of dimethylformamide. *Macromolecules*, **1999**, *32*, 1432-1437.
- ²⁹⁴ Patten, T. E.; Matyjaszewski, K. Atom transfer radical polymerization and the synthesis of polymeric materials. *Adv. Mater.*, **1998**, *10*, 901-915.
- ²⁹⁵ Horn, M.; Matyjaszewski, K. Solvent effects on the activation rate constant in atom transfer radical polymerization. *Macromolecules*, **2013**, *46*, 3350-3357.

- ²⁹⁶ Lorandi, F.; Fantin, M.; Isse, A. A.; Gennaro, A.; Matyjaszewski, K. New protocol to determine the equilibrium constant of atom transfer radical polymerization. *Electrochim. Acta*, **2018**, 260, 648-655.
- ²⁹⁷ Zhong, M.; Matyjaszewski, K. How fast can a CRP be conducted with preserved chain end functionality? *Macromolecules*, **2011**, 44, 2668-2677.
- ²⁹⁸ Li, W.; Yoon, J. A.; Zhong, M.; Matyjaszewski, K. Atom transfer radical copolymerization of monomer and cross-linker under highly dilute conditions. *Macromolecules*, **2011**, 44, 3270-3275.
- ²⁹⁹ Matyjaszewski, K. Inner and outer sphere electron transfer reactions in atom transfer radical polymerization. *Macromol. Symp.*, **1998**, 134, 105-118.
- ³⁰⁰ Wang, J.-S.; Matyjaszewski, K. "Living"/controlled radical polymerization. Transition-metal-catalyzed atom transfer radical polymerization in the presence of a conventional radical initiation. *Macromolecules*, **1995**, 28, 7572-7573.
- ³⁰¹ Xia, J.; Matyjaszewski, K. Controlled/"living" radical polymerization. Homogeneous reverse atom transfer radical polymerization using AIBN as the initiator. *Macromolecules*, **1997**, 30, 7692-7696.
- ³⁰² Gromada, J.; Matyjaszewski, K. Simultaneous reverse and normal initiation in atom transfer radical polymerization. *Macromolecules*, **2001**, 34, 7664-7671.
- ³⁰³ Kryszewski, P.; Schroeder, H.; Buback, J.; Buback, M.; Matyjaszewski, K. The borderline between simultaneous reverse and normal initiation and initiators for continuous activator regeneration ATRP. *Macromolecules*, **2016**, 49, 7793-7803.
- ³⁰⁴ Jakubowski, W.; Min, K.; Matyjaszewski, K. Activators regenerated by electron transfer for atom transfer radical polymerization of styrene. *Macromolecules*, **2006**, 39, 39-45.
- ³⁰⁵ Min, K.; Gao, H.; Matyjaszewski, K. Development of an ab initio emulsion atom transfer radical polymerization: From microemulsion to emulsion. *J. Am. Chem. Soc.*, **2006**, 128, 10521-10526.
- ³⁰⁶ Matyjaszewski, K.; Jakubowski, W.; Min, K.; Tang, W.; Huang, J.; Braunecker, W. A.; Tsarevsky, N. V. Diminishing catalyst concentration in atom transfer radical polymerization with reducing agents. *Proc. Natl. Acad. Sci. USA*, **2006**, 103, 15309-15314.
- ³⁰⁷ Matyjaszewski, K. Advanced materials by atom transfer radical polymerization. *Adv. Mater.*, **2018**, 30, 1706441.
- ³⁰⁸ Wang, Y.; Soerensen, N.; Zhong, M.; Schroeder, H.; Buback, M.; Matyjaszewski, K. Improving the "livingness" of ATRP by reducing Cu catalyst concentration. *Macromolecules*, **2013**, 46, 683-691.
- ³⁰⁹ Williams, V. A.; Ribelli, T. G.; Chmielarz, P.; Park, S.; Matyjaszewski, K. A silver bullet: Elemental silver as an efficient reducing agent for atom transfer radical polymerization of acrylates. *J. Am. Chem. Soc.* **2015**, 137, 1428-1431.
- ³¹⁰ Matyjaszewski, K.; Coca, S.; Gaynor, S. G.; Wei, M.; Woodworth, B. E. Zerovalent metals in controlled/"living" radical polymerization. *Macromolecules*, **1997**, 30, 7348-7350.
- ³¹¹ Pan, X.; Fantin, M.; Yuan, F.; Matyjaszewski, K. Externally controlled atom transfer radical polymerization. *Chem. Soc. Rev.*, **2018**, 47, 5457-5790.
- ³¹² Fantin, M.; Lorandi, F.; Gennaro, A.; Isse, A. A.; Matyjaszewski, K. Electron transfer reactions in atom transfer radical polymerization. *Synthesis*, **2017**, 49, A-L.
- ³¹³ Percec, V.; Guliyashvili, T.; Ladislav, J. S.; Wistrand, A.; Stjerndahl, A.; Sienkowska, M. J.; Monteiro, M. J.; Sahoo, S. Ultrafast synthesis of ultrahigh molar mass polymers by metal-

catalyzed living radical polymerization of acrylates, methacrylates, and vinyl chloride mediated by SET at 25 °C. *J. Am. Chem. Soc.*, **2006**, 128, 14156-14165.

³¹⁴ Fleischmann, S.; Percec, V.; SET-LRP of methyl methacrylate initiated with sulfonyl halides. *J. Polym. Sci. A. Polym. Chem.*, **2010**, 48, 2236-2242.

³¹⁵ Konkolewicz, D.; Wang, Y.; Krys, P.; Zhong, M.; Isse, A. A.; Gennaro, A.; Matyjaszewski, K. SARA ATRP or SET-LRP. End of controversy? *Polym. Chem.*, **2014**, 5, 4396-4417.

³¹⁶ Konkolewicz, D.; Krys, P.; Góis, J. R.; Mendonça, P. V.; Zhong, M.; Wang, Y.; Gennaro, A.; Isse, A. A.; Fantin, M.; Matyjaszewski, K. Aqueous RDRP in the presence of Cu⁰: The exceptional activity of Cu^I confirms the SARA ATRP mechanism. *Macromolecules* **2014**, 47, 560-570.

³¹⁷ Lorandi, F.; Fantin, M.; Isse, A. A.; Gennaro, A. RDRP in the presence of Cu⁰: The fate of Cu(I) proves the inconsistency of SET-LRP mechanism. *Polymer*, **2015**, 72, 238-245.

³¹⁸ Rosen, B.; Jiang, X.; Wilson, C. J.; Nguyen, N. H.; Monteiro, M. J.; Percec, V. The disproportionation of Cu(I)X mediated by ligand and solvent into Cu(0) and Cu(II)X₂ and its implications for SET-LRP. *J. Polym. Sci. A. Polym. Chem.*, **2009**, 47, 5606-5628.

³¹⁹ Akkapeddi, M. K. The free radical copolymerization characteristics of α -methylene- γ -butyrolactone. *Polymer* **1979**, 20, 1215-1216.

³²⁰ Ueda, M.; Takahashi, M.; Imai, Y.; Pittman Jr., C. U. Radical-initiated homo- and copolymerization of α -methylene- γ -butyrolactone. *J. Polym. Sci., Polym. Chem. Ed.* **1982**, 20, 2819-2828.

³²¹ Ueda, M.; Takahashi, M.; Imai, Y.; Pittman, Jr. C. U. Synthesis and homopolymerization kinetics of α -methylene- δ -valerolactone, an exo-methylene cyclic monomer with a nonplanar ring system spanning the radical center. *Macromolecules* **1983**, 16, 1300-1305.

³²² Pittman Jr., C. U.; Lee, H. Radical-initiated polymerization of β -methyl- α -methylene- γ -butyrolactone. *J. Polym. Sci., Polym. Chem.* **2003**, 41, 1759-1777.

³²³ Stansbury, J. W.; Antonucci, J. M. Evaluation of methylene lactone monomers in dental resins. *Dent. Mater.* **1992**, 8, 270-273.

³²⁴ Brandenburg, C.; Butler, E. P.; Erkenbrecher, C.; King, R.; Hutchins, C.; Puts, R. D. Alpha-methylene lactone homopolymer and copolymer compositions, sheets and articles made therefrom and the process for their manufacture. *US Patent* US 2003/0130414 A1, **2003**.

³²⁵ Higaki, Y.; Okazaki, R.; Takahara, A. Semirigid biobased polymer brush: Poly(α -methylene- γ -butyrolactone) brushes. *ACS Macro. Lett.* **2012**, 1, 1124-1127.

³²⁶ Trotta, J. T.; Watts, A.; Wong, A. R.; LaPointe, A. M.; Hillmyer, M. A.; Fors, B. P. Renewable thermosets and thermoplastics from itaconic acid. *ACS Sustainable Chem. Eng.* **2019**, 7, 2691-2701.

³²⁷ Wang, D.; Green, M. D.; Chen, K.; Daengngam, C.; Kotsuchibashi, Y. Stimuli-responsive polymers: Design, synthesis, characterization, and applications. *Int. J. Polym. Sci.* **2016**, Editorial.

³²⁸ Wei, M.; Gao, Y.; Li, X.; Serpe, M. J. Stimuli-responsive polymers and their applications. *Polym. Chem.* **2017**, 8, 127-143.

³²⁹ Dai, S.; Ravi, P.; Tam, K. C. pH-responsive polymers: synthesis, properties and applications. *Soft Matter* **2008**, 4, 435-449.

³³⁰ Medeiros, S. F.; Santos, A. M.; Fessi, H.; Elaissari, A. Stimuli-responsive magnetic particles for biomedical applications. *Int. J. Pharm.* **2011**, 403, 139-161.

³³¹ Seidi, F.; Jenjob, R.; Crespy, D. Designing smart polymers conjugates for controlled release of payloads. *Chem. Rev.* **2018**, 118, 3965-4036.

³³² Traitel, T.; Goldbart, R.; Kost, J. Smart polymers for responsive drug-delivery systems. *J. Biomater. Sci. Polym. Ed.* **2008**, 19, 755-767.

- ³³³ Colson, Y. L.; Grinstaff, M. W. Biologically responsive polymeric nanoparticles for drug delivery. *Adv. Mater.* **2012**, *24*, 3878-3886.
- ³³⁴ Francis, R.; Joy, N.; Sivadas, A.; Gopalan, G. P.; Baby, D. K. Chapter 9 Stimuli-responsive polymers: Biomedical applications. *Biomedical Applications of Polymeric Materials and Composites* 5th Ed. Wiley-VCH, **2017**.
- ³³⁵ Ma, Y.; Promthaveepong, K.; Li, N. CO₂-responsive polymer-functionalized Au nanoparticles for CO₂ sensor. *Anal. Chem.* **2016**, *88*, 8289-8293.
- ³³⁶ Wang, Z.; Tsarevsky, N. V. Well-defined polymers containing a single mid-chain viologen group: synthesis, environment-sensitive fluorescence, and redox activity. *Polym. Chem.* **2016**, *7*, 4402-4410.
- ³³⁷ Martin, R. T.; Camargo, L. P.; Miller, S. A. Marine-degradable polylactic acid. *Green Chem.* **2014**, *16*, 1768-1773.
- ³³⁸ Tachibana, Y.; Baba, T.; Kasuya, K.-i. Environmental biodegradation control of polymers by cleavage of disulfide bonds. *Polym. Degrad. Stab.* **2017**, *137*, 67-74.
- ³³⁹ Zhai, L. Stimuli-responsive polymer films. *Chem. Soc. Rev.* **2013**, *42*, 7148-7160.
- ³⁴⁰ Del Pezzo, R.; Bandeira, N. A. G.; Trojanowska, A.; Fernandez Prieto, S.; Underiner, T.; Giamberini, M.; Tylkowski, B. Ortho-substituted azobenzene: shedding light on new benefits. *Pure Appl. Chem.* **2019**, *91*, 1533-1546.
- ³⁴¹ Davis, D. A.; Hamilton, A.; Yang, J.; Creumar, L. D.; Van Gough, D.; Potisek, S. L.; Ong, M. T.; Braun, P. V. Martínez, T. J.; White, S. R.; Moore, J. S.; Sottos, N. R. Force-induced activation of covalent bonds in mechanoresponsive polymeric materials. *Nature* **2009**, *459*, 68-72.
- ³⁴² Johnson, J. A.; Lewis, D. R.; Díaz, D. D.; Finn, M. G.; Koberstein, J. T.; Turro, N. J. Synthesis of degradable model networks via ATRP and click chemistry. *J. Am. Chem. Soc.* **2006**, *128*, 6564-6565.
- ³⁴³ Liu, Y.; Cavicchi, K. A. Reversible addition fragmentation chain transfer (RAFT) polymerization with a polymeriz RAFT agent containing multiple trithiocarbonate groups. *Macromol. Chem. Phys.* **2009**, *210*, 1647-1653.
- ³⁴⁴ Syrett, J. A.; Mantovani, G.; Barton, W. R. S.; Price, D.; Haddleton, D. M. Self-healing polymers prepared *via* living radical polymerization. *Polym. Chem.* **2010**, *1*, 102-106.
- ³⁴⁵ Sheno, R. A.; Lai, B. F. L.; Kizhakkedathu, J. N. Synthesis, characterization, and biocompatibility of biodegradable hyperbranched polyglycerols from acid-cleavable ketal group functionalized initiators. *Biomacromolecules* **2012**, *13*, 3018-3030.
- ³⁴⁶ Fang, J.-Y.; Lin, Y.-K.; Wang, S.-W.; Yu, Y.-C.; Lee, R.-S. Acid and light dual- stimuli-cleavable polymeric micelles. *J. Polym. Res.* **2017**, *24*, 3.
- ³⁴⁷ Jazani, A. M.; Oh, J. K. Dual location, dual acidic pH/reduction-responsive degradable block copolymer: Synthesis and investigation of ketal linkage instability under ATRP conditions. *Macromolecules* **2017**, *50*, 9427-9436.
- ³⁴⁸ Moreno, A.; Ronda, J. C.; Cádiz, V.; Galià, M.; Lligadas, G.; Percec, V. SET-LRP from programmed difunctional initiators encoded with double single-cleavage and double dual-cleavage groups. *Biomacromolecules* **2019**, *20*, 3200-3210.
- ³⁴⁹ Xuan, J.; Han, D.; Xia, H.; Zhao, Y. Dual-stimuli-responsive micelle on an ABC triblock copolymer bearing a redox-cleavable unit and a photocleavable unit at two block junctions. *Langmuir* **2014**, *30*, 410-417.
- ³⁵⁰ Lee, R.-S.; Wang, S.-W.; Li, Y.-C.; Fang, J.-Y. Synthesis and characterization of thermo-responsive and photo-cleavable block copolymers as nanocarriers. *RSC Adv.* **2015**, *5*, 497-512.

- ³⁵¹ Chan, N.; An, S. Y.; Oh, J. K. Dual location disulfide degradable interlayer-crosslinked micelles with extended sheddable coronas exhibiting enhanced colloidal stability and rapid release. *Polym. Chem.* **2014**, *5*, 1637-1649.
- ³⁵² Humphrey, R. E.; Potter, J. L. Reduction of disulfides with tributylphosphine. *Anal. Chem.* **1965**, *37*, 164-165.
- ³⁵³ Tsarevsky, N. V.; Matyjaszewski, K. Combining atom transfer radical polymerization and disulfide/thiol redox chemistry: A route to well-defined (bio)degradable polymeric materials. *Macromolecules* **2005**, *38*, 3087-3092.
- ³⁵⁴ Sato, Y.; Takasu, A. Conversion of diols to dithiols via a dehydration polycondensation with a dicarboxylic acid containing a disulfide and subsequent reduction. *Polym. J.* **2010**, *42*, 956-959.
- ³⁵⁵ Tsarevsky, N. V.; Matyjaszewski, K. Reversible redox cleavage/coupling of polystyrene with disulfide or thiol groups prepared by atom transfer radical polymerization. *Macromolecules* **2002**, *35*, 9009-9014.
- ³⁵⁶ Sun, T.; Li, P.; Oh, J. K. Dual location dual reduction/photoresponsive block copolymer micelles: Disassembly and synergistic release. *Macromol. Rapid Commun.* **2015**, *36*, 1742-1748.
- ³⁵⁷ Kumar, A.; Lale, S. V.; Mahajan, S.; Choudhary, V.; Koul, V. ROP and ATRP fabricated dual targeted redox sensitive polymersomes based on pPEGMA-PCL-ss-PCL-pPEGMA triblock copolymers for breast cancer therapeutics. *ACS Appl. Mater. Interfaces* **2015**, *7*, 9211-9227.
- ³⁵⁸ Jazani, A. M.; Arezi, N.; Maruya-Li, K.; Jung, S.; Oh, J. K. Facile strategies to synthesize dual location dual acidic pH/reduction-responsive degradable block copolymers bearing acetal/disulfide block junctions and disulfide pendants. *ACS Omega* **2018**, *3*, 8980, 8991.
- ³⁵⁹ Fritze, U. F.; Craig, S. L.; von Delius, M. Disulfide-centered poly(methyl acrylates): Four different stimuli to cleave a polymer. *J. Poly. Sci. A Polym. Chem.* **2018**, *56*, 1404-1411.
- ³⁶⁰ Singh, R.; Whitesides, G. M. Thiol-disulfide interchange. *Supplement S: The chemistry of sulphur-containing functional groups*. Ed. John Wiley & Sons: New York, **1993**, p. 633-658.
- ³⁶¹ Binauld, S.; Stenzel, M. H. Acid-degradable polymers for drug delivery: a decade of innovation. *Chem. Commun.* **2013**, *49*, 2082-2102.
- ³⁶² Chen, K.; Xu, J.; Luft, J. C.; Tian, S.; Raval, J. S.; DeSimone, J. M. Design of asymmetric particles containing a charged interior and a neutral surface charge: Comparative study on *in vivo* circulation of polyelectrolyte microgels. *J. Am. Chem. Soc.* **2014**, *136*, 9947-9952.
- ³⁶³ Pohlit, H.; Leibig, D.; Frey, H. Poly(ethylene glycol) dimethacrylates with cleavable ketal sites: Precursors for cleavable PEG-hydrogels. *Macromol. Biosci.* **2017**, *17*, 1600532.
- ³⁶⁴ Miller, K. A.; Morado, E. G.; Samanta, S. R.; Walker, B. A.; Nelson, A. Z.; Sen, S.; Tran, D. T.; Whitaker, D. J.; Ewoldt, R. H.; Braun, P. V.; Zimmerman, S. C. Acid-triggered, acid-generating, and self-amplifying degradable polymers. *J. Am. Chem. Soc.* **2019**, *141*, 2838-2842.
- ³⁶⁵ Kim, S.; Linker, O.; Garth, K.; Carter, K. R. Degradation kinetics of acid-sensitive hydrogels. *Polym. Degrad. Stab.* **2015**, *121*, 303-310.
- ³⁶⁶ Sui, X.; Zhang, Z.; Guan, S.; Xu, Y.; Li, C.; Lv, Y.; Chen, A.; Yang, L.; Gao, L. A facile strategy for the synthesis of block copolymers bearing an acid-cleavable junction. *Polym. Chem.* **2015**, *6*, 2777-2782.
- ³⁶⁷ Knorr, V.; Allmendinger, L.; Walker, G. F.; Paintner, F. F.; Wagner, E. An acetal-based PEGylation reagent for pH-sensitive shielding of DNA polyplexes. *Bioconjugate Chem.* **2007**, *18*, 1218-1225.
- ³⁶⁸ Iinuma, A.; Hashimoto, T.; Urushisaki, M.; Sakaguchi, T. Vinyl ether-based polyacetal polyols with various main-chain structures and polyurethane elastomers prepared therefrom: Synthesis, structure, and functional properties. *J. Appl. Polym. Sci.* **2016**, 44088.

- ³⁶⁹ Cordes, E. H.; Bull, H. G. Mechanism and catalysis for hydrolysis of acetals, ketals, and ortho esters. *Chem. Rev.* **1974**, *74*, 581-603.
- ³⁷⁰ Satchell, D. P. N.; Satchell, R. S. Mechanisms of hydrolysis of thioacetals. *Chem. Soc. Rev.* **1990**, *19*, 55-81.
- ³⁷¹ Chelucci, G. A facile synthesis of 3-substituted glutaraldehyde monoacetal from nitriles. *Synthesis* **1991**, *1991*, 474-476.
- ³⁷² Yan, Q.; Han, D.; Zhao, Y. Main-chain photoresponsive polymers with controlled location of light-cleavable units: from synthetic strategies to structural engineering. *Polym. Chem.* **2013**, *4*, 5026-5037.
- ³⁷³ Wong, P. T.; Tang, S.; Cannon, J.; Chen, D.; Sun, R.; Lee, J.; Phan, J.; Tao, K.; Sun, K.; Chen, B.; Baker, Jr., J. R.; Choi, S. K. Photocontrolled release of doxorubicin conjugated through a thioacetal photocage in folate-targeted nanodelivery systems. *Bioconjugate Chem.* **2017**, *28*, 3016-3028.
- ³⁷⁴ Barltrop, J. A.; Plant, P. J.; Schofield, P. Photosensitive protecting groups. *Chem. Commun.* **1966**, 822-823.
- ³⁷⁵ Patchornik, A.; Amit, B. Photosensitive protecting groups. *J. Am. Chem. Soc.* **1970**, *92*, 6333-6335.
- ³⁷⁶ Holmes, C. P.; Jones, D. G. Reagents for combinatorial organic synthesis: Development of a new *o*-nitrobenzyl photolabile linker for solid phase synthesis. *J. Org. Chem.* **1995**, *60*, 2318-2319.
- ³⁷⁷ Johnson, J. A.; Finn, M. G.; Koberstein, J. T.; Turro, N. J. Synthesis of photocleavable linear macromonomers by ATRP and star macromonomers by a tandem ATRP – click reaction: Precursors to photodegradable model networks. *Macromolecules* **2007**, *40*, 3589-3598.
- ³⁷⁸ Song, C.-C.; Du, F.-S.; Li, Z.-C. Oxidation-responsive polymers for biomedical applications. *J. Mater. Chem. B* **2014**, *2*, 3413-3426.
- ³⁷⁹ Zamadar, M.; Ghosh, G.; Mahendran, A.; Minnis, M.; Kruft, B. I.; Ghogare, A.; Aebisher, D.; Greer, A. Photosensitizer drug delivery via an optical fiber. *J. Am. Chem. Soc.* **2011**, *133*, 7882-7891.
- ³⁸⁰ Deepagan, V. G.; Kwon, S.; You, D. G.; Nguyen, V. Q.; Um, W.; Ko, H.; Lee, H.; Jo, D.-G.; Kang, Y. M.; Park, J. H. *In situ* diselenide-crosslinked polymeric micelles for ROS-mediated anticancer drug delivery. *Biomaterials* **2016**, *103*, 56-66.
- ³⁸¹ Lin, G.-Q.; Yi, W.-J.; Liu, Q.; Yang, X.-J.; Zhao, Z.-G. Aromatic thioacetal-bridged ROS-responsive nanoparticles as novel gene delivery vehicles. *Molecules* **2018**, *23*, 2061.
- ³⁸² Xu, Q.; He, C.; Xiao, C.; Chen, X. Reactive oxygen species (ROS) responsive polymers for biomedical applications. *Macromol. Biosci.* **2016**, *16*, 635-646.
- ³⁸³ Wilson, D. S.; Dalmasso, G.; Wang, L.; Sitaraman, S. V.; Merlin, D.; Murthy, N. Orally delivered thioketal nanoparticles loaded with TNF- α -siRNA target inflammation and inhibit gene expression in the intestines. *Nat. Mater.* **2010**, *9*, 923-928.
- ³⁸⁴ Yuan, Y.; Liu, J.; Liu, B. Conjugated-polyelectrolyte-based polyprodrug: Targeted and image-guided photodynamic and chemotherapy with on-demand drug release upon irradiation with a single light source. *Angew. Chem. Int. Ed.* **2014**, *53*, 7163-7168.
- ³⁸⁵ Foote, C. S. Mechanisms of photosensitized oxidations. *Science* **1968**, *162*, 963-970.
- ³⁸⁶ Toutchkine, A.; Aebisher, D.; Clennan, E. L. Substituent-dictated portioning of intermediates on the sulfide singlet oxygen reaction surface. A new mechanism for oxidative C – S bond cleavage in α -hydroperoxy sulfides. *J. Am. Chem. Soc.* **2001**, *123*, 4966-4973.

- ³⁸⁷ Kice, J. L.; Rogers, T. E. Mechanism of the alkaline hydrolysis of thioisulfonates and thioisulfonates. *J. Am. Chem. Soc.* **1974**, *96*, 8009-8015.
- ³⁸⁸ Murray, R. W.; Jindal, S. L. The photosensitized oxidation of disulfides related to cysteine. *Photochem. Photobiol.* **1972**, *16*, 147-151.
- ³⁸⁹ Clennan, E. L.; Wang, D.; Clifton, C.; Chen, M.-F. Geometry-dependent quenching of singlet oxygen by dialkyl disulfides. *J. Am. Chem. Soc.* **1997**, *119*, 9081-9082.
- ³⁹⁰ Lacombe, S.; Cardy, H.; Simon, M.; Khoukh, A.; Soumillion, J. Ph.; Ayadim, M. Oxidation of sulfides and disulfides under electron transfer or singlet oxygen photosensitization using soluble or grafted sensitizers. *Photochem. Photobiol.* **2002**, *1*, 347-354.
- ³⁹¹ Kamata, M.; Sato, M.; Hasegawa, E. Photosensitized oxygenation reactions of 1,3-dithianes through cooperative single electron transfer pathway and singlet oxygen pathway. *Tetrahedron Lett.* **1992**, *33*, 5085-5088.
- ³⁹² Burghardt, T. E. Developments in the deprotection of thioacetals. *J. Sulfur Chem.* **2005**, *26*, 411-427.
- ³⁹³ Seah, G. L.; Yu, J. H.; Koo, B. I.; Lee, D. J.; Nam, Y. S. Cancer-targeted reactive oxygen species-degradable polymer nanoparticles for near infrared light-induced drug release. *J. Mater. Chem. B* **2018**, *6*, 7737-7749.
- ³⁹⁴ Cao, Z.; Ma, Y.; Sun, C.; Lu, Z.; Yao, Z.; Wang, J.; Li, D.; Yuan, Y.; Yang, X. ROS-sensitive polymeric nanocarriers with red light-activated size shrinkage for remotely controlled drug release. *Chem. Mater.* **2018**, *30*, 517-525.
- ³⁹⁵ Phua, S. Z. F.; Xue, C.; Lim, W. Q.; Yang, G.; Chen, H.; Zhang, Y.; Wijaya, C. F.; Luo, Z.; Zhao, Y. Light-responsive prodrug-based supramolecular nanosystems for site-specific combination therapy of cancer. *Chem. Mater.* **2019**, *31*, 3349-3358.
- ³⁹⁶ Dariva, C. G.; Coelho, J. F. J.; Serra, A. C. Near infrared light-triggered nanoparticles using singlet oxygen photocleavage for drug delivery systems. *J. Control. Release* **2019**, *294*, 337-354.
- ³⁹⁷ Mohammed, F.; Ke, W.; Mukerabigwi, J. F.; Japir, A. A.-W. M. M.; Ibrahim, A.; Wang, Y.; Zha, Z.; Lu, N.; Zhou, M.; Ge, Z. ROS-responsive polymeric nanocarriers with photoinduced exposure of cell-penetrating moieties for specific intracellular drug delivery. *ACS Appl. Mater. Interfaces* **2019**, *11*, 31681-31692.
- ³⁹⁸ Wang, C.; Huang, B.; Yang, G.; Ouyang, Y.; Tian, J.; Zhang, W. NIR-Triggered multifunctional and degradable nanoplatform based on an ROS-sensitive block copolymer for imaging-guided chemophototherapy. *Biomacromolecules* **2019**, *20*, 4218-4229.
- ³⁹⁹ Wang, K.; Tu, Y.; Yao, W.; Zong, Q.; Xiao, X.; Yang, R.-M.; Jiang, X.-Q.; Yuan, Y. Size-switchable nanoparticles with self-destructive and tumor penetration characteristics for site-specific phototherapy of cancer. *ACS Appl. Mater. Interfaces* **2020**, *12*, 6933-6943.
- ⁴⁰⁰ Onusseit, D. Adhesives and tapes designed to be less detrimental to paper recycling. *Henkel KGaA Düsseldorf, Germany.* **2012** <https://www.adhesives.org/resources/knowledge-center/aggregate-single/adhesives-tapes-designed-to-be-less-detrimental-to-paper-recycling> (accessed 21 November 2020).

Chapter 2

Overview and objectives

UNIVERSITAT ROVIRA I VIRGILI
STIMULI-RESPONSIVE CALIX[4]PYRROLE AND CALIX[4]ARENE BASED RECEPTORS: FROM UNIMOLECULAR
TO DIMERIC STRUCTURES

Pedro Miguel Mendonça Ferreira

2 Overview and objectives

2.1 Overview

Since the middle of the 20th century, the production of polymer materials has increased exponentially, from a global production of resins and fibers of 2 Mt in 1950 to 380 Mt in 2015. This production means a total amount of 7800 Mt manufactured since 1950. There are estimations that the 60% of the plastic waste ever produced, approx. 4900 Mt, was discarded and is accumulating in the environment, and if the global production continues to increase as expected, the waste discarded in landfills will become 12000 Mt in 2050.¹ The plastics accumulated in the environment have the potential to alter the soil biophysical properties, related to changes in microbial activity. These changes entail a long-term impact on the terrestrial ecosystem.² These effects in the environment could be related to the partial degradation of the polymer into monomers, but also for the leaching of their additives (e.g. plasticizers).³ With the actual increasing demand, caused by the development of countries and the rapid growth of global population, the global waste will keep rising during this century.⁴ This fact highlights the necessity for the development of recyclable materials which could be recovered once its useful life is over.

On the other hand, most plastics are made from petrochemicals, and even though only 7% of the world's fossil resources are used in plastic production,⁵ the fossil raw materials are limited resources. Someday they will become exhausted and its extraction entails the emission of greenhouse gasses, something that must be minimized. For these reasons is necessary to find an eco-friendly and renewable alternative to the actual petroleum-derived plastics to overcome the global waste management problem. Nowadays, it is an important goal for polymer science to obtain these renewable polymers than can compete with existing polymers in performance

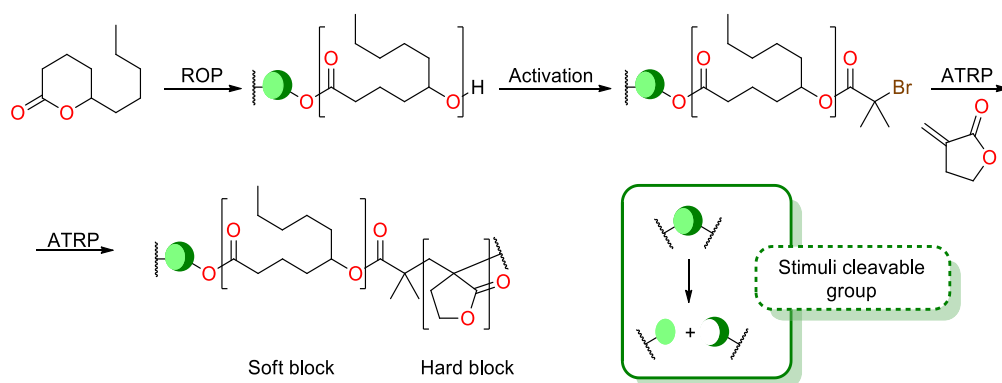
and cost but minimizing the environmental impact. Although this cannot be the only solution to the climate problem, this is a step forward to minimize the effect of human activity in the nature.

Among all the polymer materials thermoplastic elastomers (TPEs) has emerged as an attractive alternative to traditional thermoset vulcanized rubbers due to its ease processability and lower energy consumption. Nowadays, TPEs are widely used in many fields such as automotive, construction, household appliances, wires, electronic products, food packaging and medical equipment. On account of that, the global TPE market demand reached 6.7 million tons in 2019, and it is estimated to grow at a rate of 5.2% each year in the future.⁶ From this increasing demand is evidenced the necessity to find renewable alternatives to the actual fossil-derived TPE. Moreover, the recoverability of these TPEs, from the commercial products, is an important issue to consider. Not only considering the polymer itself but the recoverability of the rest of the components of the product. Adhesives, an important class of TPEs, generate great problems in paper recycling industry.⁷ For this reason, the development of TPE which could be easily eliminated has become an important target from the sustainability point of view.

Particularly, in the field of TPE Hillmyer et al. have reported the preparation of TPEs using monomers from renewable feedstocks. They synthesize ABA block copolymers through chain extension of aliphatic polyesters (e.g. polymethide synthesized by ROP), with monomers such as lactide (ROP) or tulipalin A (ATRP).^{8, 9, 10, 11} The materials obtained showed promising mechanical properties, demonstrating the viability of renewable polymers to compete with commercial TPEs.

2.2 Objectives

With the aim to break new insights and expand the realm of renewable-based specialty polymers, the objective of this thesis is to prepare ABA block copolymers suitable for TPEs applications, from renewable feedstocks. For this purpose, controlled polymerization techniques, such as ring-opening polymerization (ROP) and atom transfer radical polymerization (ATRP), will be employed. Moreover, different sensitive groups will be incorporated at the central point of the polymer, to obtain materials which can respond to different external stimuli and modify its properties under demand. By this way, the ABA block copolymer could be cleaved at the mid-point and, therefore, lose its TPE properties. δ -Decalactone (DL) will be used as renewable ROP monomer for the synthesis of the “soft” central segment of the ABA block copolymer. The DL blocks will possess different sensitive groups (disulfide, acetal or thioacetal) which could be cleaved under the appropriate stimuli. The DL blocks will be properly activated, as α -bromoisobutyryl esters, for the consecutive chain extension through ATRP. α -Methylene- γ -butyrolactone (MBL) will be used as renewable ATRP monomer for the synthesis of the “hard” end segments. The cleavage of the polymers under the appropriate stimuli (reductive, acid or oxidative media) will be studied and all the products characterized.



Scheme 2.1 Schematic representation of the synthesis of block copolymers, possessing a sensitive mid-point group, through ROP, activation, ATRP.

Specific objectives

- To synthesize a series of aliphatic polyesters from renewable δ -decalactone (DL), through ROP in a controlled manner, using different stimuli-cleavable initiators.
- To modify the end-groups of poly(DL) homopolymers to use them as macroinitiators for the synthesis of block copolymers by ATRP.
- To synthesize ABA block copolymers by chain extension from the above mentioned macroinitiators and α -methylene- γ -butyrolactone (MBL) as renewable vinylic monomer.
- To study the response of the synthesized materials upon an external stimulus and to identify the degradation products.
- To characterize the structure and properties of all poly(DL), poly(MBL) and poly(MBL)-*co*-poly(DL)-*co*-poly(MBL) and the resulting cleaved products.

-
- ¹ Greyer, R.; Jamberck, J. R.; Law, K. L. Production, use, and fate of all plastics ever made. *Sci. Adv.* **2017**, *3*, e1700782.
- ² Machado, A. A. S.; Lau, C. W.; Till, J.; Kloas, W.; Lehmann, A.; Becker, R.; Rillig, M. C. Impacts of microplastics in the soil biophysical environment. *Environ. Sci. Technol.* **2018**, *52*, 9656-9665.
- ³ Teuten, E. L.; Saquing, J. M.; Knappe, D. R. U.; Barlaz, M. A.; Jonsson, S.; Björn, A.; Rowland, S. J.; Thompson, R. C.; Galloway, T. S.; Yamashita, R.; Ochi, D.; Watanuki, Y.; Moore, C.; Viet, P. H.; Tana, T. S.; Prudente, M.; Boonyatumanond, R.; Zakaria, M. P.; Akkhavong, K.; Ogata, Y.; Hirai, H.; Iwasa, S.; Mizukawa, K.; Hagino, Y.; Imamura, A.; Saha, M.; Takada, H. Transport and release of chemicals from plastics to the environment and to wildlife. *Phil. Trans. R. Soc. B* **2009**, *364*, 2027-2045.
- ⁴ Hoornweg, D.; Bhada-Tata, P.; Kennedy, C. Waste production must peak this century. *Nature* **2013**, *502*, 615-617.
- ⁵ Yao, K.; Tang, C. Controlled polymerization of next-generation renewable monomers and beyond. *Macromolecules* **2013**, *46*, 1689-1712.
- ⁶ Jibin, H.; Wenquan, C.; Shijia, Z.; Yuan, W.; Lili, H.; Shuya, L.; Hongchi, T. The research and development of thermoplastic elastomers. *SVOA Materials Science and Technology* **2020**, *2*, 34-46.
- ⁷ Onusseit, D. Adhesives and tapes designed to be less detrimental to paper recycling. *Henkel KGaA Düsseldorf, Germany.* **2012** <https://www.adhesives.org/resources/knowledge-center/aggregate-single/adhesives-tapes-designed-to-be-less-detrimental-to-paper-recycling> (accessed 21 November 2020).
- ⁸ Wanamaker, C. L.; O'Leary, L. E.; Lynd, N. A.; Hillmyer, M. A.; Tolman, W. B. Renewable-resource thermoplastic elastomers based on polylactide and polymenthide. *Biomacromolecules*, **2007**, *8*, 3634-3640.
- ⁹ Shin, J.; Lee, Y.; Tolman, W. B.; Hillmyer, M. A. Thermoplastic elastomers derived from menthene and tulipalin A. *Biomacromolecules* **2012**, *13*, 3833-3840.
- ¹⁰ Ding, K.; John, A.; Shin, J.; Lee, Y.; Quinn, T.; Tolman, W. B.; Hillmyer, M. A. High-performance pressure-sensitive adhesives from renewable triblock copolymers. *Biomacromolecules*, **2015**, *16*, 2537-2539.
- ¹¹ Watts, A.; Kurokawa, N.; Hillmyer, M. A. Strong, resilient, and sustainable aliphatic polyester thermoplastic elastomers. *Biomacromolecules*, **2017**, *18*, 1845-1854.

UNIVERSITAT ROVIRA I VIRGILI
STIMULI-RESPONSIVE CALIX[4]PYRROLE AND CALIX[4]ARENE BASED RECEPTORS: FROM UNIMOLECULAR
TO DIMERIC STRUCTURES

Pedro Miguel Mendonça Ferreira

Chapter 3

*Stimuli-cleavable polyester macroinitiators from
renewable δ -decalactone: Synthesis, end-group
modification, and characterization*

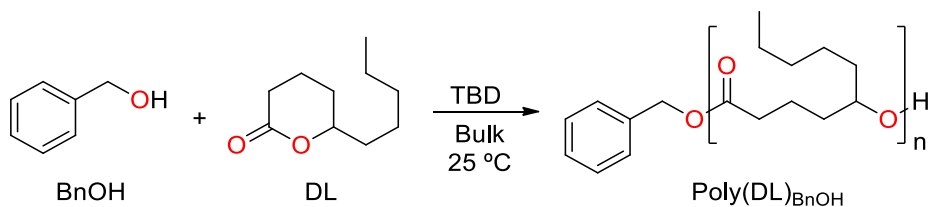
UNIVERSITAT ROVIRA I VIRGILI
STIMULI-RESPONSIVE CALIX[4]PYRROLE AND CALIX[4]ARENE BASED RECEPTORS: FROM UNIMOLECULAR
TO DIMERIC STRUCTURES

Pedro Miguel Mendonça Ferreira

3 Stimuli-cleavable polyester macroinitiators from renewable δ -decalactone: Synthesis, end-group modification, and characterization.

3.1 Synthesis of poly(δ -decalactone) as soft/rubbery block

As has been mentioned in the introduction and objectives, for the obtention of the aliphatic/rubbery block, the ring-opening polymerization (ROP) of δ -decalactone (DL) using 1,5,7-triazabicyclo[4.4.0]dec-5-ene (TBD) as organocatalyst was chosen. This catalyst allows the obtention of polymers with controlled molecular weights and narrow polydispersities, under mild conditions,^{1,2} and it has been extensively described in the literature for the polymerization of DL as well as other lactones.³⁻⁵



Scheme 3.1 ROP of DL using BnOH as initiator and TBD as catalyst.

Most of the reported procedures in ROP are carried out in a glovebox to assure complete exclusion of water, which can act as co-initiator, affecting the control over the molecular weight and the polymer end-group functionality. Due to the lack of glovebox in our facilities, at the time the polymerizations were done, we assayed the polymerization of DL using conventional Schlenk techniques with extreme care during the drying, handling and transfer operations. To check the robustness of this methodology we carried out the polymerization of DL in bulk using benzyl alcohol (BnOH) as initiator (Scheme 3.1) following a protocol based on a reported procedure (see experimental part 6.8.1).^{6,7}

Table 3.1 Conversion and molecular weight characteristics of the polyesters obtained by polymerization of DL with TBD initiated by BnOH with different TBD/BnOH ratios. Polymerization conditions [DL]:[BnOH]; 100:1, 25 °C, in bulk.

Entry	TBD/ BnOH	Time (h)	Conv. (%) ^a	Mn ^b Theor. (g/mol) (x10 ⁻³)	Mn ^c _{NMR} Ph-CH ₂ -OOC- (g/mol) (x10 ⁻³)	Mn ^d _{NMR} CH-OH (g/mol) (x10 ⁻³)	Mn ^e _{SEC} (g/mol) (x10 ⁻³)	Đ ^e
1	2.00	8	83	14.2	12.6	7.6	11.7	1.16
2	0.75	16	87	14.9	13.3	12.1	16.7	1.14

^a Determined by ¹H-NMR spectroscopy from the crude reaction mixture using the signals of monomer (4.28 ppm) and polymer backbone (4.88 ppm). ^b Calculated from the conversion degree determined by ¹H-NMR spectroscopy and the target DP. ^c Determined by ¹H-NMR spectroscopy using the signals of initiator (5.11 ppm) and the polymer backbone (4.88 ppm). ^d Determined by ¹H-NMR spectroscopy using the signals of end-group (3.59 ppm) and the polymer backbone (4.88 ppm). ^e Determined by SEC using THF as eluent and a polystyrene standards calibration curve.

In an initial experiment a degree of polymerization (DP) of 100 ([DL]:[BnOH] = 100:1) was fixed and a [TBD]/[BnOH] ratio of 2:1 (entry 1 in Table 3.1). The reaction was carried out at room temperature, in bulk. The conversion was determined by ¹H-NMR spectroscopy by comparison of the signals of the methine protons of polymer backbone, at 4.88 ppm (signal **5** in Figure 3.1-b), and the unreacted monomer, at 4.28 ppm (signal **5_M** in Figure 3.1-b). The complete initiation by BnOH was confirmed by the total disappearance of the benzylic signal, at 4.71 ppm (signal **a** in Figure 3.1-a), and the appearance of a new signal of benzyl ester, at 5.11 ppm (signal **a'** in Figure 3.1-b). In this way, a conversion of 83% was estimated after 8 hours (entry 1 in Table 3.1). The reaction was quenched using an equal volume of a 0.5 M solution of benzoic acid (PhCOOH) in dichloromethane (DCM) to neutralize the TBD.

The number average molecular weight (Mn) was determined by ¹H-NMR spectroscopy, by comparison of the signals of the polymer backbone at 4.88 ppm (signal **5**, -CH-OOC, in Figure 3.1-c) and the signals of both the initiator at 5.11 ppm (signal **a'**, Ph-CH₂-OOC-, in Figure 3.1-c) and the hydroxyl end-group at 3.59 ppm (signal **5'**, CH-OH in Figure 3.1-c). The Mn was also determined by size exclusion chromatography (SEC). The obtained chromatogram shows a monomodal distribution with narrow polydispersity (Đ = 1.16) (entry 1 in Table 3.1) but the determined Mn (relative to polystyrene) (11700

g/mol) was lower to the theoretical one (14200 g/mol). The Mn determined by $^1\text{H-NMR}$ spectroscopy using the signal corresponding to the initiator (signal **a'**, $\text{Ph-CH}_2\text{-OOC-}$, in Figure 3.1-c) is close (12600 g/mol) to the theoretical one but the Mn determined using the signal corresponding to the end-group (signal **5'**, $-\text{CH-OH}$, in Figure 3.1-c) was considerably lower (7600 g/mol) (entry 1 in Table 3.1).

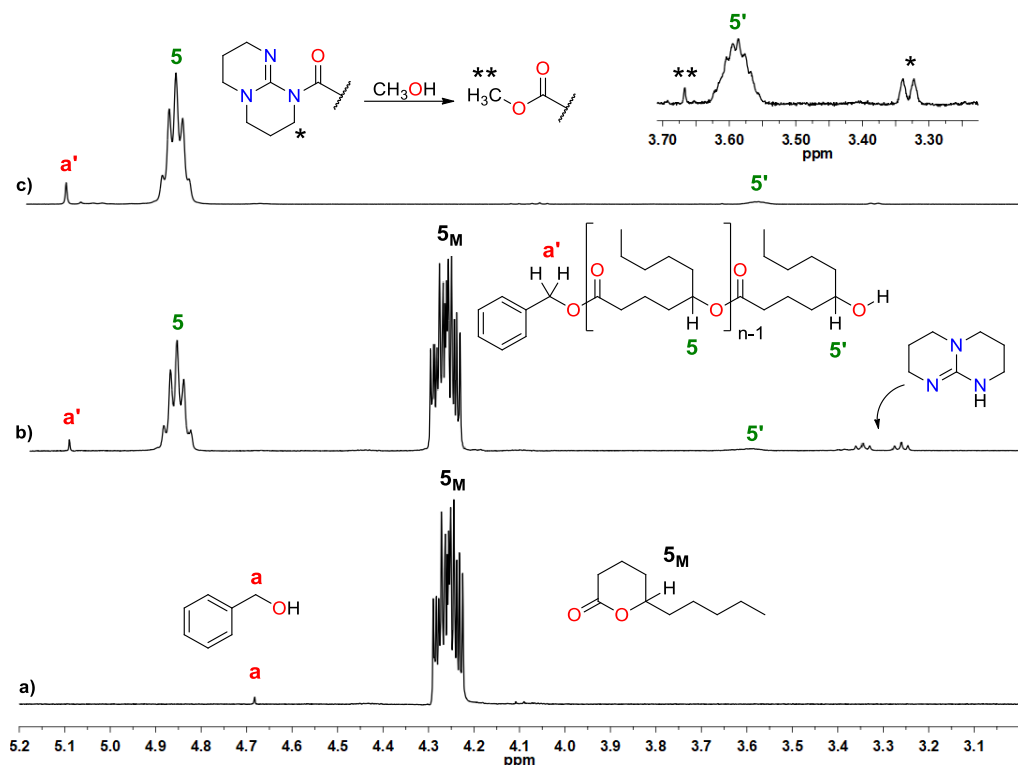


Figure 3.1 $^1\text{H-NMR}$ spectra of (a) initial monomer/initiator mixture, (b) polymerization mixture at 40 % conversion and (c) isolated polymer after precipitation with methanol.

These results seem to indicate that there are other species initiating the polymerization. The $^1\text{H-NMR}$ spectrum of the resulting polymer after precipitating in methanol, apart from the expected signals, showed a doublet at 3.31 ppm (signal ***** in Figure 3.1-c) and a singlet at 3.67 ppm (signal ****** in Figure 3.1-c). The first signal could be attributed to the polymer chains linked to TBD, according to the data described in the literature which indicate that TBD can initiate the polymerization of macrolactones.⁸

The initiation of smaller lactones by TBD (e.g. polymerization of lactide using TBD in the absence of alcohol initiator) has also been described and detected by MALDI-TOF.⁹ The second signal at 3.67 ppm (signal ** in Figure 3.1-c) could be attributed to a methyl ester, as it only appears after precipitation in methanol. The formation of this methyl ester could be explained as a result of the nucleophilic displacement of the acyl derivative of TBD by methanol during the precipitation process. It is worth to note that spectrum c) in Figure 3.1 confirms the effectiveness of the quenching protocol using benzoic acid as the signal of the free TBD (Figure 3.1-b) completely disappears.

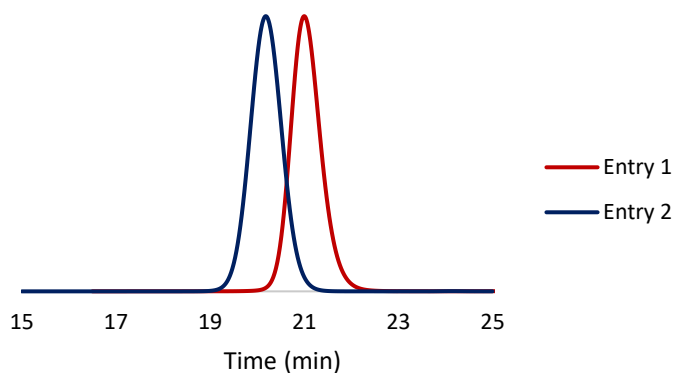
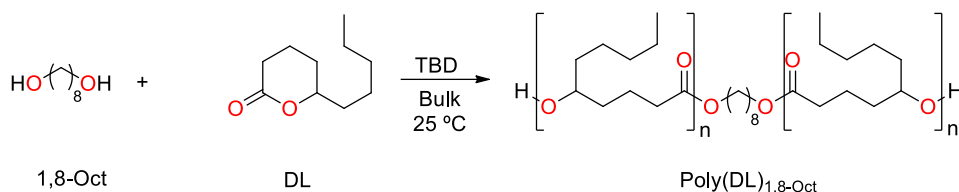


Figure 3.2 SEC chromatograms of polyesters obtained in Table 3.1: entry 1 (red) and entry 2 (blue).

According to these results, a new polymerization using a TBD/BnOH < 1 (entry 2 in Table 3.1), was tested in order to ensure an excess of initiator with respect to the catalyst and minimize the possible initiation by TBD. Thus, the target DP was maintained at 100 and the ratio TBD/BnOH was set at 0.75 (entry 2 in Table 3.1). The reaction reached 87 % of conversion within 16 hours, indicating a lower polymerization rate, as expected according to the lower catalyst concentration used. In this experiment molecular weights determined by ¹H-NMR spectroscopy using the signals of the initiator (signal a', Ph-CH₂-OOC-, in Figure 3.1-c) and the final hydroxylic group (signal 5', CH-OH, in Figure 3.1-c) match very well, with the theoretical one, indicating that the great majority of the polymer chains are initiated by BnOH. The Mn determined by SEC

(Figure 3.2 and Table 3.1) are higher than those calculated by $^1\text{H-NMR}$ spectroscopy and the theoretical ones which can be related to the differences in hydrodynamic volume. In any case, SEC traces show a monomodal distribution with narrow polydispersities ($\text{Đ}=1.14$) (entry 2 in Table 3.1 and Figure 3.2).



Scheme 3.2 Synthesis of poly(DL) using 1,8-octanediol as bifunctional initiator.

Once tested the appropriate conditions for the polymerization of DL with a monofunctional initiator, the next step was to prepare a telechelic polyester, using 1,8-octanediol (1,8-Oct) as bifunctional initiator (Scheme 3.2). This telechelic polyester will be used as model polymer for the end-group modification and chain extension tests. In this case, the selected DP was increased up to 150 and the TBD/1,8-Oct ratio was maintained at 0.75, which supposes a TBD/-OH ratio of 0.38 to further minimize any competence of TBD as initiator.⁹ The advance of polymerization was followed withdrawing samples at preset times (Table 3.2), which were analyzed by both $^1\text{H-NMR}$ spectroscopy (adding a 0.03 M solution of PhCOOH in CDCl_3) and SEC. The reaction was carried out at room temperature, in bulk. The conversion was determined in a similar way as in the prior case (Figure 3.3). The complete initiation by 1,8-Oct was confirmed by the total disappearance of the methylene signal, at 3.62 ppm (signal **a** in Figure 3.3-a), and the appearance of a new signal of methylene ester, at 4.05 ppm (signal **a'** in Figure 3.3-b).

Table 3.2 Conversion and molecular weight characteristics versus polymerization time of DL with TBD initiated with 1,8-Oct. Polymerization conditions [DL]:[1,8-Oct]; 150:1, [TBD]:[1,8-Oct]; 0.75:1, 25 °C, in bulk.

Aliquot	Time (h)	Conv. ^a (%)	Mn _{Theor.} ^b (g/mol) (x10 ⁻³)	Mn _{NMR} ^c (-CH ₂ O- (g/mol) (x10 ⁻³)	Mn _{NMR} ^d (-CH-OH (g/mol) (x10 ⁻³)	Mn _{SEC} ^e (g/mol) (x10 ⁻³)	Đ ^e
1	1	13	3.5	3.0	3.4	5.8	1.13
2	2	27	7.0	6.1	6.4	10.5	1.12
3	3	39	10.3	9.0	8.5	14.4	1.13
4	4	50	12.9	11.5	10.8	16.7	1.15
5	5	59	15.2	14.3	14.3	18.5	1.15
6	6	65	16.7	15.7	15.1	21.4	1.16
7	7.5	73	18.8	17.9	17.1	23.5	1.16

^a Determined by ¹H-NMR spectroscopy from the crude reaction mixture using the signals of monomer (4.28 ppm) and polymer backbone (4.88 ppm). ^b Calculated from the conversion degree determined by ¹H-NMR spectroscopy and the target DP. ^c Determined by ¹H-NMR spectroscopy using the signals of initiator (4.05 ppm) and the polymer backbone (4.88 ppm). ^d Determined by ¹H-NMR spectroscopy using the signals of the hydroxyl end-group (3.59 ppm) and the polymer backbone (4.88 ppm). ^e Determined by SEC using THF as eluent and a polystyrene standard calibration curve.

Figure 3.4-a (black squares) shows the evolution of the polymer conversion determined by ¹H-NMR spectroscopy versus time. As can be seen, polymer conversion reaches a plateau with 73% conversion after 7.5 hours (aliquot 7 in Table 3.2), which is close to the ceiling conversion (plateau at 88 % conversion).⁶ Moreover, the representation of the logarithm of monomer conversion versus time give a linear plot indicating the living character of the polymerization (white squares in Figure 3.4-a). Molecular weights determined by ¹H-NMR spectroscopy using the signals of the initiator (**a'**) and the hydroxyl end-group (**5'**), are very close to each other and close to the theoretical molecular weight for any conversion given (Figure 3.4-b), indicating a good end-group fidelity and confirming the telechelic structure of the polyester diol. It is noteworthy that the doublet signal at 3.32 ppm attributed to the ROP initiated by TBD is not observed for any polymerization degree confirming the effectiveness of carrying out the polymerization with TBD/I < 0.75.

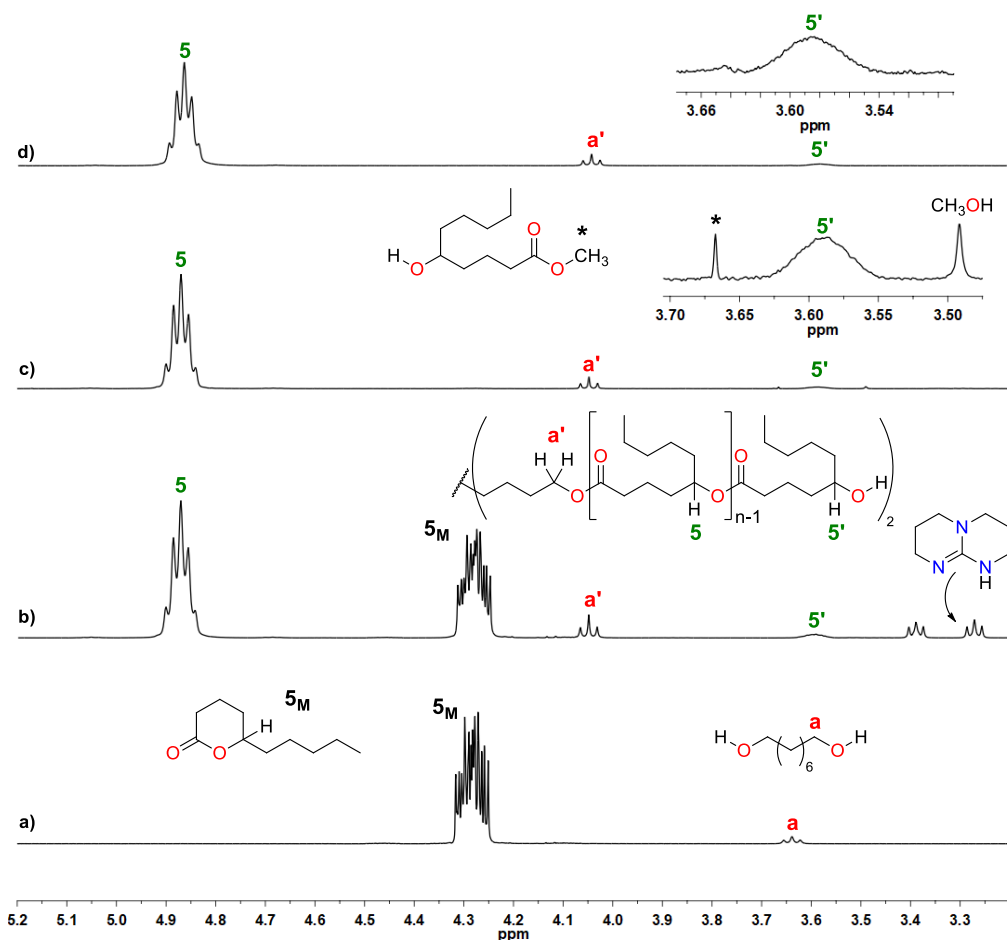


Figure 3.3 $^1\text{H-NMR}$ spectra of (a) initial DL/1,8-Oct mixture, (b) reaction mixture at 50 % conversion, (c) polymer isolated after precipitation in methanol and (d) polymer after long vacuum treatment.

Regarding to the SEC analysis, the M_n determined are higher than both the theoretical and the M_n determined by $^1\text{H-NMR}$ spectroscopy (Table 3.2) for all conversion degrees, following the same trend as before. Nevertheless, the M_n increases linearly during the progress of the polymerization (yellow triangles in Figure 3.4-b) and the polydispersities are narrow (yellow circles in Figure 3.4-b) as can be observed at the superposed chromatograms showed in Figure 3.5.

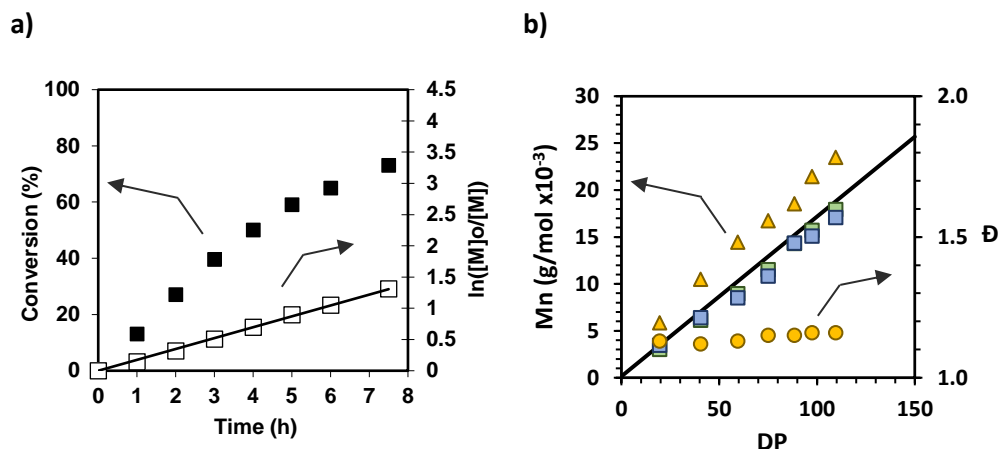


Figure 3.4 Representation of (a) the conversion versus time (black squares) and the logarithm of monomer conversion versus time (white squares) and representation of (b) Mn evolution versus, determined by both $^1\text{H-NMR}$ spectroscopy, using the signals of the initiator (green squares) and the end-group (blue squares), and by SEC (yellow triangles). Polydispersity is represented as yellow circles. The theoretical Mn is represented as a black line.

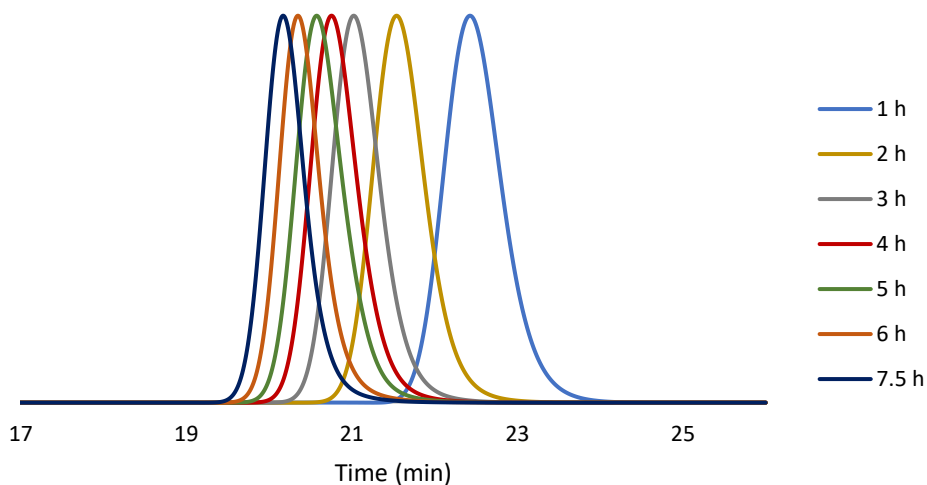


Figure 3.5 Superposed chromatograms of the withdrawn samples at preset times on ROP of DL using 1,8-Oct as initiator.

It is noteworthy to mention that the $^1\text{H-NMR}$ spectrum of the isolated polymer, after precipitation in cold methanol, apart from the expected signals, still shows a singlet signal corresponding to a methyl ester (signal * in Figure 3.3-c). Moreover, the signal corresponding to the $-\text{CHOH}$ groups seems to increase its relative intensity when

compared to the crude reaction mixture. We suspected that this signal could arise from the methanolysis of the unreacted lactone catalyzed by the TBD/PhCOOH salt during the precipitation work-up.

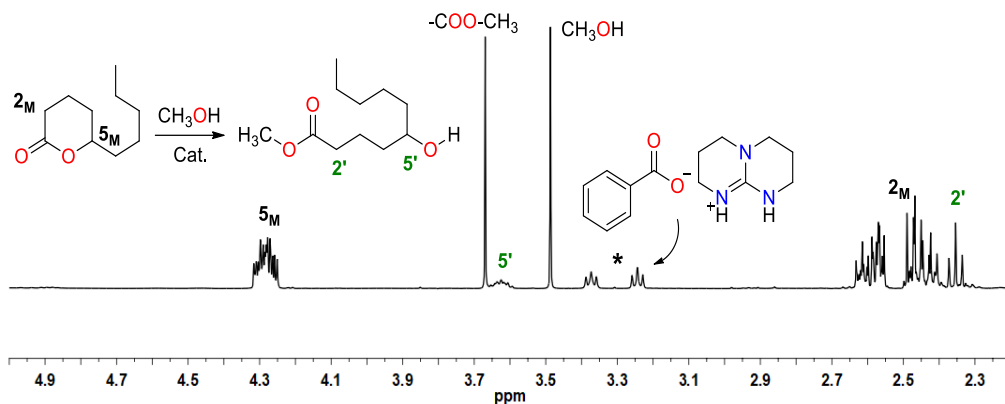


Figure 3.6 $^1\text{H-NMR}$ spectrum of residue products on methanol after precipitation.

This reaction could be confirmed by the fact that, after extensively drying of the polyester under vacuum, the singlet signal completely disappears and the intensity of the CHOH multiplet decrease significantly (signal $5'$ in Figure 3.3-d). Moreover, the $^1\text{H-NMR}$ analysis of the residue obtained after concertation of the methanolic precipitation medium, shows the presence of methyl 5-hydroxydecanoate (signals $2'$, $5'$ and $-\text{OCH}_3$ in Figure 3.6), apart from large amounts of unreacted DL (signals 2 and 5 in Figure 3.6) and the TBD/benzoic acid salt complex (signal $*$ in Figure 3.6). This alcoholysis reaction during the polyester workup has previously been described in ROP of lactones.¹⁰ The presence of traces of this type of hydroxylic impurities in the polyesters is specially undesired because leads to overestimation of the $-\text{CHOH}$ signal and entails a source of monofunctional monomolecular initiator after the activation as BriB ester for the ATRP chain extension. To avoid this undesired reaction, acetonitrile which is also polar but not nucleophilic, was tested as precipitation media instead of methanol (Table 3.3 experiment 2).

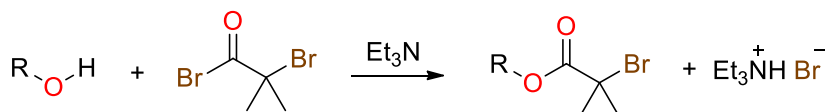
A polymerization test, using the conditions in Table 3.2, but using AcCN as precipitating media, gave a polymer which spectrum was essentially the same as in Figure 3.3-d, in which the intensity of the $-\text{CHOH}$ and $-\text{CH}_2\text{O}-$ signals showed the expected 1:2 ratio. According to these results, acetonitrile was used as precipitating media in the forthcoming ROP experiments. These results confirm the robustness of the method in terms of MW control and end-group fidelity. Then, the next step was to incorporate, at the end-groups, the appropriate functionality for the synthesis of the second block through ATRP (spectral data are collected in annex 8.13).

Table 3.3 Conversion, yield and molecular weight characteristics of poly(DL) diols obtained by ROP of DL with TBD initiated with 1,8-Oct. Polymerization conditions [DL]:[1,8-Oct]; 150:1, [TBD]:[1,8-Oct]; 0.75:1, 25 °C, in bulk. Exp. 1 polymer isolated by precipitation in MeOH, Exp. 2 polymer isolated by precipitation in AcCN.

Exp.	DL mmol	1,8- Oct mmol	Conv. ^a (%)	Mn _{Theor.} ^b (g/mol) (x10 ⁻³)	Yield (%)	Mn _{NMR} ^c -CH ₂ O- (g/mol) (x10 ⁻³)	Mn _{NMR} ^d -CH-OH (g/mol) (x10 ⁻³)	Mn _{SEC} ^e (g/mol) (x10 ⁻³)	Đ ^e
1	3.11	0.021	76.0	19.2	89	18.1	16.4	23.9	1.15
2	3.09	0.021	75.2	18.8	84	18.1	18.2	23.4	1.14

^a Determined by ¹H-NMR spectroscopy from the crude reaction mixture using the signals of monomer (4.28 ppm) and polymer backbone (4.88 ppm). ^b Calculated from the conversion degree determined by ¹H-NMR spectroscopy and the target DP. ^c Determined by ¹H-NMR spectroscopy using the signals of initiator (4.05 ppm) and the polymer backbone (4.88 ppm). ^d Determined by ¹H-NMR spectroscopy using the signals of the hydroxyl end-group (3.59 ppm) and the polymer backbone (4.88 ppm). ^e Determined by SEC using THF as eluent and a polystyrene standard calibration curve.

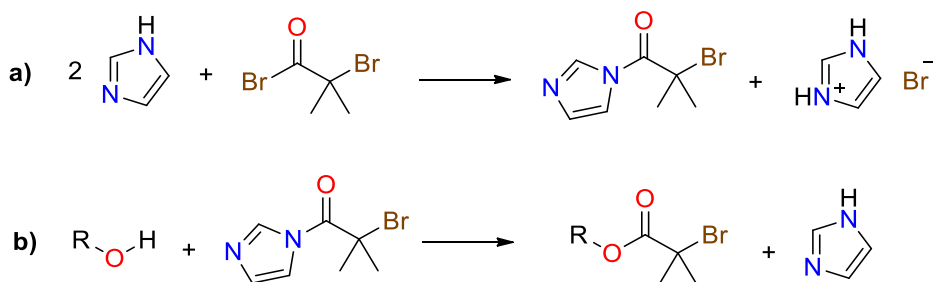
3.2 End-group modification for ATRP



Scheme 3.3 Traditional hydroxyl esterification with α -bromoisobutyryl bromide (BriBBR).

Nowadays, there are a wide range of different initiators to conduct ATRP. The choice of the appropriate initiator for a specific system is crucial to ensure a fast activation, to obtain high initiation efficiency, but also not too active than could entail terminations at early stages of the reaction. One of the most used groups to perform ATRP chain

extension on polyester macroinitiators is the 2-bromoisobutyryl (BriB) ester.^{11, 12} Although it is not the ideal initiator for methacrylate like monomers,¹³ its easy incorporation to hydroxyl end-group in polyesters usually converts the BriB derivatives in the more feasible option.¹⁴⁻¹⁶ Usually, the activation of telechelic polyesterdiols as 2-bromoisobutyrylates is performed in a multistep sequence that involves the isolation and purification of the polyester diol, the reaction with bromoisobutyryl bromide in presence of organic bases (Et₃N, DMAP) at low temperature and finally, the isolation and purification of the resulting modified ester (Scheme 3.3).^{11, 17-20} This latter step implies removing insoluble amine salts, aqueous work-up and very often an ulterior polymer purification to remove the brown impurities that usually accompanied this protocol. We sought for a more straightforward route to prepare these macroinitiators by direct functionalization of the hydroxyl end groups in the polymerization mixture once reached the ceiling conversion.



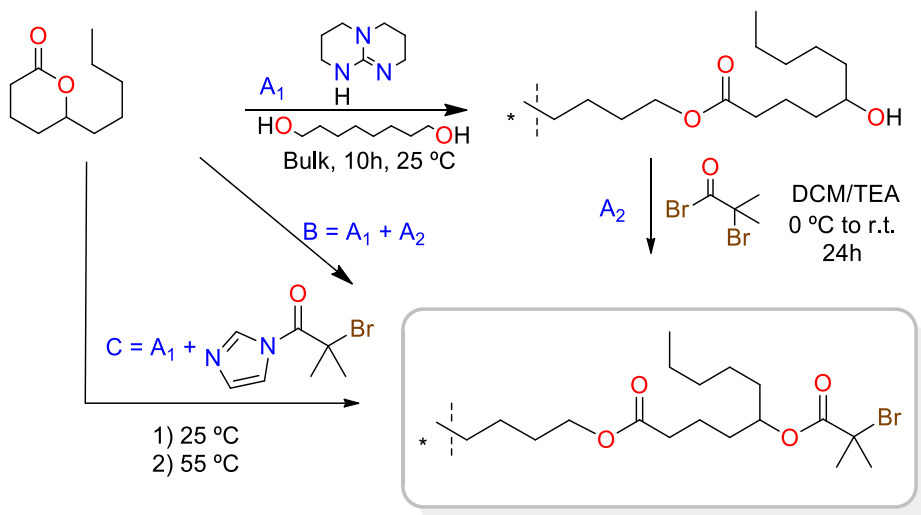
Scheme 3.4 (a) Synthesis of α -bromoisobutyryl imidazole (BriB-Im) and (b) hydroxyl esterification using BriB-Im.

Acylimidazoles have been described as effective acylating agents and can be conveniently synthesized from the corresponding acyl halide and imidazole (Scheme 3.4-a) (see experimental part 6.5) or the parent carboxylic acid and carbonyldiimidazol.²¹ They are slightly less reactive than acyl chlorides specially when bulky substituents are present or weak nucleophiles are used but this drawback can be overcome by using catalysts such as N-hydroxybenzotriazole.²² Acylimidazoles give imidazole as the only by-product (Scheme 3.4-b), which is easily removable and do not

produce strong pH changes in the medium contributing to negligible chain degradation, thus these acylating agents have previously been used to activate hydroxyl groups to perform ATRP²³ or SET-LRP²⁴⁻²⁶. Additionally, N-(2-bromoisobutryl)-imidazole (BriB-Im) is an easy to handle stable reagent that can be easily synthesized in multigram scale from the acyl bromide and an excess of imidazole (see annex 8.7).

Reaction of pristine poly(DL)_{1,8-Oct} diol with BriB-Im (4 eq) in THF at 60 °C did not afford appreciable acylation. On the contrary, after the addition of DBU or TBD (ca. 5%) the reaction proceeds smoothly, and complete esterification took place after few hours. This result prompted us to use BriB-Im directly into the bulk ROP medium once the ceiling conversion has been reached. Thus, addition of BriB-Im (4 eq) to the polymerization mixture gave the desired poly(DL)_{1,8-Oct}-(BriB) after raising the temperature to 55 °C for 24h and conventional polymer work up by dilution in DCM and precipitation over acetonitrile. To assess the method effectiveness, poly(DL)_{1,8-Oct} diol esterification, assays were carried out following three different strategies by comparing the resulting α -bromoisobutryl esters in terms of degree of modification, molecular weight and ease of isolation and purification. In all cases 1,8-octanediol was used as initiator and TBD as catalyst (following the conditions showed in Table 3.2). First methodology involved two separate steps; i) ROP of DL and isolation of the resulting poly(DL)_{1,8-Oct} diol (Scheme 3.5, A₁) and ii) conventional modification with 2-bromoisobutryl bromide in DCM/TEA (Scheme 3.5, A₂). In the second, the two steps were carried out consecutively in the same polymerization Schlenk (Scheme 3.5, B), thus after ROP of DL, the mixture was diluted in DCM and TEA and 2-bromoisobutryl bromide were added. The third, involved the same two steps one-pot procedure but using N-(2-bromoisobutryl)imidazole instead of α -bromoisobutryl bromide (Scheme 3.5, C). In this case, the temperature was increased up to 55 °C to melt the BriB-Im and decrease the medium viscosity. According to the results, polyesters with similar molecular weight (Table 3.4) and complete esterification degree were obtained in all cases. However, polyesters obtained using α -bromoisobutryl bromide as acylating

agent have a slightly higher polydispersity index and a marked brown color which required further purification steps.



Scheme 3.5 Tested strategies in the modification of poly(DL)_{1,8-Oct} as BriB ester.

Table 3.4 Molecular weight and characteristics of the polymers obtained in the two steps and one pot-two steps polymerization/modification of DL.

Exp.	Polymerization ^a				Modification ^b			
	Mn ^c (g/mol) (x10 ⁻³)	Mn ^d (g/mol) (x10 ⁻³)	Đ ^d	Reagent	Mn ^e (g/mol) (x10 ⁻³)	Mn ^d (g/mol) (x10 ⁻³)	Đ ^d	Appearance
A1	19.8 ⁽¹⁾ 20.1 ⁽²⁾	24.8	1.12	--	--	--	--	colorless
A2	--	--	--	BriBBr	20.3 ⁽¹⁾ 20.5 ⁽²⁾	24.9	1.18	brown
B	20.0 ⁽¹⁾ 20.8 ⁽²⁾	24.9	1.12	BriBBr	20.1 ⁽¹⁾ 20.8 ⁽²⁾	24.5	1.17	brown
C	20.3 ⁽¹⁾ 20.6 ⁽²⁾	24.8	1.13	BriB-Im	20.1 ⁽¹⁾ 20.6 ⁽²⁾	24.8	1.15	colorless

^a Polymerization conditions: DL/1,8-Oct (150/1), DL/TBD (200/1), bulk, 25 °C and 10 h. 78 % of conversion calculated by ¹H-NMR from the crude mixture by comparing the intensities of the signals at 4.88 and 4.28 ppm (theoretical Mn 19.900 g/mol). ^b Modification using 4 Eq of BriBBr or BriB-Im per -OH. ^c Determined by ¹H-NMR from the isolated polymer by comparing the intensities of the signal at 4.88 ppm with those at 4.05 ppm⁽¹⁾ and 3.59 ppm⁽²⁾. ^d Determined by SEC in THF using PS standards. ^e Determined by ¹H-NMR from the isolated polymer by comparing the intensities of the signal at 4.88 ppm and those at 4.05 ppm¹ and 1.93 ppm².

Thus, the use of BriB-Im, allow us to perform the lactone polymerization and the polyester BriB activation following two sequential steps in one pot reaction (Scheme 3.5, C). Precipitation in acetonitrile was found to effectively eliminate not only the unreacted δ -decalactone and TBD catalyst but also the excess of BriB-Im, the imidazole by-product and traces of N-(α -bromoisobutyryl)-1,5,7-triazabicyclo[4.4.0]dec-5-ene formed in small quantities during the modification step (Figure 3.7), which signals were assigned in basis to the data reported in literature.^{27, 28}

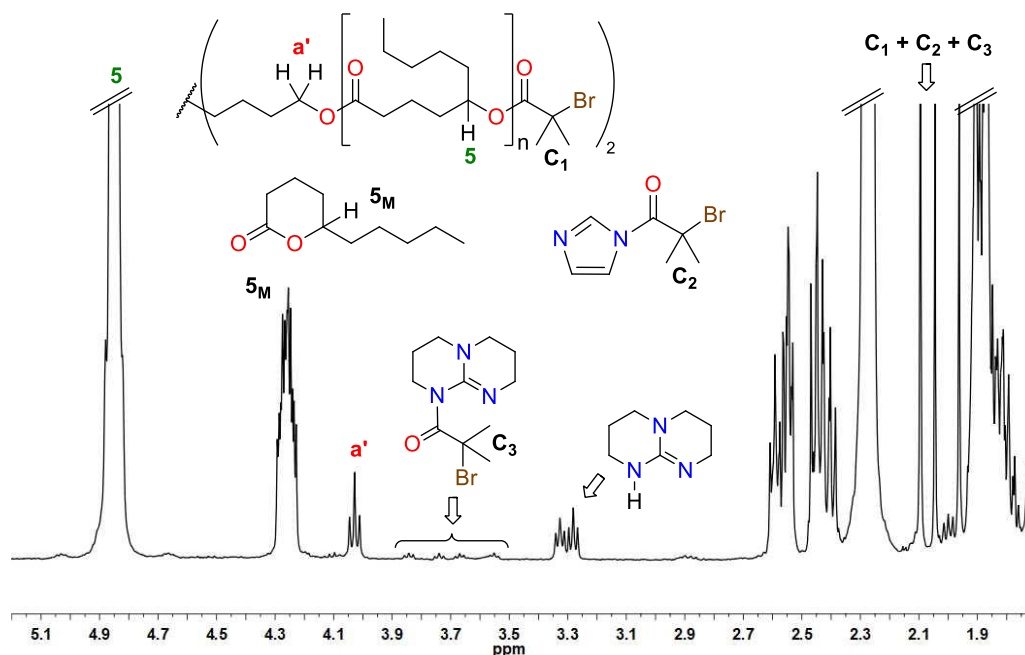


Figure 3.7 $^1\text{H-NMR}$ spectrum of crude reaction mixture in the two steps one-pot procedure for the esterification of poly(DL)_{1,8-Oct} diol using the BriB-Im.

The complete esterification of the end-groups was confirmed by $^1\text{H-NMR}$ and $^{13}\text{C-NMR}$ spectroscopy. In the case of $^1\text{H-NMR}$ spectrum the complete disappearance of the methine end-group signal at 3.59 ppm (signal 5' in Figure 3.8-a) and the appearance of a new methyl signal at 1.93 ppm (signal C in Figure 3.8-b) could be observed.

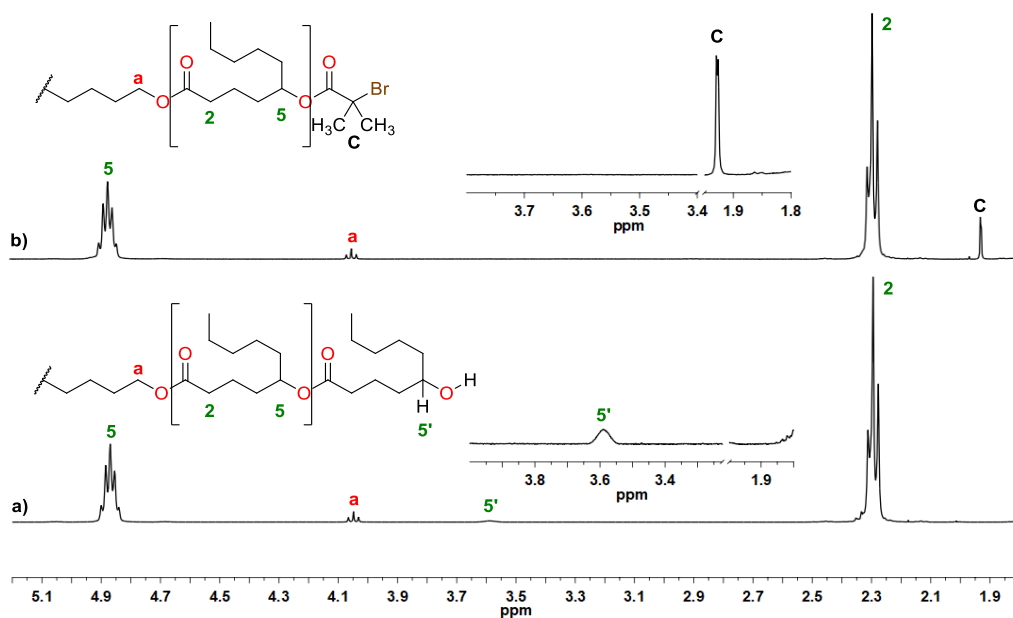


Figure 3.8 $^1\text{H-NMR}$ spectra of (a) poly(DL)_{1,8-Oct} diol and (b) poly(DL)_{1,8-Oct} BriB ester.

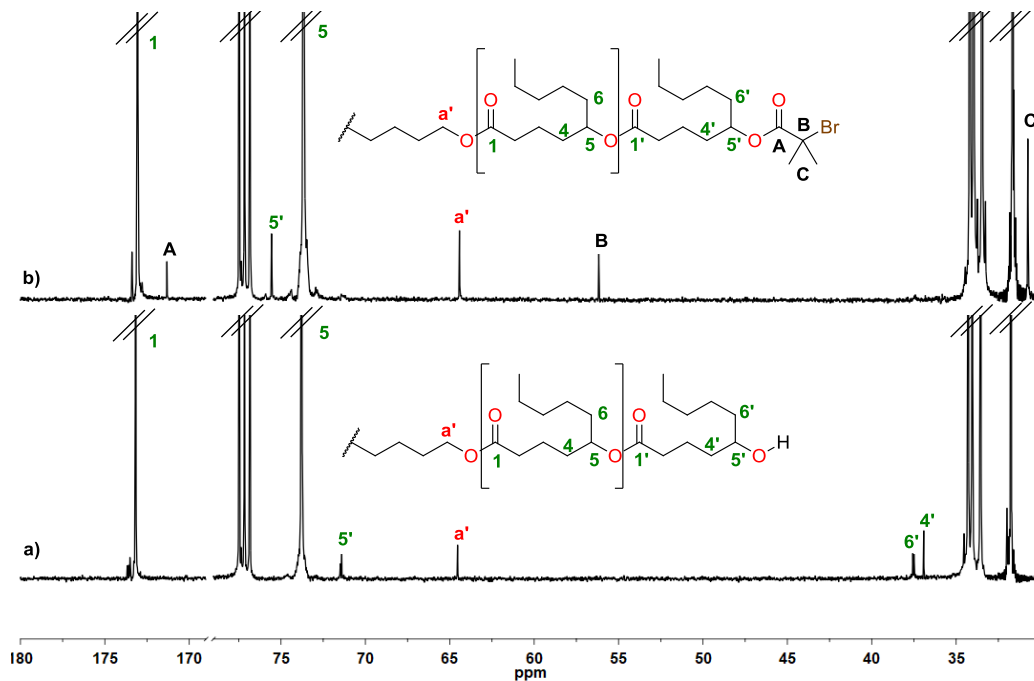


Figure 3.9 $^{13}\text{C-NMR}$ spectra of (a) poly(DL)_{1,8-Oct} diol and (b) poly(DL)_{1,8-Oct} BriB ester.

In the case of ^{13}C -NMR spectrum, the disappearance of the methine end-group signal at 71.4 ppm (signal **5'** in Figure 3.9-a) and the disappearance of the signals of the two adjacent carbons at 36.9 and 37.5 ppm (signals **4'** and **6'** respectively in Figure 3.9-a) could be observed. On the other hand, new signals at 171.3, 56.2 and 30.7 ppm corresponding to the carbonyl group, the alpha carbon and the methyls on the isobutyryl moiety, respectively (signals **A**, **B** and **C**, respectively in Figure 3.9-b) appeared.

Noticeably, ^{13}C -NMR signals of the methine ($-\underline{\text{C}}\text{H}-\text{OH}$), methylene ($-\underline{\text{C}}\text{H}_2-\text{CH}-\text{OH}$) and carbonyl ($-\underline{\text{C}}\text{O}-$) of the last repetitive units (signals **5'**, **6'** and **1'** in Figure 3.10-a and Figure 3.10-b) appears split in all the different prepared poly(DL) diols (see annex 8.13 to 8.24). This trend is not observed in the corresponding poly(DL) BriB esters (Figure 3.10-c). In fact, the carbonyl region showed a more complex pattern with some split (**1''** and **1'**) and unsplit (**1'''**) signals.

Taking into account that, as will be commented *vide infra*, the MALDI-TOF spectra show only a single species, this splitting has to be related to structural characteristics. This could be confirmed by analyzing the ^{13}C -NMR spectrum of a sample of poly(DL)_{1,8-Oct} of low molecular weight ($M_n = 1500\text{g/mol}$) which was synthesized as model for structural assignments. As can be seen in Figure 3.10-a, the intensity of the signals related to the initial and final monomeric units increases proportionally but the splitting of the signals **1'**, **5'** and **6'** remain unaffected. This fact suggests that splitting of these signals is related to sequence tacticity. This sequence sensitivity has been previously described for different six-membered lactone-based copolyesters,^{29, 30, 31, 32} but to the best of our knowledge no data referred to δ -decalactone have been reported (see annex 8.13 and 8.14).

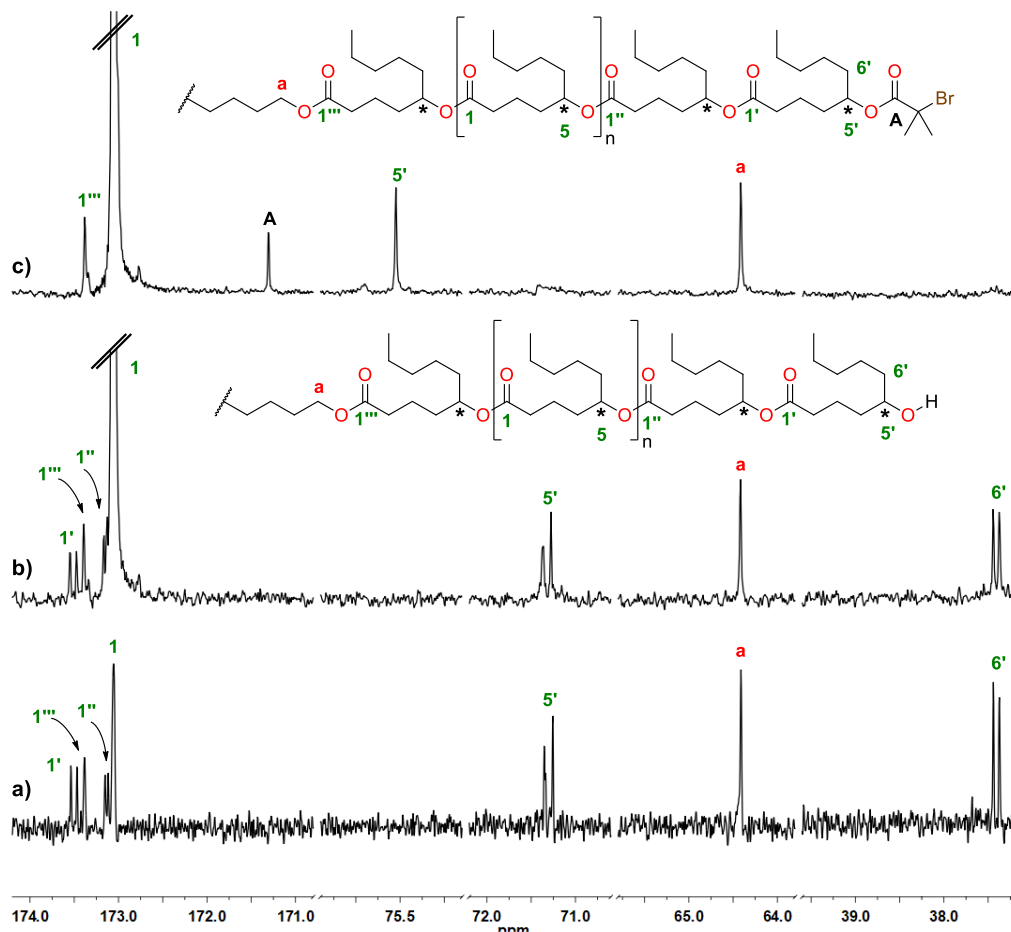


Figure 3.10 Amplification of ^{13}C -NMR spectra of (a) low molecular weight poly(DL) $_{1,8\text{-Oct}}$ diol, (b) poly(DL) $_{1,8\text{-Oct}}$ diol and (c) poly(DL) $_{1,8\text{-Oct}}$ BriB ester.

According to the ^{13}C -NMR signals pattern, this splitting is only observed in both ends of the polyester chain which could be related to different conformational environments and the existence of cyclic hydrogen bonding structures in the case of the final hydroxylic groups. The different signals could be assigned by comparison with those of model compounds (Bis(DL) $_{1,6\text{-Hex}}$ diol in Figure 3.11) (see annex 8.9), empirical calculations, and could be confirmed by the HSQC and HMBC correlation experiments (black arrow and dashed arrows respectively in Figure 3.12).

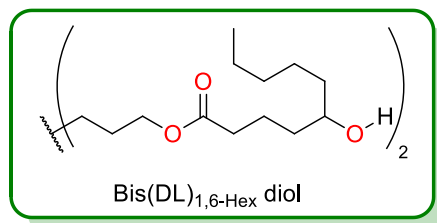


Figure 3.11 Bis(DL)_{1,6}-Hex diol as model compounds for poly(DL)_{1,8}-Oct characterization.

Thus, HSQC of poly(DL)_{1,8}-Oct diol confirms that the split signal at 71.3 and 71.4 ppm corresponds to carbon 5'' of the last monomeric unit (Figure 3.12-a) (see Figure 8.29 in annex 8.13). HMBC of poly(DL)_{1,8}-Oct BriB ester corroborates that the signal 1''' corresponds to the carbonyl from the first monomeric unit, because the existence of a 3 bonds coupling with the methylene protons from the initiator (Figure 3.12-b) (see Figure 8.34 in annex 8.14). HMBC allows also to confirm the assignment of the carbonyl A, which shows a 3-bond coupling with the methyl protons on the isobutyryl unit (Figure 3.12-b).

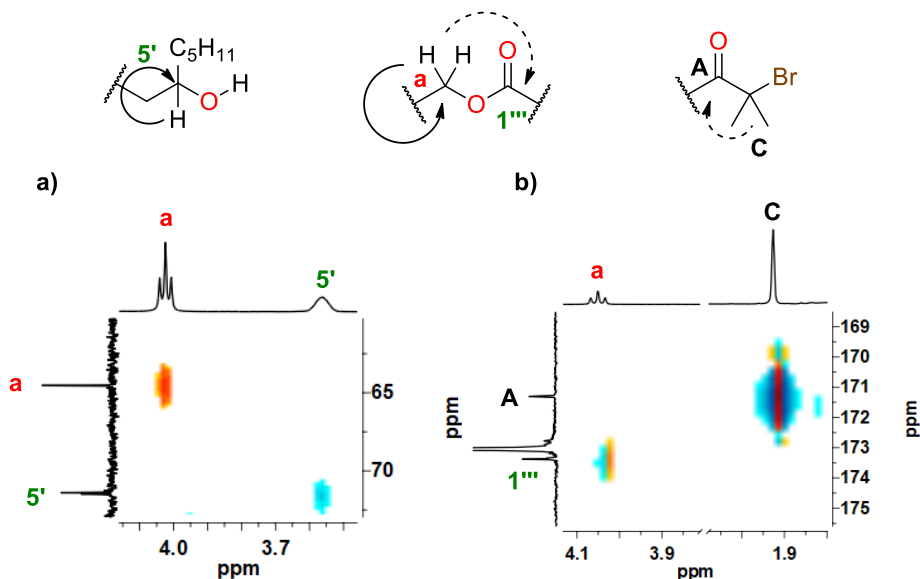


Figure 3.12 (a) HSQC of poly(DL)_{1,8}-Oct diol and (b) HMBC of poly(DL)_{1,8}-Oct BriB ester.

To further confirm the complete esterification of the hydroxyl end-groups, the polymer was analyzed by matrix-assisted laser desorption/ionization time of flight (MALDI-TOF) using *trans*-2-[3-(4-*tert*-butylphenyl)-2-methyl-2-propenylidene]malononitrile (DCTB) as matrix and potassium trifluoroacetate (KTFA) as cationization agent. As can be noted (Figure 3.13), only a single distribution can be observed in both the polyester diol and the modified polyester, which not only demonstrate the complete esterification of the hydroxylic end-groups but also confirms that all the polymer chains were initiated by 1,8-Oct. The degree of polymerization, in the case of poly(DL)_{1,8-Oct} diol, was determined by subtracting the exact masses of potassium and 1,8-Oct for each individual peak, and by dividing the obtained value by exact mass of the monomer unit. In the case of poly(DL)_{1,8-Oct} BriB ester the exact mass of two BriB units was also subtracted for each individual peak.

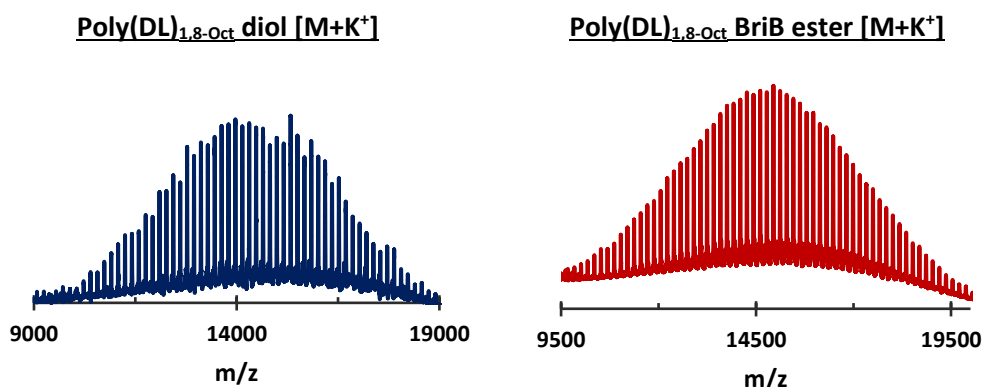


Figure 3.13 MALDI-TOF analysis of (left) poly(DL)_{1,8-Oct} diol and (right) poly(DL)_{1,8-Oct} BriB ester.

The difference between peaks corresponds to the monomeric unit exact mass (Figure 3.14) and a displacement of the peaks, within the same degree of polymerization (e.g. $n = 82$) corresponding to two BriB unit exact mass (Figure 3.14) can be observed. This fact constitutes another evidence of the complete esterification of the two hydroxyl end-groups.

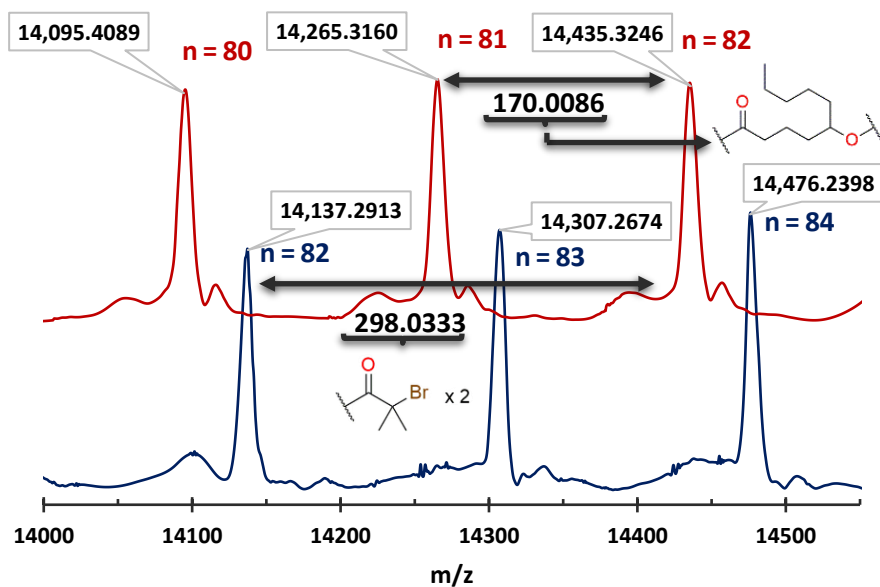
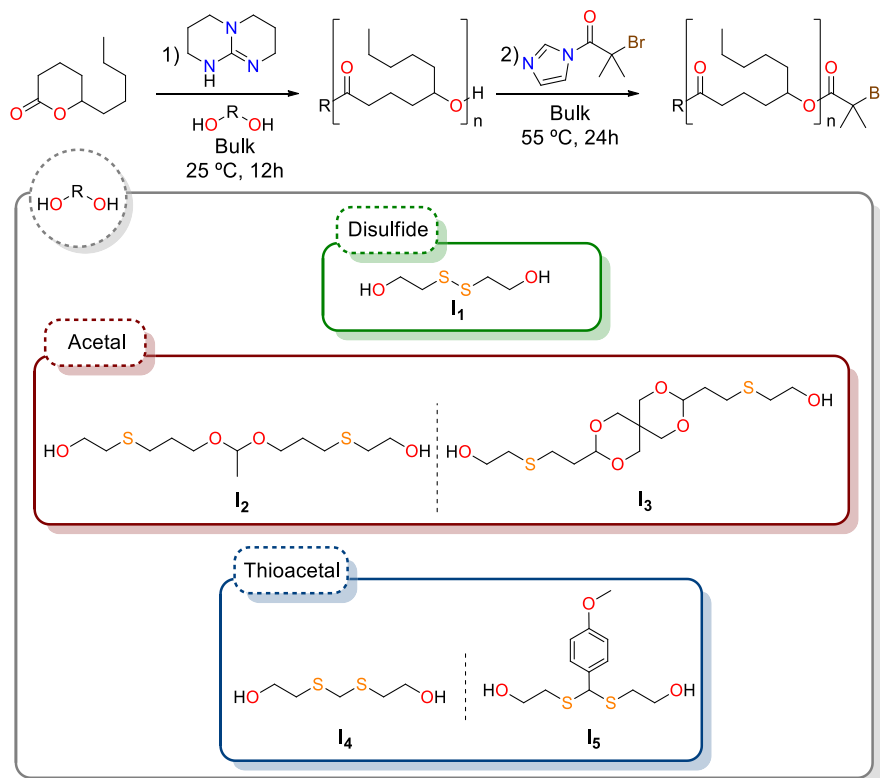


Figure 3.14 Superposition of MALDI-TOF spectra of the poly(DL)_{1,8-Oct} diol (blue) and the poly(DL)_{1,8-Oct} BriB (red).

Once tested the conditions for the polyester synthesis, as well as for its modification and purification, these conditions were applied to the synthesis of telechelic polyesters containing a cleavable mid-point moiety. The most remarkable difference between these initiators and the 1,8-Oct, in terms of polymerization, was that the drying procedures had to be modified due to the sensitive nature of some of these diol initiators.

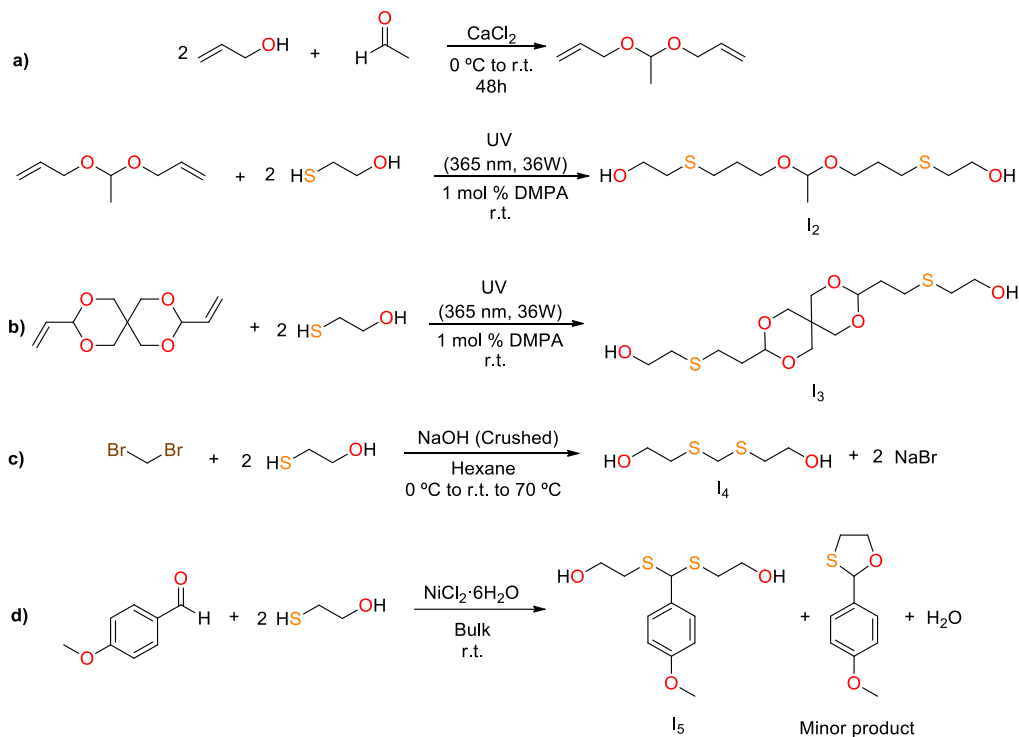
3.3 Synthesis of poly(DL) using stimuli cleavable initiators

In order to prepare telechelic poly(DL) diols with a cleavable sensitive core, different diols were chosen (Scheme 3.6): bis(2-hydroxyethyl) disulfide (*I*₁), 1,1-bis-[3-((2-hydroxyethyl)thio)propyloxy]ethane (*I*₂), 3,9-bis-[2-(ethylthio)-ethanol]-2,4,8,10-tetraoxaspiro[5.5]undecane (*I*₃), bis-((2-hydroxyethyl)thio)methane (*I*₄) and (4-methoxyphenyl)-bis-[(2-hydroxyethyl)thio]methane (*I*₅) which have disulfide, acetal or thioacetal groups. All these initiators contain terminal 2-hydroxyethylthio groups.



Scheme 3.6 ROP of DL and in-situ modification using different stimuli cleavable diol initiators.

These initiators were selected so that they contained functional groups sensitive to different external stimuli and that would have been extensively studied for the preparation of stimuli cleavable polymers. Accordingly, I₁ contains a disulfide linkage (S-S) which has been reported to be sensitive to redox conditions.³³⁻³⁸ Moreover, I₂ and I₃ contain acetal linkages (O-C-O) which are well known by its sensitive to acidic media.³⁶⁻³⁹ We also selected two initiators containing thioacetal linkages (S-C-S), I₄ and I₅. Thioacetal linkers have been far less studied but recently they have been reported as promising block linkers especially attractive due to its capability to be cleaved photochemically.⁴⁰⁻⁴⁸ Moreover, to the best of our knowledge, there are still no examples of the use of thioacetal groups as cleavable moieties in polymers for TPE applications.



Scheme 3.7 Synthesis of stimuli cleavable initiators (a) I_2 , (b) I_3 , (c) I_4 and (d) I_5 .

Diol I_1 is commercially available and only had to be purified by distillation and dried. The rest of diols were synthesized following reported procedures that were selected considering their ease to be scaled and the purification method (see experimental part 6.3). Acetals I_2 and I_3 were obtained by photo-initiated thiol-ene addition of 2-mercaptoethanol to acetaldehyde diallylacetal and 3,9-divinyl-2,4,8,10-tetraoxaspiro[5.5]undecane respectively (Scheme 3.7-a and -b respectively).⁴⁹⁻⁵² Thioacetals I_4 and I_5 were synthesized by reaction of 2-mercaptoethanol with dibromomethane in basic media (NaOH) and with anisaldehyde catalyzed by $\text{NiCl}_2 \cdot 6\text{H}_2\text{O}$ respectively (Scheme 3.7-c and -d respectively).^{53, 54} All initiators were obtained in medium to high yields (55-80%) and were purified and strictly dried as described in the experimental part (see experimental part 6.1). The chemical structure was confirmed in all cases by ESI, ^1H and ^{13}C -NMR. The assignments in NMR spectra were made based on model compounds and the data reported on the literature (see annex 8.1 to 8.5).⁴⁹⁻⁵⁴

Table 3.5 Conversion and molecular weight characteristics of the polymerization of DL with TBD initiated with different cleavable diol initiators. Polymerization conditions [DL]:[I_x]; 150:1, [TBD]:[I_x]; 0.75:1, 25 °C, in bulk.

Initiator ^a	Time (h) ^b	Conv. ^c (%)	Mn ^{Theor.} ^d (g/mol) (x10 ⁻³)	Mn ^{NMR} ^e -CH ₂ O- (g/mol) (x10 ⁻³)	Mn ^{NMR} ^f -CH ₃ x2 (g/mol) (x10 ⁻³)	Mn ^{SEC} ^g (g/mol) (x10 ⁻³)	Đ ^g
I ₁	12	80	20.7	21.7	20.4	24.8	1.29
I ₂	8	79	20.5	20.1	19.6	22.4	1.16
I ₃	15	82	21.3	22.5	22.4	24.3	1.17
I ₄	7.5	78	20.2	20.1	19.2	23.3	1.18
I ₅	7	78	20.2	19.9	19.3	22.9	1.16

^a Polymerizations were carried out at 25 °C in bulk with a DL/I_x ratio fixed at 150/1 and a TBD/I_x ratio at 0.75. Esterification of the end-groups was carried out at 55 °C in bulk using 4 eq. of BriB-Im for 24 hours. ^b The showed reaction times correspond only for the polymerization reaction and not for the esterification. ^c Determined using ¹H-NMR spectroscopy by comparison of the integrations of the signals of the polymer backbone (4.88 ppm) and the unreacted monomer (4.28 ppm). ^d Determined from the targeted DP and the obtained conversion. ^e Determined using ¹H-NMR spectroscopy by comparison of the integrations of the signals of the polymer backbone (4.88 ppm) and the initiator; I₁ = 4.33 ppm, I₂ = 4.22 ppm, I₃ = 4.21 ppm, I₄ = 4.25 ppm and I₅ = 4.17 ppm. ^f Determined using ¹H-NMR spectroscopy by comparison of the integration of the signals of the polymer backbone (4.88 ppm) and the methyl end-groups (1.93 ppm). ^g Determined using SEC in THF, relative to polystyrene standards.

ROP with these initiators were carried out using the same conditions than in Table 3.2 for 1,8-octanediol. A DP of 150 (DL/I_x = 150/1) and a TBD/I_x ratio of 0.75 (Table 3.5) were fixed. Polymer conversions were determined using ¹H-NMR spectroscopy by comparing the intensity of the polymer and monomer signals (Figure 3.3-b). Molecular weights based on the initiator were also determined using ¹H-NMR spectroscopy, in a similar way as before, by comparison of the intensity of the signals of the polymer backbone at 4.88 ppm (signal **5** in Figure 3.15) and the intensity of selected signals for each initiator at: 4.33 ppm for I₁ (signal **a**₁ in Figure 3.15-a), 4.22 ppm for I₂ (signal **a**₂ in Figure 3.15-b), 4.21 ppm for I₃ (signal **a**₃ in Figure 3.15-c), 4.25 ppm for I₄ (signal **a**₄ in Figure 3.15-d) and 4.17 ppm for signal I₅ (signal **a**₅ in Figure 3.15-e). Molecular weights according to the end-groups were determined by comparison of the intensity of ¹H-NMR signals of the polymer backbone at 4.88 ppm and the intensity of the methyl from BriB end-group at 1.93 ppm (signals **5** and **C** in Figure 3.8-b respectively) (signal -CH₃ in Figure 3.16).

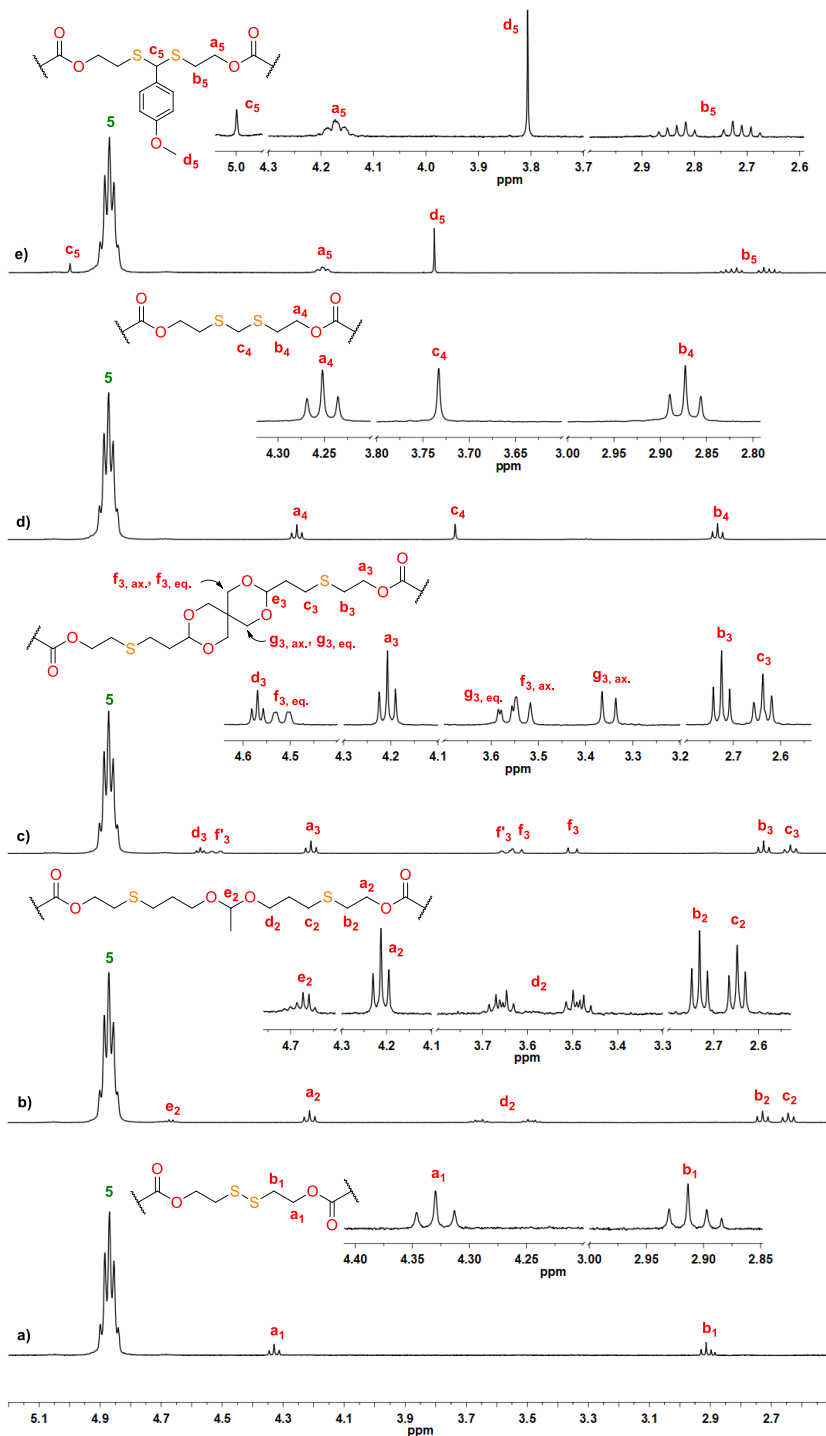


Figure 3.15 $^1\text{H-NMR}$ spectra of isolated poly(DL) BriB esters possessing different stimuli cleavable initiators.

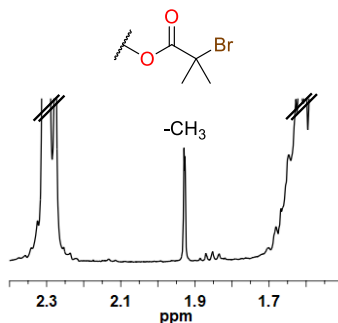


Figure 3.16 ¹H-NMR spectrum, region from 1.5 to 2.4 ppm, of poly(DL)-I₂ BriB ester.

In most cases results were similar to the obtained using 1,8-Oct as initiator, showing a good agreement between the Mn determined from the initiators, from the end-group and the theoretical ones. The SEC analysis shows molecular weights higher than the theoretical and those obtained by ¹H-NMR spectroscopy as in the prior cases (Table 3.5). Moreover, narrow polydispersities were obtained in most cases (Table 3.5 and Figure 3.17). In the case of I₁ a broader polydispersity was observed (Table 3.5). Repeated attempts to obtain a narrower molecular weight distribution with this initiator were unsuccessful, which could be related with some TBD mediated disulfide exchange with trace amounts of thiol impurities during the polymerization process.⁵⁵ Similar polydispersity values have been reported in the TBD catalyzed ROP with disulfide monomers.⁵⁶

The synthesized polymers were also analyzed by ¹³C-NMR spectroscopy, in which the signals corresponding to the initiators could be identified (see annex 8.15 to 8.24). The MALDI-TOF analysis, as in the case of 1,8-octanediol, showed only one distribution and a difference between peaks was the molecular weight of the monomer (170.13 g/mol) (see annex 8.17 to 8.24). MALDI-TOF also confirmed the complete esterification as α -bromoisobutyryl ester. In the case of the polymer containing the disulfide moiety the MALDI-TOF analysis was unsuccessful, only low molecular weight fragmentation products were observed probably caused for the instability of the disulfide bond under the MALDI-TOF conditions.⁵⁷

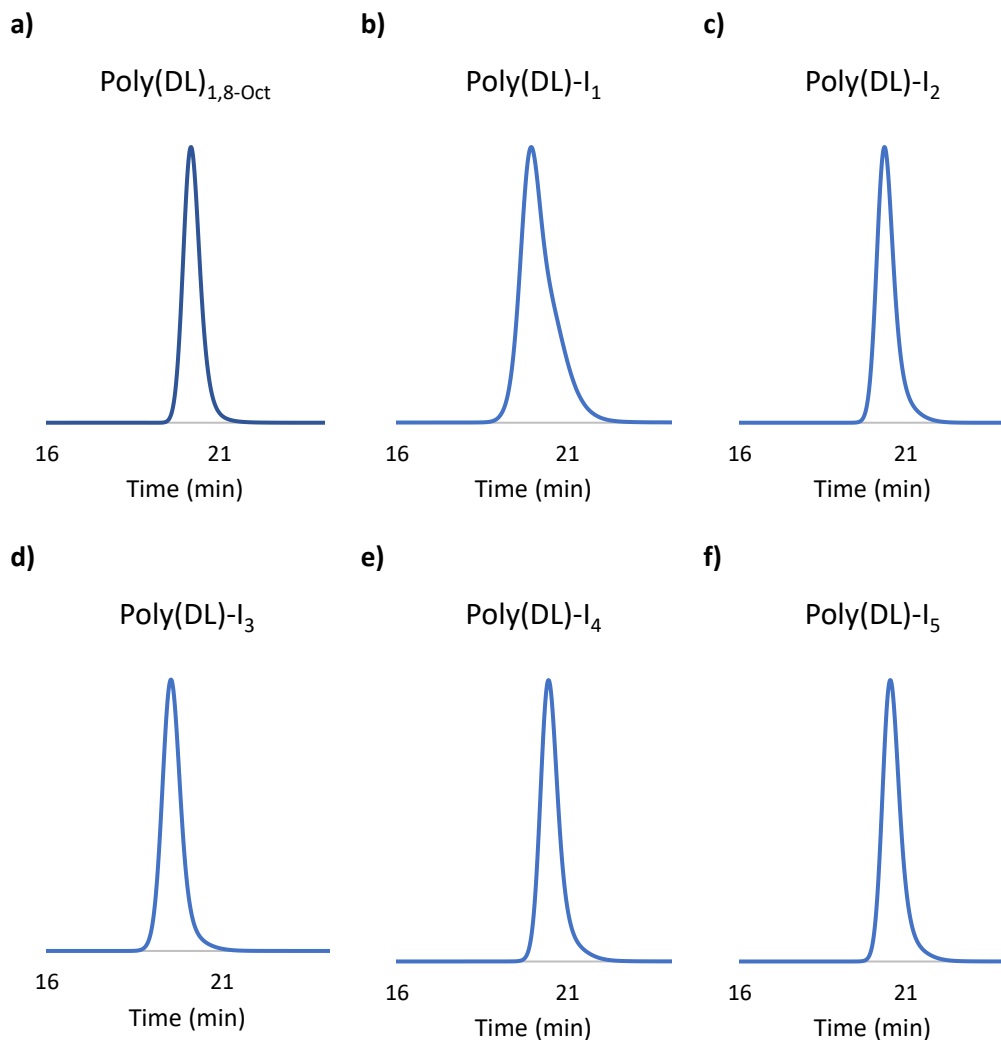


Figure 3.17 SEC (THF) chromatograms of the synthesized (a) poly(DL)_{1,8-Oct} macroinitiator and (b-f) the stimuli cleavable poly(DL)-I₁₋₅ macroinitiators.

- ¹ Kieseewetter, M. K.; Scholten, M. D.; Kirn, N.; Weber, R. L.; Hedrick, J. L.; Waymouth, R. M. Cyclic guanidine organic catalyst: What is magic about triazabicyclodecene. *J. Org. Chem.* **2009**, *74*, 9490-9496.
- ² Ruiz-Cantu, L. A.; Pearce, A. K.; Burroughs, L.; Bennett, T. M.; Vasey, C. E.; Wildman, R.; Irvine, D. J.; Alexander, C.; Taresco, V. Synthesis of methacrylate-terminated block copolymers with reduced transesterification by controlled ring-opening polymerization. *Macromol. Chem. Phys.* **2019**, *220*, 1800459.
- ³ Tang, D.; Macosko, C. W.; Hillmyer, M. A. Thermoplastic polyurethane elastomers from bio-based poly(δ -decalactone) diols. *Polym. Chem.* **2014**, *5*, 3231-3237.
- ⁴ Bandelli, D.; Helbing, C.; Weber, C.; Seifert, M.; Muljajew, I.; Jandt, K. D.; Schubert, U. S. Maintaining the hydrophilic-hydrophobic balance of polyesters with adjustable crystallinity for tailor-made nanoparticles. *Macromolecules* **2018**, *51*, 5567-5576.
- ⁵ Kim, H.; Olsson, J. V.; Hedrick, J. L.; Waymouth, R. M. Facile synthesis of functionalized lactones and organocatalytic ring-opening polymerization. *ACS Macro. Lett.* **2012**, *1*, 845-847.
- ⁶ Martello, M. T.; Burns, A.; Hillmyer, M. Bulk ring-opening transesterification polymerization of the renewable δ -decalactone using an organocatalyst. *ACS Macro Lett.* **2012**, *1*, 131-135.
- ⁷ Bansal, K. K.; Kakde, D.; Purdie, L.; Irvine, D. J.; Howdle, S. M.; Mantovani, G.; Alexander, C. New biomaterials from renewable resources – amphiphilic block copolymers from δ -decalactone. *Polym. Chem.* **2015**, *6*, 7196-7210.
- ⁸ Pascual, A.; Sardón, H.; Ruipérez, F.; Garcia, R.; Sudam, P.; Veloso, A.; Mecerreyes, D. Experimental and computational studies of ring-opening polymerization of ethylene brassylate macrolactone and copolymerization with ϵ -caprolactone and TBD-guanidine organic catalyst. *J. Polym. Sci.* **2015**, *53*, 552-561.
- ⁹ Stukenbroeker, T. S.; Bandar, J. S.; Zhang, X.; Lambert, T. H.; Waymouth, R. M. Cyclopropenimine superbases: Competitive initiation process in lactide polymerization. *ACS Macro. Lett.* **2015**, *4*, 853-856.
- ¹⁰ Bouyadhyi, M.; Pepels, M. P. F.; Heise, A.; Duchateau, R. ω -Pentadecalactone polymerization and ω -pentadecalactone/ ϵ -caprolactone copolymerization reactions using organic catalysts. *Macromolecules* **2012**, *45*, 3356-3366.
- ¹¹ Kumar, A.; Lale, S. V.; Mahajan, S.; Choudhary, V.; Koul, V. ROP and ATRP fabricated dual targeted redox sensitive polymersomes based on pPEGMA-PCL-ss-PCL-pPEGMA triblock copolymers for breast cancer therapeutics. *ACS Appl. Mater. Interfaces* **2015**, *7*, 9211-9227.
- ¹² Plichta, A.; Kowalczyk, S.; Kamiński, K.; Wasylczko, M.; Więckowski, S.; Ołędzka, E.; Nałęcz-Jawecki, G.; Zgadzaj, A.; Sobczak, M. ATRP of methacrylic derivative of camptothecin initiated with PLA toward three-arm star block copolymer conjugates with favorable drug release. *Macromolecules* **2017**, *50*, 6439-6450.
- ¹³ Magenau, A. J. D.; Kwak, Y.; Matyjaszewski, K. ATRP of methacrylates using $\text{Cu}^{\text{II}}\text{X}_2/\text{L}$ and copper wire. *Macromolecules* **2010**, *43*, 9682-9689.
- ¹⁴ Zhao, J.; Weng, Y.; Xie, D. Star-shape poly(acrylic acid)-composed glass-ionomer cements: Effect on MW and arm number on mechanical properties. *J. Appl. Polym. Sci.* **2011**, *120*, 2390-2399.
- ¹⁵ Yuan, L.; Chen, W.; Li, J.; Hu, J.; Yan, J.; Yang, D. PEG-*b*-PtBA-*b*-PHEMA well-defined amphiphilic triblock copolymer: Synthesis, self-assembly, and application in drug delivery. *J. Polym. Sci.* **2012**, *50*, 4579-4588.

- ¹⁶ Garcia, M.; Beecham, M. P.; Kempe, K.; Haddleton, D. M.; Khan, A.; Marsh, A. Water soluble triblock and pentablock poly(methacryloyl nucleosides) from copper-mediated living radical polymerisation using PEG macroinitiators. *Eur. Polym. J.* **2015**, *66*, 444-451.
- ¹⁷ Schappacher, M.; Fur, N.; Guillaume, S. M. Poly(methylmethacrylate)-poly(caprolactone) AB and ABA block copolymers by combined ring-opening polymerization and atom transfer polymerization. *Macromolecules* **2007**, *40*, 8887-8896.
- ¹⁸ Jiang, X.; Vamvakaki, M.; Narain, R. Copper-catalyzed bimolecular coupling of α,ω -dibromide-functionalized poly(ϵ -caprolactone). *Macromolecules*, **2010**, *43* 3228-3232.
- ¹⁹ Chatterjee, U.; Wang, X.; Jewrajka, S. K.; Souzek, M. D. Polyester/poly(meth)acrylate block copolymers by combined polycondensation/ATRP: Characterization and properties. *Macromol. Chem. Phys.* **2011**, *212*, 1879-1890.
- ²⁰ Sathesh, V.; Chen, J.-K.; Chang, C.-J.; Aimi, J.; Chen, Z.-C.; Hsu, Y.-C.; Huang, Y.-S.; Huang, C.-F. Synthesis of poly(ϵ -caprolactone)-based miktoarm star copolymers through ROP, SA ATRC, and ATRP. *Polymers* **2018**, *10*, 858.
- ²¹ H.A. Staab, W. Rohr in *Newer methods for preparative organic chemistry*, *Angewandte Chemie*, W. Foerst Ed. Academic Press, New York **1968**, Vol. 5, 61-108. ISBN 0122617037.
- ²² Dunn, P. J.; Hoffmann, W.; Kang, Y.; Mitchell, J. C.; Snowden, M.J. A comparison of catalysts to promote imidazolide couplings including the identification of 2-hydroxy-5-nitropyridine as a new, safe, and effective catalyst. *Org. Process Res. Dev.* **2005**, *9*, 956-961.
- ²³ Zhu, A.; Wang, Z.; Xie, M.; Zhang, Y. Synthesis of imidazole end-capped poly(*n*-butyl methacrylate)s via atom transfer radical polymerization with a new functional initiator containing imidazolium group. *e-Polymers* **2007**, 009.
- ²⁴ Voepel, J.; Edlund, U.; Albertsson, A.-C.; Percec, V. Hemicellulose-based multifunctional macroinitiator for single-electron-transfer mediated living radical polymerization. *Biomacromolecules* **2011**, *12*, 253-259.
- ²⁵ Edlund, U.; Albertsson, A.-C. Macroinitiator halide effects in galactoglucomannan-mediated single electron transfer-living radical polymerization. *J. Poly. Sci. Part A: Polym. Chem.* **2011**, *49*, 4139-4145.
- ²⁶ Navarro, J. R. G.; Wennmalm, S.; Godfrey, J.; Breitholtz, M.; Edlund, U. Luminescent nanocellulose platform: From controlled graft block copolymerization to biomarker sensing. *Biomacromolecules* **2016**, *17*, 1101-1109.
- ²⁷ Lohmeijer, B. G. G.; Pratt, R. C.; Leibfarth, F.; Logan, J. W.; Long, D. A.; Dove, A. P.; Nederberg, F.; Choi, J.; Wade, C.; Waymouth, R. M.; Hedrick, J. L. Guanidine and amidine organocatalysts for ring-opening polymerization of cyclic esters. *Macromolecules* **2006**, *39*, 8574-8583.
- ²⁸ Pratt, R. C.; Lohmeijer, B. G. G.; Long, D. A.; Waymouth, R. M.; Hedrick, J. L. Triazabicyclodecene: A simple bifunctional organocatalyst for acyl transfer and ring-opening polymerization of cyclic esters. *J. Am. Chem. Soc.* **2006**, *128*, 4556-4557.
- ²⁹ Song, Q.; Xia, Y.; Hu, S.; Zhao, J.; Zhang, G. Tuning the crystallinity and degradability of PCL by organocatalytic copolymerization with δ -hexalactone. *Polymer* **2016**, *102*, 248-255.
- ³⁰ Fernández, J.; Larrañaga, A.; Etxeberria, A.; Sarasua, J.-R. Ethylene brassylate-co- δ -hexalactone biobased polymers for application in the medical field: synthesis, characterization and cell culture studies. *RSC Adv.* **2016**, *6*, 22121-22136.
- ³¹ Fernández, J.; Etxeberria, A.; Sarasua, J.-R. Synthesis and properties of ω -pentadecalactone-co- δ -hexalactone copolymers: a biodegradable thermoplastic elastomer as an alternative to poly(ϵ -caprolactone). *RSC Adv.* **2016**, *6*, 3137-3149.

- ³² Delgove, M. A. F.; Luchies, J.; Wauters, I.; Deroover, G. G. P.; De Wildeman, S. M. A.; Bernaerts, K. V. Increasing the solubility range of polyesters by tuning their microstructure with comonomers. *Polym. Chem.* **2017**, *8*, 4696-4706.
- ³³ Tsarevsky, N. V.; Matyjaszewski, K. Combining atom transfer radical polymerization and disulfide/thiol redox chemistry: A route to well-defined (bio)degradable polymeric materials. *Macromolecules* **2005**, *38*, 3087-3092.
- ³⁴ Nelson-Mendez, A.; Aleksanian, S.; Oh, M.; Lim, H.-S.; Oh, J. K. Reductively degradable polyester-based block copolymers prepared by facile polycondensation and ATRP: synthesis, degradation, and aqueous micellization. *Soft Matter* **2011**, *7*, 7441-7452.
- ³⁵ Xuan, J.; Han, D.; Xia, H.; Zhao, Y. Dual-stimuli-responsive micelle of an ABC triblock copolymer bearing a redox-cleavable unit and a photocleavable unit at two block junctions. *Langmuir* **2014**, *30*, 410-417.
- ³⁶ Jazani, A. M.; Oh, J. K. Dual location, dual acidic pH/reduction-responsive degradable block copolymer: Synthesis and investigation of ketal linkage instability under ATRP conditions. *Macromolecules* **2017**, *50*, 9427-9436.
- ³⁷ Jazani, A. M.; Arezi, N.; Maruya-Li, K.; Jung, S.; Oh, J. K. Facile strategies to synthesize dual location dual acidic pH/reduction-responsive degradable block copolymers bearing acetal/disulfide block junctions and disulfide pendants. *ACS Omega* **2018**, *3*, 8980, 8991.
- ³⁸ Moreno, A.; Ronda, J. C.; Cádiz, V.; Galià, M.; Lligadas, G.; Percec, V. SET-LRP from programmed difunctional initiators encoded with double single-cleavage and double dual-cleavage groups. *Biomacromolecules* **2019**, *20*, 3200-3210.
- ³⁹ Zheng, L.; Zhang, X.; Wang, Y.; Liu, F.; Peng, J.; Zhao, X.; Yang, H.; Ma, L.; Wang, B.; Chang, C.; Wei, H. Fabrication of acidic pH-cleavable polymer for anticancer drug delivery using a dual functional monomer. *Macromolecules* **2018**, *19*, 3874-3882.
- ⁴⁰ Lin, G.-Q.; Yi, W.-J.; Liu, Q.; Yang, X.-J.; Zhao, Z.-G. Aromatic thioacetal-bridged ROS-responsive nanoparticles as novel gene delivery vehicles. *Molecules* **2018**, *23*, 2061.
- ⁴¹ Cao, Z.; Ma, Y.; Sun, C.; Lu, Z.; Yao, Z.; Wang, J.; Li, D.; Yuan, Y.; Yang, X. ROS-sensitive polymeric nanocarriers with red light-activated size shrinkage for remotely controlled drug release. *Chem. Mater.* **2018**, *30*, 517-525.
- ⁴² Dariva, C. G.; Coelho, J. F. J.; Serra, A. C. Near infrared light-triggered nanoparticles using singlet oxygen photocleavage for drug delivery systems. *J. Control. Release* **2019**, *294*, 337-354.
- ⁴³ Seah, G. L.; Yu, J. H.; Koo, B. I.; Lee, D. J.; Nam, Y. S. Cancer-targeted reactive oxygen species-degradable polymer nanoparticles for near infrared light-induced drug release. *J. Mater. Chem. B* **2018**, *6*, 7737-7749.
- ⁴⁴ Wang, C.; Huang, B.; Yang, G.; Ouyang, Y.; Tian, J.; Zhang, W. NIR-Triggered multifunctional and degradable nanoplatfom based on an ROS-sensitive block copolymer for imaging-guided chemophototherapy. *Biomacromolecules* **2019**, *20*, 4218-4229.
- ⁴⁵ Xu, L.; Zhao, M.; Gao, W.; Yang, Y.; Zhang, J.; Pu, Y.; He, B. Polymeric nanoparticles responsive to intracellular ROS for anticancer drug delivery. *Colloids Surf. B* **2019**, *181*, 252-260.
- ⁴⁶ Phua, S. Z. F.; Xue, C.; Lim, W. Q.; Yang, G.; Chen, H.; Zhang, Y.; Wijaya, C. F.; Luo, Z.; Zhao, Y. Light-responsive prodrug-based supramolecular nanosystems for site-specific combination therapy of cancer. *Chem. Mater.* **2019**, *31*, 3349-3358.
- ⁴⁷ Mohammed, F.; Ke, W.; Mukerabigwi, J. F.; Japir, A. A.-W. M. M.; Ibrahim, A.; Wang, Y.; Zha, Z.; Lu, N.; Zhou, M.; Ge, Z. ROS-responsive polymeric nanocarriers with photoinduced exposure of cell-penetrating moieties for specific intracellular drug delivery. *ACS Appl. Mater. Interfaces* **2019**, *11*, 31681-31692.

-
- ⁴⁸ Wang, K.; Tu, Y.; Yao, W.; Zong, Q.; Xiao, X.; Yang, R.-M.; Jiang, X.-Q.; Yuan, Y. Size-switchable nanoparticles with self-destructive and tumor penetration characteristics for site-specific phototherapy of cancer. *ACS Appl. Mater. Interfaces* **2020**, *12*, 6933-6943.
- ⁴⁹ Hurd, C. D.; Pollack, M. A. The rearrangement of vinyl ethers. *J. Am. Chem. Soc.* **1938**, *60*, 1905-1911.
- ⁵⁰ Luch, C.; Ronda, J. C.; Galià, M.; Lligadas, G.; Cádiz, V. Rapid approach to biobased telechelics through two one-pot thiol-ene click reactions. *Biomacromolecules* **2010**, *11*, 1646-1653.
- ⁵¹ Lingier, S.; Espeel, P.; Suarez, S. S.; Türünç, O.; De Wildeman, S.; Du Prez, F. E. Renewable thermoplastic polyurethanes containing rigid spiroacetal moieties. *Eur. Polym. J.* **2015**, *70*, 232-239.
- ⁵² Wróblewska, A. A.; Lingier, S.; Noordijk, J.; Du Prez, F. E.; De Wildeman, S. M. A.; Bernaerts, K. V. Polyamides based on a partially bio-based spirodiamine. *Eur. Polym. J.* **2017**, *96*, 221-231.
- ⁵³ Kaushik, M. P.; Rana, H. Facile one-step synthesis of dithiaalkanediols. *Org. Prep. Proced. Int.* **2005**, *37*, 268-272.
- ⁵⁴ Laskar, R. A.; Begum, N. A.; Mir, M. H.; Rohman, M. R.; Khan, A. T. Nickel(II) chloride hexahydrate catalyzed reaction of aromatic aldehydes with 2-mercaptoethanol: formation of supramolecular helical assemblage of the product. *Tetrahedron Lett.* **2013**, *54*, 5839-5844.
- ⁵⁵ Putzu, M.; Gräter, F.; Elstner, M.; Kubař, T. On the mechanism of spontaneous thiol-disulfide exchange in proteins. *Phys. Chem. Chem. Phys.* **2018**, *20*, 16222-16230.
- ⁵⁶ Yan, B.; Liang, B.; Hou, J.; Wei, C.; Xiao, Y.; Lang, M. Organocatalytic ring-opening polymerization of disulfide functional macrocyclic carbonates. *Eur. Polym. J.* **2020**, *123*, 109452.
- ⁵⁷ Gaillot, C.; Delolme, F.; Fabre, L.; Charreyre, M.-T.; Ladavière, C.; Favier, A. Taking advantage of oxidation to characterize thiol-containing polymer chains by MALDI-TOF mass spectrometry. *Anal. Chem.* **2020**, *92*, 3804-3809.

Chapter 4

Atom Transfer Radical Polymerization: Synthesis of homopolymers and block copolymers

UNIVERSITAT ROVIRA I VIRGILI
STIMULI-RESPONSIVE CALIX[4]PYRROLE AND CALIX[4]ARENE BASED RECEPTORS: FROM UNIMOLECULAR
TO DIMERIC STRUCTURES

Pedro Miguel Mendonça Ferreira

4 Atom Transfer Radical Polymerization: Synthesis of homopolymers and ABA block copolymers

As it has been mentioned in the introduction, atom transfer radical polymerization (ATRP) of α -methylene- γ -butyrolactone (MBL) was chosen for the obtention of the glassy/hard block. The synthesis of poly(MBL), by this polymerization technique, has already been described by Mosnáček and Matyjaszewski.¹ They synthesized an ABA block copolymer using poly(*n*-butyl acrylate) as macroinitiator. Since MBL has equal, or higher, reactivity than MMA, they used the halogen exchange effect to provide at least equal rate of initiation in comparison with the rate of propagation and for this reason the catalytic system used was CuCl/CuCl₂/bpy. They obtained well-defined triblock copolymers with narrow molecular weight distribution and predictable molecular weight.

Later, Hillmyer et. al. used a combination of ROP and ATRP for the obtention of an ABA block copolymer, using dibromo end-functionalized poly(menthide) as macroinitiator (of 100000 g/mol) and MBL as monomer.² They used the same catalytic system as Matyjaszewski et. al. obtaining a series of block copolymers with different poly(MBL) composition (from 6 to 20 % (wt)). The copolymers possessing a 15-20 % of hard block showed the best mechanical performance, being comparable to commercial SBS.

The poly(MBL) fraction can be modulated by targeting an specific degree of polymerization (DP) and reaching high conversions, however this could entail undesired termination processes and the increase of the dead chain fraction (DCF) when reaching maximum conversion. In another approach, which gives the target low DP, a higher DP is employed, and the reaction is stopped at relatively low conversions. This last approach allows a better control of the polymerization due to a higher monomer concentration, which is favorable in ATRP, especially in this case where the insolubility

usually performed in bulk or in relatively nonpolar solvents, such as toluene or xylene,³ polar solvents are necessary due to the insolubility of the poly(MBL). The use of polar solvents increases the activation rate constants while the deactivation rate constant is less affected, which often leads to limited control on the polymerization (see section 1.13.5). Moreover, polar solvents such as DMF and DMSO can compete with the ligand by complexing the metal and, therefore, affecting to the redox potential of the catalytic system.^{4,5} In fact, there are examples of ATRP in polar solvent without the addition of ligand.⁶ The copper chloride salts, instead of the copper bromide salts, are necessary to take profit of the halogen exchange (HE) effect (see section 1.13.4). The use of the HE effect is necessary to increase the initiation efficiency, as the bromine propagating specie possess higher activity than the bromine initiator due to the back-strain effect.⁷

Table 4.1 Conversion and molecular weight characteristics versus time of the polymerization of MMA with CuCl/CuCl₂/bpy initiated with EtBriB. Polymerization conditions [MMA]:[EtBriB]:[CuCl]:[CuCl₂]:[bpy]; 125:1:1.1:0.1:2.4, 50 °C, in DMF (60% v/v).

Aliquot	Time (h)	Conv. ^a (%)	Mn _{Theor.} ^b (g/mol) (x10 ⁻³)	Mn _{NMR} ^c CH ₃ CH ₂ O- (g/mol) (x10 ⁻³)	Mn _{SEC} ^d (g/mol) (x10 ⁻³)	Đ ^d
1	0.5	7.2	1.1	1.4	0.9	2.08
2	1.0	14.3	2.0	2.2	2.1	1.45
3	1.5	19.4	2.6	3.0	2.9	1.41
4	2.0	24.3	3.2	3.7	3.5	1.41
5	4.0	39.7	5.2	5.8	5.9	1.36
6	6.0	49.3	6.4	6.9	6.7	1.29
7	12.0	67.2	8.6	8.7	9.2	1.27
8	21.0	80.6	10.3	10.6	13.1	1.25

^a Determined by ¹H-NMR spectroscopy from the crude reaction mixture using the signals of monomer (3.75 ppm) and polymer backbone (3.60 ppm). ^b Calculated from the conversion degree determined by ¹H-NMR spectroscopy and the target DP. ^c Determined by ¹H-NMR spectroscopy using the signals of initiator (4.09 ppm) and the polymer backbone (3.60 ppm). ^d Determined by SEC using THF as eluent and a PMMA standard calibration curve.

The conversion was determined by ¹H-NMR spectroscopy by comparison of the signals of the methyl ester protons of the polymer backbone, at 3.60 ppm (signal **1** in Figure 4.1-a) and the unreacted monomer, at 3.75 ppm (signal **1_M** in Figure 4.1-a). The

initiation efficiency could also be determined by $^1\text{H-NMR}$ spectroscopy by comparison of the signals of the unreacted initiator 4.23 ppm (signal **a** in Figure 4.1-a) and the initiator incorporated to the polymer chain at 4.09 ppm (signal **a'** in Figure 4.1). The initiation efficiency (I_{eff}) in the first stages of the polymerization (0.5 hours) is 87%, which is in concordance with the reported in the literature for this initiator (see section 1.13.3).⁸ The advance of the polymerization was followed withdrawing samples at preset times up to high conversion degrees (Table 4.1), which were analyzed by both $^1\text{H-NMR}$ spectroscopy and SEC using PMMA standards. In this way, a conversion of 80.6% was estimated after 21 hours (aliquot 8 in Table 4.1). The I_{eff} at this conversion was 94 %. The reaction was quenched by; bubbling air though the crude reaction mixture to oxidize the catalyst, diluting with DCM, and filtering through a short basic alumina column to remove the catalyst. Finally, the polymer was isolated by precipitating in an excess of cold methanol.

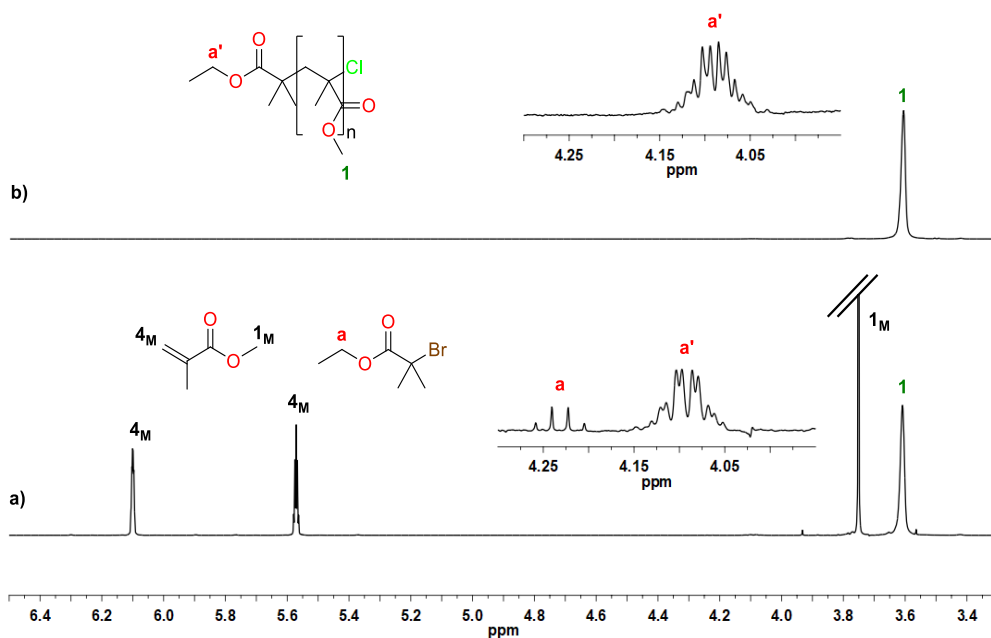


Figure 4.1 $^1\text{H-NMR}$ spectra of (a) polymerization mixture at 50% conversion and (b) isolated polymer after precipitation with methanol.

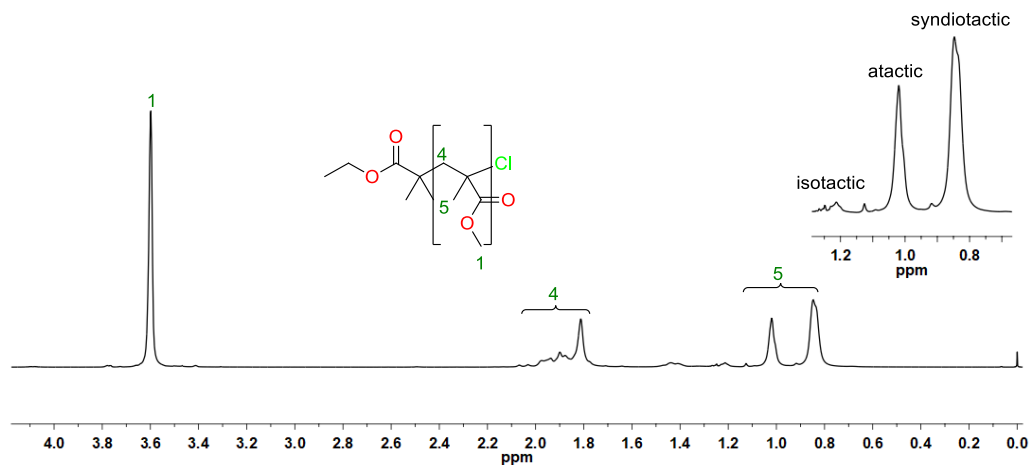


Figure 4.2 ¹H-NMR spectrum in CDCl₃ of isolated poly(MMA)_{EtBriB}.

The ¹H-NMR spectrum of the isolated poly(MMA)_{EtBriB} (Figure 4.2) shows that the obtained polymer was predominantly syndiotactic. Tacticity on poly(MMA) could be determined from the α-methyl protons (signals 5).⁹ The tacticity could also be observed in the ¹³C-NMR spectrum, in which the triads, tetrads and pentads were assigned from the data reported in the literature (see annex 8.25).

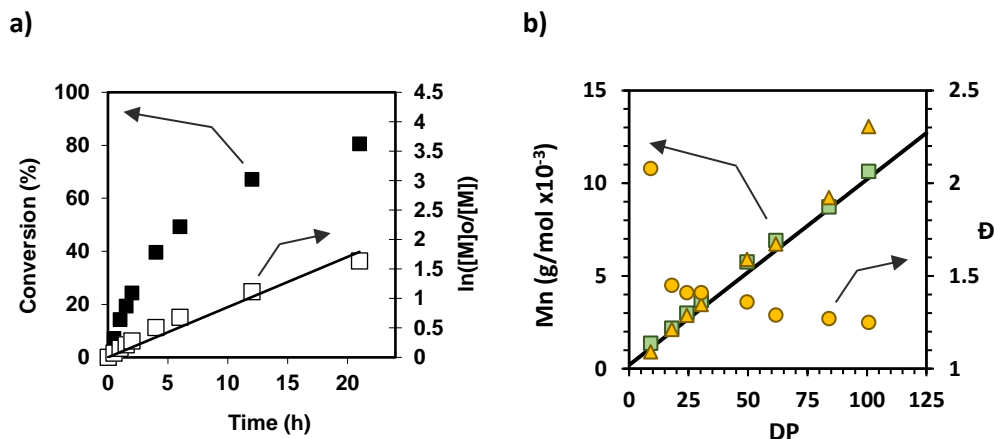


Figure 4.3 ATRP of MMA. Representation of (a) the conversion versus time (black squares) and the logarithm of monomer conversion versus time (white squares) and the representation of (b) Mn evolution, determined by both ¹H-NMR spectroscopy, using the signal of the initiator (green squares), and by SEC (yellow triangles), polydispersity is represented as yellow circles. The theoretical Mn is represented as a black line.

Figure 4.3-a (black squares) shows the evolution of the polymer conversion determined by $^1\text{H-NMR}$ spectroscopy versus time. The reaction was stopped before reaching total conversion to ensure good chain-end fidelity. Additionally, the representation of the logarithm of monomer conversion vs time give a linear plot indicating the living character of the polymerization (white squares in Figure 4.3-a).

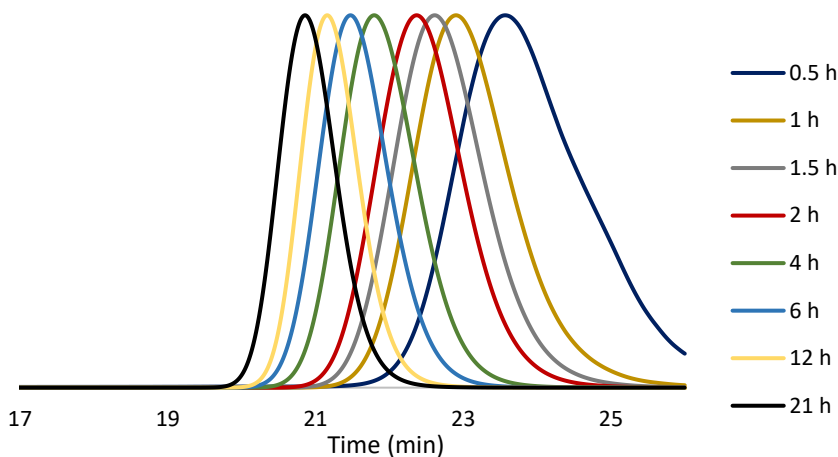
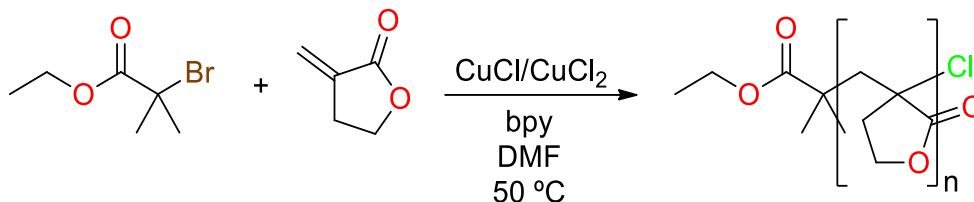


Figure 4.4 Superposed chromatograms of the withdrawn samples at preset times on ATRP of MMA using EtBrIB as initiator.

The number average molecular weight (M_n) was determined by $^1\text{H-NMR}$ spectroscopy, by comparison of the signals of the polymer backbone at 3.60 ppm (signal **1**, $\text{CH}_3\text{O-}$, in Figure 4.1-b) and the signal of the initiator at 4.09 ppm (signal **a'**, $\text{CH}_3\text{CH}_2\text{O-}$, in Figure 4.1-b). The M_n was also determined by size exclusion chromatography (SEC) using PMMA calibration standards. The M_n determined by both $^1\text{H-NMR}$ spectroscopy and SEC were slightly higher than to the theoretical one (Table 4.1), which is attributed to the unreacted initiator. Nevertheless, the M_n determined by both $^1\text{H-NMR}$ spectroscopy (green squares in Figure 4.3-b) and SEC (yellow triangles in Figure 4.3-b) increases linearly with conversion and the polydispersity decreases with increasing conversion, as usually is observed in ATRP (Table 4.1 and yellow circles in Figure 4.3-b). Narrow polydispersities were obtained as can be observed at the superposed chromatograms showed in Figure 4.4.

4.2 Synthesis of poly(MBL) by ATRP



Scheme 4.2 ATRP of MBL using EtBr as initiator and CuCl/CuCl₂/bpy as catalytic system.

Once tested the effectiveness of the reported conditions with MMA, they were applied to the MBL polymerization. Thus, using the same DP ([MBL]:[EtBr] = 125:1) and the same conditions ([EtBr]:[CuCl]:[CuCl₂]:[bpy] = 1:1.1:0.1:2.4) (Table 4.2) (see experimental part 6.8.2.2). The polymerization was monitored withdrawing samples at preset times, up to high conversions, for both ¹H-NMR spectroscopy and SEC analysis. The samples for the NMR spectroscopy were prepared in DMF-d₇ due to the insolubility of poly(MBL) in common solvents.

Table 4.2 Conversion and molecular weight characteristics versus time of the polymerization of MBL with CuCl/CuCl₂/bpy initiated with EtBr. Polymerization conditions [MBL]:[EtBr]:[CuCl]:[CuCl₂]:[bpy]: 125:1:1.1:0.1:2.4, 50 °C, in DMF (60% v/v).

Aliquot	Time (h)	Conv. ^a (%)	Mn _{Theor.} ^b (g/mol) (x10 ⁻³)	Mn _{NMR} ^c (CH ₃) ₂ -C (g/mol) (x10 ⁻³)	Mn _{SEC} ^d (g/mol) (x10 ⁻³)	Đ ^d
1	0.5	4.4	0.8	2.0	1.6	1.08
2	3.0	20.4	2.7	3.7	4.2	1.14
3	5.0	31.5	4.0	5.6	6.2	1.10
4	14.0	55.3	7.0	8.7	9.9	1.07
5	20	64.9	8.1	10.4	11.7	1.06
6	24	67.9	8.5	12.0	12.0	1.06

^a Determined by ¹H-NMR spectroscopy from the crude reaction mixture using the signals of monomer (4.40 ppm) and polymer backbone (4.49 ppm). ^b Calculated from the conversion degree determined by ¹H-NMR spectroscopy and the target DP. ^c Determined by ¹H-NMR spectroscopy using the signals of initiator (1.17 ppm) and the polymer backbone (4.49 ppm) ^d Determined by SEC using DMF (0.05% (w/w) LiBr) as eluent and a PMMA standard calibration curve.

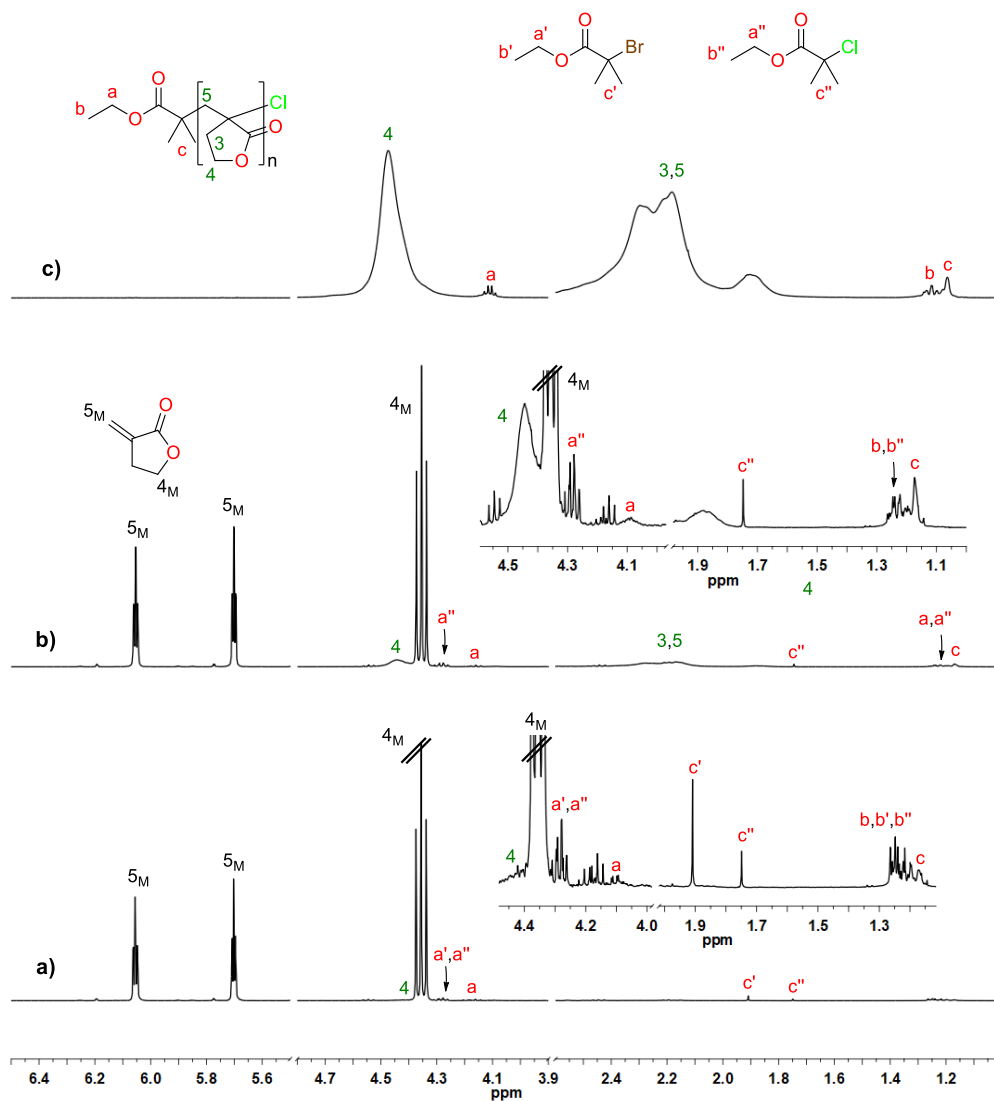
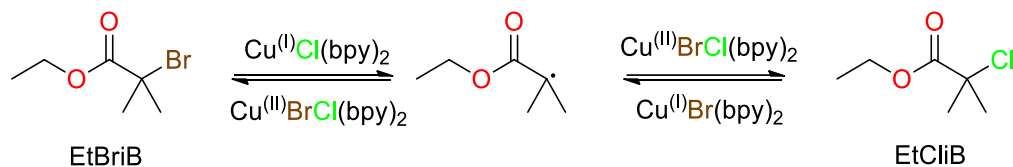


Figure 4.5 $^1\text{H-NMR}$ spectra in DMF-d_7 of (a) polymerization mixture at 4% of conversion, (b) polymerization mixture at 20% of conversion and (c) isolated polymer after precipitation with methanol.

The conversion was determined by $^1\text{H-NMR}$ spectroscopy in a similar manner as the previous experiment, by comparison of the signals of the methylene protons of the polymer backbone at 4.49 ppm (signal **4** in Figure 4.5) and the methylene protons of the unreacted monomer at 4.40 ppm (signal **4_M** in Figure 4.5). These signals were assigned by comparison of the data reported in the literature.¹⁰ Molecular weight

determined by $^1\text{H-NMR}$ spectroscopy could not be obtained using the same initiator signal as in the case of MMA (signal **a** in Figure 4.5), as this signal is partially overlapped with the signal of the polymer backbone (signal **4** in Figure 4.5). In this case, the signal of the α -methyl ($\alpha\text{-CH}_3$) of the initiator (signal **c** in Figure 4.5) was used for the determination of the molecular weight. This signal was also used for the determination of the initiation efficiency. At the early stages of the reaction (4% of conversion) can be observed the appearance of a peak at 1.17 ppm corresponding to the $\alpha\text{-CH}_3$ of the reacted initiator (signal **c** in Figure 4.5-a). The $\alpha\text{-CH}_3$ signal of the EtBrIB (1.91 ppm) (signal **c'** in Figure 4.5-a) is still present and another signal at 1.75 ppm appeared (signal **c''** in Figure 4.5-a). This new signal, according to the data reported in the literature, could correspond to ethyl α -chloroisobutyrate (EtClIB),^{11, 12} which might be formed in the deactivation process of the ethyl isobutyrate radical with the CuCl_2 before the incorporation of the first monomer (Scheme 4.3).



Scheme 4.3 Formation of ethyl α -chloroisobutyrate during the deactivation process in ATRP.

The advance of the polymerization was followed withdrawing samples at preset times (Table 4.2), which were analyzed by both $^1\text{H-NMR}$ spectroscopy and SEC in DMF (0.05% LiBr). At 20% of conversion the EtBrIB was totally consumed (Figure 4.5-b), and although the signal of the EtClIB is still present, the initiation efficiency ($I_{\text{eff.}}$) was 85%. The $I_{\text{eff.}}$ was determined by comparison of the signals of the initiator incorporated to the polymer chain (1.17 ppm, signal **c** in Figure 4.5) and the signal of the unreacted EtClIB (1.75 ppm, signal **c''** in Figure 4.5). The $I_{\text{eff.}}$ increased up to 92% at the end of the reaction. The unreacted EtClIB was eliminated in the purification process (Figure 4.5-c).

After 24 hours a conversion of 67.9% was estimated (Aliquot 6 in Table 4.2). The reaction was quenched by; bubbling air through the crude reaction mixture to oxidize the catalyst, diluting with additional DMF, and filtering through a short basic alumina column to remove the catalyst. Finally, the polymer was isolated by precipitating in an excess of cold methanol.

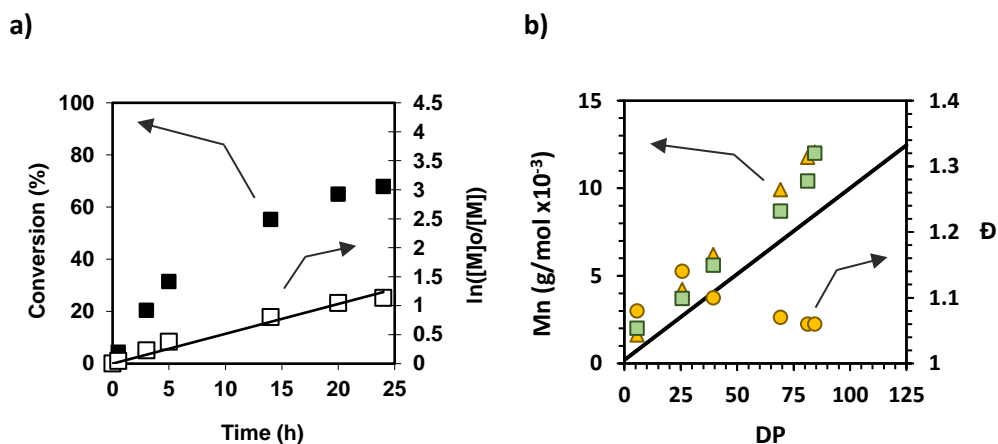


Figure 4.6 ATRP of MBL with EtBrIB. Representation of (a) the conversion versus time (black squares) and the logarithm of monomer conversion versus time (white squares) and the representation of (b) Mn evolution, determined by $^1\text{H-NMR}$ spectroscopy (green squares) and by SEC (yellow triangles), polydispersity is represented as yellow circles. The theoretical Mn is represented as a black line.

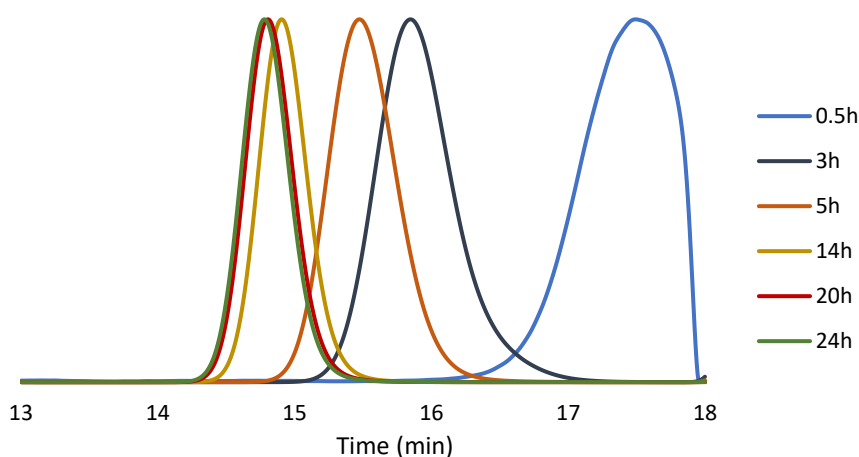
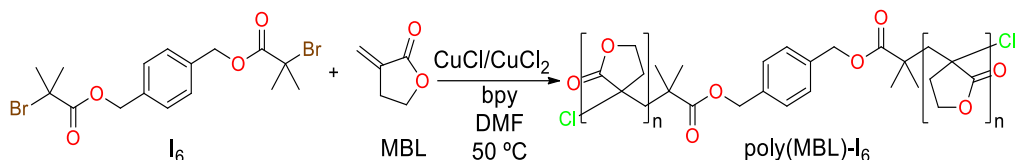


Figure 4.7 Superposed chromatograms of the withdrawn samples at preset times on ATRP of MBL using EtBrIB as initiator.

Figure 4.6-a (black squares) shows the evolution of the polymer conversion determined by $^1\text{H-NMR}$ spectroscopy versus time. The reaction was stopped before reaching total conversion to ensure good chain-end fidelity. Additionally, the representation of the logarithm of monomer conversion vs time give a linear plot indicating the living character of the polymerization (white squares in Figure 4.6-a).

The M_n was determined by both $^1\text{H-NMR}$ spectroscopy and by SEC using PMMA calibration standards. Both determined M_n were higher than the theoretical (Table 4.2). This fact is attributed to both unreacted initiator and some termination processes at early stages, unavoidable in ATRP.¹³ Nevertheless, the molecular weight increases lineally with conversion (green squares and yellow tringles in Figure 4.6-b) and the polydispersity decreases with increasing conversion (Table 4.2 and yellow circles in Figure 4.6-b), as expected in ATRP. The polydispersity at medium to high conversions was narrow as can be observed at the superposed chromatograms (Figure 4.7). The difference in polydispersity values between the poly(MMA) ($\mathcal{D} = 1.25$) and the poly(MBL) ($\mathcal{D} = 1.06$) could be related to the difference in reactivity of the two monomers. MBL is known to be more reactive than MMA, the growing chain of the poly(MBL) would react faster to form the radical and to propagate than the unreacted initiator at the first stage of the reaction. This higher reactivity can increase the probability of termination of part of the initiator. However, in the case of the MMA, the unreacted initiator at the first stage of the reaction could continue reacting with the monomer, producing more polymer chains and a slightly broader molecular weight distribution. This could also explain the better agreement between experimental and theoretical molecular weights in the case of the poly(MMA). $^{13}\text{C-NMR}$ spectroscopy was also used for the structural characterization (see annex 8.26), in which the initiator signals could be observed. The assignments were done according to the data reported in the literature.¹⁰

In order to test the reaction using a bifunctional initiator, the same reaction was carried out using 1,4-phenylenebis(methylene)-bis(2-bromoisobutyrate) (I_6) as model initiator (see experimental part 6.6).



Scheme 4.4 ATRP of MBL using I_6 as bifunctional initiator and $\text{CuCl}/\text{CuCl}_2/\text{bpy}$ as catalytic system.

As the previous example, a DP of 125 ($[\text{MBL}]:[\text{I}_6] = 125:1$) was used, and the other parameters were adjusted for a bifunctional initiator ($[\text{I}_6]:[\text{CuCl}]:[\text{CuCl}_2]:[\text{bpy}] = 1:2.2:0.2:4.8$) (Table 4.3) (see experimental part 6.8.2.3).

Table 4.3 Conversion and molecular weight characteristics versus time of the polymerization of MBL with $\text{CuCl}/\text{CuCl}_2/\text{bpy}$ initiated with I_6 . Polymerization conditions $[\text{MBL}]:[\text{I}_6]:[\text{CuCl}]:[\text{CuCl}_2]:[\text{bpy}]$; 125:1:2.2:0.2:4.8, 50 °C, in DMF (55% v/v).

Aliquot	Time (h)	Conv. ^a (%)	$M_{n\text{Theor.}}^b$ (g/mol) ($\times 10^{-3}$)	$M_{n\text{NMR}}^c$ _{PhCH₂O-} (g/mol) ($\times 10^{-3}$)	$M_{n\text{SEC}}^d$ (g/mol) ($\times 10^{-3}$)	\bar{D}^d
1	0.5	7.3	1.3	1.9	2.4	1.09
2	3.0	37.1	5.0	5.9	7.2	1.08
3	5.0	52.0	6.8	7.9	8.8	1.07
4	14.0	71.2	9.2	10.0	10.9	1.07
5	18.0	81.4	10.4	11.5	12.5	1.07
6	22.0	85.4	10.9	12.3	13.8	1.07

^a Determined by $^1\text{H-NMR}$ spectroscopy from the crude reaction mixture using the signals of monomer (4.42 ppm) and polymer backbone (4.51 ppm). ^b Calculated from the conversion degree determined by $^1\text{H-NMR}$ spectroscopy and the target DP ^c Determined by $^1\text{H-NMR}$ spectroscopy using the signals of initiator (5.28-5.14 ppm) and the polymer backbone (4.51 ppm). ^d Determined by SEC using DMF (0.05% (w/w) LiBr) as eluent and a PMMA standard calibration curve.

The conversion was determined by $^1\text{H-NMR}$ spectroscopy by comparison of the signals of the polymer backbone, at 4.51 ppm (signal **4** in Figure 4.8-a) and the unreacted monomer, at 4.42 ppm (signal **4_M** in Figure 4.8-a). The initiation efficiency (I_{eff}) could also be determined by $^1\text{H-NMR}$ spectroscopy by comparison of the signals of the

unreacted initiator 5.33 ppm (signal **a** and **a''** in Figure 4.8-a) and the initiator incorporated to the polymer chain at 5.28-5.14 ppm (signal **a'** in Figure 4.8).

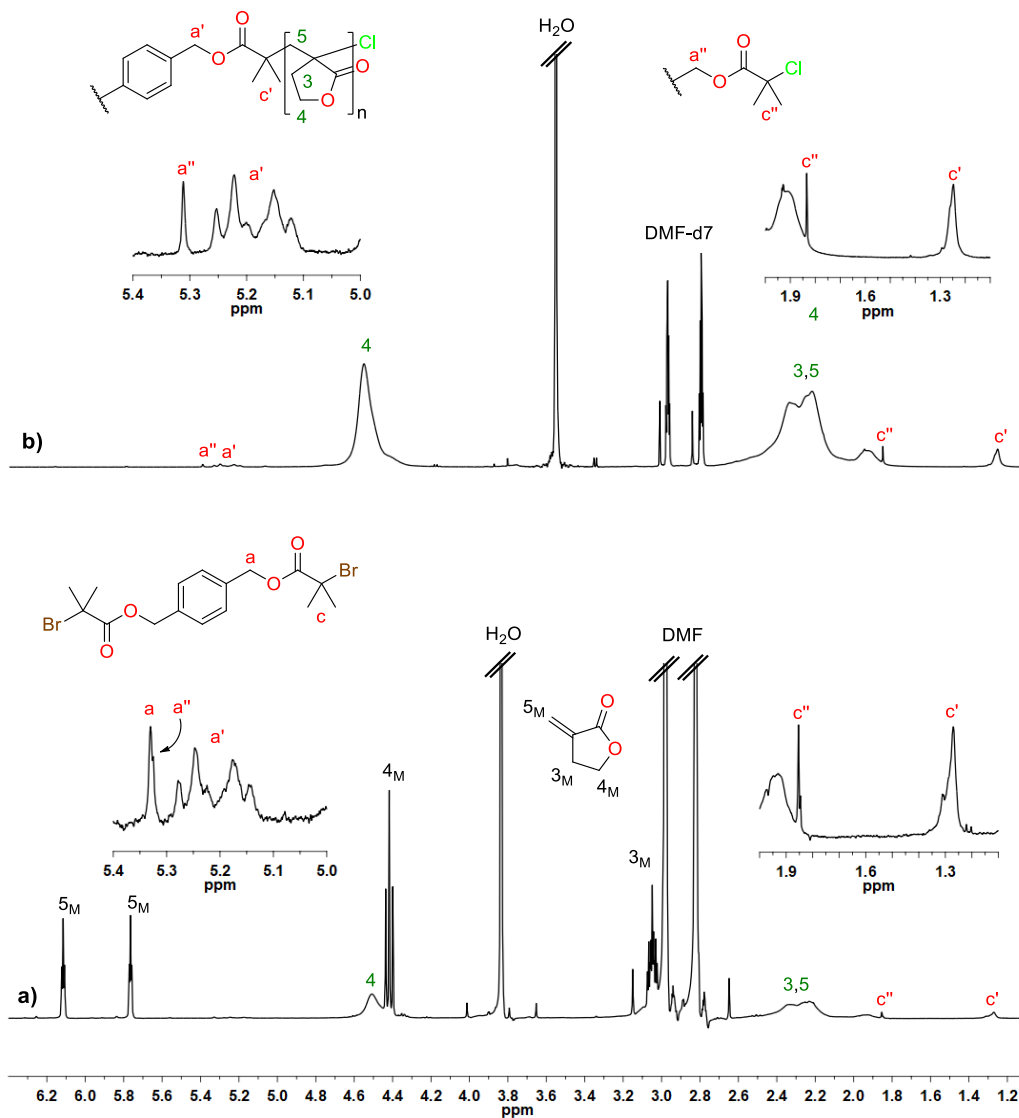


Figure 4.8 ¹H-NMR spectra in DMF-d₇ of (a) polymerization mixture at 52% conversion and (b) isolated polymer (poly(MBL)-I₆) after precipitation with methanol.

The formation of the α-chloroisobutyryl derivative could also be observed in this case by the appearance of a singlet at 1.83 ppm (signal **c''** in Figure 4.8), however the *I*_{eff}.

could not be determined from the signal c'' as it is overlapped with the polymer backbone signals (signals **3** and **5** in Figure 4.8). The initiation efficiency ($I_{eff.}$) in the first stages of the polymerization (0.5 hours) was 77%, and it increased up to 88% in the last sample (22 hours). The advance of the polymerization was followed withdrawing samples at preset times (Table 4.3), which were analyzed by both $^1\text{H-NMR}$ spectroscopy and SEC (DMF containing 0.05 % LiBr). In this way, a conversion of 85.4% was estimated after 22 hours (aliquot 6 in Table 4.3). The conversion was slightly higher than the previous case when using the monofunctional initiator. The reaction was quenched by; bubbling air through the crude reaction mixture to oxidize the catalyst, diluting with additional DMF, and filtering through a short basic alumina column to remove the catalyst. Finally, the polymer was isolated by precipitating in an excess of cold methanol. In the previous case, using a monofunctional initiator, the unreacted initiator was eliminated during the purification process (Figure 4.5-c). However, using the bifunctional initiator the signal of the α -chloroisobutyryl derivative remains after precipitation (signal c'' in Figure 4.8-b) indicating that a small fraction of monoinitiated polymer chains remained in the final product.

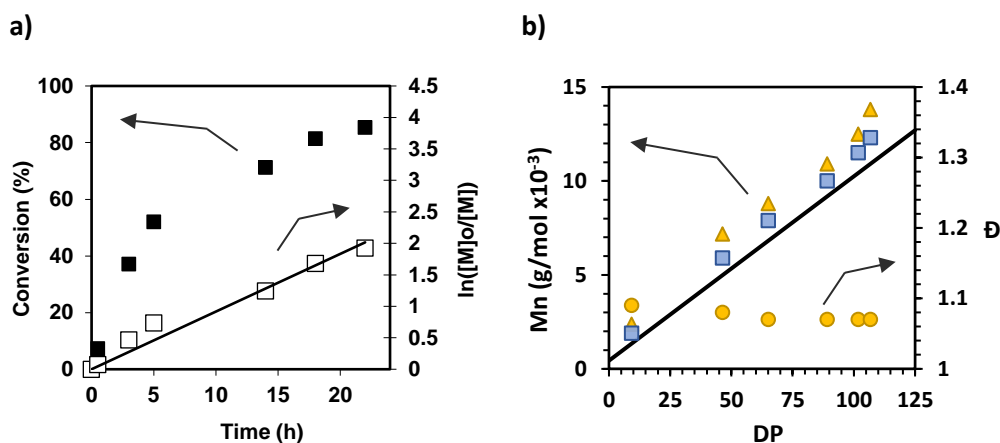


Figure 4.9 ATRP of MBL with I_6 . Representation of (a) the conversion versus time (black squares) and the logarithm of monomer conversion versus time (white squares) and the representation of (b) M_n evolution, determined $^1\text{H-NMR}$ (blue squares) and by SEC (yellow triangles), polydispersity is represented as yellow circles. The theoretical M_n is represented as a black line.

Figure 4.9-a (black squares) shows the evolution of the polymer conversion determined by $^1\text{H-NMR}$ spectroscopy versus time. The reaction was stopped before reaching total conversion to ensure good chain-end fidelity. Furthermore, as the previous case, the representation of the logarithm of monomer conversion vs time give a linear plot indicating the living character of the polymerization (white squares in Figure 4.9-a).

The M_n was determined by SEC using PMMA calibration standards, were higher than the theoretical (Table 4.3). This fact is attributed, as in the previous case, to both incomplete initiation and some termination processes at early stages. Nevertheless, the molecular weight increases lineally with conversion (blue squares and yellow triangles in Figure 4.9-b) and the polydispersity decreases with increasing conversion (Table 4.3 and yellow circles in Figure 4.9-b), as expected in ATRP. The polydispersity obtained were narrow as can be observed at the superposed chromatograms (Figure 4.10). In this case, the polydispersity was slightly higher than when using the monofunctional initiator. This difference could be attributed to the incomplete initiation, in which only one of the two α -bromoisobutyryl units has reacted. In Figure 4.8-b (signal **a**) it can be seen that the signal corresponding to the half initiated species remain in the isolated polymer, while in the case of the EtBriB the signal of unreacted initiator was completely disappeared upon precipitation. Thus, a fraction of the polymer chains has lower molecular weights, which is reflected in a “tail” in the SEC peaks (Figure 4.10). This lower molecular weight fraction is unavoidable when using BriB ester bifunctional initiators, as 100% of initiation efficiency would be unachievable for this kind of radical initiator.

The obtained polymer was also analyzed by $^{13}\text{C-NMR}$ spectroscopy (see annex 8.27). From the signal of the quaternary carbon on the $^{13}\text{C-NMR}$ spectrum (signal **2** in Figure 4.11) the tacticity of the polymer could be determined by comparison with the data reported in the literature.¹⁰ As can be seen the poly(MBL) is mostly atactic with an important fraction of syndiotactic sequences. This difference is due to a smaller

difference of activation energy between the isotactic and the syndiotactic propagation of the MBL in comparison with MMA. This fact could be related to less steric interaction in the transition state for the MBL due to the near planarity of the lactone ring. This steric interaction in the isotactic propagation involves only the cyclic methylene units of the growing chain and the approaching monomer unit. In the case of MMA, the isotactic propagation involves the less favorable methyl-methyl interaction.

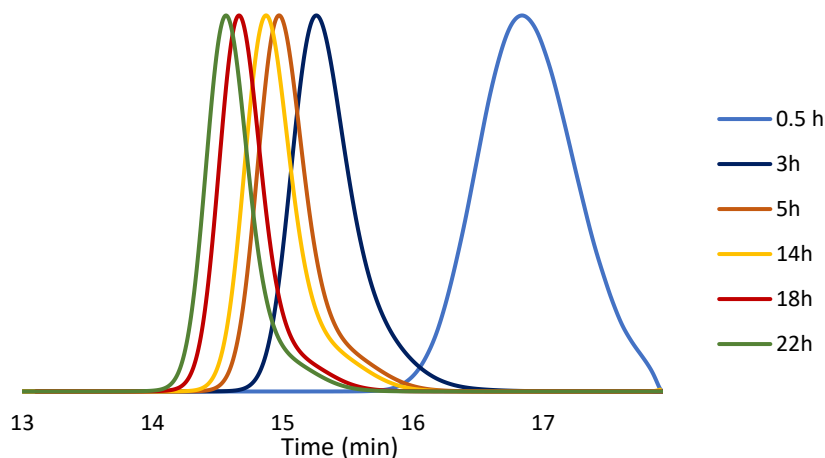


Figure 4.10 Superposed chromatograms of the withdrawn samples at preset times on ATRP of MBL using I_6 as bifunctional initiator.

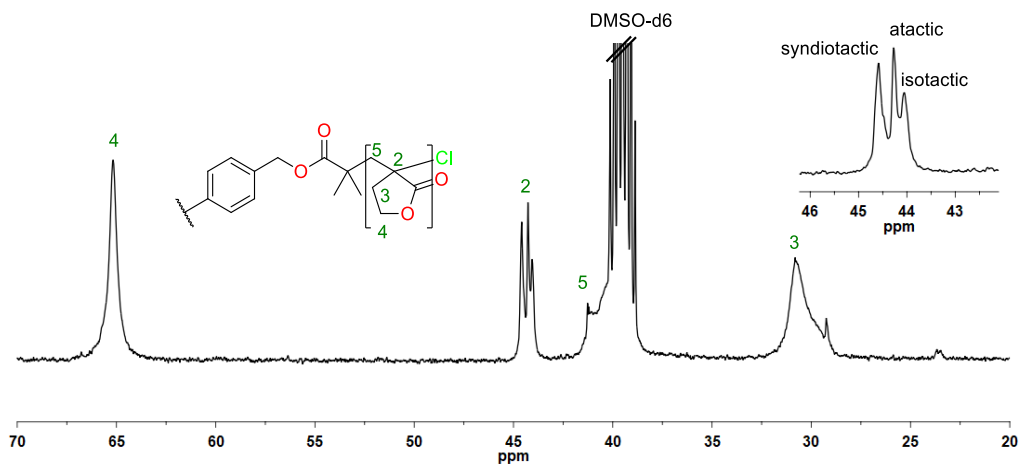


Figure 4.11 ^{13}C -NMR spectrum, region from 20 to 70 ppm, in DMSO-d_6 at $80\text{ }^\circ\text{C}$ of the isolated poly(MBL)- I_6 .

In order to prove the existence of halogen exchange in the initiator during the first stages of the polymerization an experiment was performed using the same polymerization conditions in the absence of monomer. Thus, the bifunctional initiator I_6 was solubilized in DMF-d7 and CuCl, CuCl₂ and bpy were added in the same ratio as the previous polymerization (1:2.2:0.2:4.8). The mixture was stirred at 50 °C for 15 minutes, then the catalyst was removed by filtration through basic alumina and the crude mixture was analyzed by both ¹H- and ¹³C-NMR spectroscopy.

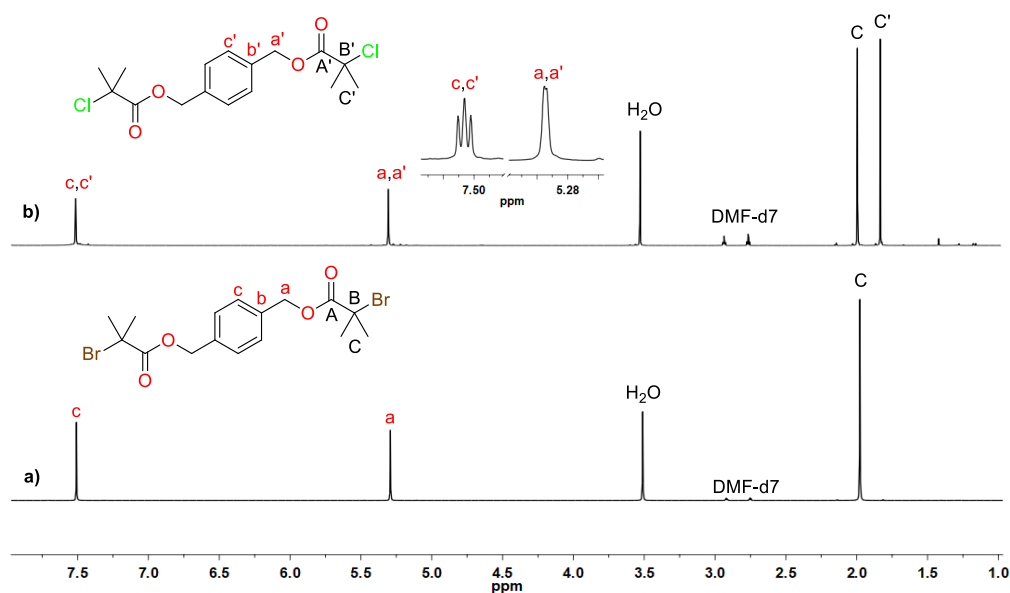


Figure 4.12 ¹H-NMR spectra of (a) pure I_6 and (b) reaction mixture (time = 15 min) of I_6 with CuCl/CuCl₂/bpy in the absence of monomer at 50 °C. Spectra recorded in DMF-d7.

In the ¹H-NMR spectra (Figure 4.12) of the resulting product a new signal at 1.82 can be observed after 15 minutes of reaction (signal **C'** in Figure 4.12-b). The chemical shift of this signal match perfectly with the chemical shift of the signal observed in the polymerization of MBL with the same initiator (1.82 ppm, signal **c''** in Figure 4.8). Moreover, it can be noticed the appearance of new benzylic and aromatic proton signals (**a'** and **c'** respectively in Figure 4.12-b). This evidence confirms the formation of the chloro-derivative during the first stages of the polymerization.

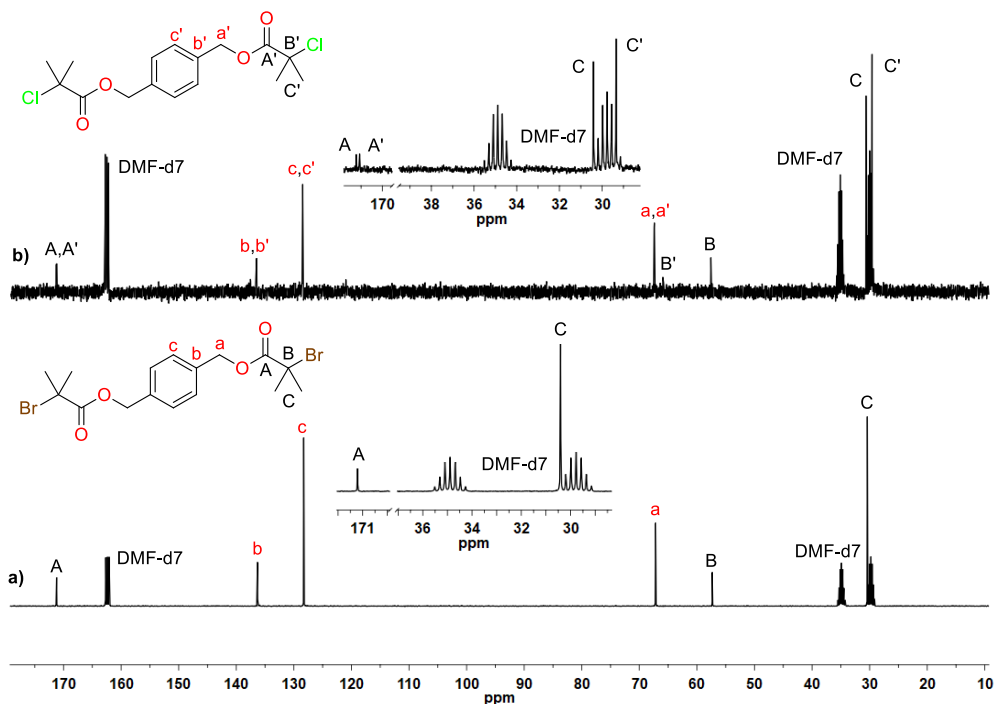
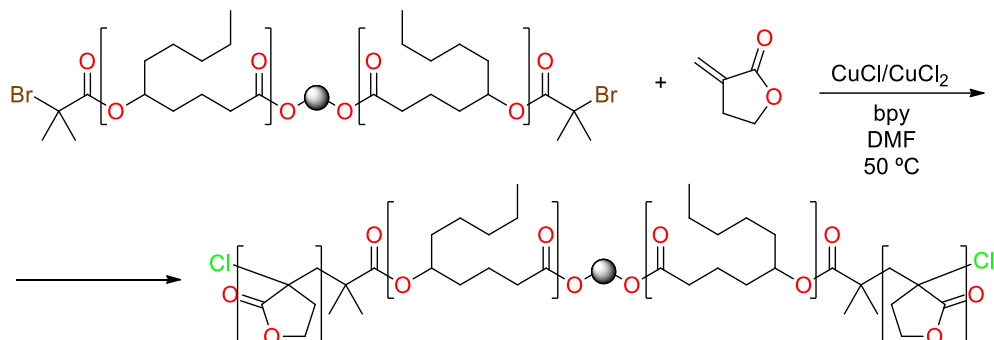


Figure 4.13 ^{13}C -NMR spectra of (a) pure I_6 and (b) reaction mixture (time = 30 min) of I_6 with $\text{CuCl}/\text{CuCl}_2/\text{bpy}$ in the absence of monomer at 50°C . Spectra recorded in DMF-d_7 .

The crude mixture was also analyzed by ^{13}C -NMR spectroscopy. The ^{13}C -NMR spectrum shows the appearance of a new methyl signal at 29.3 ppm (signal C' in Figure 4.13-b). This signal chemical shift also matches with the peak observed in the poly(MBL) (29.2 ppm, signal C'' in Figure 4.18-b). Moreover, a new carbonyl signal at 171.1 ppm appeared (signal A' in Figure 4.13-b). This undesired reaction during the first stages of the polymerization could be avoided by increasing the degree of polymerization (DP). Increasing the DP also increases the initial monomer concentration, being more probable that the initial radical formed react with a monomer molecule before being deactivated by the CuCl_2 . However, targeting a short poly(MBL) block makes unsuitable to further increase the DP considering sustainability issues. In any case, the I_{eff} obtained for the poly(MBL)- I_6 homopolymer is as high as 88 % which is good enough to prepare the desired copolymers in an economical way and reasonable good control over the molecular weight and the copolymer architecture.

4.3 Synthesis of ABA block copolymers by ATRP



Scheme 4.5 Chain extension of poly(DL) macroinitiator with MBL by ATRP.

Once tested the conditions for the homopolymerization of MBL, these were applied for the chain extension of the poly(DL) macroinitiators with MBL (see experimental part 6.8.3). As a first approach the poly(DL)_{1,8-Oct} BriB ester, molecular weight (MW) of 23500 g/mol ($\bar{D} = 1.16$) (determined by SEC in THF), was used as macroinitiator. Then, considering the macroinitiator molecular weight, targeting a 40% of conversion with a DP of 125 the final polymer will have approximately 20% of poly(MBL) in weight. The other parameters were fixed as in the case of the homopolymerization ($[\text{poly(DL)}]_{1,8\text{-Oct}} : [\text{CuCl}] : [\text{CuCl}_2] : [\text{bpy}] = 1 : 2.2 : 0.2 : 4.8$). The conversion degree was determined using ¹H-NMR spectroscopy, by comparison of the monomer signal at 5.68 ppm (signal **5_M** in Figure 4.14-a) and the signal poly(MBL) backbone at 4.38 (signal **4** in Figure 4.14-a).

The presence of the macroinitiator, increase the solubility of the copolymer, allows the ¹H-NMR analysis to be conducted in CDCl₃ instead of DMF-d₇. The reaction reached 41% of conversion within two hours. The proportion of the different block could be determined from the ¹H-NMR spectrum of the isolated polymer. By comparing the signals of the poly(DL) (signal **5** in Figure 4.14-b) and the poly(MBL) (signal **4** in Figure 4.14-b) backbones with the 1,8-octanediol signal (signal **a** in Figure 4.14-b) a MW for each block could be obtained. From the these MWs a 16.5% fraction of poly(MBL) could be estimated at the final polymer (Table 4.4).

Chapter 4. Results and discussion

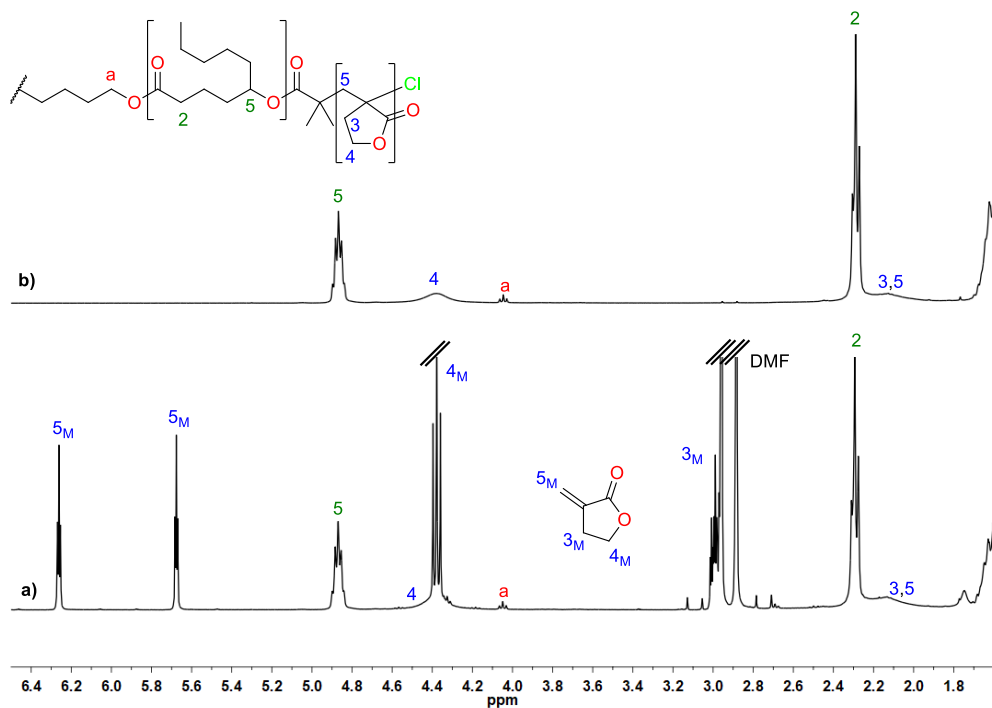


Figure 4.14 $^1\text{H-NMR}$ spectra (in CDCl_3) of (a) polymerization mixture at 41% conversion and (b) isolated polymer after precipitation with methanol.

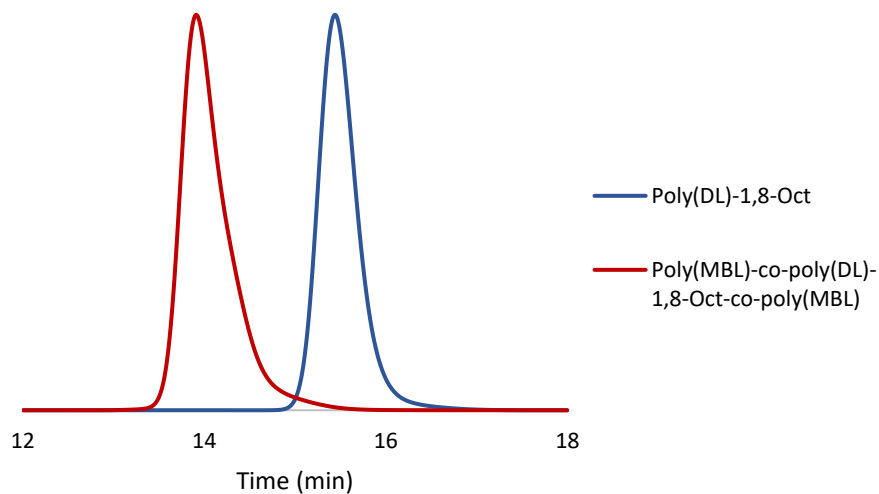


Figure 4.15 SEC traces of poly(DL)_{1,8-Oct} BriB ester (blue) and poly(MBL)-co-poly(DL)_{1,8-Oct}-co-poly(MBL).

The SEC chromatograms show that the isolated block copolymer has narrow polydispersity ($\bar{D} = 1.17$), however, some “tail” could be observed (Figure 4.15). This “tail” could be related to the incomplete initiation, leading to some AB diblock copolymers. Since complete initiation efficiency is unpractical for BriB ester bifunctional initiators a small fraction of AB diblock copolymer will be unavoidable in the final material. These lower molecular weight chains of AB diblock copolymers would not behave as a TPE, nevertheless, it only supposes a small fraction of the total material. Once tested the reaction with the macroinitiator, the same conditions were applied to the macroinitiators containing the cleavable unit (Table 4.4).

Table 4.4 Conversion and molecular weight characteristics of the polymerization of MBL with different polyester macroinitiators. Polymerization conditions [MBL]:[poly(DL)-I_x]:[CuCl]:[CuCl₂]:[bpy]:125:1:2.2:0.2:4.8, 50 °C, in DMF (67% v/v).

Initiator (Mn (g/mol) (x10 ⁻³)/ \bar{D}) ^a	Conv. ^b (%)	Mn _{SEC} ^a (g/mol) (x10 ⁻³)	\bar{D} ^a	Mn _{NMR} (g/mol) (x10 ⁻³) ^c		% (wt) of Poly(MBL)
				Poly(DL)	Poly(MBL)	
Poly(DL) _{1,8-Oct} (5.8/1.15)	41	18.9	1.17	19.2	3.8	16.5
Poly(DL)-I ₁ (5.8/1.23)	39	20.1	1.27	20.2	3.6	17.8
Poly(DL)-I ₂ (4.6/1.16)	44	20.6	1.17	19.5	4.1	17.4
Poly(DL)-I ₃ (7.3/1.11)	45	22.9	1.17	21.1	4.0	16.6
Poly(DL)-I ₄ (5.3/1.20)	42	20.0	1.18	19.0	3.9	17.0
Poly(DL)-I ₅ (6.6/1.18)	38	19.0	1.16	20.1	3.7	15.5

^a Determined by SEC using DMF (0.05% (w/w) LiBr) as eluent and a PMMA standard calibration curve. ^b Determined by ¹H-NMR spectroscopy from the crude reaction mixture using the signals of monomer (5.68 ppm) and polymer backbone (4.38 ppm). ^c Determined by ¹H-NMR spectroscopy from the isolated polymer using the signal of the ROP initiator (1,8-Oct = 4.05 ppm, I₁ = 2.91 ppm, I₂ = 2.65 ppm, I₃ = 2.64 ppm, I₄ = 2.87 ppm, I₅ = 3.81 ppm) and the poly(DL) backbone signal (4.87 ppm) and poly(MBL) backbone signal (4.38 ppm) respectively.

Polymerizations were stopped after 2 hours of reaction which supposed conversion degrees between 38 and 45 %. The molecular weight of each block was determined by ¹H-NMR spectroscopy, by comparing the intensity of the signals of the ROP initiator

(1,8-Oct = 4.05 ppm, $I_1 = 2.91$ ppm, $I_2 = 2.65$ ppm, $I_3 = 2.64$ ppm, $I_4 = 2.87$ ppm and $I_5 = 3.81$ ppm) with the poly(DL) and poly(MBL) backbone signals respectively. From these molecular weights the proportion of the poly(MBL) block could be determined (Table 4.4) being between 15.5 and 17.8 % in weight. By this way, a series of ABA block copolymers possessing a cleavable unit at de midpoint have been synthesized.

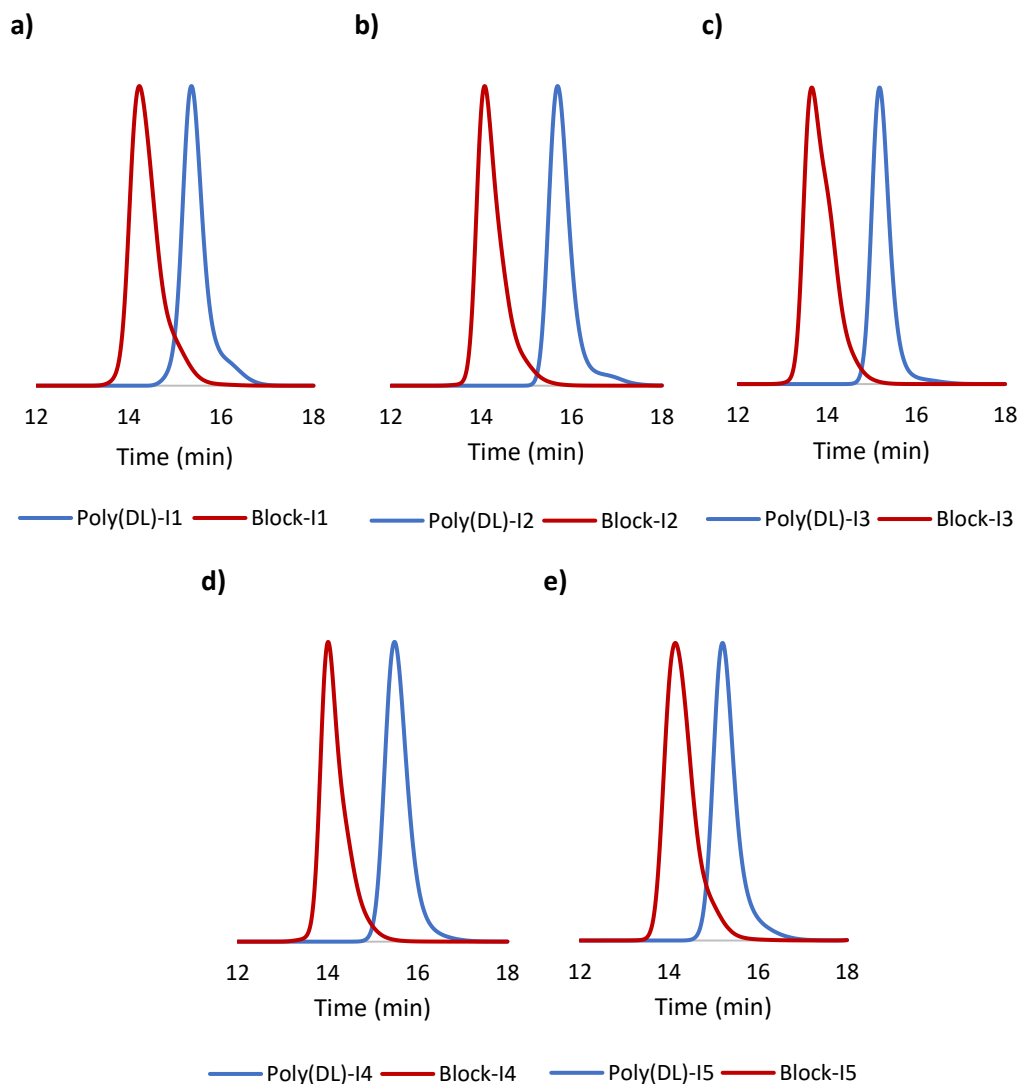


Figure 4.16 SEC traces (in DMF with 0.05% LiBr) of synthesized stimuli cleavable block copolymers (red line) compared with the SEC traces of the corresponding macroinitiator.

In all the cases chain extension proceed effectively evidenced by SEC leading to polymers with M_n between 18000 and 22000 g/mol and narrow polydispersities (Figure 4.16). The SEC traces show the presence of some low molecular weight fraction corresponding to monoinitiated macroinitiators.

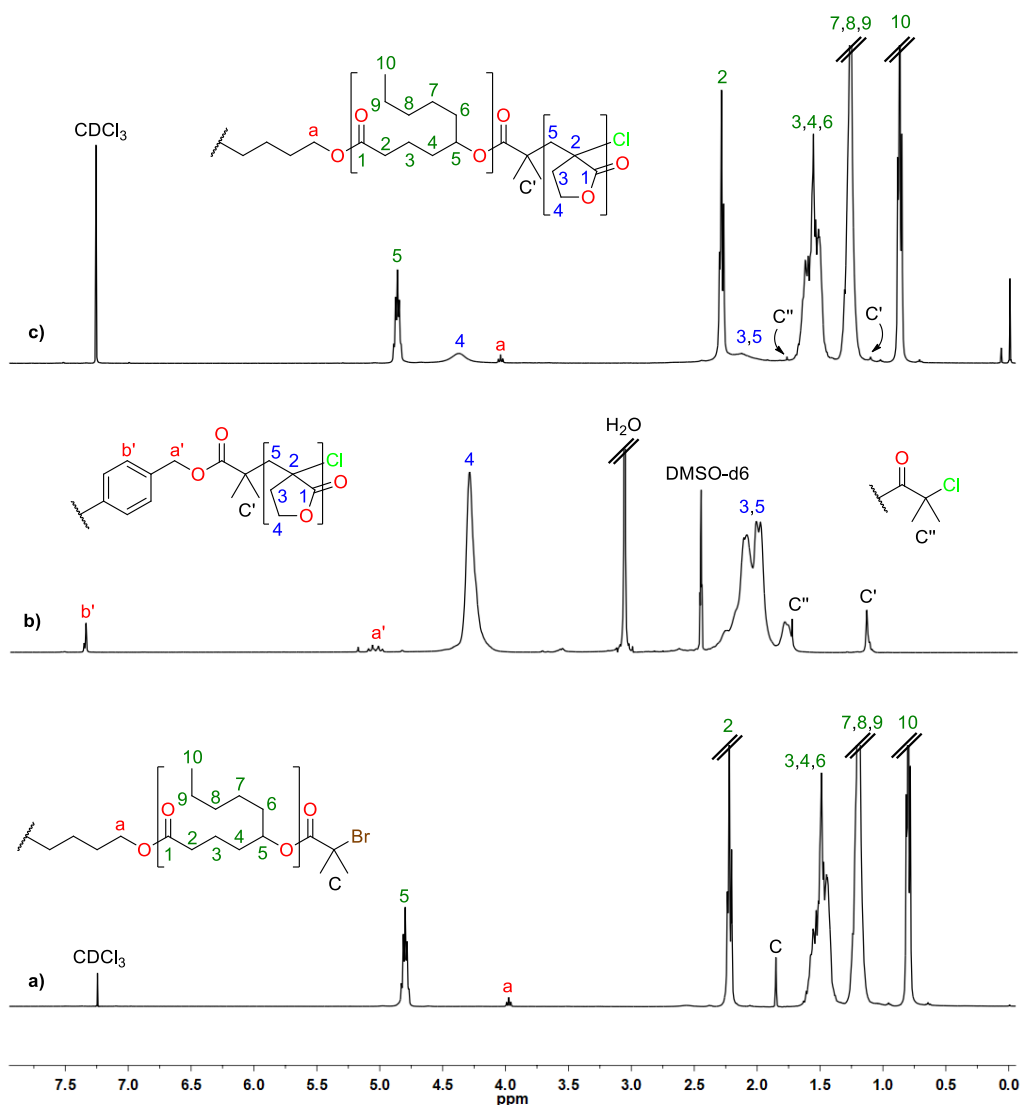


Figure 4.17 $^1\text{H-NMR}$ spectra of (a) poly(DL)-1,8-Oct BriB ester in CDCl_3 , (b) poly(MBL)-I₆ in DMSO-d_6 at 80 °C and (c) poly(MBL)-co-poly(DL)_{1,8-Oct}-co-poly(MBL) in CDCl_3 .

All the block copolymers were characterized by ^1H - and ^{13}C -NMR spectroscopy in order to confirm the effectiveness of the chain extension (see annex 8.29 to 8.34). In Figure 4.17 the ^1H -NMR spectra of the starting macroinitiator, the Poly(MBL)-I₆, used as model for the hard block and the poly(MBL)-*co*-poly(DL)_{1,8-Oct}-*co*-poly(MBL) are compared. As can be seen the methyl signal of the BriB on the macroinitiator (signal **C**) disappears upon the incorporation of the poly(MBL) block (Figure 4.17-c). The I_{eff} could not be determined due to an overlapping of the reacted initiator signal (**C'** in Figure 4.17-b) with the poly(DL) backbone signals (**7**, **8** and **9** in Figure 4.17-c). It can be notice that, as in the case of the homopolymerization, some initiator remained as chloroisobutyryl derivative (signal **C''** in Figure 4.17-c). Although I_{eff} cannot be precisely calculate, it can be assumed that the initiation efficiency must be similar as in the case of the homopolymerization using I₆ ($I_{\text{eff}} \approx 88\%$).

In the spectra of the final copolymer, the characteristic signals of the poly(MBL) block could also be observed (signals **3**, **4** and **5** in Figure 4.17-c). The block copolymers were also analyzed by ^{13}C -NMR spectroscopy. In Figure 4.18 the ^{13}C -NMR spectra of the starting macroinitiator, the Poly(MBL)-I₆, used as model for the hard block and the poly(MBL)-*co*-poly(DL)_{1,8-Oct}-*co*-poly(MBL) are compared.

The ^{13}C -NMR spectra of the block copolymer (Figure 4.18-c) showed the signals of both poly(DL) and poly(MBL) blocks (Figure 4.18-a and -b respectively). The signal of the exocyclic methylene carbon (signal **5** in Figure 4.18-c) appears as a broad multiplet partially overlapped with the DMSO-d₆ peak whereas the signal of the endocyclic methylene carbon (signal **3** in Figure 4.18-b) appears overlapped with the signals of the poly(DL) backbone. The signal corresponding to quaternary carbon show the characteristic triad pattern of atactic poly(MBL)¹⁰ (signal **2** in Figure 4.18-b and -c). However, in the block copolymer the signals of the initiator could not be observed although the spectrum was recorded at 80 °C with higher sample loading. None of the signals of the chloroisobutyryl derivative, observed in the poly(MBL) spectrum (signal

C'' in Figure 4.18-b), could be detected. The high proportion of poly(DL) and the limited solubility of the copolymer prevent the detection of the linking groups.

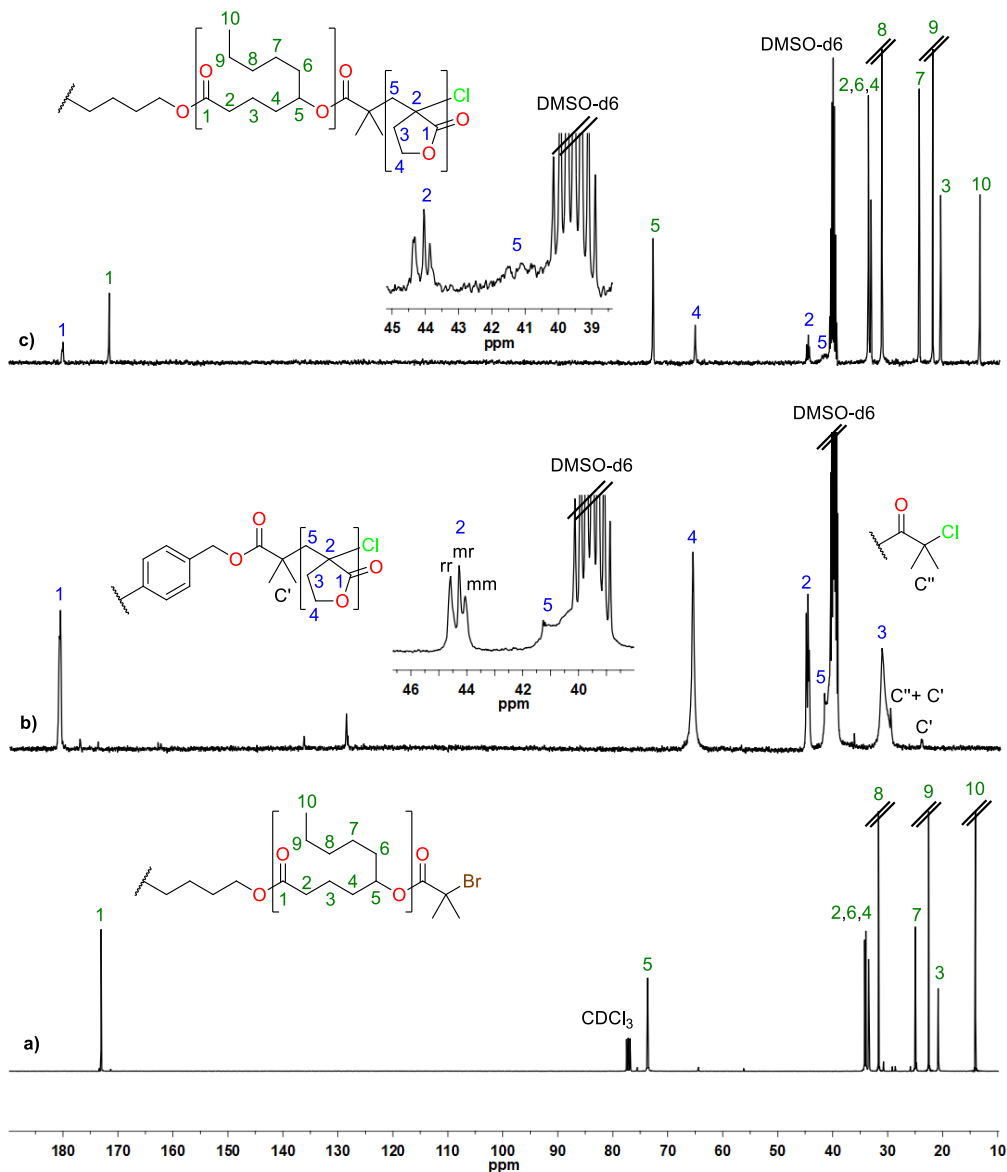


Figure 4.18 C-NMR spectra of (a) poly(DL)-1,8-Oct BriB ester in CDCl₃, (b) poly(MBL)-I₆ in DMSO-d₆ at 80 °C and (c) poly(MBL)-co-poly(DL)-1,8-Oct-co-poly(MBL) in DMSO-d₆ at 80 °C.

- Thermal and mechanical characterization:

The thermomechanical properties of the model poly(DL) and poly(MBL) homopolymers and the model block copolymer were analyzed by thermogravimetric analysis (TGA) (Figure 4.19 and Figure 4.20), differential scanning calorimetry (DSC) (Figure 4.21) and dynamo-mechanical analysis (DMA) (Figure 4.23) for comparative purposes. All the synthesized ABA block copolymers possess similar molecular weight and comparable balance between the soft and hard block and consequently must present similar thermal and mechanical properties.

The poly(DL)_{1,8-Oct} homopolymer (M_n (SEC) = 23500 g/mol/ \bar{D} = 1.16) shows a 5 % weight loss ($T_{5\%}$) at 310 °C and a maximum thermal decomposition rate (T_{max}) at 349 °C (blue dashed line in Figure 4.19 and Figure 4.20 respectively). These temperatures were considerable higher than the reported in the literature, less than 210 °C.^{14, 15} We attribute these lower reported temperatures to the presence of impurities, which could accelerate the depolymerization process. The decomposition process results in 0% of residue, which indicates that the nature of the decomposition is a depolymerization process where the δ -decalactone is reformed and evaporated. Thermal degradation behavior for lactone derived polyesters has been described in the literature, where the starting lactone was detected into the main degradation products, together with water, CO₂ and products from random chain cleavage.¹⁶ In this sense Hillmyer et al. reported recently a patent for the recovery of lactone monomers from alkyl δ -lactones-derived polymeric materials, through thermal depolymerization.¹⁷

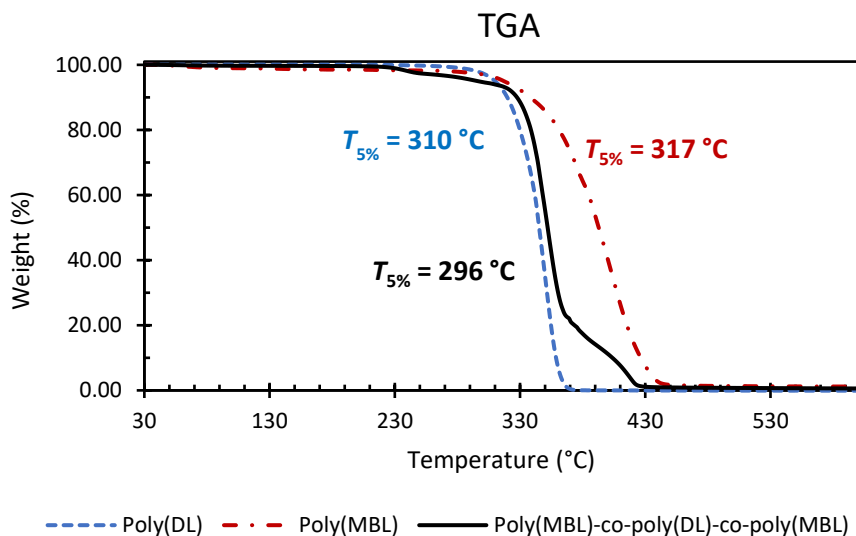


Figure 4.19 TGA decomposition patterns of poly(DL) homopolymer (blue dashed line), poly(MBL) homopolymer (red dashed line with dots) and block copolymer (black line).

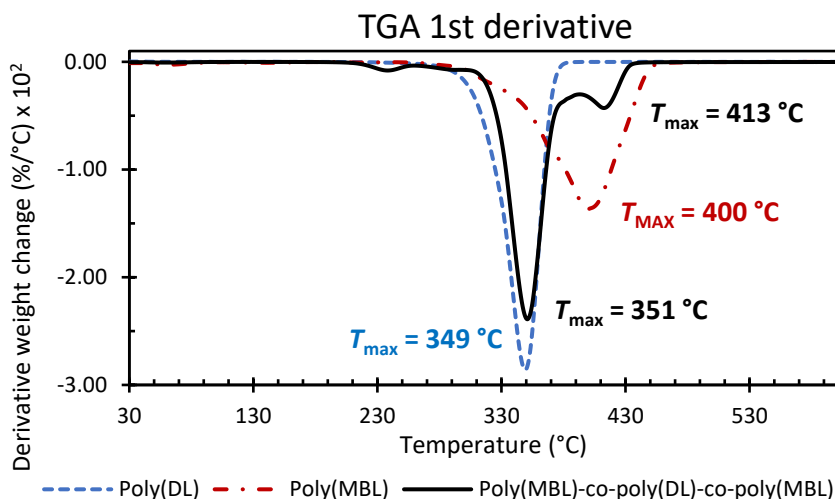


Figure 4.20 TGA first derivative plots of poly(DL) homopolymer (blue dashed line), poly(MBL) homopolymer (red dashed line with dots) and block copolymer (black line).

The TGA of poly(MBL)_{EtBrIB} homopolymer (M_n (SEC) = 12000 g/mol/ \bar{D} = 1.06) shows a $T_{5\%}$ at 317 °C and a T_{\max} at 400 °C (red dashed line with dots in Figure 4.19 and Figure 4.20 respectively). These temperatures were in accordance with those reported in the

literature where the polymer is thermally stable until 320 °C. Above this temperature the polymer tends to depolymerize reforming the MBL.¹⁰ Thus, the decomposition process results in 0 % of residue as in the case of poly(DL). The TGA of the block copolymer (M_n (SEC) = 18900 g/mol/ \bar{D} = 1.17) shows a $T_{5\%}$ at 296 °C (black line in Figure 4.19) and two T_{max} at 351 and 413 °C (black line in Figure 4.20), which seems to correspond to the poly(DL) and poly(MBL) block respectively. No solid residue remained after the thermal decomposition, as both poly(DL) and poly(MBL) depolymerize giving the starting monomer under the heating process.

The thermal transitions of the polymers were analyzed by differential scanning calorimetry (DSC) (Figure 4.21).

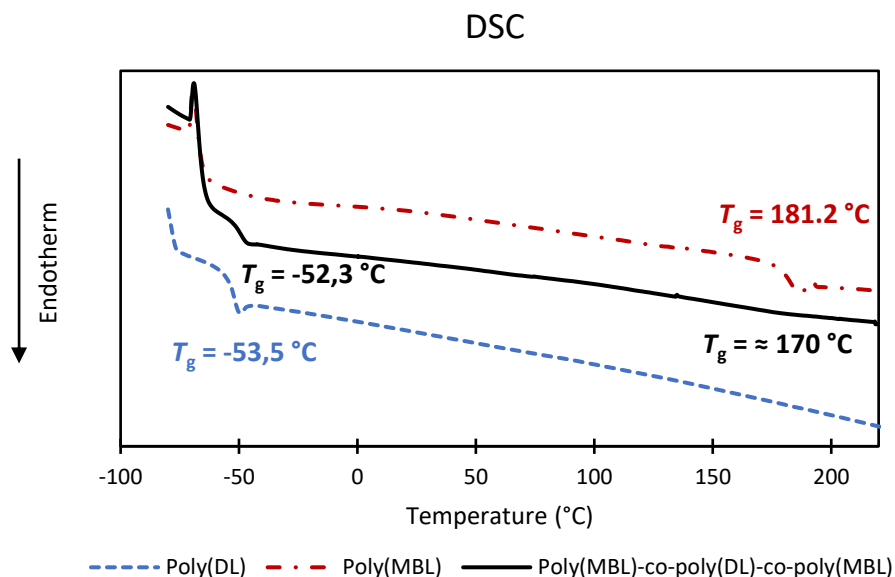


Figure 4.21 DSC plots of poly(DL) homopolymer (blue dashed line), poly(MBL) homopolymer (red dashed line with dots) and block copolymer (black line).

The poly(DL) homopolymer (M_n (SEC) = 23500 g/mol/ \bar{D} = 1.16) shows a glass transition temperature (T_g) at -53.5 °C (blue dashed line in Figure 4.21), in concordance with the values described in the literature (T_g from -56.5 to -51 °C, depending on the molecular

weight).^{18, 19} There is no evidence of melting endotherms (T_m), confirming its completely amorphous nature. According to the branched structure and the high aliphatic content of this polyester, the T_g is far below room temperature. The hard poly(MBL) homopolymer (M_n (SEC) = 12000 g/mol/ \bar{D} = 1.06) shows a T_g at 181.2 °C (red dashed line with dots in Figure 4.21), which is very close to the reported in the literature (195 °C for the atactic poly(MBL)).¹⁰ There is no evidence of T_m , confirming also its completely amorphous nature. The restricted segmental mobility of the polymer chain, originated from the conformationally rigid lactone ring perpendicular to the plane of the backbone and dipole-dipole interactions, is responsible for this high T_g value.^{10, 20} This high T_g value confirms the validity of poly(MBL) as hard segment of an ABA thermoplastic elastomer for high temperature applications. Finally, the block copolymer (M_n (SEC) = 18900 g/mol/ \bar{D} = 1.17) was also characterized by DSC (black line in Figure 4.21). The thermograph showed a first T_g at -52.3 °C corresponding to the poly(DL) block. However, the second T_g corresponding to the poly(MBL) block (around 170 °C) was hardly observed due to the above mentioned restricted mobility of the poly(MBL) chains and the low heigh percentage of the hard segment in the copolymer. Nevertheless, the T_g of the poly(DL) block remains unchanged, which is an evidence of the phase-separation.

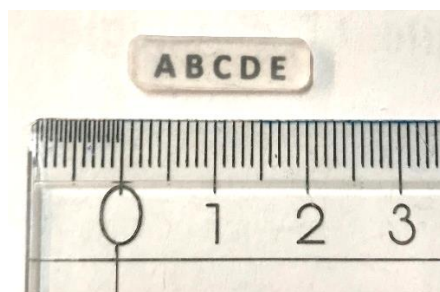


Figure 4.22 Specimen of the poly(MBL)-co-poly(DL)_{1,8-Oct}-co-poly(MBL) block copolymer for DMA.

In order to test the TPE character of these materials, representative specimens of the model block copolymer (poly(MBL)-co-poly(DL)_{1,8-Oct}-co-poly(MBL)) (Figure 4.22) were

prepared to analyze the thermomechanical properties, through dynamo-mechanical analysis (DMA), in a range of temperatures from -80 to 220 °C (Figure 4.23). The $\tan \delta$ (blue line in Figure 4.23) showed a first peak at -36.1 °C corresponding to the glass transition of the soft poly(DL). Below this temperature the material showed a storage modulus (red line in Figure 4.23) of 1674 MPa, indicating that is hard and brittle. After the first glass transition the storage modulus lowered until 11.9 MPa showing rubbery plateau from -36.1 to 164.2 °C. The second glass transition, corresponding to the hard poly(MBL) block, was observed as the second $\tan \delta$ peak at 164.2 °C. After this temperature the storage modulus was lowered until 2.4 MPa. This lower T_g of the hard block could be related to the small AB copolymer fraction, derived from an incomplete initiation, which could act as plasticizer lowering the T_g . This AB copolymer fraction would also be the responsible of the small transition around 10 °C that could be observed in Figure 4.23.

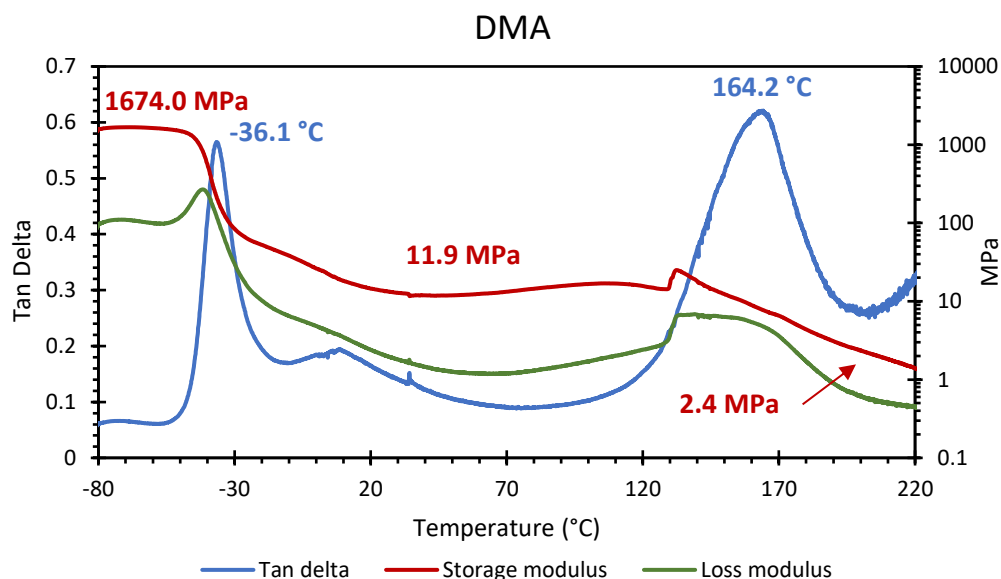


Figure 4.23 DMA plot of the block copolymer specimen.

Therefore, the range of temperature where the material can be applied as an elastomer is between -36 and 164 °C. In all this range of temperatures the $\tan \delta$ is below 1, which indicates that the elastic component on the material prevails to the viscous component.

- ¹ Mosnáček, J.; Matyjaszewski, K. Atom Transfer Radical Polymerization of Tulipalin A: A naturally renewable monomer. *Macromolecules* **2008**, *41*, 5509-5511.
- ² Shin, J.; Lee, Y.; Tolman, W. B.; Hillmyer, M. A. Thermoplastic elastomers derived from menthane and tulipalin A. *Biomacromolecules* **2012**, *13*, 3833-3840.
- ³ Bergenudd, H.; Coullerez, G.; Jonsson, M.; Malmström, E. Solvent effects on ATRP of oligo(ethylene glycol) methacrylate. Exploring the limits of control. *Macromolecules* **2009**, *42*, 3302-3308.
- ⁴ Pascual, S.; Coutin, B.; Tardi, M.; Polton, A.; Vairon, J.-P. Homogeneous atom transfer radical polymerization of styrene initiated by 1-chloro-1-phenylethane/copper(I) chloride/bipyridine in the presence of dimethylformamide. *Macromolecules*, **1999**, *32*, 1432-1437.
- ⁵ Dupayage, L.; Nouvel, C.; Six, J.-L. Copper-mediated ATRP of MMA in DMSO from unprotected dextran macroinitiators. *Polym. Bull.* **2012**, *68*, 647-665.
- ⁶ Wang, Y.; Matyjaszewski, K. ATRP of MMA in polar solvents catalyzed by FeBr₂ without additional ligand. *Macromolecules* **2010**, *43*, 4003-4005.
- ⁷ Nanda, A. K.; Matyjaszewski, K. Effect of penultimate unit on the activation process in ATRP. *Macromolecules* **2003**, *36*, 8222-8224.
- ⁸ Magenau, A. J. D.; Kwak, Y.; Matyjaszewski, K. ATRP of methacrylates using Cu^{II}X₂/L and copper wire. *Macromolecules* **2010**, *43*, 9682-9689.
- ⁹ Nishihara, M.; Teramoto, K.; Sakurai, T.; Takafuji, M.; Mashimo, T.; Ihara, H. Enhancement of isotacticity in bulk radical polymerization of poly(methyl methacrylate) under strong gravity field. *Polym. J.* **2003**, *35*, 276-279.
- ¹⁰ Akkapeddi, M. K. Poly(α -methylene- γ -butyrolactone) Synthesis, configurational structure, and properties. *Macromolecules* **1979**, *12*, 546-551.
- ¹¹ Ogata, Y.; Takagi, K.; Hayashi, E. Photochemical reduction of radical \cdot CMe₂X with toluene. *J. Org. Chem.* **1979**, *44*, 856-858.
- ¹² Duan, X.-H.; Mayr, H. Electrophilicities of α -chlorinating agents used in organocatalysis. *Org. Lett.* **2010**, *12*, 2238-2241.
- ¹³ Matyjaszewski, K. Fundamentals of controlled/living radical polymerization. *Encyclopedia of Radicals in Chemistry, Biology and Materials*. Wiley & Sons, **2012**.
- ¹⁴ Tang, D.; Macosko, C. W.; Hillmyer, M. A. Thermoplastic polyurethane elastomers from bio-based poly(δ -decalactone) diols. *Polym. Chem.* **2014**, *5*, 3231-3237.
- ¹⁵ Bandelli, D.; Helbing, C.; Weber, C.; Seifert, M.; Muljajew, I.; Jandt, K. D.; Schubert, U. S. Maintaining the hydrophilic-hydrophobic balance of polyesters with adjustable crystallinity for tailor-made nanoparticles. *Macromolecules* **2018**, *51*, 5567-5576.
- ¹⁶ Persenaire, O.; Alexandre, M.; Degée, Ph.; Dubois, Ph. Mechanism and kinetics of thermal degradation of poly(ϵ -caprolactone). *Biomacromolecules* **2001**, *2*, 288-294.
- ¹⁷ Hillmyer, M. A.; Panthani, T. R.; Vanderlaan, M. E.; Schneiderman, D. K.; Mannion, A. M. R.; Batiste, D. C.; Macosko, C. W.; Wang, J. Z.; Bates, F. S. Recovery of monomers from polyurethane materials by depolymerization. *US Patent App.* US 2017/0247350 A1, **2017**.
- ¹⁸ Martello, M. T.; Burns, A.; Hillmyer, M. Bulk ring-opening transesterification polymerization of the renewable δ -decalactone using an organocatalyst. *ACS Macro Lett.* **2012**, *1*, 131-135.
- ¹⁹ Zhao, J.; Hadjichristidis, N. Polymerization of 5-alkyl δ -lactones catalyzed by diphenyl phosphate and their sequential organocatalytic polymerization with monosubstituted epoxides. *Polym. Chem.* **2015**, *6*, 2659-2668.

²⁰ Gowda, R. R.; Chen, E. Y.-X. Sustainable polymers from biomass-derived α -methylene- γ -butyrolactones. *Encyclopedia of polymer science and technology* **2013**, John Wiley & Sons, Inc.

UNIVERSITAT ROVIRA I VIRGILI
STIMULI-RESPONSIVE CALIX[4]PYRROLE AND CALIX[4]ARENE BASED RECEPTORS: FROM UNIMOLECULAR
TO DIMERIC STRUCTURES

Pedro Miguel Mendonça Ferreira

Chapter 5

Cleavage of ABA block copolymers

UNIVERSITAT ROVIRA I VIRGILI
STIMULI-RESPONSIVE CALIX[4]PYRROLE AND CALIX[4]ARENE BASED RECEPTORS: FROM UNIMOLECULAR
TO DIMERIC STRUCTURES

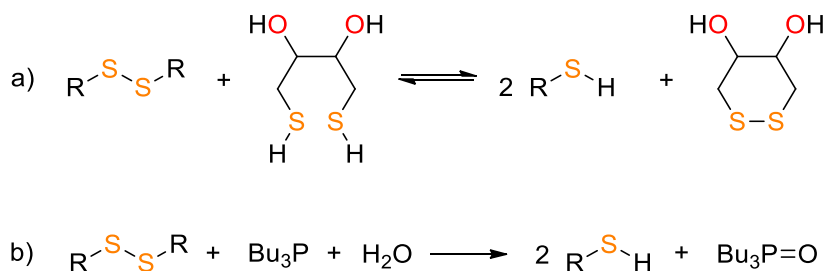
Pedro Miguel Mendonça Ferreira

5 Cleavage of ABA block copolymers

Once obtained the different stimuli cleavable block copolymers their degradation was studied, with emphasis in the degradation mechanism and the characterization of the degradation products. Three types of stimuli were applied, first the degradation of disulfides under reductive media, second the acid hydrolysis of acetal groups and finally the cleavage of thioacetals under oxidative conditions. The two first detachable groups are well known sensitive groups which have been extensively studied for their use in stimuli cleavable polymers.¹⁻⁴ However, thioacetals, although are well known as protecting groups, their deprotection under mild conditions, and avoiding environmental hazardous reagents, is still challenging. The use of thioacetal linkages, as sensitive groups, has depicted an increasing interest in the research community and have been recently employed for the synthesis of stimuli cleavable polymers, especially in the biomedical field.⁵⁻⁷

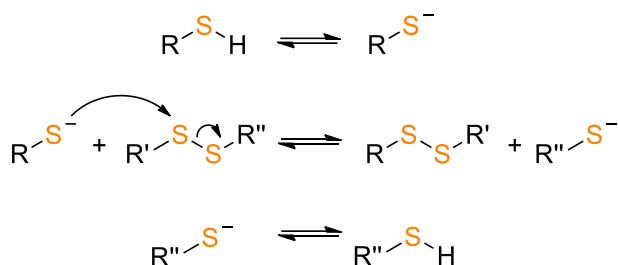
5.1 Reductive cleavable polymer

Disulfide linkages could be cleaved by two main pathways. The first one is through a thiol – disulfide exchange reaction with an excess of thiol (e.g. with dithiothreitol (DTT)). The second one involves the use of a reducing agent, such as *n*-tributylphosphine (Bu₃P) (Scheme 5.1).



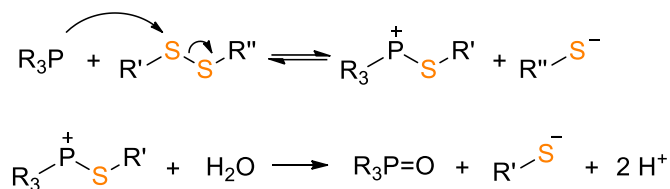
Scheme 5.1 Disulfide cleavage through (a) thiol – disulfide exchange and (b) reduction with Bu₃P.

The thiol – disulfide exchange involves three reversible steps: first, the ionization of the thiol to form thiolate anion, second, the nucleophilic attack of the thiolate anion on a sulfur atom of the disulfide moiety and third, the protonation of the product thiolate anion (Scheme 5.2).⁸ When dithiols, with 3 – 6 carbon atoms between the sulfur atoms, are used the formation of cyclic disulfides favors the equilibrium towards the desired product (e.g. formation of strain-free six-membered 1,2-dithianes).



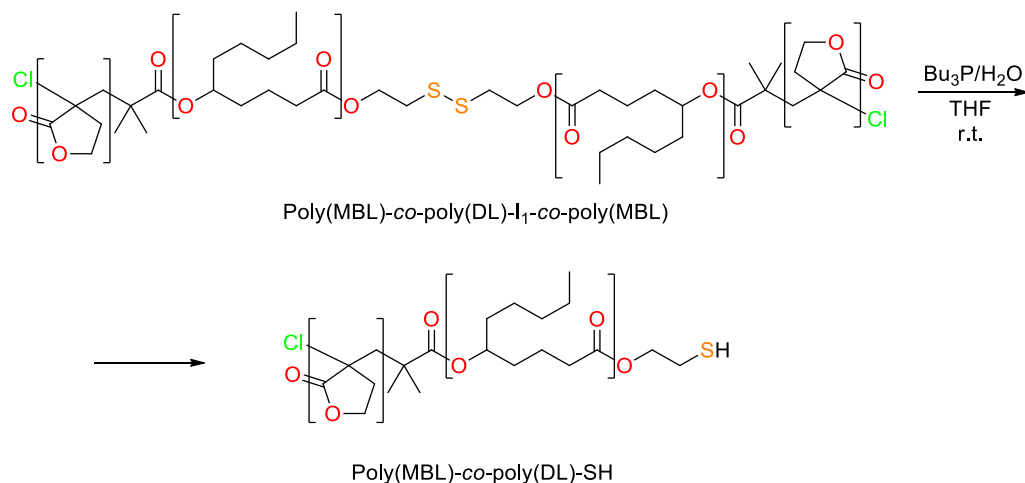
Scheme 5.2 Thiol – disulfide exchange equilibrium.

On the other hand, trialkyl phosphines (e.g. *n*-Bu₃P), in the presence of water, have been shown as efficient reducing agents for disulfides. The first step consists in a nucleophilic attack of the phosphine to the sulfur atom of the disulfide with the displacement of a thiolate anion and the formation of thioalkoxyphosphonium cation. In a subsequent step, the cationic intermediate underwent hydrolysis to form the phosphine oxide and a second thiolate anion (Scheme 5.3).⁹ The main difference with the thiol – disulfide exchange is that the reaction is irreversible due to the strength of the P=O bond formed.¹⁰ The main advantages of phosphines are their stability towards autooxidation and their great affinity of towards disulfide groups. For this reason, *n*-tributylphosphine was selected for the cleavage of the disulfide containing block copolymer.



Scheme 5.3 Reduction of disulfides using trialkylphosphines.

Thus, the synthesized poly(MBL)-*co*-poly(DL)-I₁-*co*-poly(MBL) block copolymer, was cleaved using *n*-Bu₃P following a reported procedure (Scheme 5.4) (see experimental part 6.9.1).⁴



Scheme 5.4 Reductive cleavage of poly(MBL)-*co*-poly(DL)-I₁-*co*-poly(MBL) to poly(MBL)-*co*-poly(DL)-SH using Bu₃P.

The ABA block copolymer was rapidly cleaved within 30 minutes using 150 equivalents of Bu₃P ([Bu₃P] = 0.078 M) in THF at room temperature. The molecular weight, determined by SEC, decreases from 20100 g/mol ($\bar{M}_w = 1.27$), for the initial polymer, to 9800 g/mol ($\bar{M}_w = 1.20$), for the final cleaved polymer. Moreover, the SEC traces (Figure 5.1) show the appearance of a “tail” at lower molecular weight.

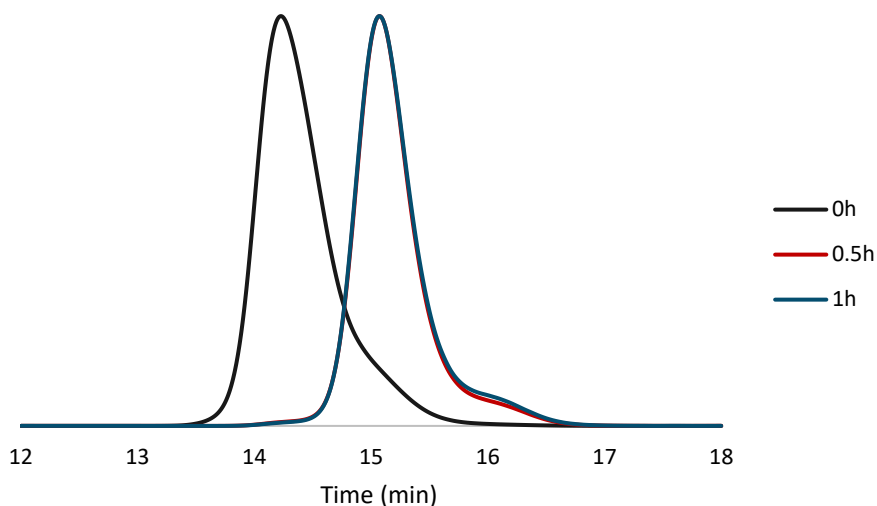
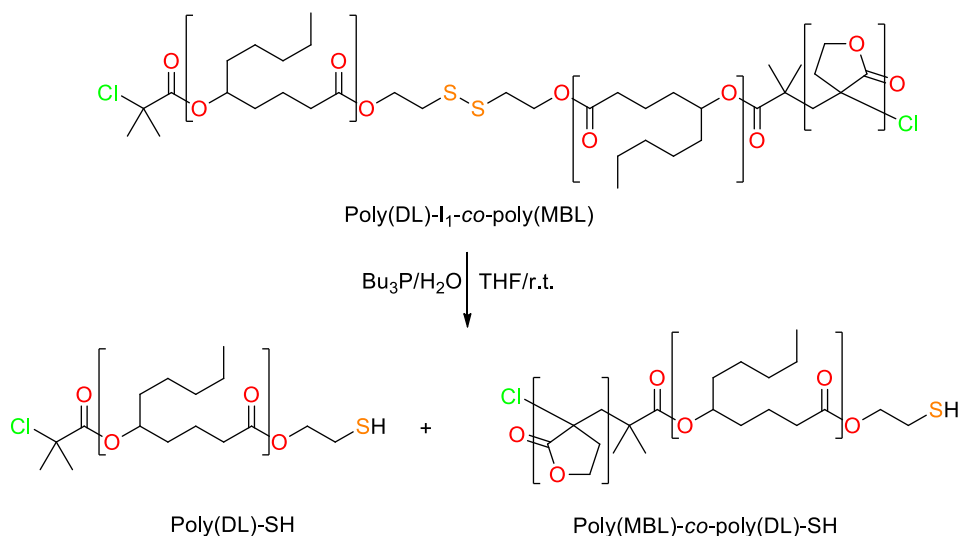


Figure 5.1 SEC traces (in DMF containing 0.05 % LiBr) of the reductive cleavage of poly(MBL)-co-poly(DL)-I₁-co-poly(MBL).



Scheme 5.5 Cleavage products of residual poly(DL)-I₁-co-poly(MBL) AB block copolymer.

This lower Mn fraction must be related to the incomplete initiation of some macroinitiator chains during ATRP. The presence of partially chain extended macroinitiator chains, consisting in a AB block copolymer (Cl-poly(DL)-I₁-co-poly(MBL)), will form two different cleavage products. One would be the same AB block copolymer

as in the cleavage of the ABA block copolymer, but the second will be a poly(DL) homopolymer with an unreacted α -chloroisobutyryl ester, with half of the molecular weight of the initial macroinitiator (Scheme 5.5).

The cleaved polymer recovered after precipitation was also analyzed by $^1\text{H-NMR}$ spectroscopy (see annex 8.35). As can be seen in Figure 5.2, the signal corresponding to the methylene protons close to the disulfide group ($\text{CH}_2\text{-S-S-}$) at 2.91 ppm completely disappeared (signal **b** in Figure 5.2-a) and a new signal at 2.74 ppm corresponding to the methylene protons near the thiol group ($\text{CH}_2\text{-SH}$) appeared (signal **b'** in Figure 5.2-b).

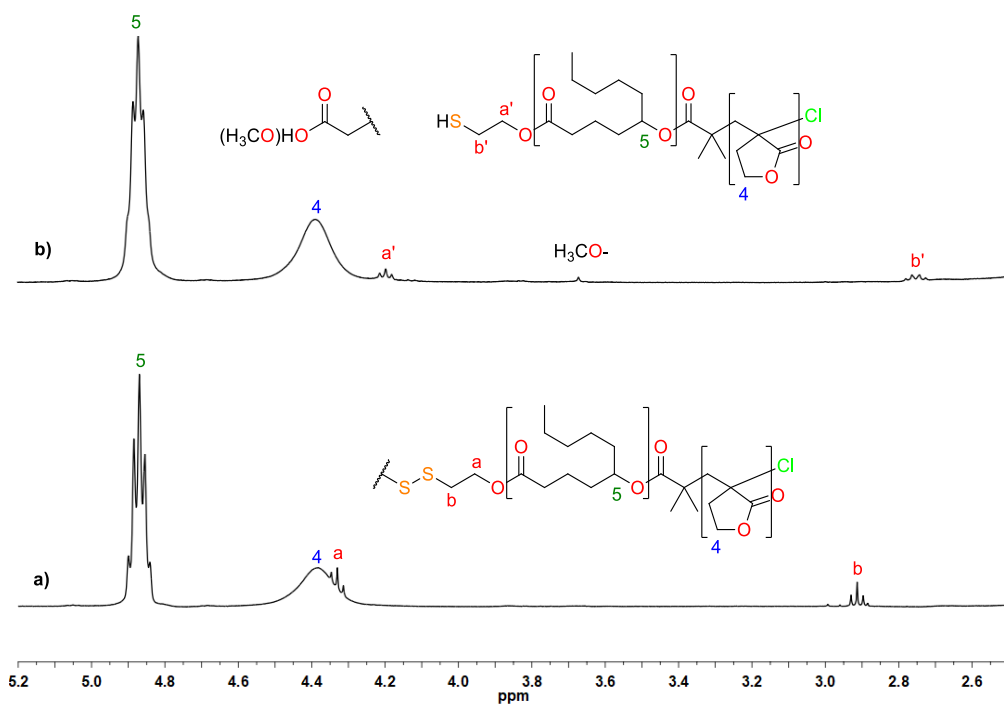
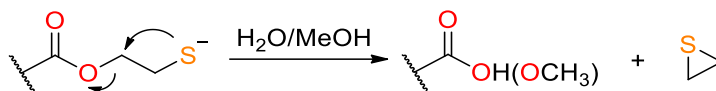


Figure 5.2 $^1\text{H-NMR}$ spectra in CDCl_3 of (a) *poly(MBL)-co-poly(DL)-I1-co-poly(MBL)* and (b) the cleaved product *poly(MBL)-co-poly(DL)-SH*.

However, it has been noticed that the intensity of the new signals is lower when compared to that of the initial signals. Moreover, a new signal that could be assigned to a methyl ester at 3.67 ppm was also observed in the spectrum of the cleaved product (Figure

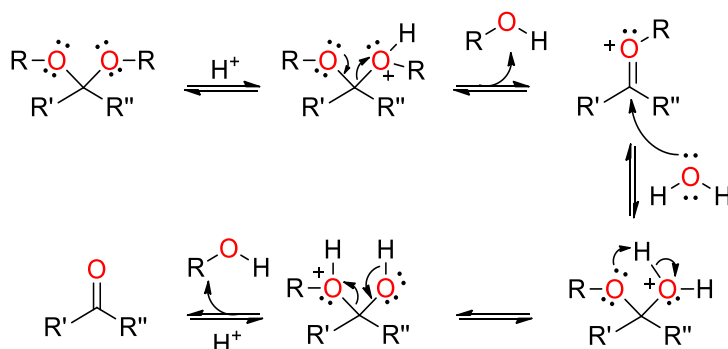
5.2-b). This fact seems to indicate that some intramolecular S_N2 displacement of the thiolate group and ulterior esterification during the methanolic work-up may also occur (Scheme 5.6) as it has been described in the literature.¹¹ Nevertheless, the effective cleavage of the block copolymer was achieved.



Scheme 5.6 Proposed mechanism for intramolecular S_N2 displacement of β -thiolate ethylester unities.

5.2 Acid cleavable polymers

Another widely used stimulus in stimuli cleavable polymers, is the acidic media.^{12, 13} Particularly, acetals and ketals have been attracted great interest due to its lability and capability of being hydrolyzed in the presence of water and acid under mild conditions.^{14, 15} Aside from the external factors (pH, temperature, etc.) the hydrolysis rate on an acetal could be modulated by changing the substituents.¹⁶ Carbocation-stabilizing substituents increase the acetal hydrolysis rate and the presence of basic groups in the molecule slows down the hydrolysis rate. The structure of the acetal also influences the hydrolysis rate, cyclic acetals are known to be more stable than linear acetals.^{10, 17}



Scheme 5.7 Acetal hydrolysis mechanism in acidic medium.

5.2.1 Cleavage of poly(MBL)-co-poly(DL)-I₂-co-poly(MBL)

Two samples of block copolymer possessing an acetal moiety (M_n (SEC) = 20600 g/mol (\mathcal{D} = 1.17)) was solubilized in THF (containing 0.5 % (w/w) of water) and trifluoroacetic acid (TFA) was added to obtain a 0.01 M and a 0.5 M solutions of acid. The mixtures were stirred at room temperature and samples were withdrawn at preset times to follow the progress of the reaction by SEC (see experimental part 6.9.2.1).

Using the 0.01 M acid concentration, the polymer was cleaved after about 24h (Figure 5.3). The obtained cleaved polymer showed a similar narrow molecular weight distribution and half of the initial molecular weight (M_n = 10000 g/mol (\mathcal{D} = 1.10)). This low polydispersity obtained is an evidence of the polymer backbone integrity during the cleavage process. Moreover, once cleaved the polymer was maintained in the acidic medium for additional 24 hours to confirm the polymer backbone stability with no signals of chain degradation (yellow line in Figure 5.3).

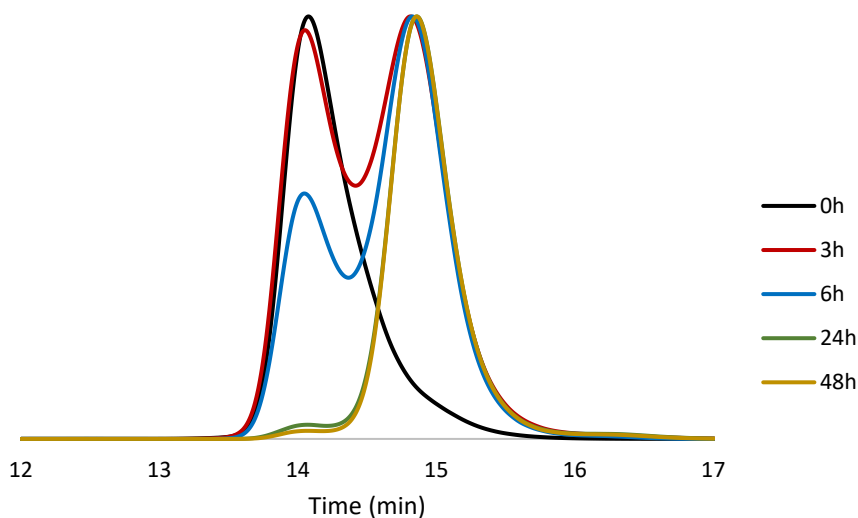


Figure 5.3 Superposed SEC traces of poly(MBL)-co-poly(DL)-I₂-co-poly(MBL) degradation in THF with [TFA] = 0.01 M at room temperature during time.

The $^1\text{H-NMR}$ shows the complete disappearance of the acetalic signal (signal **f** in Figure 5.4-a) and the appearance of a new signal at 3.75 ppm (signal **e'** in Figure 5.4-b). This signal could correspond to methylene protons close to the hydroxyl group, from the selective hydrolysis of the acetal group, of the (3-hydroxypropyl)thioethyl ester end-groups ($\text{HOCH}_2\text{CH}_2\text{CH}_2\text{SCH}_2\text{CH}_2\text{OOC-}$) (Scheme 5.8).

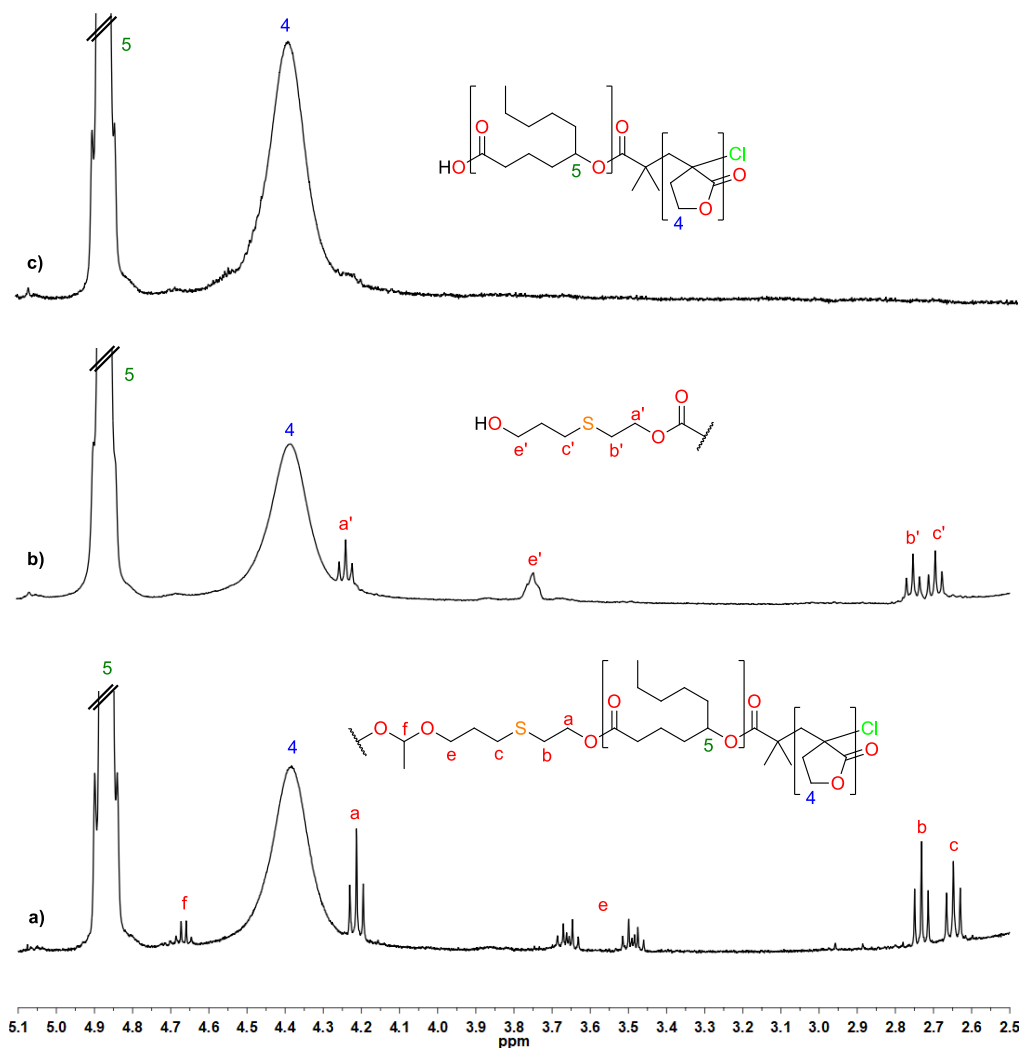
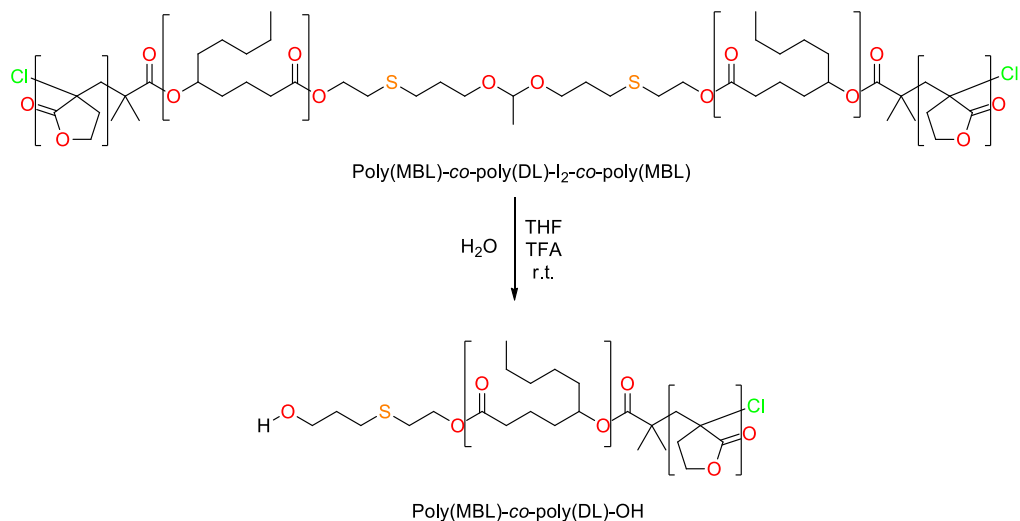


Figure 5.4 $^1\text{H-NMR}$ spectra of poly(MBL)-co-poly(DL)-l₂-co-poly(MBL) (a) before degradation, (b) after acid cleavage with $[\text{TFA}] = 0.01 \text{ M}$ and (c) after acid cleavage with $[\text{TFA}] = 0.5 \text{ M}$.



Scheme 5.8 Acid cleavage of poly(MBL)-co-poly(DL)-I₂-co-poly(MBL) to poly(MBL)-co-poly(DL)-OH using TFA.

In the other hand, using the 0.5 M solution of acid the polymer was also cleaved after about 24 hours (Figure 5.5). The obtained cleaved polymer also showed a narrow molecular weight distribution and half of the molecular weight ($M_n = 10300 \text{ g/mol}$ ($\text{Đ} = 1.10$)). The $^1\text{H-NMR}$ spectrum shows the complete disappearance of the acetalic signal (signal **f** in Figure 5.4-a), however, the expected signal corresponding to the methylene protons close to the hydroxyl group was not observed (Figure 5.4-c). This fact could be related to the selective hydrolysis of the terminal ester linkage prompted by sulfur-assistance under strong acidic conditions (Scheme 5.9).¹⁸ In fact, β -thiopropionate esters are well known as acid labile groups and have been extensively used in acid-sensitive polymeric devices.^{19, 20, 21} Nevertheless, the integrity of the polymer backbone seems to be maintained, as the poly(DL) and poly(MBL) signals remained unaffected (signals **5** and **4** in Figure 5.4-c) and, the SEC of the cleaved polymer showed a narrow molecular weight distribution.

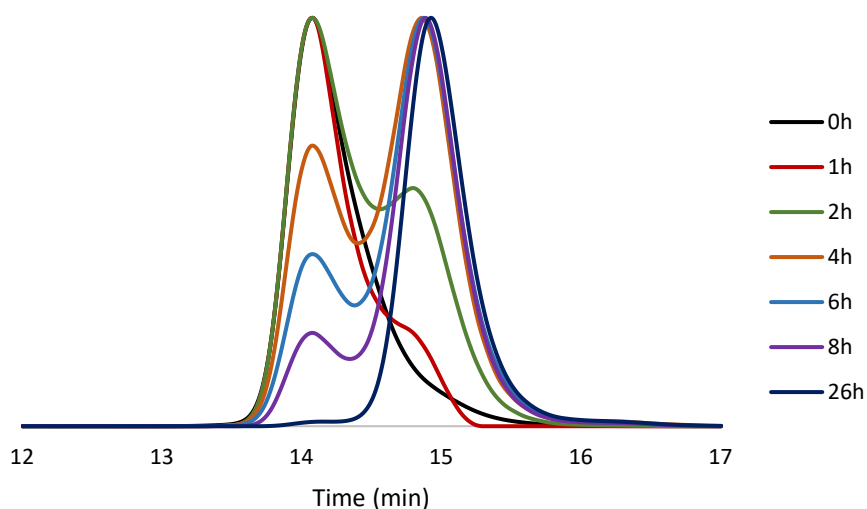
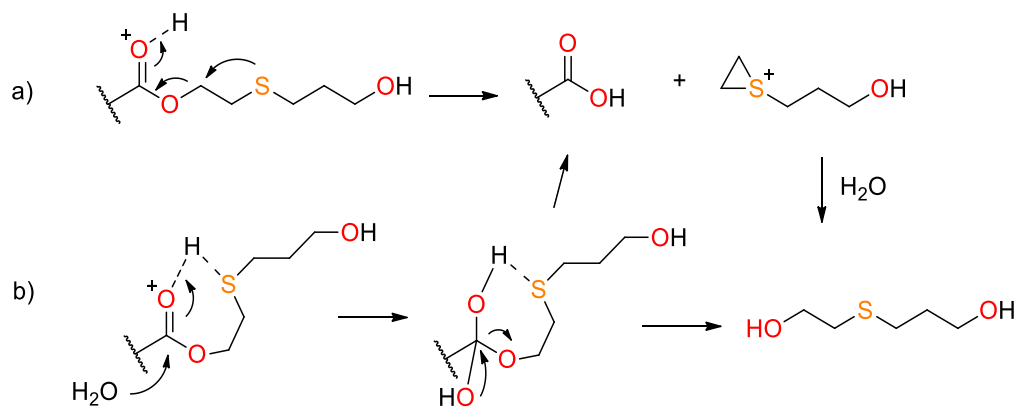


Figure 5.5 Superposed SEC traces of poly(MBL)-co-poly(DL)-I₂-co-poly(MBL) degradation in THF with [TFA] = 0.5 M at room temperature during time.



Scheme 5.9 Proposed mechanisms for the scission of the β -thioethyl ester units in 0.5 M TFA: (a) by neighboring sulfur assistance by intramolecular S_N displacement and (b) by sulfur stabilization of the hydrogen-bond cyclic intermediate.

5.2.2 Cleavage of poly(MBL)-co-poly(DL)-I₃-co-poly(MBL)

As mentioned before, cyclic acetals present higher stability towards acid hydrolysis compared with linear acetals. Nevertheless, tetraoxaspiro moieties have been described in the literature for the preparation of acid degradable polymers.^{22, 23} Considering its lower reactivity towards acid hydrolysis, initial tests were performed directly using a [TFA] = 0.5 M. Thus, the polymer containing the tetraoxaspiro moiety (M_n (SEC) = 22900 g/mol, \bar{D} = 1.17) was solubilized in THF (containing 0.5 % (w/w) of water) with a [TFA] = 0.5 M. The reaction was monitored by SEC and after 24 hours the polymer remained unaffected. Therefore, a second experiment was performed maintaining the same acid concentration ([TFA] = 0.5 M) but increasing the temperature up to 40 °C (see experimental part 6.9.2.2). At this temperature the polymer started to cleave in a progressive way. The progress of the reaction was monitored by withdrawing samples at preset times for SEC analysis (Figure 5.6). From the superposed chromatograms it can be observed that the polymer was completely cleaved after about 23 hours of reaction. Under these conditions the poly(DL) chain seems not to be affected, since prolonged hydrolysis time (33h) clearly does not affect the molecular weight distribution.

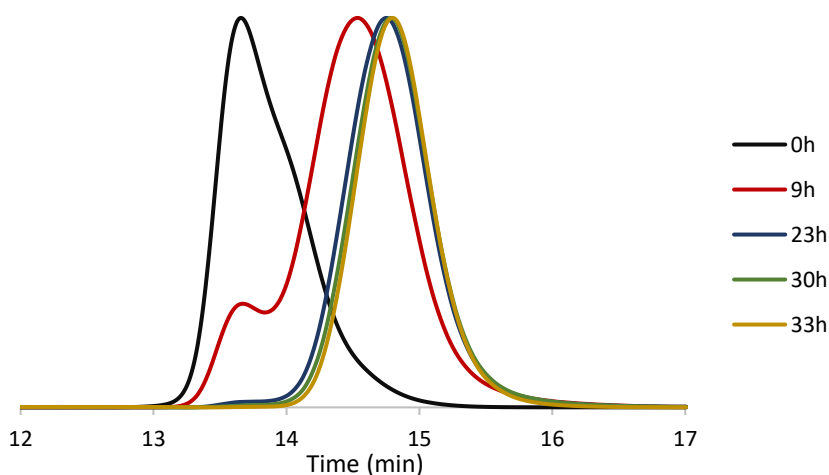


Figure 5.6 SEC traces (DMF, 0.05 % LiBr) of the acid cleavage of poly(MBL)-co-poly(DL)-I₃-co-poly(MBL).

The cleaved polymer showed a narrow polydispersity ($\mathcal{D} = 1.11$) and a molecular weight of 11500 g/mol (SEC in DMF (0.05 % LiBr)) which is about half of the molecular weight of the starting polymer. Even though, cleavage is evident from SEC traces, the $^1\text{H-NMR}$ spectrum of the recovered polymer (Figure 5.7) showed the persistence of most signals of the tetraoxospiroacetal moiety. In addition, two new signals at 3.72 and 4.11 ppm could be observed. The triplet signal at 3.72 ppm (signal ** in Figure 5.7-b) can be assigned to hydroxyethylthio end groups ($\text{HOCH}_2\text{CH}_2\text{-S-}$) arising from sulfur assisted hydrolysis of the β -thioethyl ester units under strong acidic conditions (Scheme 5.10). The singlet at 4.11 ppm (signal * in Figure 5.7-b) can be assigned to the $\text{C}(\text{CH}_2\text{OH})_2$ groups resulting from the subsequent progressive hydrolysis of the acetal units.²⁴ Thus, even though cleavage of tetraoxospiro block copolymer can be triggered under acidic conditions, mainly proceeds by β -thioethyl ester hydrolysis leading to tetraoxospiroacetal units that are hydrolyzed at slower rates.

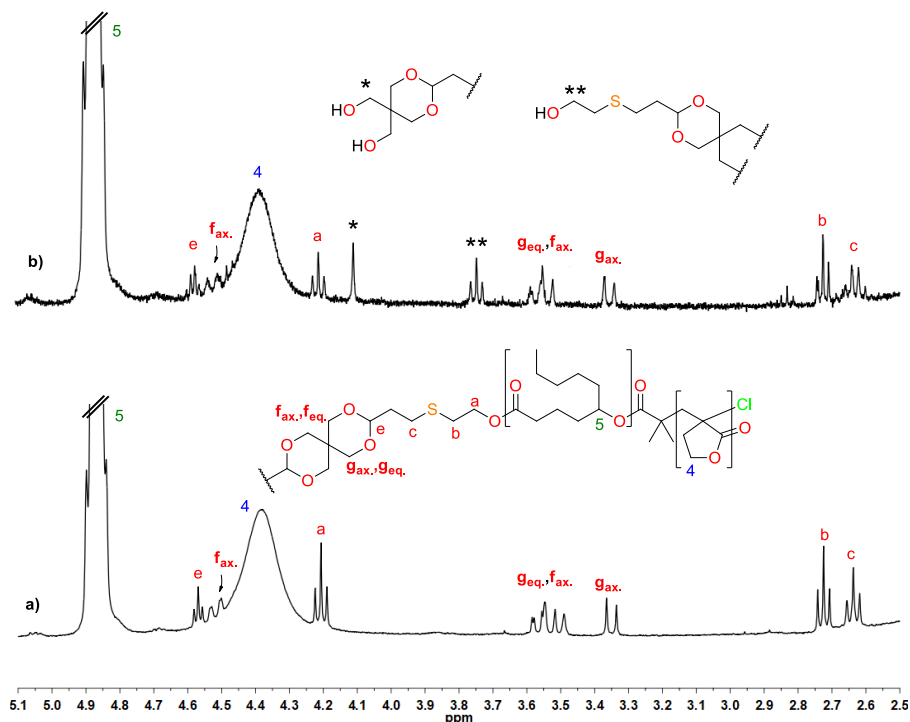
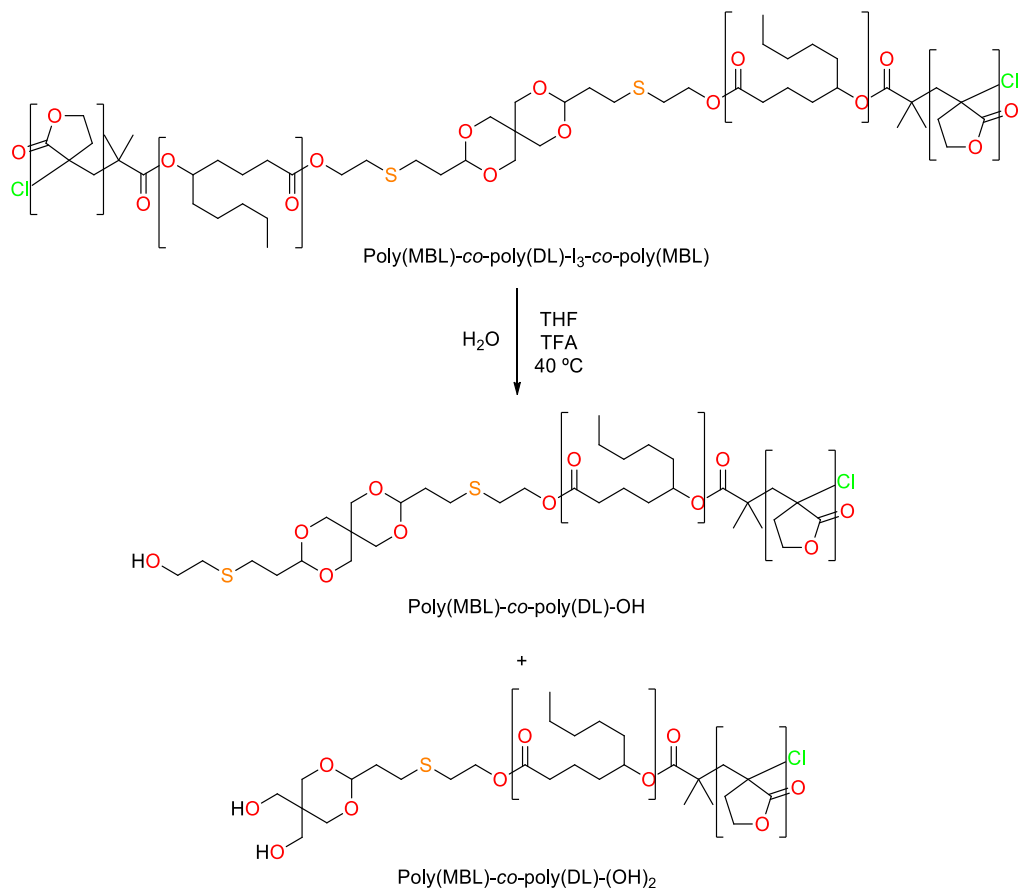


Figure 5.7 $^1\text{H-NMR}$ spectra of poly(MBL)-co-poly(DL)-I₃-co-poly(MBL) (a) before and (b) after acid cleavage.



Scheme 5.10 Acid cleavage of poly(MBL)-co-poly(DL)-I₃-co-poly(MBL) to poly(MBL)-co-poly(DL)-OH and poly(MBL)-co-poly(DL)-(OH)₂ using [TFA] = 0.5 M at 40 °C.

5.3 Reactive oxygen species (ROS) cleavable polymers

Thioacetals are well known protective groups in chemistry but chemoselective cleavage of thioacetals under mild conditions is still a challenging process, particularly in presence of sensitive substrates. Unless acetal groups, thioacetals are resistant to conventional acid and basic hydrolysis requiring quite harsh conditions due to the scarce ability of the alkyl and aryl sulfide moieties as leaving groups. As a key step in conventional synthesis, a plethora of cleavage methods have been developed which generally require heavy metal derivatives and other environmentally hazardous

reagents.²⁵ A common approach involves the transformation of thioethers into better leaving sulfonium groups by using different organic compounds as halogen sources (NBS, chloramine-T, Dess-Martin periodinane, etc.).^{25 - 27} Interestingly, catalytic amounts of iodine proved to be effective in thioacetal deprotection when DMSO is used as oxygen source.^{28, 29} Moreover, the cleavage by iodonium ions would give access to a more general procedure using chloronium ions in bleach, a common chemical used in paper processing.

In order to assess the deprotection reactions of the thioacetals, two model compounds (Dod-I₄ and Dod-I₅) were synthesized from the thioacetal diols I₄ and I₅ and dodecanoyl chloride, following an adaptation of a reported procedure (Figure 5.8).³⁰

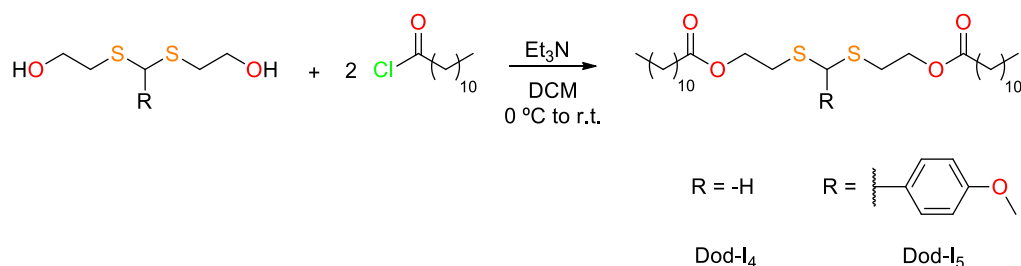
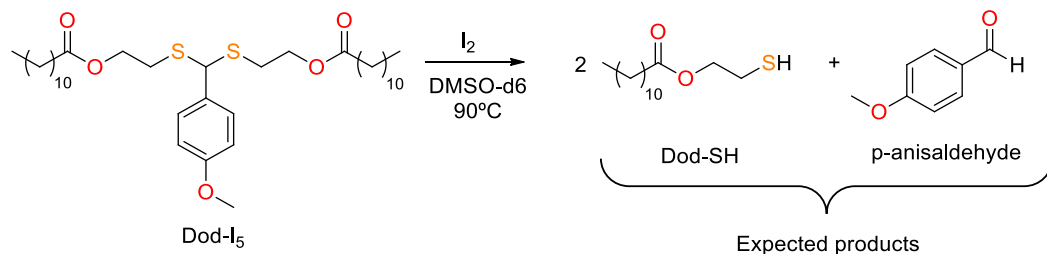


Figure 5.8 Synthesis of thioacetal model compounds Dod-I₄ and Dod-I₅.

Thus, as a first approach for the cleavage of the thioacetal moieties, the degradation of the model compound Dod-I₅, using DMSO as oxygen source with catalytic amounts of iodine, was tested (Scheme 5.11) (see experimental part 6.9.3.1).²⁹



Scheme 5.11 Expected products for thioacetal deprotection of Dod-I₅ model compound using DMSO and I₂ as catalyst.

The reaction was conducted at 90 °C and the progress of the reaction was monitored by $^1\text{H-NMR}$ spectroscopy. The spectra were recorded in CDCl_3 due to the insolubility of the products in DMSO-d_6 at room temperature.

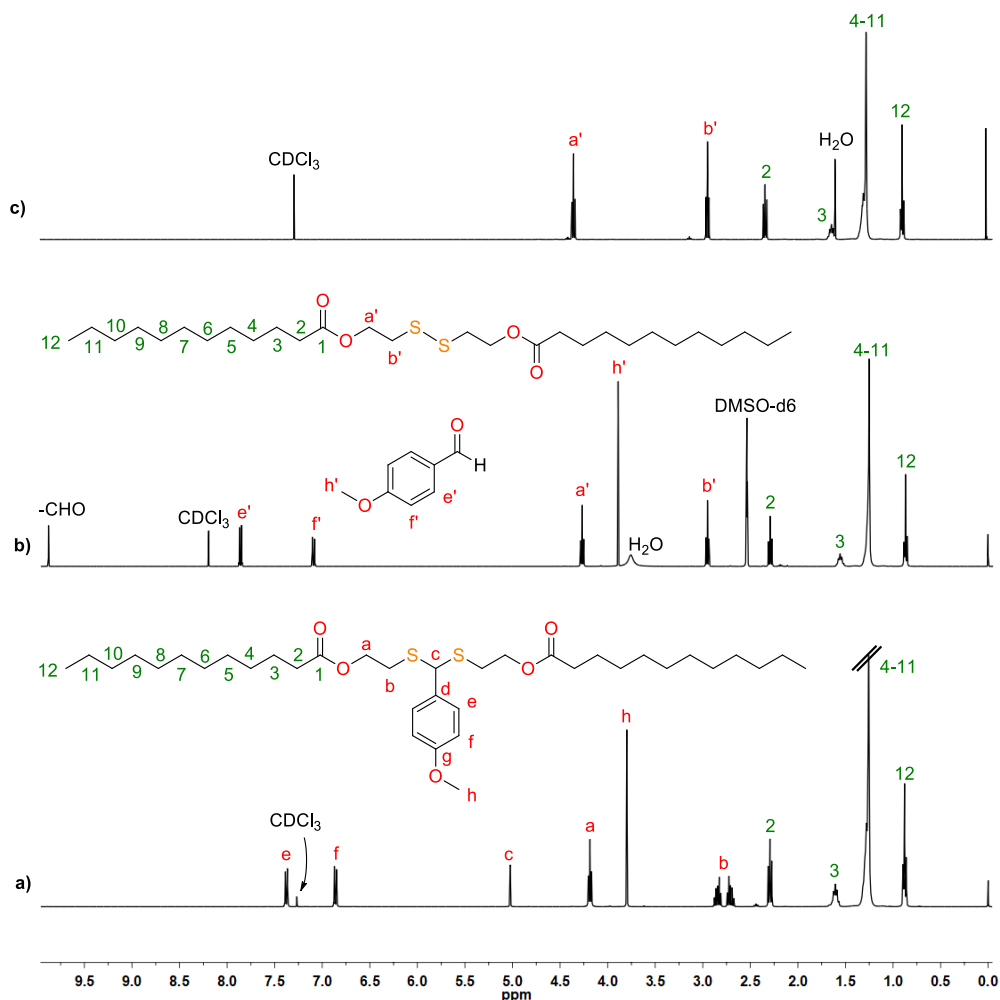


Figure 5.9 $^1\text{H-NMR}$ spectra of (a) Dod-I_5 , (b) crude reaction mixture with 1% I_2 in DMSO-d_6 after 30 min at 90 °C and (c) product after recrystallization in methanol. Spectra (a) and (c) recorded in CDCl_3 , spectrum (b) recorded in a CDCl_3 with DMSO-d_6 from the reaction mixture.

As can be seen in Figure 5.9 the signal corresponding to the thioacetal proton (5.02 ppm, signal c in Figure 5.9-a) completely disappeared within 30 minutes. Moreover, a signal at 9.83 ppm corresponding to the aldehyde proton (Figure 5.9-b) was observed,

indicating the effective deprotection of the carbonyl group. However, the expected signals of the thiol-end derivative (Dod-SH in Scheme 5.11) (around 4.20 and 2.75 ppm) were not observed. In their place, new signals at 4.33 and 2.92 ppm appeared (signals **a'** and **b'** respectively in Figure 5.9-b). That could be attributable to the corresponding disulfide compound. The formation of this product could be confirmed by comparing the $^1\text{H-NMR}$ signals with those of a model compound (Dod-I₁, Figure 5.10) prepared from diol I₁ and dodecanoyl chloride following the same procedure as in the case of Dod-I₄ and Dod-I₅. In this way, the deprotection of thioacetals with iodine as catalyst seems to proceed though the formation of disulfides, as has been recently reported in the photooxidative deprotection of thioacetals.³¹

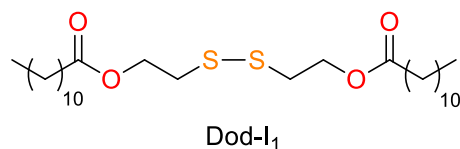
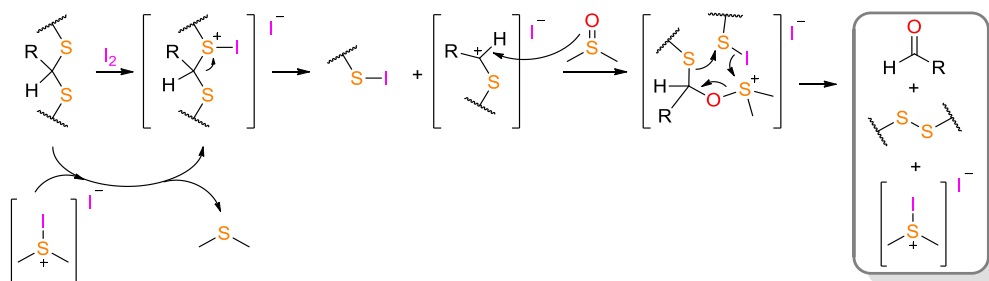


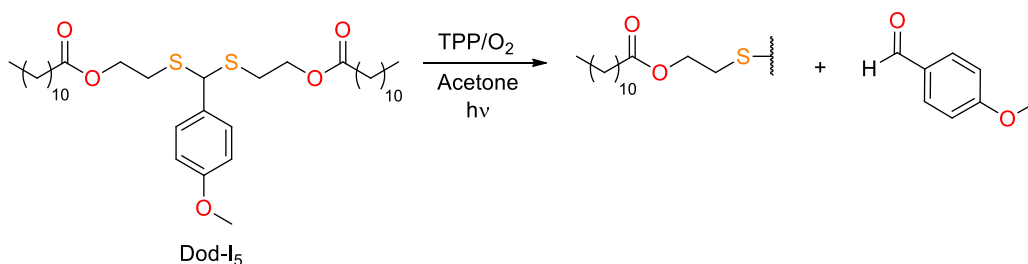
Figure 5.10 Disulfide model compound.

According to the literature, the proposed mechanism for the thioacetal deprotection catalyzed by iodine (Scheme 5.12)²⁹ involves the formation of a sulfonium complex with iodine, followed by the C-S bond cleavage and nucleophilic addition of dimethylsulfoxide. Then, the S-O bond cleavage leads to the formation of the carbonyl compound and the disulfide derivative. This result encourages us to explore the photocatalytic deprotection of thioacetals.



Scheme 5.12 Proposed mechanism for the iodonium thioacetal deprotection with DMSO.²⁹

Precisely, photooxidative cleavage is another common approach which has recently experienced an increasing interest when applied to the production of ROS-responsive polymeric drug carriers.^{32, 33} Photooxidative deprotection of cyclic and acyclic thioacetals has been described to proceed under mild conditions with light irradiation.^{31, 34, 35} Singlet oxygen (1O_2) has been proposed as reactive species in the S-C bond cleavage leading to cation-radical intermediates which evolves to different final products depending on the nature of the substituents and the redox potential of the photosensitizer used.³⁴ Thus, the Dod-I₅ was also used as model compound for the photooxidation cleavage of thioacetals (Scheme 5.13) (see experimental part 6.9.3.1).



Scheme 5.13 Photolysis of Dod-I₅ using oxygen and TPP as photosensitizer under light irradiation.

Initial tests were carried out using a 400 W high pressure sodium in a saturated oxygen atmosphere and meso-tetraphenylporphyrin (TPP) as photosensitizer. Photolysis of thioacetal Dod-I₅ in acetone solution was monitored by 1H -NMR spectroscopy (Figure 5.11). The 1H -NMR spectrum shows the formation of anisaldehyde (**d'**, **e'** and CHO in Figure 5.11-b) and the disulfide derivative (**a'** and **b'** in Figure 5.11-b) within two hours of reaction. The reaction was let to proceed and, within 6 hours of reaction, the 1H -NMR spectrum became more complex, indicating the formation of different oxidized species (Figure 5.11-c). According to the signals chemical shifts and data reported in the literature, could be attributed to a mixture of sulfinothioate (R-S-SO-S) and sulfonothioate (R-S-SO₂-R) (signals **a'''** and **b'''** in Figure 5.11-c) and other oxidation compounds.^{34, 36, 37}

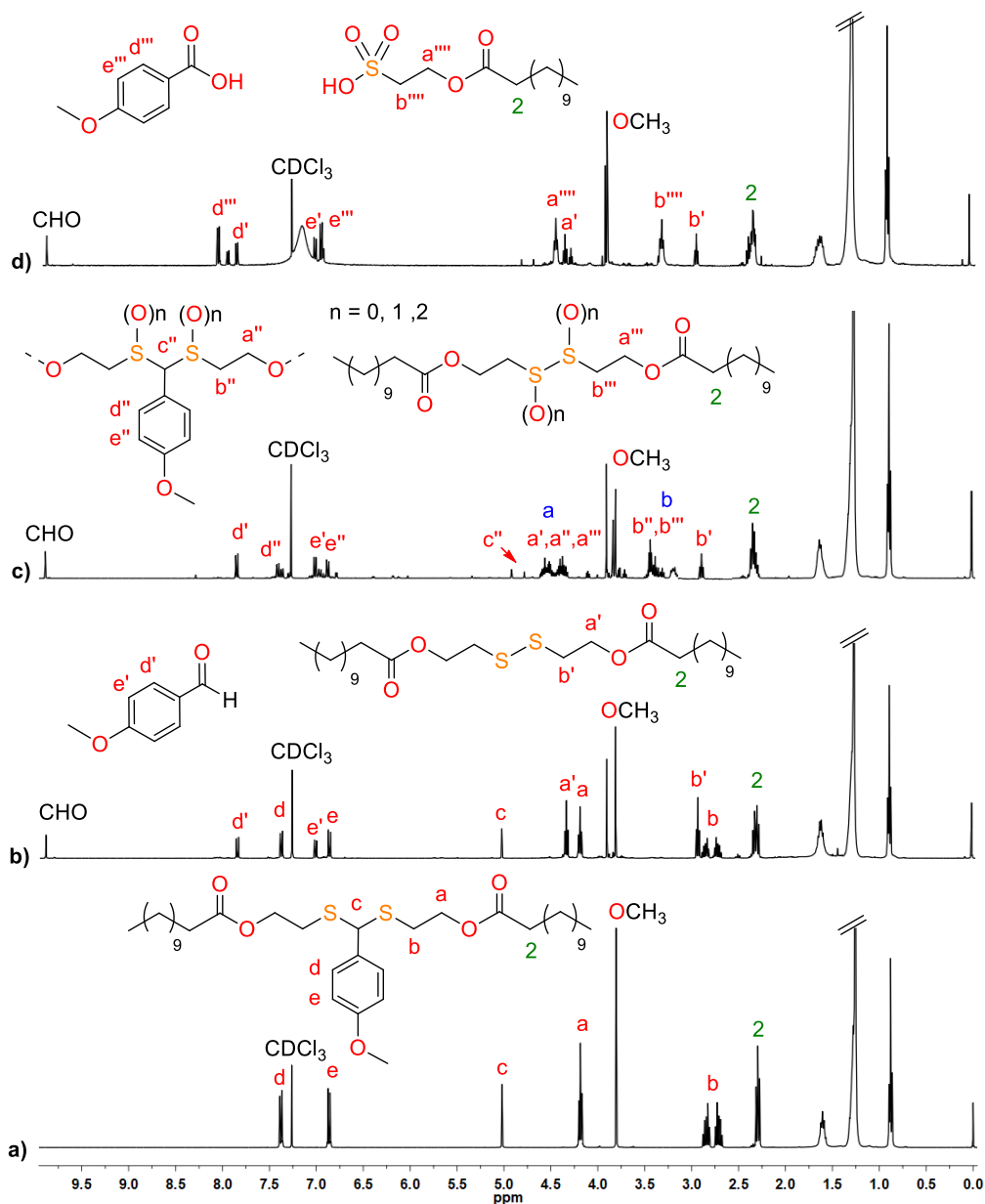
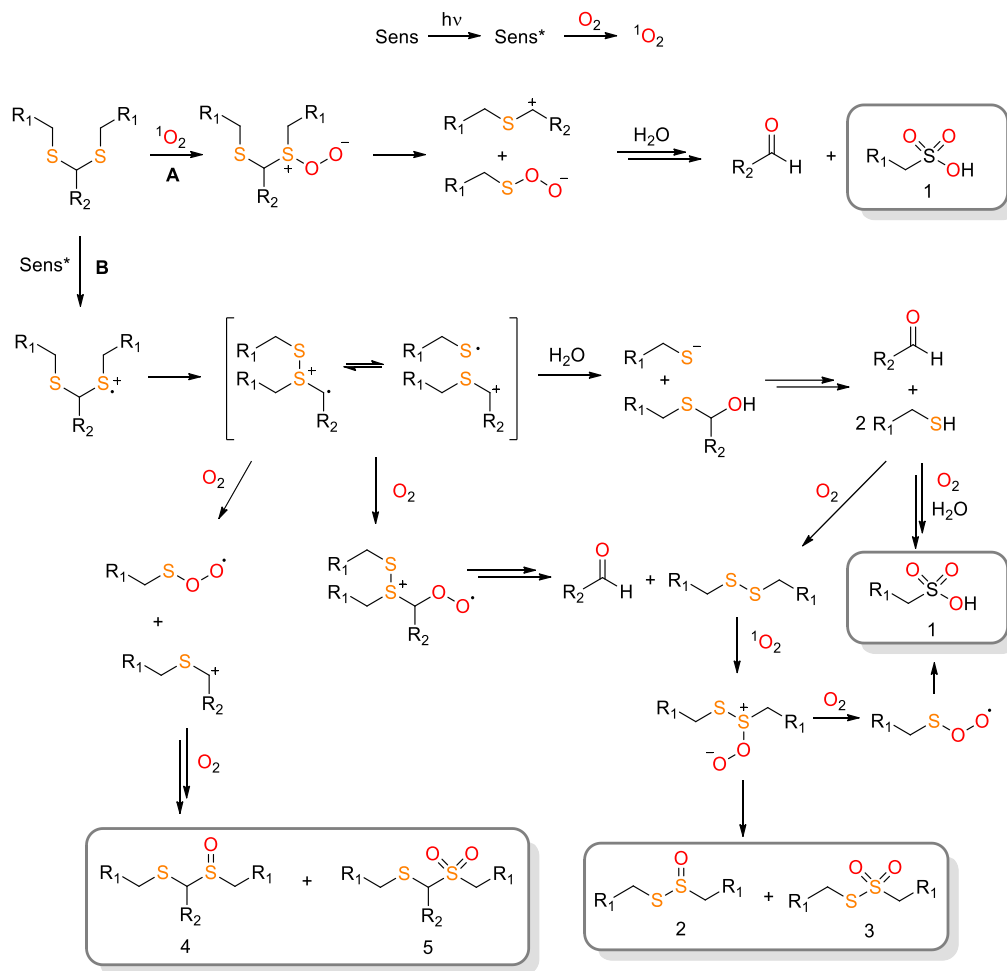


Figure 5.11 $^1\text{H-NMR}$ spectra of (a) Dod-I₅ and the products of the photolytic degradation with TPP/O₂ in acetone after (b) 2h, (c) 6h and (d) 12h. Spectra recorded in CDCl_3 .

Delightfully, after 12 hours of reaction a simpler spectrum showed the formation of a main product whose $^1\text{H-NMR}$ signals match with the alkoxyethanesulfonic derivative ($\text{COOCH}_2\text{CH}_2\text{SO}_3\text{H}$) (signals a''' and b''' in Figure 5.11-d) together with some remaining

disulfide (signals **a'** and **b'** in Figure 5.11-d).³⁸ These results seem to indicate that with this methodology an effective cleavage of the thioacetal moiety could be achieved, with a minor formation of the disulfide.



Scheme 5.14 Representative possible mechanism pathways for the photooxidative cleavage of thioacetal groups with TPP/O₂/H₂O according to the proposed photo-oxidation of 1,3-dithianes and disulfides. (A) Singlet oxygen pathway, (B) single electron transfer (SET) pathway.³⁵⁻³⁹

According to the literature, the mechanism for the photooxidation of thioacetals could follow two different pathways. The first pathway (A in Scheme 5.14) involves the generation of singlet oxygen (¹O₂) from the interaction of a sensitizer in its excited state with molecular oxygen.⁴⁰ Then, the ¹O₂ reacts with the thioacetal to form a persulfide

intermediate. The persulfoxide becomes C-S bond cleavage which products reacts with water to give the carbonyl compound and the sulfonic acid derivative (1 in Scheme 5.14). On the other hand, the second pathway involves a single electron transfer (SET) from the sensitizer in its excited state directly to the thioacetal (B in Scheme 5.14) leading to a cation radical. The thioacetal cation radical fragmentates into a distonic radical cation which could evolve in different manners. A nucleophilic attack of a water molecule would lead to the carbonyl compound and the thiol derivative, which could be overoxidized to sulfonic acid (1 in Scheme 5.14). The distonic radical cation could also react with molecular oxygen giving a peroxosulfoxide intermediate which become a C-S bond cleavage to give the carbonyl compound and the disulfide derivative. The disulfide could be overoxidized to form sulfonic acid, sulfinothioate and sulfonothioate derivatives (1, 2 and 3 in Scheme 5.14). Finally, the distonic radical cation bond cleavage, with posterior oxidation, could lead to the sulfinio and sulfono thioacetal derivative (4 and 5 in Scheme 5.14). When TPP is used as sensitizer the singlet oxygen pathway has been proposed as main pathway for the deprotection of thioacetals.^{35, 39}

With these results, the same methodology was applied to of poly(MBL)-*co*-poly(DL)-I₄-*co*-poly(MBL) (M_n 20.000 g/mol; Đ = 1.18) and poly(MBL)-*co*-poly(DL)-I₅-*co*-poly(MBL) (M_n 19.000 g/mol; Đ = 1.16) copolymers. In both cases, SEC traces (Figure 5.12 and Figure 5.13) indicate a progressive slow cleavage leading to polymers with about half the initial molecular weight. However, the process seems to be incomplete as some high molecular weight fractions remain after 24-48h. This fact is especially noteworthy in the case of poly(MBL)-*co*-poly(DL)-I₄-*co*-poly(MBL) which give rise to non-stabilized intermediates, even though additional TPP was added. These results agree with the persistence of some disulfide fractions observed in the photolysis of Dod-I₅.

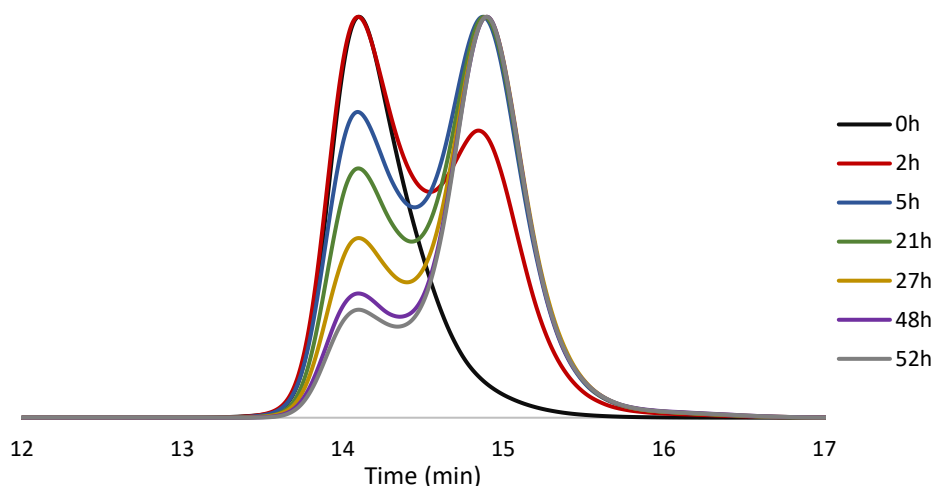


Figure 5.12 SEC traces (in DMF containing 0.05 % LiBr) of the homogeneous photolytic cleavage (TPP/O₂/hν) of poly(MBL)-co-poly(DL)-I₄-co-poly(MBL).

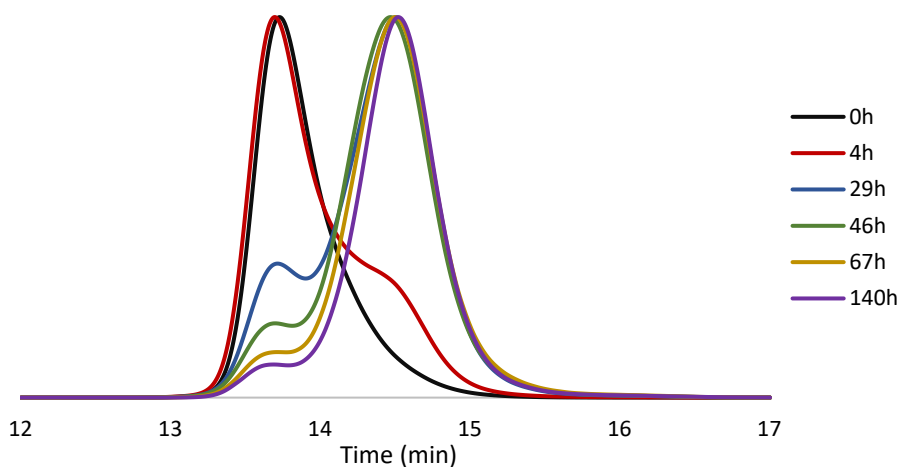


Figure 5.13 SEC traces (in DMF containing 0.05 % LiBr) of the homogeneous photolytic cleavage (TPP/O₂/hν) of poly(MBL)-co-poly(DL)-I₅-co-poly(MBL).

From the practical point of view, a much more convenient procedure for a TPE degradation might consist in the use of aqueous solutions. Hydrogen peroxide, a common paper processing chemical, has also been described as an effective source of ROS in the photolysis of thioacetals in aqueous media.^{37, 41, 42}

With the aim to improve the extend of cleavage, heterogeneous-phase photolysis, using H_2O_2 as oxygen source, was tested.

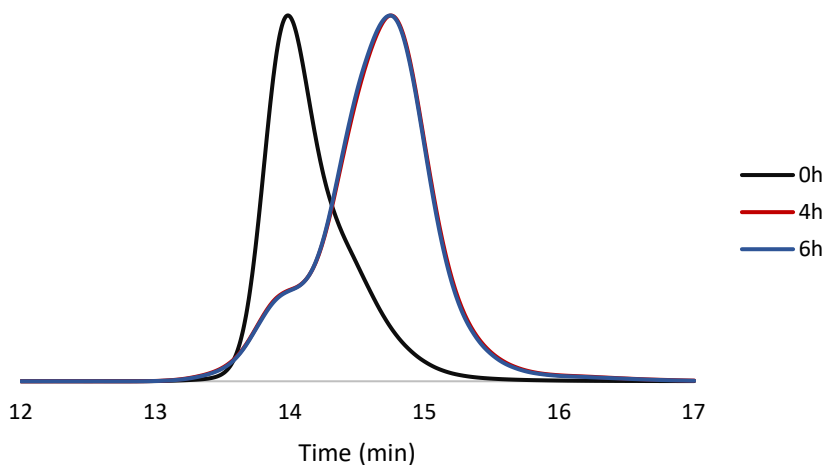


Figure 5.14 SEC traces (in DMF containing 0.05 % LiBr) of the heterogeneous photolytic cleavage (TPP/ H_2O_2 /hv) of poly(MBL)-co-poly(DL)-I₄-co-poly(MBL).

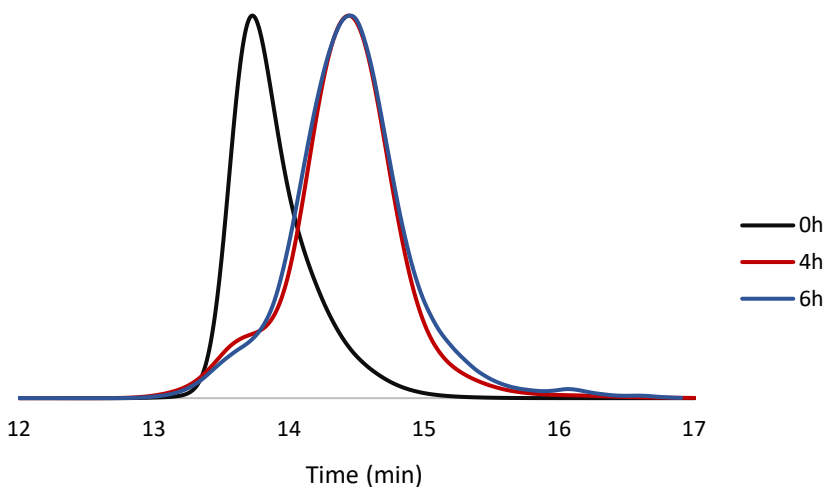


Figure 5.15 SEC traces (in DMF containing 0.05 % LiBr) of the heterogeneous photolytic cleavage (TPP/ H_2O_2 /hv) of poly(MBL)-co-poly(DL)-I₅-co-poly(MBL).

Therefore, thin films of poly(MBL)-co-poly(DL)-I₄-co-poly(MBL) and poly(MBL)-co-poly(DL)-I₅-co-poly(MBL) containing catalytic amounts of TPP were irradiated in presence of a 15 % H_2O_2 in a phosphate buffer solution (pH 7.4) (see experimental part

6.9.3.2). As can be seen in Figure 5.14 and Figure 5.15, SEC traces show fast degradation which is almost complete (>95%) in 4h in both copolymers.

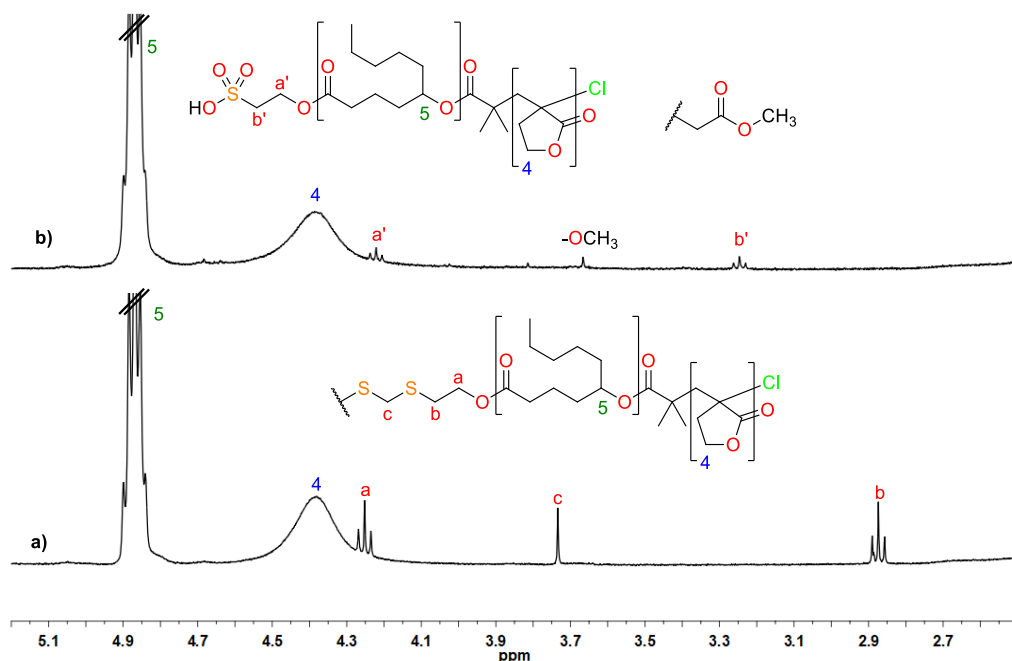


Figure 5.16 $^1\text{H-NMR}$ spectra (region between 5.2 and 2.5 ppm) of (a) pristine I_4 block copolymer and (b) the product of the oxidative degradation with H_2O_2 after 6h. Spectra recorded in CDCl_3 .

$^1\text{H-NMR}$ spectra of the resulting polymers showed the complete disappearance of the thioacetal signals (signal **c** in Figure 5.16-a and Figure 5.17-a) while the signals of the polymer backbone (signals **4** and **5** in Figure 5.16 and Figure 5.17) remained unaffected. In the case of the thioacetal I_4 the $^1\text{H-NMR}$ spectrum shows the appearance of a new triplet signal at 3.25 ppm (signal **b'** in Figure 5.16-b). This signal, according to the data reported in the literature,³⁸ could correspond to the ethanesulfonic acid derivative; however, the relative intensity of the end-group signals was considerably lower than the initiator signals in the initial polymer. This fact could arise from the hydrolysis of the ethanesulfonic ester group, leading to a carboxylic acid terminated polymer or the methyl ester derivative during the methanolic work-up (**OCH₃** in Figure 5.16-b) in a similar way as observed before (Scheme 5.9). On the other hand, the thioacetal I_5 $^1\text{H-}$

NMR spectrum didn't show the signals corresponding to sulfonic end-groups, which could be due to the above-mentioned hydrolysis (Figure 5.17-b). As in the prior case, some methyl ester end-group signal could be detected, after the methanolic work-up. Nevertheless, the effective cleavage of the block copolymers was achieved, evidenced by SEC.

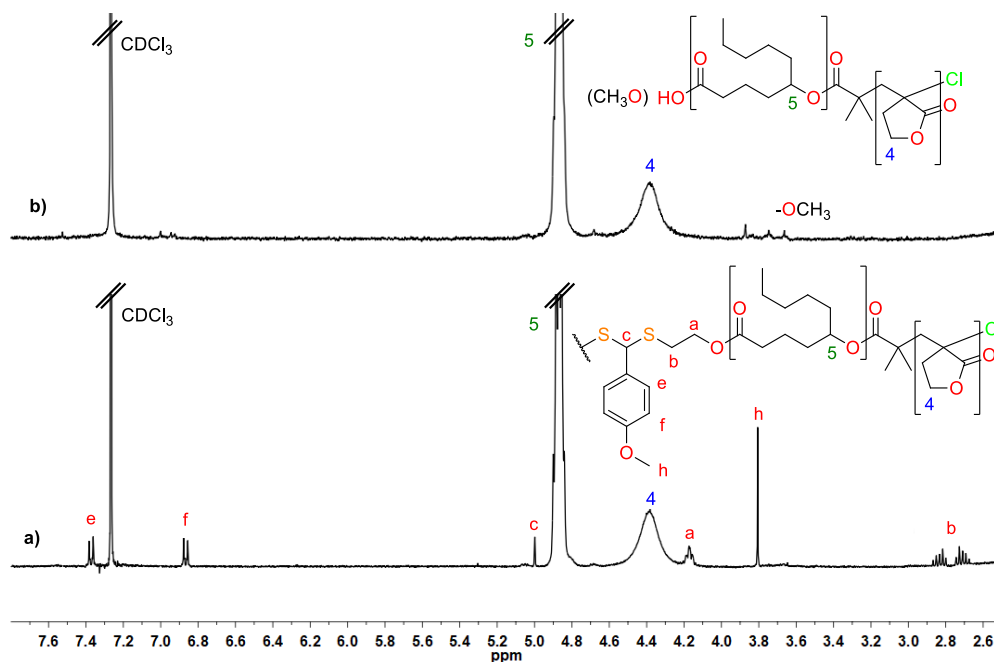
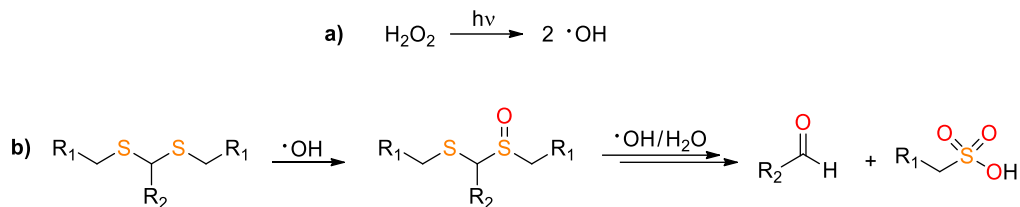


Figure 5.17 ¹H-NMR spectra (region between 7.8 and 2.5 ppm) of (a) pristine I₃ block copolymer and (b) the product of the oxidative degradation with H₂O₂ after 6h. Spectra recorded in CDCl₃.

Hydrogen peroxide becomes homolytic bond cleavage under light irradiation to form hydroxyl radicals (Scheme 5.15-a), which are also a type of ROS. These highly reactive radicals could oxidize thioacetals to form sulfoxide and disulfoxide derivatives which could be further oxidized to form the corresponding carbonyl compound and a sulfonic acid derivative (Scheme 5.15-b).⁴¹



Scheme 5.15 (a) Homolytic bond cleavage of hydrogen peroxide under light irradiation and (b) possible mechanism of thioacetal deprotection with hydroxyl radicals.

To check the influence of light in the oxidation of thioacetals with H_2O_2 a test, in the absence of light, using Dod-I₄ model compound was carried out. Thus, Dod-I₄ was solubilized in CDCl_3 and H_2O_2 (50%) containing 1% of methytrioctylammonium tetrakis (diperoxotungsto)phosphate as phase transfer catalyst (PTC) was added (see experimental part 6.9.3.1).

As can be observed in the $^1\text{H-NMR}$ spectra at the first 6 hours of reaction (Figure 5.18-b) a complex spectrum, corresponding to a mixture of oxidized products, was obtained. It can be noticed the formation of sulfoxide (blue signals at 4.29, 3.91, 3.77 and 3.30-3.10 ppm in Figure 5.18-b), disulfoxide (red signals at 4.51, 4.14 and 3.00 ppm in Figure 5.18-b) and sulfoxidesulfone (green signals at 4.60, 4.49, 4.39, 3.95, 3.41 and 3.08 ppm in Figure 5.18-b) derivatives. The spectrum simplifies within 12 hours of reaction giving the disulfone derivative as main product (purple signals at 4.71, 4.57 and 3.72 ppm in Figure 5.18-c) (Scheme 5.16). According to these results the thioacetal moiety was not cleaved under these conditions.

The effective oxidative cleavage must be related to photoactivation processes since oxidation of Dod-I₄ with 50% H_2O_2 in absence of light and photosensitizer was proved to give only the corresponding disulfone thioacetal derivatives.

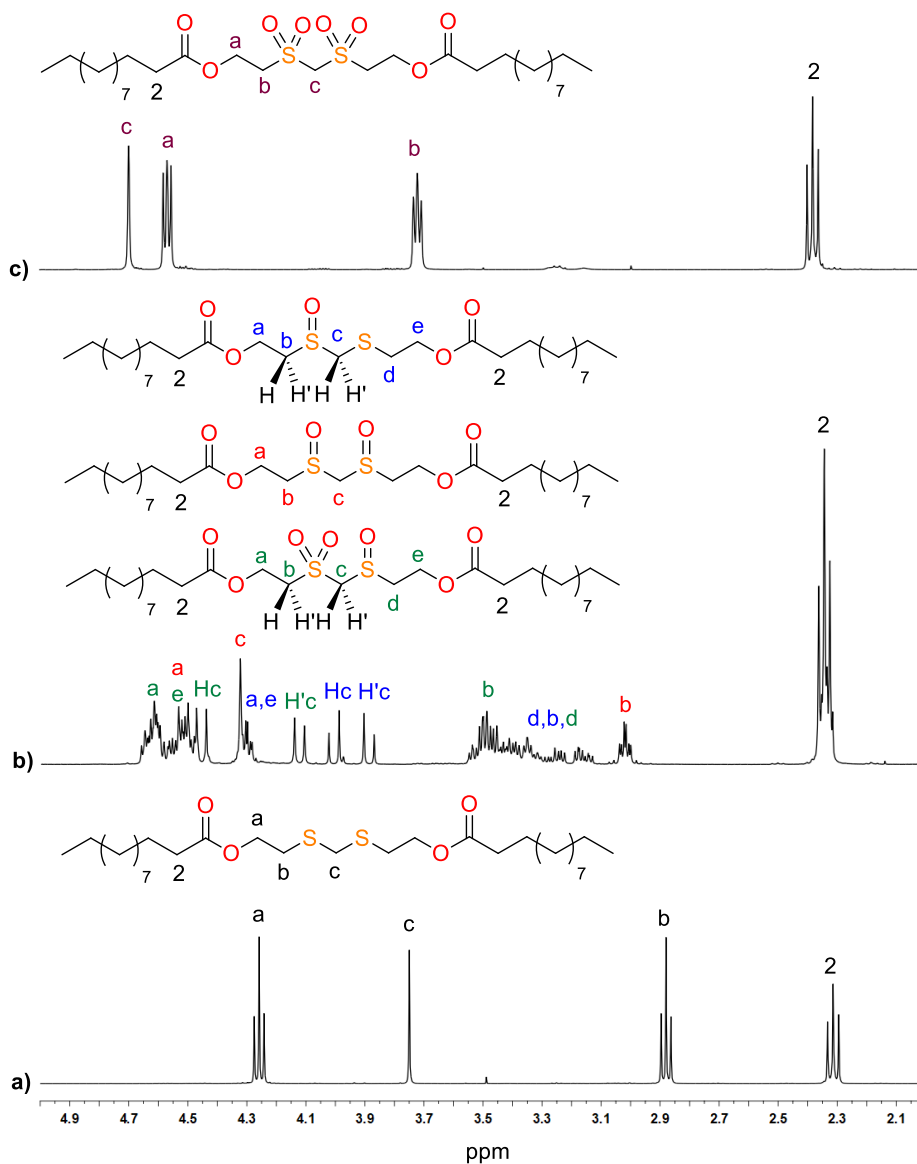
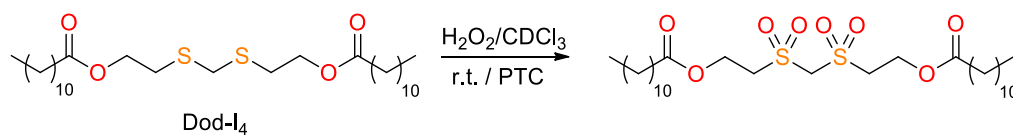


Figure 5.18 $^1\text{H-NMR}$ spectra (region between 5 and 2 ppm) of (a) *Dod-I*₄ and its oxidized products with H_2O_2 in the absence of light after (b) 6h and (c) 12h. Spectra recorded in CDCl_3 .



Scheme 5.16 Oxidative cleavage of *Dod-I*₄ with H_2O_2 under PTC.

- ¹ Xuan, J.; Han, D.; Xia, H.; Zhao, Y. Dual-stimuli-responsive micelle on an ABC triblock copolymer bearing a redox-cleavable unit and a photocleavable unit at two block junctions. *Langmuir* **2014**, *30*, 410-417.
- ² Jazani, A. M.; Oh, J. K. Dual location, dual acidic pH/reduction-responsive degradable block copolymer: Synthesis and investigation of ketal linkage instability under ATRP conditions. *Macromolecules* **2017**, *50*, 9427-9436.
- ³ Fang, J.-Y.; Lin, Y.-K.; Wang, S.-W.; Yu, Y.-C.; Lee, R.-S. Acid and light dual- stimuli-cleavable polymeric micelles. *J. Polym. Res.* **2017**, *24*, 3.
- ⁴ Moreno, A.; Ronda, J. C.; Cádiz, V.; Galià, M.; Lligadas, G.; Percec, V. SET-LRP from programmed difunctional initiators encoded with double single-cleavage and double dual-cleavage groups. *Biomacromolecules* **2019**, *20*, 3200-3210.
- ⁵ Seah, G. L.; Yu, J. H.; Koo, B. I.; Lee, D. J.; Nam, Y. S. Cancer-targeted reactive oxygen species-degradable polymer nanoparticles for near infrared light-induced drug release. *J. Mater. Chem. B* **2018**, *6*, 7737-7749.
- ⁶ Phua, S. Z. F.; Xue, C.; Lim, W. Q.; Yang, G.; Chen, H.; Zhang, Y.; Wijaya, C. F.; Luo, Z.; Zhao, Y. Light-responsive prodrug-based supramolecular nanosystems for site-specific combination therapy of cancer. *Chem. Mater.* **2019**, *31*, 3349-3358.
- ⁷ Dariva, C. G.; Coelho, J. F. J.; Serra, A. C. Near infrared light-triggered nanoparticles using singlet oxygen photocleavage for drug delivery systems. *J. Control. Release* **2019**, *294*, 337-354.
- ⁸ Houk, J.; Whitesides, G. M. Structure – reactivity relations for thiol – disulfide interchange. *J. Am. Chem. Soc.* **1987**, *109*, 6825-6836.
- ⁹ Dmitrenko, O.; Thorpe, C.; Bach, R. D. Mechanism of S_N2 disulfide bond cleavage by phosphorus nucleophiles. Implication for biochemical disulfide reducing agents. *J. Org. Chem.* **2007**, *72*, 8298-8307.
- ¹⁰ Seidi, F.; Jenjob, R.; Crespy, D. Designing smart polymers conjugates for controlled release of payloads. *Chem. Rev.* **2018**, *118*, 3965-4036.
- ¹¹ Zhang, S.; Qi, C.; Wang, C. Decomposition of 2-mercaptoethyl *o*-ester: S_N2 displacement or acyl transfer? A theoretical study. *Chin. J. Chem.* **2014**, *32*, 335-342.
- ¹² Pohlit, H.; Leibig, D.; Frey, H. Poly(ethylene glycol) dimethacrylates with cleavable ketal sites: Precursors for cleavable PEG-hydrogels. *Macromol. Biosci.* **2017**, *17*, 1600532.
- ¹³ Miller, K. A.; Morado, E. G.; Samanta, S. R.; Walker, B. A.; Nelson, A. Z.; Sen, S.; Tran, D. T.; Whitaker, D. J.; Ewoldt, R. H.; Braun, P. V.; Zimmerman, S. C. Acid-triggered, acid-generating, and self-amplifying degradable polymers. *J. Am. Chem. Soc.* **2019**, *141*, 2838-2842.
- ¹⁴ Cordes, E. H.; Bull, H. G. Mechanism and catalysis for hydrolysis of acetals, ketals, and ortho esters. *Chem. Rev.* **1974**, *74*, 581-603.
- ¹⁵ Satchell, D. P. N.; Satchell, R. S. Mechanisms of hydrolysis of thioacetals. *Chem. Soc. Rev.* **1990**, *19*, 55-81.
- ¹⁶ Liu, B.; Thayumanavan, S. Substituent effects on the pH sensitivity of acetals and ketals and their correlation with encapsulation stability in polymeric nanogels. *J. Am. Chem. Soc.* **2017**, *139*, 2306-2317.
- ¹⁷ Chelucci, G. A facile synthesis of 3-substituted glutaraldehyde monoacetal from nitriles. *Synthesis* **1991**, *1991*, 474-476.
- ¹⁸ Pramanik, P.; Halder, D.; Jana, S. S.; Ghosh, S. pH- triggered sustained drug delivery from polymer micelle having the β-thiopropionate linkage. *Macromol. Rapid Commun.* **2016**, *37*, 1499-1506.

- ¹⁹ Dan, K.; Ghosh, S. One-Pot Synthesis of an Acid-Labile Amphiphilic Triblock Copolymer and its pH-Responsive Vesicular Assembly. *Angew. Chem. Int. Ed.* **2013**, *52*, 7300-7305.
- ²⁰ Pramanik, P.; Halder, D.; Jana, S. S.; Ghosh, S. pH-Triggered Sustained Drug Delivery from a Polymer Micelle having the β -Thiopropionate Linkage. *Macromol. Rapid Commun.* **2016**, *37*, 1499-506.
- ²¹ Wu, W.-X. Lipase-catalyzed synthesis of aliphatic poly(β -thioether ester) with various methylene group contents: thermal properties, crystallization and degradation. *Polym. Int.* **2019**, *68*, 1848-1855.
- ²² Lingier, S.; Espeel, P.; Suarez, S. S.; Türünç, O.; De Wildeman, S.; Du Prez, F. E. Renewable thermoplastic polyurethanes containing rigid spiroacetal moieties. *Eur. Polym. J.* **2015**, *70*, 232-239.
- ²³ Wróblewska, A. A.; Lingier, S.; Noordijk, J.; Du Prez, F. E.; De Wildeman, S. M. A.; Bernaerts, K. V. Polyamides based on a partially bio-based spirodiamine. *Eur. Polym. J.* **2017**, *96*, 221-231.
- ²⁴ Herbinski, A.; Métaay, E.; Da Silva, E.; Illous, E.; Aubry, J.-M.; Lemaire, M. An eco-compatible pathway to new hydrotropes from tetraols. *Green Chem.* **2018**, *20*, 1250-1261.
- ²⁵ Burghardt, T. E. Developments in the deprotection of thioacetals. *J. Sulphur Chem.* **2005**, *26*, 411-427.
- ²⁶ Langille, N.; Dakin, L. A.; Panek, J. S. A mild, chemoselective protocol for the removal of thioketals and thioacetals mediated by Dess-Martin periodinane. *Org. Lett.* **2003**, *5*, 575-578.
- ²⁷ Shaterian, H. R.; Hadadzadeh, H. Efficient chemoselective mild deprotection of S,S- and S,O-acetals and ketals with electrophilic halogens. *Phosphorus Sulfur Silicon Relat. Elem.* **2006**, *181*, 1059-1071.
- ²⁸ Das, S.; Borah, R.; Devi, R. R.; Thakur, A. J. Molecular Iodine in Protection and Deprotection Chemistry. *Synlett.* **2008**, *18*, 2741-2762.
- ²⁹ Chattopahyaya, J. B.; Rao, A. V. R. A novel oxidative desulphurisation of s-trithianes and thioacetals with iodine in dimethylsulphoxide. *Tetrahedron Lett.* **1973**, *38*, 3735-3736.
- ³⁰ He, T.; Adams, D. J.; Butler, M. F.; Yeoh, C. T.; Cooper, A. I.; Rannard, S. P. Direct synthesis of anisotropic polymer nanoparticles. *Angew. Chem. Int. Ed.* **2007**, *46*, 9243-9247.
- ³¹ Krumb, M.; Kammer, L. M.; Forster, R.; Grundke, C.; Opatz, T. Visible-Light-Induced Cleavage of C-S Bonds in Thioacetals and Thioketals with Iodine as a Photocatalyst. *ChemPhotoChem* **2020**, *4*, 101-104.
- ³² Lin, G. Q.; Yi, W. J.; Liu, Q.; Yang, X. J.; Zhao, Z. G. Aromatic Thioacetal-Bridged ROS-Responsive Nanoparticles as Novel Gene Delivery Vehicles. *Molecules.* **2018**, *23*, 2061.
- ³³ Wang, C.; Huang, B.; Yang, G.; Ouyang, Y.; Tian, J.; Zhang, W. NIR-Triggered Multifunctional and Degradable Nanoplatform Based on an ROS-Sensitive Block Copolymer for Imaging-Guided Chemo-Phototherapy. *Biomacromolecules* **2019**, *20*, 4218-4229.
- ³⁴ McHale, W. A.; Kutateladze, A. G. An Efficient Photo-SET-Induced Cleavage of Dithiane-Carbonyl Adducts and Its Relevance to the Development of Photoremovable Protecting Groups for Ketones and Aldehydes. *J. Org. Chem.* **1998**, *63*, 9924-9931.
- ³⁵ Oksdath-Mansilla, G.; Hajj, V.; Andrada, D. M.; Argüello, J. E.; Bonin, J.; Robert, M.; Peñeñory, A. B. Photoremoval of protecting groups: mechanistic aspects of 1,3-dithiane conversion to a carbonyl group. *J. Org. Chem.* **2015**, *80*, 2733-2739.
- ³⁶ Kouokam, J. C.; Zapp, J.; Becker, H. Oxygen-containing sulfur-rich compounds from the bark of the tropical garlic tree *Scorodophloeus zenkeri* Harms. *Phytochemistry* **2002**, *60*, 403-407.
- ³⁷ Liu, B.; Thayumanavan, S. Mechanistic investigation on oxidative degradation of ROS-responsive thioacetal/thioketal moieties and their implications. *Cell. Rep.* **2020**, *1*, 100271.

-
- ³⁸ Lacombe, S.; Cardy, H.; Simon, M.; Khoukh, A.; Soumillion, J. Ph.; Ayadim, M. Oxidation of sulfides and disulfides under electron transfer or singlet oxygen photosensitization using soluble or grafted sensitizers. *Photochem. Photobiol. Sci.* **2002**, *1*, 347-354.
- ³⁹ Kamata, M.; Sato, M.; Hasegawa, E. Photosensitized oxygenation reactions of 1,3-dithianes through cooperative single electron transfer pathway and singlet oxygen pathway. *Tetrahedron Lett.* **1992**, *33*, 5085-5088.
- ⁴⁰ DeRosa, M. C.; Crutchley, R. J. Photosensitized singlet oxygen and its applications. *Coord. Chem. Rev.* **2002**, *233-234*, 351-371.
- ⁴¹ Habibi, M. H.; Tangestaninejad, S.; Mohammadpoor-Baltork, I.; Montazerzohori, M. Photochemical oxidative deprotection of 1,3-dithianes to carbonyl compounds with hydrogen peroxide. *Phosphorus Sulfur Silicon Relat. Elem.* **2004**, *179*, 597-600.
- ⁴² Delehanty, J. B.; Das, S.; Goldberg, E.; Sangtani, A.; Knight, D. A. Synthesis of a Reactive Oxygen Species-Responsive Doxorubicin Derivative. *Molecules* **2018**, *23*, 1809.

UNIVERSITAT ROVIRA I VIRGILI
STIMULI-RESPONSIVE CALIX[4]PYRROLE AND CALIX[4]ARENE BASED RECEPTORS: FROM UNIMOLECULAR
TO DIMERIC STRUCTURES

Pedro Miguel Mendonça Ferreira

Chapter 6

Experimental part

UNIVERSITAT ROVIRA I VIRGILI
STIMULI-RESPONSIVE CALIX[4]PYRROLE AND CALIX[4]ARENE BASED RECEPTORS: FROM UNIMOLECULAR
TO DIMERIC STRUCTURES

Pedro Miguel Mendonça Ferreira

6 Experimental part

6.1 Materials

The following chemicals were purchased from Sigma-Aldrich and used as received unless specified: Acetaldehyde (99.5%), allyl alcohol (99%), p-anisaldehyde (98%), Barium oxide (97%), Benzyl alcohol, 2,2'-bipyridine ($\geq 99\%$), 2-bromo-2-methylpropionyl bromide (98%), γ -butyrolactone ($\geq 98\%$), calcium hydride ($\geq 90\%$, powder), copper (II) chloride (99.999%), δ -decalactone ($\geq 98\%$), 1,6-dibromohexane (96%), dibromomethane (99%), 2,2-dimethoxy-2-phenylacetophenone (DMPA) (99%), 3,9-divinyl-2,4,8,10-tetraoxaspiro[5.5]undecane (98%), ethyl 2-bromo-2-methylpropionate (98%), ethyl formate ($\geq 97\%$), hydrogen peroxide (50%), imidazole ($\geq 98\%$), lithium bromide (99%), 2-mercaptoethanol (99%), methyl methacrylate (99% stabilized with MEHQ), nickel (II) chloride hexahydrate (98%), 1,8-octanediol (98%), paraformaldehyde (95%), potassium trifluoroacetate (98%), sodium hydride (60% in mineral oil), tetrabutylammonium hydrogensulfate (TBAH) (97%), *meso*-tetraphenylporphyrin (TPP) (99%), trans-2-[3-(4-tert-Butylphenyl)-2-methyl-2-propenylidene]malononitrile (DCTB) (99%), tri-*n*-butylphosphine (97%), 1,5,7-triazabicyclo[4.4.0]dec-5-ene (TBD) (98%), trichlorofluoromethane (99.5%), triethylamine (97%), trifluoroacetic acid (99%), trifluoroacetic anhydride (99%) were purchased from Sigma-Aldrich. 2-hydroxyethyl disulfide was supplied by from Chevron Phillips Co. Phosphomolybdic acid (99%) was purchased from Panreac and used as received. Benzene dimethanol was purchased from Acros Organics and used as received.

Anhydrous magnesium sulfate, basic aluminum oxide, diphosphorous pentoxide, calcium chloride, potassium carbonate, potassium hydroxide, sodium hydrogen-carbonate, and sodium hydroxide were purchased from Scharlab and used as received.

Chloroform-d (CDCl_3), dimethylformamide-d7 (DMF-d7), dimethylsulfoxide-d6 (DMSO-d6) and tetramethylsilane (TMS) (99%) were purchased from Eurisotop and used as received.

Acetonitrile (HPLC grade), dichloromethane (DCM) (synthesis grade), diethyl ether (synthesis grade), dimethylformamide (DMF) (HPLC grade), ethanol (synthesis grade), ethyl acetate (synthesis grade), hexane (synthesis grade, mixture of isomers), methanol (MeOH) (synthesis grade), tetrahydrofuran (THF) (synthesis and GPC grade) and toluene (synthesis grade) were purchased from Scharlab.

Anhydrous diethyl ether and tetrahydrofuran were dried over sodium-benzophenone and used freshly distilled.

Dichloromethane, ethyl formate, γ -butyrolactone and triethylamine were distilled over CaH_2 prior use. Anhydrous ethanol was obtained by refluxing over Mg/I_2 and used freshly distilled. Methyl methacrylate was passed through basic aluminum oxide prior to use.

1,8-Octanediol was distilled under vacuum over calcium hydride. 2-Hydroxyethyl disulfide was distilled under vacuum. 1,8-Octanediol and initiators I_1 to I_5 were dried under vacuum at 50 °C for 24 hours prior to use. TBD was sublimated under vacuum at 70 °C and dried under vacuum 48 hours prior to use. δ -Decalactone was refluxed under vacuum over CaH_2 for 12 hours and collected prior to use.

TLC was carried out on DC-Fertigfolien ALUGRAM Xtra SIL G/UV 254 (Macherey-Nagel) using phosphomolybdic acid as dyeing agent (4.8 g in 100 mL absolute ethanol).

6.2 Instruments and methods

6.2.1 Nuclear Magnetic resonance (NMR) spectroscopy

^1H -NMR (400 MHz), ^{19}F (376.8 MHz) and ^{13}C -NMR (100.6 MHz) were recorded using a Varian Gemini 400 spectrometer. Spectra were recorded using 10-15 mg (^1H -NMR) or 30-40 mg (^{13}C -NMR) of sample at 25 °C in CDCl_3 (using TMS as internal standard for ^1H -NMR or CFCl_3 for ^{19}F -NMR) or DMSO- d_6 (at 25 or 80 °C) and DMF- d_7 (using the residual solvent peak as internal standard). In ^{13}C -NMR the central peak of the deuterated solvent was taken as reference and the chemical shifts given in ppm. Two-dimensional ^1H - ^1H homonuclear and ^{13}C - ^1H heteronuclear shift correlation spectra were recorded with the COSY, HSQC and HMBC pulse sequences.

^{13}C -NMR spectra of polymer samples were recorded using 80-100 mg of sample in CDCl_3 , DMF- d_7 or DMSO- d_6 with an acquisition time (at) of 0.5 s, decoupling mode (dm) 'nny', a delay time (d1) of 0.5 s and a number of scans (nt) of 30,000.

6.2.2 Size exclusion chromatography (SEC)

The number-average molecular weight (M_n) and molecular weight distribution (\mathcal{D}) were measured by SEC. Polyesters and polymethacrylate chromatograms were performed with an Agilent 1200 series system equipped with a precolumn; PLgel 5 μm Guard column and a three-serial column system; PLgel Mixed-E (3 μm), PLgel Mixed-D (5 μm) and PLgel Mixed-A (20 μm) and with an Agilent 1290 Infinity II series refractive index detector. Chromatograms were carried out in THF (HPLC grade, stabilized with BHT) with a flow rate of 1 mL/min at 35 °C. Samples were prepared at a concentration of 0.1% (w/w), filtered through 0.22 μm Teflon syringe filter and 100 μL of the polymer solution was injected using an Agilent 1260 autosampler. M_n and \mathcal{D} were determined using monodisperse polystyrene standards (Agilent EasiVial PS-M) or poly(methyl methacrylate) standards (Polymer Standards Service ReadyCal Kit) calibration curve and toluene was used as flow rate marker.

Poly(MBL) homopolymers and block copolymers were analyzed using an Agilent 1200 series system equipped with a precolumn; PLgel 5 μm Guard column and a two-serial column system; 2x PLgel Mixed-D (5 μm) and with an Agilent 1100 series refractive index detector. Chromatograms were carried out in DMF (HPLC grade) containing 0.05% (w/w) of LiBr with a flow rate of 1 mL/min at 50 °C. Samples were prepared at a concentration of 0.1% (w/w), filtered through 0.22 μm Teflon syringe filter and 20 μL of the polymer solution was injected using a manual sample injector Rheodyne Model 7125. M_n and \bar{M}_w were determined using monodisperse poly(methyl methacrylate) standards (Polymer Standards Service ReadyCal Kit) calibration curve and toluene was used as flow rate marker.

6.2.3 Matrix-Assisted Laser Desorption/Ionization Time-Of-Flight (MALDI-TOF)

MALDI-TOF analysis was performed on a Voyager DE (Applied Biosystems) instrument with a 337 nm nitrogen laser (3 ns pulse width). For all the polymers the accelerating voltage was 25 kV. For linear mode, the grid voltage was 89%, the laser intensity was 2068 (arb. unit) and a delay time of 375 ns in positive ionization mode was used. For reflector mode, the grid voltage was 70%, the laser intensity was 1997 (arb. unit) and a delay time of 150 ns in positive ionization mode was used. The samples were prepared using *trans*-2-[3-(4-*tert*-butylphenyl)-2-methyl-2-propenyldiene]malononitrile (DCTB) as matrix. THF solutions of DCTB (40 mg/mL), potassium trifluoroacetate (KTFA) as cationization agent (15 mg/mL) and polymer (10 mg/mL) were prepared separately. The solutions for the MALDI-TOF analysis were obtained by mixing the matrix, salt and polymer solutions in a 4:1:1 volumetric ratio. Then, 1 μL of the mixture was deposited onto the sample plate and dried onto air at room temperature before the analysis.

6.2.4 Differential Scanning Calorimetry (DSC)

DSC measurements were carried out with Mettler DSC3+ thermal analyzer with N_2 as the purge gas (50 mL/min) using heating rates of 10 °C/min and cooling rates of 30 °C/min in a -80 to 220 °C temperature range. Calibration was performed using indium

standards for the heat flow calibration and zinc standards for temperature calibration. Samples of 10 mg of polymer were sealed in aluminum pans and the second heating was used for the determination of the glass transition temperature (T_g).

6.2.5 Thermogravimetric Analysis (TGA)

Thermal stability studies were carried out on a Mettler TGA/SDTA851e/LF/1100 with N_2 as the purge gas at a scanning rate of 10 °C/min in a 30 to 600 °C temperature range.

6.2.6 Specimen preparation

Polymer specimens, for mechanical test, were prepared using stainless steel molds (60 x 30 x 10 mm), with an inner cavity of (20 x 6 x 1.25 mm). The mold's cover has a counter mold with the following dimensions (20 x 6 x 1 mm) (Figure 6.1). 250 – 300 mg of the polymer was introduced into the mold and was subjected to 5 t of pressure at 100 °C for 30 minutes in a press model Specac. The specimen obtained was a colorless and transparent elastic solid (Figure 6.2).



Figure 6.1 Stainless steel mold used for the specimen preparation for DMTA analysis.

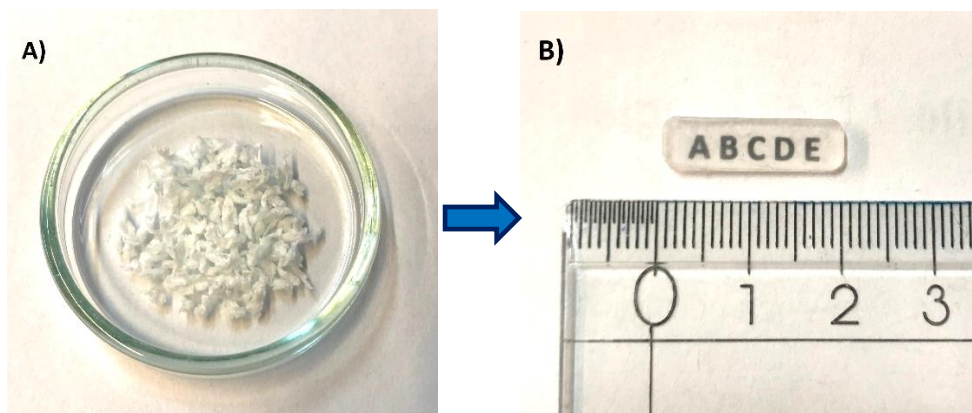


Figure 6.2 Block copolymer before (A) and after (B) specimen preparation

6.2.7 Dynamic Mechanical Analysis (DMA)

The thermomechanical properties were evaluated using DMA Q800 (TA Instrument) equipped with a three-point bending clamp. Rectangular samples of 1.25 x 5.5 x 20 mm were analyzed from -80 to 220 °C, at 1 Hz, 0.07 % (10 μ m of amplitude) strain and with a heating rate 2 °C/min.

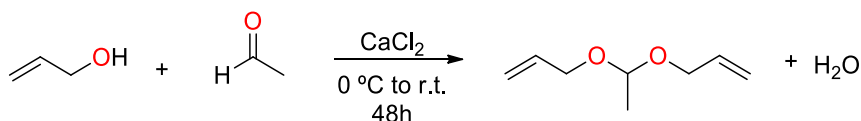
6.2.8 Electrospray ionization-Mass Spectrometry (ESI-MS)

ESI-MS measurements were carried out using an Agilent 1200 liquid chromatography coupled to 6210 Time of Flight (TOF) mass spectrometer from Agilent Technologies (Waldbronn, Germany) with an ESI interface.

6.3 Synthesis of stimuli-cleavable initiators

6.3.1 Synthesis of 1,1-bis-[3-((2-hydroxyethyl)thio)propyloxy]ethane (I₂)

6.3.1.1 Synthesis of acetaldehyde diallyl acetal



Scheme 6.1 Synthesis of acetaldehyde diallyl acetal.

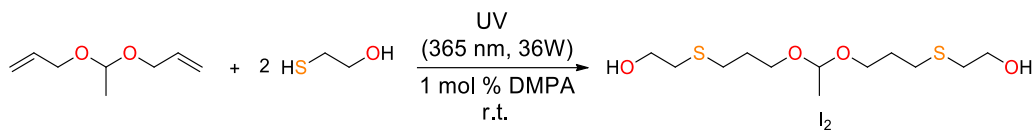
Based on a reported procedure,¹ in a 500 mL round bottom flask 20 g (0.18 mol) of anhydrous CaCl₂ were dissolved by shaking in 155 mL (132.0 g, 2.27 mol) of allyl alcohol. The solution was cooled to 0°C in a crushed ice bath and 64 mL (50.0 g, 1.13 mol) of freshly distilled acetaldehyde (precooled to 0°C) were added. The flask was stopped, and shaken vigorously during 10 min, whereas cool, and occasionally at room temperature during 48h. The clear upper layer was decanted and washed with three portions of cool water (3x40 mL) and dried over anhydrous magnesium sulphate. The product was purified by fractionated distillation collecting the fraction at 147-149 °C as a colourless liquid (82.3g, 52%) which was essentially pure by ¹H-NMR (spectra are shown in annex 8.1).

ESI-MS, exact mass m/z 142.0994 [M] (Theoretical mass: 142.0994).

¹H-NMR (CDCl₃, 400 MHz, TMS, δ ppm): 5.97-5.87 (m, 2H, CH₂=CH-), 5.31-5.26 (dq, ³J_{trans} = 17.2 Hz, ⁴J = 1.6 Hz, 2H_{cis}, CH₂=CH-), 5.18-5.14 (dq, ³J_{cis} = 10.4 Hz, ⁴J = 1.6 Hz, 2H_{trans} CH₂=CH-), 4.80 (q, ³J = 5.2 Hz, 1H, O-CH-O), 4.14-3.98 (m, 4H, O-CH₂-), 1.34 (d, 3H, CH₃).

¹³C-NMR (CDCl₃, 100.6 MHz, TMS δ ppm): 134.8 (-CH=CH₂), 116.7 (-CH=CH₂), 98.8 (O-CH-O), 66.0 (-OCH₂), 19.8 (CH₃).

6.3.1.2 Synthesis of 1,1-bis-[3-((2-hydroxyethyl)thio)propyloxy]ethane (I_2)



Scheme 6.2 Synthesis of 1,1-bis-[3-((2-hydroxyethyl)thio)propyloxy]ethane (I_2).

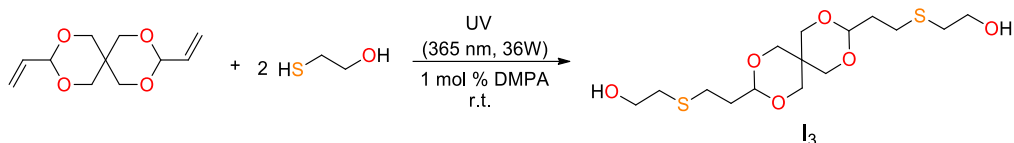
Based on a general reported procedure,² in a 100 mL round flask with a Teflon coated stir bar, 0.76 g (3.0 mmol, 1 mol% for each double bond) of 2,2-dimethoxy-2-phenylacetophenone (DMPA) were dissolved in 21.0 g (150 mmol) of acetaldehyde diallylacetal and desoxygenated by bubbling argon through. Next, 23.4 g (300 mmol) of 2-mercaptoethanol were added and the mixture stirred and irradiated with UV light (365 nm, 36 w). After 60 min, a sample ¹H-NMR spectrum indicates that the reaction was complete. Thus, direct vacuum was applied for 2 h to remove traces of unreacted 2-mercaptoethanol. The product was purified through flash column chromatography with Hexane:AcOEt (1:1) (1% triethylamine) yielding 15.4 g (35%) of a colourless oil (spectra are shown in annex 8.2).

ESI-MS, exact mass m/z 298.1268 [M] (Theoretical mass: 298.1273).

¹H-NMR (CDCl₃, 400 MHz, TMS, δ ppm): 4.67 (q, ³J = 5.6 Hz, 1H, O-CH-O), 3.73 (t, ³J = 6.0 Hz, 4H, SCH₂-CH₂OH), 3.71-3.48 (m, 4H, O-CH-O-CH₂-), 2.73 (t, ³J = 6.0 Hz, 4H, SCH₂-CH₂O-), 2.64 (t, ³J = 7.2 Hz, 4H, CH₂SCH₂-CH₂O-), 1.86 (quint, ³J = 6.8 Hz, 4 H, O-CH-O-CH₂-CH₂), 1.30 (d, ³J = 5.2 Hz, 3H, (O)₂-CHCH₃).

¹³C-NMR (CDCl₃, 100.6 MHz, TMS δ ppm): 100.0 (O-CH-O), 63.6 (O-CH-O-CH₂-), 60.4 (SCH₂-CH₂OH), 35.2 (SCH₂-CH₂OH), 29.8 (O-CH-O-CH₂CH₂), 28.5 (O-CH-O-CH₂CH₂CH₂), 19.7 ((O)₂-CHCH₃).

6.3.2 Synthesis of 3,9-bis-[2-(ethylthio)ethanol]- 2,4,8,10-tetraoxaspiro-[5.5]undecane (**I₃**)



Scheme 6.3 Synthesis of 3,9-bis-[2-(ethylthio)ethanol]- 2,4,8,10-tetraoxaspiro-[5.5]undecane (**I₃**).

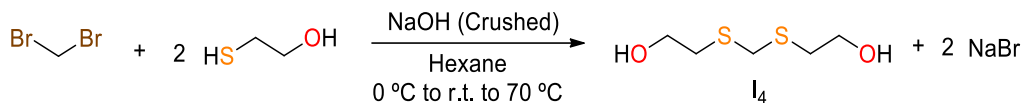
Based on reported procedures [3,4] in a 100 mL round flask with a Teflon coated stir bar, 0.11 g (0.44 mmol, 1 mol% for each double bond) of DMPA, 4.67 g (22 mmol) of 3,9-divinyl-2,4,8,10-tetraoxaspiro[5.5]undecane were melted at 60 °C and deoxygenated by bubbling argon through. Next, 3.10 mL (3.44 g, 45 mmol) of 2-mercaptoethanol were added and the mixture cooled on a water bath. The mixture was stirred and irradiated with UV light (365 nm, 36 w). After 30 min, a transparent mass is formed and a sample ¹H NMR spectrum indicates that the reaction was complete. Thus, direct vacuum was applied for 2 h to remove traces of unreacted 2-mercaptoethanol and the product cooled on a freezer to solidify. The resulting solid was purified by recrystallization in diethyl ether/hexanes (1:1) at – 10 °C, yielding 5.9 g (72 %) of white needles mp. 48-50 °C (spectra are shown in annex 8.3).

ESI-MS, exact mass m/z 368.1329 [M] (Theoretical mass: 368.1327).

¹H-NMR (CDCl₃, 400 MHz, TMS, δ ppm): 4.57 (t, ³J = 4.8 Hz, 2H, O-CH-O), 4.51 (dd, ³J = 11.2 Hz, ⁴J = 2.0 Hz, 2H_{eq.}, -OCH₂C-), 3.71 (q, ³J = 5.9 Hz, 4H, SCH₂-CH₂OH), 3.56 (dd, ³J = 11.6 Hz, ⁴J = 2.4 Hz, 2H_{eq.}, -OCH₂C-), 3.53 (d, ³J = 12.0 Hz, 2H_{ax.}, -OCH₂C-), 3.34 (d, ³J = 11.6 Hz, 2H_{ax.}, -OCH₂C-), 2.71 (t, ³J = 5.8 Hz, 4H, SCH₂-CH₂OH), 2.61 (t, ³J = 7.6 Hz, 4H, CH₂SCH₂-CH₂O-), 2.24 (t, ³J = 6.0 Hz, 2H, -OH), 1.92-1.87 (m, 4H, (O)₂CHCH₂-).

¹³C-NMR (CDCl₃, 100.6 MHz, TMS δ ppm): 101.1 (O-CH-O), 70.5 (-OCH₂C-), 70.0 (OCH₂C), 60.2 (SCH₂-CH₂OH), 35.3 (SCH₂-CH₂O-), 34.7 ((O)₂CHCH₂-), 32.4 (-OCH₂C-), 25.7 (CH₂SCH₂-CH₂OH).

6.3.3 Synthesis of bis-((2-hydroxyethyl)thio)methane (**I₄**)



Scheme 6.4 Synthesis of bis-((2-hydroxyethyl)thio)methane (**I₄**).

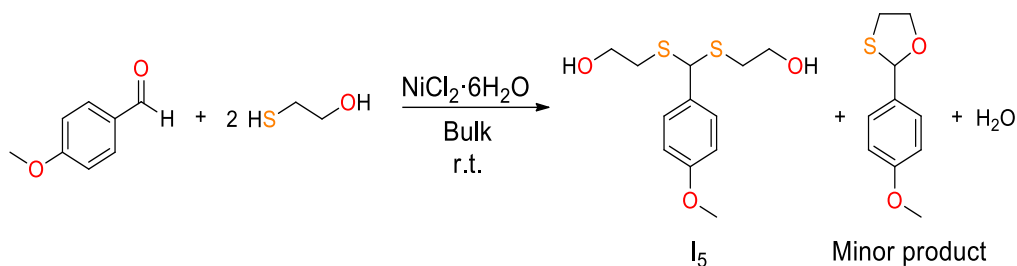
Following a reported procedure,⁵ in a 250 mL, three-necked, round-bottom flask equipped with a magnetic stir bar, a condenser and a calcium chloride guard tube, 21.5 mL (306 mmol) of 2-mercaptoethanol, 20 mL of hexane and 12.6 g (314 mmol) of crushed NaOH were introduced. The flask was cooled to 0 °C in an ice bath and 8,5 ml (121 mmol) of dibromomethane were added dropwise using an addition funnel at a rate that kept the temperature below 60 °C. After the addition, the reaction was brought to room temperature and then stirred at 70 °C for 2 hours. Progress of the reaction was monitored by ¹H-NMR and once completed, the resulting solid mass was extracted several times with dichloromethane, filtered and the solvent removed under vacuum. The resulting crude product was distilled under reduced pressure over BaO (150-152 °C, 0.3 mbar; lit. 115 °C, 0.6 mbar)⁵ (mp 16-17 °C (DSC) (lit. 18 °C))⁶ yielding 14.1 g (69%) of a colourless liquid (spectra are shown in annex 8.4).

ESI-MS, exact mass m/z 168.0281 [M] (Theoretical mass: 168.0279).

¹H-NMR (CDCl₃, 400 MHz, TMS, δ ppm): 3.81 (t, ³J = 5.8 Hz, 4H, SCH₂-CH₂OH), 3.74 (s, 2H, , S-CH₂-S), 2.88 (t, ³J = 5.8 Hz, 4H, SCH₂-CH₂O-), 2.30 (s, 2H, -OH).

¹³C-NMR (CDCl₃, 100.6 MHz, TMS δ ppm): 60.9 (SCH₂-CH₂OH), 35.6 (S-CH₂-S), 34.3 (SCH₂-CH₂OH).

6.3.4 Synthesis of (4-methoxyphenyl)-bis-[(2-hydroxyethyl)thio]methane (I₅)



Scheme 6.5 Synthesis of (4-methoxyphenyl)-bis-[(2-hydroxyethyl)thio]methane (I₅).

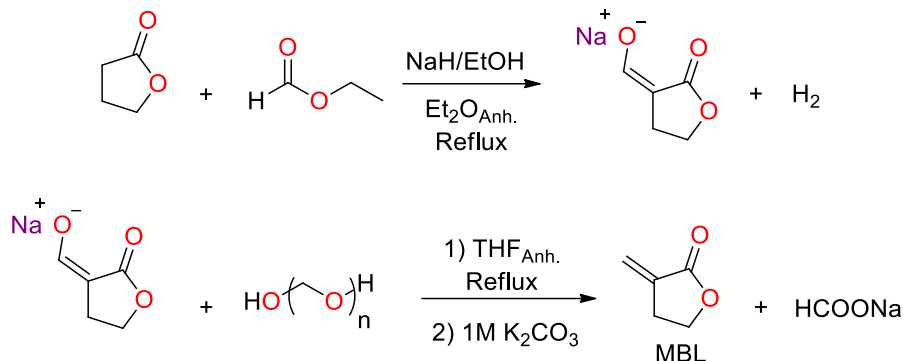
Following a reported procedure,⁷ in a 50 mL round-bottom flask, equipped with a magnetic stir bar, 10 ml (82 mmol) of 4-methoxybenzaldehyde and 15 mL (214 mmol) of 2-mercaptoethanol were added. Once homogenized, 1 g (4.2 mmol, 5 mol %) of nickel (II) chloride hexahydrate was added and the progress of the reaction monitored by TLC using acetone:toluene (1:9) as eluent. After 30 minutes, the reaction was complete. 500 mL of DCM were added, and the insoluble catalyst removed by filtration. The DCM was washed with brine and water and the organic phase was dried with anhydrous magnesium sulphate. After removing the solvent under vacuum, crude product was recrystallized in hot toluene (3.0 L) yielding 16.5 g of white crystals (73%) with mp. 85-86 °C (lit. 83 °C)⁷ (spectra are shown in annex 8.5).

ESI-MS, exact mass m/z 274.0696 [M] (Theoretical mass: 274.0697).

¹H-NMR (CDCl₃, 400 MHz, TMS, δ ppm): 7.38 (d, ³J = 8.4 Hz, 2H, CH₂-C-CH, Ar.), 6.87 (d, ³J = 8.8 Hz, 2H, CH₂-C-OCH₃, Ar.), 5.06 (s, 1H, S-CH-S), 3.80 (s, 3H, -OCH₃), 3.73 (t, ³J = 5.6 Hz, 4H, SCH₂-CH₂OH), 2.85-2.67 (m, 4H, SCH₂-CH₂OH), 2.38 (br. s, -OH).

¹³C-NMR (CDCl₃, 100.6 MHz, TMS δ ppm): 159.5 (C-OCH₃, Ar.), 132.0 (C-CH, Ar.), 129.0 (CH₂-C-CH, Ar.), 114.2 (CH₂-C-OCH₃, Ar.), 61.4 (SCH₂-CH₂OH), 55.4 (OCH₃), 52.6 (S-CH-S), 35.7 (SCH₂-CH₂OH).

6.4 Synthesis of α -methylene- γ -butyrolactone (MBL)



Scheme 6.6 Synthesis of α -methylene- γ -butyrolactone (MBL) from γ -butyrolactone.

This monomer was synthesized from γ -butyrolactone based on the procedures described in the literature.^{8, 9, 10, 11, 12} First, under Ar atmosphere, 17,6 g (439.0 mmol) of sodium hydride (60% in mineral oil) was placed in a 1 L two necked round-bottom Schleck flask equipped with a Teflon coated magnetic stir bar. After rinsing three times with anhydrous hexanes, sodium hydride was suspended in 350 mL of anhydrous diethyl ether. Subsequently, 2.8 mL (48.0 mmol) of anhydrous ethanol was added, and then a mixture of 30.0 ml (394 mmol) of anhydrous γ -butyrolactone and 42.0 ml (507 mmol) of anhydrous ethyl formate was added dropwise through an addition funnel. The resulting mixture was heated up to reflux for 2 hours, under argon atmosphere. The resulting yellowish solid was filtered under argon and washed several times with anhydrous diethyl ether and finally dried under vacuum to give of α -hydroxymethylene- γ -butyrolactone sodium salt in almost quantitative yield (54.0 g) as a pale cream solid. In a second step, 55.9 g (1786 mmol) of paraformaldehyde and 600 mL of anhydrous tetrahydrofuran were introduced in a 1 L two-necked round-bottom flask equipped with a magnetic stir bar, a condenser and a calcium chloride guard tube. Next, the above α -hydroxymethylene- γ -butyrolactone sodium salt was added under argon flow and the mixture was brought to reflux for three hours. Once finished, the reaction mixture was cooled to 10 °C and filtered to remove the unreacted paraformaldehyde.

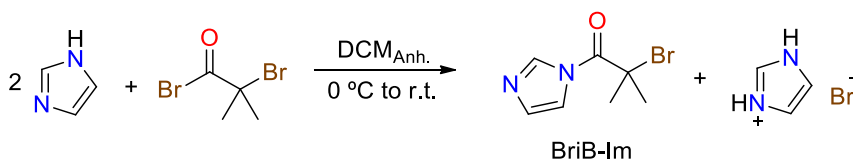
Then, 125 mL of 1 M potassium carbonate solution was added, followed by 400 mL of diethyl ether. The organic phase was dried over anhydrous magnesium sulphate and the solvent evaporated under vacuum. The crude product was purified by vacuum distillation obtaining 20.1 g (53% yield) of a clear colourless oil (spectra are shown in annex 8.6).

ESI-MS, exact mass m/z 98.0371 [M] (Theoretical mass: 98.0368).

$^1\text{H-NMR}$ (CDCl_3 , 400 MHz, TMS, δ ppm): 6.25 (t, $^4J = 2.8$ Hz, 1H, $\text{H}_{\text{C}=\text{C}}$), 5.67 (t, $^4J = 2.8$ Hz, 1H, $\text{H}_{\text{C}=\text{C}}$), 4.37 (t, $^3J = 7.6$ Hz, 2H, $-\text{CH}_2-\text{CH}_2-\text{C}=\text{CH}_2$), 2.99 (tt, $^3J = 7.6$ Hz, $^4J = 2.80$ Hz, 2H, $-\text{CH}_2-\text{CH}_2-\text{C}=\text{CH}_2$).

$^{13}\text{C-NMR}$ (CDCl_3 , 100.6 MHz, δ ppm): 169.7 ($-\text{O}-\text{C}=\text{O}-$), 132.6 ($\text{CH}_2-\text{CH}_2-\text{C}=\text{CH}_2$), 121.1 ($\text{CH}_2-\text{CH}_2-\text{C}=\text{CH}_2$), 64.3 ($\text{CH}_2-\text{CH}_2-\text{C}=\text{CH}_2$), 26.3 ($\text{CH}_2-\text{CH}_2-\text{C}=\text{CH}_2$).

6.5 Synthesis of N-(2-bromoisobutyryl)imidazole (BriB-Im)



Scheme 6.7 Synthesis of N-(2-bromoisobutyryl)imidazole (BriB-Im).

Following a reported procedure,¹³ in a 250 mL round-bottom Schleck flask, dried at 200 °C and cooled under argon, 4.5 ml (35.7 mmol) of α -bromoisobutyryl bromide and 30 mL of anhydrous DCM were introduced. The mixture was kept under stirring in an ice bath for a few minutes and then 4.9 g (72.2 mmol) of imidazole in 50 ml of anhydrous DCM was added dropwise. The mixture was let to reach room temperature for two hours and the formed salt removed by filtration and the solution concentrated under vacuum. The resulting oil was extracted twice with dry hexanes (2x75 mL) and the solution cooled to -18 °C. The obtained with crystals were collected by filtration and

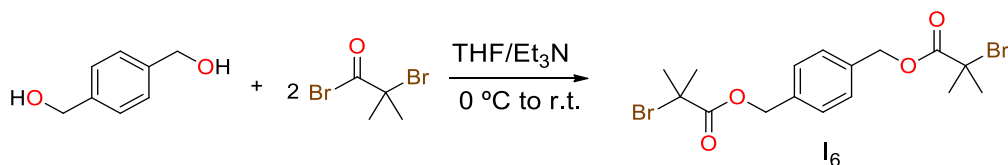
dried under argon to produce 5.6 g (72 %) of the pure product (mp. 43-44 °C; lit. 43-44 °C)¹³ (spectra are shown in annex 8.7).

ESI-MS, exact mass m/z 215.9889 [M] (Theoretical mass: 215.9898).

¹H-NMR (CDCl₃, 400 MHz, TMS, δ ppm): 8.52 (s, 1H, N=CH-N), 7.76 (t, ³J = 1.4 Hz, 1H, =CH-N-CO), 7.08 (m, 1H, =N-CH-), 2.11 (s, 6H, -CH₃).

¹³C-NMR (CDCl₃, 100.6 MHz, δ ppm): 168.1 (CO), 138.3 (CH, N=CH-N), 130.3 (=N-CH-), 118.4 (=CH-N-CO), 55.0 (C-Br), 31.9 (CH₃).

6.6 Synthesis of 1,4-phenylenebis(methylene)-bis(2-bromoisobutyrate) (I₆)



Scheme 6.8 Synthesis of 1,4-phenylenebis(methylene)-bis(2-bromoisobutyrate) (I₆).

Following a reported procedure.¹⁴ In a 250 ml round-bottom Schlenk flask, dried at 200 °C and cooled under argon, 3.0 g (21.7 mmol) of 1,4-benzenedimethanol were dissolved in 100 mL of anhydrous THF and, after cooling in an ice bath, 18.5 mL (132.7 mmol) of anhydrous Et₃N was added. Then 11.5 mL (93.0 mmol) of 2-bromoisobutyryl bromide was added dropwise during 30 min. with gentle stirring. Once added, the reaction mixture was brought to room temperature for 6 hours. The formed triethylammonium bromide was filtered off and the solvent evaporated under vacuum. The resulting oil was solved in dichloromethane and washed twice with sodium hydrogencarbonate solution and water. The organic phase was dried with anhydrous magnesium sulphate and the solvent eliminated under vacuum. The crude product was purified by crystallization in hexane at -20 °C after activated charcoal treatment. After filtration,

rinsing with cool hexane and drying under vacuum, 6.4 g (67%) of white crystals with m.p 62-64 °C (spectra are shown in annex 8.8).

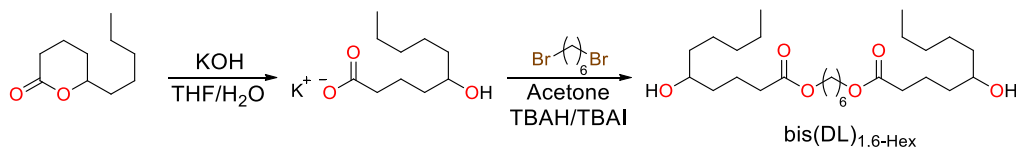
ESI-MS, exact mass m/z 472.9362 [M+K] (Theoretical mass: 433.9728).

$^1\text{H-NMR}$ (CDCl_3 , 400 MHz, TMS, δ ppm): 7.39 (s, 4H, Ar.), 5.21 (s, 4H, $-\text{CH}_2-$), 1.96 (s, 12H, $-\text{CH}_3$).

$^{13}\text{C-NMR}$ (CDCl_3 , 100.6 MHz, δ ppm): 171.5 ($-\text{CO}-$), 135.6 ($-\text{C}-$, Ar.), 128.1 ($-\text{CH}-$, Ar.), 67.2 ($-\text{CH}_2-$), 55.6 ($-\text{C-Br}$), 30.8 ($-\text{CH}_3$).

6.7 Synthesis of model compounds.

6.7.1 Synthesis of bis(DL)_{1,6}-Hex diol



Scheme 6.9 Synthesis of bis(DL)_{1,6}-Hex diol.

Following an adapted procedure described for nonalactone and benzyl bromide,¹⁵ in a 250 mL round flask 18.0 mL (17.9 g, 100 mmol) of δ -decalactone were dissolved in 50 mL of THF. Next, a cooled solution of 85% potassium hydroxide in 100 mL of water (6.6 g, 100 mmol) was added. The mixture raises its temperature, and two phases are observed. The mixture was heated under reflux for 2h until it became homogeneous. Finally, THF and water were completely removed on the rotary evaporator until a white syrup was obtained. In the next step, the crude salt was suspended in 150 mL of acetone and 7.90 mL (12.6 g, 50 mmol) of 1,6-dibromohexane, 0.2 g of tetrabutylammonium hydrogensulphate (TBAH) and 0.2 g of tetrabutylammonium iodide (TBAI) were added. The mixture was heated under reflux for 48 h and the resulting orange suspension concentrated under vacuum and extracted using 100 mL of water and 100 mL of diethyl ether. The organic phase was washed several times with

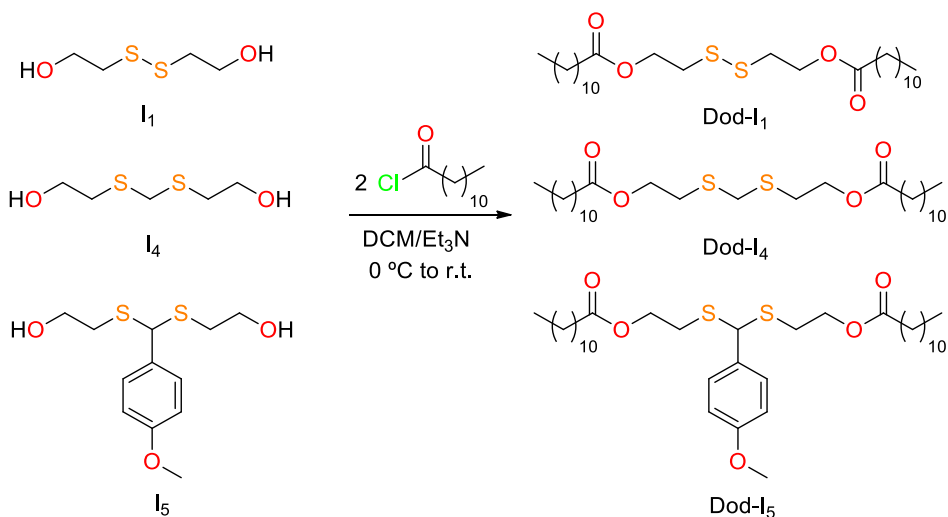
brine, dried with anhydrous magnesium sulphate and concentrated under vacuum to give a yellow liquid that solidifies on the refrigerator. The product was purified by recrystallization in 200 mL of a mixture of hexane/diethyl ether (2:1) and keeping on the freezer overnight. The solid product was collected by filtration, washed several times with cool pentane and dried under vacuum over anhydrous CaCl_2 to yield 16.5 g (72 %) of a fine white solid (spectra are shown in annex 8.9).

ESI-MS, exact mass m/z 458.3610 [M] (Theoretical mass: 458.3607).

$^1\text{H-NMR}$ (CDCl_3 , 400 MHz, TMS, δ ppm): 4.07 (t, $^3J = 6.6$ Hz, 4H, $-\text{CH}_2\text{OCO}$), 3.59 (m, 2H, $-\text{CH-OH}$), 2.34 (t, $^3J = 7.4$ Hz, CH_2COO), 1.89 (br. s, 2H, $-\text{OH}$), 1.68-1.27 (m, $-(\text{CH}_2)_n-$), 0.89 (t, $^3J = 7.0$ Hz, CH_2-CH_3).

$^{13}\text{C-NMR}$ (CDCl_3 , 100.6 MHz, TMS δ ppm): 173.9 (CH_2COO), 71.4 ($-\text{CH-OH}$), 64.3 ($-\text{CH}_2\text{OCO}$), 37.5 ($\text{CH}_3\text{CH}_2\text{CH}_2\text{CH}_2\text{CH}_2\text{CH-}$), 36.8 ($\text{OOC-CH}_2\text{CH}_2\text{CH}_2\text{CH-}$), 34.2 (CH_2COO), 31.9 ($\text{CH}_3\text{CH}_2\text{CH}_2\text{CH}_2\text{-CH}_2\text{CH-}$), 28.5 ($-\text{CH}_2\text{CH}_2\text{OCO}$), 25.6 ($\text{CH}_2\text{CH}_2\text{CH}_2\text{OCO}$), 25.3 ($\text{CH}_3\text{CH}_2\text{CH}_2\text{CH}_2\text{CH}_2\text{CH-}$), 22.6 ($\text{CH}_3\text{CH}_2\text{CH}_2\text{CH}_2\text{-CH}_2\text{CH-}$), 21.1 ($\text{OOC-CH}_2\text{CH}_2\text{CH}_2\text{CH-}$), 14.1 ($\text{CH}_3\text{CH}_2\text{CH}_2\text{CH}_2\text{CH}_2\text{-CH-}$).

6.7.2 Synthesis of model cleavable compounds Dod-I₁, Dod-I₄ and Dod-I₅



Scheme 6.10 Synthesis of disulfide and thioacetal stimuli cleavable model compounds.

In a 100 mL 2-necked round-bottom flask, 6 mmols of diol (0.93 g for I₁, 1.00 g for I₄ and 1.65 g for I₅) was dissolved in 50 mL of anhydrous DCM. The flask was cooled in an ice bath and 2.1 mL (15 mmols) of triethylamine were added. Then, 3.0 mL (13 mmols) of dodecanoyl chloride, solved in 10 mL of anhydrous DCM were added dropwise in a period of 30 min. Once added, the reaction mixture was brought to room temperature for 6 hours. The formed triethylammonium bromide was filtered off and the organic phase was washed with sodium hydrogencarbonate solution, brine and water. The organic phase was dried over anhydrous magnesium sulphate and the solvent evaporated under vacuum. The crude product was purified by crystallization in hexane at -20 °C. After filtration, rinsing with cool hexane and drying under vacuum, 2.57 g (82%) for Dod-I₁, 2.87 g (87%) for Dod-I₄ and 3.43 g (89%) for Dod-I₅ as white crystals with m.p 57-59 °C, 62-64 °C and 51-53 °C respectively.

Dod-I₁: ESI-MS, exact mass m/z 518.3474 [M] (Theoretical mass: 518.3464).

Dod-I₄: ESI-MS, exact mass m/z 532.3629 [M] (Theoretical mass: 532.3620).

Dod-I₅: ESI-MS, exact mass m/z 638.4049 [M] (Theoretical mass: 638.4039).

- Dod-I₁ (Annex 8.10):

¹H-NMR (CDCl₃, 400 MHz, TMS, δ ppm): 4.33 (t, ³J = 6.4 Hz, 4H, SCH₂-CH₂OCO), 2.92 (t, ³J = 6.4 Hz, 4H, SCH₂-CH₂OCO), 2.32 (t, ³J = 7.6 Hz, 4H, OOC-CH₂-), 1.61 (quint, ³J = 7.2 Hz, 4H, OOC-CH₂CH₂), 1.32-1.25 (br. s, 32 H, -CH₂- dodecanoyl), 0.88 (t, ³J = 6.4 Hz, 6H, CH₃)

¹³C-NMR (CDCl₃, 100.6 MHz, TMS δ ppm): 173.6 (CH₂COO), 62.0 (CH₂O-), 37.4 (SCH₂), 34.2 (OOC-CH₂), 31.9 (CH₂CH₂CH₃), 29.6 - 29.2 (CH₂ x 6), 24.9 (OOC-CH₂CH₂), 22.7 (CH₂CH₂CH₃), 14.1 (CH₂CH₂CH₃)

- Dod-I₄ (Annex 8.11):

¹H-NMR (CDCl₃, 400 MHz, TMS, δ ppm): 4.26 (t, ³J = 6.4 Hz, 4H, SCH₂-CH₂OCO), 3.75 (s, 2H, S-CH₂-S), 2.88 (t, ³J = 6.4 Hz, 4H, SCH₂-CH₂OCO), 2.32 (t, ³J = 7.6 Hz, 4H, OOC-CH₂-), 1.61 (quint, ³J = 7.2 Hz, 4H, OOC-CH₂CH₂), 1.32-1.25 (br. s, 32 H, -CH₂- dodecanoyl), 0.88 (t, ³J = 6.4 Hz, 6H, CH₃)

¹³C-NMR (CDCl₃, 100.6 MHz, TMS δ ppm): 173.7 (CH₂COO), 62.9 (CH₂O-), 35.8 (SCH₂S), 34.3 (OOC-CH₂), 32.0 (CH₂CH₂CH₃), 29.7 - 29.3 (CH₂ x 6), 29.2 (SCH₂), 25.0 (OOC-CH₂CH₂), 22.8 (CH₂CH₂CH₃), 14.2 (CH₂CH₂CH₃)

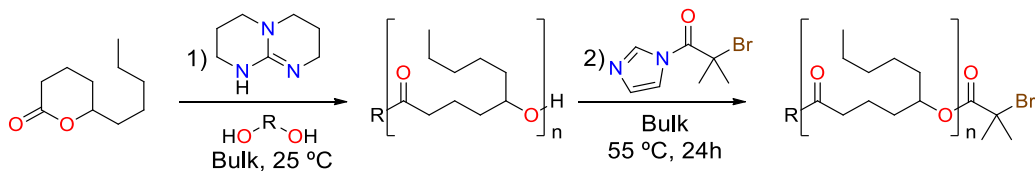
- Dod-I₅ (Annex 8.12):

¹H-NMR (CDCl₃, 400 MHz, TMS, δ ppm): 7.38 (d, ³J = 8.4 Hz, 2H, CH₂-C-CH, Ar.), 6.86 (d, ³J = 8.8 Hz, 2H, CH₂C-OCH₃, Ar.), 5.02 (s, 1H, S-CH-S), 4.19 (t, ³J = 5.6 Hz, 4H, SCH₂-CH₂OCO), 3.80 (s, 3H, -OCH₃), 2.88-2.67 (m, 4H, SCH₂-CH₂OCO), 2.32 (t, ³J = 7.6 Hz, 4H, OOC-CH₂-), 1.61 (quint, ³J = 7.2 Hz, 4H, OOC-CH₂CH₂), 1.32-1.25 (br. s, 32 H, -CH₂- dodecanoyl), 0.88 (t, ³J = 6.4 Hz, 6H, CH₃).

¹³C-NMR (CDCl₃, 100.6 MHz, TMS δ ppm): 173.5 (CH₂COO), 159.4 (C-OCH₃, Ar.), 131.4 (C-CH, Ar.), 129.0 (CH₂-C-CH, Ar.), 114.1 (CH₂-C-OCH₃, Ar.), 62.8 (CH₂O-), 55.3 (CH₃O-), 52.8 (SCHS), 34.2 (OOC-CH₂), 31.9 (CH₂CH₂CH₃), 30.9 (SCH₂), 29.7 - 29.3 (CH₂ x 6), 25.0 (OOC-CH₂CH₂), 22.8 (CH₂CH₂CH₃), 14.2 (CH₂CH₂CH₃).

6.8 Synthesis of poly(MBL-co-DL-co-MBL) block copolymers

6.8.1 Synthesis of poly(DL) soft macroinitiators



Scheme 6.11 Synthesis of poly(DL) macroinitiators.

Using conventional inert atmosphere handling techniques, the appropriate amount of initiator (0.37 mmol; 1,8-Oct 54.1 mg, I₁ 57.1 mg, I₂ 110.4 mg, I₃ 136.3 mg, I₄ 62.3 mg and I₅ 101.5 mg) and 9.90 mL of δ -decalactone (DL) (55.48 mmol) were placed in a flame dried cylindrical 25 mL Schlenk flask with a magnetic stir bar to prepare a stock solution with [DL]:[I] = 150:1 ratio (DP = 150) (checked by ¹H-NMR). The mixture was stirred until the initiator was completely solubilized. Separately, 0.06 mmol of TBD (8.4 mg) was placed in another flame dried cylindrical 20 mL Schlenk flask with a magnetic stirrer. Then, the Schlenk containing the TBD was placed in a water bath (25 ± 2 °C) and 2 mL of the stock solution was transferred through a gas tight syringe under positive argon pressure ([TBD]:[-OH] = 0.40, [TBD] = 30 mM). The mixture was gently stirred until the desired conversion. The samples for ¹H-NMR analysis were withdrawn under argon flow and dissolved in a 0.03 M solution of benzoic acid (PhCOOH) in CDCl₃. Then, under argon flow, 130 mg of BriB-Im (4 Eq. with respect to -OH) were added and the temperature was increased up to 55 °C and let react overnight. The samples were precipitated in cold acetonitrile prior to NMR analysis. Once totally esterified, the crude reaction mixture was brought to room temperature and 2 mL of 0.5 M solution of PhCOOH in DCM was added to neutralize the TBD and the imidazole formed. The crude reaction mixture was diluted with additional 4 mL of DCM and was precipitated twice into 600 mL of cold acetonitrile. The pure polymer was recovered by dissolving in DCM

and dried under vacuum at 50 °C for 24 hours. Conversion, reaction time, yield and molecular weight characteristics for all the initiators are showed in Table 6.1.

Table 6.1 Conversion and molecular weight characteristics of the polymerization of DL with TBD initiated with different diol initiators. Polymerization conditions [DL]:[I]; 150:1, [TBD]:[-OH]; 0.4:1, 25 °C, in bulk.

I ^a	Time (h) ^b	Conv. ^c (%)	Yield ^d (%)	Mn _{Theor.} ^e (g/mol) (x10 ⁻³)	Mn _{NMR} ^f CH ₂ O- (g/mol) (x10 ⁻³)	Mn _{NMR} ^g CH ₃ x2 (g/mol) (x10 ⁻³)	Mn _{SEC} ^h (g/mol) (x10 ⁻³)	Đ ^h
Oct	7.5	73	68	18.8	17.9	17.1	23.5	1.16
I ₁	24	89	81	22.8	29.7	21.4	24.8	1.30
I ₂	8	70	66	18.2	19.1	18.6	22.4	1.16
I ₃	15	82	75	21.3	22.5	22.4	29.3	1.17
I ₄	7.5	72	65	18.5	20.1	18.0	23.3	1.18
I ₅	7	68	62	17.6	18.8	17.3	21.9	1.16

^a Polymerizations were carried out at 25 °C in bulk with a DL/I_x ratio fixed at 150/1 and a TBD/-OH ratio at 0.4. Esterification of the end-groups was carried out at 55 °C in bulk using 4 eq. of BriB-Im for 24 hours. ^b The showed reaction times correspond only for the polymerization reaction and not for the esterification. ^c Determined using ¹H-NMR spectroscopy by comparison of the integrations of the signals of the polymer backbone (4.88 ppm) and the unreacted monomer (4.28 ppm). ^d Polymer recovery after precipitation in cold acetonitrile. ^e Determined from the targeted DP and the obtained conversion. ^f Determined using ¹H-NMR spectroscopy by comparison of the integrations of the signals of the polymer backbone (4.88 ppm) and the initiator; Oct = 4.05 ppm, I₁ = 4.33 ppm, I₂ = 4.21 ppm, I₃ = 4.21 ppm, I₄ = 4.25 ppm and I₅ = 4.17 ppm. ^g Determined using ¹H-NMR spectroscopy by comparison of the integration of the signals of the polymer backbone (4.88 ppm) and the methyl end-groups (1.93 ppm). ^h Determined using SEC in THF, relative to polystyrene standards.

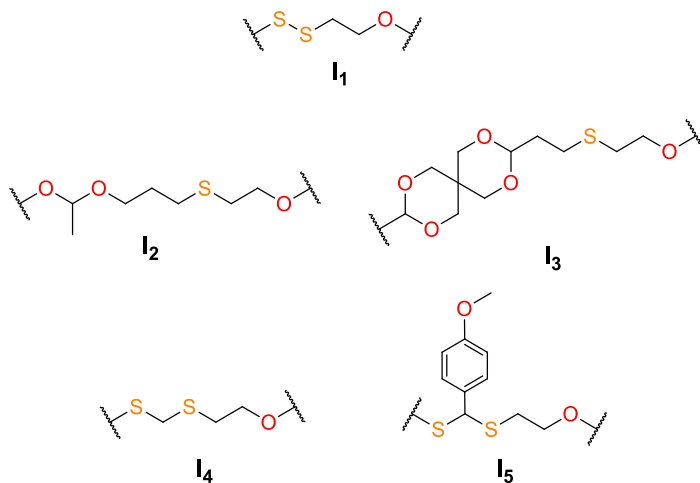


Figure 6.3 Structure of stimuli cleavable initiators

- Spectral data of poly(DL)-I_x diols:

• Poly(DL)_{1,8-Oct} diol (Annex 8.13)

¹H-NMR (CDCl₃, 400 MHz, TMS, δ ppm): 4.87 (m, CH-OOC-), 4.05 (**1,8-Oct**, t, ³J = 6.8 Hz, 4H, OCH₂), 3.59 (br. s, 2H, -CH-OH), 2.30 (t, ³J = 6.8 Hz, CH₂COO), 1.68-1.27 (m, (CH₂)_n), 0.87 (t, ³J = 7.0 Hz, CH₂-CH₃).

¹³C-NMR (CDCl₃, 100.6 MHz, TMS δ ppm): 173.1 (CH₂COO), 73.7 (CH-OOC-), 71.4-71.3 (-CH-OH), 64.4 (**1,8-Oct**, CH₂O-), 34.2 (CH₂COO), 33.9 (CH₃CH₂CH₂CH₂CH-), 33.5 (OOC-CH₂CH₂CH₂CH-), 31.6 (CH₃CH₂CH₂CH₂-CH₂CH-), 29.2 (**1,8-Oct**, CH₂CH₂CH₂CH₂O), 28.6 (**1,8-Oct**, CH₂CH₂O), 25.9 (**1,8-Oct**, CH₂CH₂CH₂O), 24.9 (CH₃CH₂CH₂CH₂CH-), 22.5 (CH₃CH₂CH₂CH₂-CH₂CH-), 20.8 (OOC-CH₂CH₂CH₂CH-), 14.0 (CH₃CH₂CH₂CH₂CH-).

• Poly(DL)-I₁ diol (Annex 8.15)

¹H-NMR (CDCl₃, 400 MHz, TMS, δ ppm): 4.87 (m, CH-OOC-), 4.33 (I₁, t, ³J = 6.6 Hz, 4H, SCH₂-CH₂O-), 3.59 (br. s, 2H, -CH-OH), 2.91 (I₁, t, ³J = 6.6 Hz, 4H, SCH₂-CH₂O-), 2.30 (t, ³J = 6.8 Hz, CH₂COO), 1.68-1.27 (m, -(CH₂)_n-), 0.87 (t, ³J = 7.0 Hz, CH₂-CH₃).

¹³C-NMR (CDCl₃, 100.6 MHz, TMS δ ppm): 173.1 (CH₂COO), 73.7 (CH-OOC-), 71.4-71.3 (-CH-OH), 62.1 (I₁, SCH₂-CH₂O-), 37.2 (I₁, SCH₂-CH₂O-), 34.2 (CH₂COO), 33.9 (CH₃CH₂CH₂CH₂CH-), 33.5 (OOC-CH₂CH₂CH₂CH-), 31.6 (CH₃CH₂CH₂CH₂-CH₂CH-), 24.9 (CH₃CH₂CH₂CH₂CH-), 22.5 (CH₃CH₂CH₂CH₂-CH₂CH-), 20.8 (OOC-CH₂CH₂CH₂CH-), 14.0 (CH₃CH₂CH₂CH₂CH-).

• Poly(DL)-I₂ diol (Annex 8.17)

¹H-NMR (CDCl₃, 400 MHz, TMS, δ ppm): 4.87 (m, CH-OOC-), 4.67 (I₂, q, ³J = 5.6 Hz, 1H, O-CH-O), 4.22 (I₂, t, ³J = 7.0 Hz, 4H, SCH₂-CH₂O-), 3.69-3.46 (I₂, m, 4H, O-CH-O-CH₂-), 3.59 (br. s, 2H, -CH-OH), 2.73 (I₂, t, ³J = 7.0 Hz, 4H, SCH₂-CH₂O-), 2.65 (I₂, t, ³J = 7.2 Hz, 4H, CH₂SCH₂-CH₂O-), 2.30 (t, ³J = 6.8 Hz, CH₂COO), 1.85 (I₂, quint, ³J = 6.8 Hz, 4H, O-CH-O-CH₂CH₂), 1.68-1.27 (m, -(CH₂)_n-), 0.87 (t, ³J = 7.0 Hz, CH₂-CH₃).

^{13}C -NMR (CDCl_3 , 100.6 MHz, TMS δ ppm): 173.1 (CH_2COO), 99.9 (I_2 , O-CH-O), 73.7 (CH-OOC-), 71.4-71.3 (-CH-OH), 63.6 (I_2 , O-CH-O- CH_2 -), 63.3 (I_2 , SCH_2 - CH_2 O-), 34.2 (CH_2COO), 33.9 ($\text{CH}_3\text{CH}_2\text{CH}_2\text{CH}_2\text{CH}_2\text{CH-}$), 33.5 ($\text{OOC-CH}_2\text{CH}_2\text{CH}_2\text{CH-}$), 31.6 ($\text{CH}_3\text{CH}_2\text{CH}_2\text{CH}_2\text{-CH}_2\text{CH-}$), 30.4 (I_2 , SCH_2 - CH_2 O-), 29.8 (I_2 , O-CH-O- CH_2CH_2), 29.0 (I_2 , O-CH-O- $\text{CH}_2\text{CH}_2\text{CH}_2$), 24.9 ($\text{CH}_3\text{CH}_2\text{CH}_2\text{CH}_2\text{CH}_2\text{CH-}$), 22.5 ($\text{CH}_3\text{CH}_2\text{CH}_2\text{CH}_2\text{-CH}_2\text{CH-}$), 20.8 ($\text{OOC-CH}_2\text{CH}_2\text{CH}_2\text{CH-}$), 19.7 (I_2 , $(\text{O})_2\text{-CHCH}_3$), 14.0 ($\text{CH}_3\text{CH}_2\text{CH}_2\text{CH}_2\text{CH}_2\text{-CH-}$).

- Poly(DL)- I_3 diol (Annex 8.19)

^1H -NMR (CDCl_3 , 400 MHz, TMS, δ ppm): 4.87 (m, CH-OOC-), 4.57 (I_3 , t, $^3J = 5.0$ Hz, 2H, O-CH-O), 4.51 (I_3 , dd, $^3J = 11.2$ Hz, $^4J = 2.0$ Hz, $2\text{H}_{\text{eq.}}$, -OCH $_2$ C-), 4.21 (I_3 , t, $^3J = 7.0$ Hz, 4H, SCH_2 - CH_2 O-), 3.59 (br. s, 2H, -CH-OH), 3.56 (I_3 , dd, $^3J = 11.6$ Hz, $^4J = 2.4$ Hz, $2\text{H}_{\text{eq.}}$, -OCH $_2$ C-), 3.53 (I_3 , d, $^3J = 12.0$ Hz, $2\text{H}_{\text{ax.}}$, -OCH $_2$ C-), 3.34 (I_3 , d, $^3J = 11.6$ Hz, $2\text{H}_{\text{ax.}}$, -OCH $_2$ C-), 2.71 (I_3 , t, $^3J = 6.8$ Hz, 4H, SCH_2 - CH_2 O-), 2.61 (I_3 , t, $^3J = 7.6$ Hz, 4H, CH_2SCH_2 - CH_2 O-), 2.30 (t, $^3J = 6.8$ Hz, CH_2COO), 1.92-1.87 (I_3 , m, 4H, $(\text{O})_2\text{CHCH}_2$ -), 1.68-1.27 (m, $-(\text{CH}_2)_n$ -), 0.87 (t, $^3J = 7.0$ Hz, $\text{CH}_2\text{-CH}_3$).

^{13}C -NMR (CDCl_3 , 100.6 MHz, TMS δ ppm): 173.1 (CH_2COO), 101.1 (I_3 , O-CH-O), 73.7 (CH-OOC-), 71.4-71.3 (-CH-OH), 70.5 (I_3 , -OCH $_2$ C-), 70.0 (I_3 , -OCH $_2$ C-), 63.2 (I_3 , SCH_2 - CH_2 O-), 34.7 (I_3 , $(\text{O})_2\text{CHCH}_2$ -), 34.2 (CH_2COO), 33.9 ($\text{CH}_3\text{CH}_2\text{CH}_2\text{CH}_2\text{CH}_2\text{CH-}$), 33.5 ($\text{OOC-CH}_2\text{CH}_2\text{CH}_2\text{CH-}$), 32.4 (I_3 , -OCH $_2$ C-), 31.6 ($\text{CH}_3\text{CH}_2\text{CH}_2\text{CH}_2\text{-CH}_2\text{CH-}$), 30.5 (I_3 , SCH_2 - CH_2 O-), 26.4 (I_3 , CH_2SCH_2 - CH_2 O-), 24.9 ($\text{CH}_3\text{CH}_2\text{CH}_2\text{CH}_2\text{CH}_2\text{CH-}$), 22.5 ($\text{CH}_3\text{CH}_2\text{CH}_2\text{CH}_2\text{-CH}_2\text{CH-}$), 20.8 ($\text{OOC-CH}_2\text{CH}_2\text{CH}_2\text{CH-}$), 14.0 ($\text{CH}_3\text{CH}_2\text{CH}_2\text{CH}_2\text{CH}_2\text{-CH-}$).

- Poly(DL)-I₄ diol (Annex 8.21)

¹H-NMR (CDCl₃, 400 MHz, TMS, δ ppm): 4.87 (m, CH-OOC-), 4.25 (I₄, t, ³J = 6.8 Hz, 4H, SCH₂-CH₂O-), 3.74 (I₄, s, 2H, S-CH₂-S), 3.59 (br. s, 2H, -CH-OH), 2.87 (I₄, t, ³J = 6.6 Hz, 4H, SCH₂-CH₂O-), 2.30 (t, ³J = 6.8 Hz, CH₂COO), 1.68-1.27 (m, -(CH₂)_n-), 0.87 (t, ³J = 7.0 Hz, CH₂-CH₃).

¹³C-NMR (CDCl₃, 100.6 MHz, TMS δ ppm): 173.1 (CH₂COO), 73.7 (CH-OOC-), 71.4-71.3 (-CH-OH), 62.9 (I₄, SCH₂-CH₂O-), 35.6 (I₄, S-CH₂-S), 34.2 (CH₂COO), 33.9 (CH₃CH₂CH₂CH₂CH₂CH-), 33.5 (OOC-CH₂CH₂CH₂CH-), 31.6 (CH₃CH₂CH₂CH₂-CH₂CH-), 29.0 (I₄, SCH₂-CH₂O-), 24.9 (CH₃CH₂CH₂CH₂CH₂CH-), 22.5 (CH₃CH₂CH₂CH₂-CH₂CH-), 20.8 (OOC-CH₂CH₂CH₂CH-), 14.0 (CH₃CH₂CH₂CH₂CH₂-CH-).

- Poly(DL)-I₅ diol (Annex 8.23)

¹H-NMR (CDCl₃, 400 MHz, TMS, δ ppm): 7.37 (I₅, d, ³J = 8.4 Hz, 2H, CH₂-C-CH, Ar.), 6.87 (I₅, d, ³J = 8.8 Hz, 2H, CH₂-C-OCH₃, Ar.), 5.00 (I₅, s, 1H, S-CH-S), 4.87 (m, CH-OOC-), 4.17 (I₅, m, 4H, SCH₂-CH₂O-), 3.80 (I₅, s, 3H, -OCH₃), 3.59 (br. s, 2H, -CH-OH), 2.85-2.67 (I₅, m, 4H, SCH₂-CH₂O-), 2.30 (t, ³J = 6.8 Hz, CH₂COO), 1.68-1.27 (m, -(CH₂)_n-), 0.87 (t, ³J = 7.0 Hz, CH₂-CH₃).

¹³C-NMR (CDCl₃, 100.6 MHz, TMS δ ppm): 173.1 (CH₂COO), 159.5 (I₅, C-OCH₃, Ar.), 131.4 (I₅, C-CH, Ar.), 129.0 (I₅, CH₂-C-CH, Ar.), 114.1 (I₅, CH₂-C-OCH₃, Ar.), 73.7 (CH-OOC-), 71.4-71.3 (-CH-OH), 62.8 (I₅, SCH₂-CH₂O-), 55.3 (I₅, OCH₃), 52.7 (I₅, S-CH-S), 34.2 (CH₂COO), 33.9 (CH₃CH₂CH₂CH₂CH₂CH-), 33.5 (OOC-CH₂CH₂CH₂CH-), 31.6 (CH₃CH₂CH₂CH₂-CH₂CH-), 30.9 (I₅, SCH₂-CH₂O-), 24.9 (CH₃CH₂CH₂CH₂CH₂CH-), 22.5 (CH₃CH₂CH₂CH₂-CH₂CH-), 20.8 (OOC-CH₂CH₂-CH₂CH-), 14.0 (CH₃CH₂CH₂CH₂CH₂-CH-).

- Spectral data of poly(DL)-I_x BriB esters:

• Poly(DL)_{1,8-Oct} BriB ester (Annex 8.14)

¹H-NMR (CDCl₃, 400 MHz, TMS, δ ppm): 4.87 (m, CH-OOC-), 4.05 (**1,8-Oct**, t, ³J = 6.8 Hz, 4H, OCH₂), 2.30 (t, ³J = 6.8 Hz, CH₂COO), 1.93 (**BriB**, s, 12H, -CH₃), 1.68-1.27 (m, -(CH₂)_n-), 0.87 (t, ³J = 7.0 Hz, CH₂-CH₃).

¹³C-NMR (CDCl₃, 100.6 MHz, TMS δ ppm): 173.1 (CH₂C=O), 171.3 (OOC-C-Br), 75.6 (CH-OOC-C-Br), 73.7 (CH-OOC-), 64.4 (**1,8-Oct**, CH₂O-), 56.2 (OOC-C-Br), 34.2 (CH₂COO), 33.9 (CH₃CH₂CH₂CH₂CH₂CH-), 33.5 (OOC-CH₂CH₂CH₂CH-), 31.6 (CH₃CH₂CH₂CH₂CH₂CH-), 30.7 (**BriB**, -CH₃), 29.2 (**1,8-Oct**, CH₂CH₂CH₂CH₂O), 28.6 (**1,8-Oct**, CH₂CH₂O), 25.9 (**1,8-Oct**, CH₂CH₂CH₂O), 24.9 (CH₃CH₂CH₂CH₂CH₂CH-), 22.5 (CH₃CH₂CH₂CH₂CH₂CH-), 20.8 (OOC-CH₂CH₂CH₂CH-), 14.0 (CH₃CH₂CH₂CH₂CH₂CH-).

• Poly(DL)-I₁ BriB ester (Annex 8.16)

¹H-NMR (CDCl₃, 400 MHz, TMS, δ ppm): 4.87 (m, CH-OOC-), 4.33 (**I₁**, t, ³J = 6.6 Hz, 4H, SCH₂-CH₂O-), 2.91 (**I₁**, t, ³J = 6.6 Hz, 4H, SCH₂-CH₂O-), 2.30 (t, ³J = 6.8 Hz, CH₂COO), 1.93 (**BriB**, s, 12H, -CH₃), 1.68-1.27 (m, -(CH₂)_n-), 0.87 (t, ³J = 7.0 Hz, CH₂-CH₃).

¹³C-NMR (CDCl₃, 100.6 MHz, TMS δ ppm): 173.1 (CH₂C=O), 171.3 (OOC-C-Br), 75.6 (CH-OOC-C-Br), 73.7 (CH-OOC-), 62.1 (**I₁**, SCH₂-CH₂O-), 56.2 (OOC-C-Br), 37.2 (**I₁**, SCH₂-CH₂O-), 34.2 (CH₂COO), 33.9 (CH₃CH₂CH₂CH₂CH₂CH-), 33.5 (OOC-CH₂CH₂CH₂CH-), 31.6 (CH₃CH₂CH₂CH₂CH₂CH-), 30.7 (**BriB**, -CH₃), 24.9 (CH₃CH₂CH₂CH₂CH₂CH-), 22.5 (CH₃CH₂CH₂CH₂CH₂CH-), 20.8 (OOC-CH₂CH₂CH₂CH-), 14.0 (CH₃CH₂CH₂CH₂CH₂CH-).

• Poly(DL)-I₂ BriB ester (Annex 8.18)

¹H-NMR (CDCl₃, 400 MHz, TMS, δ ppm): 4.87 (m, CH-OOC-), 4.67 (**I₂**, q, ³J = 5.6 Hz, 1H, O-CH-O), 4.22 (**I₂**, t, ³J = 7.0 Hz, 4H, SCH₂-CH₂O-), 3.69-3.46 (**I₂**, m, 4H, O-CH-O-CH₂-), 2.73 (**I₂**, t, ³J = 7.0 Hz, 4H, SCH₂-CH₂O-), 2.65 (**I₂**, t, ³J = 7.2 Hz, 4H, CH₂SCH₂-CH₂O-), 2.30 (t, ³J = 6.8 Hz, CH₂COO), 1.93 (**BriB**, s, 12H, -CH₃), 1.85 (**I₂**, quint, ³J = 6.8 Hz, 4H, O-CH-O-CH₂CH₂), 1.68-1.27 (m, -(CH₂)_n-), 0.87 (t, ³J = 7.0 Hz, CH₂-CH₃).

^{13}C -NMR (CDCl_3 , 100.6 MHz, TMS δ ppm): 173.1 (CH_2COO), 171.3 (OOC-C-Br), 99.9 (I_2 , O-CH-O), 75.6 (CH-OOC-C-Br), 73.7 (CH-OOC-), 63.6 (I_2 , O-CH-O- CH_2 -), 63.3 (I_2 , $\text{SCH}_2\text{-CH}_2\text{-O-}$), 56.2 (OOC-C-Br), 34.2 (CH_2COO), 33.9 ($\text{CH}_3\text{CH}_2\text{CH}_2\text{-CH}_2\text{CH}_2\text{CH-}$), 33.5 ($\text{OOC-CH}_2\text{CH}_2\text{CH}_2\text{CH-}$), 31.6 ($\text{CH}_3\text{CH}_2\text{CH}_2\text{CH}_2\text{-CH}_2\text{CH-}$), 30.7 (**BriB**, - CH_3), 30.4 (I_2 , $\text{SCH}_2\text{-CH}_2\text{-O-}$), 29.8 (I_2 , O-CH-O- CH_2CH_2), 29.0 (I_2 , O-CH-O- $\text{CH}_2\text{CH}_2\text{CH}_2$), 24.9 ($\text{CH}_3\text{CH}_2\text{CH}_2\text{CH}_2\text{CH}_2\text{CH-}$), 22.5 ($\text{CH}_3\text{CH}_2\text{CH}_2\text{CH}_2\text{-CH}_2\text{CH-}$), 20.8 ($\text{OOC-CH}_2\text{CH}_2\text{CH}_2\text{CH-}$), 19.7 (I_2 , (O) $_2\text{-CHCH}_3$), 14.0 ($\text{CH}_3\text{CH}_2\text{CH}_2\text{CH}_2\text{CH}_2\text{-CH-}$).

- Poly(DL)- I_3 BriB ester (Annex 8.20)

^1H -NMR (CDCl_3 , 400 MHz, TMS, δ ppm): 4.87 (m, CH-OOC-), 4.57 (I_3 , t, $^3J = 5.0$ Hz, 2H, O-CH-O), 4.51 (I_3 , dd, $^3J = 11.2$ Hz, $^4J = 2.0$ Hz, 2H_{eq} , - $\text{OCH}_2\text{C-}$), 4.21 (I_3 , t, $^3J = 7.0$ Hz, 4H, $\text{SCH}_2\text{-CH}_2\text{O-}$), 3.56 (I_3 , dd, $^3J = 11.6$ Hz, $^4J = 2.4$ Hz, 2H_{eq} , - $\text{OCH}_2\text{C-}$), 3.53 (I_3 , d, $^3J = 12.0$ Hz, 2H_{ax} , - $\text{OCH}_2\text{C-}$), 3.34 (I_3 , d, $^3J = 11.6$ Hz, 2H_{ax} , - $\text{OCH}_2\text{C-}$), 2.71 (I_3 , t, $^3J = 6.8$ Hz, 4H, $\text{SCH}_2\text{-CH}_2\text{O-}$), 2.61 (I_3 , t, $^3J = 7.6$ Hz, 4H, $\text{CH}_2\text{SCH}_2\text{-CH}_2\text{O-}$), 2.30 (t, $^3J = 6.8$ Hz, CH_2COO), 1.93 (**BriB**, s, 12H, - CH_3), 1.92-1.87 (I_3 , m, 4H, (O) $_2\text{CHCH}_2$ -), 1.68-1.27 (m, $-(\text{CH}_2)_n$ -), 0.87 (t, $^3J = 7.0$ Hz, $\text{CH}_2\text{-CH}_3$).

^{13}C -NMR (CDCl_3 , 100.6 MHz, TMS δ ppm): 173.1 (CH_2COO), 171.3 (OOC-C-Br), 101.1 (I_3 , O-CH-O), 75.6 (CH-OOC-C-Br), 73.7 (CH-OOC-), 70.5 (I_3 , - $\text{OCH}_2\text{C-}$), 70.0 (I_3 , - $\text{OCH}_2\text{C-}$), 63.2 (I_3 , $\text{SCH}_2\text{-CH}_2\text{O-}$), 56.2 (OOC-C-Br), 34.7 (I_3 , (O) $_2\text{CHCH}_2$ -), 34.2 (CH_2COO), 33.9 ($\text{CH}_3\text{CH}_2\text{CH}_2\text{CH}_2\text{CH}_2\text{CH-}$), 33.5 ($\text{OOC-CH}_2\text{CH}_2\text{CH}_2\text{CH-}$), 32.4 (I_3 , - $\text{OCH}_2\text{C-}$), 31.6 ($\text{CH}_3\text{CH}_2\text{CH}_2\text{CH}_2\text{CH}_2\text{-CH}_2\text{CH-}$), 30.7 (**BriB**, - CH_3), 30.5 (I_3 , $\text{SCH}_2\text{-CH}_2\text{O-}$), 26.4 (I_3 , $\text{CH}_2\text{SCH}_2\text{-CH}_2\text{O-}$), 24.9 ($\text{CH}_3\text{CH}_2\text{CH}_2\text{CH}_2\text{CH}_2\text{CH-}$), 22.5 ($\text{CH}_3\text{CH}_2\text{CH}_2\text{CH}_2\text{-CH}_2\text{CH-}$), 20.8 ($\text{OOC-CH}_2\text{CH}_2\text{CH}_2\text{CH-}$), 14.0 ($\text{CH}_3\text{CH}_2\text{CH}_2\text{CH}_2\text{CH}_2\text{-CH-}$).

- Poly(DL)-I₄ BriB ester (Annex 8.22)

¹H-NMR (CDCl₃, 400 MHz, TMS, δ ppm): 4.87 (m, CH-OOC-), 4.25 (**I**₄, t, ³J = 6.8 Hz, 4H, SCH₂-CH₂O-), 3.74 (**I**₄, s, 2H, S-CH₂-S), 2.87 (**I**₄, t, ³J = 6.6 Hz, 4H, SCH₂-CH₂O-), 2.30 (t, ³J = 6.8 Hz, CH₂COO), 1.93 (**BriB**, s, 12H, -CH₃), 1.68-1.27 (m, -(CH₂)_n-), 0.87 (t, ³J = 7.0 Hz, CH₂-CH₃).

¹³C-NMR (CDCl₃, 100.6 MHz, TMS δ ppm): 173.1 (CH₂COO), 171.3 (OOC-C-Br), 75.6 (CH-OOC-C-Br), 73.7 (CH-OOC-), 62.9 (**I**₄, SCH₂-CH₂O-), 56.2 (OOC-C-Br), 35.6 (**I**₄, S-CH₂-S), 34.2 (CH₂COO), 33.9 (CH₃CH₂CH₂CH₂CH₂CH-), 33.5 (OOC-CH₂CH₂CH₂CH-), 31.6 (CH₃CH₂CH₂CH₂-CH₂CH-), 30.7 (**BriB**, -CH₃), 29.0 (**I**₄, SCH₂-CH₂O-), 24.9 (CH₃CH₂CH₂CH₂CH₂CH-), 22.5 (CH₃CH₂CH₂CH₂-CH₂CH-), 20.8 (OOC-CH₂CH₂CH₂CH-), 19.7 (**I**₂, (O)₂-CHCH₃), 14.0 (CH₃CH₂CH₂CH₂CH₂-CH-).

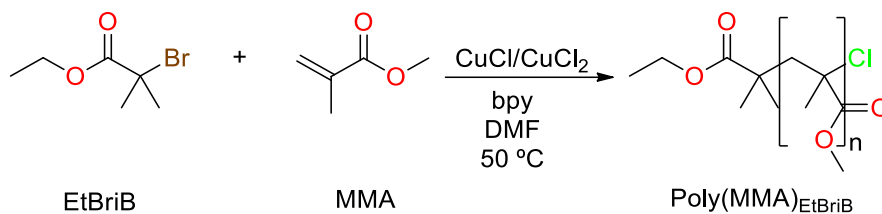
- Poly(DL)-I₅ BriB ester (Annex 8.24)

¹H-NMR (CDCl₃, 400 MHz, TMS, δ ppm): 7.37 (**I**₅, d, ³J = 8.4 Hz, 2H, CH₂-C-CH, Ar.), 6.87 (**I**₅, d, ³J = 8.8 Hz, 2H, CH₂C-OCH₃, Ar.), 5.00 (**I**₅, s, 1H, S-CH-S), 4.87 (m, CH-OOC-), 4.17 (**I**₅, m, 4H, SCH₂-CH₂O-), 3.80 (**I**₅, s, 3H, -OCH₃), 2.85-2.67 (**I**₅, m, 4H, SCH₂-CH₂O-), 2.30 (t, ³J = 6.8 Hz, CH₂COO), 1.93 (**BriB**, s, 12H, -CH₃), 1.68-1.27 (m, -(CH₂)_n-), 0.87 (t, ³J = 7.0 Hz, CH₂-CH₃).

¹³C-NMR (CDCl₃, 100.6 MHz, TMS δ ppm): 173.1 (CH₂COO), 171.3 (OOC-C-Br), 159.5 (**I**₅, C-OCH₃, Ar.), 131.4 (**I**₅, C-CH, Ar.), 129.0 (**I**₅, CH₂-C-CH, Ar.), 114.1 (**I**₅, CH₂-C-OCH₃, Ar.), 75.6 (CH-OOC-C-Br), 73.7 (CH-OOC-), 62.8 (**I**₅, SCH₂-CH₂O-), 56.2 (OOC-C-Br), 55.3 (**I**₅, OCH₃), 52.7 (**I**₅, S-CH-S), 34.2 (CH₂COO), 33.9 (CH₃CH₂CH₂CH₂CH₂CH-), 33.5 (OOC-CH₂CH₂CH₂CH-), 31.6 (CH₃CH₂CH₂CH₂-CH₂CH-), 30.9 (**I**₅, SCH₂-CH₂O-), 30.7 (**BriB**, -CH₃), 24.9 (CH₃CH₂CH₂CH₂CH₂CH-), 22.5 (CH₃CH₂CH₂CH₂-CH₂CH-), 20.8 (OOC-CH₂CH₂CH₂CH), 14.0 (CH₃CH₂CH₂-CH₂CH₂-CH-).

6.8.2 Synthesis poly(MBL) hard blocks

6.8.2.1 Synthesis of poly(MMA)_{EtBriB} homopolymer



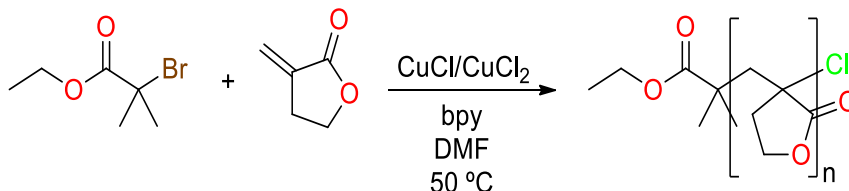
Scheme 6.12 Synthesis of poly(MMA) using EtBriB as initiator by ATRP.

In a typical experiment, 2.00 mg (0.015 mmol) of copper(II) chloride and 4.65 mg (0.030 mmol) of 2,2'-bipyridine (bpy) was placed into a 25 mL cylindrical Schlenk flask equipped with a Teflon coated magnetic stir bar. Then, 21.8 μ L (0.15 mmols) of ethyl 2-bromoisobutyrate (EtBriB), 2 mL of DMF and 2.0 mL (18.70 mmols) of methyl methacrylate (MMA) were added. The mixture was stirred at 50 °C until homogenization. In another Schlenk flask, equipped with a magnetic stir bar, 0.1620 g (1.64 mmols) of copper(I) chloride, 0.5205 g (3.33 mmols) of bpy and 10 mL of DMF (previously deoxygenated by bubbling argon for 15 minutes) were placed to prepare a stock solution. The mixture of MMA, CuCl₂, bpy and EtBriB was degassed through 4 freeze-pump-thaw cycles and was placed into a preheated bath at 50 °C. Then, 1.0 mL of the CuCl/bpy stock solution (0.16 and 0.33 mmols respectively) was added, within a period of 5 minutes, through a gas tight syringe. Samples were withdrawn at preset times, solubilized in CDCl₃, passed through basic alumina to remove the catalyst and analyzed by ¹H-NMR spectroscopy. The same samples were used for size exclusion chromatography (SEC) by removing the chloroform under vacuum and solubilizing in THF. The polymerization was stopped, at 80% of conversion (21 hours), by bubbling air through the reaction mixture, diluting with DCM (2 mL), passing through basic alumina, and precipitating in cold methanol (spectra are shown in annex 8.25).

$^1\text{H-NMR}$ (CDCl_3 , 400 MHz, TMS, δ ppm): 4.13-4.06 (m, 2H, $\text{CH}_3\text{CH}_2\text{O-}$), 3.60 (br. s, CH_3O), 2.07-1.41 (m, $-\text{CH}_2-$), 1.25 (m, $\text{CH}_3\text{CH}_2\text{O}$), 1.21-0.85 (m, $-\text{CH}_3$).

$^{13}\text{C-NMR}$ (CDCl_3 , 100.6 MHz, TMS δ ppm): 178.4-176.2 ($-\text{COO-}$), 60.5 ($\text{CH}_3\text{CH}_2\text{O}$), 54.4-52.5 ($-\text{CH}_2-$), 51.8 ($\text{CH}_3\text{O-}$), 45.5-44.5 ($-\text{C-}$), 21.1-16.5 ($-\text{CH}_3$), 14.0 ($\text{CH}_3\text{CH}_2\text{O}$).

6.8.2.2 Synthesis of poly(MBL)_{EtBrIB} homopolymer



Scheme 6.13 Synthesis of poly(MBL) using EtBrIB as initiator by ATRP.

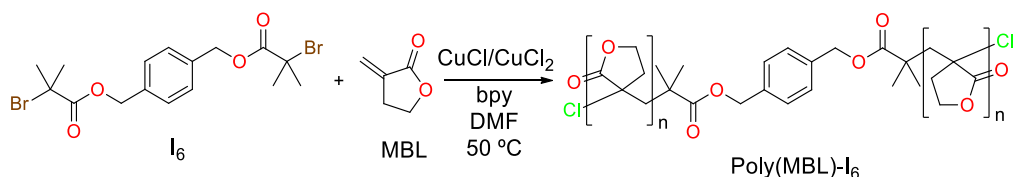
Following the previous procedure, 2.85 mg (0.021 mmols) of CuCl_2 and 6.56 mg (0.042 mmols) of bpy was placed into a 25 mL cylindrical Schlenk flask equipped with a Teflon coated magnetic stir bar. Then, 29.2 μL (0.20 mmols) of EtBrIB, 1.15 mL of DMF and 1.75 mL (20.0 mmol) of α -methylene- γ -butyrolactone (MBL) were added. The mixture was stirred at 50 °C until homogenization. The mixture was degassed through 4 freeze-pump-thaw cycles and was placed into a preheated bath at 50 °C. In another Schlenk flask, equipped with a magnetic stir bar, 0.0814 g (0.82 mmols) of copper(I) chloride, 0.2614 g (1.67 mmols) of bpy and 4 mL of DMF (previously deoxygenated by bubbling argon for 15 minutes) were placed to prepare a stock solution. Then, 1.1 mL of the CuCl/bpy stock solution (0.23 and 0.46 mmols respectively) was added, within a period of 5 minutes, through a gas tight syringe. Samples were withdrawn at preset times, solubilized in DMF-d_7 , passed through basic alumina to remove the catalyst and analyzed by $^1\text{H-NMR}$ spectroscopy. The same samples were used for size exclusion chromatography (SEC) analysis in DMF (0.05% (w/w) LiBr). The polymerization was stopped, at 68% of conversion (24 hours), by bubbling air through the reaction mixture,

diluting with additional DMF (2 mL), passing through basic alumina, and precipitating in cold methanol (spectra are shown in annex 8.26).

$^1\text{H-NMR}$ (DMSO- d_6 , 400 MHz, δ ppm): 4.35 (br. s, $\text{CH}_2\text{CH}_2\text{OOC-}$), 4.04 (br. s, $\text{CH}_3\text{CH}_2\text{O-}$), 2.33-1.74 (m, $\text{CH}_2\text{CH}_2\text{OOC-}$ and $\text{CH}_2\text{C-}$), 1.18 (m, $\text{CH}_3\text{CH}_2\text{O-}$).

$^{13}\text{C-NMR}$ (DMSO- d_6 , 100.6 MHz, δ ppm): 180.2 ($\text{C=OCH}_2\text{CH}_2$), 173.2 ($\text{C=OCH}_2\text{CH}_3$), 65.1 ($\text{COOCH}_2\text{CH}_2$), 60.4 ($\text{COOCH}_2\text{CH}_3$), 44.4 ($\text{C-COOCH}_2\text{CH}_2$), 41.1 (CH_2C), 30.8 ($\text{COOCH}_2\text{CH}_2$), 13.8 ($\text{COOCH}_2\text{CH}_3$).

6.8.2.3 Synthesis of poly(MBL)- I_6 homopolymer



Scheme 6.14 Synthesis of poly(MBL) using I_6 as initiator by ATRP.

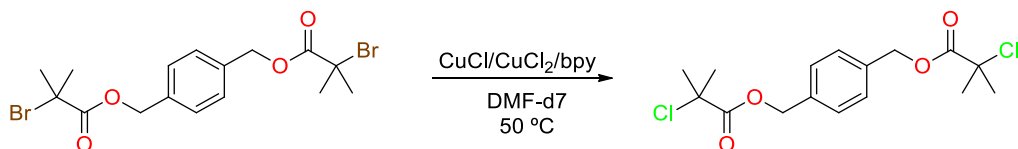
Following the previous procedure, 4.10 mg (0.030 mmols) of CuCl_2 and 9.52 mg (0.061 mmols) of bpy was placed into a 25 mL cylindrical Schlenk flask equipped with a Teflon coated magnetic stir bar. Then, 66.50 mg (0.15 mmols) of I_6 , 0.8 mL of DMF and 1.30 mL (14.83 mmols) of MBL were added. The mixture was stirred at $50\text{ }^\circ\text{C}$ until homogenization. The mixture was degassed through 4 freeze-pump-thaw cycles and was placed into a preheated bath at $50\text{ }^\circ\text{C}$. A CuCl/bpy stock solution containing 330 mg (3.34 mmols) of CuCl , 1050 mg (6.72 mmols) of bpy and 10 mL of deoxygenated DMF was prepared. Then, 1.00 mL of the CuCl/bpy stock solution (0.33 and 0.67 mmol respectively) was added, within a period of 5 minutes, through a gas tight syringe. Samples were withdrawn at preset times, solubilized in DMF- d_7 , passed through basic alumina to remove the catalyst, and analyzed by $^1\text{H-NMR}$ spectroscopy. The same samples were used for size exclusion chromatography (SEC) analysis in DMF (0.05% (w/w) LiBr). The polymerization was stopped, at 85% of conversion (22 hours), by

bubbling air through the reaction mixture, diluting with additional DMF (2 mL), passing through basic alumina, and precipitating in cold methanol (spectra are shown in annex 8.27).

$^1\text{H-NMR}$ (DMSO- d_6 , 400 MHz, δ ppm): 7.36 (s, Ar.), 5.11-5.00 (m, Bn., $-\text{CH}_2-$), 4.31 (br. s, $\text{CH}_2\text{CH}_2\text{OOC-}$), 2.28-1.78 (m, $\text{CH}_2\text{CH}_2\text{OOC-}$ and $\text{CH}_2\text{C-}$), 1.74 (CH_3).

$^{13}\text{C-NMR}$ (DMSO- d_6 , 100.6 MHz, δ ppm): 180.7 ($\text{C=OCH}_2\text{CH}_2$), 173.9 ($\text{OOC-C(CH}_3)_2$), 136.7 ($-\text{C-}$, Ar.), 128.5 ($-\text{CH-}$, Ar.), 67.1 (Bn., $-\text{CH}_2-$), 65.5 ($\text{COOCH}_2\text{CH}_2$), 44.6 ($\text{C-COOCH}_2\text{CH}_2$), 41.6 (CH_2C), 31.2 ($\text{COOCH}_2\text{CH}_2$), 29.6 (CH_3).

6.8.2.4 Halogen exchange of initiator I_6



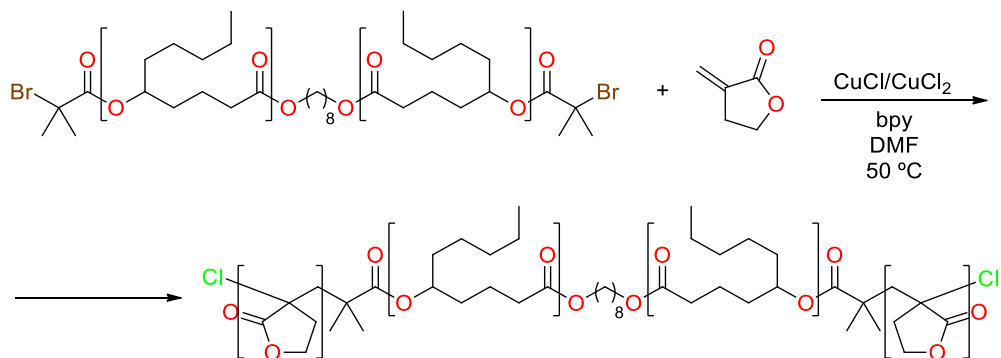
Scheme 6.15 Halogen exchange reaction of initiator I_6 with $\text{CuCl/CuCl}_2/\text{bpy}$ system.

In a 20 mL vials, equipped with a magnetic stir bar, 44.2 mg (0.10 mmol) of initiator I_6 , 78.1 mg (0.50 mmol) of bpy, 2.9 mg (0.02 mmol) of CuCl_2 and 20.0 mg (0.20 mmol) of CuCl was placed. The vial was closed with a rubber septum and was purged with argon. Then, 1 mL of DMF-d_7 , previously degassed by bubbling argon for 15 minutes, was added. The mixture was introduced into a preheated thermostatic bath at $50\text{ }^\circ\text{C}$ under stirring. After 30 minutes the conversion was quantitative. The reaction was stopped by bubbling air through the solution to oxidize the catalyst and the crude mixture was filtrated through basic alumina to remove the copper. The product was directly analyzed by NMR spectroscopy without further purification (spectra are shown in annex 8.28).

$^1\text{H-NMR}$ (DMF-d_7 , 400 MHz, δ ppm): 7.51 (s, 4H, Ar.), 5.31 (s, 4H, $-\text{CH}_2-$), 1.83 (s, 12H, CH_3).

^{13}C -NMR (DMF- d_7 , 100.6 MHz, δ ppm): 171.1 (-COO-), 136.3 (-C-, Ar.), 128.3 (-CH-, Ar.), 67.2 (-CH $_2$ -), 65.7 (C-Cl), 29.4 (CH $_3$).

6.8.3 Synthesis of block copolymers



Scheme 6.16 Synthesis of block copolymer by chain extension of poly(DL)_{1,8-Oct} macroinitiator with MBL by ATRP.

In a typical experiment, 0.747 g (0.04 mmols) of the poly(DL) BriB ester macroinitiator (M_n (^1H -NMR) = 18900 g/mol) was transferred to a 25 mL cylindrical schlenk flask equipped with a Teflon coated magnetic stir bar. Then, 1.23 mg (0.009 mmols) of CuCl₂, 2.85 mg (0.018 mmols) of bipyridine, 460 μL (5.25 mmol) of MBL and 0.49 mL of DMF were added. The reaction mixture was introduced into a preheated bath at 50 °C until complete homogenization. Once the macroinitiator was completely solubilized, the mixture was degassed through 4 freeze-pump-thaw cycles. After the deoxygenation process the reaction mixture was introduced again at the thermostatic bath at 50 °C and let a 10-15 minutes until complete homogenization. A CuCl/bpy stock solution containing 0.0814 g (0.82 mmols) of CuCl, 0.2614 g (1.67 mmols) of bpy and 4 mL of deoxygenated DMF was prepared. Finally, 0.45 mL of the CuCl/bpy stock solution (0.092 and 0.188 mmols respectively) were added within a period of 5 minutes. The reaction was stopped at 41% of conversion diluting with 0.5 mL of DMF and bubbling air through the reaction mixture. The crude of the reaction was diluted with 8 mL of

DCM and passed through a short basic alumina column to remove the catalyst. Finally, the polymer was isolated by precipitation in cold methanol.

- Spectral data of block copolymers:
 - Poly(MBL)-*co*-poly(DL)_{1,8-Oct}-*co*-poly(MBL) (Annex 8.29):

¹H-NMR (CDCl₃, 400 MHz, TMS, δ ppm): 4.87 (m, CH-OOC- (DL)), 4.38 (br. s, CH₂OOC- (MBL)), 4.05 (**1,8-Oct**, t, ³J = 6.8 Hz, 4H, OCH₂), 2.29 (t, ³J = 7.0 Hz, CH₂COO (DL)), 2.17-2.13 (m, (-CH₂)_{x2} (MBL)), 1.68-1.26 (m, -(CH₂)_n- (DL)), 0.88 (t, ³J = 7.2 Hz, CH₂-CH₃ (DL)).

¹³C-NMR (DMSO-d₆, 80 °C, 100.6 MHz, δ ppm): 179.7-179.5 (C-COO, (MBL)), 171.1 (CH₂C=O (DL)), 72.2 (CH-OOC- (DL)), 64.6 (CH₂OOC- (MBL)), 44.3-43.9 (C-COO, (MBL)), 41.5-40.7 (-CH₂-C- (MBL)), 33.1 (CH₂COO (DL)), 33.0 (CH₃CH₂-CH₂CH₂CH₂CH- (DL)), 32.6 (OOC-CH₂CH₂CH₂CH- (DL)), 30.7 (CH₃CH₂CH₂CH₂-CH₂CH- (DL)), 23.9 (CH₃CH₂CH₂-CH₂CH₂CH- (DL)), 21.4 (CH₃CH₂CH₂CH₂-CH₂CH-(DL)), 20.0 (OOC-CH₂CH₂CH₂CH- (DL)), 12.9 (CH₃CH₂CH₂CH₂CH₂-CH- (DL)).

- Poly(MBL)-*co*-poly(DL)-I₁-*co*-poly(MBL) (Annex 8.30):

¹H-NMR (CDCl₃, 400 MHz, TMS, δ ppm): 4.87 (m, CH-OOC- (DL)), 4.38 (br. s, CH₂OOC- (MBL)), 4.33 (I₁, t, ³J = 6.8 Hz, 4H, SCH₂-CH₂O-), 2.91 (I₁, t, ³J = 6.8 Hz, 4H, SCH₂-CH₂O-), 2.30 (t, ³J = 7.0 Hz, CH₂COO (DL)), 2.17-2.13 (m, (-CH₂)_{x2} (MBL)), 1.68-1.26 (m, -(CH₂)_n- (DL)), 0.88 (t, ³J = 7.2 Hz, CH₂-CH₃ (DL)).

¹³C-NMR (DMSO-d₆, 80 °C, 100.6 MHz, δ ppm): 179.7-179.3 (C-COO, (MBL)), 171.0 (CH₂C=O (DL)), 72.2 (CH-OOC- (DL)), 64.6 (CH₂OOC- (MBL)), 44.3-43.9 (C-COO, (MBL)), 41.7-40.5 (-CH₂-C- (MBL)), 33.1 (CH₂COO (DL)), 33.0 (CH₃CH₂-CH₂CH₂CH₂CH- (DL)), 32.6 (OOC-CH₂CH₂CH₂CH- (DL)), 30.6 (CH₃CH₂CH₂CH₂-CH₂CH- (DL)), 23.9 (CH₃CH₂CH₂-CH₂CH₂CH- (DL)), 21.4 (CH₃CH₂CH₂CH₂-CH₂CH-(DL)), 20.0 (OOC-CH₂CH₂CH₂CH- (DL)), 12.9 (CH₃CH₂CH₂CH₂CH₂-CH- (DL)).

- Poly(MBL)-co-poly(DL)-I₂-co-poly(MBL) (Annex 8.31):

¹H-NMR (CDCl₃, 400 MHz, TMS, δ ppm): 4.87 (m, CH-OOC- (DL)), 4.67 (I₂, q, ³J = 5.6 Hz, 1H, O-CH-O), 4.38 (br. s, CH₂OOC- (MBL)), 4.21 (I₂, t, ³J = 7.0 Hz, 4H, SCH₂-CH₂O-), 3.69-3.46 (I₂, m, 4H, O-CH-O-CH₂-), 2.73 (I₂, t, ³J = 7.0 Hz, 4H, SCH₂-CH₂O-), 2.65 (I₂, t, ³J = 7.2 Hz, 4H, CH₂SCH₂-CH₂O-), 2.30 (t, ³J = 7.0 Hz, CH₂COO (DL)), 2.17-2.13 (m, (-CH₂-)x2 (MBL)), 1.85 (I₂, quint, ³J = 6.8 Hz, 4H, O-CH-O-CH₂CH₂), 1.68-1.26 (m, -(CH₂)_n- (DL)), 0.88 (t, ³J = 7.2 Hz, CH₂-CH₃ (DL)).

¹³C-NMR (DMSO-d₆, 80 °C, 100.6 MHz, δ ppm): 179.7-179.5 (C-COO, (MBL)), 171.1 (CH₂C=O (DL)), 72.2 (CH-OOC- (DL)), 64.6 (CH₂OOC- (MBL)), 44.3-43.9 (C-COO, (MBL)), 41.7-40.5 (-CH₂-C- (MBL)), 33.1 (CH₂COO (DL)), 33.0 (CH₃CH₂-CH₂CH₂CH₂CH- (DL)), 32.6 (OOC-CH₂CH₂CH₂CH- (DL)), 30.6 (CH₃CH₂CH₂CH₂-CH₂CH- (DL)), 23.9 (CH₃CH₂CH₂-CH₂CH₂CH- (DL)), 21.4 (CH₃CH₂CH₂CH₂-CH₂CH- (DL)), 20.0 (OOC-CH₂CH₂CH₂CH- (DL)), 12.9 (CH₃CH₂CH₂CH₂CH₂-CH- (DL)).

- Poly(MBL)-co-poly(DL)-I₃-co-poly(MBL) (Annex 8.32):

¹H-NMR (CDCl₃, 400 MHz, TMS, δ ppm): 4.87 (m, CH-OOC- (DL)), 4.57 (I₃, t, ³J = 5.0 Hz, 2H, O-CH-O), 4.52 (I₃, dd, ³J = 11.2 Hz, ⁴J = 2.0 Hz, 2H_{eq.}, -OCH₂C-), 4.38 (br. s, CH₂OOC- (MBL)), 4.21 (I₃, t, ³J = 7.0 Hz, 4H, SCH₂-CH₂O-), 3.56 (I₃, dd, ³J = 11.6 Hz, ⁴J = 2.4 Hz, 2H_{eq.}, -OCH₂C-), 3.53 (I₃, d, ³J = 12.0 Hz, 2H_{ax.}, -OCH₂C-), 3.34 (I₃, d, ³J = 11.6 Hz, 2H_{ax.}, -OCH₂C-), 2.71 (I₃, t, ³J = 6.8 Hz, 4H, SCH₂-CH₂O-), 2.61 (I₃, t, ³J = 7.6 Hz, 4H, CH₂SCH₂-CH₂O-), 2.30 (t, ³J = 6.8 Hz, CH₂COO (DL)), 2.17-2.13 (m, (-CH₂-)x2 (MBL)), 1.92-1.87 (I₃, m, 4H, (O)₂CHCH₂-), 1.68-1.27 (m, -(CH₂)_n- (DL)), 0.87 (t, ³J = 7.0 Hz, CH₂-CH₃ (DL)).

¹³C-NMR (DMSO-d₆, 80 °C, 100.6 MHz, δ ppm): 179.7-179.5 (C-COO, (MBL)), 171.1 (CH₂C=O (DL)), 72.2 (CH-OOC- (DL)), 64.6 (CH₂OOC- (MBL)), 44.3-43.9 (C-COO, (MBL)), 41.7-40.5 (-CH₂-C- (MBL)), 33.1 (CH₂COO (DL)), 33.0 (CH₃CH₂-CH₂CH₂CH₂CH- (DL)), 32.6 (OOC-CH₂CH₂CH₂CH- (DL)), 30.6 (CH₃CH₂CH₂CH₂-CH₂CH- (DL)), 30.2-29.8 (CH₂-CH₂-OOC-

(MBL)), 23.9 (CH₃CH₂CH₂-CH₂CH₂CH- (DL)), 21.4 (CH₃CH₂CH₂CH₂-CH₂CH-(DL)), 20.0 (OOC-CH₂CH₂CH₂CH- (DL)), 12.9 (CH₃CH₂CH₂CH₂CH₂-CH- (DL)).

- Poly(MBL)-*co*-poly(DL)-I₄-*co*-poly(MBL) (Annex 8.33):

¹H-NMR (CDCl₃, 400 MHz, TMS, δ ppm): 4.87 (m, CH-OOC- (DL)), 4.38 (br. s, CH₂OOC- (MBL)), 4.25 (I₄, t, ³J = 6.8 Hz, 4H, SCH₂-CH₂O-), 3.74 (I₄, s, 2H, S-CH₂-S), 2.87 (I₄, t, ³J = 6.6 Hz, 4H, SCH₂-CH₂O-), 2.30 (t, ³J = 7.0 Hz, CH₂COO (DL)), 2.17-2.13 (m, (-CH₂-)x2 (MBL)), 1.68-1.26 (m, -(CH₂)_n- (DL)), 0.88 (t, ³J = 7.2 Hz, CH₂-CH₃ (DL)).

¹³C-NMR (DMSO-d₆, 80 °C, 100.6 MHz, δ ppm): 179.7-179.5 (C-COO, (MBL)), 171.1 (CH₂COO (DL)), 72.2 (CH-OOC- (DL)), 64.6 (CH₂OOC- (MBL)), 44.3-43.9 (C-COO, (MBL)), 41.7-40.5 (-CH₂-C- (MBL)), 33.1 (CH₂COO (DL)), 33.0 (CH₃CH₂-CH₂CH₂CH₂CH- (DL)), 32.6 (OOC-CH₂CH₂CH₂CH- (DL)), 30.6 (CH₃CH₂CH₂CH₂-CH₂CH- (DL)), 23.9 (CH₃CH₂CH₂-CH₂CH₂CH- (DL)), 21.4 (CH₃CH₂CH₂CH₂-CH₂CH-(DL)), 20.0 (OOC-CH₂CH₂CH₂CH- (DL)), 12.9 (CH₃CH₂CH₂CH₂CH₂-CH- (DL)).

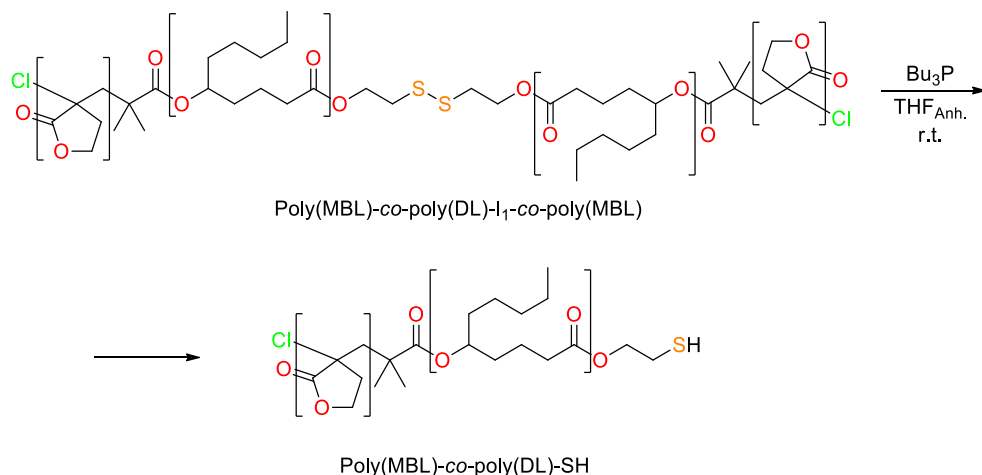
- Poly(MBL)-*co*-poly(DL)-I₅-*co*-poly(MBL) (Annex 8.34):

¹H-NMR (CDCl₃, 400 MHz, TMS, δ ppm): 7.37 (I₅, d, ³J = 8.4 Hz, 2H, CH₂-C-CH, Ar.), 6.87 (I₅, d, ³J = 8.8 Hz, 2H, CH₂C-OCH₃, Ar.), 5.00 (I₅, s, 1H, S-CH-S), 4.87 (m, CH-OOC- (DL)), 4.38 (br. s, CH₂OOC- (MBL)), 4.17 (I₅, m, 4H, SCH₂-CH₂O-), 3.80 (I₅, s, 3H, -OCH₃), 2.85-2.67 (I₅, m, 4H, SCH₂-CH₂O-), 2.30 (t, ³J = 6.8 Hz, CH₂COO (DL)), 2.17-2.13 (m, (-CH₂-)x2 (MBL)), 1.68-1.27 (m, -(CH₂)_n- (DL)), 0.87 (t, ³J = 7.0 Hz, CH₂-CH₃ (DL)).

¹³C-NMR (DMSO-d₆, 80 °C, 100.6 MHz, δ ppm): 179.7-179.5 (C-COO, (MBL)), 171.1 (CH₂COO (DL)), 72.2 (CH-OOC- (DL)), 64.6 (CH₂OOC- (MBL)), 44.3-43.9 (C-COO, (MBL)), 41.7-40.5 (-CH₂-C- (MBL)), 33.1 (CH₂COO (DL)), 33.0 (CH₃CH₂-CH₂CH₂CH₂CH- (DL)), 32.6 (OOC-CH₂CH₂CH₂CH- (DL)), 30.6 (CH₃CH₂CH₂CH₂-CH₂CH- (DL)), 23.9 (CH₃CH₂CH₂-CH₂CH₂CH- (DL)), 21.4 (CH₃CH₂CH₂CH₂-CH₂CH-(DL)), 20.0 (OOC-CH₂CH₂CH₂CH- (DL)), 12.9 (CH₃CH₂CH₂CH₂CH₂-CH- (DL)).

6.9 Degradation of stimuli-cleavable block copolymers

6.9.1 Reductive cleavable block copolymer poly(MBL)-co-poly(DL)-I₁-co-poly(MBL)



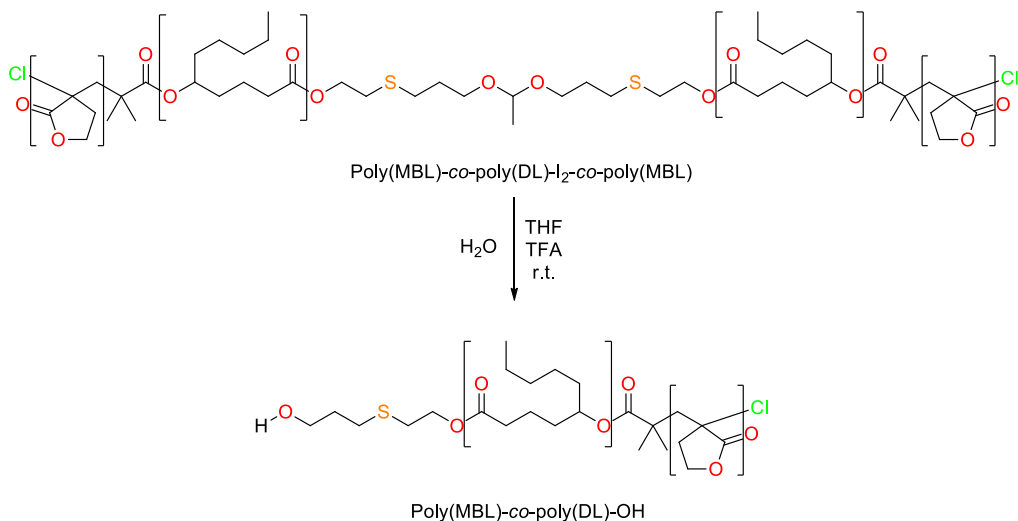
Scheme 6.17 Reductive cleavage of poly(MBL)-co-poly(DL)-I₁-co-poly(MBL) to poly(MBL)-co-poly(DL)-SH using Bu₃P.

In a typical experiment, 68.6 mg of the disulfide containing block copolymer (M_n (SEC) = 20100 g/mol (\bar{D} = 1.27)) was introduced into a 5 mL round-bottom flask and was solubilized in 5 mL of anhydrous THF. Then, 0.1 mL of tributylphosphine (Bu₃P) (0.4 mmol) was added. The reaction mixture was stirred at room temperature for 0.5 hours, then, a sample was withdrawn for SEC (DMF (0.05 % (w/w) LiBr)) analysis. Finally, the solvent was partially eliminated under vacuum and the resulting cleaved polymer was precipitated in cold methanol (spectrum is shown in annex 8.35).

¹H-NMR (CDCl₃, 400 MHz, TMS, δ ppm): 4.87 (m, CH-OOC- (DL)), 4.39 (br. s, CH₂OOC- (MBL)), 4.19 (l₁, t, ³J = 6.8 Hz, 2H, SCH₂-CH₂O-), 2.75 (l₁, m, 2H, SCH₂-CH₂O-), 2.30 (t, ³J = 7.0 Hz, CH₂COO (DL)), 2.17-2.13 (m, (-CH₂-)_x2 (MBL)), 1.68-1.26 (m, -(CH₂)_n- (DL)), 0.88 (t, ³J = 7.2 Hz, CH₂-CH₃ (DL)).

6.9.2 Acid cleavable block copolymers

6.9.2.1 Cleavage of poly(MBL)-co-poly(DL)-I₂-co-poly(MBL)



Scheme 6.18 Acid cleavage of poly(MBL)-co-poly(DL)-I₂-co-poly(MBL) to poly(MBL)-co-poly(DL)-OH using TFA.

In a typical experiment, 235.0 mg of the acetal containing block copolymer ($M_n(\text{SEC}) = 20600 \text{ g/mol}$ ($\bar{D} = 1.17$)) was introduced into a 50 mL round-bottom flask and was solubilized in 32 mL of THF (0.5 % water). Then, 24.5 μL or 1.25 mL of trifluoroacetic acid (TFA) was added to obtain a 0.01 or 0.5 M solution respectively. The reaction mixture was stirred at room temperature and samples were withdrawn at preset times to follow the progress of the reaction. Each sample was neutralized with solid sodium bicarbonate, filtered, and the solvent eliminated prior to SEC (DMF (0.05 % (w/w) LiBr)) analysis. The polymer was completely cleaved within 24 hours in both cases. Finally, the crude reaction mixture was neutralized with sodium bicarbonate, filtered and the solvent was partially eliminated under vacuum and the resulting cleaved polymer was precipitated in cold methanol.

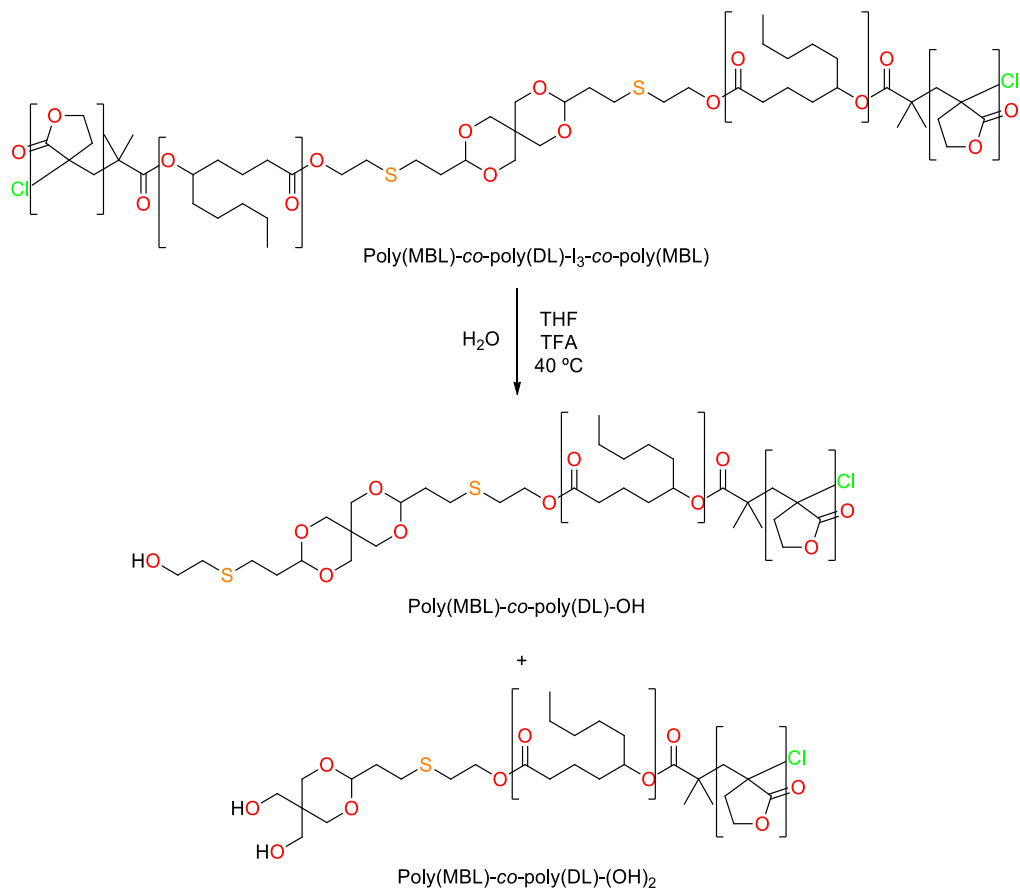
- [TFA] = 0.01 M (Annex 8.36):

$^1\text{H-NMR}$ (CDCl_3 , 400 MHz, TMS, δ ppm): 4.87 (m, CH-OOC- (DL)), 4.38 (br. s, $\text{CH}_2\text{OOC-}$ (MBL)), 4.24 (l₂, t, $^3J = 6.8$ Hz, 2H, $\text{SCH}_2\text{-CH}_2\text{O-}$), 3.75 (l₂, m, 2H, HO- $\text{CH}_2\text{-}$), 2.75 (l₂, t, $^3J = 6.8$ Hz, 2H, $\text{SCH}_2\text{-CH}_2\text{O-}$), 2.70 (l₂, t, $^3J = 7.2$ Hz, 2H, $\text{CH}_2\text{SCH}_2\text{-CH}_2\text{O-}$), 2.30 (t, $^3J = 7.0$ Hz, CH_2COO (DL)), 2.17-2.13 (m, $(\text{-CH}_2\text{-})\times 2$ (MBL)), 1.85 (l₂, m, 2H, HO- $\text{CH}_2\text{CH}_2\text{-}$), 1.68-1.26 (m, $(\text{-CH}_2)_n\text{-}$ (DL)), 0.88 (t, $^3J = 7.2$ Hz, $\text{CH}_2\text{-CH}_3$ (DL)).

- [TFA] = 0.5 M (Annex 8.37):

$^1\text{H-NMR}$ (CDCl_3 , 400 MHz, TMS, δ ppm): 4.87 (m, CH-OOC- (DL)), 4.38 (br. s, $\text{CH}_2\text{OOC-}$ (MBL)), 2.30 (t, $^3J = 7.0$ Hz, CH_2COO (DL)), 2.17-2.13 (m, $(\text{-CH}_2\text{-})\times 2$ (MBL)), 1.68-1.26 (m, $(\text{-CH}_2)_n\text{-}$ (DL)), 0.88 (t, $^3J = 7.2$ Hz, $\text{CH}_2\text{-CH}_3$ (DL)).

6.9.2.2 Cleavage of poly(MBL)-co-poly(DL)-I₃-co-poly(MBL)



Scheme 6.19 Acid cleavage of poly(MBL)-co-poly(DL)-I₃-co-poly(MBL) to poly(MBL)-co-poly(DL)-OH and poly(MBL)-co-poly(DL)-(OH)₂ using [TFA] = 0.5 M at 40 °C.

In a typical experiment, 415.3 mg of the tetraoxaspiro containing block copolymer (M_n (SEC) = 22900 g/mol (\bar{D} = 1.17)) was introduced into a 100 mL round-bottom flask and was solubilized in 37 mL of THF (0.5 % water). Then, 1.47 mL of trifluoroacetic acid (TFA) was added to obtain a 0.5 M solution. The reaction mixture was stirred at 40 °C and samples were withdrawn at preset times to follow the progress of the reaction. Each sample was neutralized with sodium bicarbonate, filtered, and the solvent eliminated prior to SEC (DMF (0.05 % (w/w) LiBr)) analysis. The polymer was completely cleaved within 23 hours. Finally, the crude reaction mixture was neutralized with

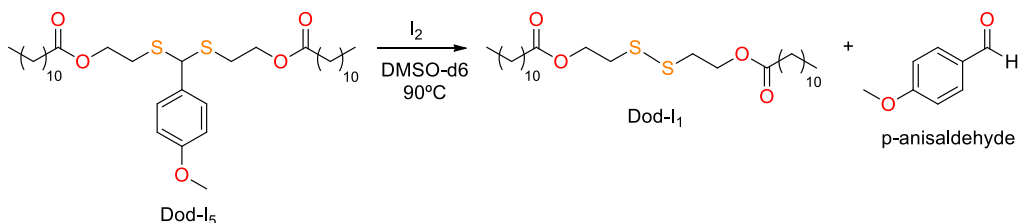
sodium bicarbonate, filtered and the solvent was partially eliminated under vacuum and the resulting cleaved polymer was precipitated in cold methanol (spectrum is shown in annex 8.38).

$^1\text{H-NMR}$ (CDCl_3 , 400 MHz, TMS, δ ppm): 4.87 (m, CH-OOC- (DL)), 4.57 (I_3 , m, O-CH-O), 4.52 (I_3 , m, $\text{H}_{\text{eq.}}$, -OCH₂C-), 4.38 (br. s, CH₂OOC- (MBL)), 4.21 (I_3 , t, $^3J = 6.8$ Hz, SCH₂-CH₂O-), 4.11 (I_3 , s, HO-CH₂-), 3.72 (I_3 , s, HO-CH₂-CH₂-S-), 3.56 (I_3 , m, $\text{H}_{\text{eq.}}$, -OCH₂C-), 3.53 (I_3 , d, $^3J = 12.0$ Hz, $\text{H}_{\text{ax.}}$, -OCH₂C-), 3.34 (I_3 , d, $^3J = 12.0$ Hz, $\text{H}_{\text{ax.}}$, -OCH₂C-), 2.73 (I_3 , t, $^3J = 6.8$ Hz, SCH₂-CH₂O-), 2.63 (I_3 , m, CH₂SCH₂-CH₂O-), 2.30 (t, $^3J = 6.8$ Hz, CH₂COO (DL)), 2.17-2.13 (m, (-CH₂)_x (MBL)), 1.68-1.27 (m, -(CH₂)_n- (DL)), 0.87 (t, $^3J = 7.0$ Hz, CH₂-CH₃ (DL)).

6.9.3 ROS cleavable block copolymers

6.9.3.1 Cleavage of thioacetal model compounds

- Thioacetal deprotection of Dod-I₅ using I₂/DMSO

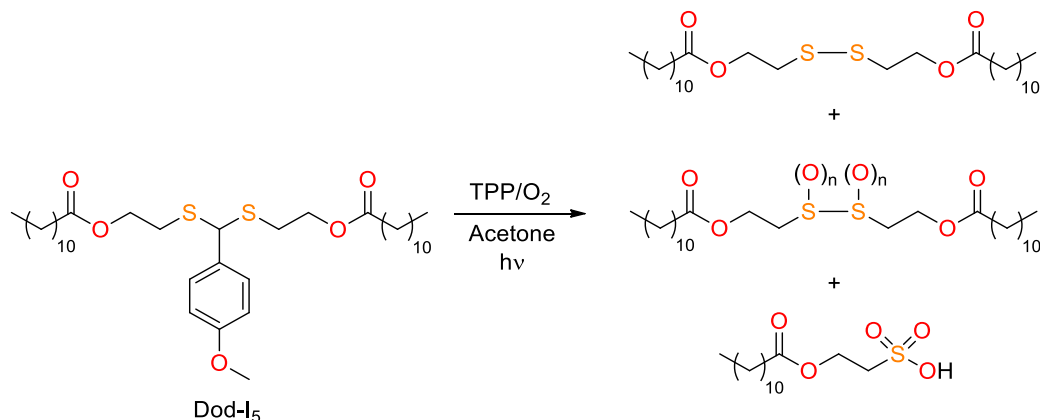


Scheme 6.20 Deprotection of Dod-I₅ with I₂ in DMSO at 90 °C.

In rubber septa sealed tubes, about 50 mg of Dod-I₅ was dissolved in 2 mL of DMSO-d₆ in presence of iodine (1%) and the mixture heated at 90 °C. Samples were withdrawn at pre-set times and analyzed by $^1\text{H-NMR}$ spectroscopy. After 1h, the remaining reaction mixture was brought to room temperature, the product precipitate in DMSO at room temperature. The crude product was recovered by filtration and purified by recrystallization in methanol (spectrum is shown in annex 8.39).

$^1\text{H-NMR}$ (CDCl_3 , 400 MHz, TMS, δ ppm): 4.33 (t, $^3J = 6.4$ Hz, 4H, $\text{SCH}_2\text{-CH}_2\text{OCO}$), 2.92 (t, $^3J = 6.4$ Hz, 4H, $\text{SCH}_2\text{-CH}_2\text{OCO}$), 2.32 (t, $^3J = 7.6$ Hz, 4H, $\text{OOC-CH}_2\text{-}$), 2.32 (quint, $^3J = 7.2$ Hz, 4H, $\text{OOC-CH}_2\text{CH}_2$), 1.32-1.25 (br. s, 32 H, $-\text{CH}_2\text{-}$ dodecanoyl), 0.88 (t, $^3J = 6.4$ Hz, 6H, CH_3)

- Homogeneous photolysis of Dod-I₅ with TPP/O₂

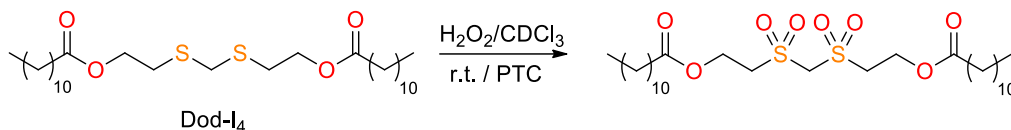


Scheme 6.21 Cleavage of Dod-I₅ under photolytic conditions using TPP/O₂/hv.

In a 50 ml cylindrical flask with a Teflon-coated magnetic stirrer, 80 mg of the thioacetal Dod-I₅ were dissolved in 15 mL of a 10⁻⁵ M solution of meso-tetraphenylporphyrin (TPP) in acetone. A gentle oxygen stream was bubbled throughout the reaction mixture while the solution was irradiated. Samples were withdrawn at pre-set times, evaporated to dryness, and analyzed by $^1\text{H-NMR}$ spectroscopy (spectrum is shown in annex 8.40).

$^1\text{H-NMR}$ (CDCl_3 , 400 MHz, TMS, δ ppm): 4.43 (t, $^3J = 5.2$ Hz, 4H, $\text{O}_2\text{S-CH}_2\text{CH}_2\text{-O}$), 3.29 (t, $^3J = 5.2$ Hz, 4H, $\text{O}_2\text{S-CH}_2\text{CH}_2\text{-O}$), 2.30 (t, $^3J = 7.6$ Hz, 4H, $\text{OOC-CH}_2\text{-}$), 1.64 (quint, $^3J = 7.2$ Hz, 4H, $\text{OOC-CH}_2\text{CH}_2$), 1.32-1.25 (br. s, 32 H, $-\text{CH}_2\text{-}$ dodecanoyl), 0.88 (t, $^3J = 6.4$ Hz, 6H, CH_3)

- Oxidation of Dod-I₄ with H₂O₂



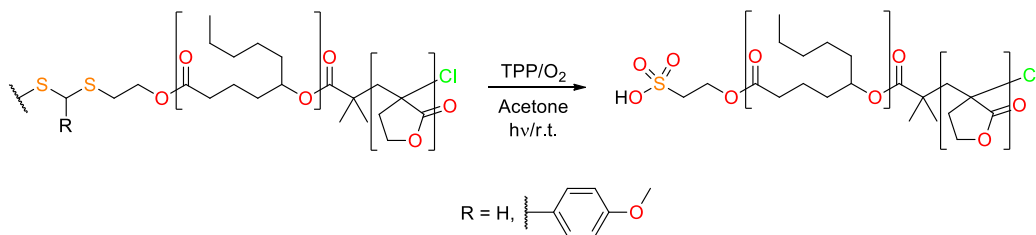
Scheme 6.22 Oxidative cleavage of Dod-I₄ with H₂O₂ under PTC.

In a 50 mL round bottom flask about 100 mg of Dod-I₄ were dissolved in 5 mL of CDCl₃. 5 mL of 50% H₂O₂ containing 1% methytrioctylammonium tetrakis (diperoxotungsto)-phosphate were added. The mixture was vigorously stirred at room temperature and samples were withdrawn at preset times, washed with water, dried with anhydrous magnesium sulfate, and finally analyzed by ¹H-NMR spectroscopy (spectrum is shown in annex 8.41).

¹H-NMR (CDCl₃, 400 MHz, TMS, δ ppm): 4.70 (s, 2H, O₂S-CH₂-SO₂), 4.57 (t, ³J = 5.2 Hz, 4H, O₂S-CH₂CH₂-O), 3.72 (t, ³J = 5.2 Hz, 4H, O₂S-CH₂CH₂-O), 2.37 (t, ³J = 7.6 Hz, 4H, OOC-CH₂-), 1.64 (quint, ³J = 7.2 Hz, 4H, OOC-CH₂CH₂), 1.32-1.25 (br. s, 32 H, -CH₂-dodecanoyl), 0.88 (t, ³J = 6.4 Hz, 6H, CH₃).

6.9.3.2 Cleavage of thioacetal containing block copolymer

- Homogeneous system:

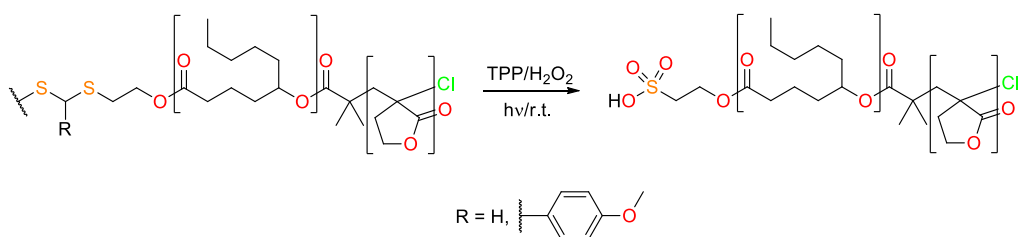


Scheme 6.23 Photolytic cleavage of thioacetal containing block copolymers.

About 100 mg of the thioacetal containing block copolymer (M_n (SEC) = 20.000 g/mol (Đ = 1.18) and M_n (SEC) = 19.000 g/mol (Đ = 1.16) for I₄ and I₅ block copolymers respectively) were placed in a 50 mL cylindrical flask equipped with a Teflon-coated

magnetic stirrer. Then, 20 mL of a 10^{-5} M solution of meso-tetraphenylporphyrin (TPP) in acetone were added. Once the polymer was completely solubilized, a gentle oxygen stream was bubbled throughout the reaction mixture while the solution was irradiated. Samples were withdrawn at pre-set times to follow the reaction progress through SEC analysis. After 48 h a new amount of TPP was added and the irradiation and monitoring were continued.

- Heterogeneous system:



Scheme 6.24 Thioacetal containing block copolymers degradation under oxidation media.

About 150 mg of the thioacetal containing block copolymer (M_n (SEC) = 20.000 g/mol (\bar{D} = 1.18) and M_n (SEC) = 19.000 g/mol (\bar{D} = 1.16) for I_4 and I_5 block copolymers respectively) were solubilized in 30 mL of a 10^{-5} M solution of TPP in acetone. The polymer solution was split into three 25 mL cylindrical flask and the solvent evaporated under vacuum to form thin films. Then, 15 mL of a 15% hydrogen peroxide in phosphate buffer solution (pH 7.4) was added to each flask which were irradiated. After pre-set times (3h and 6h) the aqueous phase was removed and the polymer dissolved in chloroform, dried with anhydrous magnesium sulphate, filtered, and concentrated under vacuum. Two samples of each polymer (I_4 and I_5 block copolymers) were used for SEC measurements. The third sample was precipitated over cold methanol, recovered by centrifugation, dried under vacuum, and characterized by $^1\text{H-NMR}$.

- Poly(MBL)-*co*-poly(DL)-I₄-*co*-poly(MBL) (Annex 8.42):

¹H-NMR (CDCl₃, 400 MHz, TMS, δ ppm): 4.87 (m, CH-OOC- (DL)), 4.38 (br. s, CH₂OOC- (MBL)), 4.22 (t, ³J = 6.4 Hz, SCH₂-CH₂O-), 3.67 (s, H₃C-O₃S-CH₂), 3.25 (t, ³J = 6.4 Hz, O₃S-CH₂), 2.30 (t, ³J = 6.8 Hz, CH₂COO (DL)), 2.17-2.13 (m, (-CH₂)_{x2} (MBL)), 1.68-1.27 (m, -(CH₂)_n- (DL)), 0.87 (t, ³J = 7.0 Hz, CH₂-CH₃ (DL)).

- Poly(MBL)-*co*-poly(DL)-I₅-*co*-poly(MBL) (Annex 8.43):

¹H-NMR (CDCl₃, 400 MHz, TMS, δ ppm): 4.87 (m, CH-OOC- (DL)), 4.38 (br. s, CH₂OOC- (MBL)), 2.30 (t, ³J = 6.8 Hz, CH₂COO (DL)), 2.17-2.13 (m, (-CH₂)_{x2} (MBL)), 1.68-1.27 (m, -(CH₂)_n- (DL)), 0.87 (t, ³J = 7.0 Hz, CH₂-CH₃ (DL)).

- ¹ Hurd, C. D.; Pollack, M. A. The rearrangement of vinyl allyl ethers. *J. Am. Chem. Soc.* **1938**, *60*, 1905-1911.
- ² LLuch, C.; Ronda, J. C.; Galià, M.; LLigadas, G.; Cádiz, V. Rapid approach to biobased telechelics through two one-pot thiol-ene click reactions. *Biomacromolecules* **2010**, *11*, 1646-1653.
- ³ Lingier, S.; Espeel, P.; Suarez, S. S.; Türünç, O.; De Wildeman, S.; Du Prez, F. E. Renewable thermoplastic polyurethanes containing rigid spiroacetal moieties. *Eur. Polym. J.* **2015**, *70*, 232-239.
- ⁴ Wróblewska, A. A.; Lingier, S.; Noordijk, J.; Du Prez, F. E.; De Wildeman, S. M. A.; Bernaerts, K. V. Polyamides based on a partially bio-based spirodiamine. *Eur. Polym. J.* **2017**, *96*, 221-231.
- ⁵ Kaushik, M. P.; Rana, H. Facile one-step synthesis of dithiaalkanediols. *Org. Prep. Proced. Int.* **2005**, *37*, 268-272.
- ⁶ Gasson, E. J.; McCombie, H.; Williams, H.; Woodward, F. N. New organic Sulphur vesicants. Part IV. 1: 2-Di-(2-chloroethylthio)ethane and its analogues. *J. Chem. Soc.* **1948**, 44-46.
- ⁷ Laskar, R. A.; Begum, N. A.; Mir, M. H.; Rohman, Md. R.; Khan, A. T. Nickel(II) chloride hexahydrate catalyzed reaction of aromatic aldehydes with 2-mercaptoethanol: formation of supramolecular helical assemblage of the product. *Tetrahedron Lett.* **2013**, *54*, 5839-5844.
- ⁸ Zhou, J.; Schmidt, A. M.; Ritter, H. Bicomponent Transparent Polyester Network with Shape Memory Effect. *Macromolecules* **2010**, *43*, 939-942.
- ⁹ Hutchinson, C. R. A synthesis of tulipalin A and B and the acylglucoside, tuliposide A, fungitoxic agents from *tulipa gesneriana*. Carbon-13 nuclear magnetic resonance analysis of anomeric configurations in acylglucosides. *J. Org. Chem.* **1974**, *39*, 1854-1858.
- ¹⁰ Murray, A. W.; Reid, R. G. Convenient synthesis of α -epoxylactones (4-Oxo-1,5-dioxaspiro[2.4]heptanes and -[2.5]octanes). *Synthesis* **1985**, *1*, 35-38.
- ¹¹ Jenkins, S. M.; Wadsworth, H. J.; Bromidge, S.; Orlek, B. S.; Wyman, P. A.; Riley, G. J.; Hawkins, J. Substituent variation in azabicyclic triazole- and tetrazole-based muscarinic receptor ligands. *J. Med. Chem.* **1992**, *35*, 2392-2406.
- ¹² Gazivoda, T.; Raić-Malić, S.; Hergold-Brundić, A.; Cetina, M. Synthesis and structural characterization of the 5-(2-haloethyl)pyrimidines – Hydrogen-bonded chains in alpha-(1-carbamyliminomethylene)-gamma-butyrolactone. *Molecules* **2008**, *13*, 2786-2795.
- ¹³ Zhu, A.; Wang, Z.; Xie, M.; Zhang, Y. Synthesis of imidazole end-capped poly(n-butyl methacrylate)s via atom transfer radical polymerization with a new functional initiator containing imidazolium group. *e-Polymers*, **2007**, 009.
- ¹⁴ He, T.; Adams, D. J.; Butler, M. F.; Yeoh, C. T.; Cooper, A. I.; Rannard, S. P. Direct synthesis of anisotropic polymer nanoparticles. *Angew. Chem. Int. Ed.* **2007**, *46*, 9243-9247.
- ¹⁵ Weber, A. E.; Steiner, M. G.; Krieter, P. A.; Colletti, A. E.; Tata, J. R.; Halgren, T. A.; Ball, R. G.; Doyle, J. J.; Schorn, T. W.; Stearns, R. A.; Miller, R. R.; Siegl, P. K. S.; Greenlee, W. J.; Patchett, A. A. Highly potent, orally active diester macrocyclic human renin inhibitors. *J. Med. Chem.* **1992**, *35*, 3755-3773.

Chapter 7

General conclusions

UNIVERSITAT ROVIRA I VIRGILI
STIMULI-RESPONSIVE CALIX[4]PYRROLE AND CALIX[4]ARENE BASED RECEPTORS: FROM UNIMOLECULAR
TO DIMERIC STRUCTURES

Pedro Miguel Mendonça Ferreira

7 General conclusions

This thesis intends to be a contribution to the feasibility of biobased materials for the preparation of ABA block copolymer-based materials with potential applications as thermoplastic elastomers. The general conclusions of this research are summarized as follows:

- ABA triblock copolymers containing different central stimuli cleavable groups have been successfully prepared from bio-based δ -decalactone (DL) and α -methylene- γ -butyrolactone (MBL) using the ROP / end-group activation / ATRP chain extension approach.
- ROP of DL with difunctional diol initiators using TBD as catalyst at room temperature, proceeds with high control over the molecular weight and the polymer architecture yielding telechelic poly(DL) diols with the targeted molecular weight.
- BriB-Im has proved to be an efficient acylating agent in the poly(DL)-diol end group esterification. By using this reagent, a one-pot two-step protocol has been established which results in high end-group fidelity skipping the conventional isolation and purification steps.
- The one-pot two-step, polymerization of DL and modification with BriB-Im, allowed to prepare different ATRP macroinitiators containing a central cleavable group in high yields and high chain end fidelity as inferred by the MALDI-TOF analysis.
- trans-2-[3-(4-tert-butylphenyl)-2-methyl-2-propenylidene]malononitrile (DCTB) has been proved as an adequate matrix for the MALDI-TOF analysis of the poly(DL)-diols and the corresponding BriB esters with molecular weight around 20000 g/mol. Polymers with disulfide linkages had been found to decompose under ionization conditions.

- ATRP of MBL targeting relatively high MBL conversions in order to maximize monomer usage have been tested with monofunctional and difunctional model initiators. Under the tested conditions, good molecular weight control and reasonably high initiation efficiencies were achieved up to 80% conversion.
- The use of the halogen exchange technique in the ATRP of MBL, allowed to control the molecular weight and the polydispersity of the resulting polymers but entails the formation of 2-chloroisobutiryl groups that prevents full extend of the initiation.
- ATRP chain extension with MBL has been successfully applied to the different macroinitiators. Targeting 40% MBL conversion, poly(MBL)-poly(DL)-poly(MBL) block copolymers with an adequate balance of the hard MBL block ($\approx 20\%$ w/w) were achieved in all cases.
- Detailed structural characterization by ^1H and ^{13}C NMR of poly(DL)-OH, poly(DL)-BriB, poly(MBL) and poly(MBL)-poly(DL)-poly(MBL) homo- and block copolymers allowed to confirm their structure and the presence of small percentages of poly(DL)-poly(MBL) in the case of the poly(MBL)-poly(DL)-poly(MBL) block copolymers.
- Thermal and thermomechanical characterization of poly(MBL)-poly(DL)-poly(MBL) initiated with 1,8-octanediol as representative ABA copolymer, confirmed its thermoplastic elastomeric behavior with a service temperature range of $200\text{ }^\circ\text{C}$ (-36 to $164\text{ }^\circ\text{C}$).
- Reductive and acidic cleavage of poly(MBL)-poly(DL)-poly(MBL) containing disulfide and acetal groups proceeds under mild conditions yielding poly(DL)-poly(MBL) AB block copolymers with the expected thiol and hydroxyl end groups.
- Cleavage of poly(MBL)-poly(DL)-poly(MBL) containing tetraoxospiroacetal group requires stronger acidic conditions and occurs mainly by hydrolysis of the β -thioethyl ester linking groups.

- Photooxidative conditions in presence of TTP as sensitizer using either O₂ or H₂O₂ as oxygen source, lead to almost complete cleavage of poly(MBL)-poly(DL)-poly(MBL) containing thioacetal groups. The concomitant formation of intermediate disulfide compounds and their oxidized derivatives seem to prevent complete cleavage in the case of the methylene thioacetal.

UNIVERSITAT ROVIRA I VIRGILI
STIMULI-RESPONSIVE CALIX[4]PYRROLE AND CALIX[4]ARENE BASED RECEPTORS: FROM UNIMOLECULAR
TO DIMERIC STRUCTURES

Pedro Miguel Mendonça Ferreira

Annex

UNIVERSITAT ROVIRA I VIRGILI
STIMULI-RESPONSIVE CALIX[4]PYRROLE AND CALIX[4]ARENE BASED RECEPTORS: FROM UNIMOLECULAR
TO DIMERIC STRUCTURES

Pedro Miguel Mendonça Ferreira

8 Annex

8.1 Acetaldehyde diallylacetal

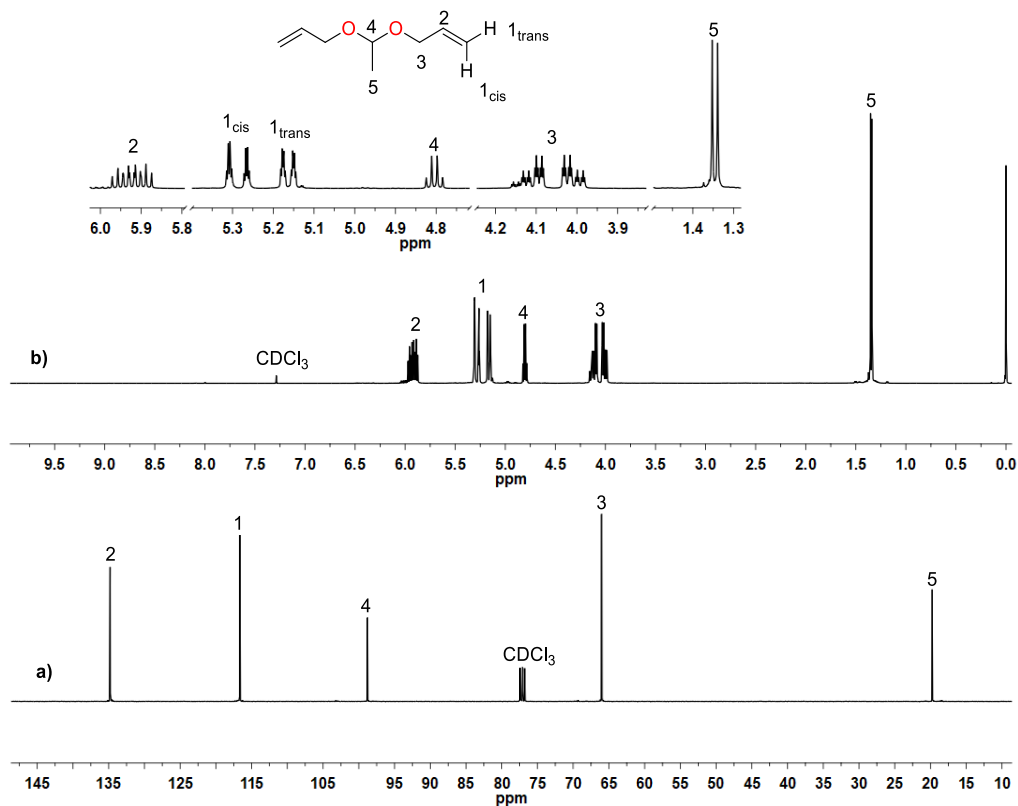


Figure 8.1 (a) ¹³C-NMR and (b) ¹H-NMR spectra of acetaldehyde diallylacetal in CDCl₃.

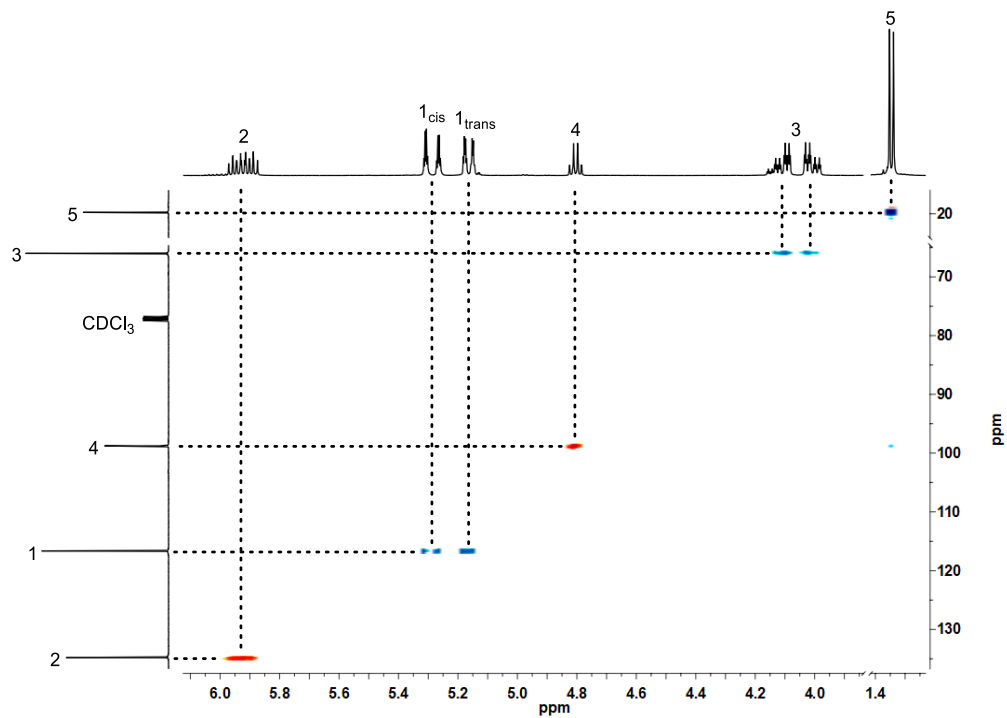


Figure 8.2 HSQC spectrum of acetaldehyde diallylacetal in CDCl₃.

8.2 1,1-Bis-[3-(2-hydroxyethyl)thio]propoxy]ethane (I_2)

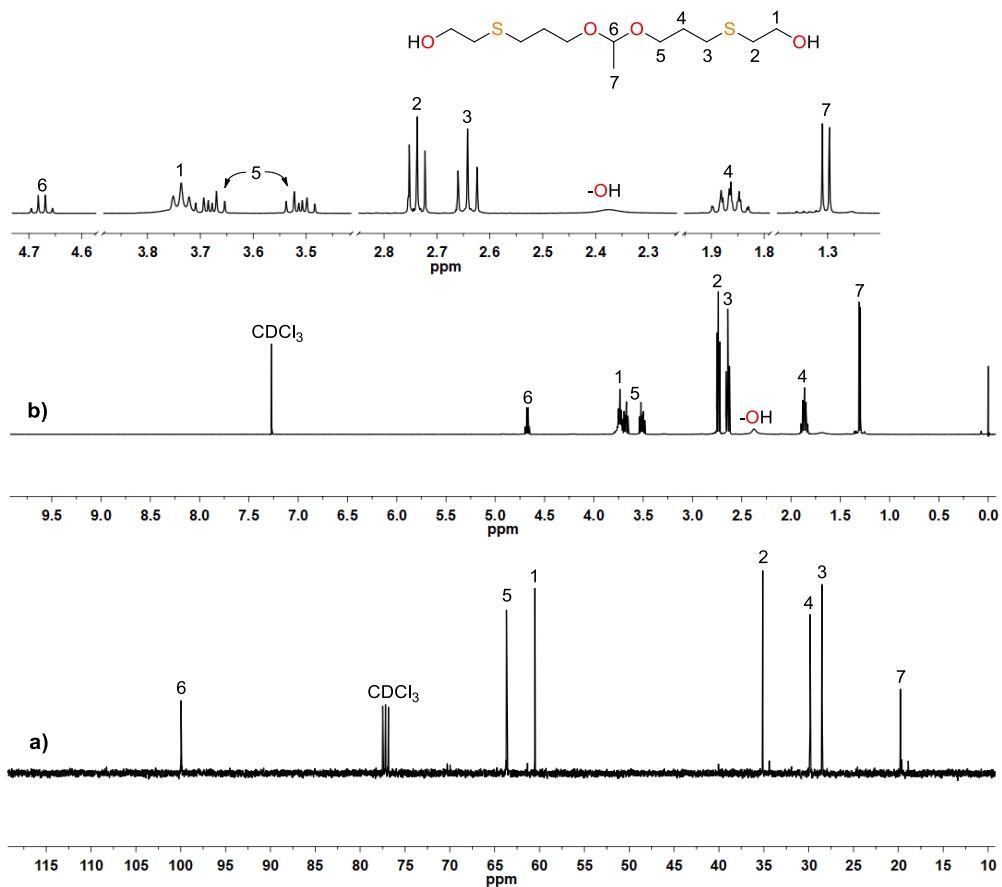


Figure 8.3 (a) ^{13}C -NMR and (b) ^1H -NMR spectra of I_2 in CDCl_3 .

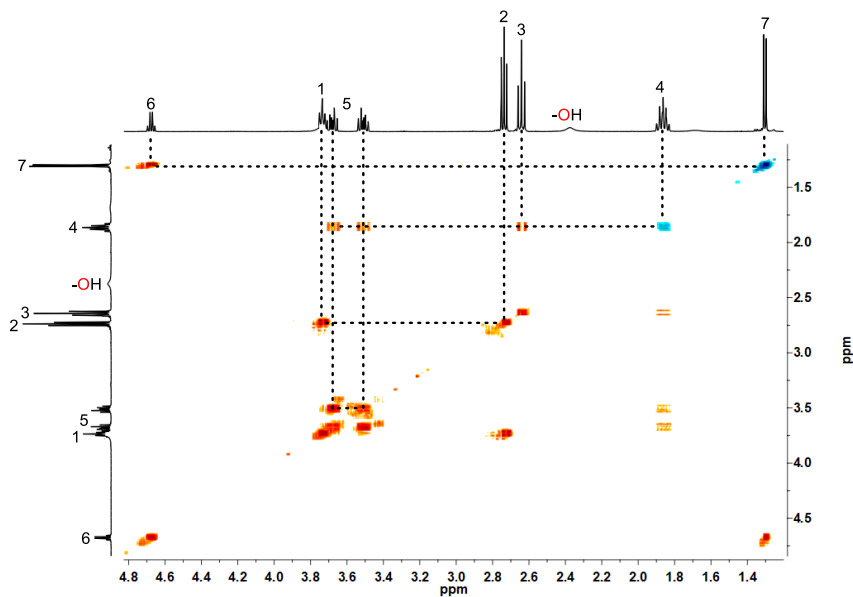


Figure 8.4 COSY spectrum of I_2 in $CDCl_3$.

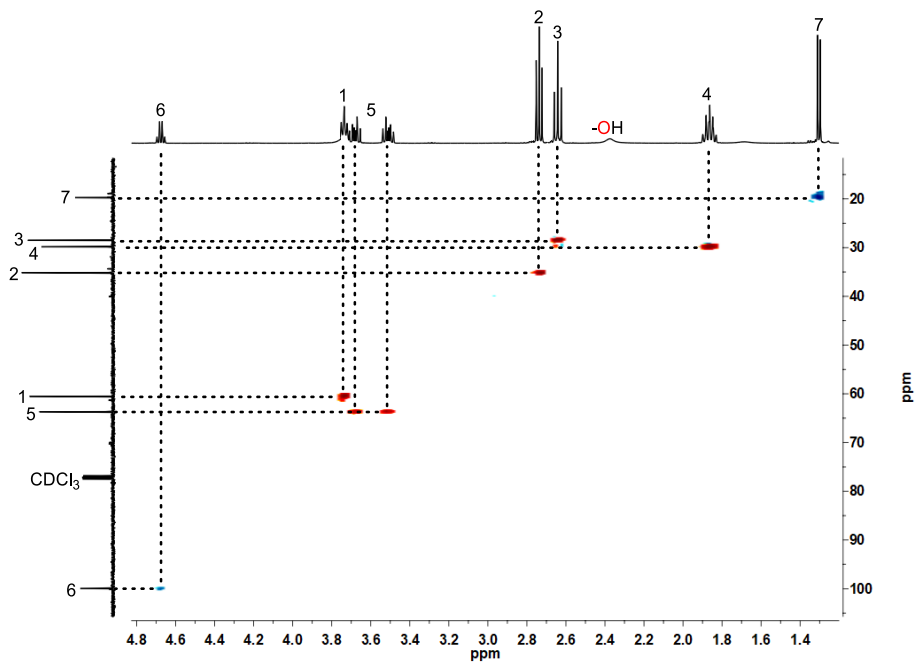


Figure 8.5 HSQC spectrum of I_2 in $CDCl_3$.

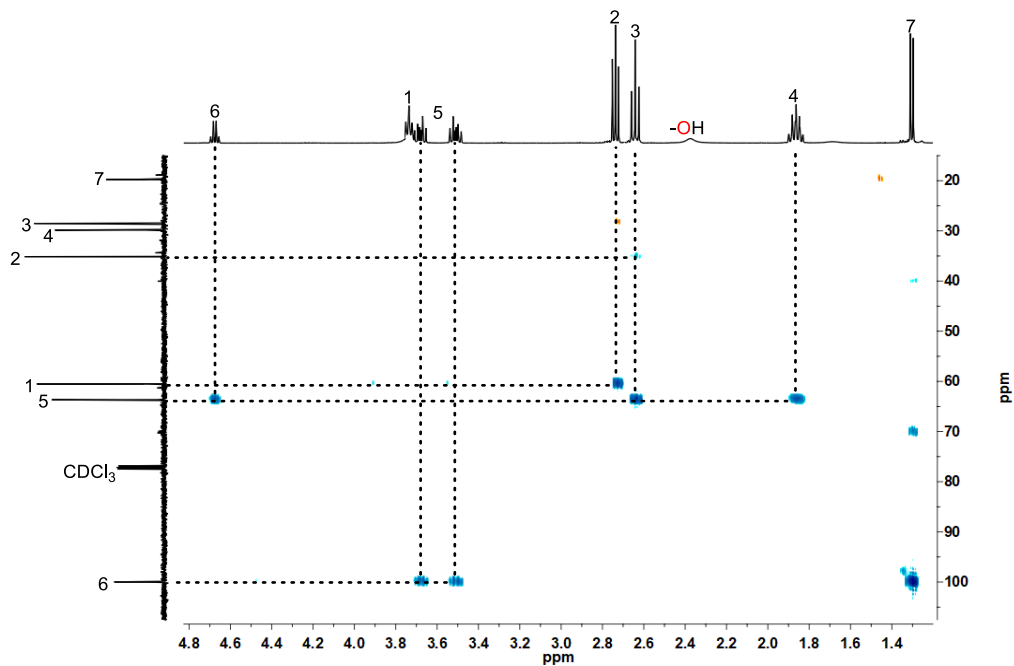


Figure 8.6 HMBC spectrum of 12 in CDCl₃.

8.3 3,9-Bis-[2-(ethylthio)ethanol]- 2,4,8,10-tetraoxaspiro-[5.5]undecane (**I₃**)

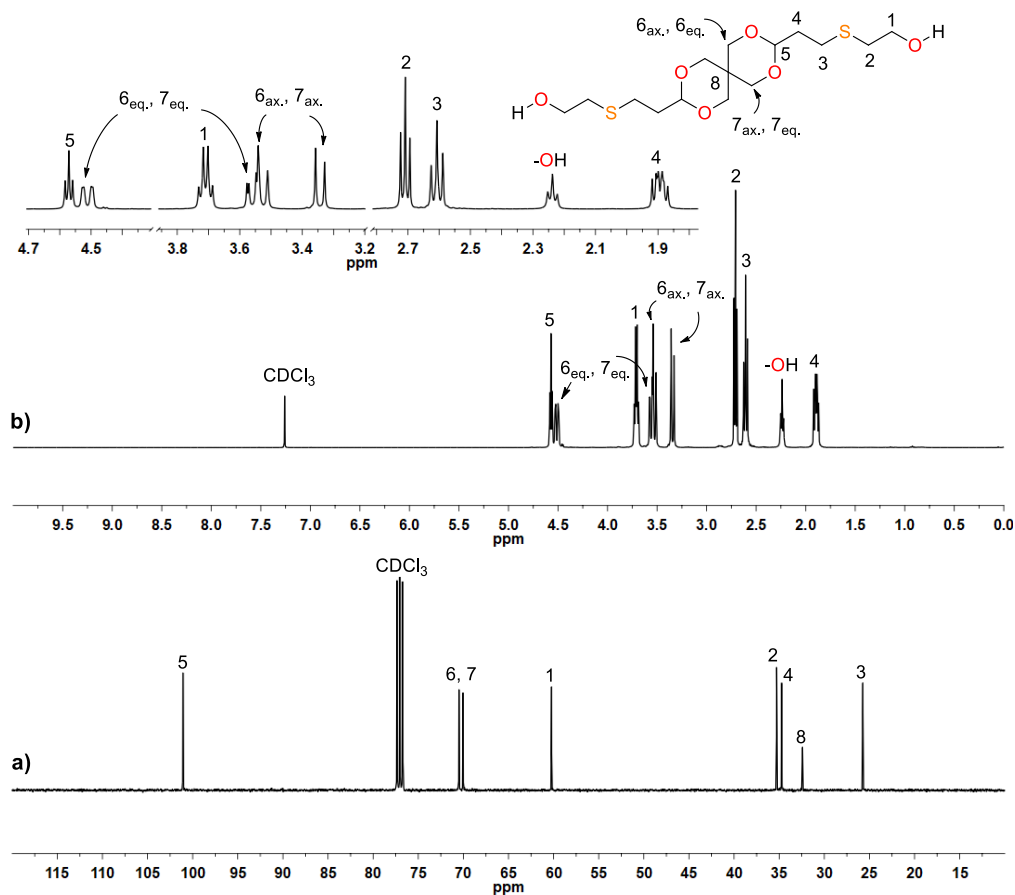


Figure 8.7 (a) ^{13}C -NMR and (b) ^1H -NMR spectra of **I₃** in CDCl_3 .

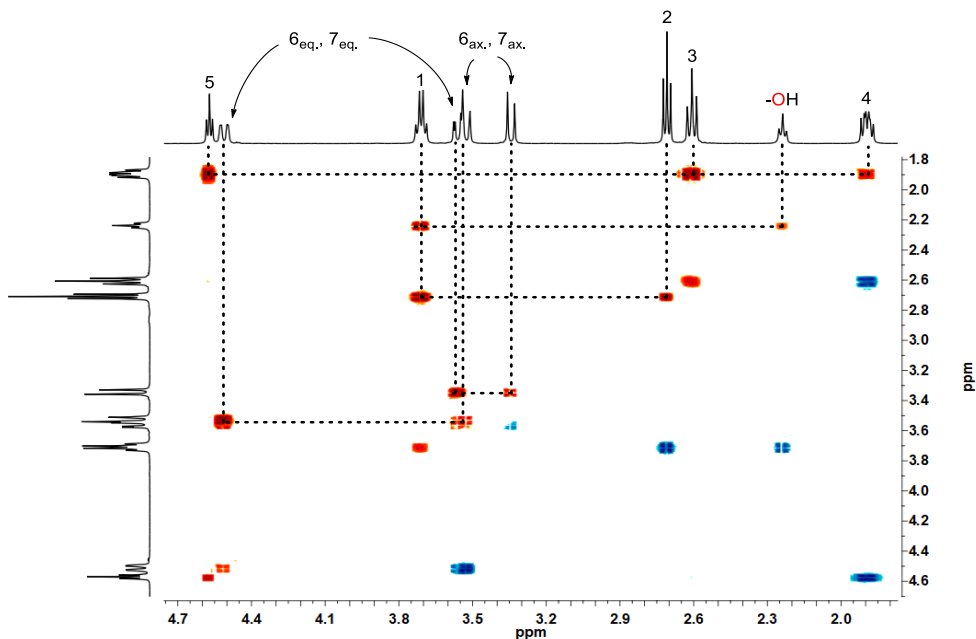


Figure 8.8 COSY spectrum of I_3 in $CDCl_3$.

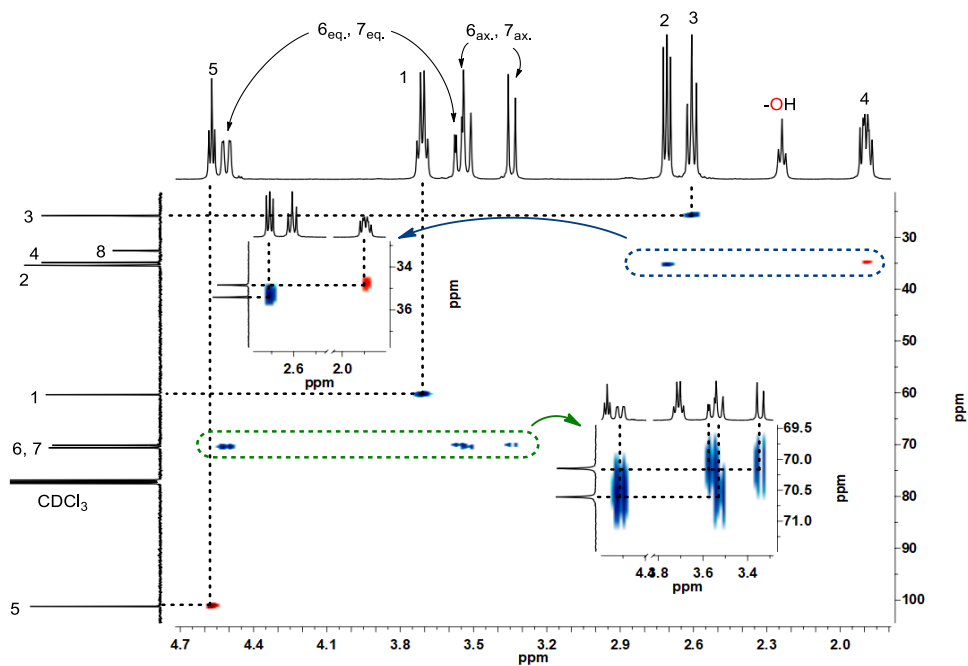


Figure 8.9 HSQC spectrum of I_3 in $CDCl_3$.

8.4 Bis-((2-hydroxyethyl)thio)methane (I_4)

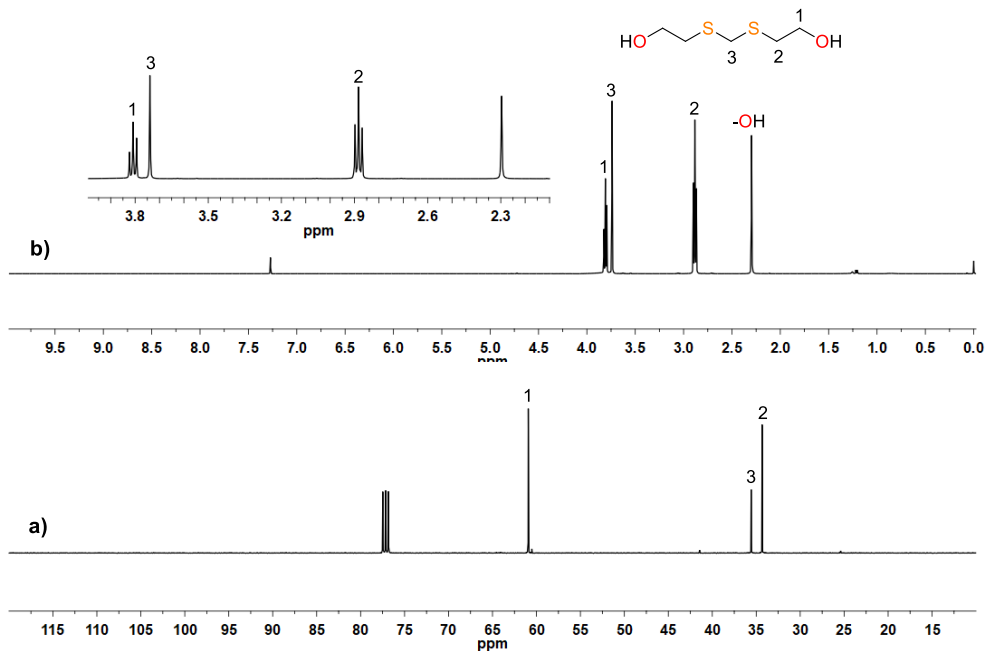


Figure 8.10 (a) ^{13}C -NMR and (b) ^1H -NMR spectra of I_4 in CDCl_3 .

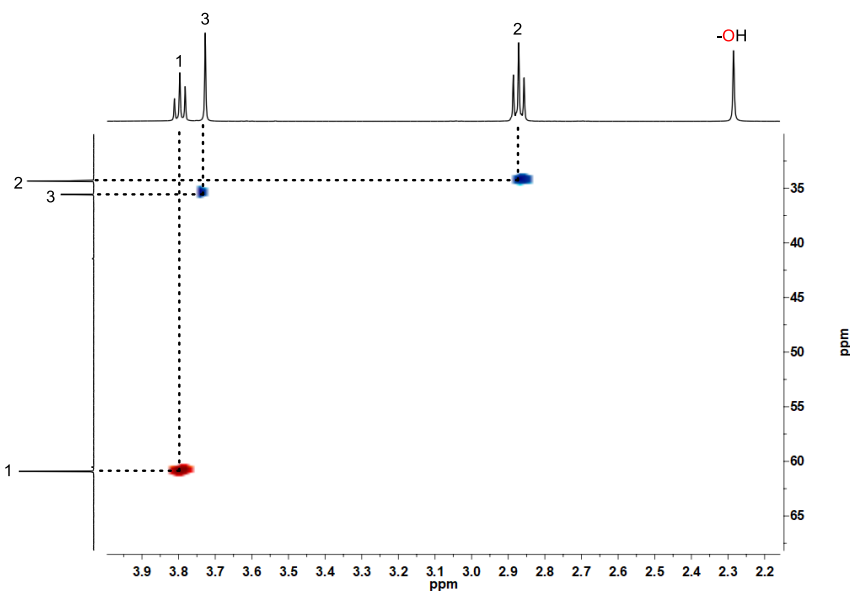


Figure 8.11 HSQC spectrum of I_4 in CDCl_3 .

8.5 (4-Methoxyphenyl)-bis-[(2-hydroxyethyl)thio]methane (I_5)

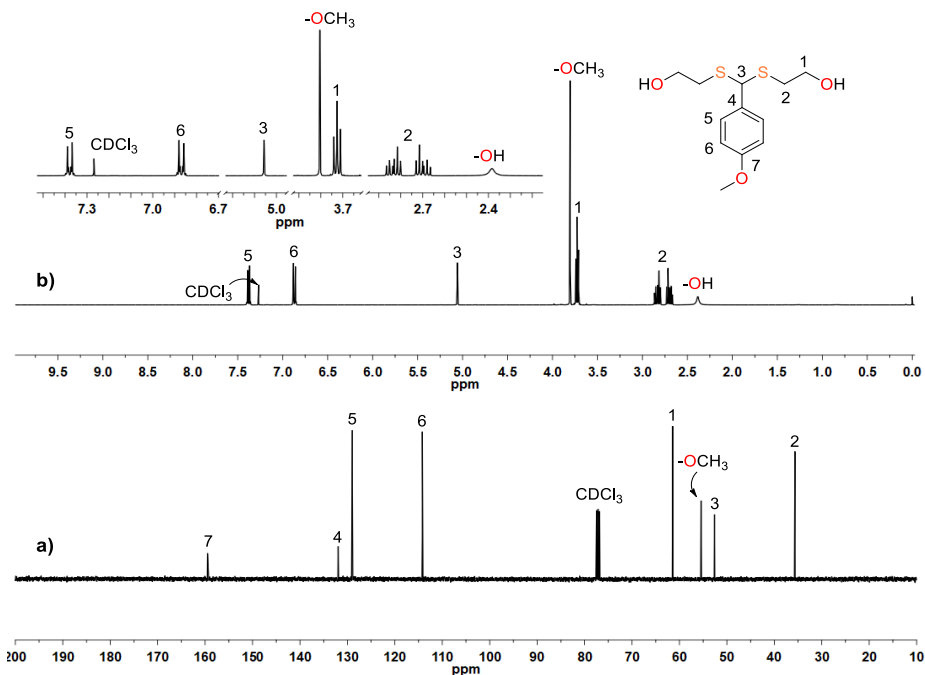


Figure 8.12 (a) ^{13}C -NMR and (b) ^1H -NMR spectra of I_5 in CDCl_3 .

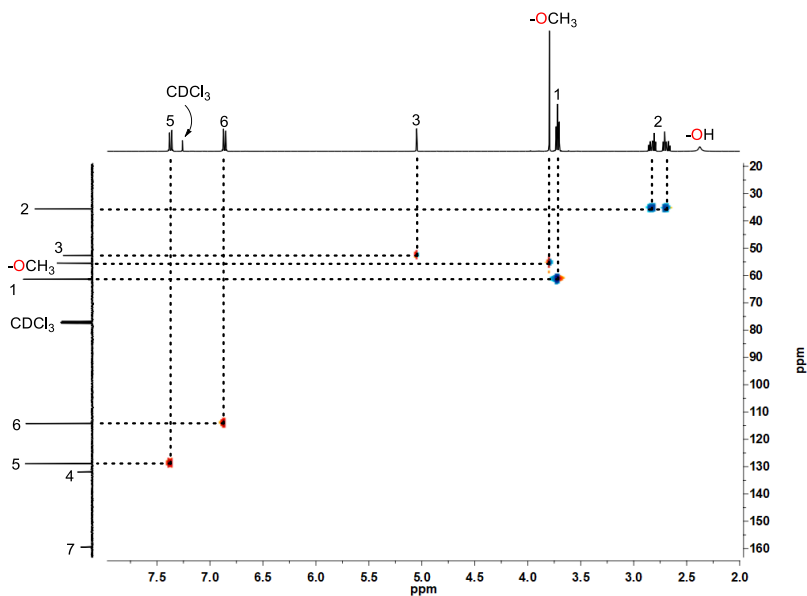


Figure 8.13 HSQC spectrum of I_5 in CDCl_3 .

8.6 α -Methylene- γ -butyrolactone (MBL)

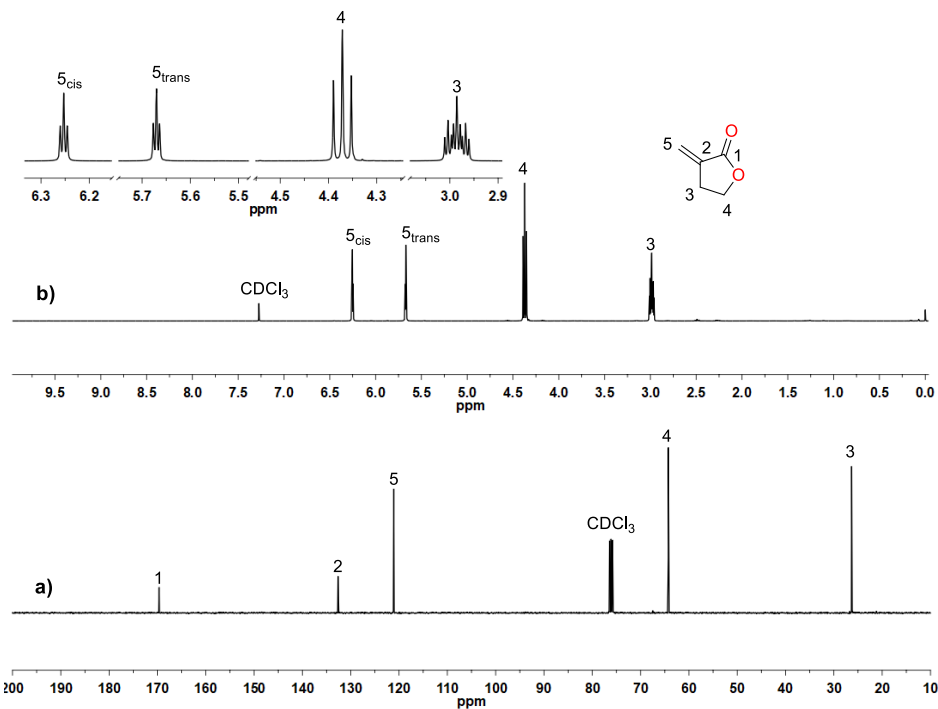


Figure 8.14 (a) ^{13}C -NMR and (b) ^1H -NMR spectra of MBL in CDCl_3 .

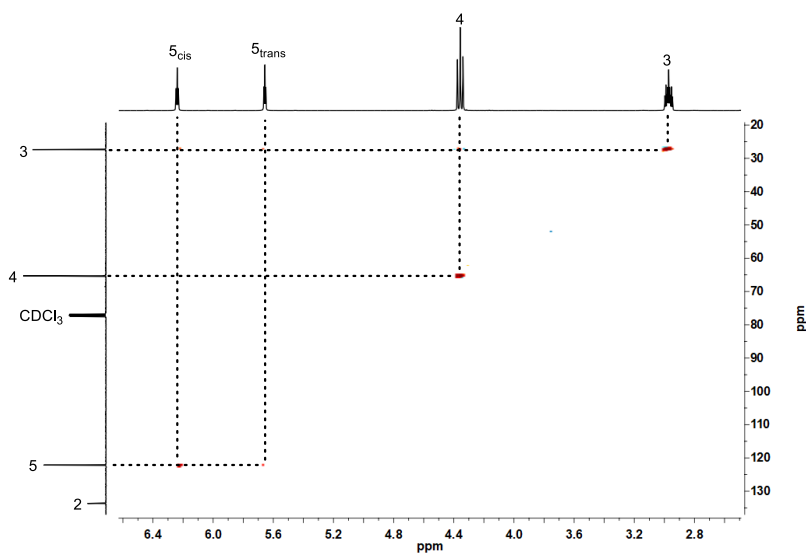


Figure 8.15 HSQC spectrum of MBL in CDCl_3 .

8.7 N-(2-bromoisobutyryl)imidazole (BriB-Im)

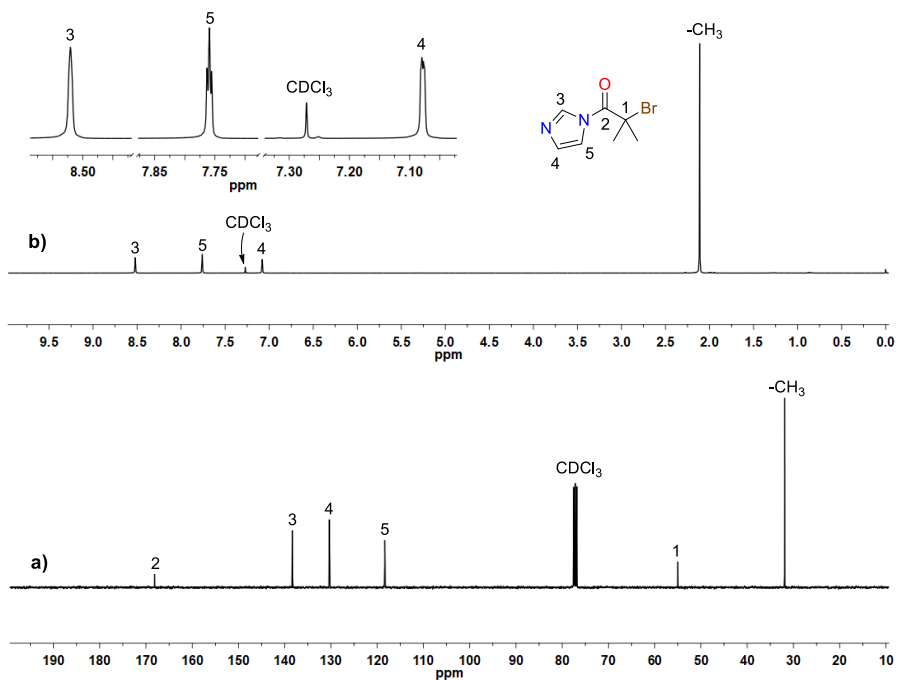


Figure 8.16 (a) ^{13}C -NMR and (b) ^1H -NMR spectra of BriB-Im in CDCl_3 .

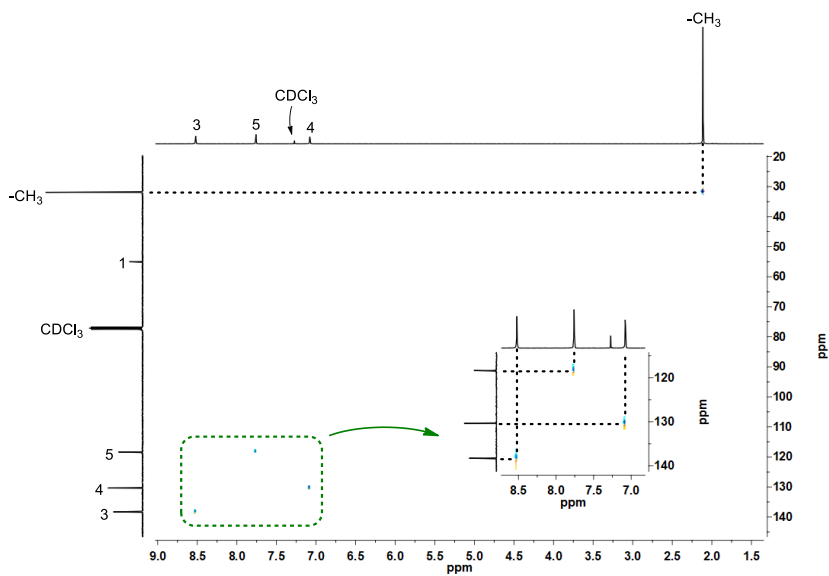


Figure 8.17 HSQC spectrum of BriB-Im in CDCl_3 .

8.8 1,4-Phenylenebis(methylene)-bis(2-bromoisobutyrate) (**I₆**)

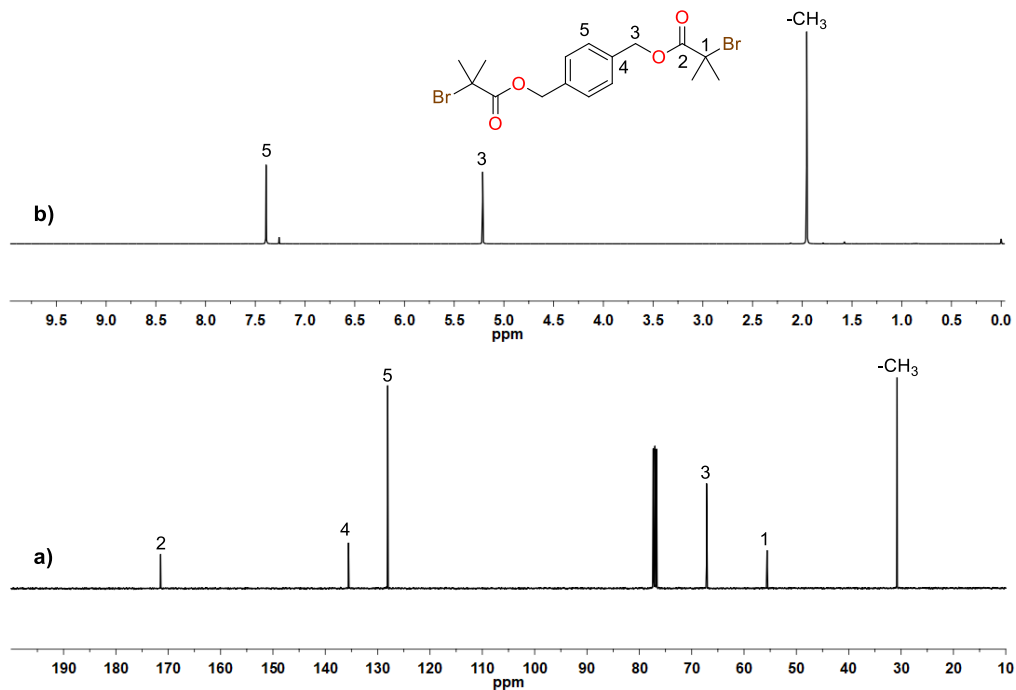


Figure 8.18 (a) ¹³C-NMR and (b) ¹H-NMR spectra of **I₆** in CDCl₃.

8.9 Bis(DL)_{1,6}-Hex diol

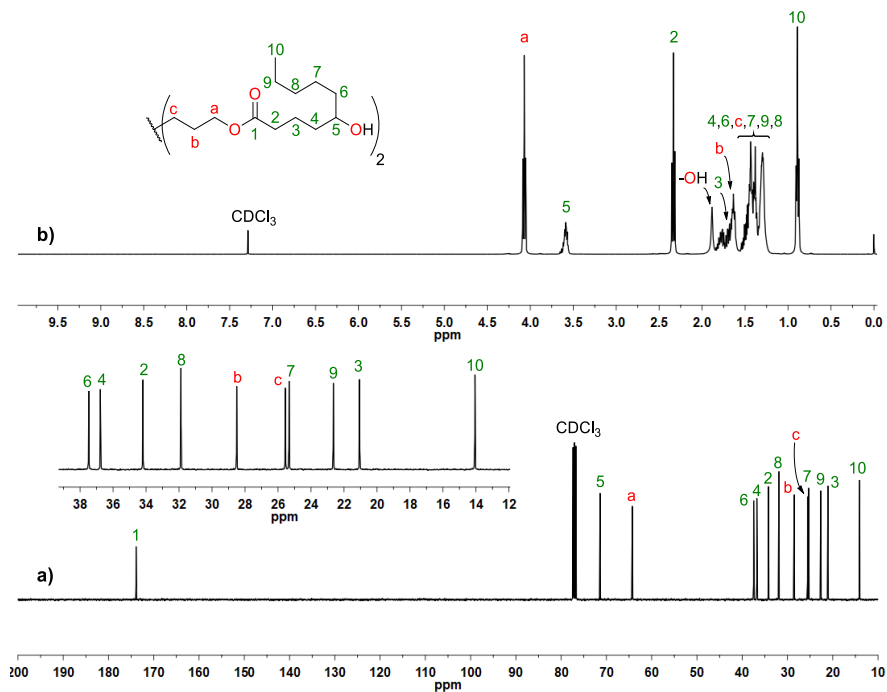


Figure 8.19 (a) ¹³C-NMR and (b) ¹H-NMR spectra of bis(DL)_{1,6}-Hex diol in CDCl₃.

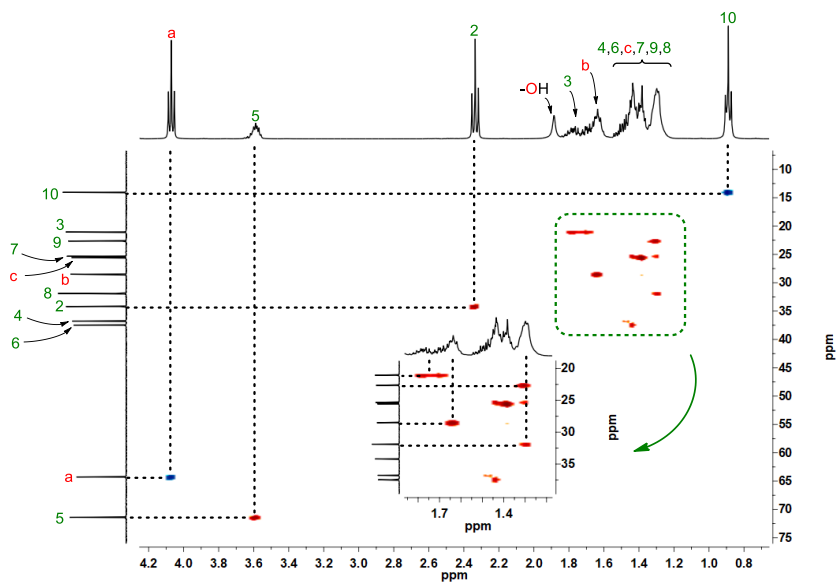


Figure 8.20 HSQC spectrum of bis(DL)_{1,6}-Hex diol in CDCl₃.

8.10 2,2'-Disulfanediyl diethanol didodecanoate (Dod-I₁)

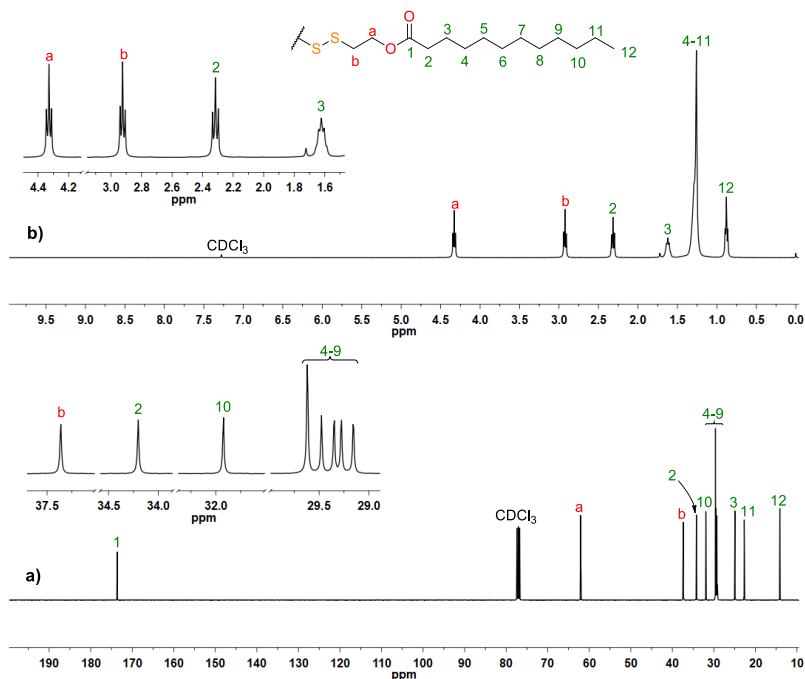


Figure 8.21 (a) ^{13}C -NMR and (b) ^1H -NMR spectra of Dod-I₁ in CDCl_3 .

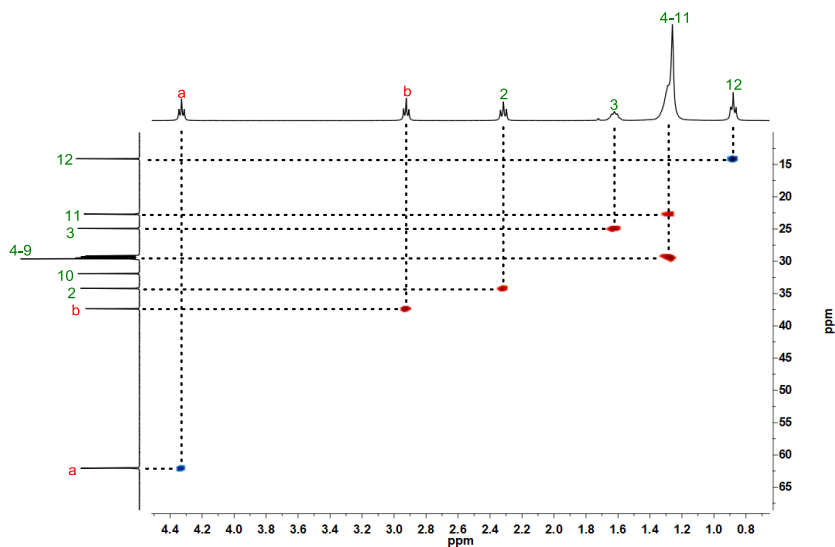


Figure 8.22 HSQC spectrum of Dod-I₁ in CDCl_3 .

8.11 Bis-[(2-ethylthio)dodecanoate)methane (Dod-I₄)

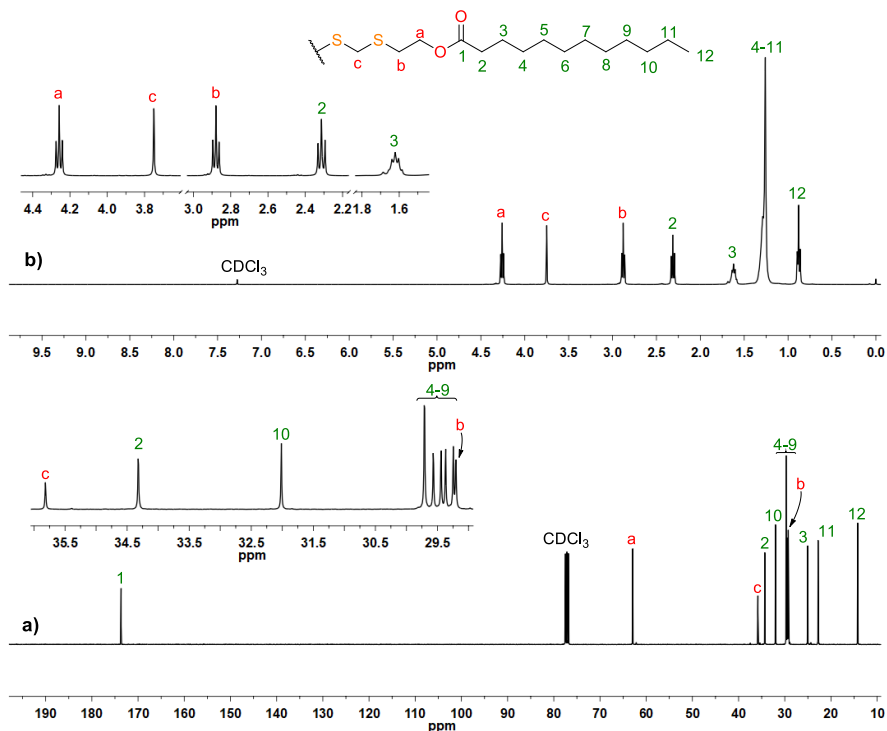


Figure 8.23 (a) ¹³C-NMR and (b) ¹H-NMR spectra of Dod-I₄ in CDCl₃.

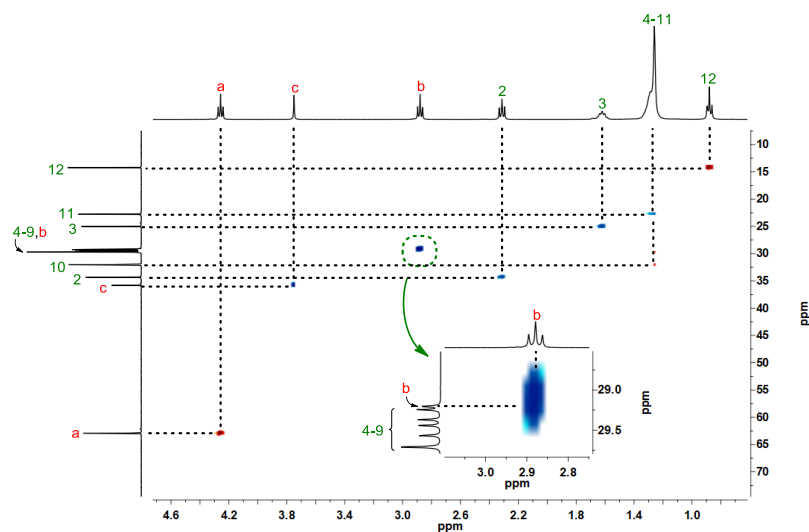


Figure 8.24 HSQC spectrum of Dod-I₄ in CDCl₃.

8.12 (4-Methoxyphenyl)-bis-[(2-ethylthio)dodecanoate]-methane (Dod-I₅)

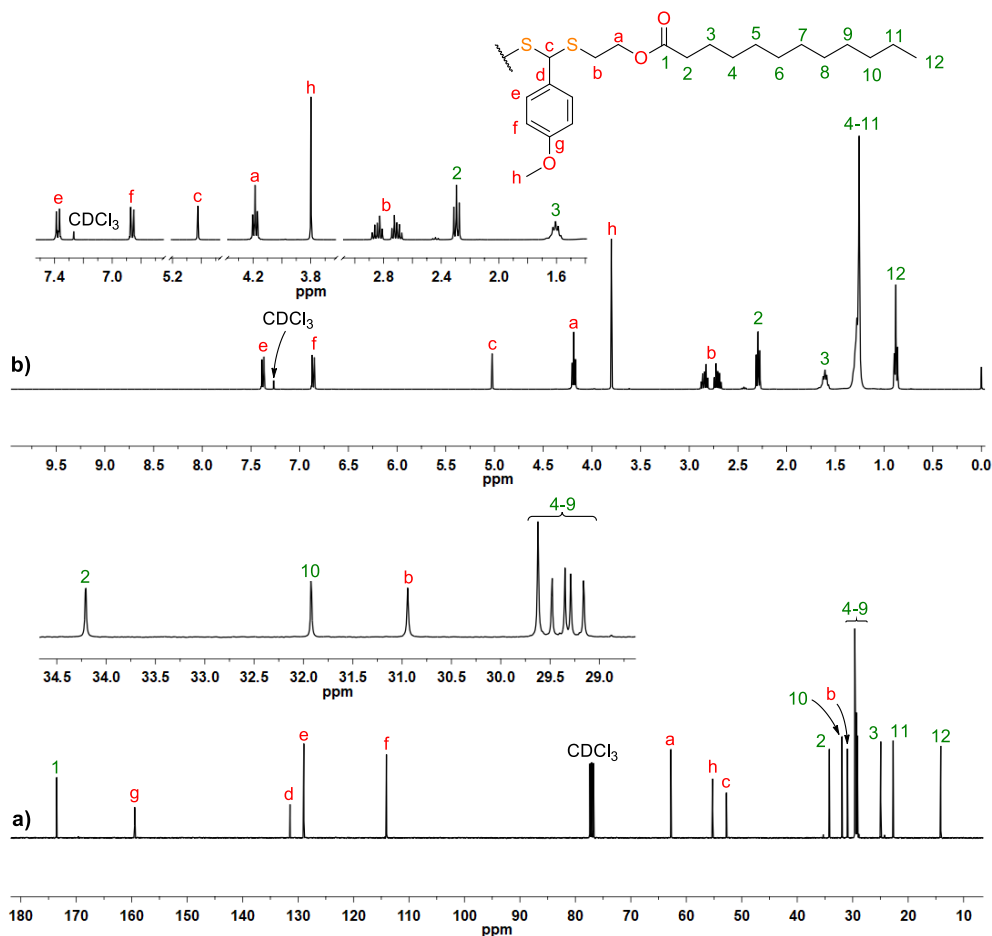


Figure 8.25 (a) ¹³C-NMR and (b) ¹H-NMR spectra of Dod-I₅ in CDCl₃.

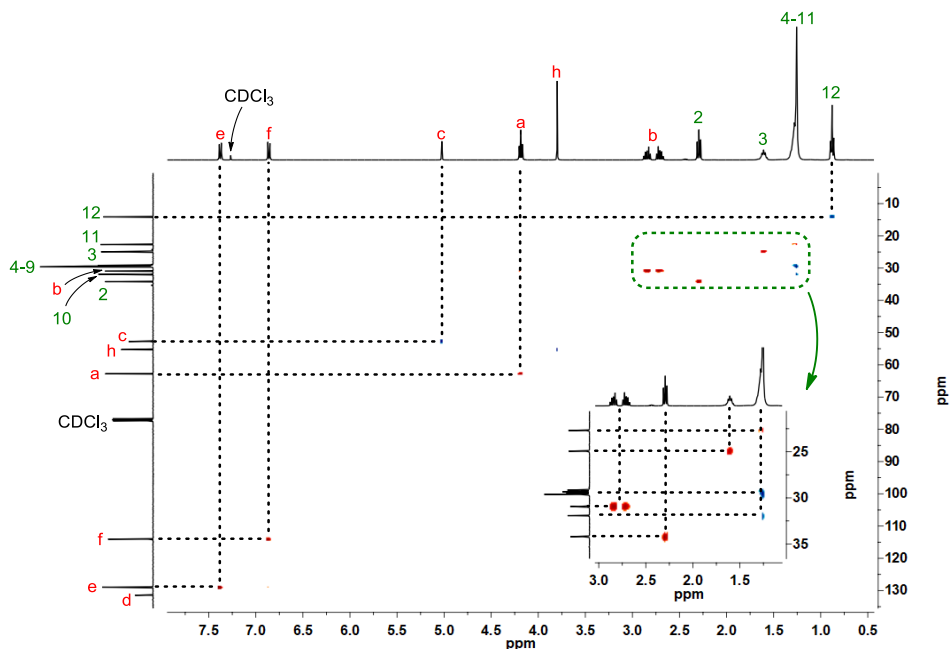


Figure 8.26 HSQC spectrum of *Dod-I₅* in $CDCl_3$.

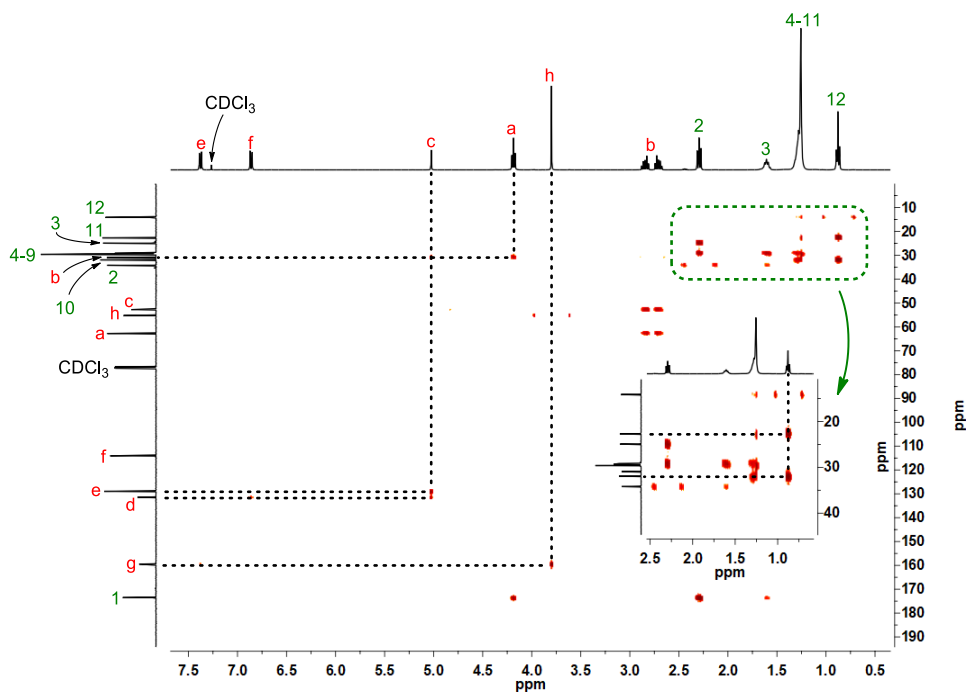


Figure 8.27 HMBC spectrum of *Dod-I₅* in $CDCl_3$.

8.13 Poly(DL)_{1,8}-Oct diol

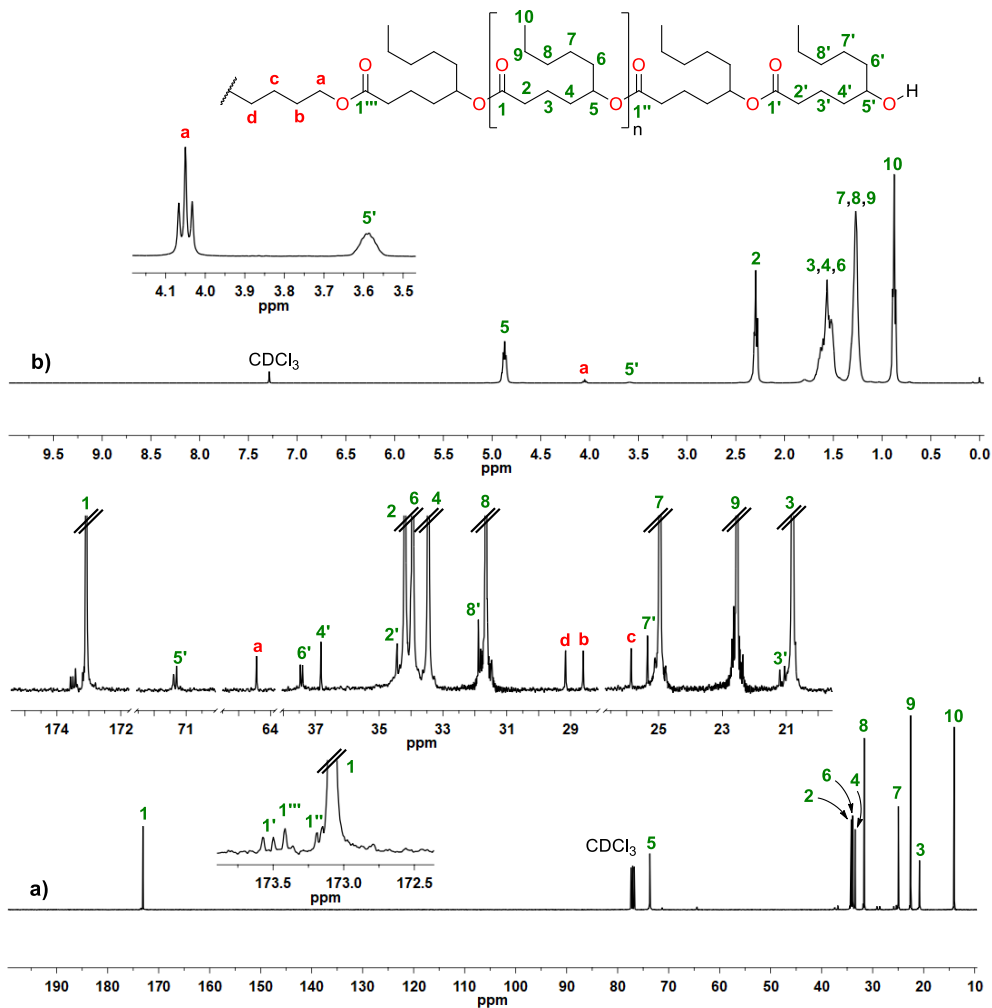


Figure 8.28 (a) ¹³C-NMR and (b) ¹H-NMR spectra of poly(DL)_{1,8}-Oct diol in CDCl₃.

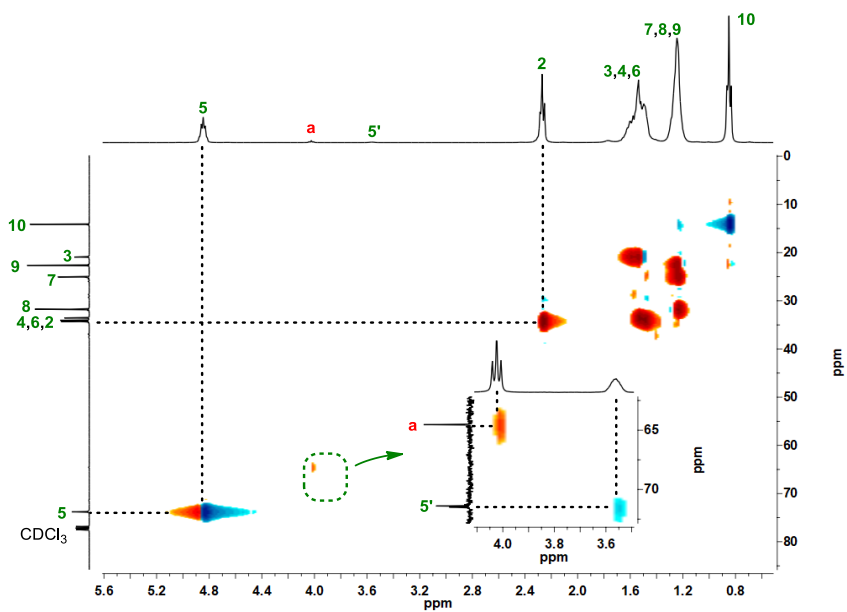


Figure 8.29 HSQC spectrum of poly(DL)_{1,8-Oct} diol in CDCl₃.

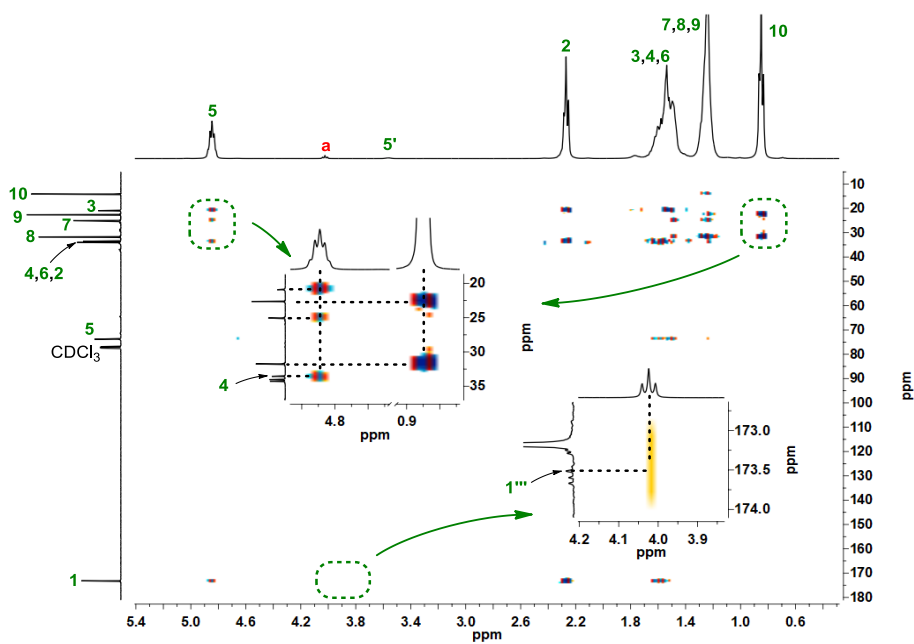


Figure 8.30 HMBC spectrum of poly(DL)_{1,8-Oct} diol in CDCl₃.

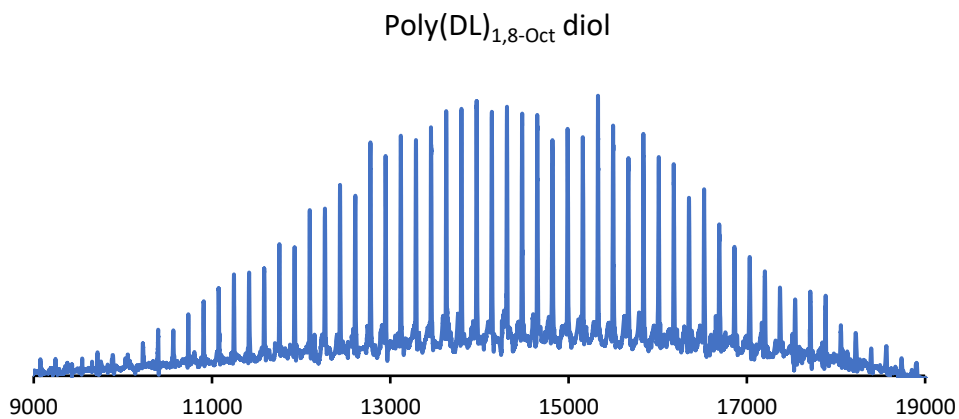


Figure 8.31 MALDI-TOF spectrum of poly(DL)_{1,8-Oct} diol.

8.14 Poly(DL)_{1,8}-Oct BriB ester

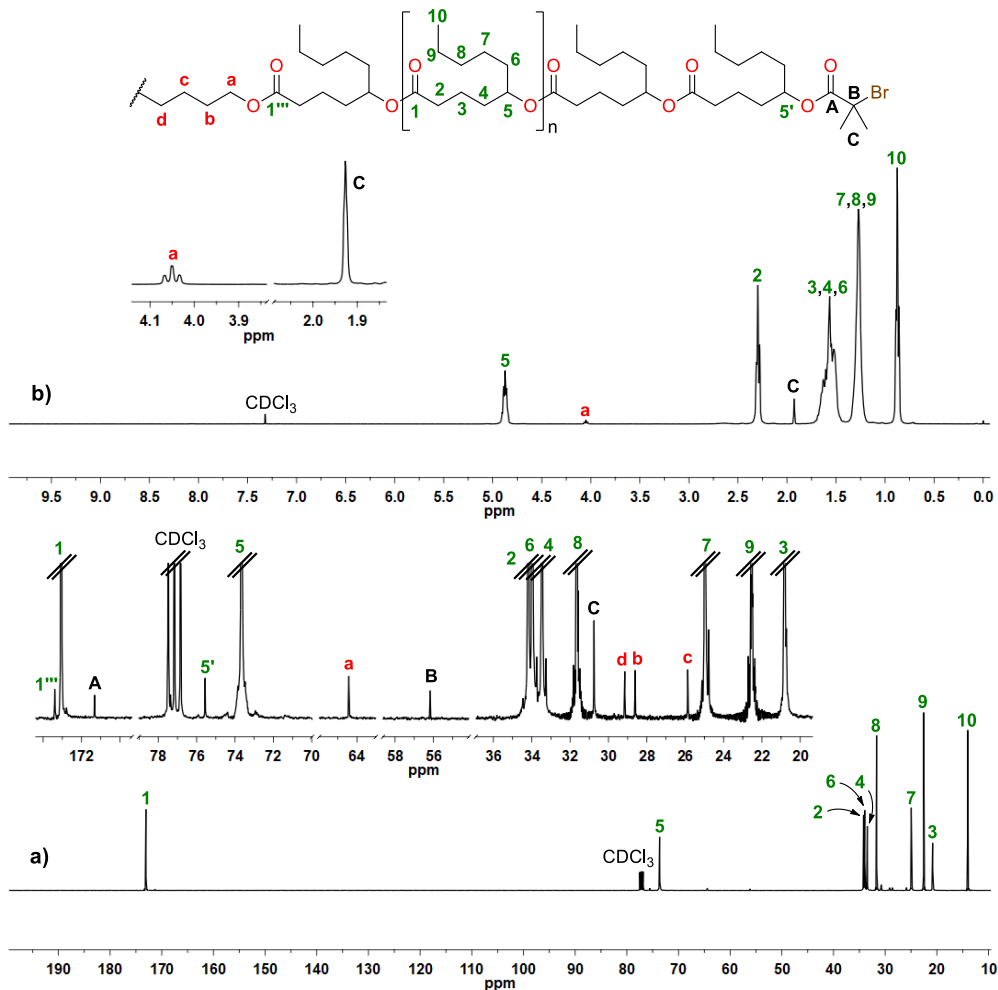


Figure 8.32 (a) ¹³C-NMR and (b) ¹H-NMR spectra of poly(DL)_{1,8}-Oct BriB ester in CDCl₃.

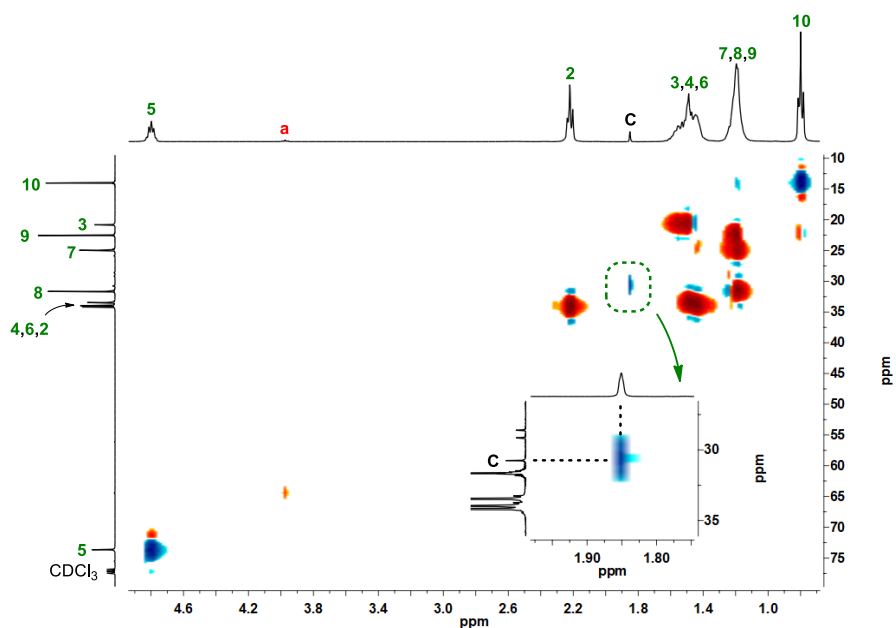


Figure 8.33 HSQC spectrum of poly(DL)_{1,8-Oct} BriB ester in CDCl₃.

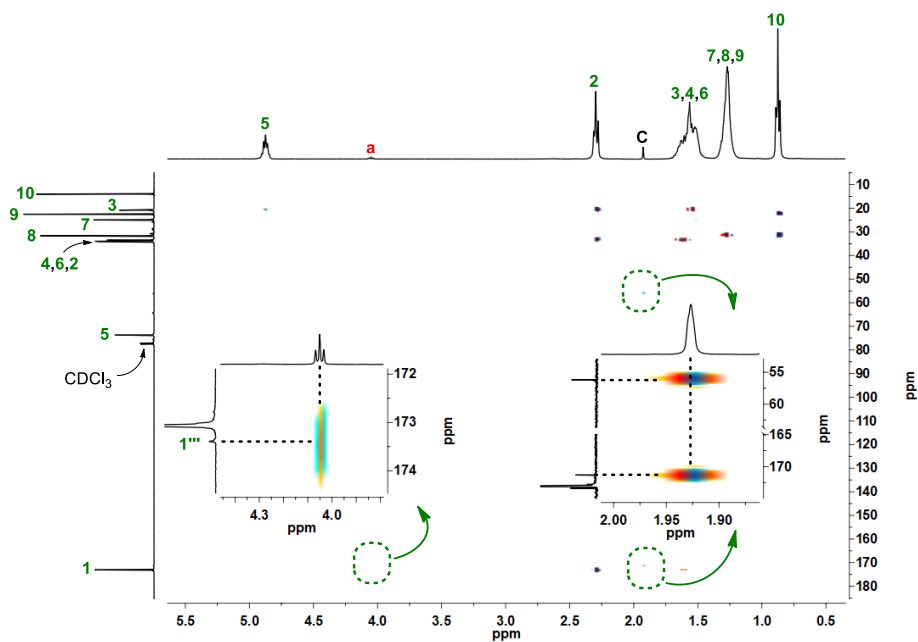


Figure 8.34 HMBC spectrum of poly(DL)_{1,8-Oct} BriB ester in CDCl₃.

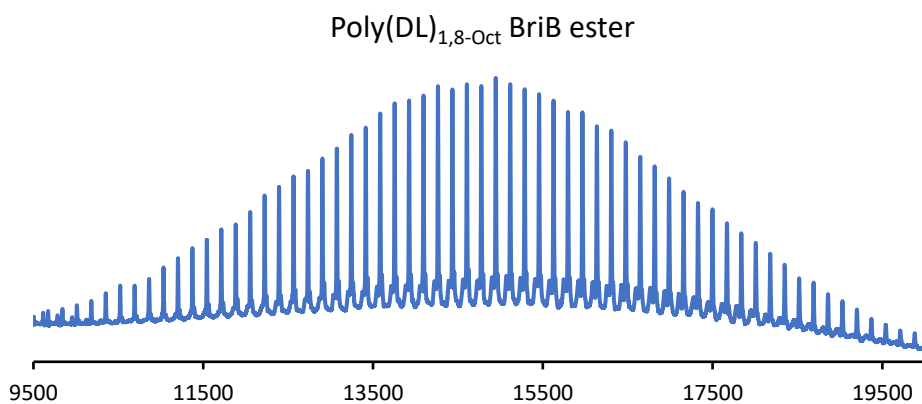


Figure 8.35 MALDI-TOF spectrum of poly(DL)_{1,8-Oct} BriB ester.

8.15 Poly(DL)-I₁ diol

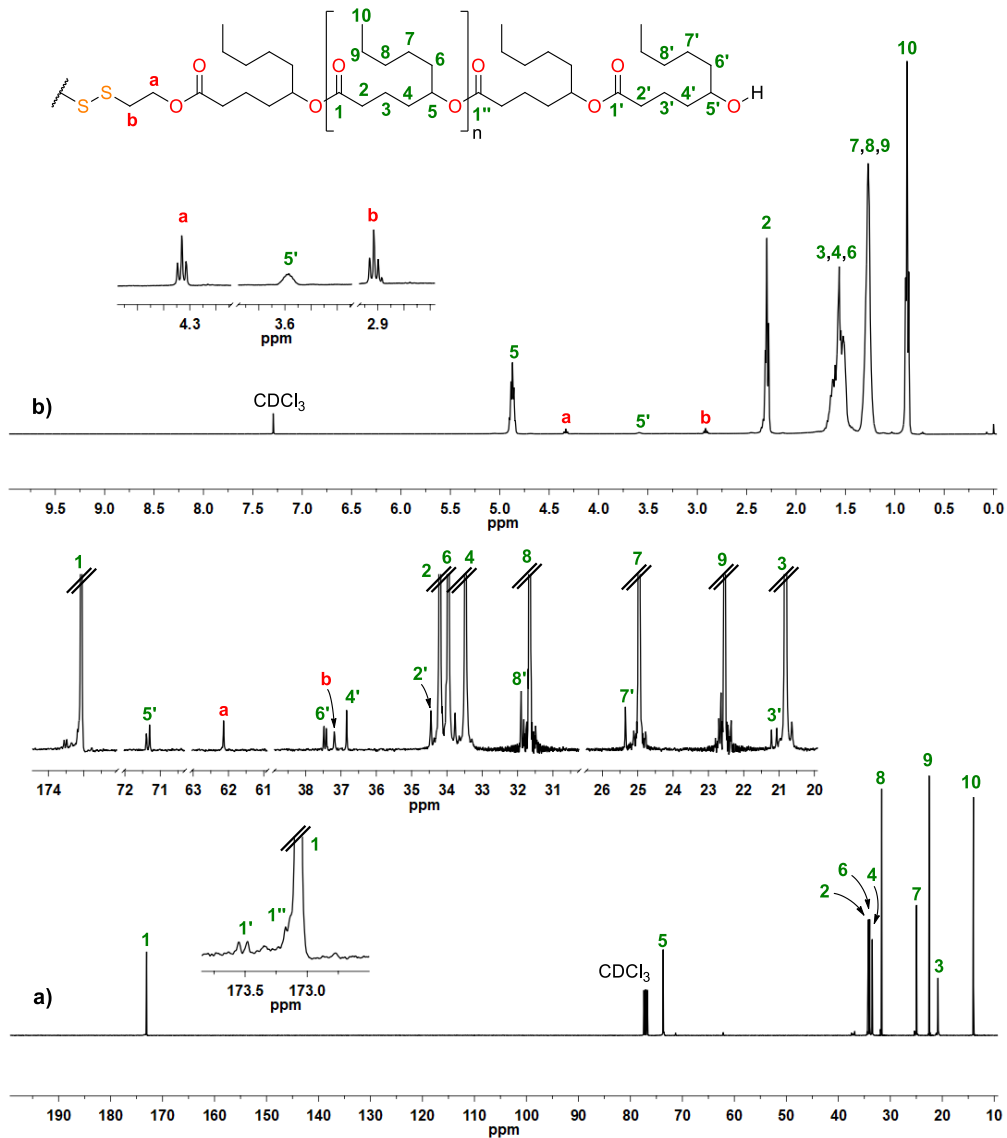


Figure 8.36 (a) ¹³C-NMR and (b) ¹H-NMR spectra of poly(DL)-I₁ diol in CDCl₃.

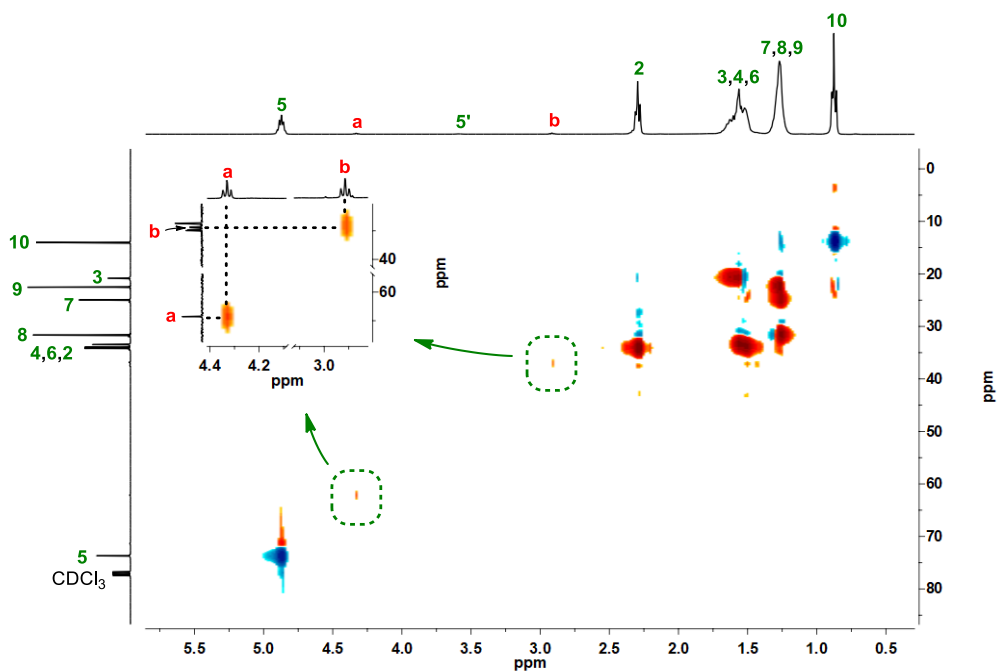


Figure 8.37 HSQC spectrum of poly(DL)-I₁ diol in CDCl₃.

8.16 Poly(DL)-I₁ BriB ester

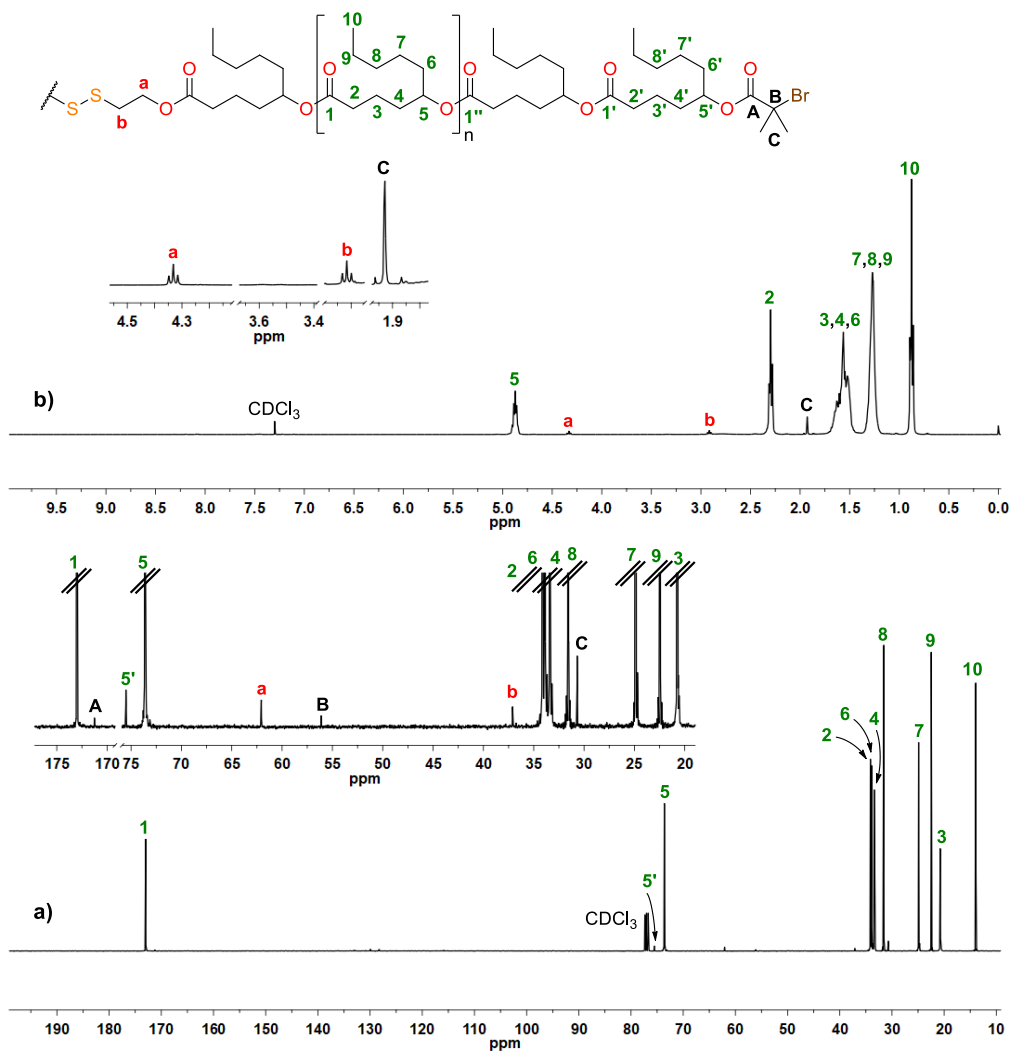


Figure 8.38 (a) ¹³C-NMR and (b) ¹H-NMR spectra of poly(DL)-I₁ BriB ester in CDCl₃.

8.17 Poly(DL)-I₂ diol

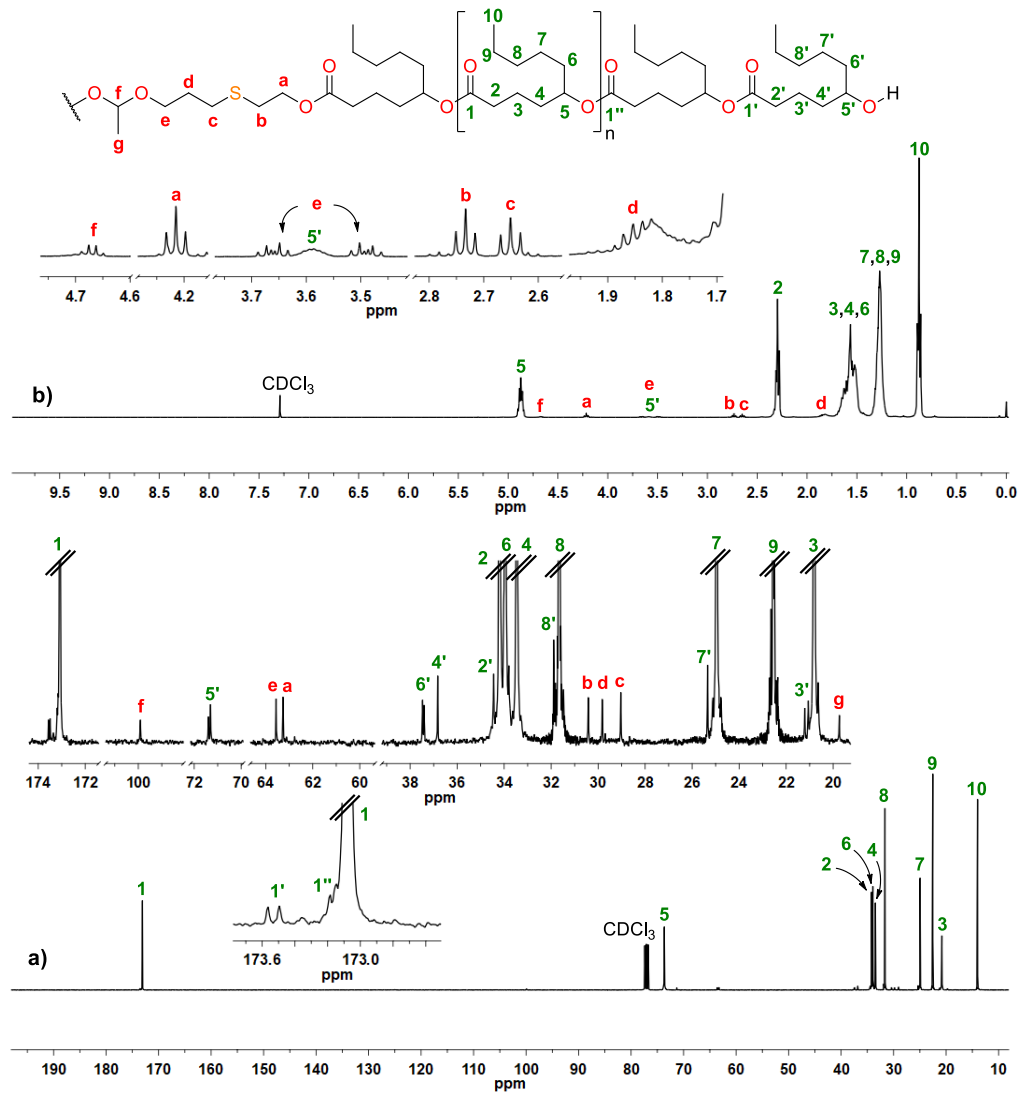


Figure 8.39 (a) ¹³C-NMR and (b) ¹H-NMR spectra of poly(DL)-I₂ diol in CDCl₃.

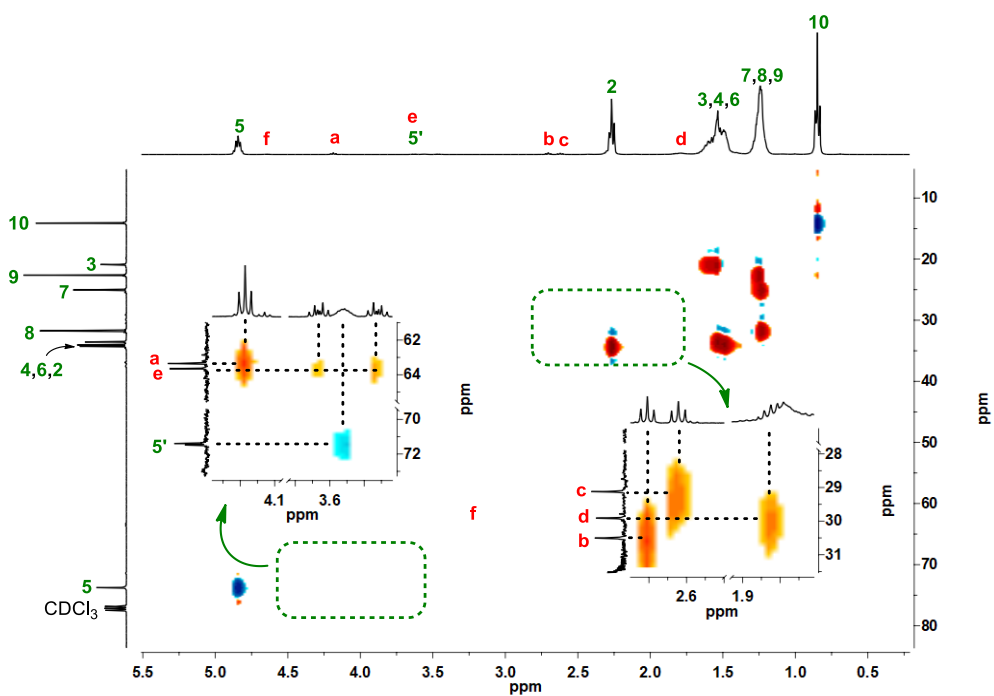


Figure 8.40 HSQC spectrum of poly(DL)-l₂ diol in CDCl₃.

Poly(DL)-l₂ diol

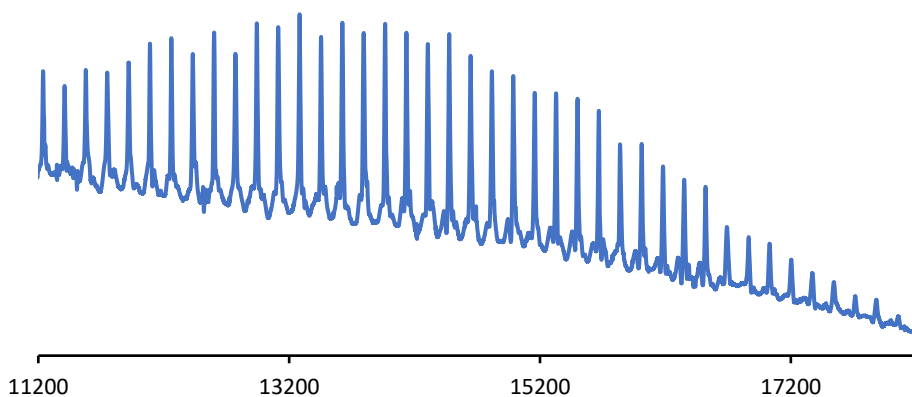


Figure 8.41 MALDI-TOF spectrum of poly(DL)-l₂ diol.

8.18 Poly(DL)-I₂ BriB ester

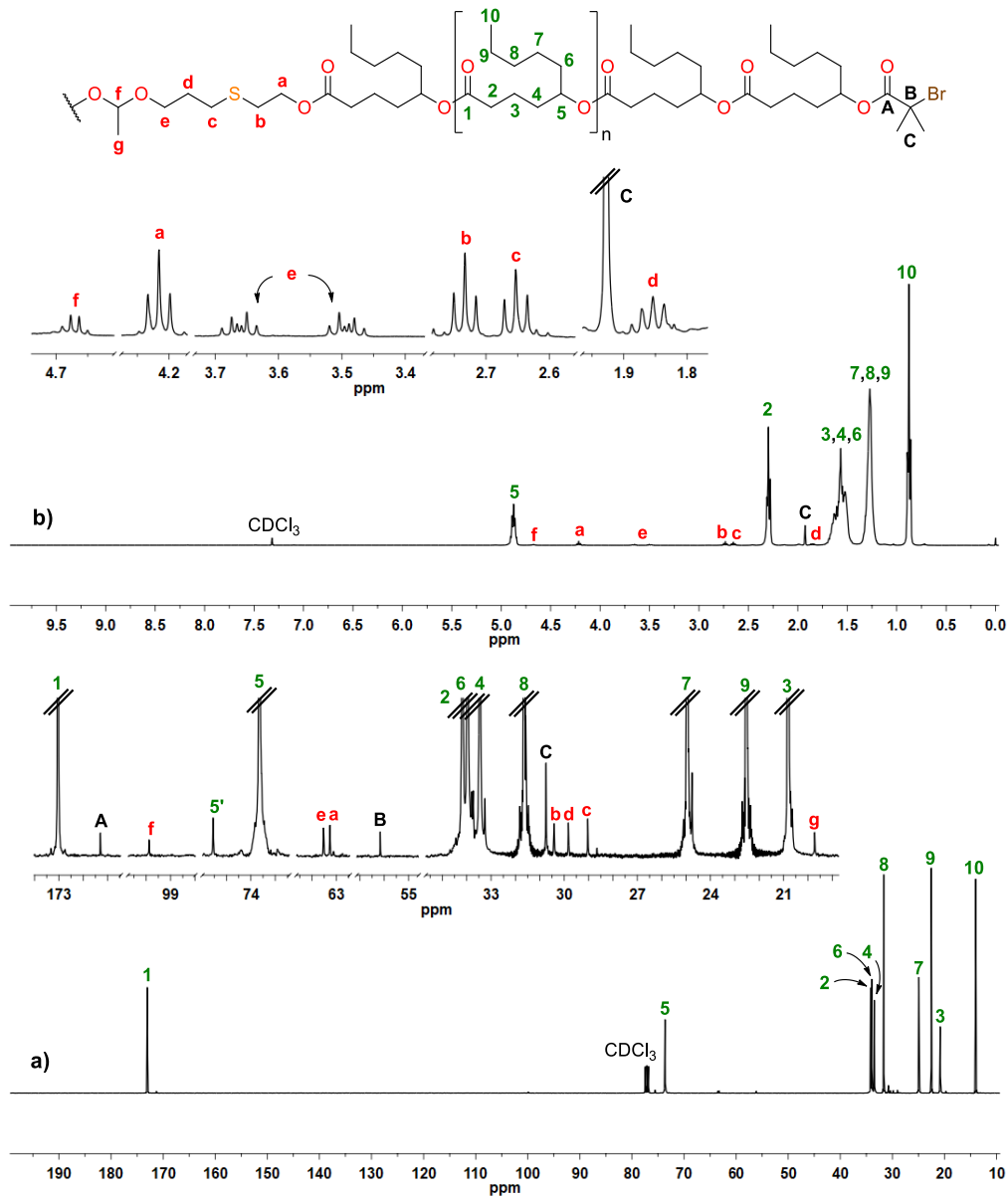


Figure 8.42 (a) ¹³C-NMR and (b) ¹H-NMR spectra of poly(DL)-I₂ BriB ester in CDCl₃.

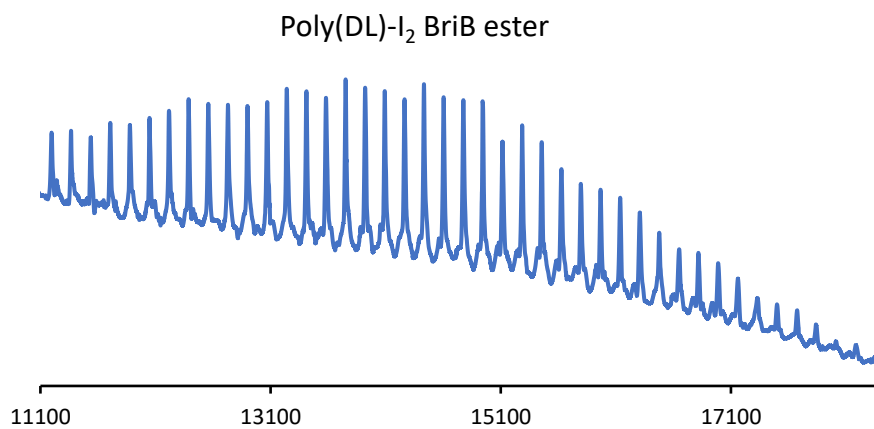


Figure 8.43 MALDI-TOF spectrum of poly(DL)-I₂ BriB ester.

8.19 Poly(DL)-I₃ diol

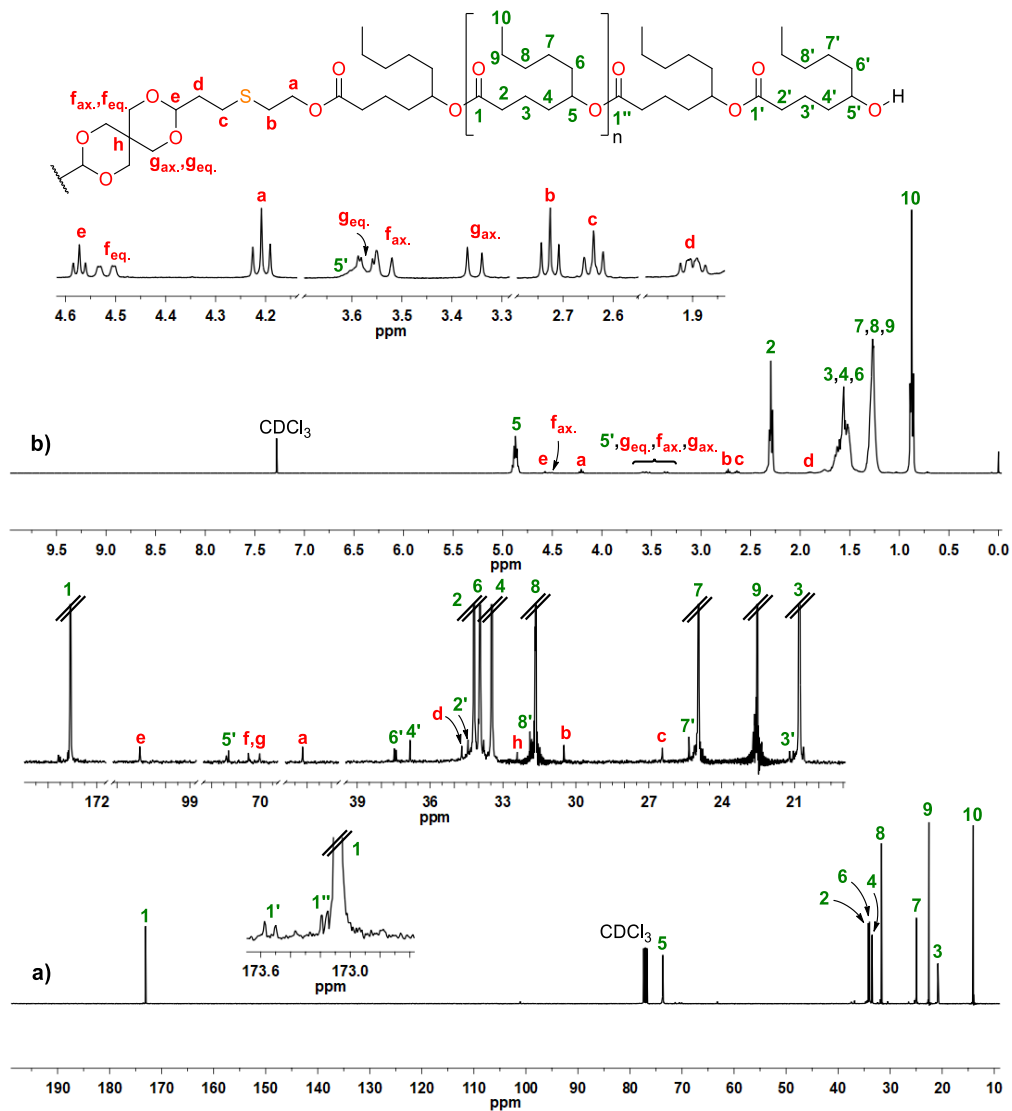


Figure 8.44 (a) ¹³C-NMR and (b) ¹H-NMR spectra of poly(DL)-I₃ diol in CDCl₃.

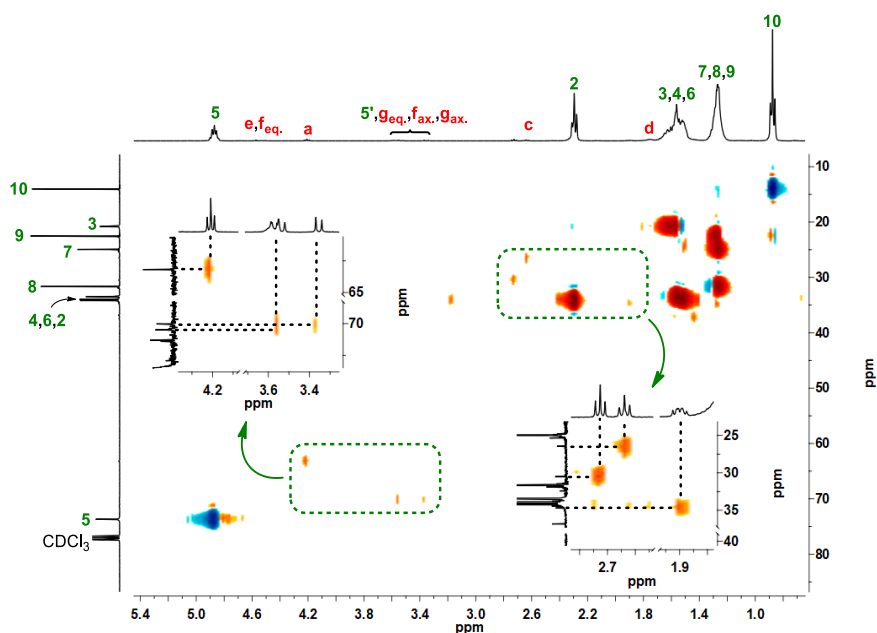


Figure 8.45 HSQC spectrum of poly(DL)-I₃ diol in CDCl₃.

Poly(DL)-I₃ diol

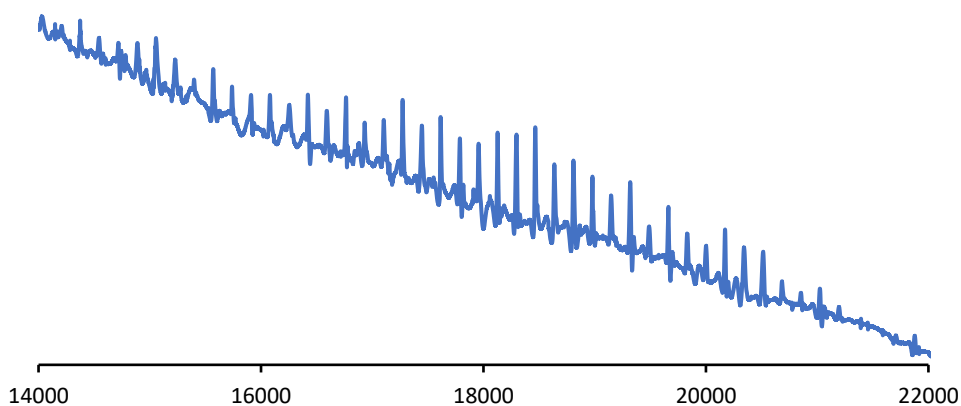


Figure 8.46 MALDI-TOF spectrum of poly(DL)-I₃ diol.

8.20 Poly(DL)-I₃ BriB ester

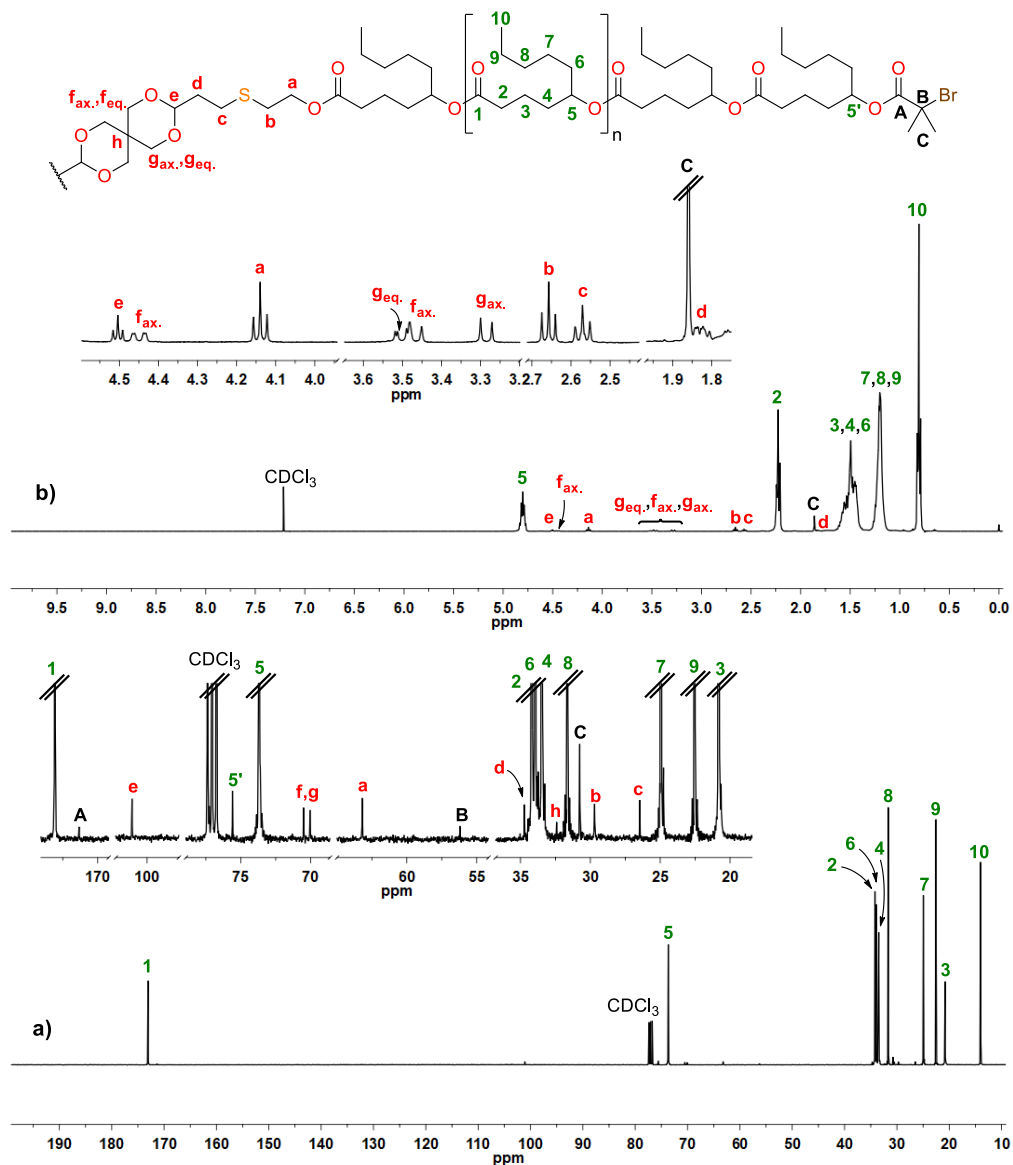


Figure 8.47 (a) ¹³C-NMR and (b) ¹H-NMR spectra of poly(DL)-I₃ BriB ester in CDCl₃.

8.21 Poly(DL)-I₄ diol

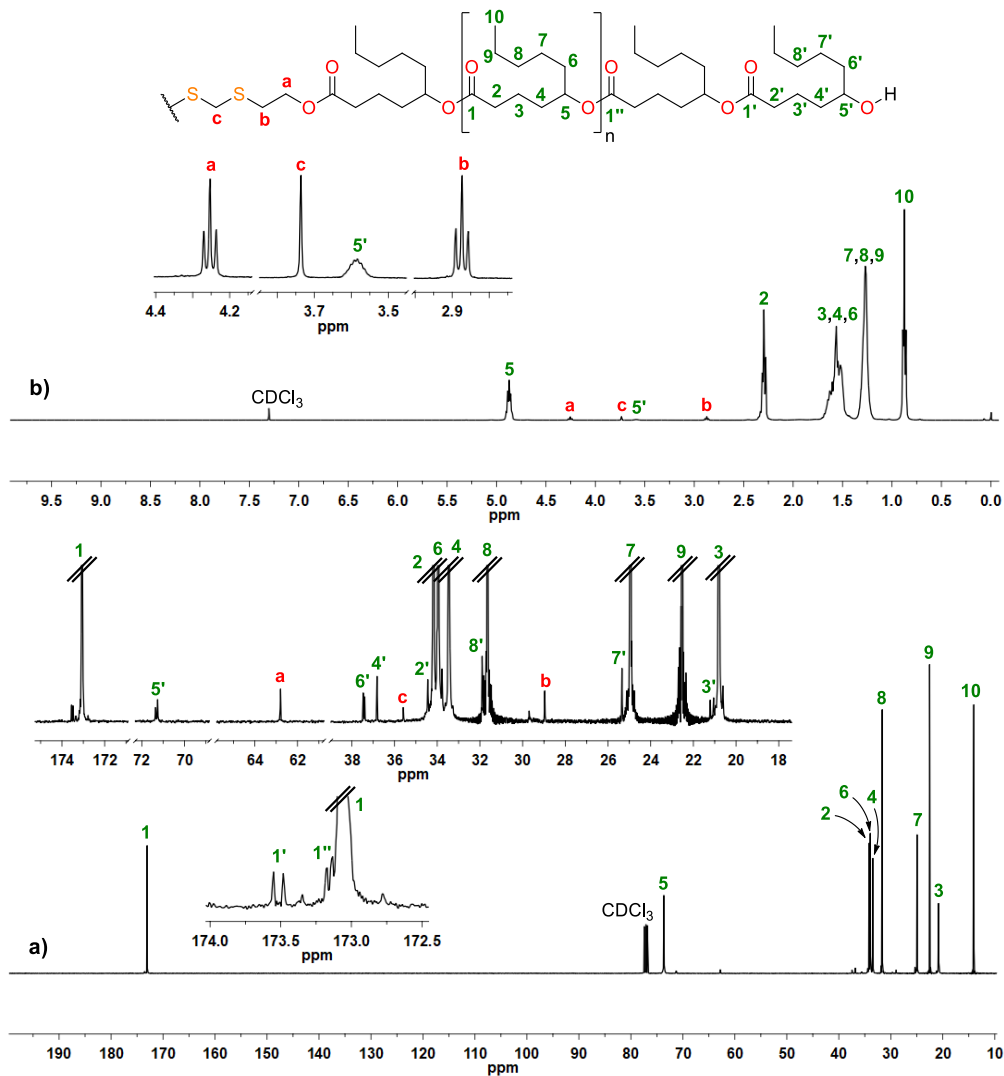


Figure 8.48 (a) ¹³C-NMR and (b) ¹H-NMR spectra of poly(DL)-I₄ diol in CDCl₃.

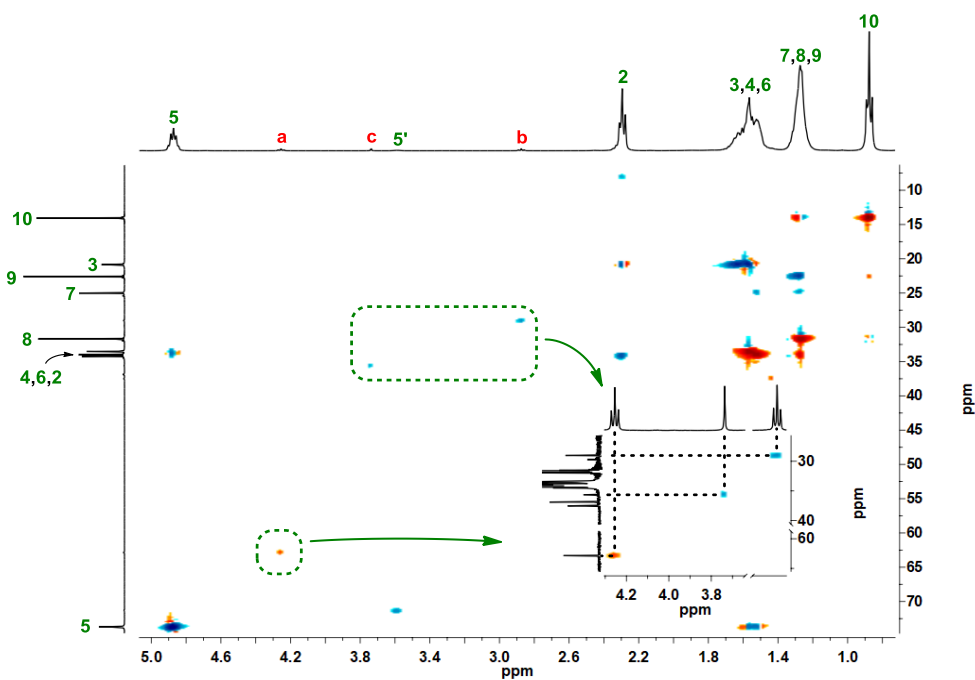


Figure 8.49 HSQC spectrum of poly(DL)-I₄ diol in CDCl₃.

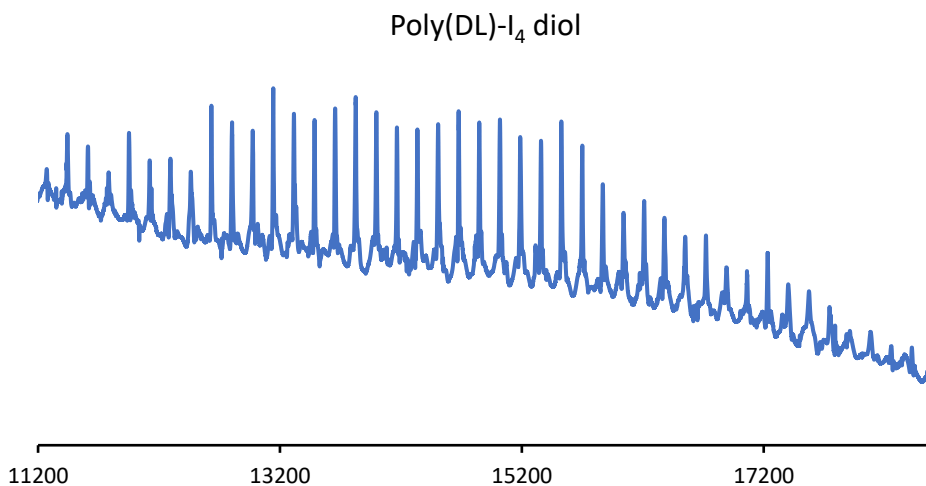


Figure 8.50 MALDI-TOF spectrum of poly(DL)-I₄ diol.

8.22 Poly(DL)-I₄ BriB ester

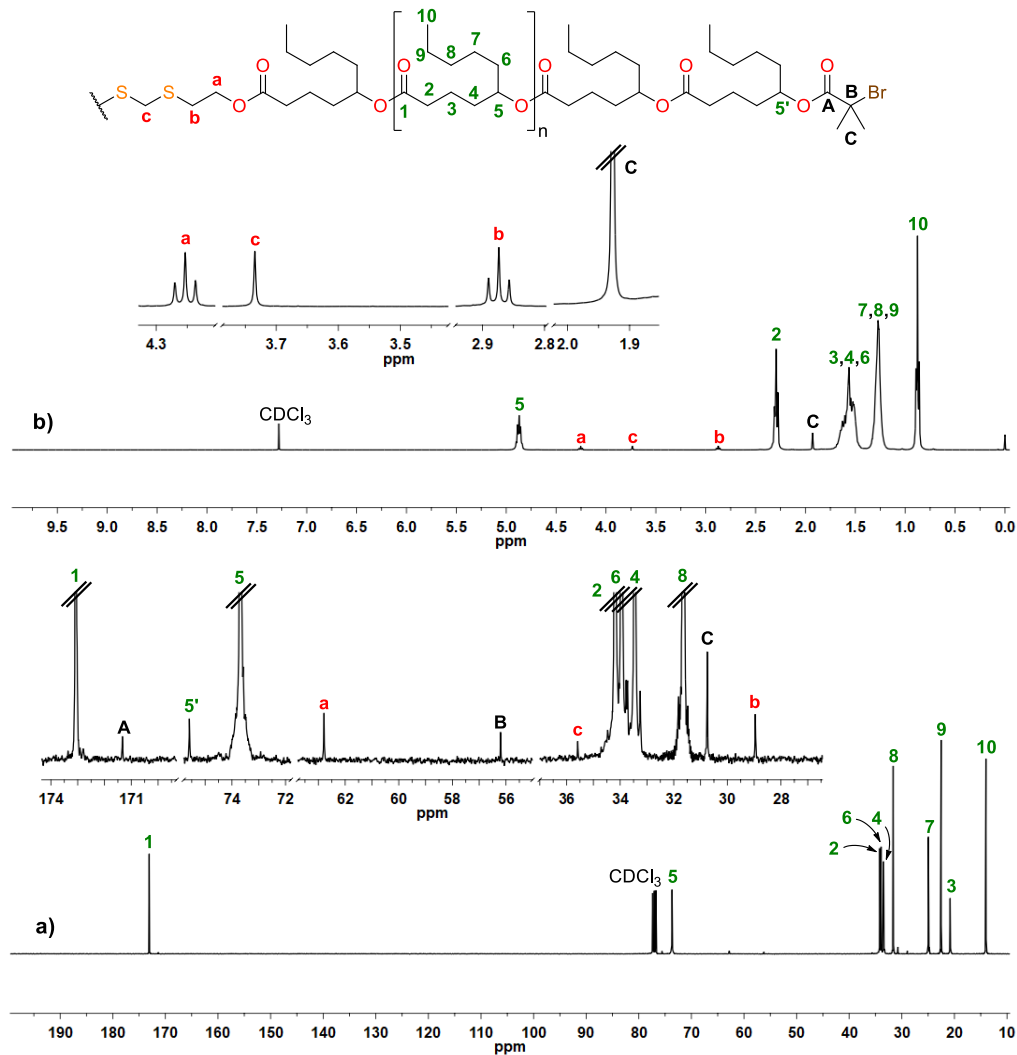


Figure 8.51 (a) ¹³C-NMR and (b) ¹H-NMR spectra of poly(DL)-I₄ BriB ester in CDCl₃.

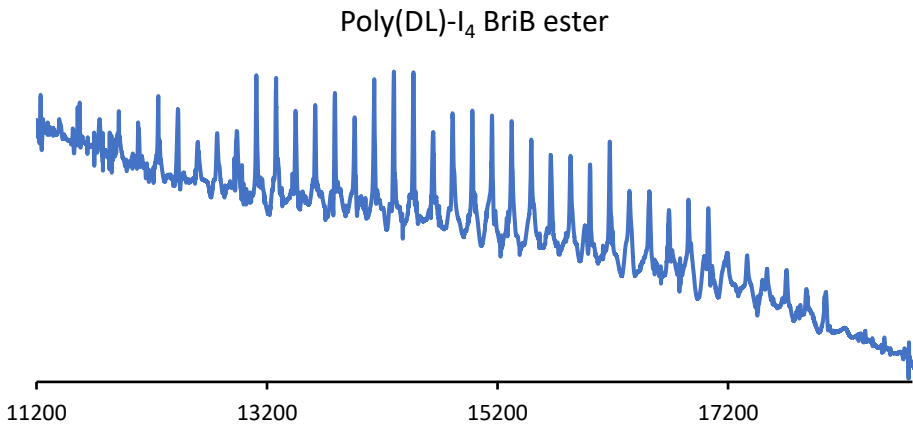


Figure 8.52 MALDI-TOF spectrum of poly(DL)-I₄ BriB ester.

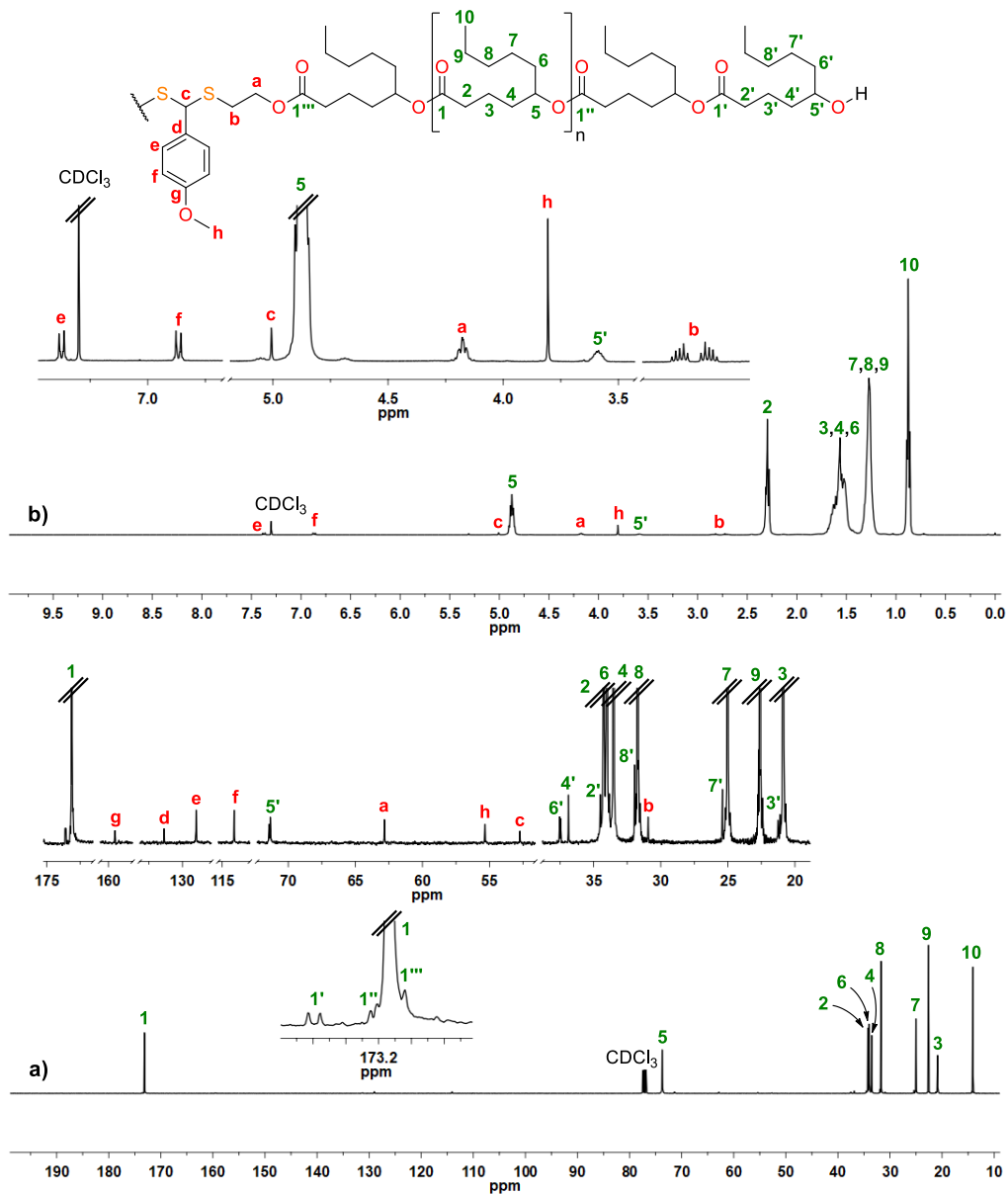
8.23 Poly(DL)-I₅ diol

Figure 8.53 (a) ^{13}C -NMR and (b) ^1H -NMR spectra of poly(DL)-I₅ diol in CDCl_3 .

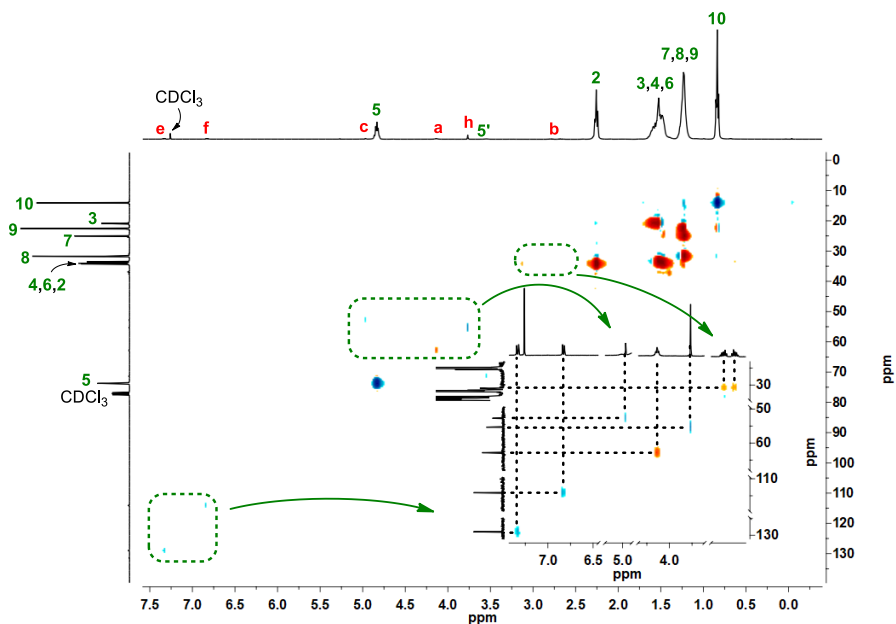


Figure 8.54 HSQC spectrum of poly(DL)-I₅ diol in CDCl₃.

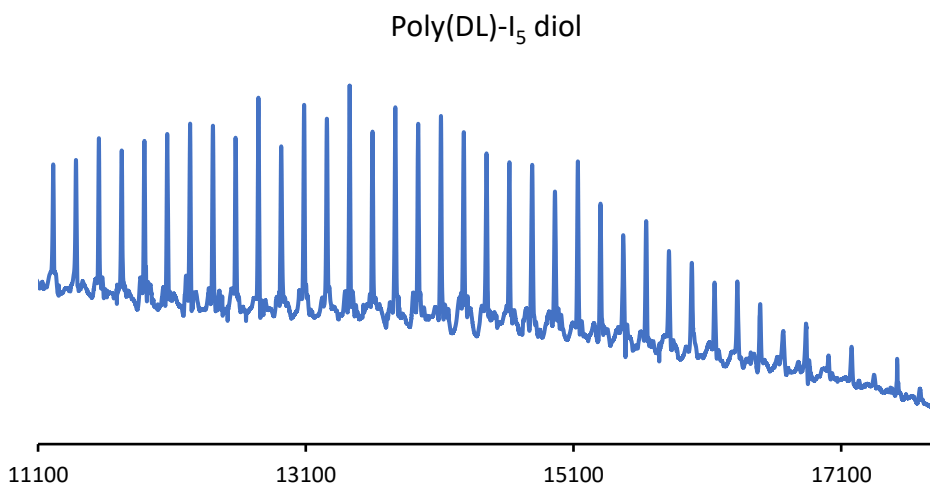


Figure 8.55 MALDI-TOF spectrum of poly(DL)-I₅ diol.

8.24 Poly(DL)-I₅ BriB ester

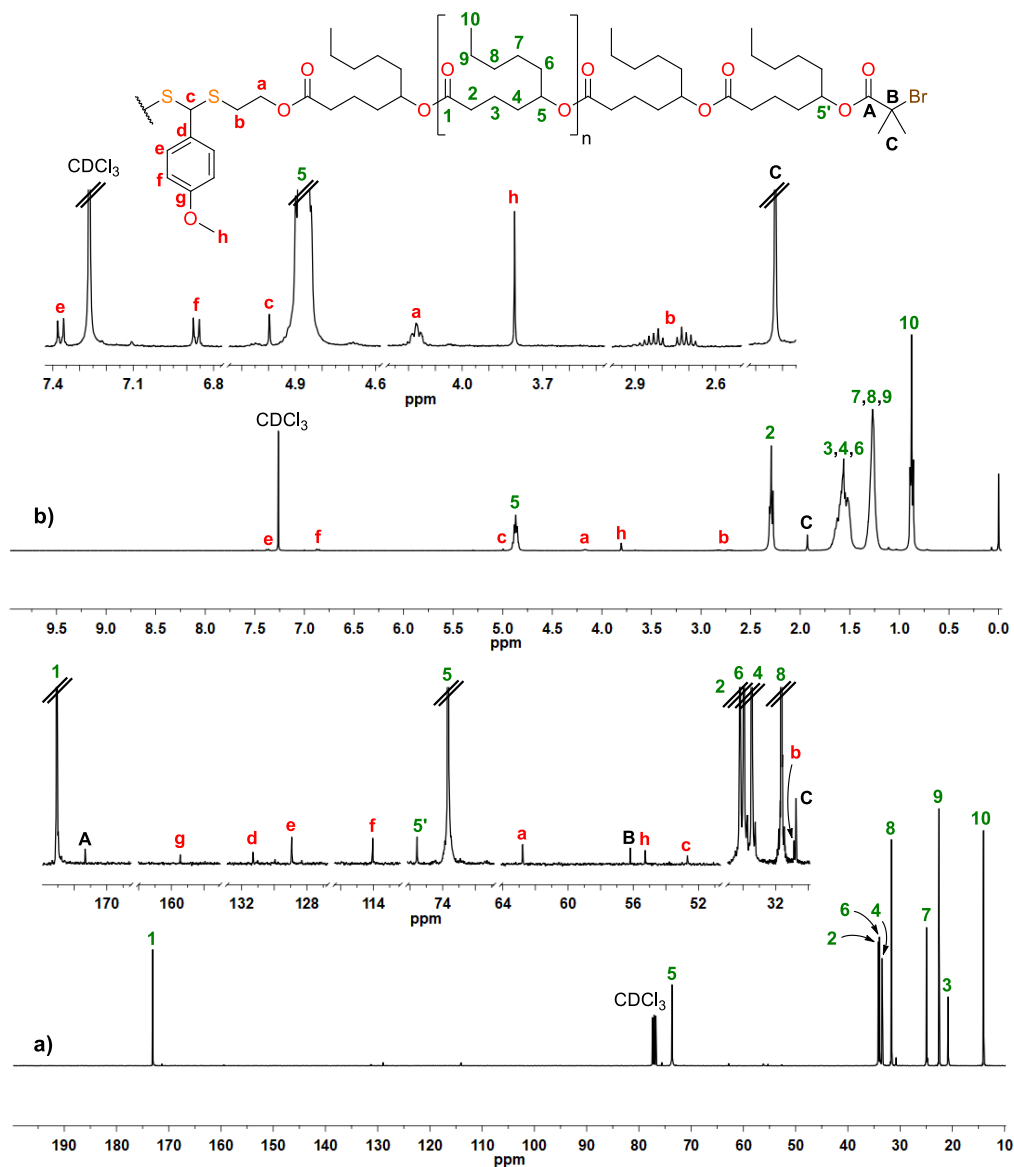


Figure 8.56 (a) ¹³C-NMR and (b) ¹H-NMR spectra of poly(DL)-I₅ BriB ester in CDCl₃.

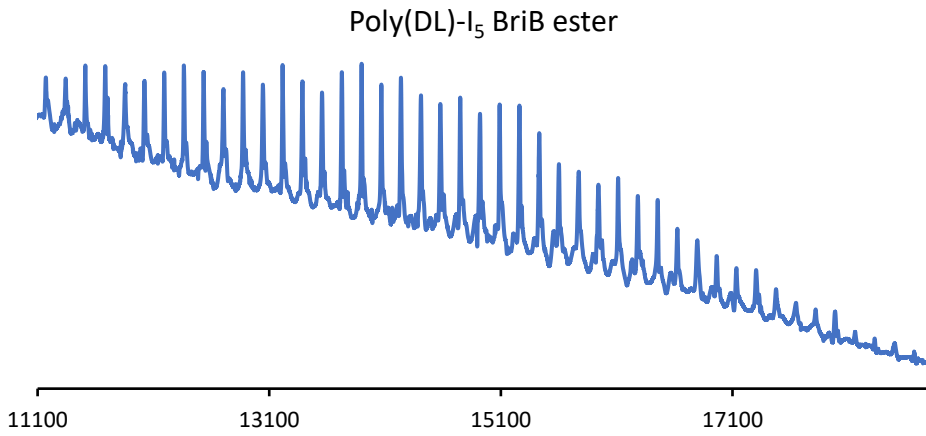


Figure 8.57 MALDI-TOF spectrum of poly(DL)-I₅ BriB ester.

8.25 Poly(MMA)_{EtBrIB}

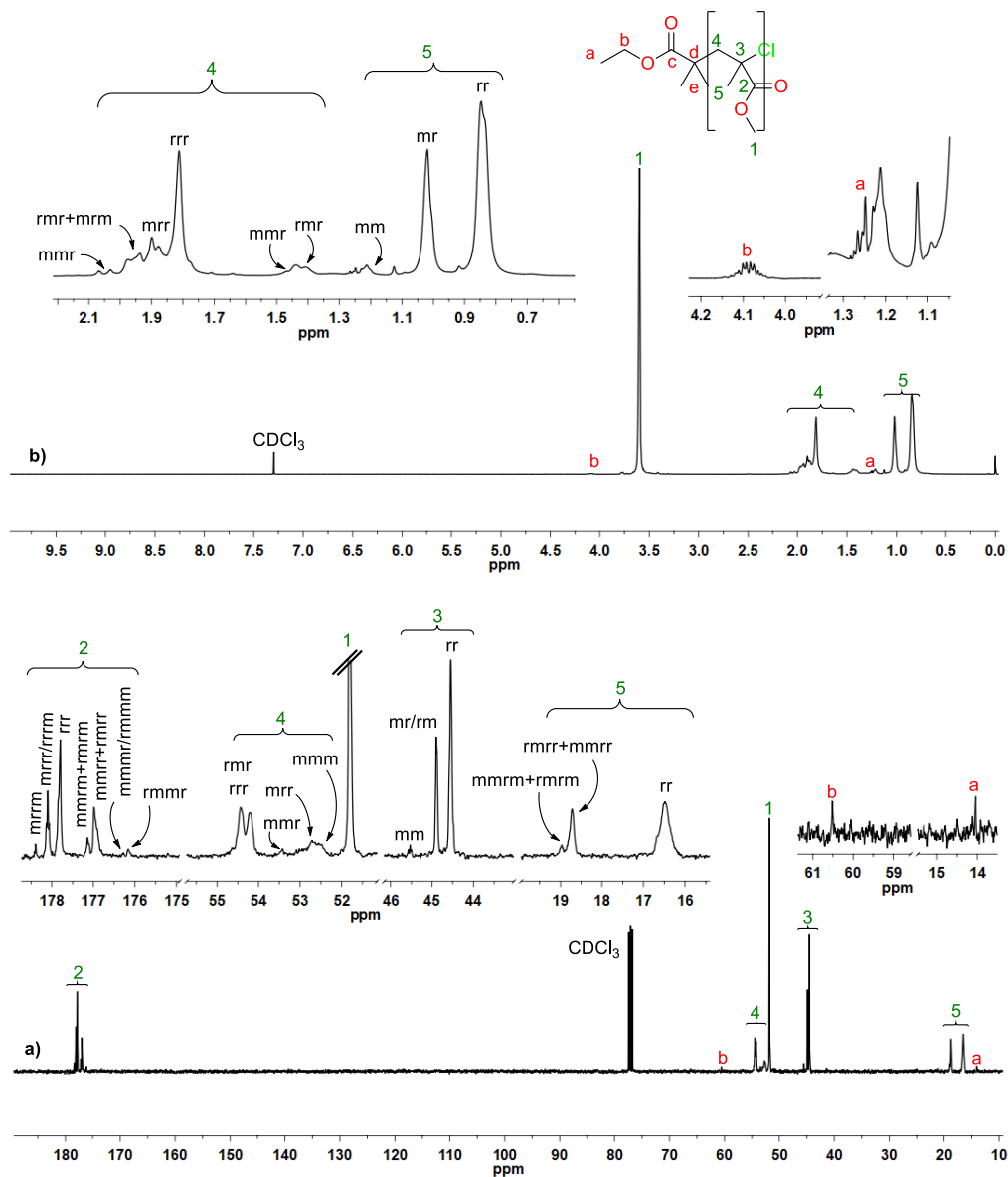


Figure 8.58 (a) ¹³C-NMR and (b) ¹H-NMR spectra of poly(MMA)_{EtBrIB} in CDCl₃. Triads, tetrads and pentads were assigned from data reported in the literature (*m* = meso; *r* = racemo).¹

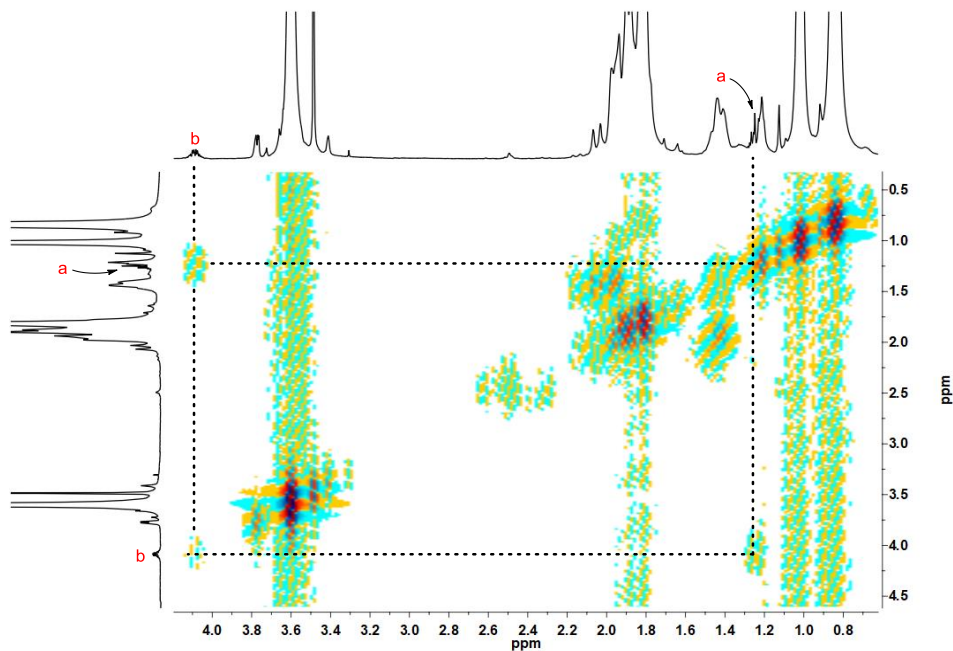


Figure 8.59 COSY spectrum of poly(MMA)_{EtBrIB} in CDCl₃.

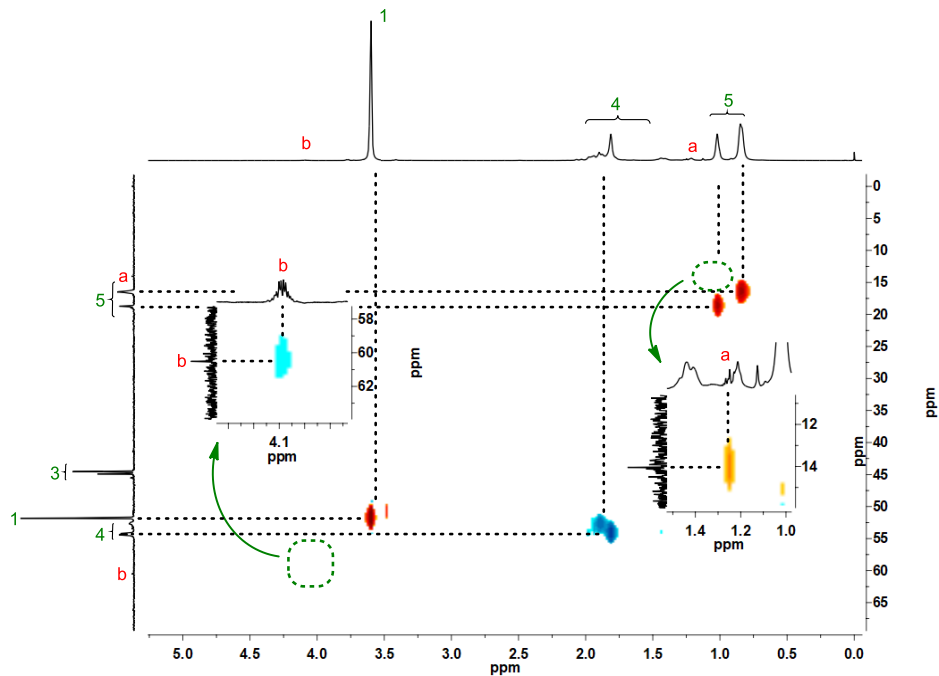


Figure 8.60 HSQC spectrum of poly(MMA)_{EtBrIB} in CDCl₃.

8.26 Poly(MBL)_{EtBriB}

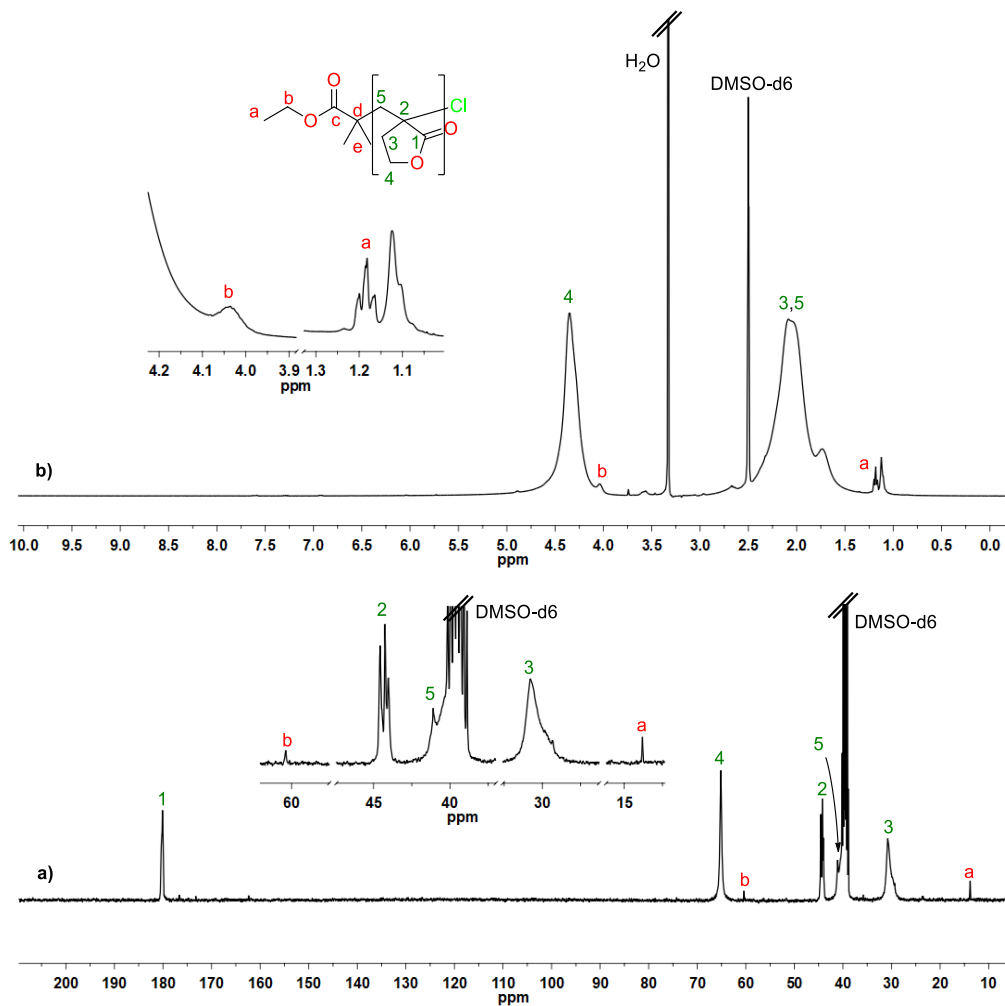


Figure 8.61 (a) ¹³C-NMR and (b) ¹H-NMR spectra of poly(MBL)_{EtBriB} in DMSO-d₆. The signals from the polymer backbone were assigned from data reported in the literature.^{2,3}

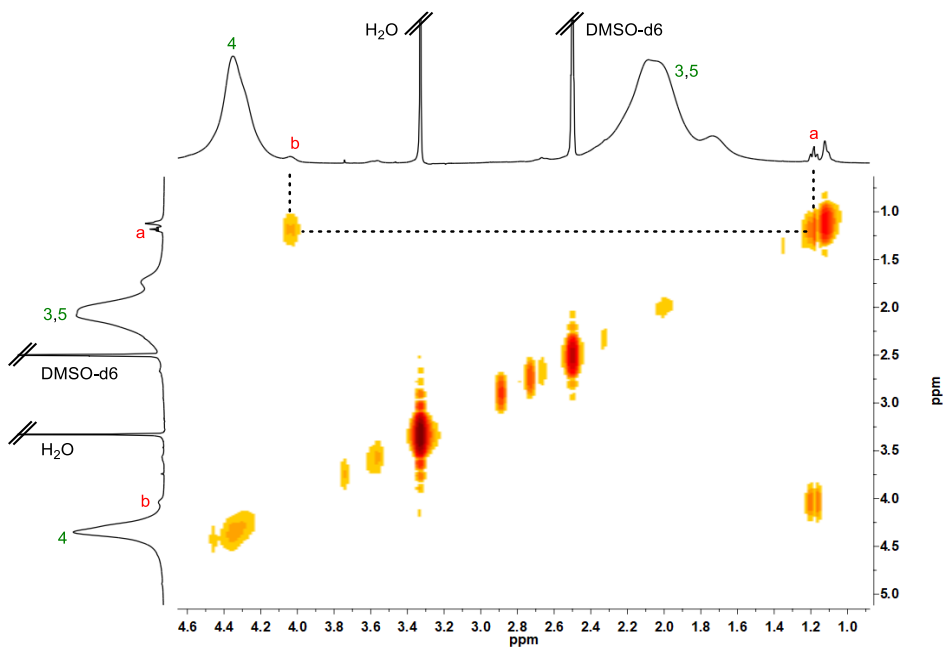


Figure 8.62 COSY spectrum of poly(MBL)_{EtBrIB} in DMSO-d₆.

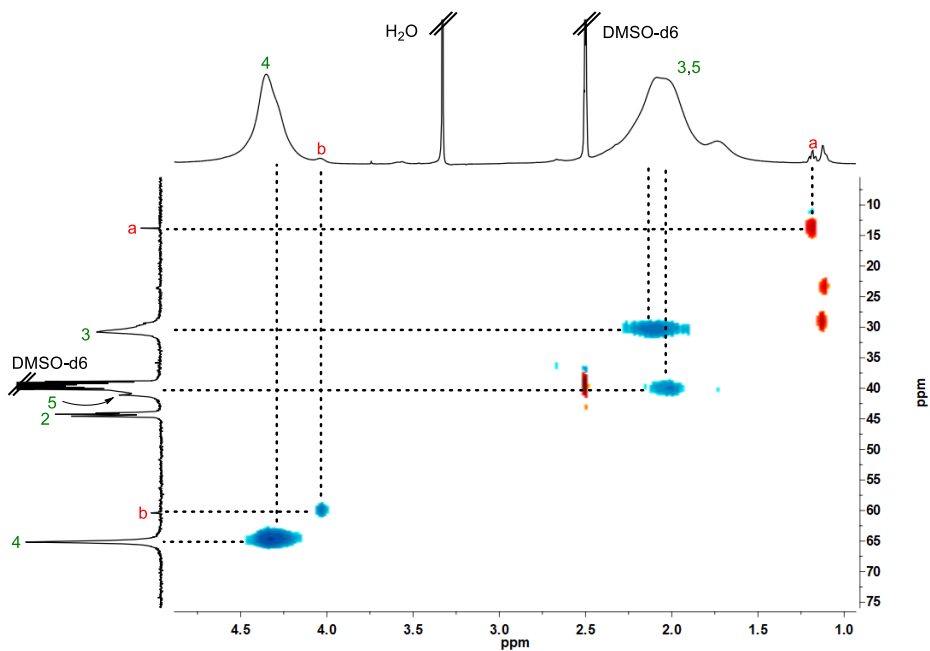


Figure 8.63 HSQC spectrum of poly(MBL)_{EtBrIB} in DMSO-d₆.

8.27 Poly(MBL)-I₆

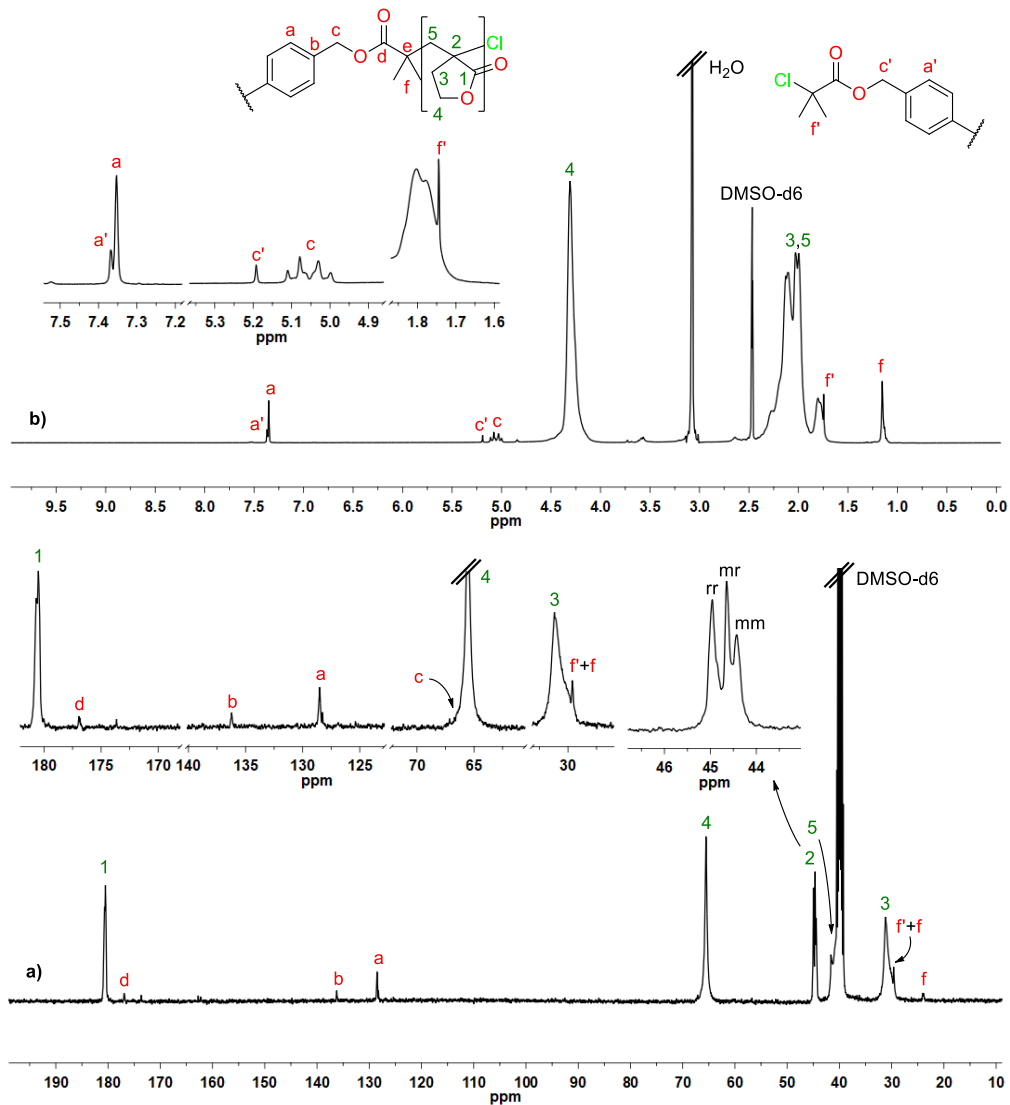


Figure 8.64 (a) ¹³C-NMR and (b) ¹H-NMR spectra (recorded at 80 °C) of poly(MBL)-I₆ in DMSO-d₆. Triads of the quaternary carbon were assigned according to the described in the literature.^{2,4}

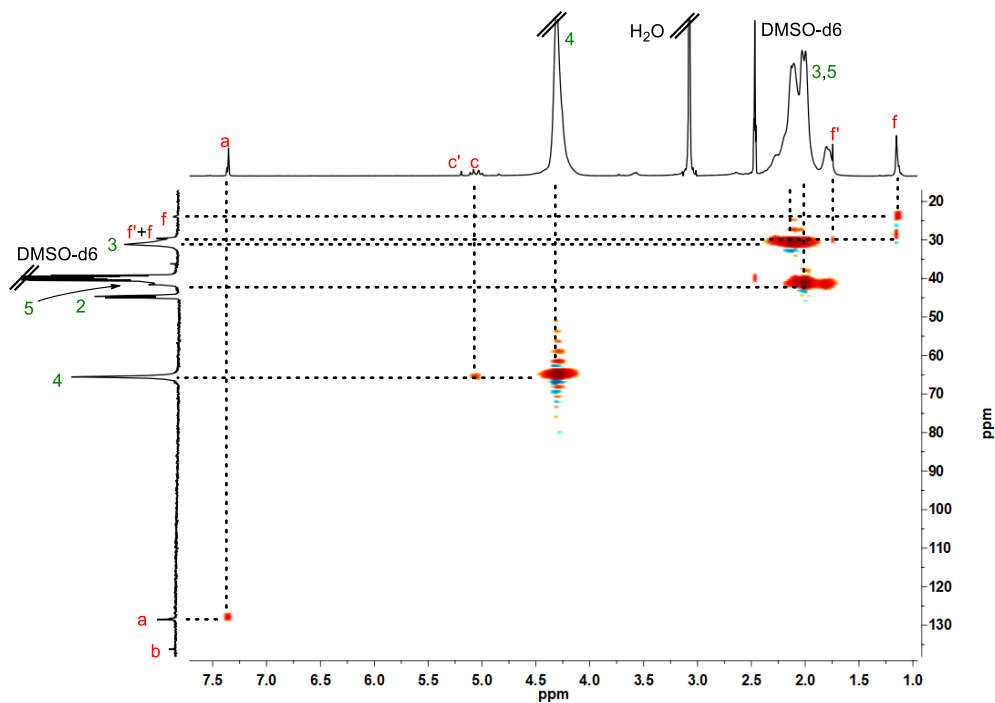


Figure 8.65 HSQC spectrum of poly(MBL)-I₆ in DMSO-d₆.

8.28 1,4-phenylenebis(methylene)-bis(2-chloroisobutyrate)

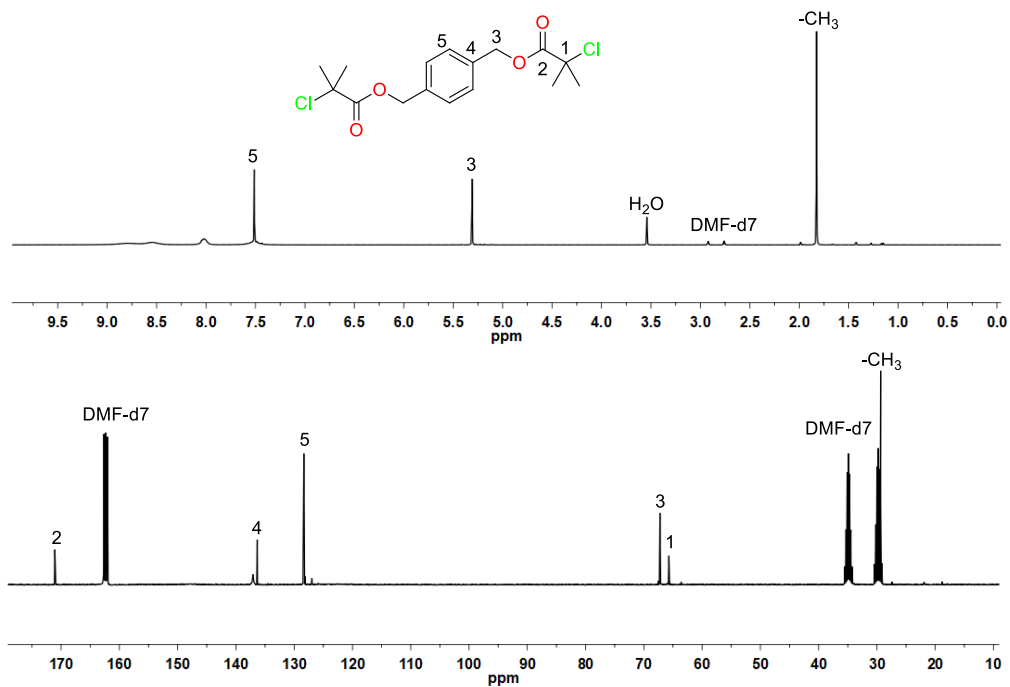


Figure 8.66 (a) ^{13}C -NMR and (b) ^1H -NMR spectra of 1,4-chloro-derivative in DMF-d₇.

8.29 Poly(MBL)-*co*-poly(DL)_{1,8-Oct}-*co*-poly(MBL)

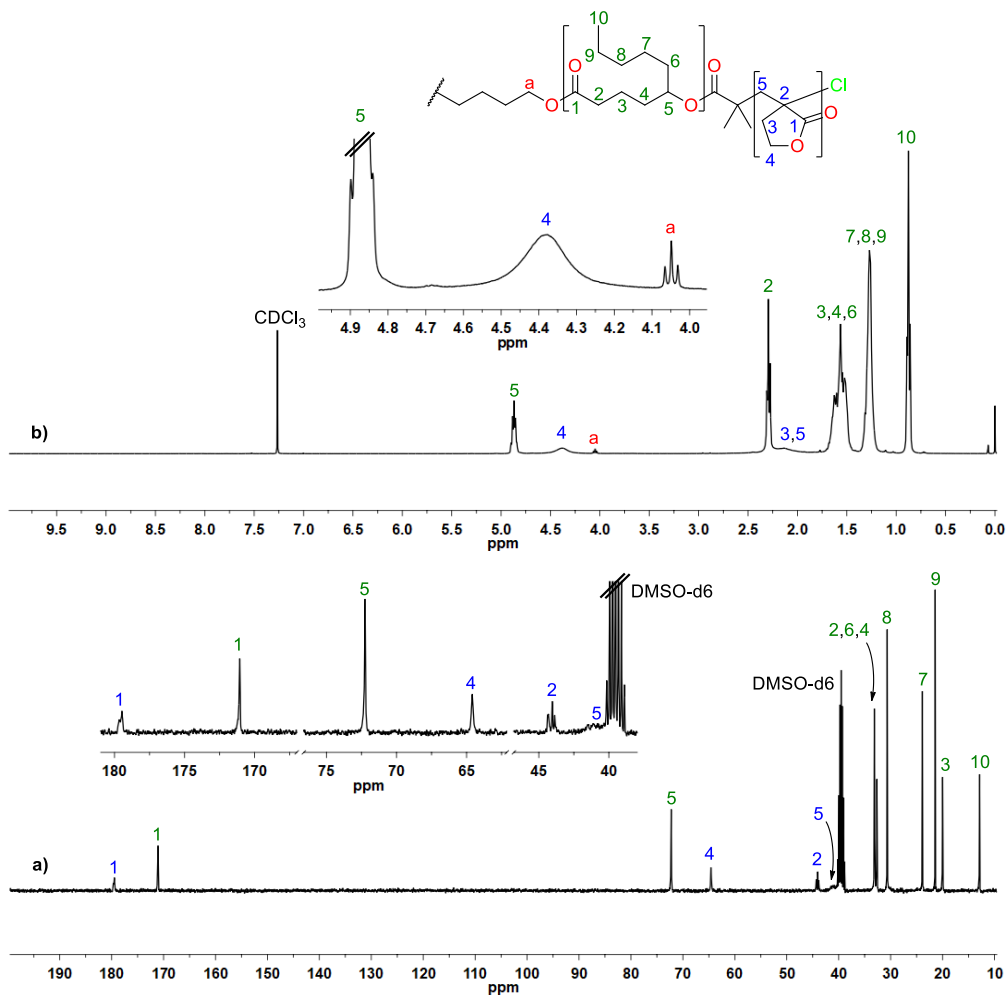


Figure 8.67 (a) ¹³C-NMR spectrum in DMSO-d₆ (recorded at 80 °C) and (b) ¹H-NMR spectrum in CDCl₃ of poly(MBL)-*co*-poly(DL)_{1,8-Oct}-*co*-poly(MBL).

8.30 Poly(MBL)-*co*-poly(DL)-I₁-*co*-poly(MBL)

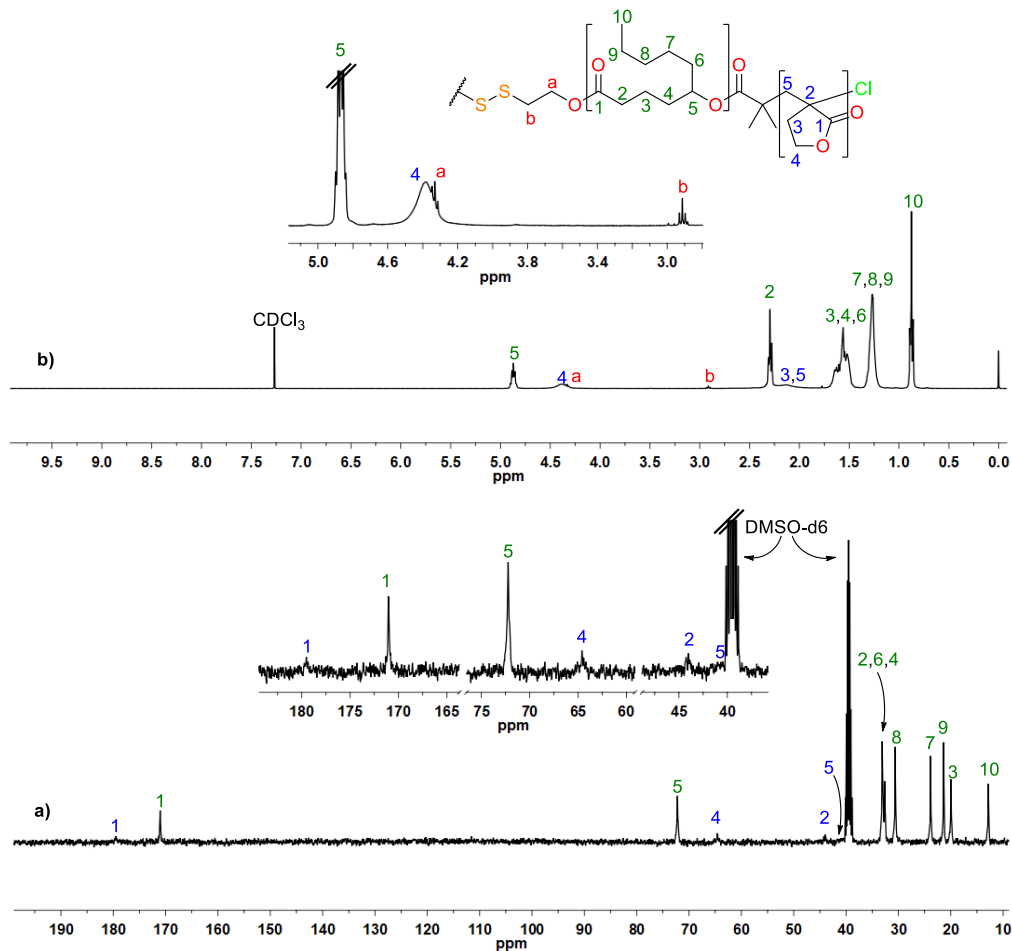


Figure 8.68 (a) ^{13}C -NMR spectrum in DMSO- d_6 (recorded at 80 °C) and (b) ^1H -NMR spectrum in CDCl_3 of poly(MBL)-*co*-poly(DL)-I₁-*co*-poly(MBL).

8.31 Poly(MBL)-*co*-poly(DL)-I₂-*co*-poly(MBL)

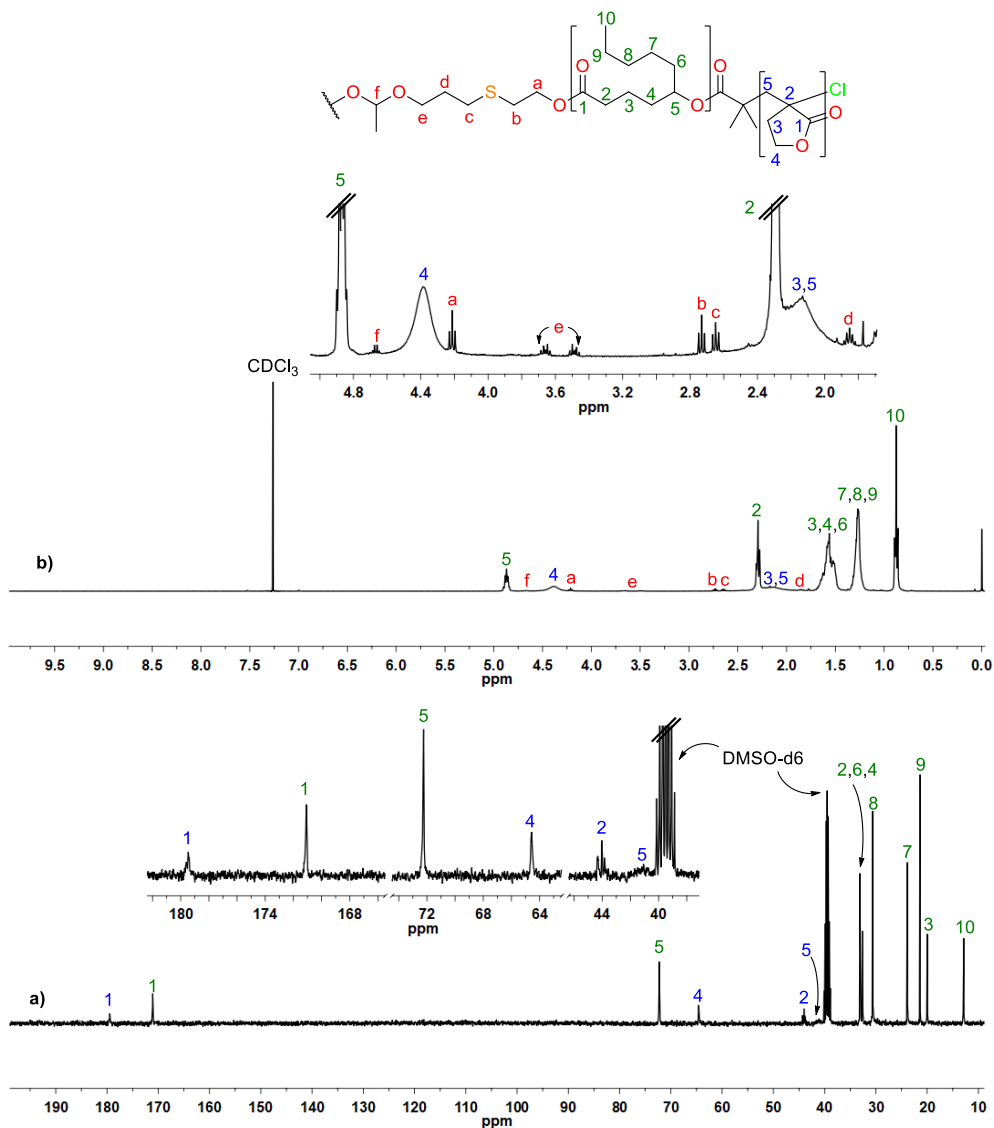


Figure 8.69 (a) ¹³C-NMR spectrum in DMSO-d₆ (recorded at 80 °C) and (b) ¹H-NMR spectrum in CDCl₃ of poly(MBL)-*co*-poly(DL)-I₂-*co*-poly(MBL).

8.32 Poly(MBL)-*co*-poly(DL)-I₃-*co*-poly(MBL)

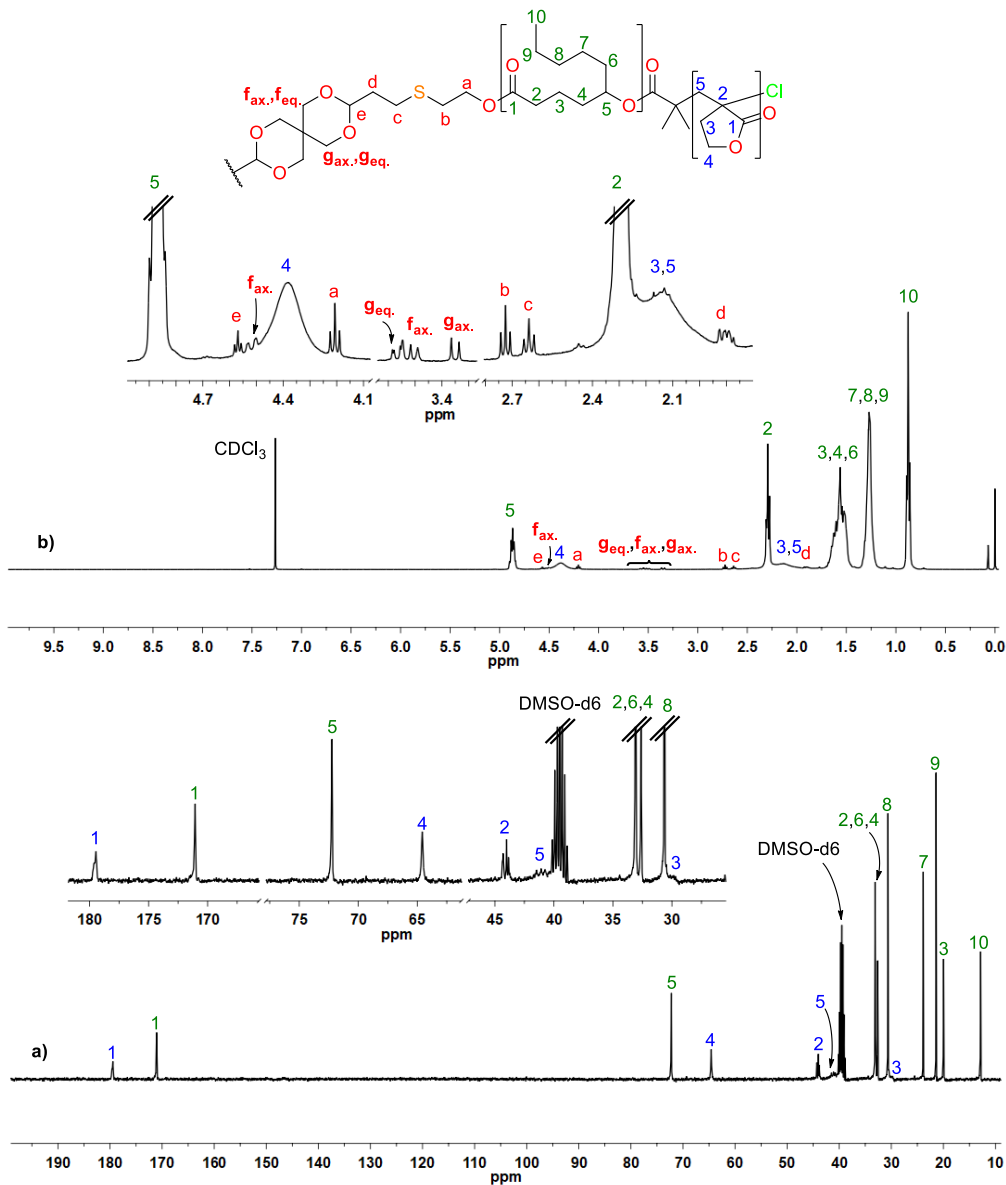


Figure 8.70 (a) ¹³C-NMR spectrum in DMSO-d₆ (recorded at 80 °C) and (b) ¹H-NMR spectrum in CDCl₃ of poly(MBL)-*co*-poly(DL)-I₃-*co*-poly(MBL).

8.33 Poly(MBL)-co-poly(DL)-I₄-co-poly(MBL)

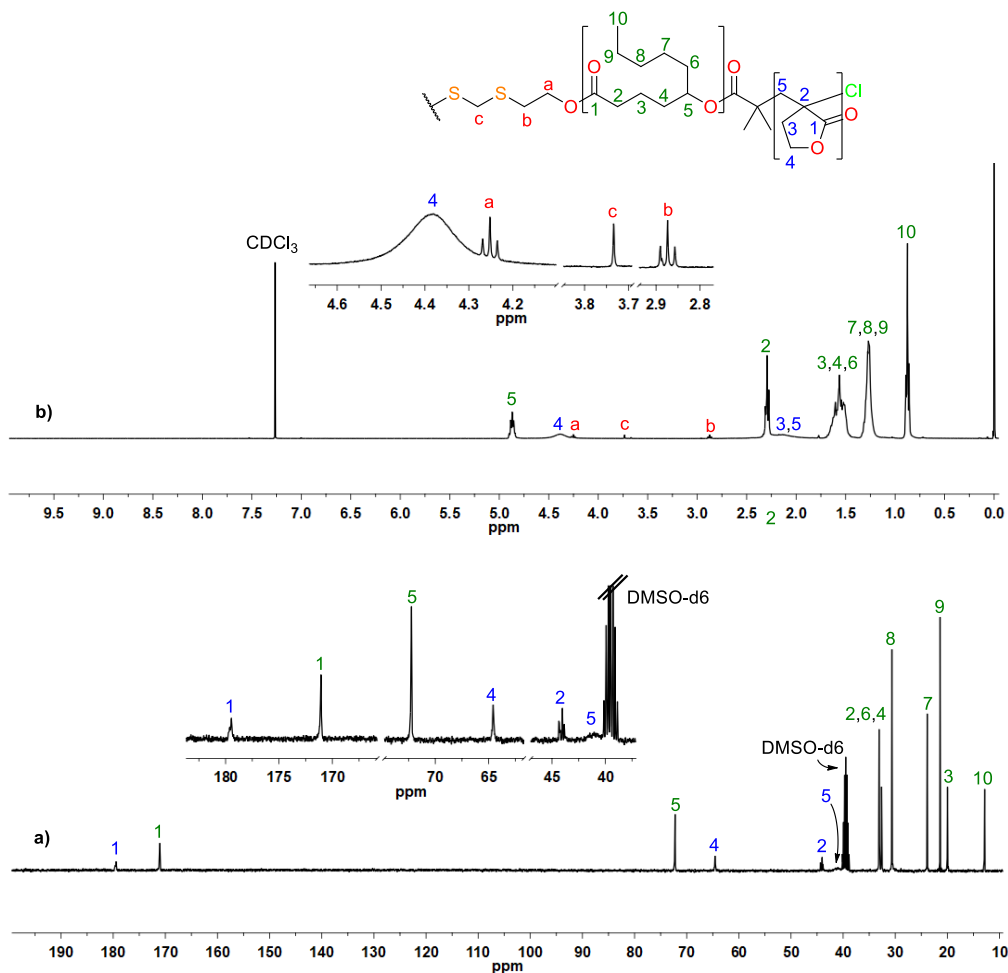


Figure 8.71 (a) ¹³C-NMR spectrum in DMSO-d₆ (recorded at 80 °C) and (b) ¹H-NMR spectrum in CDCl₃ of poly(MBL)-co-poly(DL)-I₄-co-poly(MBL).

8.34 Poly(MBL)-co-poly(DL)-I₅-co-poly(MBL)

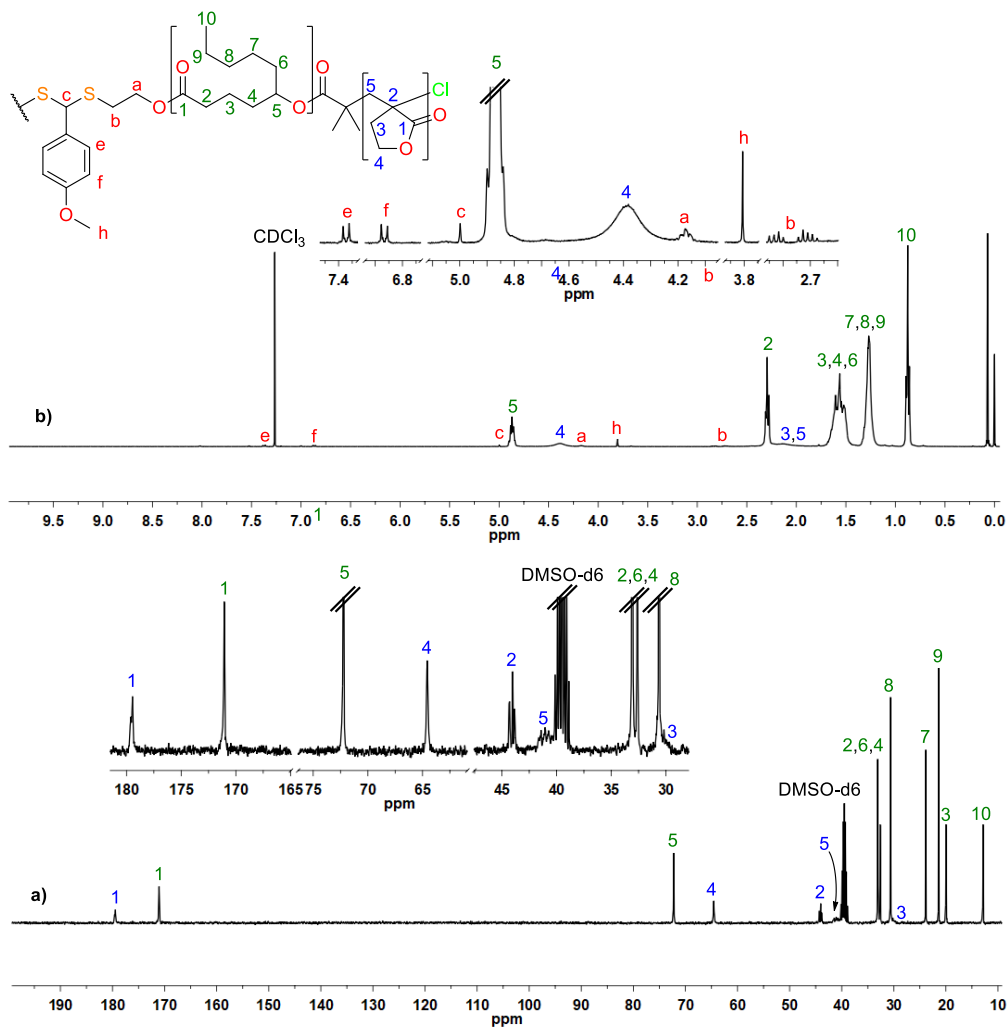


Figure 8.72 (a) ¹³C-NMR spectrum in DMSO-d₆ (recorded at 80 °C) and (b) ¹H-NMR spectrum in CDCl₃ of poly(MBL)-co-poly(DL)-I₅-co-poly(MBL).

8.35 Cleavage product of poly(MBL)-co-poly(DL)-I₁-co-poly(MBL) with Bu₃P

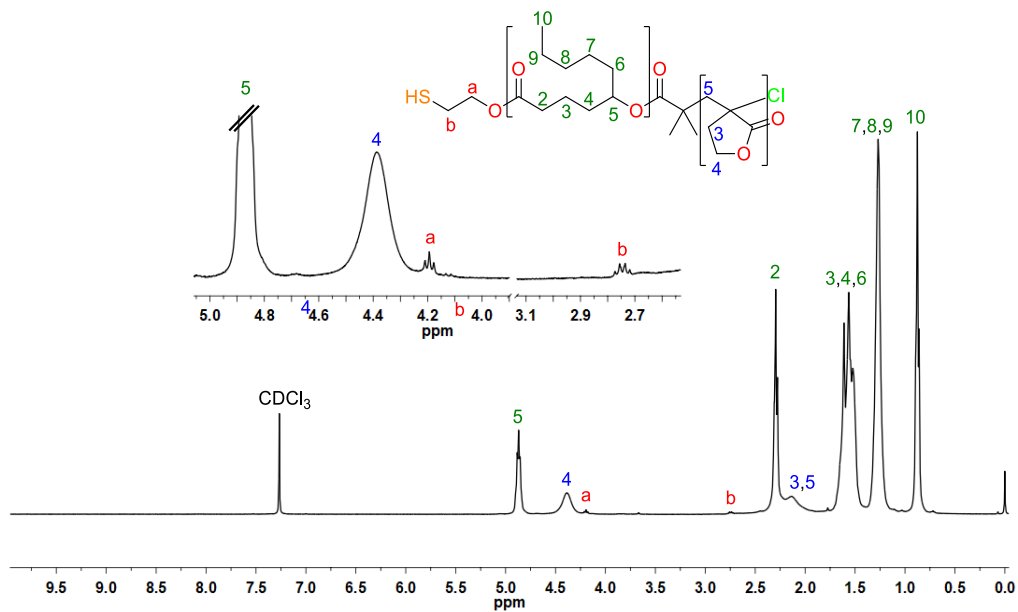


Figure 8.73 ¹H-NMR spectrum in CDCl₃ of the cleavage product of poly(MBL)-co-poly(DL)-I₁-co-poly(MBL).

8.36 Cleavage product of poly(MBL)-co-poly(DL)-I₂-co-poly(MBL)

with [TFA] = 0.01 M

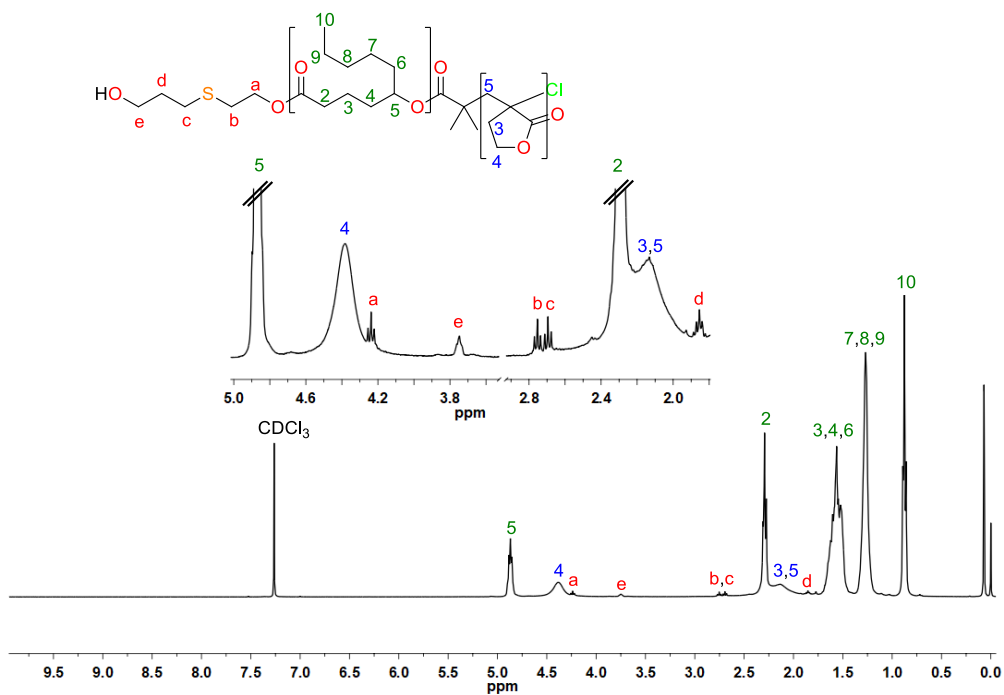


Figure 8.74 ¹H-NMR spectrum in CDCl₃ of the cleavage product of poly(MBL)-co-poly(DL)-I₂-co-poly(MBL) with [TFA] = 0.01 M.

8.37 Cleavage product of poly(MBL)-co-poly(DL)-l₂-co-poly(MBL) with [TFA] = 0.5 M

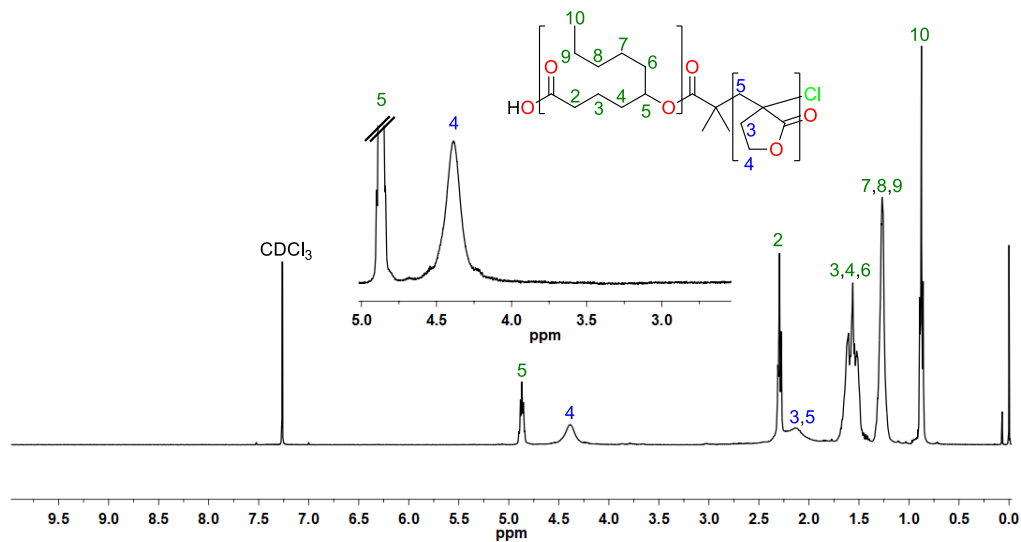


Figure 8.75 ¹H-NMR spectrum in CDCl₃ of the cleavage product of poly(MBL)-co-poly(DL)-l₂-co-poly(MBL) with [TFA] = 0.5 M.

8.38 Cleavage product of poly(MBL)-co-poly(DL)-I₃-co-poly(MBL) with [TFA] = 0.5 M at 40°C

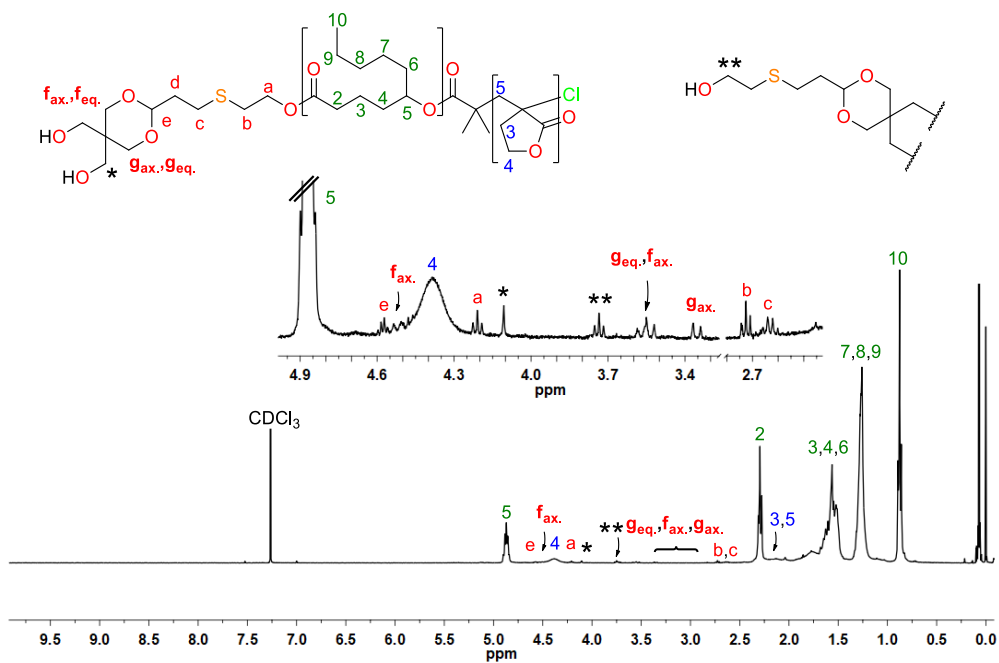


Figure 8.76 ¹H-NMR spectrum in CDCl₃ of the cleavage product of poly(MBL)-co-poly(DL)-I₃-co-poly(MBL) with [TFA] = 0.5 M at 40 °C..

8.39 Deprotection product of Dod-I₅ with DMSO/I₂ at 90 °C

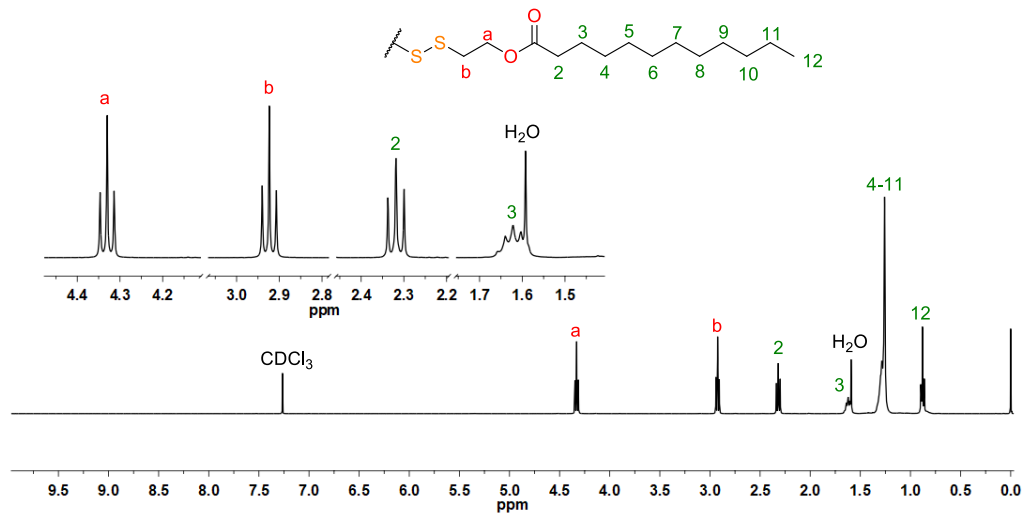


Figure 8.77 ¹H-NMR spectrum in CDCl₃ of Dod-I₅ deprotection product with DMSO containing 1 % of I₂ at 90 °C.

8.40 Cleavage products of Dod-I₅ with TPP/O₂/hv

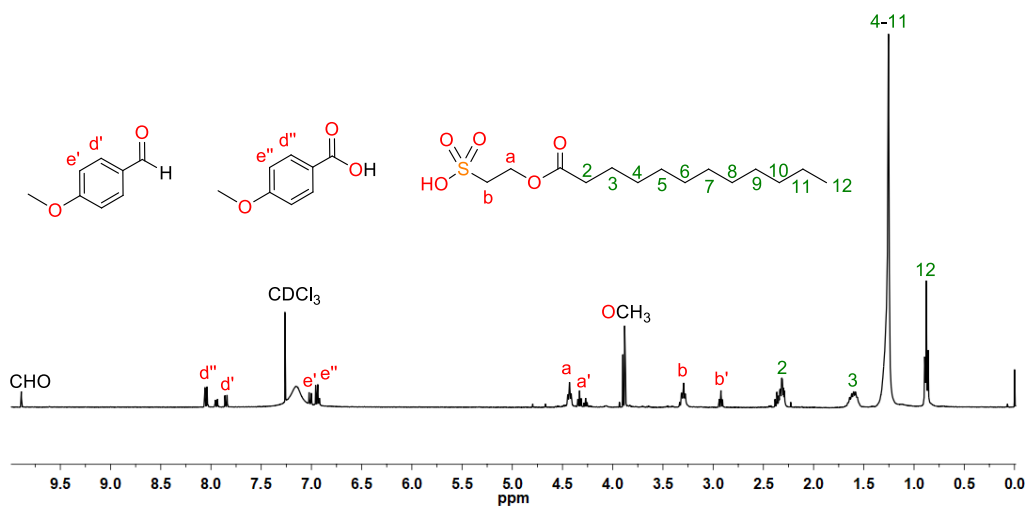


Figure 8.78 ¹H-NMR spectrum in CDCl₃ of Dod-I₅ cleavage products with TPP/O₂/hv.

8.41 Oxidation product of Dod-I₄ with H₂O₂/PTC

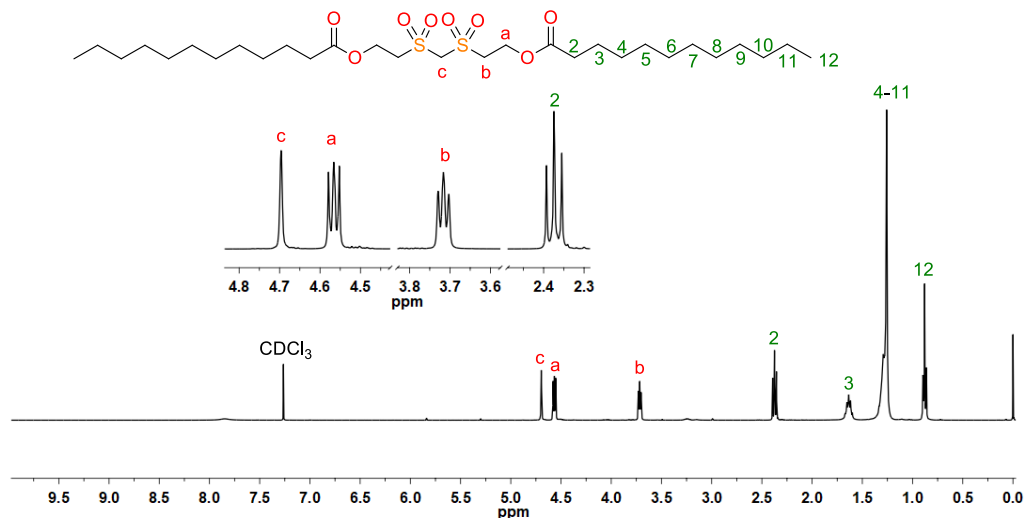


Figure 8.79 ¹H-NMR spectrum in CDCl₃ of Dod-I₄ oxidation product with H₂O₂/PTC.

8.42 Cleavage product of poly(MBL)-co-poly(DL)-I₄-co-poly(MBL) with H₂O₂/TPP/hν

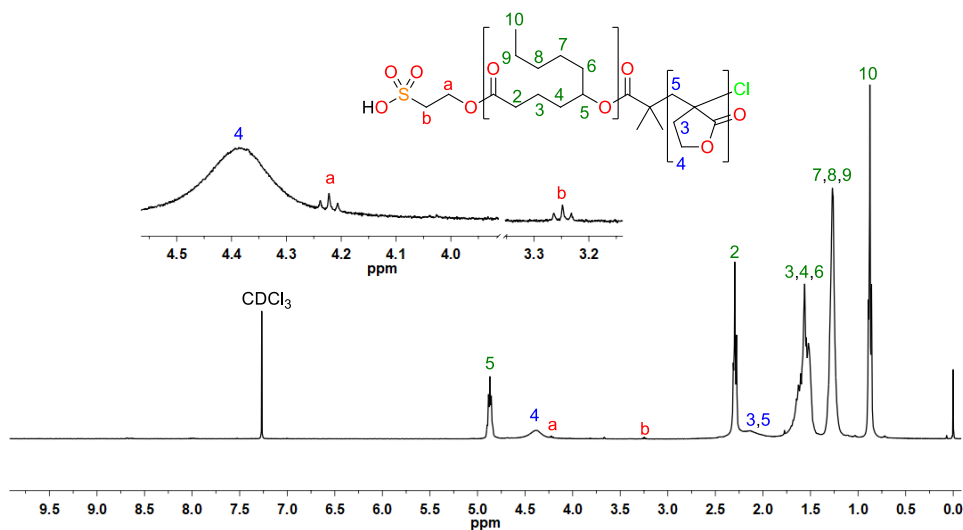


Figure 8.80 ¹H-NMR spectrum in CDCl₃ of the cleavage product of poly(MBL)-co-poly(DL)-I₄-co-poly(MBL) with H₂O₂/TPP/hν.

8.43 Cleavage product of poly(MBL)-co-poly(DL)-I₅-co-poly(MBL) with H₂O₂/TPP/hv

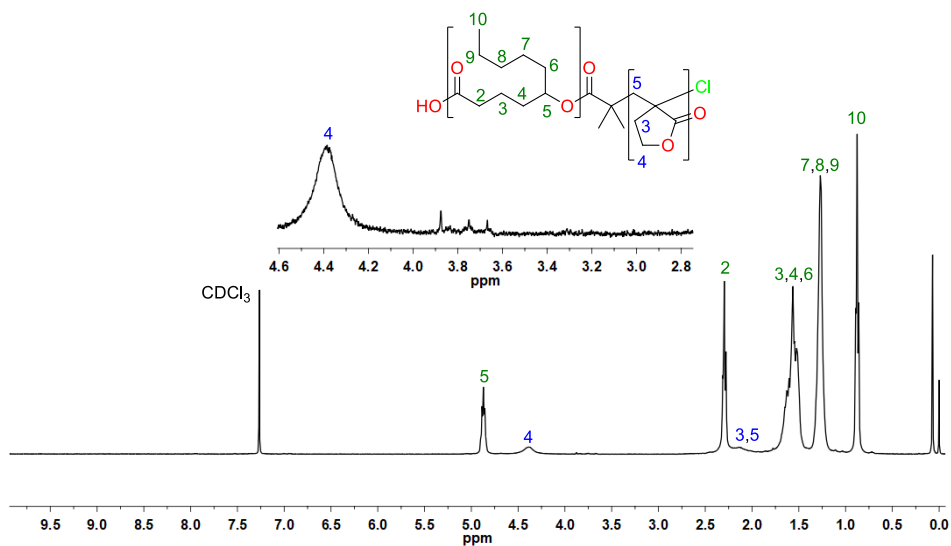


Figure 8.81 ¹H-NMR spectrum in CDCl₃ of the cleavage product of poly(MBL)-co-poly(DL)-I₅-co-poly(MBL) with H₂O₂/TPP/hv.

-
- ¹ Brar, A. S.; Singh, G.; Shankar, R. Structural investigations of poly(methyl methacrylate) by two-dimensional NMR. *J. Mol. Struct.* **2004**, *703*, 69-81.
 - ² Akkapeddi, M. K. Poly(α -methylene- γ -butyrolactone). Synthesis, configurational structure, and properties. *Macromolecules* **1979**, *12*, 546-551.
 - ³ Lee, C. W.; Nakamura, S.; Kimura, Y. Synthesis and characterization of polytulipalin-*g*-polylactide copolymers. *J. Polym. Sci. A: Polym. Chem.* **2012**, *50*, 1111-1119.
 - ⁴ Higaki, Y.; Okazaki, R.; Ishikawa, T.; Kikuchi, M.; Ohta, N.; Takahara, A. Chain stiffness and chain conformation of poly(α -methylene- γ -butyrolactone) in dilute solutions. *Polymer* **2014**, *55*, 6539-6545.

LIST OF ABBREVIATIONS

ΔG_p	Free Gibbs energy of polymerization
ΔH_p	Enthalpy of polymerization
ΔS_p	Entropy of polymerization
1O_2	Singlet oxygen
2-MTHF	2-Methyltetrahydrofuran
AcCN	Acetonitrile
AFM	Atomic Force Microscopy
AIBN	2,2'-Azobis(2-methylpropionitrile)
ARGET	Activators ReGenerated by Electron Transfer
ATRA	Atom Transfer Radical Addition
ATRP	Atom Transfer Radical Polymerization
BDE	Bond Dissociation Energy
BL	γ -Butyrolactone
BPN	2-Bromopropionitrile
bpy	2,2'-Bipyridine
BriBBr	2-Bromoisobutyryl bromide
BriBBr	2-Bromoisobutyryl bromide
CHOMP	Change-Of-Mechanism Polymerization
COPAs	Polyamide-based thermoplastic elastomers
COPEs	Polyetherester-based thermoplastic elastomer
CRP	Controlled Radical Polymerization
\bar{D}	Polydispersity index
DBU	1,8-Diazabicyclo[5.4.0]undec-7-ene
DCA	9,10-Dicyanoanthracene
DCF	Dead Chain Fraction
DCM	Dichloromethane
DL	δ -Decalactone
DMA	Dynamic Mechanical Analysis
DMAP	Dimethyl amino pyridine
DMF	<i>N,N</i> -Dimethylformamide
DMSO	Dimethyl sulfoxide
dNbpy	4,4'-Di-(5-nonyl-2,2'-dipyridyl)
DP	Degree of Polymerization
DPP	Diphenyl phosphate
DSC	Differential Scanning Calorimetry
DTT	Dithiothreitol
EA	Electron Affinity
EBPA	Ethyl 2-bromophenylacetate
ESI-MS	Electrospray Ionization-Mass Spectrometry

ET	Electron Transfer
EtBrIB	Ethyl 2-bromoisobutyrate
FRP	Free Radical Polymerization
GSH	Glutathione
HE	Halogen Exchange
I ₁	bis(2-hydroxyethyl) disulfide
I ₂	1,1-bis-[3-((2-hydroxyethyl)thio)propyloxy]ethane
I ₃	3,9-bis-[2-(ethylthio)-ethanol]-2,4,8,10-tetraoxaspiro[5.5]undecane
I ₄	bis-((2-hydroxyethyl)thio)methane
I ₅	(4-methoxyphenyl)-bis-[(2-hydroxyethyl)thio]methane
I ₆	1,4-phenylenebis(methylene)-bis(2-bromoisobutyrate)
ICAR	Initiators for Continuous Activator Regeneration
KTFA	Potassium trifluoroacetate
MALDI-TOF	Matrix Assisted Laser Desorption ionization Time of Flight
MB	Methylene blue
MBCs	Multiblock copolymers
MBL	α -Methylene- γ -butyrolactone
MBrP	Methyl 2-bromopropionate
MDI	Diphenylmethane-4,4'-diisocyanate
Me ₆ TREN	tris[2-(Dimethylamino)ethyl]amine
MMA	Methyl methacrylate
Mn	Average molecular weight
MTBD	<i>N</i> -methyl-TBD
MVL	α -Methylene- γ -valerolactone
NMP	Nitroxide Mediated Polymerization
NMR	Nuclear Magnetic Resonance
OBA	<i>o</i> -Nitrosobenzaldehyde
ONB	<i>o</i> -Nitrobenzyl
PBA	Poly(butyl acrylate)
PCL	Poly(ϵ -caprolactone)
PE	Polyethylene
PEBr	1-Phenylethyl bromide
PET	Poly(ethylene terephthalate)
PHA	Poly(hydroxyalkanoates)
PI	Polyisoprene
PLA	Poly(lactic acid)
PM	Poly(menthide)
PMA	Poly(methyl acrylate)
PMBL	Poly(α -methylene- γ -butyrolactone)
PMDETA	<i>N,N,N',N'',N'''</i> -Pentamethyl-diethylenetriamine
PMMA	Poly(methyl methacrylate)
PS	Polystyrene

PVC	Poly(vinyl chloride)
RAFT	Reversible Addition-Fragmentation Chain-Transfer polymerization
ROMP	Ring Opening Metathesis Polymerization
ROP	Ring-Opening Polymerization
ROS	Reactive Oxygen Species
ROTEP	Ring-Opening Transesterification Polymerization
SARA	Supplemental Activator and Reducing Agent
SBS	Styrene-butadiene-styrene
SEC	Size Exclusion Chromatography
SET	Single Electron Transfer
SET-LRP	Single-Electron Transfer Living Radical Polymerization
SIS	Styrene-isoprene-styrene
SR&NI	Simultaneous Reverse and Normal Initiation
TBD	1,5,7-Triazabicyclo[4.4.0]dec-5-ene
TCPPClO ₄	2,4,6-tri-(<i>p</i> -chlorophenyl)pyrylium perchlorate
TDI	2,4-Toluene-diisocyanate
TEA	Triethylamine
T_g	Glass transition temperature
TGA	Thermogravimetric analysis
THF	Tetrahydrofuran
T_m	Melting temperature
TPE	Thermoplastic elastomer
TPOs	Thermoplastic polyolefin blends
TPP	<i>meso</i> -Tetraphenylporphyrin
TPVs	Dynamically vulcanized polymer blends
TRA	Truxillic acid
TU	Thiourea

PUBLICATION

Title: Bio-based ABA triblock copolymers with central degradable moieties.

Authors: Verdugo, P.; Lligadas, G.; Ronda, J. C.; Galià, M.; Cádiz, V.

Reference: *Eur. Polym. J.* (Sent) (EUROPOL-D-20-01108)

MEETING CONTRIBUTIONS

- 1) Authors:** Verdugo, P. M.; Ronda, J. C.; Lligadas, G.; Galià, M. Cádiz, V.
Title: “Stimuli cleavable bio-based thermoplastic block copolymers”
Type of contribution: Poster
Scientific meeting: XIV Congreso del Grupo Especializado de Polímeros (GEP).
Place: Huelva, Spain
Date: 24/09/2018 – 27/09/2018

- 2) Authors:** Verdugo, P. M.; Ronda, J. C.; Lligadas, G.; Galià, M. Cádiz, V.
Title: “Stimuli cleavable bio-based thermoplastic block copolymers”
Type of contribution: Oral communication
Scientific meeting: X Congreso de Jóvenes Investigadores en Polímeros (JIP).
Place: Burgos, Spain
Date: 20/05/2019 – 23/05/2019

UNIVERSITAT ROVIRA I VIRGILI
STIMULI-RESPONSIVE CALIX[4]PYRROLE AND CALIX[4]ARENE BASED RECEPTORS: FROM UNIMOLECULAR
TO DIMERIC STRUCTURES

Pedro Miguel Mendonça Ferreira

UNIVERSITAT ROVIRA I VIRGILI
STIMULI-RESPONSIVE CALIX[4]PYRROLE AND CALIX[4]ARENE BASED RECEPTORS: FROM UNIMOLECULAR
TO DIMERIC STRUCTURES

Pedro Miguel Mendonça Ferreira

UNIVERSITAT ROVIRA I VIRGILI
STIMULI-RESPONSIVE CALIX[4]PYRROLE AND CALIX[4]ARENE BASED RECEPTORS: FROM UNIMOLECULAR
TO DIMERIC STRUCTURES

Pedro Miguel Mendonça Ferreira

UNIVERSITAT ROVIRA I VIRGILI
STIMULI-RESPONSIVE CALIX[4]PYRROLE AND CALIX[4]ARENE BASED RECEPTORS: FROM UNIMOLECULAR
TO DIMERIC STRUCTURES

Pedro Miguel Mendonça Ferreira



UNIVERSITAT ROVIRA I VIRGILI